ELASTIC-PLASTIC FRACTURE TEST METHODS

SECOND VOLUME

The User's Experience

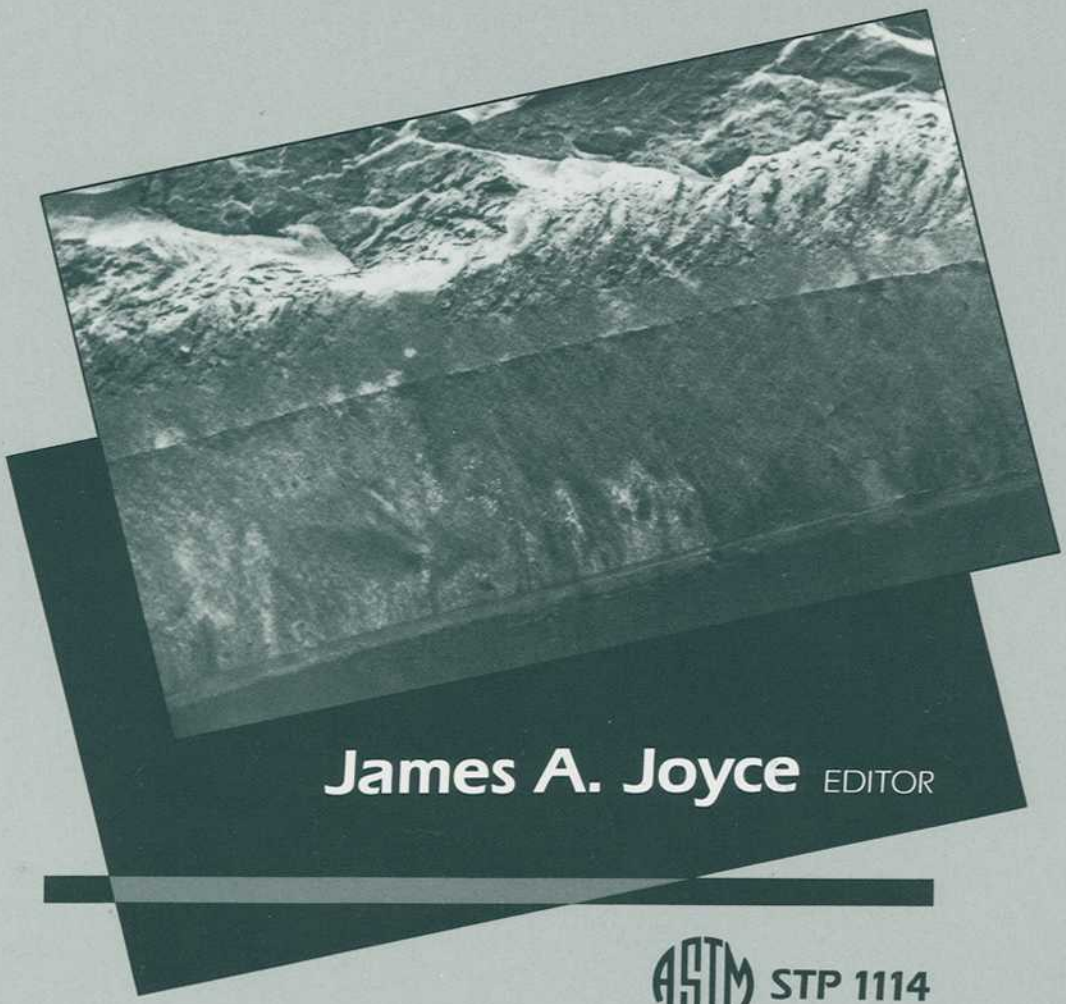

James A. Joyce EDITOR

ASTM STP 1114

STP 1114

Elastic-Plastic Fracture Test Methods: The User's Experience (Second Volume)

James A. Joyce, editor

ASTM Publication Code Number (PCN)
04-011140-30

ASTM
1916 Race Street
Philadelphia, PA 19103

ASTM Publication Code Number (PCN): 04-011140-30
ISBN: 0-8031-1418-4
ISSN: 055-8497

Photocopy Rights

Peer Review Policy

Each paper published in this volume was evaluated by three peer reviewers. The authors addressed all of the reviewers' comments to the satisfaction of both the technical editor(s) and the ASTM Committee on Publications.

The quality of the papers in this publication reflects not only the obvious efforts of the authors and the technical editor(s), but also the work of these peer reviewers. The ASTM Committee on Publications acknowledges with appreciation their dedication and contribution to time and effort on behalf of ASTM.

Printed in Baltimore, MD
August 1991

Foreword

The papers in this publication, *Elastic-Plastic Fracture Test Methods; The User's Experience (Second Volume)*, were presented at a symposium held in Lake Buena Vista, Florida, 8–9 November 1989. The symposium was sponsored by ASTM Committee E24 on Fracture Testing. James A. Joyce, U.S. Navy Academy, presided as chairman and is editor of this publication.

Contents

Overview 1

Experience with the Use of the New ASTM E 813-87—W. ALAN VAN DER SLUYS AND CHARLES S. WADE 2

A Comparison of the *J*-Integral and CTOD Parameters for Short Crack Specimen Testing—WILLIAM A. SOREM, ROBERT H. DODDS, JR., AND STANLEY T. ROLFE 19

Normalization: An Experimental Method for Developing *J-R* Curves—ZHEN ZHOU, KANG LEE, RUBEN HERRERA, AND JOHN D. LANDES 42

Quantification of Engineering Limits to *J* Control of Ductile Crack Growth—JAMES A. JOYCE 57

Specimen Size Requirements for Elastic-Plastic Crack Growth Resistance Curves—J. ROBIN GORDON AND RICHARD L. JONES 81

A Fracture Instability Data Qualification Limit—BRUCE D. MACDONALD, R. H. OBERDICK, AND A. L. HISER, JR. 102

Development of Eta Factors in Elastic-Plastic Fracture Testing Using a Load Separation Technique—MONIR H. SHAROBEAM, JOHN D. LANDES, AND RUBEN HERRERA 114

Obtaining *J*-Resistance Curves Using the Key-Curve and Elastic Unloading Compliance Methods: An Integrity Assessment Study—SABU J. JOHN 133

Nonincremental Evaluation of Modified *J-R* Curve—NAOTAKE OHTSUKA 150

Experience in Using Direct Current Electric Potential to Monitor Crack Growth in Ductile Metals—MARK P. LANDOW AND CHARLES W. MARSCHALL 163

Analysis of Deformation Behavior During Plastic Fracture—JUN MING HU AND PEDRO ALBRECHT 178

Fracture Toughness and Fatigue Crack Initiation Tests of Welded Precipitation-Hardening Stainless Steel—JOHN H. UNDERWOOD, RICHARD A. FARRARA, G. PETER O'HARA, JOHN J. ZALINKA, AND JOHN R. SENICK 197

Experience with *J* Testing of Type 304/308 Stainless Steel Weldment—STEPHEN M. GRAHAM, W. RANDOLPH LLOYD, AND WALTER G. REUTER 213

Key-Curve Analysis of Linde 80 Welds—KENNETH K. YOON, W. ALAN VAN DER SLUYS, AND ARTHUR L. LOWE, JR. 225

Observations in Conducting *J-R* Curve Tests on Nuclear Piping Materials—CHARLES W. MARSCHALL AND MARK P. LANDOW 238

Effect of Residual Stress on the *J-R* Curve of HY-100 Steel—ANDREA D. GALLANT, ISA BAR-ON, AND FLOYD R. TULER 260

Dynamic Fracture Toughness of Modified SA508C12 in the Ductile-to-Brittle Transition Region—MARIE T. MIGLIN, C. SCOTT WADE, JAMES A. JOYCE, AND W. ALAN VAN DER SLUYS 273

Discussion 289

The Application of the Multispecimen *J*-Integral Technique to Toughened Polymers—DONALD D. HUANG 290

Fracture Toughness of Polycarbonate as Characterized by the *J*-Integral—HENRY L. BERNSTEIN 306

Determination of J_{Ic} for Polymer Using the Single Specimen Method—WAI N. CHUNG AND JAMES G. WILLIAMS 320

Author Index 341

Subject Index 343

Overview

User experience with elastic-plastic test methods dates to 1981 when the first test standard in this field, ASTM E 813-81, J_{Ic}, A Measure of Fracture Toughness, became a part of the ASTM Standards. This original standard provided a starting point for standards development in elastic-plastic fracture mechanics throughout the world. In 1983 the first symposium on User's Experience with Elastic-Plastic Fracture Test Methods was sponsored by ASTM Committee E24 and held in Knoxville, Tennessee. Papers and discussion presented at this symposium was published in *ASTM STP 856* in 1985. The work presented included not only criticism of E 813 but also new and improved test techniques and many suggestions for improvement of elastic-plastic test technology.

This forum of new work and criticism had direct application to the development of a dramatically improved version of E 813 as well as the completion of a second test standard, ASTM E 1152, Determining *J-R* Curves, both of which were first included in the ASTM Book of Standards in 1987.

Much work has continued in the field of elastic-plastic fracture mechanics, and the new work is again having a direct impact on the ASTM test standards. The Second Symposium on User Experience with Elastic-Plastic Fracture Test Methods was held in Orlando, Florida, in November of 1989 to again bring together the experts with experience to share in testing of elastic-plastic and fully plastic materials. Papers presented cover experiences with the test standards, suggestions for improvements and modifications, possible redefinition of the limits of applicability, and applications to a range of materials including polymers. Generally the presentations and discussions at this symposium demonstrate a higher level of satisfaction with the E 813-87 standard than there was with the E 813-81 standard. Many suggestions for improvements were made and will become a basis for a continued evaluation of elastic-plastic test standards.

The editor would like to acknowledge the assistance of Dorothy Savini of ASTM, E. M. Hackett and J. P. Gudas of DTRC, Annapolis, Maryland, in planning and organizing the symposium. I thank the authors for making their presentations and submitting their formal papers which make up this publication, and I thank the attendees whose open discussions, questions, and comments resulted in a stimulating symposium. I especially thank the reviewers who read and critiqued the papers and who have helped me ensure a high degree of professionalism and technical quality in this publication.

I wish to thank Portia Wells and Inez Johnson of the U. S. Naval Academy Mechanical Engineering Department for their aid with document preparation and correspondence associated with both the symposium and this publication, and I wish to thank ASTM publications staff for their many contributions, including supplying deadlines, suggestions, and advice during the preparation of this special technical publication.

James A. Joyce
Mechanical Engineering Department, U. S. Naval Academy, Annapolis, MD 21402; symposium chairman and editor.

W. Alan Van Der Sluys[1] *and Charles S. Wade*[1]

Experience with the Use of the New ASTM E 813-87

REFERENCE: Van Der Sluys, W. A. and Wade, C. S., **"Experience with the Use of the New ASTM E 813-87,"** *Elastic-Plastic Fracture Test Methods: The User's Experience (Second Volume), ASTM STP 1114*, J. A. Joyce, Ed., American Society for Testing and Materials, Philadelphia, 1991, pp. 2–18.

ABSTRACT: In this paper the impact of recent changes in ASTM Test Method for J_{Ic}, a Measure of Fracture Toughness (E 813) are evaluated. J_{Ic} was determined from a large number of *J-R* curves using both the 1981 and the 1987 versions of ASTM E 813. The value of J_{Ic} is usually from 10 to 15% higher when measured according to the new version of the standard. The scatter in the measured J_{Ic} values was not affected by the revisions. Although the revisions to the standard removed a number of difficulties with its use, one problem still remains to be resolved. ASTM E 813 should be revised to include some guidance for correcting a_0 so that the blunting line fits the data in the early portion of the *J-R* curve when a *J-R* curve from ASTM Test Method for Determining *J-R* Curves (E 1152-87) is used.

KEY WORDS: elastic-plastic fracture, test methods, *J-R* curve, J_{Ic} test standards, fracture toughness

The J_{Ic} value of a material was first defined in Ref *1* in 1972. This parameter is now used as a measure of a material's resistance to the initiation of ductile testing. In 1981, the ASTM issued the Test Method for J_{Ic}, a Measure of Fracture Toughness (E 813-81). This method was extensively revised and reissued in 1987. The objective of this paper is, in part, to evaluate the impact on measured values of J_{Ic} made by the changes to ASTM E 813 in the 1987 revision. Two major modifications were made to the ASTM E 813-81 version in creating the ASTM E 813-87 version. The most significant involved changing the method of determining the value of J_{Ic} from the *J-R* curve. The 1981 version of the method uses the intersection of the blunting line and a linear line fit to a portion of the *J-R* curve as the measuring point. This procedure was changed in the 1987 version of the method to use the intersection of a power law fit to the same portion of the data and a construction line parallel to the blunting line that is offset by an amount representing 0.2 mm (0.008 in.) of crack extension.

The second major revision to the 1981 version modified the equation used to evaluate *J* from load, displacement, and crack length information. The expression used in the 1981 version evaluated *J* from the total area under the load displacement curve. The expression was changed so that the elastic and plastic parts of *J* are evaluated separately in the 1987 version. The elastic term is evaluated from the elastic stress intensity, *K*, defined in ASTM Test Method for Plane-Strain Fracture Toughness of Metallic Materials (E 399-83). The plastic term is determined from the plastic portion of the area under the load displacement

[1]Scientist and group supervisor, respectively, Babcock & Wilcox, Research and Development Division, Alliance, OH 44601.

curve. The combination of the modified relationship for calculating J and the new procedure for determining J_{Ic} were intended to improve the accuracy in calculating J and decrease the variability in J_{Ic}. Differences observed in data sets analyzed by both versions of the method will be discussed in this paper.

In addition to the two revisions just described, ASTM issued a new standard in 1987, ASTM Test Method for Determining J-R Curves (E 1152-87). ASTM E 813-87 allows the use of the J-R curve determined by ASTM E 1152-87 for the determination of J_{Ic}.

A second objective of this study is to evaluate problem areas that still exist in the method and to recommend solutions to these problems. The method of correcting a_0 so that the blunting line fits data in the initial portion of the J-R curve is still a problem in the standard. A discussion of this problem and difficulties meeting validity criteria will be included in this paper.

Finally, various procedures for fitting mathematical models to a J-R curve will be reviewed. The procedures will be evaluated in terms of the goodness of the fit to the J-R curve and the ability to extrapolate the J-R curve from small-sized specimens.

Comparison of Data

The important issue to be addressed is the effect of the changes in the method on the measured value of J_{Ic}. Difficulties were encountered with the 1981 version that were identified at the 1983 user's experience symposium [*2*]. One major problem with the 1981 version was a significant variation in J_{Ic} with repeated evaluation of the same data set. By omitting alternate points between the exclusion lines, variations in valid measures of J_{Ic} were as high as 10% for a given test. This problem is related to the use of a linear fit to the data between the 0.15-mm (0.006-in.) and 1.5-mm (0.060-in.) exclusion lines for the determination of J_{Ic}.

The shape of a J-R curve between the exclusion lines is often best represented by a power law relationship rather than a linear relationship. In this situation, the linear relationship is strongly influenced by the number and spacing of points between the exclusion lines. In the 1981 version, J_{Ic} was determined from the intersection of a linear fit to the data between the exclusion lines and the theoretical blunting line. Therefore, J_{Ic} was also sensitive to the number and spacing of points on the J-R curve that fell between the exclusion lines. As a solution to this problem, the 1987 version uses a power law fit to the data between the exclusion lines. This relationship is much less sensitive to the number and spacing of points between the exclusion lines. The intersection of the power law fit and a construction line define J_{Ic}. The construction line has a slope equivalent to the theoretical blunting line but is offset by an amount representing 0.2 mm (0.008 in.) of crack extension.

A second concern identified in the 1983 symposium was scatter in J_{Ic} values obtained from the analysis of data sets generated from testing several specimens from the same material. The modifications made in the 1987 version of the method were intended to address these concerns.

To reveal the changes in measured J_{Ic} values that are induced by the modifications to the method, results from a large number of J tests were reviewed. Data generated in several testing programs were used to make the comparisons. It was desired to evaluate test results over a range in measured J_{Ic} values. Therefore, the data reviewed includes that obtained from tests conducted for ORNL that were reported in Refs *3* and *4* and represent relatively low J_{Ic} results for ferritic materials. Data obtained in a ferritic steel piping program conducted for both Babcock & Wilcox (B&W) and the Electric Power Research Institute (EPRI) and reported in Ref *5* was also used in the J_{Ic} comparison. This data set contained a range in J_{Ic} results. For those tests that were conducted prior to 1987, the results were reanalyzed using ASTM E 813-87 procedures. For tests completed according to the 1987 version of

ASTM E 813, the results were reanalyzed to the 1981 version of the method. As will be discussed later, a procedure was used that resulted in a consistent correction of the initial crack length, a_0. This correction method provides for good agreement between the data in the initial portion of the *J-R* curve and the blunting line. The method described in ASTM E 1152-87 for determination of a_0 can result in inappropriate placement of the blunting line and erroneous J_{Ic} values.

All *J* tests used in this comparison were conducted using the computer-controlled single-specimen technique described in Ref *6*. Load and displacement data were stored directly. Crack length information was inferred from unloading compliance data.

The data presented in Figs. 1 and 2 are used to evaluate the changes in the measured values of J_{Ic} produced by the modifications of the method. Figure 1 presents the J_{Ic} values determined on seven different materials over a range in test temperatures all on the Charpy upper shelf. The materials included in this figure are four submerged-arc-weld metals (Refs *3–5*), two ferritic steels [*5*], and a manual metal weld [*5*]. In all cases, the values analyzed to the 1987 method are higher than those calculated in accordance with the 1981 version of the method. The difference in the submerged-arc-weld metal data ranges from a 0 to 30% increase in the measured value of J_{Ic} from the 1981 to the 1987 versions. The average increase is 11% for the 12 results reported. In the case of the ferritic materials and the manual weld, the increase ranges from 6 to 32%. The average increase is 18% for the six values reported.

Figure 2 shows the results from two series of tests conducted at 149°C (300°F) on submerged-arc-weld metal [*3,4*]. These two weldments were fabricated using the same welding procedures and with the same heat of weld wire and lot of flux. They were each subjected to identical post-weld heat treatment cycles. There is significant scatter in these test results from each weldment. However, the difference between the results of the two test series is not significant. Bars are shown in the figure showing the plus and minus one standard deviation about the mean value of J_{Ic}. The 1987 version of the analysis resulted in an increase of the measured J_{Ic} value of approximately 10% as compared to the 1981 analysis. However, use of the 1987 analysis procedure did not reduce the scatter in the measured J_{Ic} data as evidenced by the standard deviations.

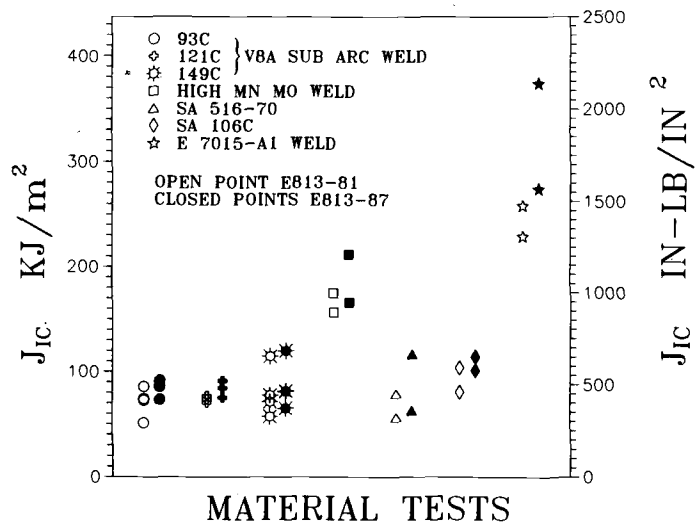

FIG. 1—J_{Ic} *values determined using ASTM E 813-81 compared with values obtained using ASTM E 813-87 for several materials.*

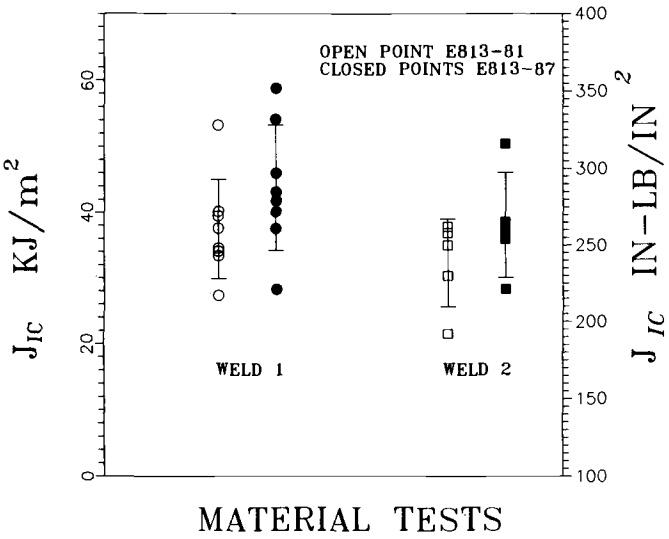

FIG. 2—J_{Ic} *values determined using ASTM E 813-81 compared with values obtained using ASTM E 813-87 for one material.*

Figure 3 is a plot of the *J-R* curves obtained from the analysis of test data for three specimens, from a single material, using both versions of the method. There is very little difference in the *J-R* curves obtained using the two versions of the method. This similarity indicates that the change in the *J* formulation yields a negligible change in a material's *J-R* curve. However, the differences in the measured J_{Ic} values for the two versions of the analyses are significant. The change in J_{Ic} values can be attributed to the changes in the measuring point used for J_{Ic} determination and not the *J* formulation.

A detailed review of two *J-R* curves from a single material that exhibited a large amount of variability in J_{Ic} was performed to determine the causes of the scatter in the J_{Ic} data. Figure 4 presents the two *J-R* curves from which the J_{Ic} values for the high magnesium-molybdenum (Mn-Mo) submerged-arc-weld metal in Fig. 1 were obtained. The J_{Ic} values obtained from these tests were 166 and 212 kJ/m^2 (947 and 1210 in. · lb/in.^{2}). While this represents a 21% difference in the J_{Ic} value, the *J-R* curves are very similar. They differ slightly in the region very close to the blunting line, yielding the difference in the measured J_{Ic} values. The *J-R* curves have a steep slope between the exclusion line for these two specimens. Large variations in J_{Ic} values would be obtained from small variations to a_o. It is conceivable that Test 3912T could easily have yielded a J_{Ic} value higher than Test 3922T using a slightly different, but acceptable, correction to a_o to obtain the best agreement between data in the early portion of the *J-R* curve and the blunting line. This topic is discussed in the next section.

The revision to ASTM E 813 invoking a power law fit rather than a linear fit to data between the exclusion lines should improve the determination of J_{Ic}. The power law more accurately defines the *J-R* curve between the exclusion lines. In addition, the revised measuring point is between the exclusion lines thereby using the power law fit to interpolate the data to determine the J_{Ic} value. In contrast, the 81 version of ASTM E 813 makes use of the linear fit to extrapolate the fit line to the blunting line to determine J_{Ic}. For these reasons the revised procedure should be less sensitive to slight changes to the data points between the exclusion lines. The data analyzed in this report does, however, not show an improve-

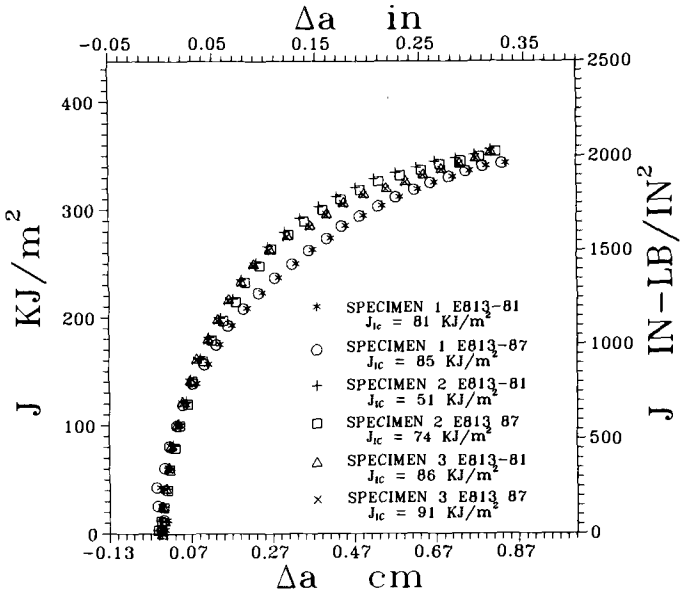

FIG. 3—J-R *curve plots of ORNL V8A submerged-arc-weld metal comparing the 1981 with the 1987 version of ASTM E 813.*

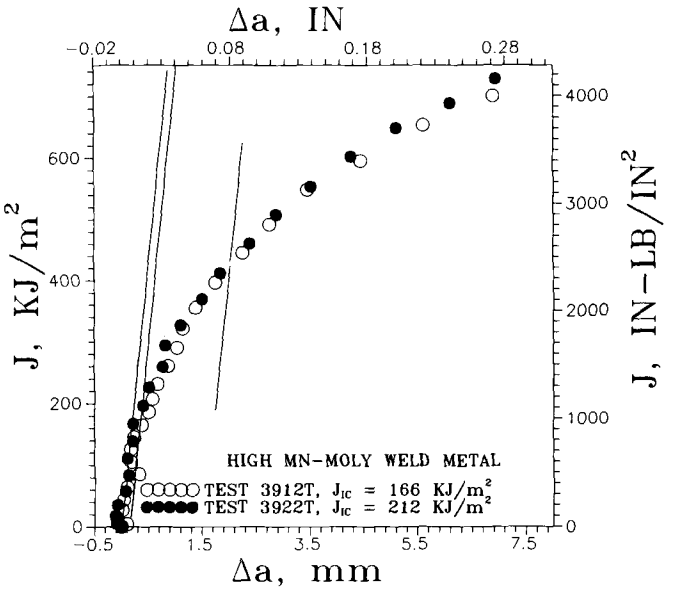

FIG. 4—*Comparison of* J-R *curves yielding significantly differing* J_{Ic} *values for the same material.*

ment. All of the *J-R* curves used in this study were determined using the procedures of ASTM E 1152-87. This may have influenced the lack of observed improvements between the 1981 and the 1987 versions of the method.

Blunting Line Data Fit

ASTM E 813 gives well-defined procedures for performing tests and reducing acquired data to obtain J_{Ic} values. After reducing load, displacement, and crack length information into *J*-integral values, the user is left to determine the critical J_{Ic} value. If the multiple-specimen procedure is used, the determination of the J_{Ic} value is well defined and adequate. If, however, a *J-R* curve is determined from a single specimen using ASTM E 1152-87, a major problem has been identified in determining an appropriate value for the initial crack length.

ASTM E 1152-87 suggests that the crack length measured at the start of the test (using compliance or other techniques) be compared with the optically measured initial crack length (measured after post-test heat tinting and specimen fracture) and any errors be corrected by determining an effective modulus value. All the crack length information used in determining the *J-R* curve is then corrected using this effective modulus. If there is a significant error in the initial crack length value, the blunting line will not fit the data in the early portion of the *J-R* curve and the effective modulus procedure will not improve the fit between the blunting line and the *J-R* curve. Because of the small load changes required in initial unloading compliance measurements, initial crack length values will have the largest errors of any of the crack lengths used to determine the *J-R* curve. Therefore, it is important to review the *J-R* curve data closely and possibly adjust the initial crack length value to obtain the best agreement between the *J-R* curve and the theoretical blunting line.

Reviewing Fig. 4, it is clear that the value of J_{Ic} is strongly dependent on the placement of the *J-R* curve data on the blunting line. The slope of the *J-R* curve may be steep in the early portion of the curve. Significant variations in J_{Ic} would then be obtained from slight differences in placement of the data on the blunting line.

Table 1 lists results obtained by the authors and an independent laboratory after analyzing identical load, displacement, and crack extension data sets. Although the *J-R* curve data calculated by the two laboratories were nearly identical, the differences in J_{Ic} were often extreme. The reason for the disparity is clear upon reviewing the position of the individual *J-R* curves with respect to the theoretical blunting line. The authors corrected a_o to obtain the best agreement between data in the initial portion of the *J-R* curve and the blunting line. The independent laboratory simply placed the first point of the *J-R* curve on the blunting line as suggested by ASTM E 1152-87. Plots of the *J-R* curves demonstrating the effect of

TABLE 1—*Comparison of* J_{Ic} *measurements obtained by two separate laboratories using identical data sets.*

	J_{Ic}, Author's		J_{Ic}, Independent Laboratory	
Data Set	kJ/m²	in. · lb/in.²	kJ/m²	in. · lb/in.²
1	266	1519	188	1076
2	180	1028	78	448
3	268	1530	132	754
4	476	2717	296	1689
5	309	1763	85	487
6	178	1016	82	470

correcting a_o are displayed in Figs. 5 and 6. Using only one crack length value to fit the *J-R* curve to the blunting line obviously yields incorrect J_{Ic} values in the cases discussed. More representative values of J_{Ic} will be obtained when an attempt is made to place a number of points from the initial portion of the *J-R* curve on the theoretical blunting line.

The authors have adopted a procedure for correcting a_o so that the initial *J-R* curve data best fit the blunting line. The data analysis computer code prompts the user to select points on the *J-R* curve that define a line with a slope nearly equal to that of the blunting line. These points are then used in a linear regression to define a new initial crack length value. All crack length values are then adjusted to be in agreement with this new initial crack length value. The initial test data will then scatter around the blunting line. This method requires judgment on the part of the experimentalist in choosing which points should fall on the blunting line. However, it forces the user to consider more than one point in the data set when fitting data to the blunting line. When using this procedure, very little error is usually seen between the initial crack length values measured by compliance and the optically measured values. If an error still exists at this point, the effective modulus procedure can be applied.

ASTM E 813 should be revised to require that a fit to more than one data point be used to establish the initial crack length value and therefore the blunting line location when a single-specimen *J-R* curve is going to be used to determine a value of J_{Ic}.

Crack Extension Requirements

ASTM E 813-87 has validity requirements relating to the uniformity of crack extension and accuracy in the measurement of the crack extension experienced during testing. Based on the authors' experience in conducting several hundred *J* tests on various materials, the requirements described in Sections 9.4.1.6 and 9.4.1.7 are often violated.

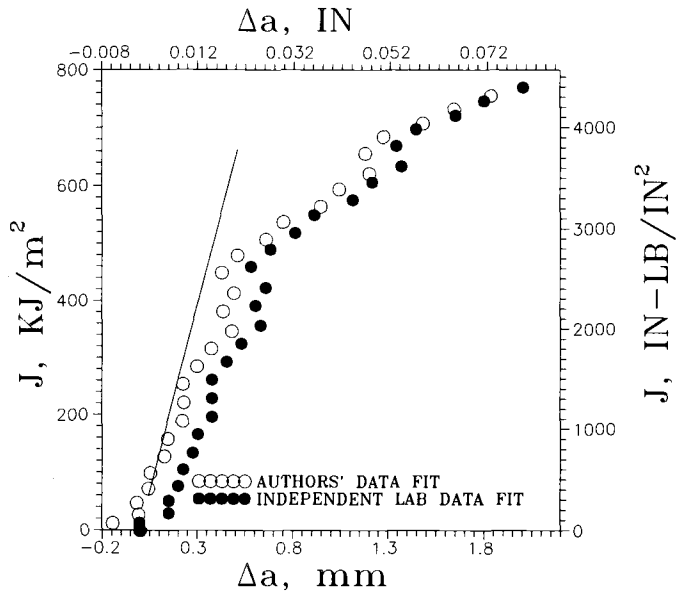

FIG. 5—*Comparison of* J-R *curve fits to the blunting line from two laboratories.*

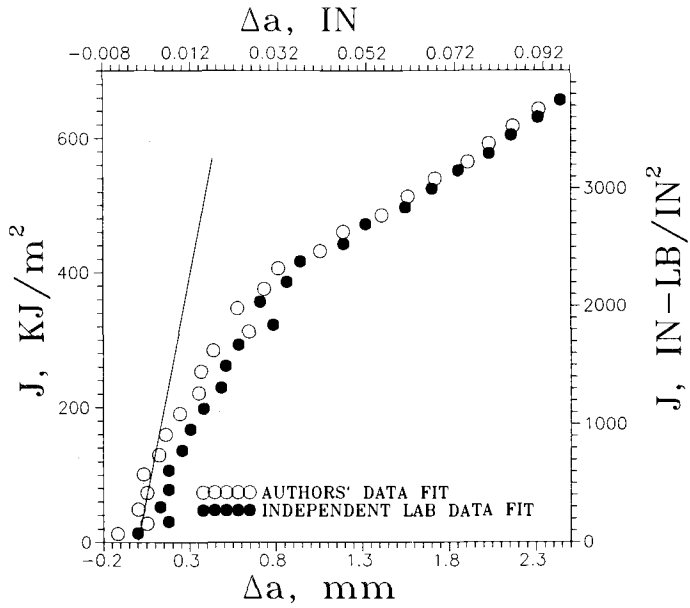

FIG. 6—*Comparison of* J-R *curve fits to the blunting line from two laboratories.*

Section 9.4.1.6 relates to the uniformity of crack extension through specimen thickness. To satisfy this J_{Ic} validity check, the crack extension at the two near-surface measuring points must not differ from that at the center of the specimen by more than $0.02W$. This criterion is often violated using side-grooved specimens due to the crack front geometries induced by precracking (before side grooving), side grooving, and subsequent testing. The crack front is usually shorter at the specimen surface than in the center after fatigue precracking. By side grooving the specimen, the crack front tends towards straightness during testing. Often times the crack extension at the surface will then exceed that in the center by an amount that violates Section 9.4.1.6.

The validity requirement of Section 9.4.1.6 appears to be overly restrictive considering the flexibility given in the crack front straightness requirement of 9.4.1.5. Section 9.4.1.5 requires that any of the nine crack length measurements taken across the crack front be within 7% of the average crack length. As a comparison of the two requirements, consider performing a test using a 1T compact specimen containing a curved initial crack front. Assume a typical initial average crack length of 33 mm (1.3 in.). The crack length at the specimen surface could differ from the average by as much as 2.3 mm (0.091 in.) and still satisfy Section 9.4.1.5. Correspondingly, the crack length at the center of the specimen could be 2.3 mm longer or shorter than the average crack length. An example of this is shown schematically in Fig. 7. If the crack became perfectly straight during testing, the crack extension at the surface would be 4.6 mm (0.182 in.) larger than that at the center. This difference is more than four times that allowed by Section 9.4.1.6, which is 1.0 mm (0.040 in.) for this example. Clearly, a discrepancy exists between these validity checks indicating that uniformity of crack extension is more important than crack front straightness. Changing the requirement to be based on crack front straightness and not uniformity of crack extension should be considered.

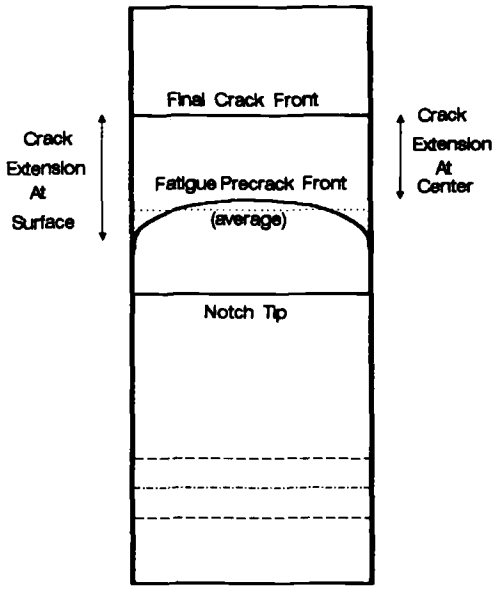

FIG. 7—*Schematic of crack extension through the thickness of a specimen.*

Section 9.4.1.7 deals with the required accuracy of the measure of crack extension. This validity check requires that the crack extension predicted by the last compliance measurement (or other method of indication) not differ from the actual physical measurement of crack extension according to the following limits.

a The difference does not exceed 0.15 Δa_p for crack extensions less than $\Delta a_{p\max}$.
b The difference does not exceed 0.15 $\Delta a_{p\max}$ for crack extensions greater than $\Delta a_{p\max}$.

The parameter $\Delta a_{p\max}$ is defined as the crack extension value where the *J-R* curve intersects the 1.5 mm (0.060 in.) exclusion line defined by ASTM E 813.

For cases in which data are desired for crack extension well beyond the second exclusion line, the requirements of 9.4.1.7 are difficult to meet. The validity of the J_{Ic} value measured from the early portion of the test is based on data obtained from the end of the test. This prohibits the user from measuring J_{Ic} and determining the material's *J-R* curve in a single test.

The accuracy and crack straightness requirements in ASTM E 813 should be revised to eliminate the problems just discussed. It is suggested that the crack extension uniformity requirement be modified to require a crack straightness rather than a uniformity of crack extension. The crack length accuracy requirement should be changed to require an accuracy based on final crack length rather than one based on the crack length at the second exclusion line.

R-Curve Fit Equations

There are a number of reasons for determining an equation for the *J-R* curve. Most instability analyses that make use of the *J-R* curve are performed with the use of a computer

program. The use of the *J-R* curve in the form of an equation greatly simplifies the instability analysis. To determine the instability condition, an extrapolation of the *J-R* curve to crack extension values well past the measuring capacity of the specimen is often required by such analyses. The ideal fit to the data should then fit the data accurately in the region where the data exist and in addition allow for the conservative extrapolation of the *J-R* curve.

There are several popular relationships used to describe the form of *J-R* curves obtained from various materials. These functions include:

1. Four Coefficient Fit [*6*], $J = C_0 + C_1A + C_2(C_3 + A)^{-2}$
2. Power Law Fit, $J = C_0A^{C_1}$
3. Eason Fit [*7*], $J = C_0A^{C_1} \exp(C_2/A)$

where A = crack extension, and C_0 through C_3 are constants.

In order to evaluate these models, each were applied to a series of *J-R* curves obtained from a single forging using a variety of specimen sizes. The ability of the model to extrapolate the small specimen data to predict the large specimen results could be evaluated.

The data sets used for the comparison of models were obtained from Refs *8* and *9*. This reference reports *J*-test results obtained on a large SA508 Cl 2 forging. Reference *10* describes a problem with inhomogeneity in the forging used to develop this fracture toughness data. The results detailed by Ref *10* were found to be ordered in accordance with the strength of the material at particular locations in the forging and were divided into four strength categories. All the specimens selected for this comparison were chosen from the same strength category as defined in Ref *10*. Specimens included two 10Ts, two 4Ts, and two 1Ts. Load, displacement, and crack length information given in Ref *8* for these specimens was used to determine *J-R* curves using the 1987 version of ASTM E 1152-87. The *J-R* curves for each specimen were fit from the blunting line to the last point before Δa exceeded $0.35b_0$ using the three models just described. These fits are well beyond limits set in ASTM E 1152-87 but were used to demonstrate the relative effectiveness of the mathematical models. The relationships obtained from each of the fit models were then used to extrapolate the *J-R* curves to a crack extension value of 127 mm (5.0 in.). Plots of *J* versus $dJ/d\Delta a$ were used to evaluate the use of each model for predicting large specimen results from the extrapolation of results from a small specimen. Both *J*-deformation (*J*-def) and *J*-modified (*J*-mod) data from the data sets were examined. The values of *J*-mod were determined in accordance with the procedures outlined in Ref *11*.

The four coefficient relationship fits the *J-R* curves very well. Representative examples are shown in Fig. 8. However, the extrapolation of this equation did not work well with some of the *J*-def and *J*-mod data sets examined in this review. When the *J-R* curve remains linear and does not asymptotically approach a maximum, this fit will yield a constant for $dJ/d\Delta a$ at large crack extensions. This result is obtained because the four-coefficient relationship has enough degrees of freedom to fit the *J-R* curve exactly. It does not force the fit to asymptotically approach some minimum $dJ/d\Delta a$ value at large crack extensions. Plots of $dJ/d\Delta a$ using extrapolations of the four-coefficient fits obtained for each specimen are given in Fig. 9 for both *J*-def and *J*-mod. The extrapolation of the fits obtained from the smaller specimens did not predict those obtained from the larger specimens for either *J*-def or *J*-mod. Even though the model fits the *J-R* curve well, it does not allow for accurate prediction of the response of a large specimen using data from a small specimen.

Eason's equation also fits most of the *J-R* curves reviewed quite well. Examples are given in Fig. 10. The extrapolation of the equations obtained from these fits appeared to yield more consistent results between specimen sizes than the extrapolation of the four-coefficient

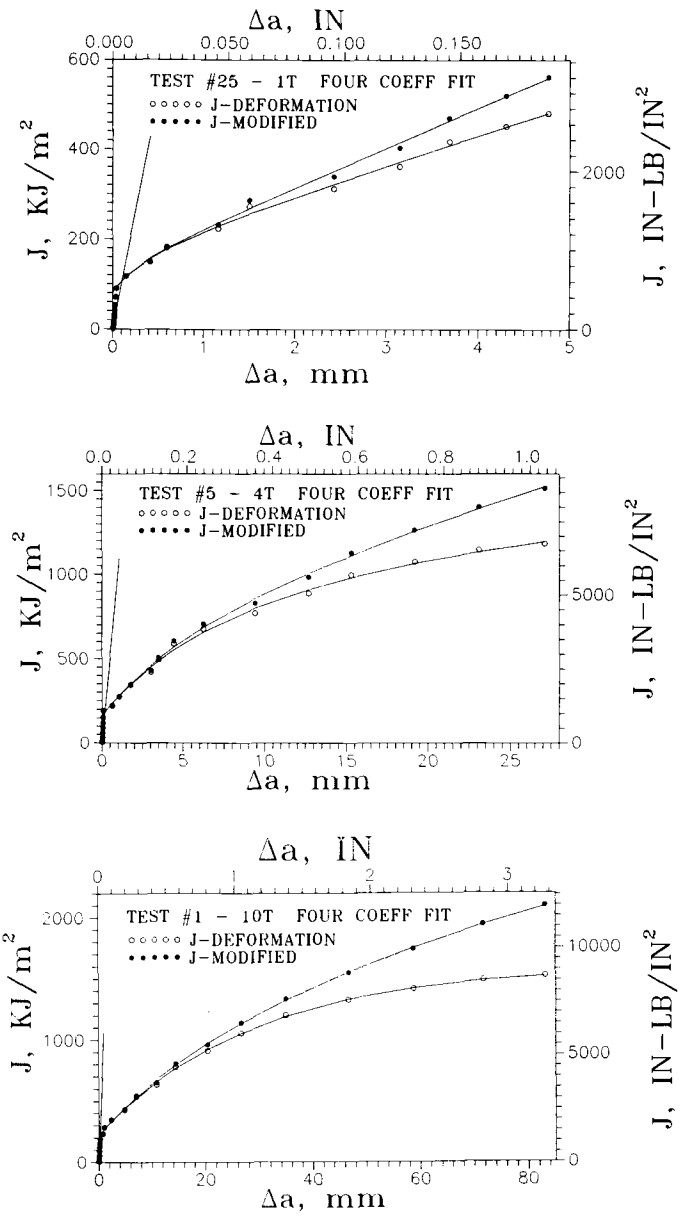

FIG. 8—*Fit of the four-coefficient model to the* J-R *curve for three specimen sizes.*

fits. Figure 11 displays J versus $dJ/d\Delta a$ for the six specimens reviewed. The data in this figure does not order by specimen size, indicating little specimen-size effect. All curves scatter around a common trend line related to material tearing properties.

The power law fit does not adequately describe many of the J-R curves reviewed when it is desired to fit the data outside the exclusion lines. Examples are given in Fig. 12. The form of this relationship does not allow for a good representation of the data throughout

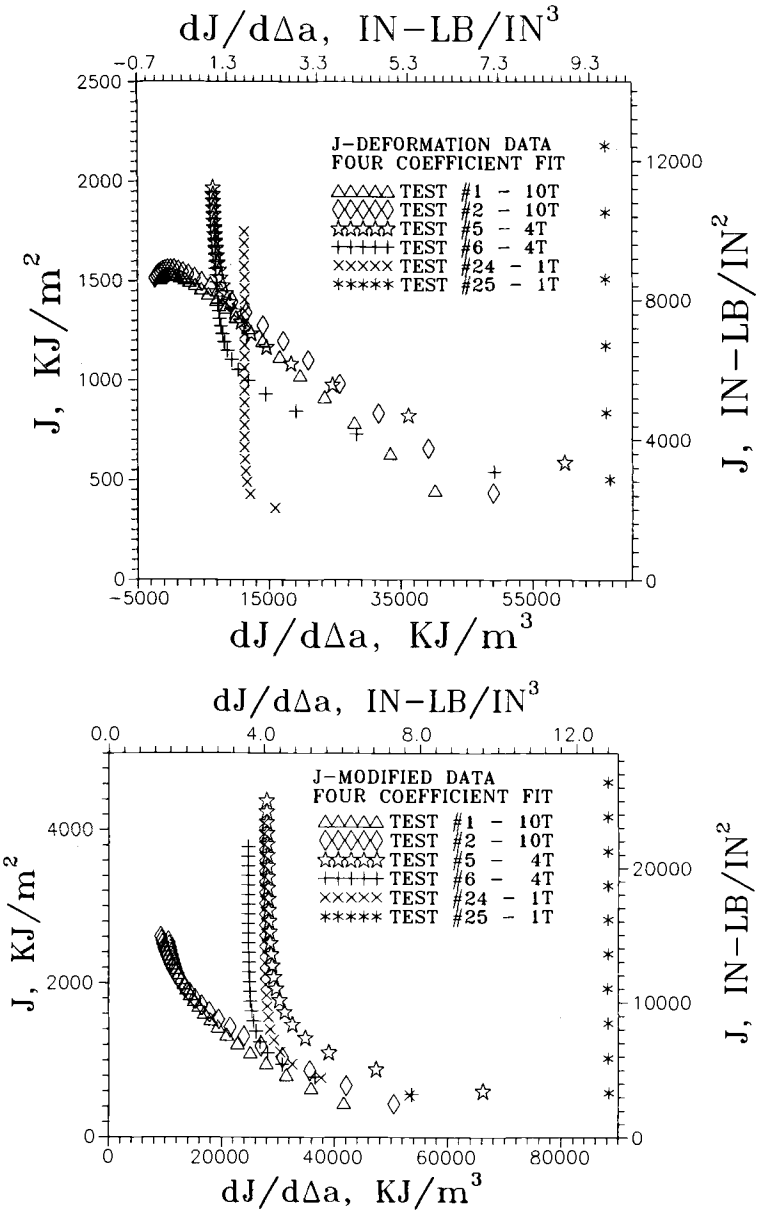

FIG. 9—*Plot of extrapolations of the four-coefficient models for each specimen.*

the entire *J-R* curve. Plots of *J* versus $dJ/d\Delta a$ obtained from these fits are given in Fig. 13. The curves order around a common trend line indicating material tearing properties. However, the results exhibit some ordering with respect to specimen size.

In summary, it appears from the data sets reviewed that Eason's relationship yields the best results for fitting *J-R* curves and predicting the results for large specimens from small specimens. The relationship fits most *J-R* curves nearly as well as the four-coefficient type and better than the power law. When the equation is extrapolated to large crack extensions,

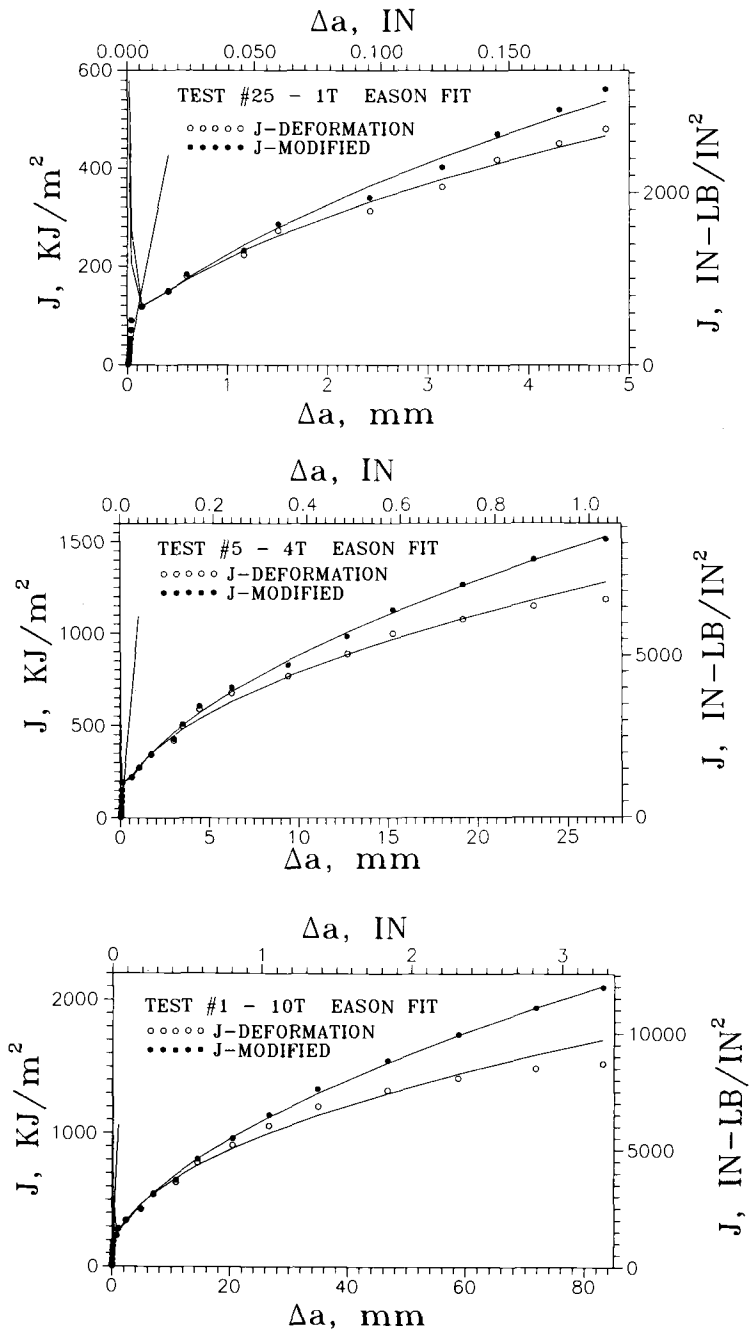

FIG. 10—*Fit of the Eason model to the* J-R *curve for the three specimen sizes.*

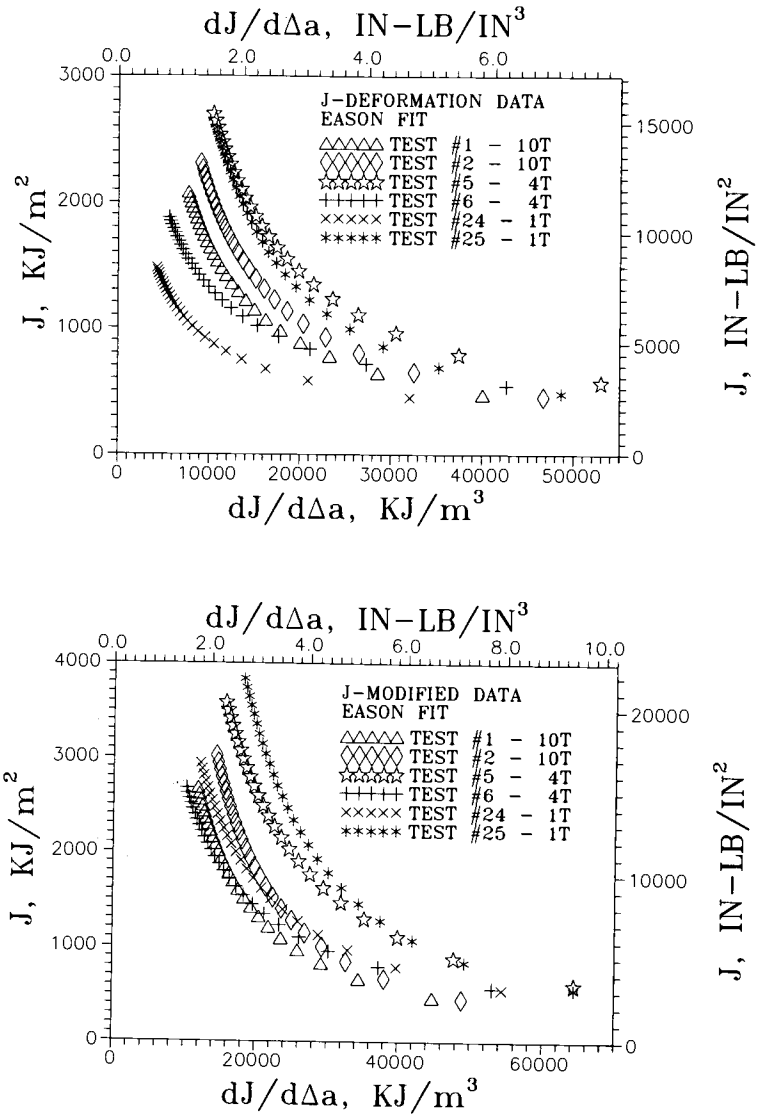

FIG. 11—*Plot of extrapolations of the Eason model for each specimen.*

plots of $dJ/d\Delta a$ are most consistent between differing specimen sizes for the Eason fit as compared to the other fits. This combination of factors makes the Eason relationship the most promising for modeling *J-R* curves.

Conclusions

From the results of this study a number of conclusions regarding the use of ASTM E 813-87 for determining values of J_{Ic} can be reached. In addition, methods of fitting and extrapolating *J-R* curves were evaluated.

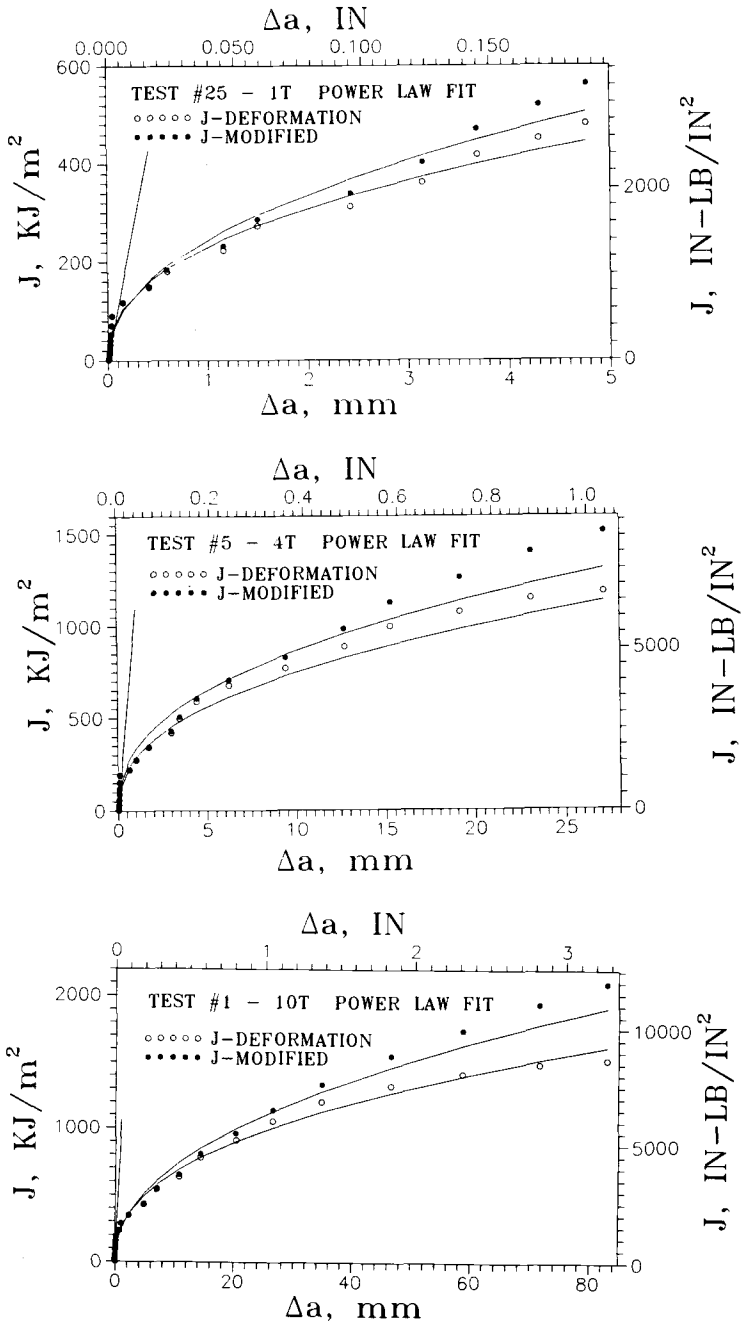

FIG. 12—*Fit of the power law model to the* J-R *curve for three specimen sizes.*

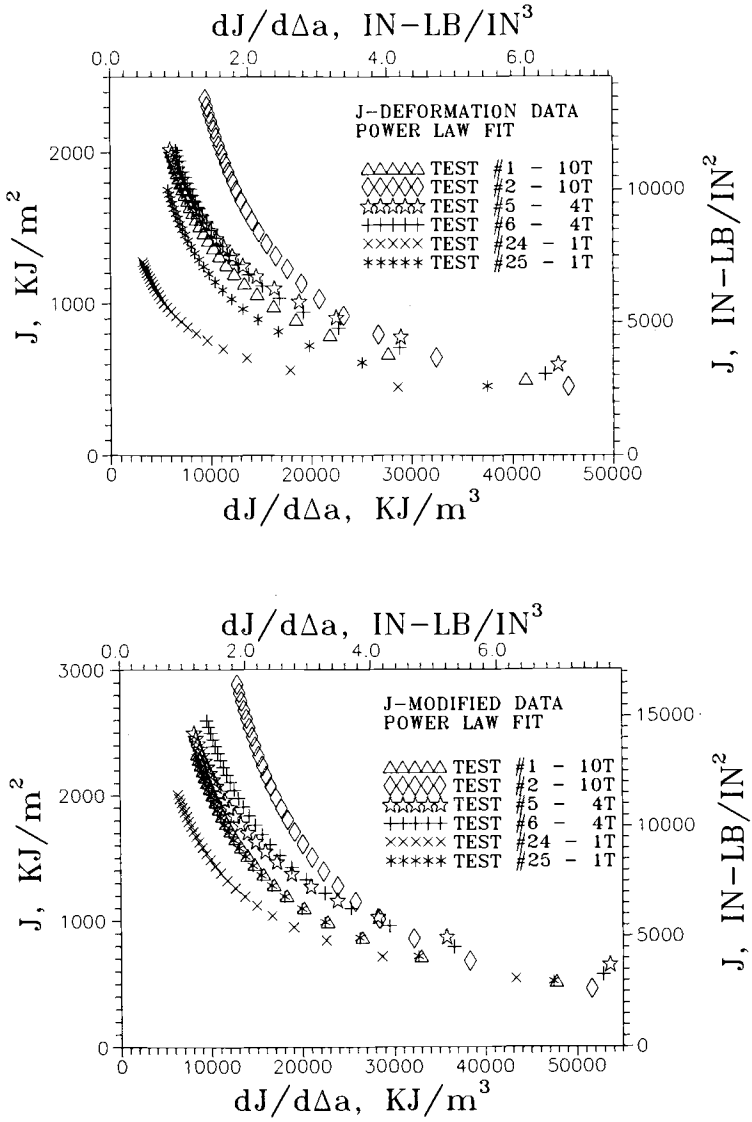

FIG. 13—*Plot of extrapolations of the power law model for each specimen.*

The following conclusions can be reached based on the results of the studies reported in this paper.

1. The revisions made to ASTM E 813 in 1987 result in increasing the measured value of J_{Ic} by an amount generally of about 10 to 15%. In some specific instances slightly greater amounts were observed.
2. The changes in the expression used to calculate the value of J made to ASTM E 813 did not substantially change the J-R curve properties measure for a material.

3. When J-R curves determined from ASTM E 1152-87 are to be used to determine J_{Ic}, a better procedure for determining the initial crack length is needed.
4. The requirements of Section 9.4.1.6 in ASTM E 813-87 should be revised. Section 9.4.1.6 should be revised to allow a set maximum variation in crack length across the width of the specimen. This could be that the maximum and minimum values of Δa cannot vary from the average Δa by more than 10% of the average Δa.
5. The requirement of Section 9.4.1.7 should be revised to base the allowable error in final crack measurements (that is, optical versus compliance) on the final crack length.
6. The fit procedure suggested by Eason appears to be the best of the procedures evaluated.

References

[1] Begley, J. A. and Landes, J. D., "The J Integral as a Fracture Criterion," *Fracture Toughness, ASTM STP 514*, American Society for Testing and Materials, Philadelphia, 1972, pp. 1–20.

[2] Futato, R. J., Aadland, J. D., Van Der Sluys, W. A., and Lowe, A. L., "A Sensitivity Study of the Unloading Compliance Single-Specimen J-Test Technique," *Elastic-Plastic Fracture Test Methods: The User's Experience, ASTM STP 856*, E. T. Wessel and F. J. Loss, Eds., American Society for Testing and Materials, Philadelphia, 1985, pp. 84–103.

[3] Domian, H. A., "Vessel V-8 Repair and Preparation of Low Upper-Shelf Weldment," Final Report to Oak Ridge National Laboratory, ORNL/Sub/81-85813/1, NUREG/CR-2676, U.S. Nuclear Regulatory Commission, Washington, DC, June 1982.

[4] Domian, H. A. and Futato, R. J., "J-Integral Test Results of HSST-ITV8A Low Upper Shelf Weld," B&W Letter Report RDD:83:4083-01:01, Babcock and Wilcox, Alliance, OH, 25 Feb. 1983.

[5] Van Der Sluys, W. A. and Emanuelson, R. H., "Toughness of Ferritic Piping Steels," Final Report, NP-6264, Research Project 2455-8, Electric Power Research Institute, Palo Alto, CA, April 1989.

[6] Van Der Sluys, W. A. and Futato, R. J., "Computer-Controlled Single-Specimen J-Test," *Elastic-Plastic Fracture: Second Symposium, Volume II: Fracture Curves and Engineering Applications, ASTM STP 803*, C. F. Shih and J. P. Gudas, Eds., American Society for Testing and Materials, Philadelphia, 1983, pp. II-646–II-482.

[7] Eason, E. D. and Nelson, E. E., "Improved Model for Predicting J-R Curves from Charpy Data," Phase I Final Report, NUREG/CR-5356, MCS 890301, U.S. Nuclear Regulatory Commission, Washington, DC, April 1989.

[8] McCabe, D. E. and Landes, J. D., "Elastic-Plastic Methodology to Establish R-Curves and Instability Criteria, R&D Report 81-2D7-ELASP-R1, Westinghouse R&D Center, Pittsburgh, PA, 11 Dec. 1981.

[9] McCabe, D. E. and Landes, J. D., "J_R-Curve Testing of Large Compact Specimens," *Elastic-Plastic Fracture: Second Symposium, Volume II: Fracture Curves and Engineering Applications, ASTM STP 803*, C. F. Shih and J. P. Gudas, Eds., American Society for Testing and Materials, Philadelphia, 1983, pp. II-353–II-371.

[10] McCabe, D. E., Landes, J. D., and Ernst, H. A., "An Evaluation of the J_R-Curve Method for Fracture Toughness Characterization," *Elastic-Plastic Fracture: Second Symposium, Volume II: Fracture Curves and Engineering Applications, ASTM STP 803*, C. F. Shih and J. P. Gudas, Eds., American Society for Testing and Materials, Philadelphia, 1983, pp. II-562–II-581.

[11] Ernst, H. A., "Materials Resistance and Instability Beyond J-Controlled Crack Growth," *Elastic-Plastic Fracture, Volume I: Inelastic Crack Analysis, ASTM STP 803*, C. F. Shih and J. P. Gudas, Eds., American Society for Testing and Materials, Philadelphia, pp. I-191–I-213.

William A. Sorem,[1] *Robert H. Dodds, Jr.,*[2] *and Stanley T. Rolfe*[3]

A Comparison of the *J*-Integral and CTOD Parameters for Short Crack Specimen Testing

REFERENCE: Sorem, W. A., Dodds, R. H., Jr., and Rolfe, S. T., **"A Comparison of the *J*-Integral and CTOD Parameters for Short Crack Specimen Testing,"** *Elastic-Plastic Fracture Test Methods: The User's Experience (Second Volume), ASTM STP 1114*, J. A. Joyce, Ed., American Society for Testing and Materials, Philadelphia, 1991, pp. 19–41.

ABSTRACT: This study investigates the applicability of the *J*-integral test procedure to test short crack specimens in the temperature region below the initiation of ductile tearing where J_{Ic} cannot be measured. The current *J*-integral test procedure is restricted to determining the initiation of ductile tearing and requires that no specimen demonstrates brittle cleavage fracture. The J_{Ic} test specimen is also limited to crack-depth to specimen-width ratios (a/W) between 0.50 and 0.75. In contrast, the crack tip opening displacement (CTOD) test procedure can be used for testing throughout the entire temperature-toughness transition region from brittle to fully ductile behavior. Also, extensive research is being conducted to extend the CTOD test procedure to the testing of short crack specimens (a/W ratios of approximately 0.15).

The CTOD and *J*-integral fracture parameters are compared both analytically and experimentally using square (cross-section) three-point bend specimens of A36 steel with a/W ratios of 0.50 (deep crack) and 0.15 (short crack). Three-dimensional elastic-plastic finite element analyses are conducted on both the deep crack and the short crack specimens. The measured *J*-integral and CTOD results are compared at various levels of linear-elastic and elastic-plastic behavior. Experimental testing is conducted throughout the lower shelf and lower transition regions where stable crack growth does not occur. Very good agreement exists between the analytical and experimental results for both the short crack and deep crack specimens.

Results of this study show that both the *J*-integral and the CTOD fracture parameters work well for testing in the lower shelf and lower transition regions where stable crack growth does not occur. A linear relationship is shown to exist between *J*-integral and CTOD throughout these regions for both the short and the deep crack specimens. These observations support the consideration to extend the *J*-integral test procedure into the temperature region of brittle fracture rather than limiting it to J_{Ic} at the initiation of ductile tearing. Also, analyzing short crack three-point bend specimen ($a/W < 0.15$) records using the load versus load-line displacement (LLD) record has great potential as an experimental technique. The problems of accurately measuring the CMOD of short crack specimens in the laboratory without affecting the crack tip behavior may be eliminated using the *J*-integral test procedure.

KEY WORDS: *J*-integral, CMOD, CTOD, elastic-plastic fracture mechanics, short crack, finite element analysis, transition fracture toughness

[1]Research engineer, Exxon Production Research Company, Houston, TX 77252-2189.
[2]Associate professor, Civil Engineering, University of Illinois, Urbana-Champaign, IL 61801.
[3]Professor, Civil Engineering, University of Kansas, Lawrence, KS 66045.

Currently, there is no ASTM standard procedure for fracture mechanics testing of three-point bend specimens with small crack-depth to specimen-width ratios (a/W). However, in the linear-elastic regime, the plastic zone at the crack tip is so small that the fracture toughness (K_c) obtained from short crack specimens is identical to the fracture toughness (K_{Ic}) of deep crack specimens (consistent with the single parameter characterization of the fracture event). The authors have previously shown [*1,2*] that in the elastic-plastic regime, large plastic zones are developed prior to brittle fracture. Moreover, three-point bend specimens frequently develop a full plastic hinge prior to brittle fracture. For short crack specimens, plastic zones at the crack tip extend to the free surface behind the crack; this response differs considerably from the ligament confined plasticity of deep crack specimens as shown in Fig. 1. Yielding to the free surface causes a loss of crack tip "constraint." Consequently, short crack specimens must undergo considerably more crack tip blunting and plastic deformation than deep crack specimens to develop the same critical stress at the crack tip required to cause brittle fracture.

The British Standard crack tip opening displacement (CTOD) test procedure (BS5762) "Methods for Crack Opening Displacement Testing," can be used for testing throughout the entire temperature-toughness transition region from brittle to fully ductile behavior (Fig. 2). Critical CTOD results can be obtained in the lower-shelf, lower-transition, upper-transition, and upper-shelf regions. The British standard allows the testing of specimens with a/W ratios between 0.15 and 0.70, but considerably more research is needed before the behavior of short crack specimens is fully understood.

The ASTM draft standard for CTOD testing limits the a/W ratio to the range of 0.45 to 0.55 until the relation between CTOD and laboratory measured crack mouth opening displacement (CMOD) is better developed for short crack specimens. Extensive studies are underway [*1–11*] to extend the ASTM CTOD standard to include the testing of short crack specimens. The relation between CTOD and CMOD appears dependent on both the a/W ratio and the strain hardening properties of the material. Development of a characteristic

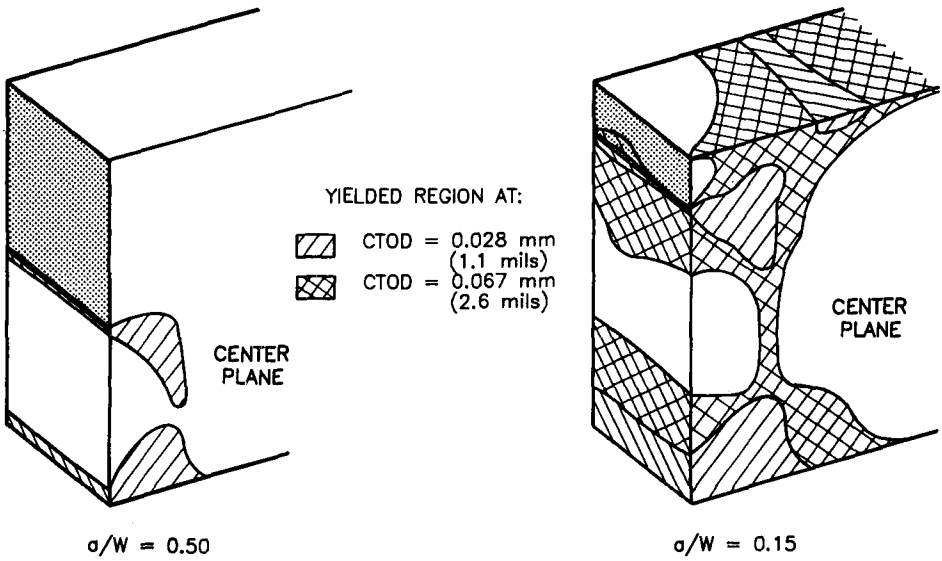

FIG. 1—*Von Mises stress distribution for 31.8 by 31.8 mm steel specimens.*

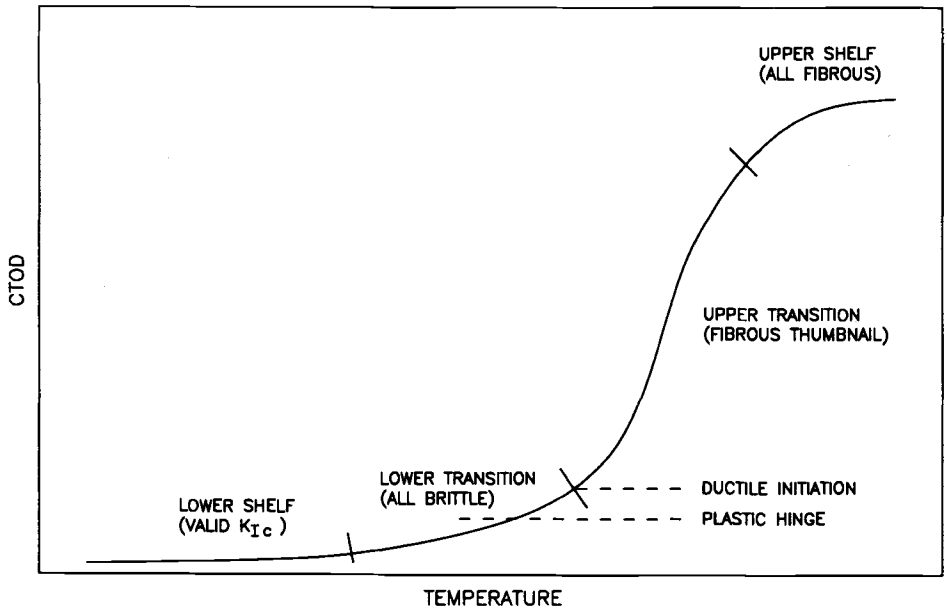

FIG. 2—*Schematic CTOD temperature transition curve.*

relationship between CTOD and CMOD for short crack specimens will rely on experimental (crack infiltration, lasers, etc.) and numerical (finite element analysis) investigations.

A major concern in testing short crack specimens is the ability to measure the CMOD without physically affecting the behavior of the crack tip region. Measurement of CMOD becomes much more difficult as the physical size of the crack decreases. Very small and precise instrumentation is required; the procedure is further complicated by plastic deformation extending from the crack tip to the measuring surface, as shown in Fig. 1. The clip gage must be contained between the two regions where the plastic zone has extended from the crack tip to the free tension surface on both sides of the crack mouth. Figure 3 illustrates warping of the top tension surface that develops as the plastic zone extends to the surface of the short crack specimen. The CMOD is measured in this region and is potentially affected by the near surface plasticity. These problems make the laboratory measurement of CMOD on short crack specimens more complicated than for deep crack specimens.

The ASTM *J*-integral test procedure (E 813), "Standard Test Method for J_{Ic}, a Measure of Fracture Toughness," is restricted currently to testing for the initiation of ductile tearing. However, several investigators have extended the *J*-integral parameter (and test procedure) to quantify brittle fracture (J_c) in the lower shelf and lower transition regions [*12–14*]. The *J*-integral test also is limited to *a*/*W* ratios between 0.50 and 0.75. Several investigations [*7–9,12,13*] have been conducted using the *J*-integral procedure to analyze specimens with *a*/*W* ratios between 0.10 and 0.30.

Experimentally, the *J*-integral procedure offers the advantage of measuring either load versus load-line displacement (LLD) or load versus CMOD. Although accurately measuring LLD can be difficult in the laboratory, LLD measurements are less dependent on the effects of crack depth than are CMOD measurements. The load-line displacement of the specimen itself must be measured; instrumentation must exclude local deformation at the loading rollers and deformation of the loading frame. Also, the measurements are generally taken

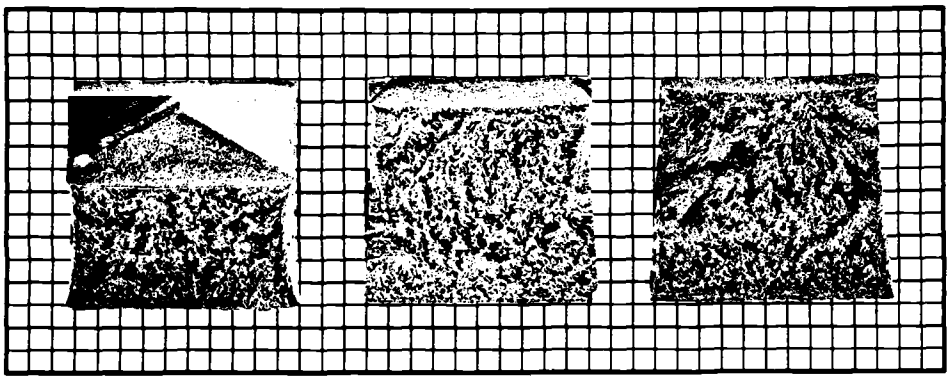

FIG. 3—*Fracture surfaces of A36 steel specimens (31.8 by 31.8 mm) tested at 21°C (70°F).*

at the outside surface of the specimen rather than at the center plane. But, becuase LLD is measured at a distance away from the crack tip and away from the top tension surface where short crack specimens plastically deform, LLD measurements have less potential of affecting the crack tip behavior and therefore may better characterize the elastic-plastic fracture toughness of short crack specimens.

This study compares the two elastic-plastic fracture parameters (CTOD and *J*-integral) for characterizing both short crack and deep crack three-point bend specimens. Square (cross-section) three-point bend specimens (31.8 by 31.8 by 127 mm (1.25 by 1.25 by 5.00 in.)) are analyzed with crack-depth to specimen-width ratios (a/W) of 0.15 and 0.50. The study focuses on the response in the lower-transition region where brittle initiation is preceded by extensive plastic deformation and crack tip blunting. Finite element analyses are utilized to compare the displacement, strain, and stress distributions of the short crack specimen ($a/W = 0.15$) to the deep crack specimen ($a/W = 0.50$) at similar values of J and CTOD. Finite element values of J-integral and CTOD [*1*] are combined with load-displacement records to develop relationships between laboratory measured quantities and the crack tip parameters. Experimental tests previously conducted using the CTOD procedure [*2*] are reanalyzed using the J-integral procedure. Both the analytical and the experimental results are compared to develop a relationship between J and CTOD.

Material Properties

A 31.8-mm (1.25-in.)-thick, as-rolled plate of A36 steel was used in this study. Tables 1 and 2 provide the chemical analysis and mechanical properties of the material. Table 3 provides the yield strength of the A36 steel plate at various temperatures as determined previously by Shoemaker and Seeley [*15*]. The estimated flow strengths at equivalent temperatures are also shown in Table 3. The flow strength (σ_{fl}) was estimated using the equation $\sigma_{fl} = (\sigma_{ys} + \sigma_u)/2$. Clausing [*16*] observed that yield strength and tensile strength of construction steels undergo parallel increases as the temperature is decreased from 21°C (70°F)

TABLE 1—*Chemical analysis, %.*

Steel	C	Mn	P	S	Si
A36	0.20	1.11	0.007	0.023	0.029

TABLE 2—*Mechanical properties.*

Steel	Yield Strength @ 0.2% Offset	Tensile Strength	Elongation in 50.8 mm	Reduction in Area
A36	248 MPa 36 ksi	460 MPa 66.8 ksi	38%	67%

TABLE 3—*Yield strength adjusted to temperature.*

Steel	Temperature, °C	Yield Strength		Flow Strength	
		MPa	(ksi)	MPa	(ksi)
A36	21 to 0	248	(36)	351	(51)
	−18	262	(38)	365	(53)
	−43	290	(42)	393	(57)
	−76	345	(50)	448	(65)
	−112	462	(67)	565	(82)
	−195	793	(115)	896	(130)

to −195°C (−320°F). Since the yield strength and ultimate strength undergo parallel increases, the room temperature relation $\sigma_u = \sigma_{ys} + 206$ MPa (30 ksi) should also be applicable as the temperature decreases. Therefore, the low temperature flow strength of the A36 steel corresponded to the equivalent temperature yield strength +103 MPa (15 ksi). Figure 4 shows the engineering stress-strain curve obtained from a standard 12.8-mm (0.505-in.)-diameter-longitudinal tensile test conducted at room temperature and a slow loading rate. A piecewise linear representation of the uniaxial stress-strain curve was utilized in the finite element analyses as shown in Fig. 4. A36 steel is a low strength, high strain-hardening material with an ultimate stress to yield stress ratio of 1.86 and a strain hardening exponent (n) of 0.23 at room temperature.

Finite Element Analysis

Elastic-plastic finite element analyses were conducted on the short crack and deep crack three-point bend specimens using the models shown in Fig. 5. Two-dimensional models were analyzed for both plane-strain and plane-stress conditions. Three-dimensional models were analyzed to assess the effect of through-thickness constraint. Quadratic, isoparametric elements were utilized in the meshes with degenerated crack tip elements to model the singularity. The size of the crack tip elements for the short crack and deep crack specimens was less than 5% of the corresponding crack depths. Convergence studies demonstrated that these finite element models were sufficiently detailed to extract values of the J-integral and CTOD. No simulation of crack growth was attempted in the analyses. The finite element solutions employed the conventional, linear strain-displacement relations based on small geometry change assumptions. Plasticity was modeled using incremental theory with a von

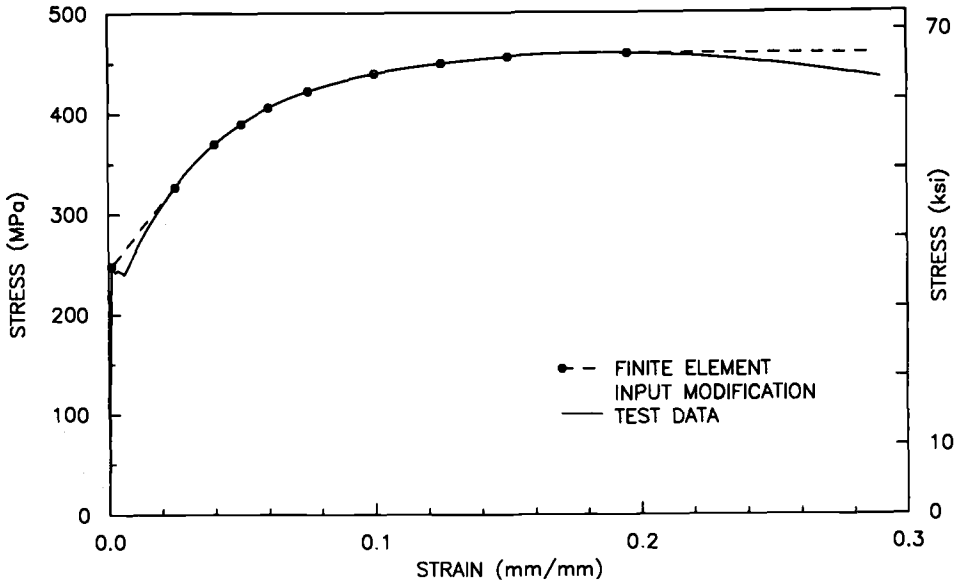

FIG. 4—*A36 steel tension test showing modification for finite element analysis.*

Mises yield surface, associated flow rule, and isotropic hardening. Numerical computations were performed with the POLO-FINITE structural mechanics system [*17,18*]. Complete details of the analysis procedure have been described by Sorem et al. [*1*].

The load versus LLD results from the finite element analyses are compared to the experimental results in Figs. 6 and 7. LLD is measured at the crack plane midway between

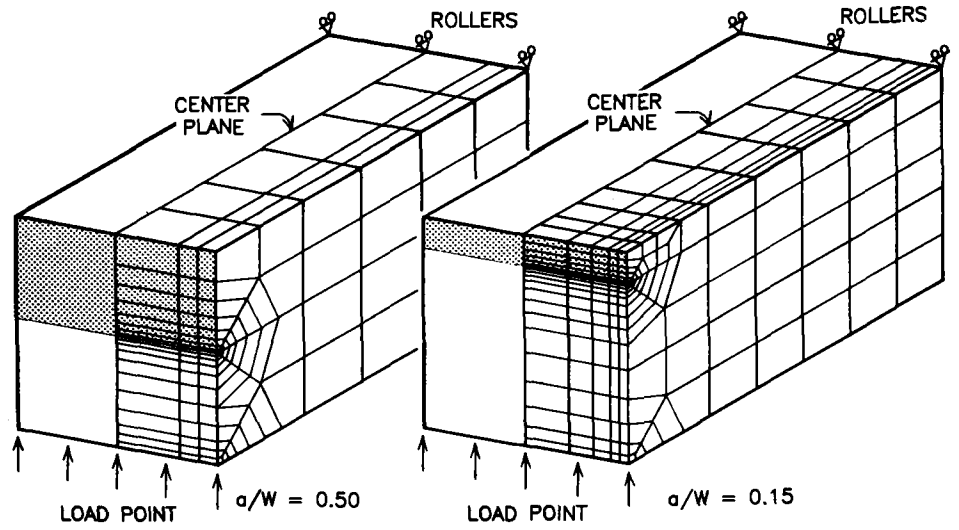

FIG. 5—*Three-dimensional finite element analysis mesh for the three-point bend specimens.*

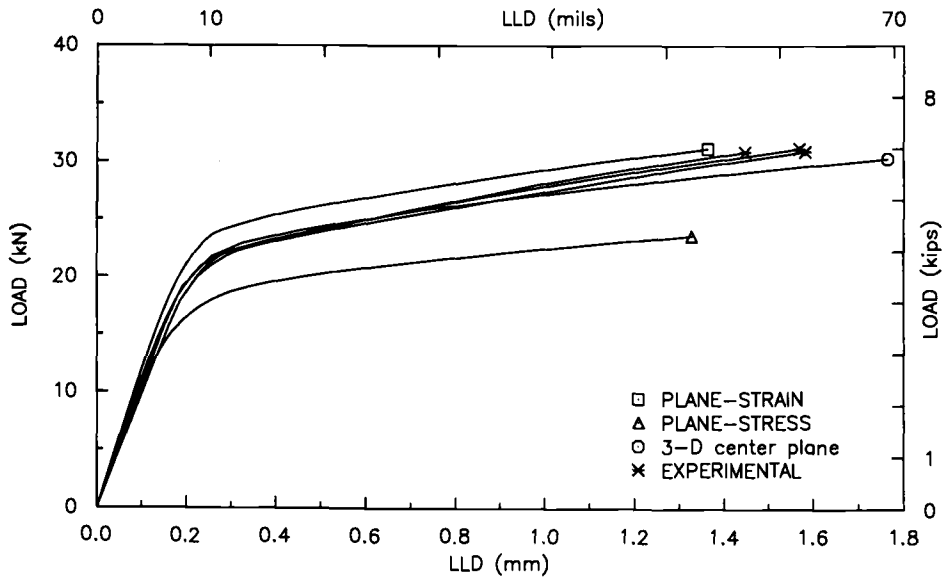

FIG. 6—*Load versus LLD for square (31.8 by 31.8 mm) A36 steel specimens with* a/W = *0.50.*

the crack tip and the point of load application (loading roller) of the finite element model and therefore is not affected by local deformations at the load and reaction points. The load-LLD results for the deep crack specimen are shown in Fig. 6, and the results of the short crack specimen are shown in Fig. 7. For both *a/W* ratios, the plane-strain analysis provides an upper bound load-LLD relation, and the plane-stress analysis provides a lower

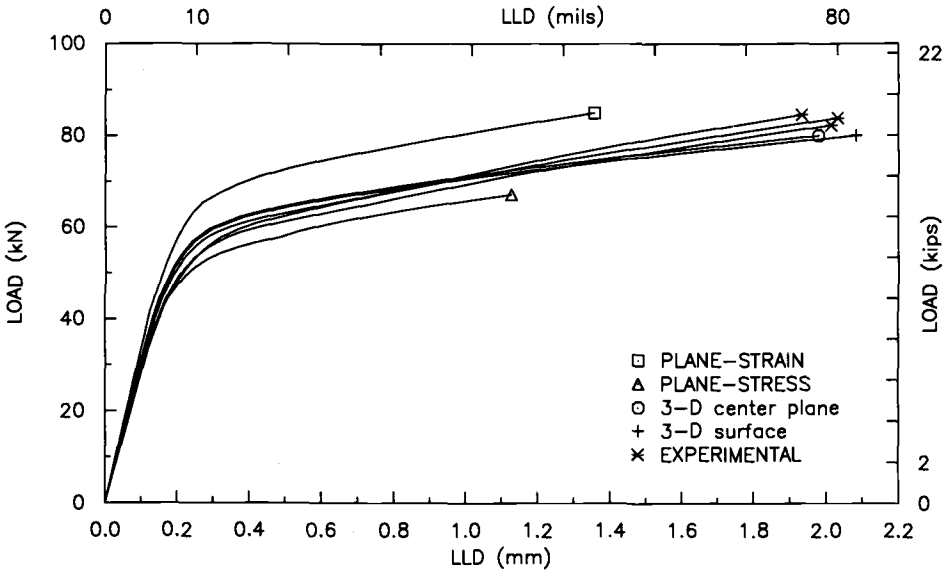

FIG. 7—*Load versus LLD for square (31.8 by 31.8 mm) A36 steel specimens with* a/W = *0.15.*

bound relation. The three-dimensional analyses very closely approximate the load-LLD records of the laboratory specimens. The LLD is nearly constant through the thickness of the deep crack specimen with less than 2% variation from center plane to surface. For the short crack specimen, the LLD is constant through the thickness of the specimen for linear elastic specimen behavior, but, in the elastic-plastic regime, the surface LLD is up to 5% greater than the center plane LLD due to distortion of the cross section from the initially square configuration.

J-Integral Analysis

J-integral values are computed from the finite element results using a domain integral formulation (line integrals and area integrals) as described by Dodds et al. [*19*]. Pointwise values of the applied *J* along the crack front are numerically computed with the POLO-FINITE system.

In three-dimensions, the applied *J* at each location on the crack front includes contributions from both line integrals and area integrals.

$$J(\eta) = \int_\Gamma \left(w^e n_1 - T_i \frac{\partial u_i}{\partial x_1} \right) d\Gamma + \int_\Gamma w^p n_1 \, d\Gamma - \int_A \partial \left[\sigma_{i3} \frac{\partial u_i}{\partial x_1} \right] / \partial x_3 \, dA \qquad (1)$$

The line integral is evaluated over a remote contour that lies in the principal normal plane of the crack front at location "η" and that encloses the crack tip as shown in Fig. 8*a*. The area integral is evaluated over the planar area (surface) enclosed by the contour and includes the crack tip elements. Dodds et al. [*19*] demonstrated path independence of the *J*-integral defined by Eq 1 when the area integral was added to the contour integrals.

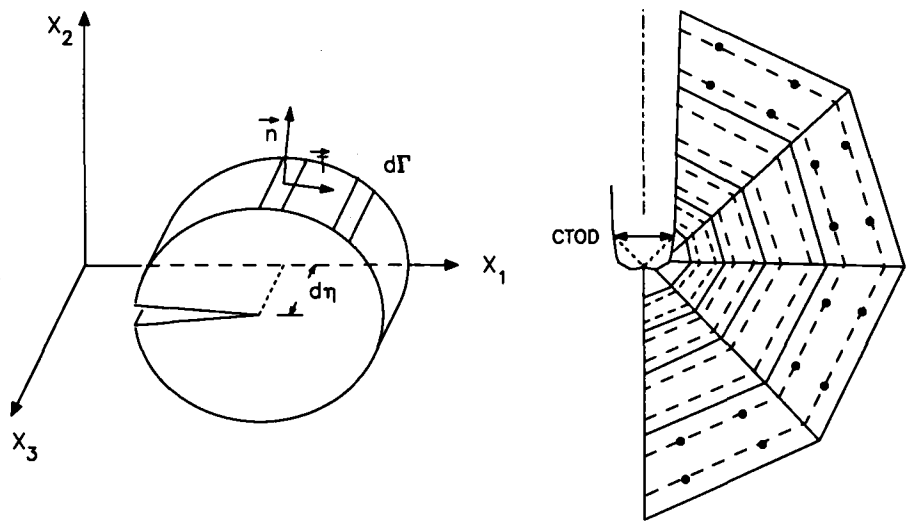

a) CONTOUR AND AREA INTEGRAL EVALUATION

b) INTEGRATIONS PATHS THROUGH THE GAUSS POINTS

FIG. 8—*Contour* J*-integral formulation at the crack tip.*

Both the contour and the area integrals are evaluated at each Gauss plane through the specimen half thickness. A sequence of contours for the line integrals are defined that pass through Gauss points of elements excluding the ring of crack tip elements as shown in Fig. 8*b*. Eight such contour paths are evaluated at each Gauss plane. The area integrals are computed in the Gauss point planes for the concentric rings of elements that enclose the crack tip.

J-values, $J(\eta)$, for these paths surrounding the crack tip at the center plane, middle, and surface elements are shown in Fig. 9 and demonstrate path independence of *J*. The center-plane elements and middle elements show less than 3% variation of the *J*-values over the paths investigated. The surface elements show an 8% variation in *J* over the same paths. This larger variation arises from the steep stress gradients that occur in the boundary layer at the free surface, that is, $\sigma_z \rightarrow 0$ combined with the limited mesh refinement in the thickness direction.

The variation of *J* through the thickness of the specimen is shown in Fig. 10 at center-plane *J* levels of 0.014, 0.057, and 0.140 MPa-m (0.080, 0.326, and 0.805 ksi in.). *J* remains nearly constant over the center 60% of the specimen thickness and decreases rapidly as the outside free surface is approached. CTOD levels through the thickness of the specimen at identical load levels are shown in Fig. 11. The levels shown correspond to center-plane CTOD values of 0.028, 0.102, and 0.251 mm (1.1, 4.0, and 9.9 mil). The through-thickness variations of CTOD are similar to the *J* variations, but the CTOD values near the outside surface decrease less rapidly than the *J*-values. Consequently, the relationship between CTOD and *J* will vary at each location through the thickness of the specimen. Since the maximum values of both *J* and CTOD occur at the center plane of the specimen, subsequent development of the relation between CTOD and *J* is based on the center-plane values.

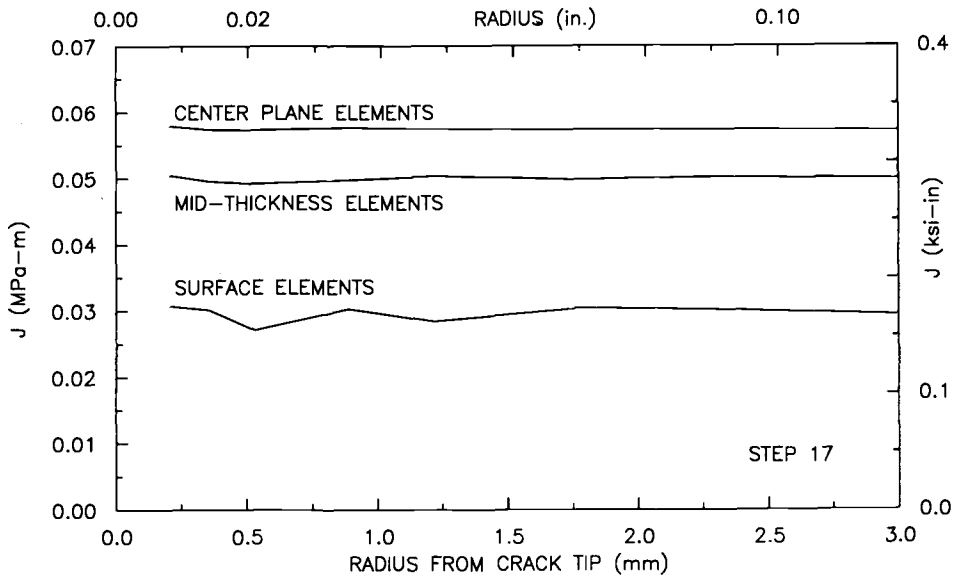

FIG. 9—*Path independence of* J*-integral for the square (31.8 by 31.8 mm) A36 steel specimens with* a/W = *0.15.*

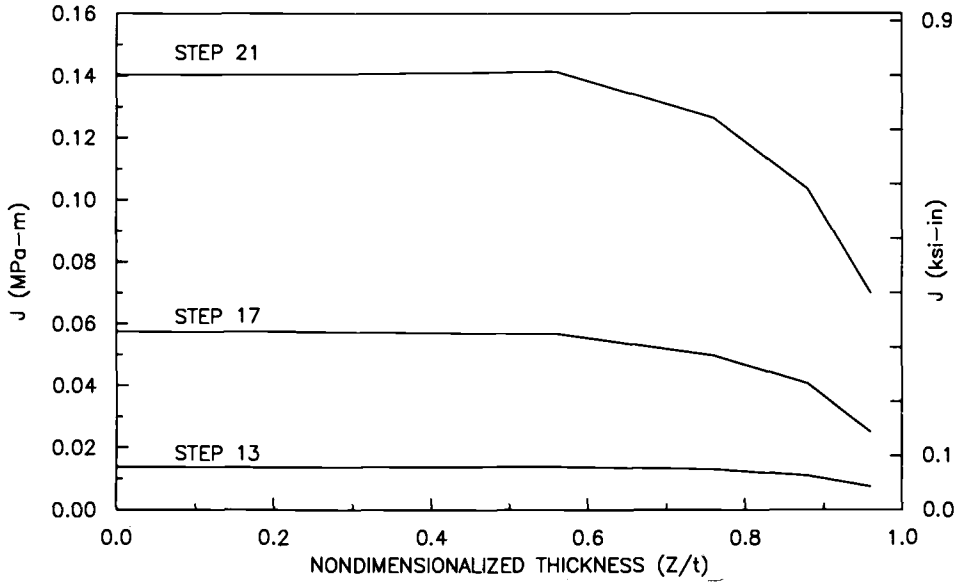

FIG. 10—*J-integral values through the thickness of the square (31.8 by 31.8 mm) A36 steel specimens with* a/W = *0.15.*

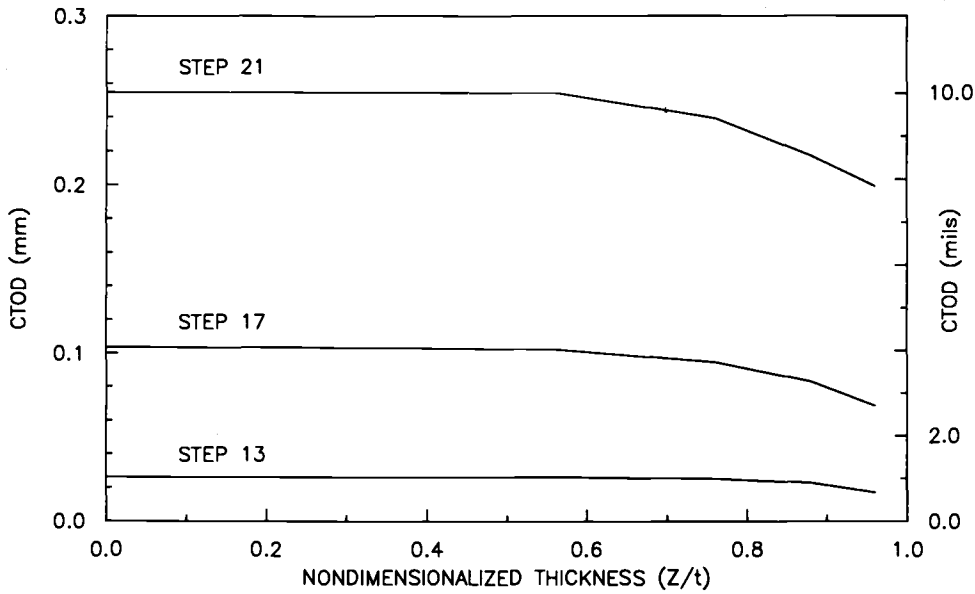

FIG. 11—*CTOD values through the thickness of the square (31.8 by 31.8 mm) A36 steel specimens with* a/W = *0.15.*

J-Integral Computation

Early work in relating the *J*-integral fracture concept [*20*] to laboratory measurements stemmed from LEFM studies by Rice et al. [*21*] and Turner [*22*] which related the Griffith energy release rate to the elastic energy, U_e

$$J = \frac{\eta_e U_e}{B(W - a)} \tag{2}$$

where

η_e = dimensionless elastic factor based on specimen compliance,
U_e = area beneath the elastic load versus LLD record,
B = specimen thickness,
W = specimen depth, and
a = effective crack depth.

This relation, while applicable for linear-elastic conditions, was extended to include plastic deformation. Sumpter and Turner [*12*] separated the total energy into elastic and plastic energy contributions which correspond respectively to the elastic area, U_e, and plastic area, U_p, beneath the load-LLD record.

$$J = J_e + J_p = \frac{\eta_e U_e}{B(W - a)} + \frac{\eta_p U_p}{B(W - a)} \tag{3}$$

where

J_e = elastic contribution to J,
J_p = plastic contribution to J,
η_p = dimensionless plastic factor, and
U_p = plastic area beneath the load-LLD record.

Both η_e and η_p are dependent on specimen geometry, loading conditions, and a/W ratio; the two factors generally are not equivalent.

The η_e and η_p factors of Eq 3 for both the short crack and the deep crack specimens are determined from the area beneath the finite element load-LLD records and the domain integral values for J. η_e is determined from the first finite element analysis (FEA) load increment (linear-elastic) where the elastic area equals the total area and the elastic J equals the total J. For the deep crack specimen, $a/W = 0.50$, $\eta_e = 1.95$. For the short crack specimen, $a/W = 0.15$, $\eta_e = 1.25$.

To calculate η_p, the plastic area (U_p) and the plastic component of J-integral (J_p) are calculated at each load increment. To obtain U_p, the elastic component of the area (based on the initial slope of the load-LLD record) is subtracted from the total area, U_t. In the elastic-plastic regime, the LLD for the short crack specimen is as much as 5% greater at the outside surface than at the center plane. The plastic area beneath the curve is thus 5% greater at the outside surface than at the center plane. Since the LLD is measured experimentally at the outside surface, the plastic area is based on the surface LLD rather than the center plane LLD to maintain consistency. Therefore, to develop the relation between LLD and J-integral, the maximum value of J (at the center plane) is compared to the measured LLD (at the surface). To obtain J_p, the elastic component of J (based on η_e and U_e) is subtracted from the domain integral value. For the deep crack specimen, $a/W = 0.50$, $\eta_p = 2.10$. For the short crack specimen, $a/W = 0.15$, η_p is not constant but rather decreases with increasing plastic deformation to a low of 1.25 in the final load increment of the finite element analysis.

Sumpter [*13*] describes a relationship between η_p and a/W ratio for shallow notch bend specimens using the limit load estimates of Haigh and Richards [*23*] for pure bending.

$$\eta_p = 0.32 + 12(a/W) - 49.5(a/W)^2 + 99(a/W)^3 \tag{4}$$

Using this expression for $a/W = 0.50$, $\eta_p = 2.0$, and for $a/W = 0.15$, $\eta_p = 1.34$. Sumpter [*13*] argues that the plastic term of Eq 3 is accurate only for a perfectly plastic, homogeneous material after limit load is reached. He further argues that there is no obvious reason why the expression should successfully provide the plastic component of J which accrues prior to limit load or account precisely for work hardening effects. Paris et al. [*24*] argues that η_p only exists where the dependence on specimen configuration (a/W ratio) and plastic deformation can be separated.

Srawley [*25*] returned to the original formulation and supported the substitution of the total η factor (η_t) for η_e and the total energy, (U_t) for U_e.

$$J = \frac{\eta_t U_t}{B(W - a)} \tag{5}$$

For the three-point bend specimen with $a/W > 0.05$:

$$\eta_t = 2 - (0.3 - 0.7\, a/W)(1 - a/W) - \exp(0.5 - 7\, a/W) \tag{6}$$

Therefore, for the deep crack specimen, $a/W = 0.50$, $\eta_t = 1.98$ and for the short crack specimen, $a/W = 0.15$, $\eta_t = 1.26$. Because η_e and η_p for the deep crack bend specimen are both nearly equal to 2, it has become common practice to use Eq 5 with $\eta_t = 2$ for J-integral testing.

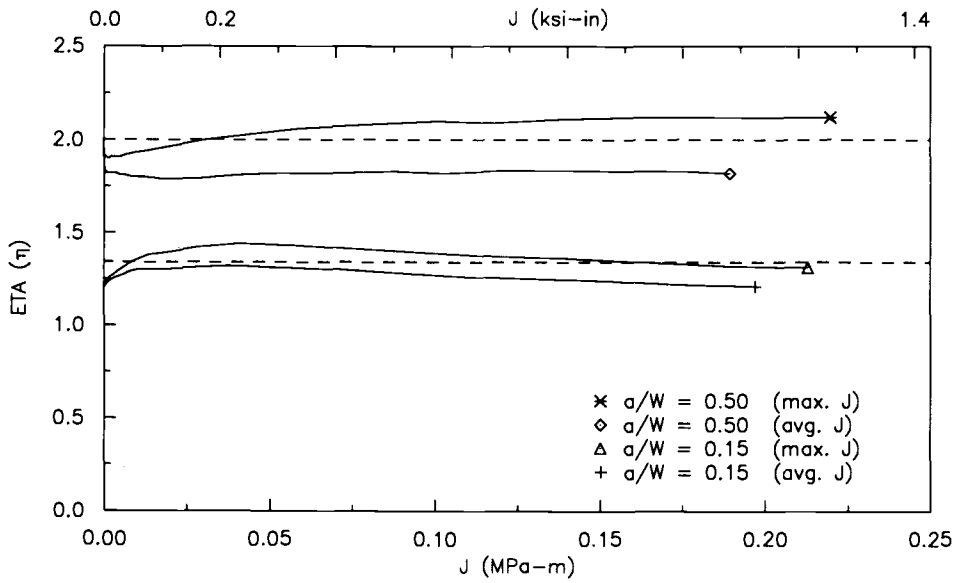

FIG. 12—J-*integral* η *factor from the load LLD record for square (31.8 by 31.8 mm) steel specimens.*

The relationship of the area beneath the finite element load-LLD curve to the finite element J-values is developed for both short crack and deep crack three-point bend specimens as follows. Using Eq 5, η_t is calculated and plotted as a function of the domain integral J in Fig. 12. Both the average values of J and the maximum values of J (at the center plane) are compared. For the deep crack specimen, Eq 2 with $\eta_e = 1.95$ and $\eta_p = 2.1$ describes the relation between area and maximum J better than Eq 5 with $\eta_t = 2.0$. For the short crack specimen, η_t varies from 1.25 to 1.44 and eventually settles at 1.31. Thus, the energy separation model to estimate J (Eq 2) for the short crack specimen does not perform as well: the total energy model (Eq 5) is adopted with $\eta_t = 1.34$. These results agree with Turner's [*26*] observations that η_t is more nearly independent of the degree of plasticity than η_p for a wider range of cases (variety of a/W ratios 0.50 to 0.025 in three-point bend specimens).

Using these η_t values in Eq 5 and the area beneath the finite element load-LLD records, J is calculated and compared to the FEA J-integral as shown in Fig. 13. Over the entire loading range, the calculated values of J for the deep crack specimen are within 6% of the FEA J-values; for the short crack specimen the calculated J-values are within 7% of the FEA J-values.

Experimental Procedure

Three-point bend specimens were machined from the A36 steel plate in the as-rolled condition with crack planes oriented perpendicular to the rolling direction of the plate (L-T orientation). Due to the difficulty in obtaining straight fatigue cracks from a shallow machined notch, the short crack specimens were originally over-sized and incorporated deep chevron notches. After the fatigue cracks were grown, the specimens were remachined to the square cross-section (31.8 by 31.8 by 127 mm (1.25 by 1.25 by 5.00 in.)) with an a/W

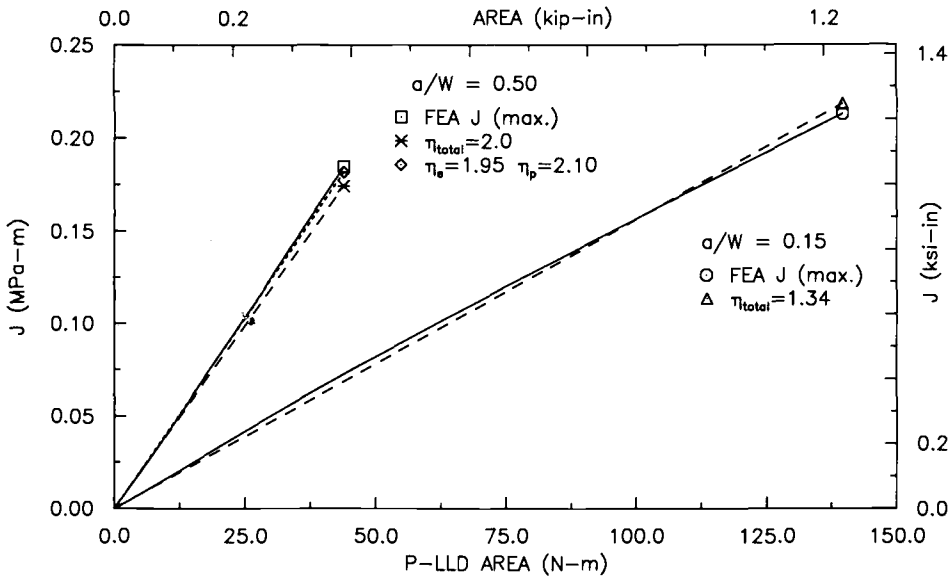

FIG. 13—*J-integral versus area beneath the load LLD record for square (31.8 by 31.8 mm) steel specimens.*

ratio of 0.15 as shown in Fig. 14. Figure 14 also illustrates the deep crack specimen with $a/W = 0.50$.

A 200 kN universal closed-loop testing machine was used for both fatigue cracking and the final ramp load to failure. CMOD was measured by a clip-gage mounted on knife edges machined into the specimen. The dove-tailed slot was approximately 0.051 mm (0.020 in.) deep with an initial gage length of 4.3 mm (0.170 in.). LLD for the short crack specimens was measured using a comparator bar attached at the specimen neutral bending axis. LLD for the deep crack specimens was measured from the loading rollers and the localized displacement of the loading rollers was later subtracted from the measured LLD. Results of typical load versus LLD records for the deep crack and short crack specimens tested at room temperature are shown in Figs. 6 and 7, respectively.

Experimental Results

Both deep crack and short crack specimens were tested throughout the lower-shelf and lower-transition regions. Results for the deep crack specimen tests ($a/W = 0.50$) are shown in Fig. 15. J-integral values were calculated using the load-LLD measurements and Eq 5 with $\eta_t = 2.0$. Specimens tested between −195°C (−320°F) and −18°C (0°F) failed by brittle initiation (J_c). Many of the specimens tested at 0, 10, and 21°C (32, 50, and 70°F) exhibited ductile thumbnails prior to brittle fracture and therefore were in the upper-transition region. Ductile initiation was determined for the deep crack specimen using crack growth resistance curves from the previous experimental CTOD analysis [2]. Ductile tearing (0.2 mm (8 mil) of crack growth) initiated at a CTOD of 0.30 mm (12 mil) which corresponded to $J_{Ic} = 0.18$ MPa·m (1.0 ksi·in.).

Results for the short crack specimen tests ($a/W = 0.15$) are shown in Fig. 16. J-integral values were calculated using the load-LLD measurements and Eq 5 with $\eta_t = 1.34$. Specimens tested between −195°C (−320°F) and −43°C (−45°F) failed by brittle initiation (J_c). Specimens tested at −18°C (0°F) and 21°C (70°F) exhibited ductile thumbnails prior to

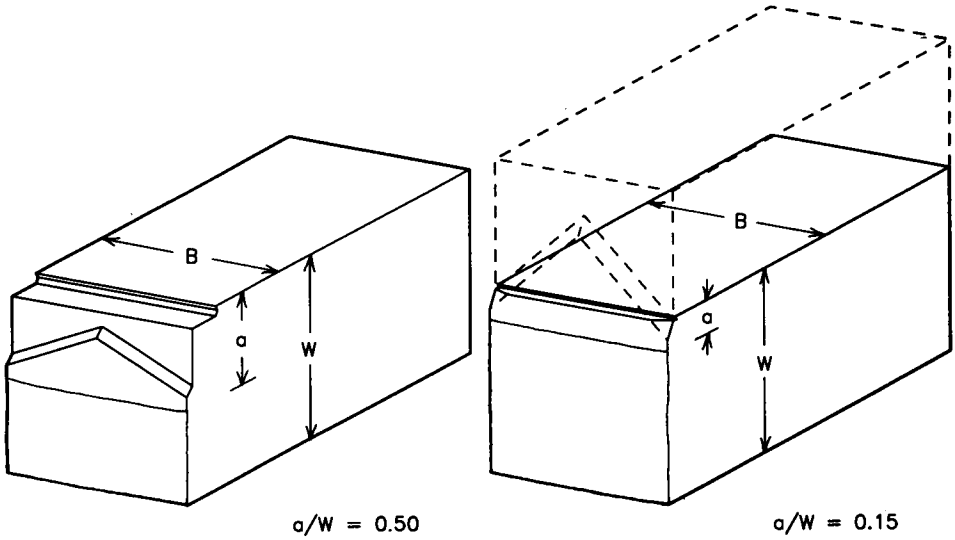

FIG. 14—*Square cross section (31.8 by 31.8 mm) three-point bend laboratory specimens.*

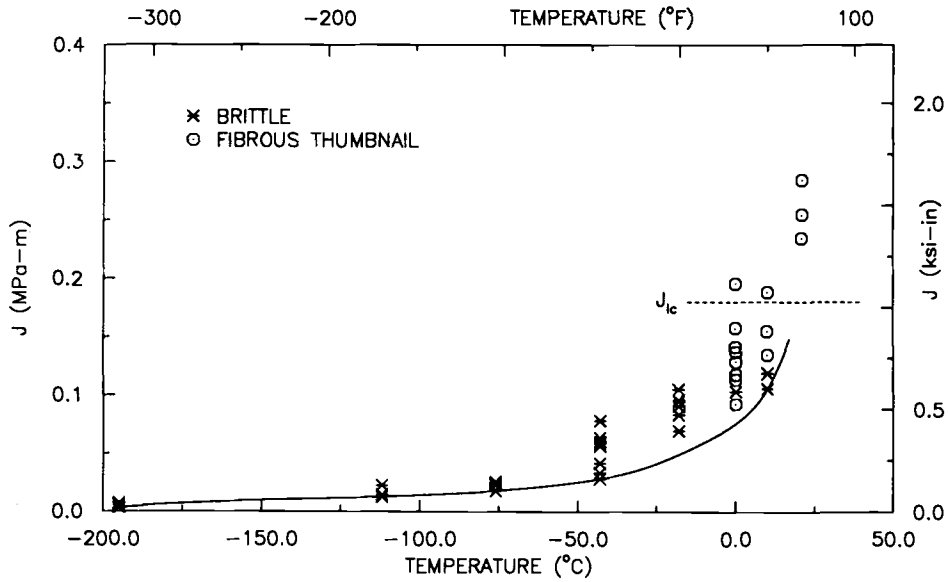

FIG. 15—J *versus temperature for A36 steel specimens (31.8 by 31.8 mm) with* a/W *ratios of 0.50.*

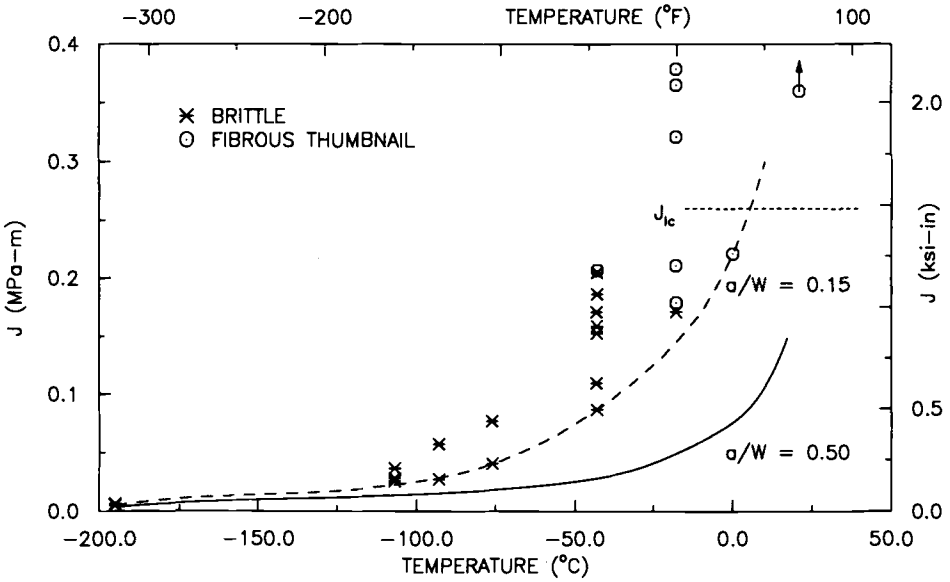

FIG. 16—J *versus temperature for A36 steel specimens (31.8 by 31.8 mm) with* a/W *ratios of 0.15.*

brittle fracture and therefore were in the upper-transition region. Ductile tearing initiated at a CTOD of 0.46 mm (18 mil) which corresponded to J_{Ic} = 0.26 MPa·m (1.5 ksi·in.).

Critical J-values for the short crack specimen and the lower bound estimate of the deep crack specimen are compared in Fig. 16. In the lower-shelf region (−195°C (−320°F)), no significant effect of crack depth was observed in the J_c-values. In the lower-transition region, the short crack specimens exhibited significantly larger J_c-values than the deep crack specimens. At −107°C (−160°F), the lower bound J_c-values of the short crack specimen (a/W = 0.15) were approximately two times higher than the lower bound J_c-values of the deep crack specimen (a/W = 0.50). As the temperature increased, the difference between the short crack and deep crack J_c results increased until at −18°C (0°F) the short crack specimen J_c-values were about three times greater than the deep crack specimen J_c-values.

CTOD Analysis

The CTOD from the finite element analysis is directly measured from the displaced mesh using the 90° intercept method [*20*] as shown in Fig. 8*b*. A line is constructed from the crack tip at an angle of 45° from the crack plane; the intersection of this line with the crack profile defines the CTOD.

Experimentally, CTOD is calculated using the load-CMOD record and the British standard equation

$$\delta = \frac{K^2(1 - \nu^2)}{2\,\sigma_{ys}\,E} + \frac{\mathrm{RF}(W - a)\,V_p}{\mathrm{RF}(W - a) + a} \tag{7}$$

The first term of this equation is the small-scale yielding (SSY) contribution which is often referred to as the elastic contribution. The second term is the large-scale yielding (LSY) or plastic contribution which is based on the assumed rigid body rotation of the specimen about a point ahead of the crack tip. The plastic rotation factor (RF) is dependent on both crack-depth to specimen-width ratio (a/W) and material strain hardening [*1–11*]. The rotation factors for the A36 steel specimens were determined from the corresponding FEA [*1*]. The adjusted rotation factor was 0.37 for the deep crack specimen and 0.20 for the short crack specimen. Using the finite element load-CMOD record and Eq 7 with the adjusted rotation factors, the CTOD was calculated for the deep crack and the short crack specimen. A comparison of the calculated CTOD and the measured CTOD (using the 90° intercept method) is shown in Fig. 17. The maximum error in the elastic-plastic regime was a 24% over-estimate of CTOD (at CTOD = 0.032 mm (1.26 mil)) for the deep crack specimen and a 20% over-estimate of CTOD (at CTOD = 0.034 mm (1.35 mil)) for the short crack specimen.

An alternative method of calculating CTOD from the load-CMOD record is being studied by the authors [*27*]. The SSY contribution of CTOD remains the same, but the LSY contribution is based on the strain-energy or plastic area beneath the load-CMOD record.

$$\delta = \frac{K^2(1 - \nu^2)}{2\,\sigma_{ys}\,E} + \frac{\eta_\delta\,U_\delta}{B(W - a)\,\sigma_{fl}} \tag{8}$$

where

U_δ = plastic area beneath the load-CMOD record,
η_δ = dimensionless factor based on a/W ratio and material properties, and
σ_{fl} = flow stress = $\sigma_{ys} + \sigma_u/2$.

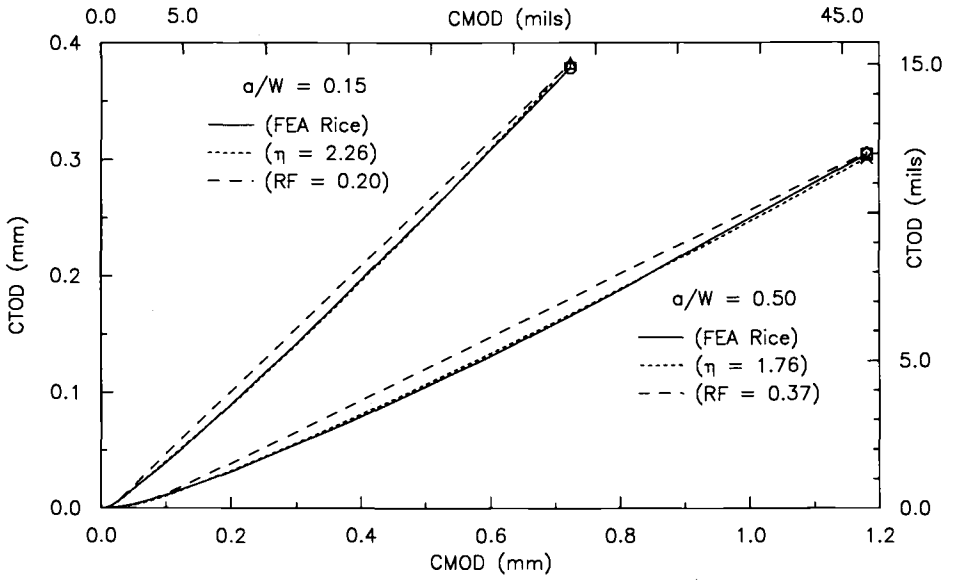

FIG. 17—*CTOD versus CMOD for square (31.8 by 31.8 mm) A36 steel specimens with* a/W = *0.15 and 0.50.*

The η_δ factors are determined from the finite element analyses and are dependent on the material properties and specimen *a/W* ratio. Throughout the elastic-plastic finite element analyses of the A36 steel, η_δ is 1.76 for the deep crack specimen and 2.26 for the short crack specimen. The CTOD calculated using the load-CMOD record and Eq 8 very closely approximates the 90° intercept CTOD as shown in Fig. 17. Throughout the elastic-plastic regime, the calculated CTOD is within 3% of the measured CTOD for both the short crack and the deep crack specimens.

J-CTOD Relation

The relationship between the *J* and CTOD fracture parameters for the deep crack specimen is shown in Fig. 18. Throughout the elastic-plastic regime, the finite element *J* and the 90° intercept CTOD are linearly related. A linear relationship between *J* and CTOD was previously described by Dawes [*14*] using yield stress and by Wellman et al. [*28*] using flow stress.

$$J = m \sigma_{fl} \delta \tag{9}$$

where m = constraint factor dependent on loading conditions and stress state.

For the deep crack specimen, the constraint factor equals 1.7, as shown in Fig. 18. The calculated CTOD (from the load-CMOD results and Eq 8) and the calculated *J*-integral (from the load-LLD results and Eq 5) also are compared in Fig. 18. Both the correlated finite element results and the experimental results exhibit a nearly linear relationship between *J* and CTOD and closely match the finite element results.

Comparisons of the *J*-integral and the CTOD fracture parameters for the short crack specimen are shown in Fig. 19. A linear relationship exists between the finite element *J*-

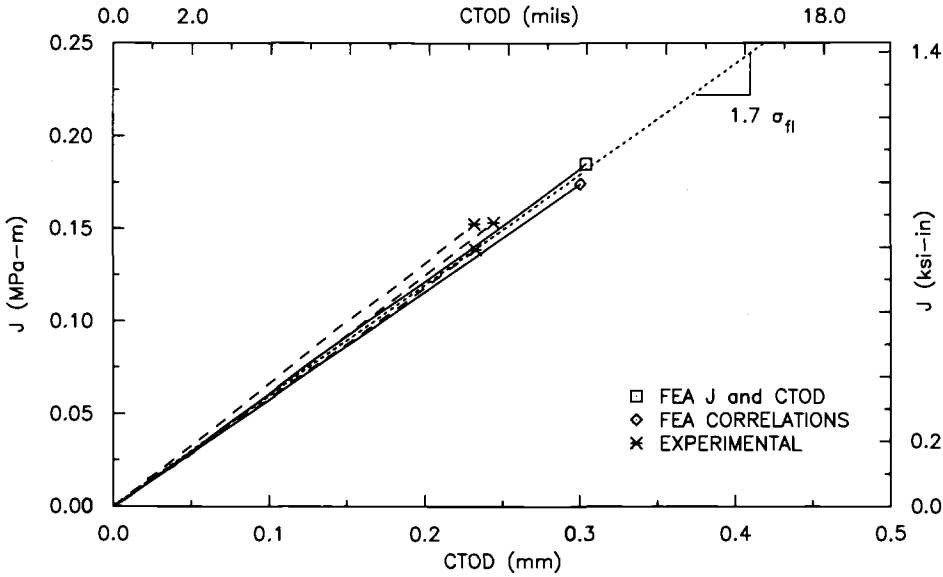

FIG. 18—J-*integral versus CTOD for square (31.8 by 31.8 mm) A36 steel specimens with* a/W = *0.50.*

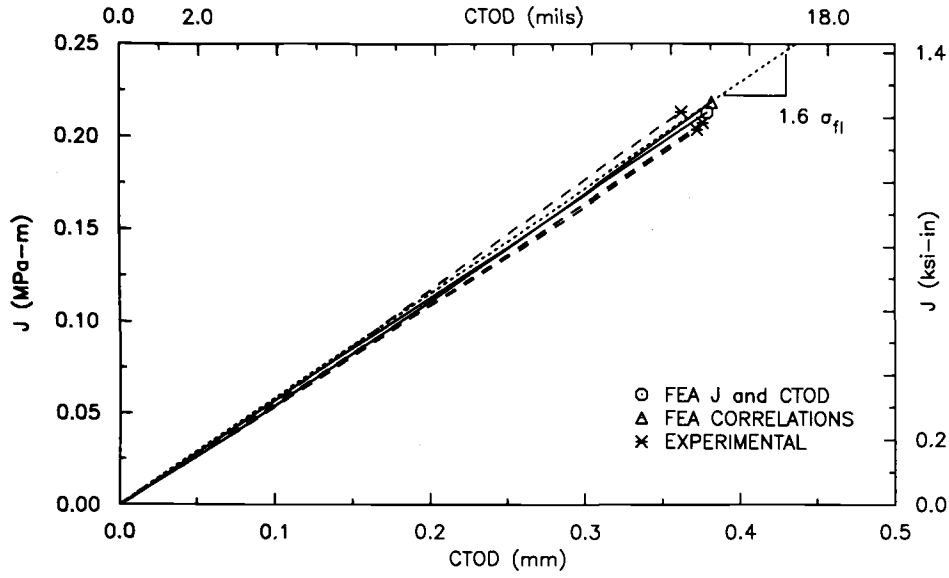

FIG. 19—J-*integral versus CTOD for square (31.8 by 31.8 mm) A36 steel specimens with* a/W = *0.15.*

integral and the 90° intercept CTOD. For the short crack specimen the constraint factor (m) equals 1.6. A similar relationship is exhibited between J calculated from the load-LLD records and CTOD calculated from the load-CMOD records. From the results of the experimental load-LLD records and load-CMOD records, the same linear relationship exists between the J and CTOD fracture parameters throughout the elastic-plastic regime.

The relationship between J and CTOD in Eq 9 is shown to work very well for the room temperature material properties of the A36 steel. Because the material properties deviate as the temperature decreases, the J and CTOD results experimentally determined throughout the lower-shelf and lower-transition regions are compared and shown in Fig. 20. Critical J-integral values are calculated for each specimen using Eq 5 and $\eta_t = 1.34$. Critical CTOD values are calculated for the same specimens using Eq 8 and $\eta_\delta = 2.26$. Throughout the lower-shelf and lower-transition regions, the experimental results show a linear relationship of $J = 1.7\,\sigma_{fl}\,\delta$. Since σ_{fl} increases with decreasing temperature, the slope of the relationship, $1.7\,\sigma_{fl}$, also increases with decreasing temperature. Experimentally the same linear relationship exists between the J and CTOD fracture parameters in the upper transition region after the initiation of stable crack growth. This is not analytically verified since crack growth is not simulated in the finite element models.

Discussion

Many problems exist in accurately measuring fracture toughness using short crack specimens in the laboratory. The J-integral fracture parameter can be measured using load-line displacement which may be a more accurate laboratory measurement for estimating the fracture toughness of short crack specimens. LLD is measured at some distance away from the crack tip, and the measurement is not affected by the plastic zone extending to the outside surface of the short crack specimens. Because the LLD is measured away from the crack tip, it does not affect the crack tip behavior. In contrast, CMOD is measured in a critical location near the crack tip, particularly for very small a/W ratios. Displacement of the load-line is relatively consistent for both the short and the deep crack specimen at the same J-values where as the displacement of the crack mouth is much less for the short crack specimen than for the deep crack specimen at the same CTOD values.

The relationship between specimen energy (area beneath the load-LLD record) and J-integral is greatly affected by the a/W ratio. The strain hardening properties of the material also affect this relationship but to a lesser extent. Finite element analyses were previously conducted by the authors on similar three-point bend specimens with a/W ratios of 0.10 using stress-strain properties of the A36 steel and an elastic-perfectly plastic (E-PP) material ($\sigma_{ys} = \sigma_u = 344$ MPa (50 ksi)). The η_t versus J relations for the $a/W = 0.10$ specimens are shown in Fig. 21. η_e from Eq 2 was equal to 0.93 for both materials. For the E-PP analysis, η_p was a constant 1.15 which agreed quite closely to Eq 4 where $\eta_p = 1.12$ for $a/W = 0.10$. For the A36 steel analysis, η_p was not constant but rather decreased with greater plastic zone development to a low of 0.88. Therefore η_p does appear to be both specimen geometry dependent and material dependent.

The results of this study show a linear relation of the J and CTOD fracture parameters ($J = m\,\sigma_{fl}\,\delta$) for both the short and the deep crack specimens. The a/W ratio appears to have very little affect on the constraint factor (m) in this relation. The J versus CTOD relations of the previously described FEA of the $a/W = 0.10$ specimens are shown in Fig. 22. The J-CTOD relation is linear for both materials, but the constraint factor (m) for the A36 steel is 1.6 and for the E-PP material is 1.4. This implies the stress parameter possibly should be based on something other than flow stress or yield stress in order for the relationship to be material independent. The linear relationship is encouraging because CTOD

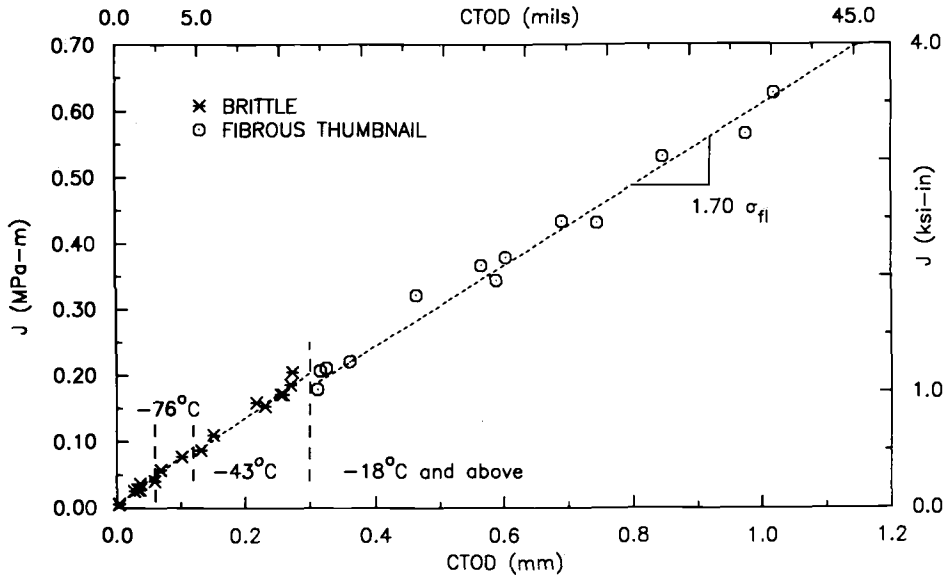

FIG. 20—*J-integral versus CTOD for square (31.8 by 31.8 mm) A36 steel specimens with* a/W = *0.15.*

or J can be determined in the laboratory using either load versus CMOD or load versus LLD and the preferred fracture parameter (CTOD or J) can be used for structural assessment studies.

Summary and Conclusions

Three-dimensional finite element analyses and experimental tests were conducted on a low-strength structural steel (A36) to determine the effect of crack depth on J-integral fracture toughness of square three-point bend specimens. Specimens with crack-depth to specimen-width ratios (a/W) of 0.50 (deep crack) and 0.15 (short crack) were compared in the linear-elastic regime and the elastic-plastic regime where considerable crack tip blunting and plastic zone development precedes brittle fracture. The J-integral results were compared to the CTOD results of both the short crack and deep crack specimens previously reported by Sorem et al. [*1,2*]. The results of this study may be summarized as follows:

1. J-integral values can be determined from the load versus load-line displacement records of three-point bend specimens with the relation

$$J = \frac{\eta_t U_t}{B(W - a)}$$

Using $\eta_t = 2.0$ for the deep crack specimen, the calculated J-values are within 6% of the FEA J-integral values over the entire loading range. Using $\eta_t = 1.34$ for the short crack specimen, the calculated J-values are within 7% of the FEA J-integral values over the entire loading range.

2. The J-integral and CTOD fracture parameters are linearly related throughout the elastic-plastic FEA for both the short crack and the deep crack specimens. Using the relation

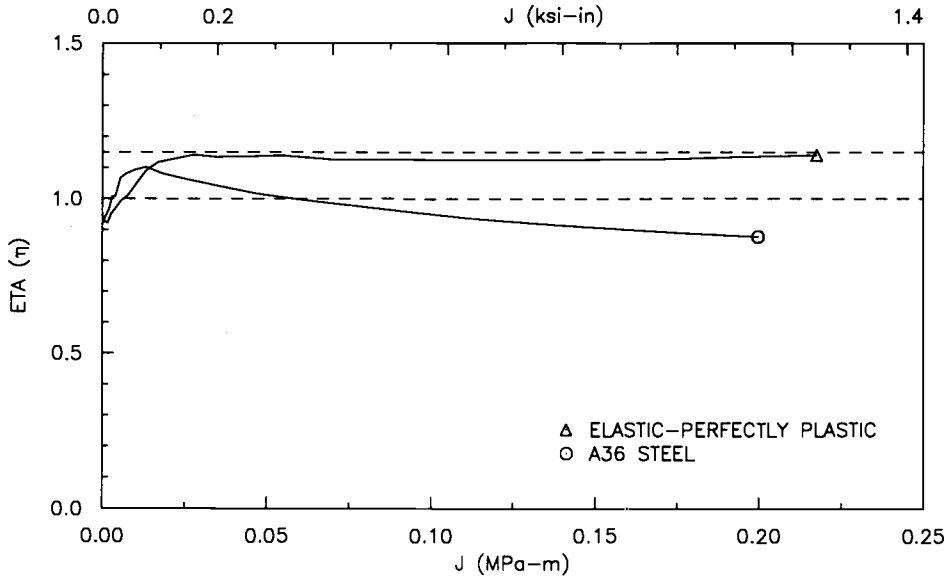

FIG. 21—J-*integral* η *factor from the load LLD record for square (31.8 by 31.8 mm) specimens with* a/W = *0.10.*

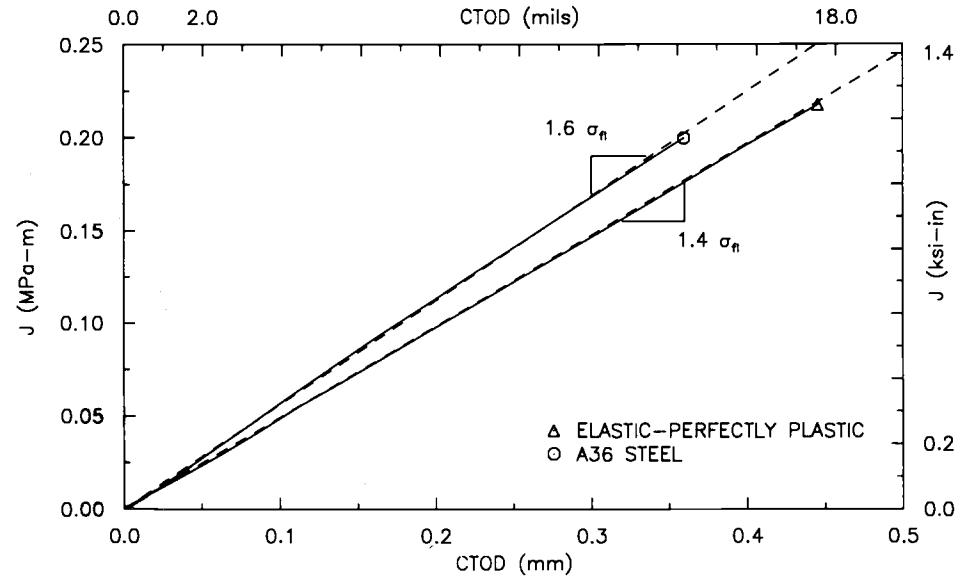

FIG. 22—J-*integral versus CTOD for square (31.8 by 31.8 mm) three-point bend specimens with* a/W = *0.10.*

$J = m\,\sigma_{fl}\,\delta$, the constraint factor (m) is equal to 1.7 for the deep crack specimen and 1.6 for the short crack specimen.

3. In the lower-shelf region, the J_c results of the short crack specimens are similar to the J_c results of the deep crack specimens. This implies the fracture toughness can be expressed as a single parameter characterization of the stress field which is independent of specimen size and crack depth in the lower shelf region.

4. In the lower-transition region, the J_c-values of the short crack specimen were two to three times larger than the J_c results of the deep crack specimens at identical temperatures. Thus the fracture toughness of the three-point bend specimen in the lower-transition region increases significantly as the a/W ratio decreases.

5. The critical CTOD results and critical J-integral results of the short crack experimental tests are linearly related throughout the lower-shelf and lower-transition regions and into the upper-transition region. The constraint factor (m) is equal to 1.7 for the short crack specimen.

In summary, the results of this study show that both the J-integral and the CTOD fracture parameters are equally applicable for testing in the lower-shelf and lower-transition regions where brittle fracture occurs prior to stable crack growth. The results support proposals to extend the current ASTM E 813 J-integral test procedure into the region of brittle fracture rather than limiting it to J_{Ic} at the initiation of ductile tearing. Testing short crack specimens ($a/W < 0.15$) using the load versus LLD record has potential experimental advantages. The laboratory measurement can be taken at a significant distance from the crack tip in order to facilitate easier measurement, yet characterize the fracture behavior of the crack tip region.

References

[1] Sorem, W. A., Dodds, R. H., Jr., and Rolfe, S. T., "An Analytical Comparison of Short Crack and Deep Crack CTOD Fracture Specimens of an A36 Steel," *Fracture Mechanics: Twenty-First Symposium, ASTM STP 1079*, American Society for Testing and Materials, Philadelphia, 1990, pp. 3–23.

[2] Sorem, W. A., Rolfe, S. T. and Dodds, R. H., Jr., "An Experimental Comparison of Short Crack and Deep Crack CTOD Fracture Specimens of an A36 Steel," to be published.

[3] Matsoukas, G., Cotterell, B., and Mai, Y.-W., "Hydrostatic Stress and Crack Opening Displacement in Three-Point Bend Specimens with Shallow Cracks, "*Journal of the Mechanics and Physics of Solids*, Vol. 34, No. 5, 1986, pp. 499–510.

[4] de Castro, P. M. S. T., Spurrier, J., and Hancock, P., "An Experimental Study of the Crack Length/Specimen Width (a/W) Ratio Dependence on the Crack Opening Displacement (COD) Test Using Small-Scale Specimens," *Fracture Mechanics, ASTM STP 677*, C. W. Smith, Ed., American Society for Testing and Materials, Philadelphia, 1979, pp. 486–497.

[5] Sumpter, J. D. G., "The Effect of Notch Depth and Orientation on the Fracture Toughness of Multi-Pass Weldments," *International Journal of Pressure Vessel and Piping*, 1982, Vol. 10, pp. 169–180.

[6] Cotterell, B., Li, Q.-F., Zhang, D.-Z., and Mai, Y.-W., "On the Effect of Plastic Constraint on Ductile Tearing in a Structural Steel," *Engineering Fracture Mechanics*, Vol. 21, No. 2, 1985, pp. 239–244.

[7] Li, Q.-F., "A Study About J_i and δ_i in Three-Point Bend Specimens With Deep and Shallow Notches," *Engineering Fracture Mechanics*, Vol. 22, No. 1, 1985, pp. 9–15.

[8] Li, Q.-F., Zhou, L. and Li, S., "The Effect of a/W Ratio on Crack Initiation Values of COD and J-integral," *Engineering Fracture Mechanics*, Vol. 23, No. 5, 1986, pp. 925–928.

[9] Zhang, D. Z. and Wang, H., "On the Effect of the Ratio a/W on the Values of δ_i and J_i in a Structural Steel," *Engineering Fracture Mechanics*, Vol. 26, No. 2, 1987, pp. 247–250.

[10] Anderson, T. L., McHenry, H. I., and Dawes, M. G., "Elastic-Plastic Fracture Toughness Tests with Single-Edge Notched Bend Specimens," *ASTM STP 856*, American Society for Testing and Materials, Philadelphia, 1985, pp. 210–229.

[11] Ebrahimi, F., "A Study of Crack Initiation in the Ductile-to-Brittle Transition Region of a Weld," *ASTM STP 945*, American Society for Testing and Materials, Philadelphia, 1988, pp. 555–580.

[12] Sumpter, J. D. G. and Turner, C. E., "Method for Laboratory Determination of J_c," *Cracks and Fracture, ASTM STP 601*, American Society for Testing and Materials, Philadelphia, 1976, pp. 3–18.

[13] Sumpter, J. D. G., "J_c Determination for Shallow Notch Welded Bend Specimens," *Fatigue Fracture Engineering Materials Structures*, Vol. 10, No. 6, 1987, pp. 479–493.

[14] Dawes, M. G., "Elastic-Plastic Fracture Toughness Based on the COD and J-Contour Integral Concepts," *Elastic-Plastic Fracture, ASTM STP 668*, J. D. Landes, J. A. Begley and G. A. Clarke, Eds., American Society for Testing and Materials, Philadelphia, 1979, pp. 307–333.

[15] Shoemaker, A. K. and Seeley, R. R., "Summary Report of Round Robin Testing by ASTM Task Group E24.01.06 on Rapid Loading Plane-Strain Fracture Toughness K_{Ic} Testing," *Journal of Testing and Evaluation*, JTEVA, Vol. 11, No. 4, July 1983, pp. 261–272.

[16] Clausing, D. P., "Tensile Properties of Eight Constructional Steels Between 70 and −320 F," *Journal of Materials*, Vol. 4, No. 2, June 1969, pp. 473–492.

[17] Lopez, L. A., "Finite: An Approach to Structural Mechanics Systems," *International Journal for Numerical Methods in Engineering*, Vol. 11, No. 5, 1977, pp. 851–866.

[18] Dodds, R. H. and Lopez, L. A., "A Generalized Software System for Nonlinear Analysis," *International Journal for Advances in Engineering Software*, Vol. 2, No. 4, 1980.

[19] Dodds, R. H., Jr., Carpenter, W. C., and Sorem, W. A., "Numerical Evaluation of a 3-D J-Integral and Comparison with Experimental Results for a 3-Point Bend Specimen," *Engineering Fracture Mechanics*, Vol. 29, No. 3, 1988, pp. 275–285.

[20] Rice, J. R., "A Path Independent Integral and the Approximate Analysis of Strain Concentration by Notches and Cracks," *Journal of Applied Mechanics*, Transactions of the American Society of Mechanical Engineers, Vol. 35, June 1968, pp. 379–386.

[21] Rice, J. R., Paris, P. C., and Merkle, J. G., "Some Further Results of J-Integral Analysis and Estimates," *ASTM STP 536*, American Society for Testing and Materials, Philadelphia, 1973, pp. 231–245.

[22] Turner, C. E., *Material Science Engineering*, Vol. 11, 1973, pp. 275–282.

[23] Haigh, J. R. and Richards, C. E., "Yield Point Loads and Compliance Functions of Fracture Mechanics Specimens," CEGB Report RD/L/M461.

[24] Paris, P. C., Ernst, Hugo, and Turner, C. E., "A J-Integral Approach to Development of η-Factors," *Fracture Mechanics: Twelfth Conference, ASTM STP 700*, American Society for Testing and Materials, Philadelphia, 1980, pp. 338–351.

[25] Srawley, J., "On the Relation of J_1 to Work Done per Unit Area: 'Total,' or Component 'Due to Crack'," *International Journal of Fracture*, Vol. 12, 1976, pp. 470–474.

[26] Turner, C. E., "The Ubiquitous η Factor," *Fracture Mechanics: Twelfth Conference, ASTM STP 700*, American Society for Testing and Materials, Philadelphia, 1980, pp. 314–337.

[27] Correspondence between Sorem, Rolfe, and Dodds, currently unpublished.

[28] Wellman, G. W., Rolfe, S. T., and Dodds, R. H., Jr., "Three-Dimensional Elastic-Plastic Finite Element Analysis of Three-Point Bend Specimens," *Fracture Mechanics: Sixteenth Symposium, ASTM STP 868*, American Society for Testing and Materials, Philadelphia, 1985, pp. 214–237.

Zhen Zhou,[1] *Kang Lee,*[1] *Ruben Herrera,*[1] *and John D. Landes*[1]

Normalization: An Experimental Method for Developing *J-R* Curves

REFERENCE: Zhou, Z., Lee, K., Herrera, R., and Landes, J. D., **"Normalization: An Experimental Method for Developing *J-R* Curves,"** *Elastic-Plastic Fracture Test Methods: The User's Experience (Second Volume), ASTM STP 1114*, J. A. Joyce, Ed., American Society for Testing and Materials, Philadelphia, 1991, pp. 42–56.

ABSTRACT: The method of normalization has been used to develop *J-R* curves for metallic materials based only on analysis of load and displacement pairs in a ductile fracture test record. This method eliminates the need for crack length monitoring equipment. It not only provides a method for more easily conducting and evaluating *J-R* curve tests; but it could be useful for tests conducted under special conditions such as under dynamic loading, in restructive facilities such as a hot cell, or even in a facility with limited instrumentation.

The method uses a normalized deformation curve which has a functional relationship resembling a power law in the beginning and a straight line later. A functional form is proposed to fit this material deformation pattern. This form was used along with the load versus displacement records to evaluate *J-R* curves for many materials. The results showed that the new method was a more accurate and versatile one for the assessment of the *J-R* curve. Compared with previous application of this method, the accuracy is remarkably improved in the beginning stages of the *J-R* curve where a J_{Ic} point is determined. The J_{Ic} point was analyzed on more than 60 specimens and found to be consistent with methods used in the ASTM test standards.

KEY WORDS: fracture testing, *J-R* curve, elastic compliance, normalization, J_{Ic}, test methods

J_{Ic} fracture toughness values from ASTM Standard Test Method for J_{Ic}, a Measure of Fracture Toughness, (E 813) have traditionally been developed using two techniques. The first, called the multiple specimen method, uses a series of specimens, each developing a single point of *J* versus crack extension. The second, called the single specimen method, uses instrumentation to develop values of *J* versus crack extension from one specimen. The single specimen method can also be used to develop the full *J-R* curves in accordance with ASTM Standard Test Method for Determining *J-R* Curves (E 1152).

Obviously the single specimen technique has advantages. It develops more information, namely the full *J-R* curve, requires fewer specimens, and gives a more satisfactory result. The instrumentation required to measure crack extension for the single specimen technique however is sometimes a problem. Most often the elastic unloading compliance is used [*1,2*], but this requires sophisticated equipment and an advanced testing technique that may not be available to some laboratories. Other methods for single specimen testing such as d-c potential drop [*3*] can equally cause experimental difficulties.

Recently a method of normalization has been introduced [*4,5*] to evaluate the *J-R* curve from load-displacement records with no crack extension monitoring equipment. This method

[1]Graduate assistant, graduate assistant, research associate, and professor, respectively, University of Tennessee, Knoxville, TN 37996. Mr. Herrera is presently a professor at National University of Mar Del Plata, Argentina.

was based on the key curve approach [*6*] but uses the results from a single test record to develop all needed information to get a *J* versus crack extension analysis. This method gives the information needed to develop both the J_{Ic} values of E 813 and the *J-R* curves of E 1152.

This paper will show how the method of normalization can be used with the standard ASTM ductile fracture test methods, first giving some background on the method. The latest approach uses a new functional form to relate normalized load and plastic displacement. This new approach will be explained and examples will be presented of both J_{Ic} and *J-R* curves analyzed by this method as well as by the elastic compliance method.

Normalization—Background

The method of normalization was derived from the early key curve analysis [*6*]. It assumes that the load carried by a test specimen can be represented by separable multiplicative functions of crack length (a/W) and material deformation (v_{pl}/W) [*7,8*]

$$P = G\left(\frac{a}{W}\right) H\left(\frac{v_{pl}}{W}\right) \tag{1}$$

If both of these functions are known the load, displacement and crack length have a unique relationship. Hence if load and displacement pairs are taken, for example, from a test record, the crack length can be determined [*4,5*].

The function $G(a/W)$ is dependent on the particular specimen geometry and can be determined for a specimen type if the *J* calibration is known. This was demonstrated by the analyses of Ernst et al. [*8*] and Sharobeam and Landes [*9,10*] in which the plastic eta factor, η_{pl}, was used to determine $G(a/W)$ using the relationship

$$\eta_{pl} = -\left(\frac{b}{W}\right)\left[\frac{G'(a/W)}{G(a/W)}\right] \tag{2}$$

The deformation function $H(v_{pl}/W)$ is material dependent and varies from one material to another. It depends on flow strength, hardening character and other material features. The approach assumes that a functional form could be inferred for $H(v_{pl}/W)$ that is general for metals. This functional form would have unknown constants that could be determined from details of the test.

The first suggestion for this function was a power law [*4,5,11*] with unknown fitting constants which could be determined from test details at the original and final crack length. This function worked satisfactorily for materials that did not have extensive deformation during the fracture process. For materials with extensive deformation the function $H(v_{pl}/W)$ appeared to approach a straight line. Therefore, to generalize $H(v_{pl}/W)$, a functional form that started as a power law but later changed to a straight line was suggested [*12*]. The power law plus straight line function gave better results than the pure power law method because it more generally described the deformation character observed in a test specimen. However, the function was awkward to use because a point of transition from power law to straight line was needed. This point had to be chosen and fitting constants determined from points in the test record where crack length was not known.

Figures 1 and 2 show results from the normalization method using both the power law assumption and the power law plus straight line (labeled combination). In both cases the *J-R* curve agreement between normalization and compliance is reasonable, especially at larger crack extension. However, the agreement at the early range of crack extension is not

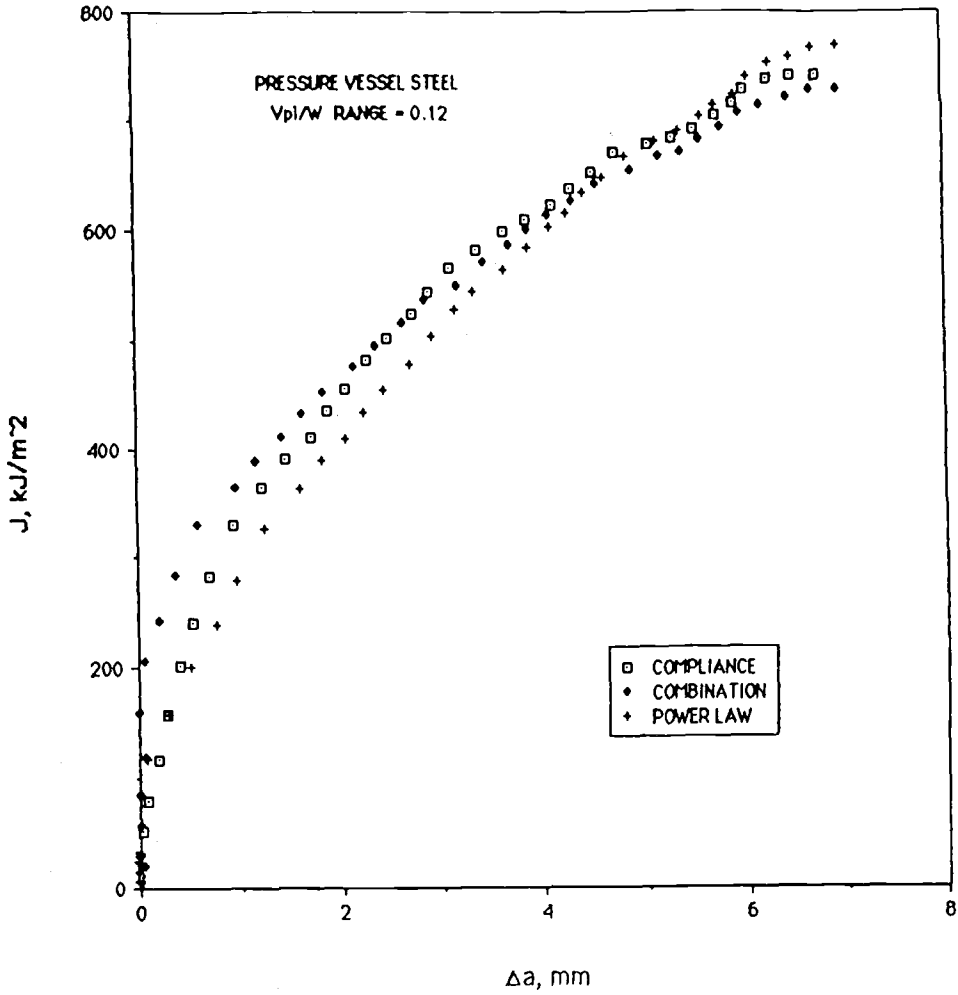

FIG. 1—J-R *curve from previous analysis for a pressure vessel steel.*

so good. Since this is the region where J_{Ic} is determined for the cases analyzed in Figs. 1 and 2, the J_{Ic} consistency would not be good.

To try to improve the normalization analysis a new fitting function called the LMN function was taken from the work of Orange [*13*]. This function has the general form

$$H(v_{pl}/W) = \frac{\left[L + M\left(\frac{v_{pl}}{W}\right)\right]\left(v_{pl}/W\right)}{N + v_{pl}/W} \tag{3}$$

where L, M, and N are fitting constants. This function has the character of resembling a power law (or polynomial) for small v_{pl}/W and a straight line for large v_{pl}/W. The transition between the two behaviors is smooth. This new function is used along with a different analysis procedure to introduce a new method for normalization analysis of J-R curves from

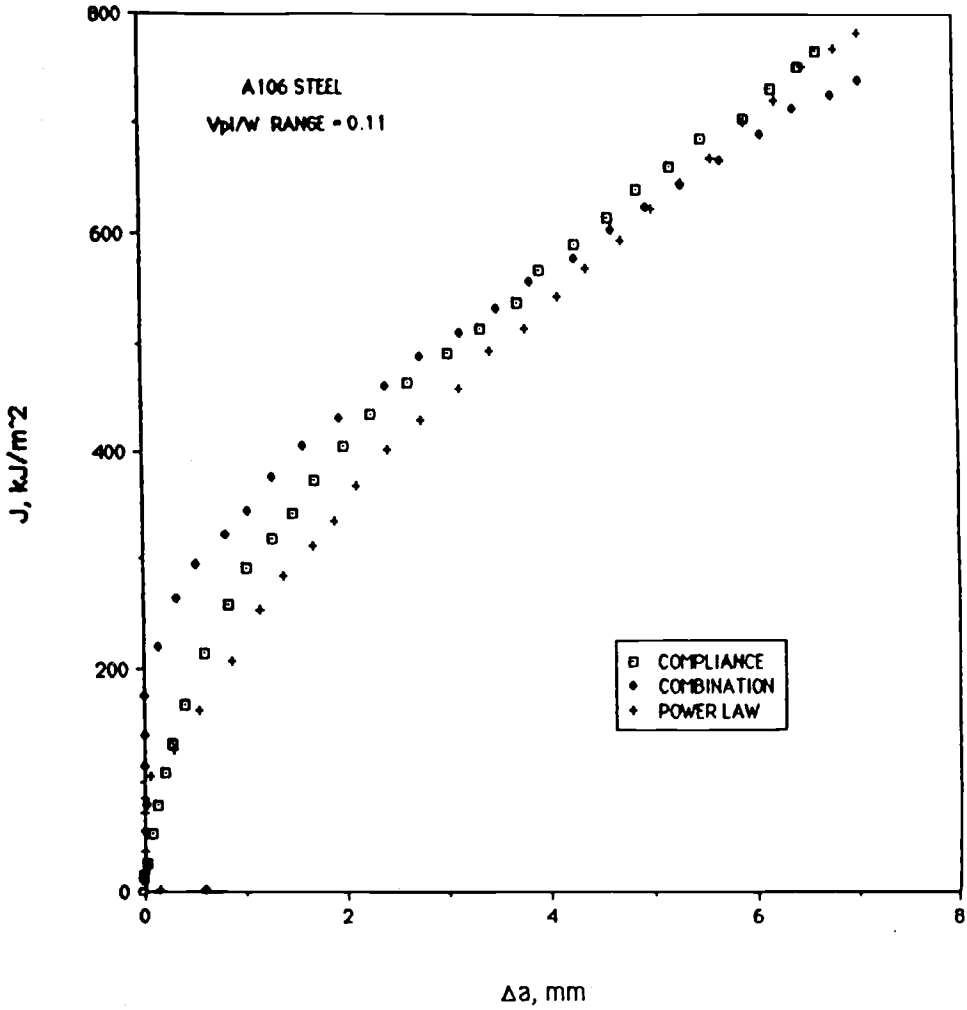

FIG. 2—J-R *curve from previous analysis for A106 steel.*

load versus displacement records. It will be demonstrated that this new method gives more accurate results, especially for determining J_{Ic}.

New Features of the Method

The new normalization method has some additional features which makes it more generally applicable to metallic materials. The two new features which will be discussed here are an assumed artificial blunting behavior and an intermediate calibration point.

The original normalization using either the power law or power law plus straight line did not reproduce the blunting behavior observed in the *J-R* curve results from either multiple specimen or single specimen techniques. The point of crack initiation tended to be somewhat artificially established; hence, the J_{Ic} values were not very reliable. As illustrated in Figs. 1 and 2, results showed excellent agreement between normalization and other methods like elastic compliance for larger crack extensions but did not agree well at the very beginning

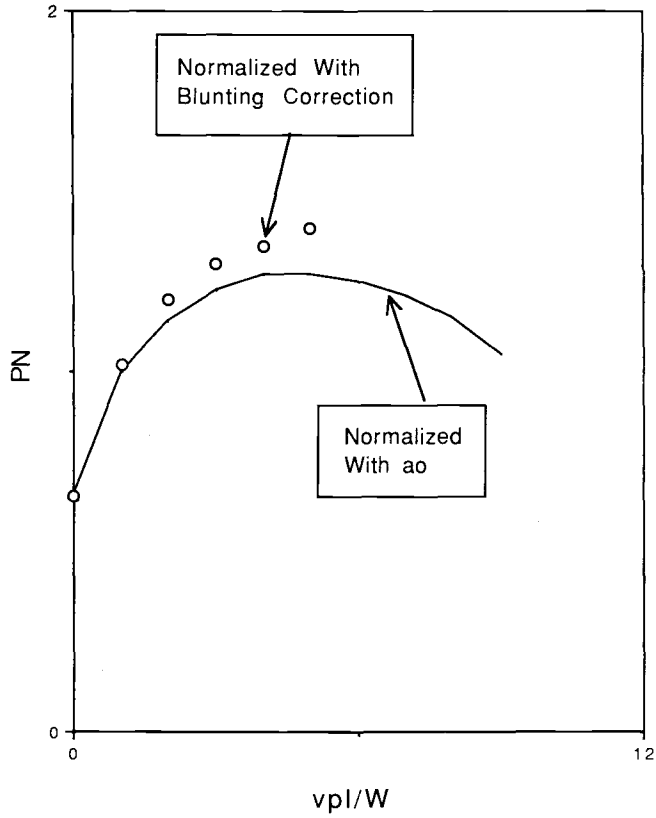

FIG. 3—*Enforced blunting line correction.*

of crack extension [*12*]. In order to get better agreement over this initial part of the *J-R* curve where J_{Ic} is determined and to give more realistic looking results, an artifically produced blunting was given to this new normalization method. Details of artificial blunting are given later.

The second new feature of the new method is the introduction of a new intermediate calibration point in the normalized load versus plastic displacement curve. The power law fit had two constants which were determined from load and displacement values at the initial and final crack lengths [*4*]. The power law plus straight line fits required an additional constant which was somewhat arbitrarily taken only from the load versus displacement record [*12*]. The LMN function has three constants and therefore also needs a third calibration point. The definition of this point was selected based on a careful study of the deformation character of metals [*14*] and was taken over an intermediate range of the deformation. The use of this point along with enforced blunting and a final calibration at the final value of crack length determines the LMN function which specifies the deformation behavior of the test specimen.

Summary of the Method

A detailed description of how to use the new normalization method is given elsewhere [*15*]. Here a summary of important steps will be presented. The first part of the method

involves the determination of the LMN function from the test record. The calibration requires a physically measured initial and final crack size. The methods in ASTM E 813 and E 1152 for measuring crack length are recommended. These values of crack length along with the appropriate load versus load line displacement points are required. Some additional information about the material tensile properties are also needed.

The first part of the analysis requires putting in an assumed blunting behavior. The ASTM E 813 blunting equation has been used although an alternate form may also work. This is

$$\Delta a = J/2\sigma_Y \tag{4}$$

where

σ_Y = yield stress or effective yield stress, and
Δa = crack extension.

The construction is schematically shown in Fig. 3. Here the measured load versus displacement is first normalized based on the initial crack length a_0. Normalization of the load by crack lengths between a_0 and a_f produces values of normalized load for a given plastic displacement. Hence the enforced blunting line gives calibration points above the a_0 normalized curve.

The second part of the construction requires an intermediate calibration point which cannot be determined for a known crack length. The idea for this point came from a study of normalized deformation behavior of many different steel specimens. It was observed that by dividing the normalized load, P_N, by flow stress, σ_Y and dividing v_{pl}/W by $\alpha\varepsilon_0$ where α is the coefficient of the nonlinear term in a Ramberg-Osgood power hardening stress-strain description and ε_0 is σ_Y/E, where E is the elastic modulus, gives a fairly consistent normalized deformation curve for all materials. This is illustrated in Fig. 4. In particular there was a point near the transition between the power law curve and the straight line behavior where all of the curves appeared to converge [*14*]. This point is approximately at $P_N = 0.32\ \sigma_Y$

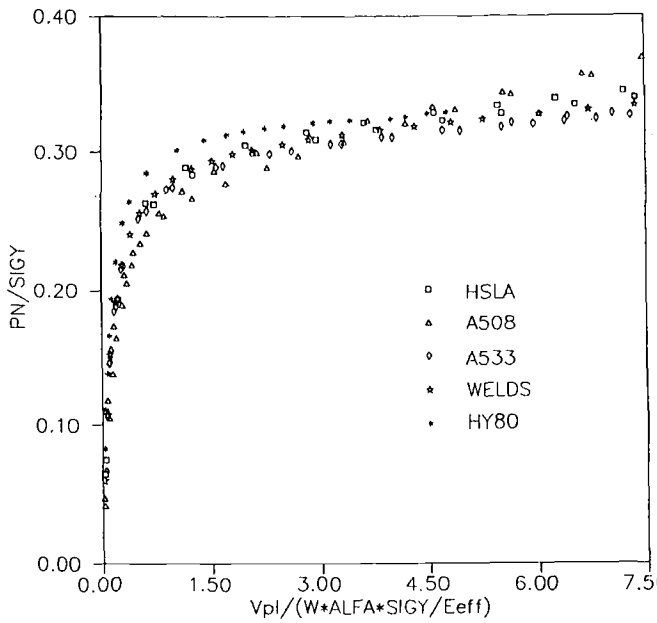

FIG. 4—*Normalized load versus plastic displacement.*

and $v_{pl}/W = 4\alpha\varepsilon_0$. This was first adopted as a fixed point. However in using this point, slight material variations caused scatter in results, because it was in a sensitive region for *J-R* curve analysis. The new method then picks this as an intermediate calibration point which can vary slightly. To choose the correct intermediate point a range of P_N values at $v_{pl}/W = 4\alpha\varepsilon_0$ is chosen.

The third calibration point is the final load, normalized by a_f, versus the final normalized plastic displacement. Figure 5 shows schematically all of the experimental calibration points and the variation of the intermediate calibration point.

The fitting of the LMN function then proceeds using the three types of calibration points described; the assumed blunting points, the intermediate point, and the final calibration point. The intermediate calibration point is varied and fits of the function in Eq 3 are made. The selection of the intermediate point is one that minimizes fitting error. A full description of this procedure is given in Ref *15*.

Once the LMN function is determined, the crack length values can be determined continuously or at discrete points. The LMN function uniquely relates load, plastic load line displacement, and crack length. This taken with a compliance calibration function for elastic displacement uniquely determines the crack length for given pairs of load and displacement.

Once the crack length values are determined, the value of *J* can be evaluated from load, displacement, and crack length. This can be done by directly integrating the deformation function [*16*] or from the E 1152 formula. The calculations in this paper used the latter.

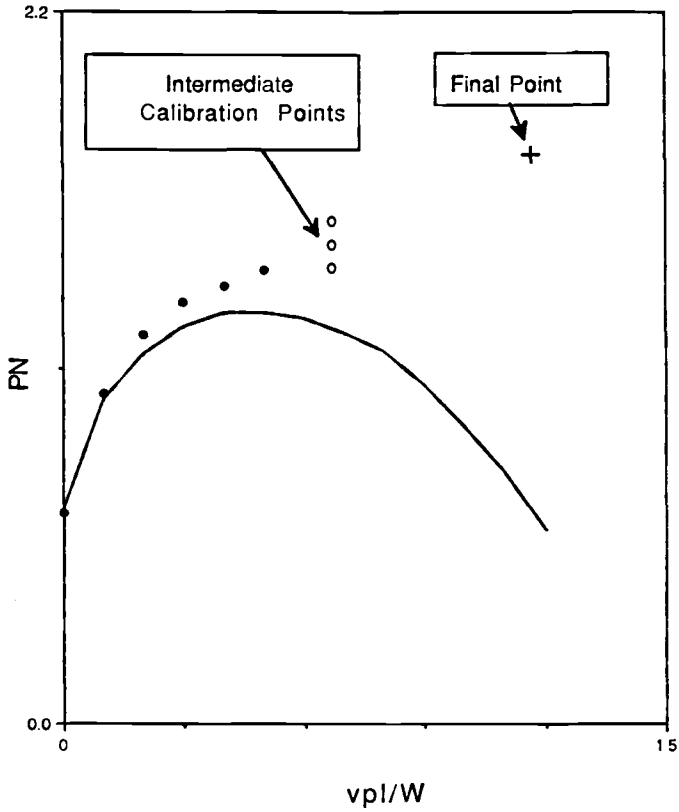

FIG. 5—*Schematic of points for LMN function fit.*

Results

The results of the normalization analysis are presented for five different materials. The emphasis is on how the method works along with the ASTM Standards for J_{Ic} determination (E 813) and for *J-R* curve evaluation (E 1152). For *J-R* curves the method works extremely well. This is illustrated in Figs. 6 through 12. Figure 6 shows results for an A508 pressure vessel steel [*17*]. The elastic compliance crack lengths measured in this test agreed very well with physical crack length measurement. Both compliance and the new method of normalization agree well throughout the range of Δa including the short Δa region. Figure 7 is the same material but for an 10T-CT specimen. Previous attempts to analyze this with normalization did not work well [*12*]. The new method works well, especially for the smaller crack extensions. The disagreement for larger crack extension represents a region where elastic compliance did not agree with physical crack measurements, whereas the normalization result must fit the final physical crack length exactly.

Figure 8 shows results for a weld metal. This was a difficult case to analyze because of the disruption caused on the deformation pattern by the composite weld metal/base metal structure. However, here the results look good.

Figures 9 and 10 are for an A106 steel [*18*]. Figure 9 is the same specimen shown in Fig. 2 but with the new normalization method. The agreement between compliance and normalization is much improved. Figure 10 shows a case where elastic compliance causes a short negative slope at the end of the *J-R* curve. This is removed by the normalization

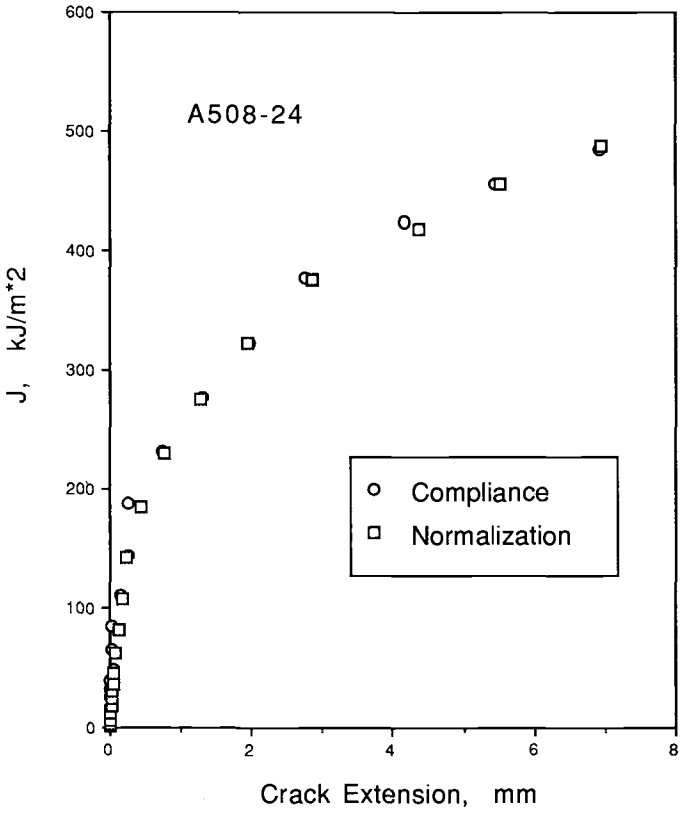

FIG. 6—J-R *curve for A508 steel, 1T-CT.*

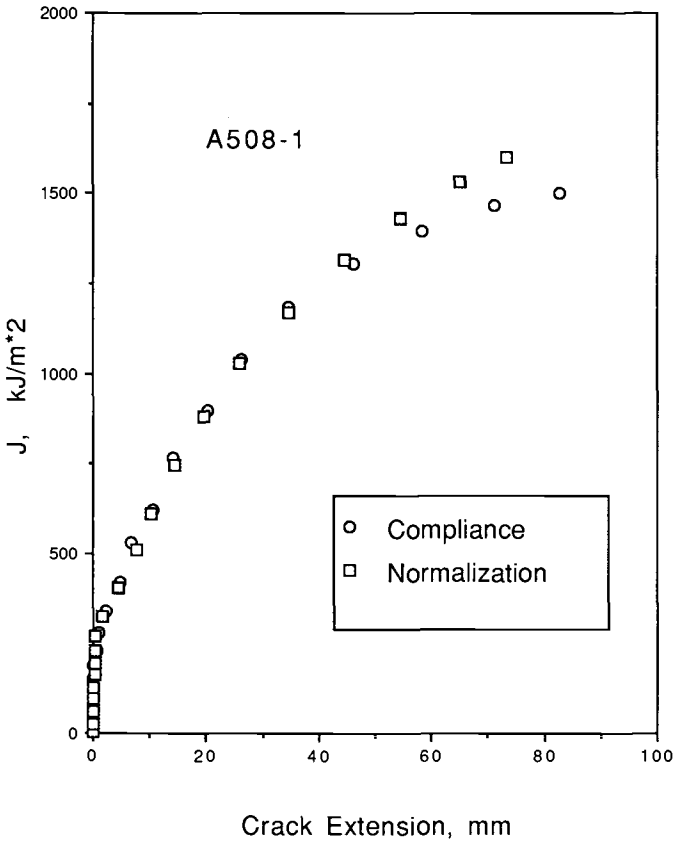

FIG. 7—J-R *curve for A508 steel, 10T-CT.*

analysis. Most cases of negative *J-R* slope were found to be caused by artifacts of the analysis and could be removed by the normalization analysis [*19*].

Figures 11 and 12 show results for an HY80 steel and HSLA steel [*18*]. These represent the low and high toughness range for the materials analyzed. The HSLA material shows the most plastic deformation of all materials and had the most scatter. This represents the worst agreement between elastic compliance and normalization of all cases analyzed for this paper.

The new method of normalization was used also to analyze J_{Ic} for various cases. Six materials were included, the five analyzed for *J-R* curves and an A533B steel [*18*]. A total of 67 specimens of the compact geometry were evaluated ranging from 1/2 T-CT to 10 T-CT. The results of the J_{Ic} analysis are given in Table 1. As would be expected from the good agreement throughout the range of the *J-R* curve, the J_{Ic} values were consistent. For each material a mean value of J_{Ic} and the standard deviation were determined. The absolute minimum and maximum in the group were also included. Figure 13 shows the mean value of J_{Ic} along with standard deviation range for all materials and both methods of analysis. Figure 14 shows the mean values of J_{Ic} with minimum and maximum values. For every material the mean value is consistent between the two methods of analysis. The scatter of results is sometimes greater for the normalization analysis and sometimes for elastic com-

pliance. In the cases where there were many specimens, the A508 and HSLA steels, the elastic compliance showed more scatter.

Table 2 gives a summary of J_{Ic} differences. It is important to note that the elastic compliance method of analysis is subject to results not fitting into the standard deviation range at least as often as the normalization method. Based on this the normalization is judged to work as well as elastic compliance for J_{Ic} evaluation on these materials. It would be interesting to look at more materials.

Discussion and Summary

The new method of normalization has many advantages. First it does not require automatic crack length monitoring equipment. This can be a great advantage for laboratories which do not have this equipment or have not developed sufficient technique. Essentially tests can be conducted following the multiple specimen J_{Ic} technique. When multiple specimen tests are conducted an R curve can be developed for each specimen. Tests conducted by the multiple specimen method before crack length monitoring equipment was available can now be reanalyzed to develop full *J-R* curves [*20*]. The method can even be used as a backup technique for single specimen tests which have crack length monitoring equipment.

In terms of the accuracy of the method the following observations can be made. When a single specimen crack monitoring system is working well, that is accurately predicting final

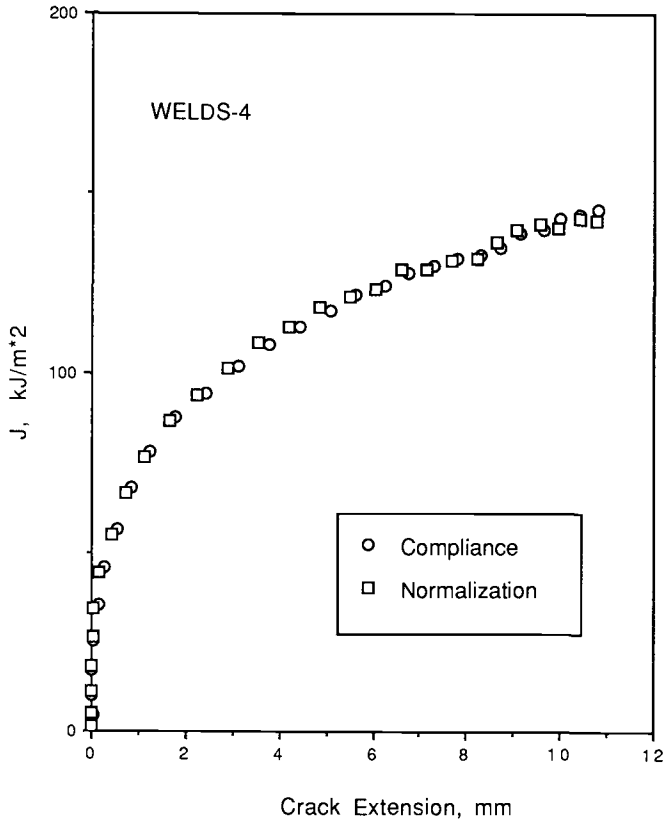

FIG. 8—J-R *curve for weld metal.*

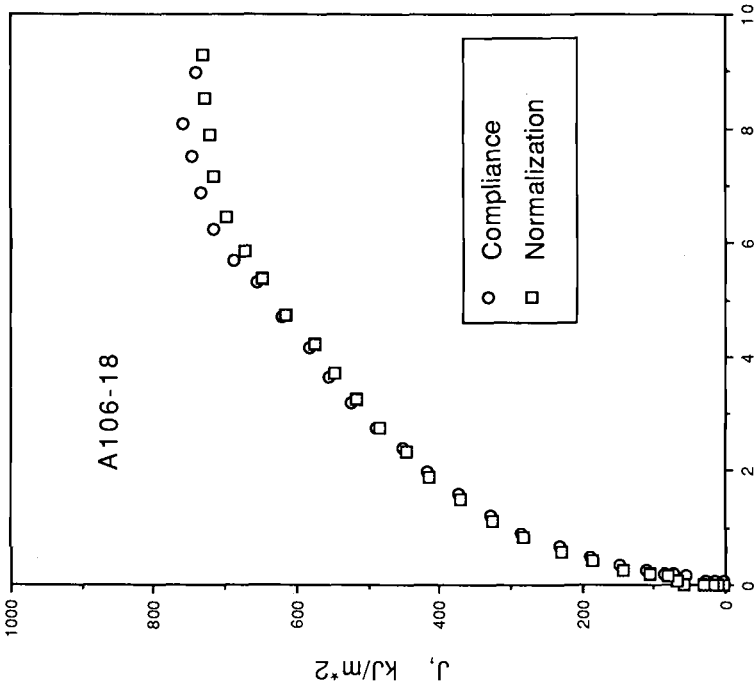

FIG. 10—J-R *curve for A106 steel.*

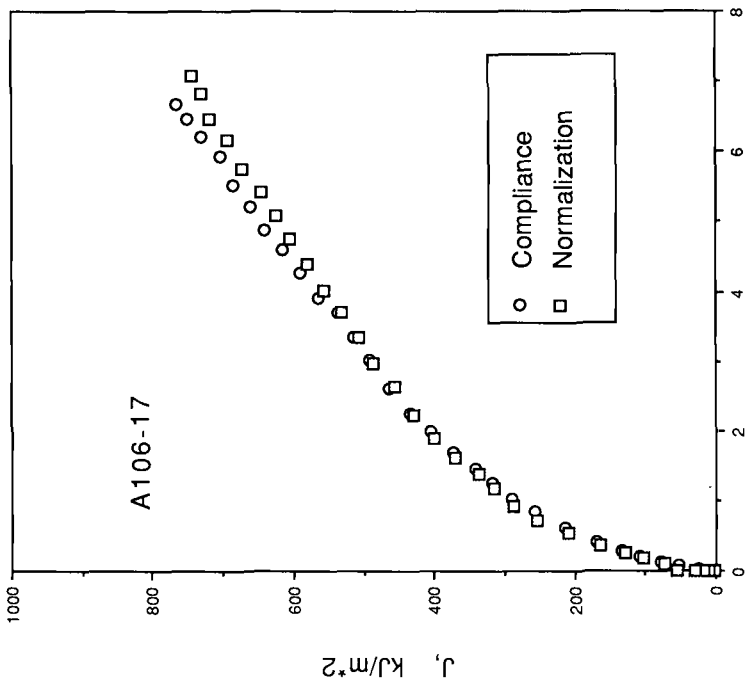

FIG. 9—J-R *curve for A106 steel.*

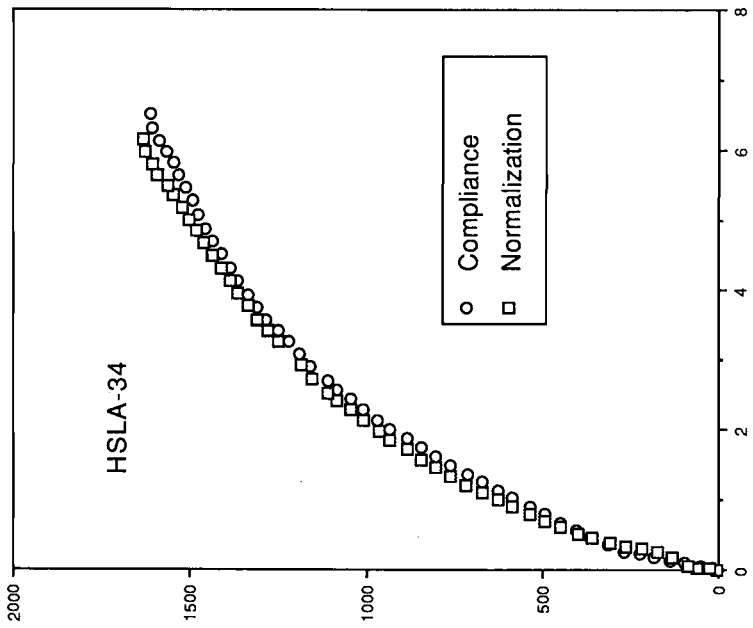

FIG. 12—J-R *curve for HSLA steel.*

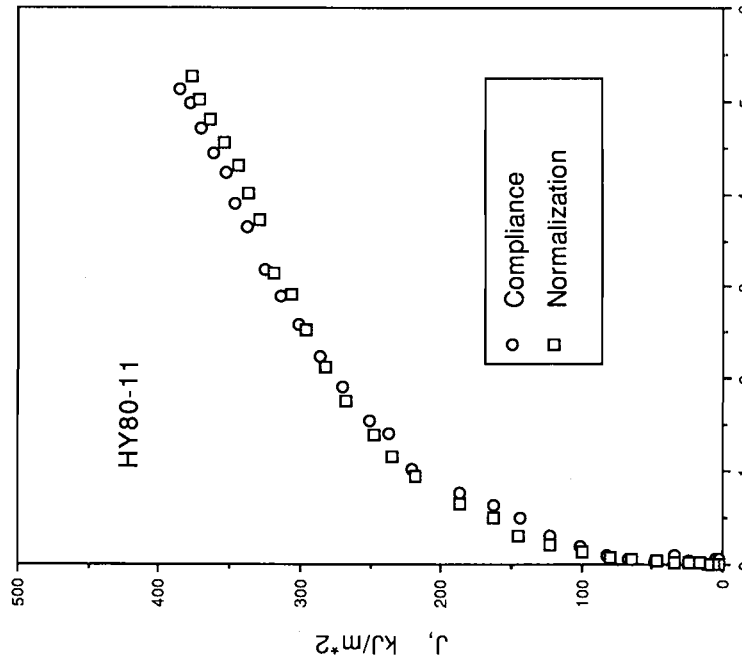

FIG. 11—J-R *curve for HY-80 steel.*

TABLE 1—J_{Ic} *Statistical analysis.*

Material	Curves Analyzed	J_{Ic} Mean, kJ/m²	Standard Deviation, kJ/m²	Max J_{Ic}, kJ/m²	Min J_{Ic}, kJ/m²
		NORMALIZATION ANALYSIS			
A508	34	188.8	49.9	175	98.6
HY80	3	123.8	11.73	138.2	109.6
A106	3	164.1	26.6	183.9	126.3
A533	3	226	25.0	261	205
HSLA	16	286	132.7	531	103.3
Weld	8	52.0	7.88	67.2	40.5
		ELASTIC COMPLIANCE ANALYSIS			
A508	34	171.1	67.9	454	57.8
HY80	3	105.1	21.7	131.5	78.1
A106	3	159.9	20.5	165.5	142.1
A533	3	227	14.0	240	108
HSLA	16	288	186.0	707	22.4
Weld	8	45.9	5.25	55.7	36.9

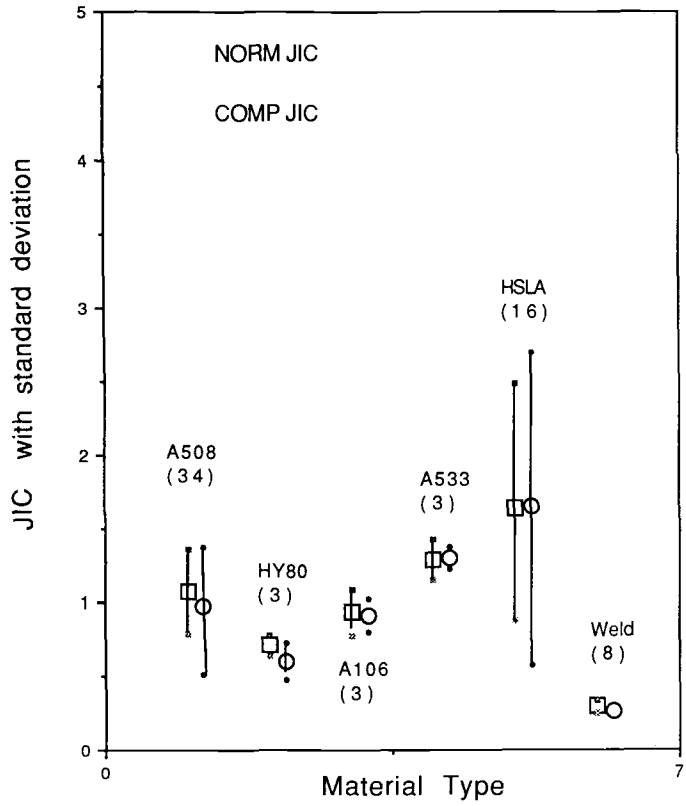

FIG. 13—J_{Ic} *with standard deviation for normalization and compliance.*

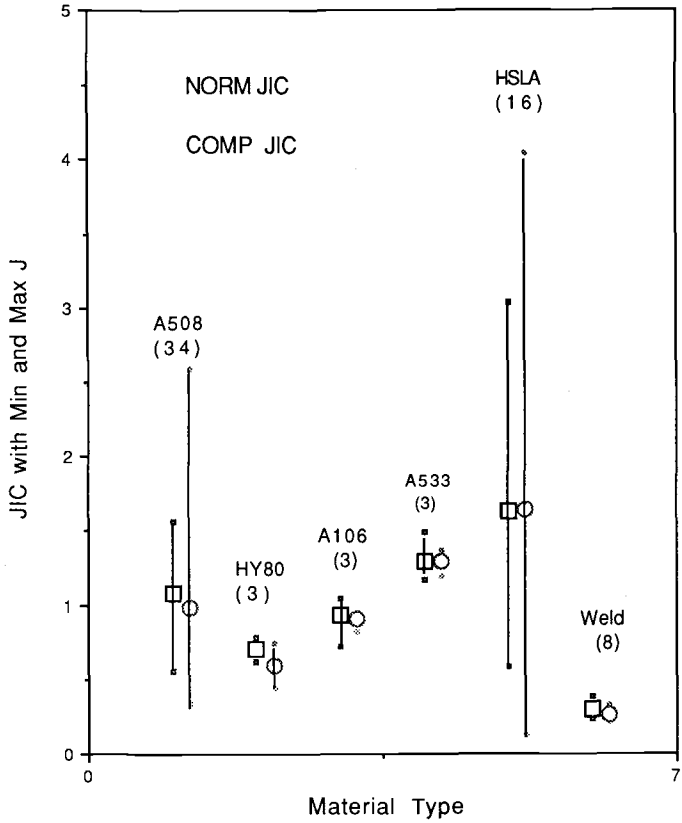

FIG. 14—J_{Ic} *with minimum and maximum* J_{Ic} *for normalization and compliance.*

crack length, the new method of normalization gives nearly identical results. In cases where the crack monitoring system failed to predict final crack length accurately, the new method appeared to give better results. Based on these observations, the new method could be judged to give overall more satisfactory results. The least success for the materials analyzed in this paper was for the HSLA steel which had the most plastic deformation as well as the most scatter in J_{Ic}.

TABLE 2—*Comparison of* J_{Ic} *difference normalization versus compliance.*

Percent Difference	No. of Cases	Percent of Total
Greater than 50%	7	10
25 to 50%	15	22
Less than 25%	45	67
For Cases Greater than 50% Method out of Standard Deviation Range		
Compliance	3	
Normalization	2	
Neither	2	

As an overall assessment of the new method of normalization, it appears satisfactory for use with the ASTM standards and is offered as a candidate to incorporate into the standards. However, before it could be adopted by consensus, experience is needed by a larger number of laboratories. Therefore it is recommended now as a second method to use along with the other primary methods of *J-R* curve analysis.

References

[*1*] Clarke, G. A., Andrews, W. R., Paris, P. C., and Schmidt, D. W., "Single Speciment Tests for J_{Ic} Determination," *Mechanics of Crack Growth, ASTM STP 590*, American Society for Testing and Materials, Philadelphia, 1976, pp. 24–42.

[*2*] Joyce, J. A. and Gudas, J. P., "Computer Interactive J_{Ic} Testing of Navy Alloys," *Elastic-Plastic Fracture, ASTM STP 668*, J. D. Landes, J. A. Begley, and G. A. Clarke, Eds., American Society for Testing and Materials, Philadelphia, 1979, pp. 451–468.

[*3*] Wilkowsky, G. M. and Maxey, W. A., *Fracture Mechanics: Fourteenth Symposium—Volume II: Testing and Applications, ASTM STP 791*, J. C. Lewis and G. Sines, Eds., American Society for Testing and Materials, Philadelphia, 1983, pp. II-226–II-294.

[*4*] Landes, J. D. and Herrera, R., "A New Look at *J-R* Curve Analysis," *International Journal of Fracture*, Vol. 36, 1988, pp. R9–R14.

[*5*] Herrera, R. and Landes, J. D., "A Direct *J-R* Curve Analysis of Fracture Toughness Tests," *Journal of Testing and Evaluation*, Vol. 16, No. 5, Sept. 1988, pp. 427–449.

[*6*] Joyce, J. A., Ernst, H. A., and Paris, P. C., "Direct Evaluation of J-Resistance Curves from Load Displacement Records," *Fracture Mechanics: Twelfth Conference, ASTM STP 700*, American Society for Testing and Materials, Philadelphia, 1980, pp. 222–236.

[*7*] Ernst, H. A., Paris, P. C., Rossow, M., and Hutchinson, J. W., "Analysis of Load Displacement Relationship to Determine *J-R* Curve and Tearing Instability Material Properties," *Fracture Mechanics, ASTM STP 677*, C. W. Smith, Ed., American Society for Testing and Materials, Philadelphia, 1979, pp. 581–599.

[*8*] Ernst, H. A., Paris, P. C. and Landes, J. D., "Estimations on *J*-integral and Tearing Modulus T From a Single Specimen Test Record," *Fracture Mechanics, Thirteenth Conference, ASTM STP 743*, Richard Roberts, Ed., American Society for Testing and Materials, Philadelphia, 1981, pp. 476–502.

[*9*] Sharobeam, M. H. and Landes, J. D., "The Separation Criterion and Methodology in Ductile Fracture Mechanics," *International Journal of Fracture*, Vol. 47, 1991, pp. 81–104.

[*10*] Sharobeam, M. H., Landes, J. D., and Herrera, R., this publication, pp. 114–132.

[*11*] Joyce, J. A. and Hackett, E. M., "An Advanced Procedure for *J-R* Curve Testing using a Drop Tower," *Nonlinear Fracture Mechanics: Volume I—Time Dependent Fracture, ASTM STP 995*, A. Saxena, J. D. Landes, and J. L. Bassani, Eds., American Society for Testing and Materials, Philadelphia, 1989, pp. 298–317.

[*12*] Herrera, R. and Landes, J. D., "Direct *J-R* Curve Analysis: A Guide to the Methodology," *Fracture Mechanics: Twenty-First Symposium, ASTM STP 1074*, American Society for Testing and Materials, Philadelphia, 1990, pp. 24–43.

[*13*] Orange, T. W., "Methods and Models for *R*-Curve Instability Calculations," *Fracture Mechanics: Twenty-First Symposium, ASTM STP 1074*, American Society for Testing and Materials, Philadelphia, 1990, pp. 545–599.

[*14*] Landes, J. D. and Herrera, R., unreported results.

[*15*] Landes, J. D., Herrera, R., Lee, K., and Zhou, Z., "The Normalization Method to Develop *J-R* Curve with the LMN Fraction," *Journal of Testing and Evaluation*, to be published.

[*16*] Landes, J. D. and Herrera, R., "Calculation of *J* From Test Records for the Growing Crack," *International Journal of Fracture*, Vol. 36, 1988, pp. R15–R20.

[*17*] Landes, J. D., McCabe, D. E., and Ernst, H. A., "Fracture Testing of Ductile Steels," MP-5014, Final Report of Project 1238-2, Electric Power Research Institute, Palo Alto, CA, Jan. 1987.

[*18*] Joyce, J. A., Davis, D. A., Hays, R. A., and Hackett, E. H., "Application of the *J*-Integral and Modified *J*-Integral to Cases of Large Crack Extension," NUREG CR-5143, Nuclear Regulatory Commission, Washington, DC, Feb. 1989.

[*19*] Landes, J. D. and Herrera, R., "Correcting *J-R* Curve Mismatch Twist with Normalization," *Advances in Fracture Research*, Vol. 1, Proceedings of ICF-7, March 1989, pp. 403–411.

[*20*] Wong, R., Herrera, R., Zhou, Z., and Landes, J. D., "Development of *J-R* Curves from Obsolete Data Using Normalization Techniques," *Engineering Fracture Mechanics*, to be published.

James A. Joyce[1]

Quantification of Engineering Limits to *J* Control of Ductile Crack Growth

REFERENCE: Joyce, J. A., "**Quantification of Engineering Limits to *J* Control of Ductile Crack Growth,**" *Elastic-Plastic Fracture Test Methods: The User's Experience (Second Volume), ASTM STP 1114*, J. A. Joyce, Ed., American Society for Testing and Materials, Philadelphia, 1991, pp. 57–80.

ABSTRACT: The *J*-integral has been developed as a ductile fracture parameter over the past 15 years and has been applied to an ever-expanding range of applications and materials. Limits originally placed on the application of *J* by analytical considerations have, in most cases, proven too stringent—and in some cases the analytical limits have even seemed to be inapplicable or irrelevant. This has been particularly true of the omega (ω) criterion introduced by Hutchinson and Paris. Experimental work has seemed to show little correspondence between the limits predicted by this criterion and the experimentally measured size limitations.

Recent experimental work by Joyce et al. has shown that the *J*-integral is applicable to much larger crack extensions than previously proposed. Using these experiments Joyce and Hackett have proposed an experimental method to define the limit to *J*-integral controlled crack growth.

This paper now shows that the ω criterion is consistent with the collected data set, except that the limiting value for ω is on the order of one, not the value of 5 to 10 originally proposed. Three simple analyses are presented using the ω criterion to develop proposed limits on *J* and crack extension that can be used in a predictive manner for fracture analysis.

KEY WORDS: elastic-plastic fracture, test methods, crack growth, *J*-integral, crack initiation

The *J*-integral has been developed as a ductile fracture parameter over the past 15 years and has been applied to an ever-expanding range of applications and materials. Initially, because of the deformation plasticity assumptions utilized in its mathematical derivation, the *J*-integral was applied only to crack initiation. It was clear that crack growth causes some material to be unloaded, and that this possibly eliminates the *J*-integral singularity. *J*-resistance curves were originally developed not as a measure of material toughness but only as a means of evaluating the J_{Ic} initiation parameter. The development of single-specimen *J*-resistance curve techniques [*1*] allowed high-quality *J*-resistance curves to be evaluated from each test sample, and the amount of *J*-resistance curve data available grew rapidly. It soon became apparent that small amounts of crack extension did not immediately eliminate the *J*-integral singularity or at least *J* control of crack growth but also that a considerable degree of size independence was present in *J*-resistance curves as well as J_{Ic} values.

In many structural applications, little crack growth is expected during normal operation, but considerable growth could occur during accident conditions. To assess the residual toughness of a structure during accident conditions, *J*-resistance curves have been developed and incorporated into engineering safety analyses [*2*]. Work has continued on the definition of both experimental and analytical limits to the utilization of the *J*-integral in terms of

[1]Professor of Mechanical Engineering, U. S. Naval Academy, Annapolis, MD 21402.

specimen size, toughness, and crack extension. An experimental limit has been recently proposed by Joyce and Hackett [*3*] utilizing a plot of plastic crack mouth opening displacement, normalized by specimen width, versus crack extension, normalized by specimen width. A region of "*J*-controlled growth" is defined on this plot and its limit is evaluated and used as a definition of "*J*-controlled crack growth." The basic point of view is taken that the initial crack extension occurred due to singularity-controlled conditions, and if subsequent growth occurs at an equivalent rate, it can be used in an engineering sense as being at least nearly equivalent to what would occur if the singularity had somehow been maintained. This limit is applied in this work to seek an analytical quantity that defines the limit of *J*-controlled growth and is independent of specimen type, size, and material.

Analytical Limits to *J*-Controlled Growth

The work of Hutchinson [*4*] and Rice and Rosengren [*5*] showed that the *J*-integral defines the intensity of the stress and strain fields near a stationary crack. This gives a strong analytical basis for a stationary crack problem but a weak basis for cases where crack growth is present. As just described, however, experimental and engineering expendiency caused a large effort to be expended on development of *J*-integral-based crack growth resistance curves. Hutchinson and Paris [*6*] gave some analytical legitimacy to this application when they showed that, for small amounts of crack extension, nearly proportional plastic deformation and strains occur in an annular region completely surrounding the crack tip. They showed that a zone of nonproportional strain occurs at the crack tip, and they proposed that, when this nonproportional strain zone was small compared to the size of the plastic annular region, and hence specimen dimensions, crack growth could occur under *J*-integral control.

In the Hutchinson and Paris analysis, plastic strain is related to stress according to

$$\epsilon_{PL} = A\sigma^n \tag{1}$$

and then using the singularity solution of Refs (*4*) and (*5*) gives (Ref 6, Eq 1)

$$\epsilon_{ij} = k_n J^{n/(n+1)} r^{-n/(n+1)} \tilde{\epsilon}_{ij}(\theta, n) \tag{2}$$

Strain increments can be calculated as (Ref 6, Eq 4)

$$d\epsilon_{ij} = k_n J^{n/(n+1)} r^{-n(n+1)} \tilde{\epsilon}_{ij}(\theta, n) \left[\frac{n}{n+1} \frac{dJ}{J} \tilde{\epsilon}_{ij} + \frac{da}{r} \tilde{\beta}_{ij} \right] \tag{3}$$

where (Ref 6, Eq 4*a*)

$$\tilde{\beta}_{ij}(\theta) \approx \frac{n}{n+1} \cos\theta \, \tilde{\epsilon}_{ij} + \sin\theta \frac{\partial}{\partial\theta} \tilde{\epsilon}_{ij} \tag{4}$$

Comparing Eqs 2 and 3 shows that the first term in the brackets in Eq 3 gives strain increments proportional to strain components, while the second term is not proportional. Recognizing that $\tilde{\epsilon}_{ij} = \tilde{\beta}_{ij}$, then in a zone near the crack tip if

$$\frac{da}{r} \geq \frac{dJ}{J} \tag{5}$$

it follows that in this region nonproportional strain increments will predominate and the J-integral singularity may be eliminated. Referring to Fig. 1, a parameter, ω, is defined as the ratio of the J-integral controlled outer annular radius, R, to the inner nonproportional radius, D, that is

$$\omega = \frac{R}{D} \tag{6}$$

Combining Eqs 5 and 6 and assuming $r = D$ gives

$$\frac{1}{D} = \frac{\omega}{R} = \frac{dJ}{da}\frac{1}{J} \tag{7}$$

A practical upper limit for R is the specimen uncracked ligament, b, where in the usual notation

$$b = W - a \tag{8}$$

giving

$$\frac{R}{D} = \omega = \frac{b}{J} = \frac{dJ}{da} \tag{9}$$

This is the omega (ω) parameter defined by Hutchinson and Paris, who expected that, for J-controlled growth to exist, it would be necessary that $\omega >> 1$. However, Hutchinson and Paris [6] were not more specific—nor did they look at the practical limits proposed by this condition on the applicability of the J-integral resistance curve method.

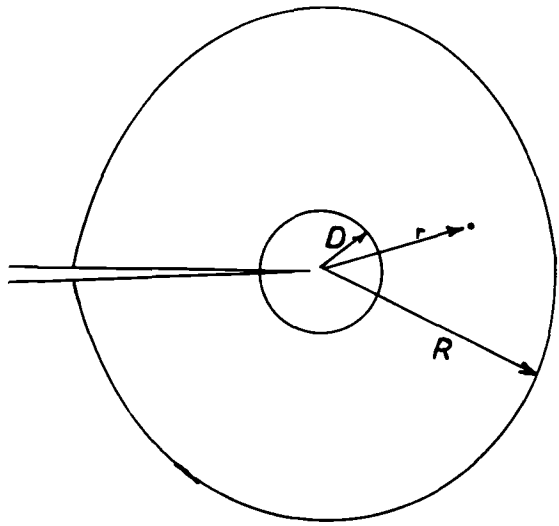

FIG. 1—*Zones of proportional and nonproportional strain increments near a crack tip.*

Other *J*-Integral Limits

Two other limits are generally applied to *J*-resistance curves and these need to be explored here as well. The first size requirement was proposed by Paris [*7*] in reference to the first application by Landes and Begley [*8*] of the *J*-integral as an elastic-plastic fracture criterion. This requirement was that

$$M = \frac{b\sigma_F}{J} >> 1 \ (\approx 25 \text{ to } 40) \tag{10}$$

and is essentially a requirement that the crack tip opening displacement be small in comparison with the ligament dimension, b. This requirement is generally applied to both crack initiation and growth. The values of M have been discussed by many researchers including McMeeking and Parks [*9*], Joyce and Gudas [*1*], Davis et al. [*10*], and McCabe et al. [*11*], and the range 25 to 40 is generally used for initiation, while 20 is used by ASTM Test Method for Determining *J-R* Curves (E 1152-87) for crack growth. No consistent value of M has been obtained by these researchers.

A third limit has been proposed by Shih and German [*12*] limiting the amount of crack extension to 6% of the initial uncracked ligament, that is, that

$$\Delta a \leq 0.06\, b_o = \gamma b_o \tag{11}$$

This result is generally felt to be too stringent and was modified in ASTM E 1152-87 to

$$\Delta a \leq 0.1\, b_o \tag{12}$$

based on more recent computational results of Booth [*13*].

Experimental Verification

Experimental verification of these results, as for example in Ref [*14*], has been attempted and generally shows that Eqs 10 and 12 are overly stringent for bend-type specimens, though the amount of conservatism is not consistent across the range of materials and specimen geometries tested.

Of the three parameters (ω, M, γ), experimental work has been least favorable to ω, with work showing that no effect is present on the *J-R* curve as ω falls below, say, 10 or 5 or even, in some cases, 1. This result has generally caused ω to be omitted when limits to valid *J*-resistance curves are set, as is the case in both ASTM Test Method for J_{Ic}, a Measure of Fracture Toughness (E 813-87) and ASTM E 1152-87. Problems have arisen, especially in the nuclear power area, which would be much more tractable if the *J*-integral limits could be clearly defined from both an analytical and an experimental viewpoint. To this end, much recent work has again been directed.

Recent work by the present author and coworkers [*11*] has proposed that it is possible to greatly expand the limits of applicability of the *J*-integral, at least in terms of the amount of crack extension allowed. Typical data from this study are shown in Fig. 2 that shows consistency of *J*-resistance curves between specimen sizes to large crack extension. Data presented in Ref *14*, over a range of material toughnesses, and for geometries from 1/2T to 2T compact tension (CT) specimens and 1/2T to 2T three-point bend (3PB) specimens, have been very consistent in showing that the limits defined previously need considerable modification.

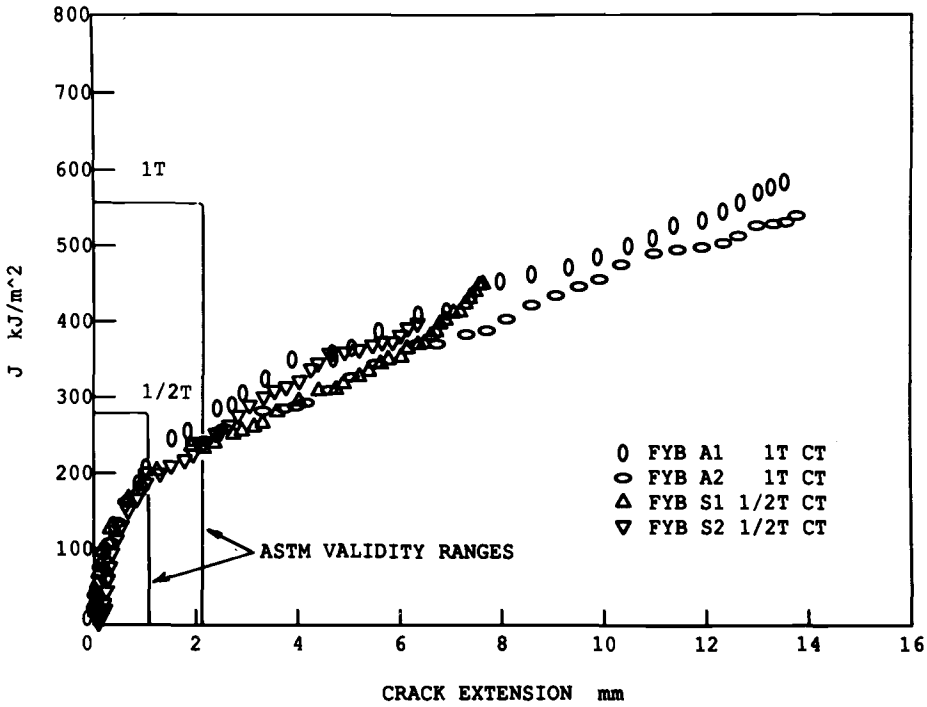

FIG. 2—J-*resistance curve data showing the insensitivity to specimen size to large crack extensions for an HY80 structural steel* [1].

Another step was the development of an experimentally determinable limit to *J*-controlled crack growth in Ref *3* using data plotted as shown in Fig. 3. The *J*-control limit is evaluated by fitting a straight line to the initial data in the *J*-control region, and then locating the first data point that deviates by 5% or more above this straight line. Repeating this process iteratively until the region of fit exceeds two-thirds of the *J*-control zone, as shown in Fig. 3, seems to give a well-defined limit.

Results obtained by the application of this method to three sets of data are presented in Tables 1 to 6. The material codes FYB and FYD correspond to 3% nickel alloy structural steels, while the FGN material is a CS19 structural aluminum alloy. Tensile mechanical properties of these materials are shown in Table 7. These materials codes are used in the remainder of this report. Tables 1 to 3 are calculated using the standard deformation *J* as defined by ASTM E 1152-87, and Tables 4 to 6 are calculated using the modified *J* (denoted usually as J_M) introduced by Ernst [*15*].

These tables contain fractional crack growth parameters, γ_o, based on initial remaining ligament, and γ_f, based on the uncracked ligament when the singularity limit was reached. Likewise, the tables contain crack-tip opening displacement (CTOD) parameters, M_o, based on the initial remaining ligament and M_f, based on the uncracked ligament when the singularity limit was reached. In both cases, the *J* used was the total *J* at the *J*-control limit. Also present in the tables are two CTOD parameters based on the plastic *J* component and again on both the initial and singularity limit values of the uncracked ligament.

Four ω quantities have likewise been evaluated for each specimen. To obtain these, a power law form of the *J*-resistance curve was assumed and fit to the measured *J*-resistance

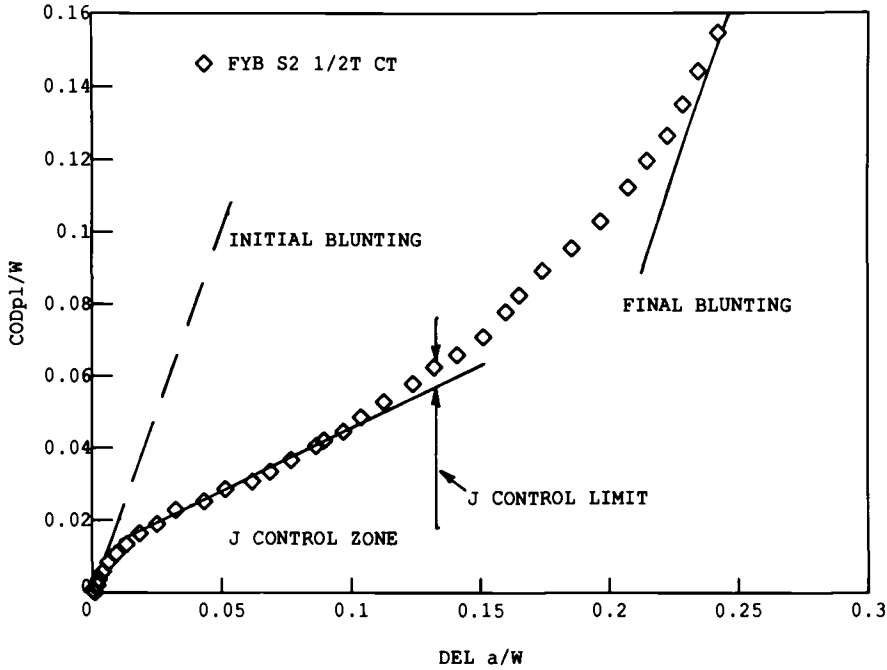

FIG. 3—*Definition of an engineering limit to J-controlled crack growth.*

curve using all data beyond initiation and before the predicted J-control limit. This equation was taken in the form

$$J = A\left[\frac{\Delta a}{W}\right]^N \tag{13}$$

This form fits the J-R curves of most materials very well as long as the R curve is rising, which is certainly the case if $\omega > 0$.

Differentiation then gives

$$\frac{dJ}{da} = \frac{NA}{W}\left[\Delta a/W\right]^{N-1} \tag{14}$$

and ω can be obtained from

$$\omega = \frac{b}{J}\frac{dJ}{da}N/[\Delta a/b] \tag{15}$$

Using Eq 15, four cases were again evaluated using the total J with b_o and b_f, and the J_{PL} component with b_o and b_f.

All four are presented in the results tables referenced earlier. The simple interdependency of $\Delta a/b$ and ω for materials whose J-R curves are of a power law form is consistent with the observations in Tables 1 through 6 that both of these quantities give consistent definitions of the region J-controlled crack growth.

TABLE 1—J-*controlled growth limit quantities—HY80 alloy steel (FYB).*

Specimen Identification	Type	Size	Δa_{LIM}, in.	$\Delta a_{LIM}/b_o$, γ_o (1)	$\Delta a_{LIM}/b_i$, γ_f (2)	J_{LIM}, kJ/m^2 (3)	$b_o\sigma_f/J_{LIM}$ M_o (4)	$b_i\sigma_f/J_{LIM}$, M_i (5)	$J_{PL\ LIM}$, kJ/m^2 (6)	$b_o\sigma_f/J_{PL\ LIM}$, M_{PLo} (7)	$b_i\sigma_f/J_{PL\ LIM}$, M_{PLf} (8)	ω_o (9)	ω_i (10)	ω_{PLo} (11)	ω_{PLi} (12)
FYBA1	CT	1T	0.314	0.397	0.658	452	28.2	17.0	395	32.4	19.5	1.412	0.852	1.247	0.752
FYBA2	CT	1T	0.265	0.338	0.510	370	34.1	22.6	308	41.1	27.2	1.677	1.111	1.522	1.008
FYBA8	CT	1T	0.368	0.411	0.698	436	33.0	19.4	374	38.6	22.7	1.488	0.876	1.150	0.677
FYBA9	CT	1T	0.236	0.405	0.680	465	20.1	12.0	421	22.3	13.3	1.505	0.896	1.448	0.862
FYBA10	CT	1T	0.246	0.308	0.445	388	33.1	22.9	326	39.5	27.4	1.480	1.024	1.421	0.984
FYBS1	CT	1/2T	0.159	0.403	0.674	299	21.6	12.9	263	24.2	14.4	1.056	0.631	0.957	0.572
FYBS2	CT	1/2T	0.132	0.337	0.507	298	21.2	14.1	264	24.0	15.9	1.638	1.087	1.535	1.018
FYBS4	CT	1/2T	0.171	0.431	0.758	316	20.2	11.5	283	22.6	12.8	1.171	0.666	1.090	0.620
FYBV5	3PB	1/2T	0.127	0.340	0.516	389	15.4	10.2	362	16.6	10.9	1.177	1.776	1.169	0.771
FYBV10	3PB	1/2T	0.138	0.341	0.518	396	16.4	10.8	365	17.8	11.7	1.394	0.918	1.379	0.908
FYBV12	3PB	1/2T	0.125	0.357	0.556	397	14.2	9.1	368	15.3	9.8	1.055	0.678	1.047	0.673
FYBV14	3PB	1/2T	0.141	0.464	0.867	416	11.7	6.3	397	12.3	6.6	1.151	0.617	1.114	0.596
FYB507	3PB	1/2T	0.294	0.374	0.598	501	25.3	15.8	457	27.8	17.4	1.389	0.869	1.264	0.791
Mean				0.377	0.614	399	22.65	14.2	352	25.73	16.12	1.353	0.846	1.257	0.787
σ				0.045	0.121	63.5	7.55	5.11	60.2	9.58	6.49	0.41	0.167	0.189	0.158
Combined Values, Tables 1, 2, and 3															
Mean				0.414	0.731	252	50.26	29.05	209	68.12	39.4	0.857	0.531	1.232	0.736
σ				0.066	0.222	140.4	31.48	18.1	127.3	52.2	30.4	0.447	0.298	0.369	0.268

TABLE 2—J-*controlled growth limit quantities—HY100 alloy steel (FYO).*

Specimen Identification	Type	Size	Δa_{LIM}, in.	$\Delta a_{LIM}/b_o$, γ_o (1)	$\Delta a_{LIM}/b_i$, γ_f (2)	J_{LIM}, kJ/m^2 (3)	$b_o\sigma_f/J_{LIM}$ M_o (4)	$b_i\sigma_f/J_{LIM}$, M_f (5)	$J_{PL\ LIM}$, kJ/m^2 (6)	$b_o\sigma_f/J_{PL\ LIM}$, M_{PLo} (7)	$b_i\sigma_f/J_{PL\ LIM}$, M_{PLf} (8)	ω_o (9)	ω_i (10)	ω_{PLo} (11)	ω_{PLi} (12)
FYOM1	CT	1/2T	0.186	0.487	0.950	230	33.1	16.9	199	38.3	19.6	0.516	0.264	0.929	0.477
FYOM2	CT	1/2T	0.237	0.623	1.651	168	45.3	17.1	145	52.4	19.7	0.167	0.063	0.482	0.182
FYOM3	CT	1/2T	0.128	0.435	0.771	185	31.8	18.0	161	36.6	20.7	0.912	0.515	1.291	0.729
FYOM4	CT	1/2T	0.125	0.429	0.751	228	25.5	14.6	197	29.5	16.8	1.434	0.819	1.992	1.138
FYOM10	CT	1/2T	0.136	0.404	0.678	154	43.4	25.9	125	53.7	32.0	0.757	0.451	1.222	0.728
FYOM11	CT	1/2T	0.198	0.491	0.963	190	42.4	21.6	157	51.2	26.1	0.352	0.179	0.734	0.374
FYON5	CT	1T	0.270	0.338	0.510	308	51.9	34.4	226	70.6	46.8	0.928	0.615	1.723	1.141
FYON10	CT	1T	0.282	0.354	0.549	356	44.6	28.8	271	58.6	37.8	1.183	0.764	2.099	1.356
FYON9	CT	1T	0.301	0.518	1.076	326	35.5	17.1	237	48.8	23.5	0.691	0.333	1.524	0.734
FYON1	CT	1T	0.173	0.405	0.682	385	22.1	13.1	342	24.9	14.8	1.360	0.809	1.786	1.062
FYOB1	CT	2T	0.749	0.468	0.880	258	123.7	65.8	154	207.5	110.3	0.163	0.087	0.976	0.519
FYOB2	CT	2T	0.579	0.419	0.722	252	109.1	63.3	151	183.1	106.3	0.515	0.299	1.470	0.854
FYOB3	CT	2T	0.600	0.503	1.011	238	100.2	49.8	163	146.8	73.0	0.200	0.099	0.950	0.472
FYOB4	CT	2T	0.418	0.408	0.689	269	77.4	45.8	189	108.2	64.1	0.457	0.271	1.239	0.733
FYOJ3	3PB	1T	0.290	0.380	0.612	370	41.1	25.5	296	51.5	31.9	0.922	0.572	1.578	0.979
FYOJ4	3PB	1T	0.307	0.395	0.654	403	38.4	23.2	332	46.7	28.3	1.033	0.625	1.701	1.028
FYOL4B	3PB	2T	0.491	0.355	0.551	423	65.2	42.0	301	91.6	59.1	0.900	0.580	1.966	1.268
FYOH6	3PB	1/2T	0.133	0.333	0.500	310	25.6	17.1	271	29.5	19.7	1.078	0.719	1.418	0.946
FYOH7	3PB	1/2T	0.131	0.328	0.489	360	22.2	14.9	319	25.0	16.8	1.433	0.962	1.819	1.222
Mean				0.425	0.773	285	51.5	29.2	223	71.28	40.38	0.790	0.475	1.416	0.839
σ				0.076	0.278	83.1	30.12	16.5	71.3	53.4	29.3	0.415	0.275	0.453	0.330

TABLE 3—J-*controlled growth limit quantities—CS-19 alloy aluminum (FGN).*

Specimen Identification	Type	Size	Δa_{LIM}, in.	$\Delta a_{LIM}/b_o$, γ_o (1)	$\Delta a_{LIM}/b_i$, γ_f (2)	J_{LIM}, kJ/m^2 (3)	$b_o\sigma_f/J_{LIM}$, M_o (4)	$b_i\sigma_f/J_{LIM}$, M_f (5)	$J_{PL\ LIM}$, kJ/m^2 (6)	$b_o\sigma_f/J_{PL\ LIM}$, M_{PLo} (7)	$b_i\sigma_f/J_{PL\ LIM}$, M_{PLf} (8)	ω_o (9)	ω_i (10)	ω_{PLo} (11)	ω_{PLi} (12)
FGN30	CT	1T	0.395	0.440	0.787	72	114.0	63.8	50	162.9	91.1	0.289	0.162	0.749	0.419
FGN31	CT	1T	0.235	0.460	0.852	71	65.8	35.5	53	87.6	47.3	0.588	0.317	1.147	0.619
FGN32	CT	1T	0.282	0.322	0.474	85	94.0	63.8	55	145.6	98.8	0.571	0.387	1.209	0.820
FGN33	CT	1T	0.270	0.311	0.452	75	106.0	73.0	45	176.5	121.5	0.555	0.382	1.253	0.863
FGN51	CT	1T	0.374	0.469	0.884	63	114.3	60.7	42	173.7	92.2	0.274	0.146	0.918	0.487
FGN52	CT	1T	0.281	0.461	0.856	78	71.3	38.4	58	95.4	51.4	0.484	0.261	1.017	0.548
FGN58	CT	1T	0.255	0.423	0.734	82	67.2	38.7	62	88.7	51.1	0.482	0.278	0.991	0.572
FGN70	CT	1/2T	0.132	0.414	0.708	81	35.8	20.9	70	41.6	24.4	0.588	0.344	0.867	0.507
FGN72	CT	1/2T	0.177	0.436	0.773	83	44.6	25.2	69	54.0	30.4	0.634	0.357	1.053	0.594
FGN74	CT	1/2T	0.218	0.540	1.174	78	47.1	21.7	66	56.1	25.8	0.490	0.225	0.853	0.392
FGN10	3PB	1T	0.319	0.424	0.736	76	89.7	51.7	55	125.2	72.1	0.449	0.259	0.900	0.519
FGN17	3PB	1T	0.355	0.444	0.799	80	91.4	50.8	60	120.8	67.1	0.437	0.243	0.896	0.498
FGN24	3PB	1/2T	0.190	0.477	0.911	74	48.9	25.6	63	57.9	30.3	0.526	0.275	0.847	0.443
FGN25	3PB	1/2T	0.167	0.444	0.797	70	48.9	27.2	59	58.6	32.6	0.465	0.259	0.732	0.407
Mean				0.433	0.781	76	74.2	42.6	58	103.2	59.7	0.488	0.314	0.959	0.549
σ				0.058	0.177	6.0	27.2	17.8	8.3	47.6	31.31	0.105	0.153	0.160	0.142

TABLE 4—J_M-*controlled growth limit quantities—HY80 alloy steel (FYB).*

Specimen Identification	Type	Size	Δa_{LIM}, in.	$\Delta a_{LIM}/b_o$, γ_o (1)	$\Delta a_{LIM}/b_i$, γ_f (2)	J_{LIM}, kJ/m^2 (3)	$b_o\sigma_f/J_{LIM}$, M_o (4)	$b_i\sigma_f/J_{LIM}$, M_f (5)	$J_{PL\ LIM}$, kJ/m^2 (6)	$b_o\sigma_f/J_{PL\ LIM}$, M_{PLo} (7)	$b_i\sigma_f/J_{PL\ LIM}$, M_{PLf} (8)	ω_o (9)	ω_i (10)	ω_{PLo} (11)	ω_{PLi} (12)
FYBA1	CT	1T	0.314	0.397	0.658	626	20.4	12.3	568	22.5	13.6	1.277	0.770	1.127	0.680
FYBA2	CT	1T	0.265	0.338	0.510	482	26.2	17.3	420	30.1	19.9	1.454	0.963	1.479	0.979
FYBA8	CT	1T	0.368	0.411	0.698	625	23.0	13.6	563	25.6	15.1	1.167	0.687	1.155	0.680
FYBA9	CT	1T	0.236	0.405	0.680	638	14.7	8.7	593	15.8	9.4	1.612	0.959	1.182	0.704
FYBA10	CT	1T	0.246	0.308	0.445	492	26.1	18.1	431	29.9	20.7	1.482	1.026	1.336	0.925
FYBS1	CT	1/2T	0.159	0.403	0.674	421	15.1	9.0	390	16.3	9.7	1.092	0.652	0.796	0.475
FYBS2	CT	1/2T	0.132	0.337	0.507	387	9.0	10.8	353	17.9	11.9	1.597	1.059	1.383	0.917
FYBS4	CT	1/2T	0.171	0.431	0.758	464	13.8	7.8	436	14.8	8.4	1.244	0.708	0.859	0.489
FYBV5	3PB	1/2T	0.127	0.340	0.516	502	11.9	7.9	476	12.6	8.3	1.417	0.935	0.956	0.636
FYBV10	3PB	1/2T	0.138	0.341	0.518	522	12.5	8.2	492	13.2	8.7	1.576	1.038	1.122	0.739
FYBV12	3PB	1/2T	0.125	0.357	0.556	527	10.7	6.9	495	11.4	7.3	1.340	0.861	0.847	0.544
FYBV14	3PB	1/2T	0.141	0.464	0.867	600	8.1	4.4	581	8.4	4.5	1.424	0.763	0.826	0.443
FYB507	3PB	1T	0.294	0.374	0.598	650	19.5	12.2	601	20.9	13.1	1.318	0.825	1.150	0.720
Mean					0.614	533	16.8	10.55	492	18.4	11.58	1.39	0.865	1.094	0.687
σ				0.045	0.121	86.8	5.81	4.03	83.9	6.94	4.81	0.166	0.141	0.224	0.174
Combined values, Tables 4, 5, and 6															
Mean				0.414	0.731	340	36.8	21.37	297	45.5	26.6	1.16	0.693	1.518	0.899
σ				0.066	0.222	183	23.1	13.7	170.8	33.2	19.9	0.35	0.254	0.452	0.315

TABLE 5—J_M-*controlled growth limit quantities—HY100 alloy steel (FYO).*

Specimen Identification	Type	Size	Δa_{LIM}, in.	$\Delta a_{LIM}/b_o$, γ_o (1)	$\Delta a_{LIM}/b_i$, γ_f (2)	J_{LIM}, kJ/m^2 (3)	$b_o\sigma_f/J_{LIM}$, M_o (4)	$b_i\sigma_f/J_{LIM}$, M_f (5)	$J_{PL\ LIM}$, kJ/m^2 (6)	$b_o\sigma_f/J_{PL\ LIM}$, M_{PLo} (7)	$b_i\sigma_f/J_{PL\ LIM}$, M_{PLf} (8)	ω_o (9)	ω_i (10)	ω_{PLo} (11)	ω_{PLi} (12)
FYOM1	CT	1/2T	0.186	0.487	0.950	343	22.2	11.4	312	24.4	12.5	0.932	0.478	1.369	0.702
FYOM2	CT	1/2T	0.237	0.623	1.651	302	25.2	9.5	279	27.3	10.3	0.581	0.219	0.938	0.354
FYOM3	CT	1/2T	0.128	0.435	0.771	260	22.6	12.0	236	25.0	14.1	1.436	0.811	1.822	1.029
FYOM4	CT	1/2T	0.125	0.429	0.751	307	18.9	10.8	276	21.0	12.0	1.962	1.121	2.501	1.428
FYOM10	CT	1/2T	0.136	0.404	0.678	208	32.2	19.2	179	37.5	22.4	1.275	0.760	1.781	1.062
FYOM11	CT	1/2T	0.198	0.491	0.963	292	27.7	14.1	258	31.3	15.9	0.887	0.452	1.316	0.670
FYON5	CT	1T	0.270	0.338	0.510	387	41.2	27.3	306	52.2	34.6	1.425	0.944	2.309	1.529
FYON10	CT	1T	0.282	0.354	0.549	449	35.3	22.3	365	43.6	28.1	1.611	1.040	2.567	1.657
FYON9	CT	1T	0.301	0.528	1.076	413	28.0	13.5	325	35.7	17.2	0.969	0.467	1.827	0.880
FYON1	CT	1T	0.173	0.405	0.682	513	16.6	9.9	470	18.1	10.8	1.826	1.086	2.255	1.341
FYOB1	CT	2T	0.749	0.468	0.880	366	87.1	46.3	263	121.7	64.7	0.591	0.314	1.598	0.850
FYOB2	CT	2T	0.579	0.419	0.722	325	84.6	49.1	224	123.2	71.6	0.882	0.512	1.919	1.114
FYOB3	CT	2T	0.600	0.503	1.011	336	70.8	35.2	261	91.3	45.4	0.661	0.328	1.488	0.740
FYOB4	CT	2T	0.418	0.408	0.689	349	59.4	35.2	269	76.1	45.0	0.784	0.464	1.629	0.964
FYOJ3	3PB	1T	0.290	0.380	0.612	469	32.4	20.1	396	38.5	23.9	1.203	0.747	1.888	1.171
FYOJ4	3PB	1T	0.307	0.395	0.654	517	30.0	18.1	446	34.8	21.0	1.286	0.778	1.970	1.191
FYOL4B	3PB	2T	0.491	0.355	0.551	510	54.0	34.8	388	71.1	45.8	1.194	0.770	2.316	1.493
FYOH6	3PB	1/2T	0.133	0.333	0.500	396	20.1	13.4	356	22.4	14.9	1.535	1.024	1.900	1.267
FYOH7	3PB	1/2T	0.131	0.328	0.489	453	17.6	11.8	412	19.4	13.0	1.791	1.203	2.188	1.470
Mean				0.425	0.773	378	38.19	21.76	317	48.14	27.54	1.202	0.711	1.873	1.100
σ				0.076	0.278	89.4	22.3	12.5	79.5	33.11	18.64	0.426	0.304	0.425	0.346

TABLE 6—J_M-*controlled growth limit quantities—CS-19 alloy aluminum (FGN).*

Specimen Identification	Type	Size	Δa_{LIM}, in.	$\Delta a_{LIM}/b_o$, γ_o (1)	$\Delta a_{LIM}/b_i$, γ_f (2)	J_{LIM}, kJ/m^2 (3)	$b_o\sigma_f/J_{LIM}$, M_o (4)	$b_i\sigma_f/J_{LIM}$, M_f (5)	$J_{PL\ LIM}$, kJ/m^2 (6)	$b_o\sigma_f/J_{PL\ LIM}$, M_{PLo} (7)	$b_i\sigma_f/J_{PL\ LIM}$, M_{PLf} (8)	ω_o (9)	ω_i (10)	ω_{PLo} (11)	ω_{PLi} (12)
FGN30	CT	1T	0.395	0.440	0.787	112	73.0	40.9	90	90.4	50.6	0.711	0.398	1.274	0.713
FGN31	CT	1T	0.235	0.460	0.852	97	47.7	25.8	80	58.3	31.5	1.006	0.543	1.633	0.881
FGN32	CT	1T	0.282	0.322	0.474	106	75.2	51.0	76	104.9	71.2	0.966	0.655	1.728	1.172
FGN33	CT	1T	0.270	0.311	0.452	93	85.1	58.6	63	125.3	86.3	0.982	0.676	1.844	1.270
FGN51	CT	1T	0.374	0.469	0.884	92	78.5	41.7	71	102.6	54.5	0.710	0.377	1.462	0.776
FGN52	CT	1T	0.281	0.461	0.856	110	50.5	27.2	90	61.4	33.1	0.889	0.479	1.474	0.794
FGN58	CT	1T	0.255	0.423	0.734	110	49.7	28.7	91	60.5	34.9	0.910	0.525	1.484	0.856
FGN70	CT	1/2T	0.132	0.415	0.708	118	24.6	14.4	107	27.3	16.0	1.089	0.638	1.407	0.824
FGN72	CT	1/2T	0.177	0.436	0.773	120	30.9	17.4	105	35.1	19.8	1.041	0.587	1.501	0.847
FGN74	CT	1/2T	0.218	0.540	1.174	128	28.6	13.1	116	31.6	14.5	0.873	0.402	1.250	0.575
FGN10	3PB	1T	0.319	0.424	0.736	100	68.8	39.6	78	87.9	50.6	0.762	0.439	1.281	0.738
FGN17	3PB	1T	0.355	0.444	0.799	109	66.5	37.0	90	80.8	44.9	0.803	0.446	1.322	0.735
FGN24	3PB	1/2T	0.190	0.477	0.911	109	33.1	17.3	98	37.0	19.3	0.884	0.463	1.227	0.642
FGN25	3PB	1/2T	0.167	0.444	0.797	98	34.9	19.4	87	39.6	22.0	0.841	0.468	1.148	0.639
Mean				0.433	0.781	107	53.36	30.86	88.8	67.34	39.23	0.8905	0.507	1.431	0.819
σ				0.058	0.177	10.5	20.87	14.23	14.6	31.53	21.66	0.1182	0.099	0.201	0.193

TABLE 7—*Tensile properties of materials.*

Material Code	Yield Strength, MPa	Ultimate Strength, MPa	Elongation, %
FYB	614	731	23
FGN	251	408	24
FYO	753	836	22

Discussion of the Tabulated Results

The desired quantity is one that defines the limit to *J*-controlled crack growth and is independent of specimen type, specimen size, initial crack length, and material. The results shown in Tables 1 to 6 encompass, at least in a limited way, all of these variations. Given the small number of data and wide range of variations present, it is not possible to make statements strongly supported by statistical theory, but the following observations seem to be supported by trends in the data.

There appears to be little effect of specimen type, that is, CT or 3PB, on any of the parameters presented in the tables. Likewise, little effect of initial crack length is present in this data set. There also seems to be no difference between quantities evaluated in terms of deformation, J or J_M. In all of the following work, comparisons will be made in terms of deformation, J, but identical conclusions would follow if J_M was used. The M parameters do appear to be dependent on specimen scale, being larger for specimens of larger scale. This is shown graphically in terms of M_o in Fig. 4. The γ and ω factors appear to be much less dependent on specimen scale, a plot of ω_o versus specimen size is shown in Fig. 5.

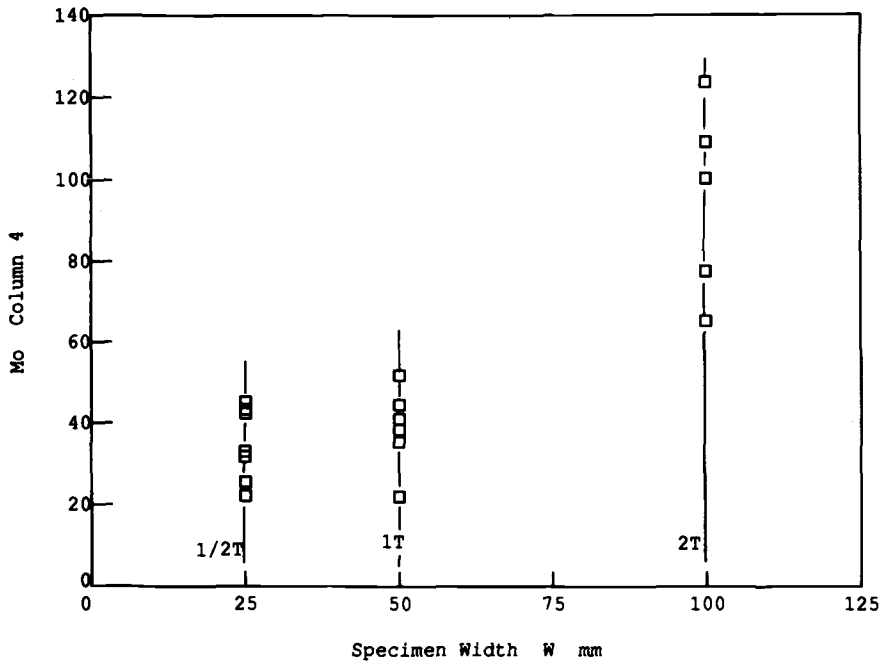

FIG. 4—*Demonstration of the dependence of an* M_o *parameter on specimen scale.*

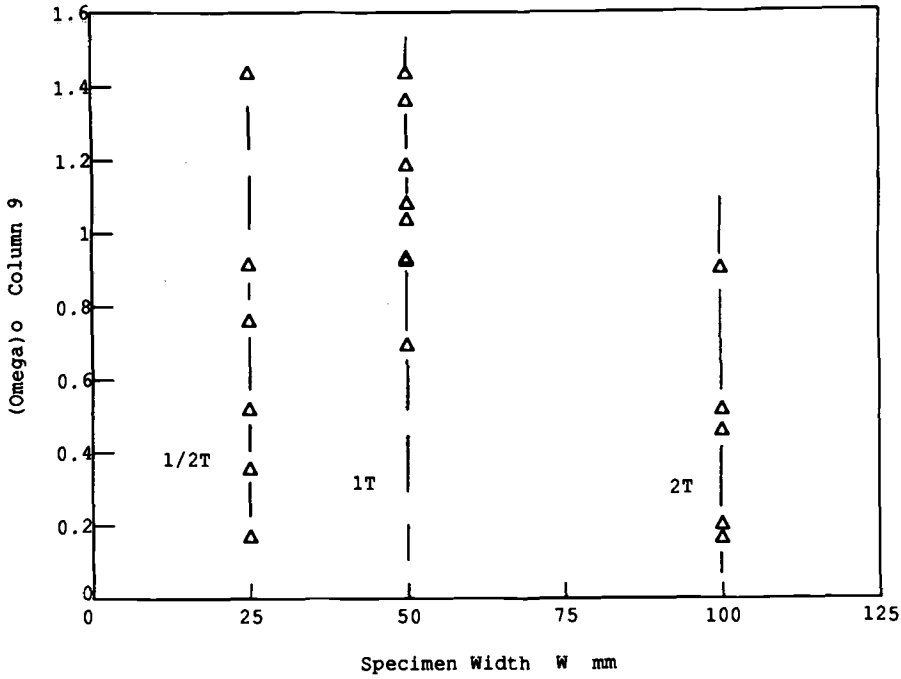

FIG. 5—*Demonstration of the independence of an ω_o parameter on specimen scale.*

A strong material effect is also demonstrated by the M parameters. This can be observed by comparing the average values of each parameter calculated for a given material with the averages calculated for all the materials combined. This comparison is done in a systematic fashion in Table 8. The number in the first column corresponds to the column number in Tables 4, 5, and 6. The third column is the mean value of each column taken over all three materials. The next three columns are means taken for each material separately. The seventh column gives a measure of the difference of the individual mean values and the mean value of the full set of data in each column.

If this value is low, it is felt that the mean value of that column is consistent across material type and hence that this parameter is a relatively material independent measure of the limit of J-controlled crack growth. The last column in Table 8 ranks the columns on this basis, with a low number implying the preferred behavior. The rank column clearly shows that material dependence is smallest for the γ_o, γ_f, and ω_{PLo} quantities, that is, Columns 1, 2, and 11.

Histograms are presented in Fig. 6 showing γ_o (a good case) and M_o (a bad case). Separate histograms for each material are present along with a histogram combining the three materials. For the γ_o case the independence of the parameters distribution over the three materials is clearly observable, while the M_o parameter histograms show a much more nearly uniform distribution with each material defining a separate distribution. Similar histograms for γ_f and M_f are presented in Fig. 7, again comparing good and bad cases, and finally the two plastic ω quantities are shown in histograms in Fig. 8.

These results show that the best parameters to define the extent of J-controlled growth appear to be γ_o, γ_f, and ω_{PLo}, at least based on the data presented here. The initial γ_o values, based on the experimental limit to J control presented in the previous section, falls between

TABLE 8—*Comparison of parameter mean values for each material and the overall mean for each parameter using a root mean square percent difference.*

Column	Parameter	Super Mean	% Difference $\left(\frac{M - SM}{SM}\right) \times 100$ FYB	FGN	FYO	$\sqrt{\Sigma(\%\text{Difference})^2}$	Rank
1	γ_o	0.414	−8.9	4.6	2.7	10.4	1
2	γ_F	0.731	−16.0	6.8	5.4	18.2	2
3	J_{LIM}	252	56	−70	12.9	90.6	11
4	M_o	50.26	−55	+47.6	−2.4	72.8	7
5	M_F	29.05	−51.1	46.6	0.52	69.2	5
6	J_{PLUM}	209	68	−72.5	6.6	99.6	12
7	M_{PLO}	68.12	−62	51.5	4.7	80.7	10
8	M_{PLF}	39.4	−59.1	51.5	2.5	78.4	9
9	ω_o	0.857	57.9	−43	−7.8	72.5	6
10	ω_i	0.531	59.3	−40.9	−10.5	72.9	8
11	ω_{PLO}	1.232	2.1	−22	14.9	26.6	3
12	ω_{PLi}	0.736	−6.9	−45.1	14.0	47.6	4

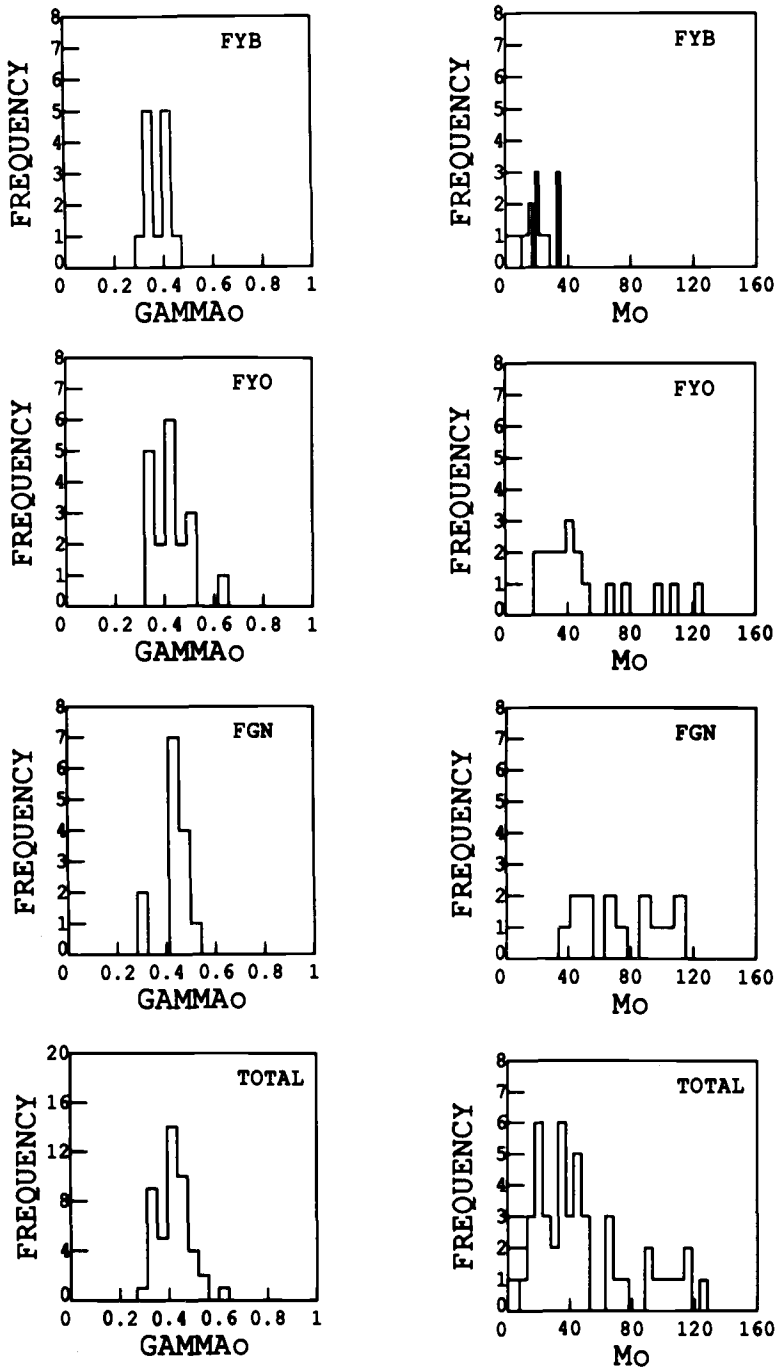

FIG. 6—*Histograms showing a comparison of the* γ_o *and* M_o *parameter distributions for each material and for the full data set.*

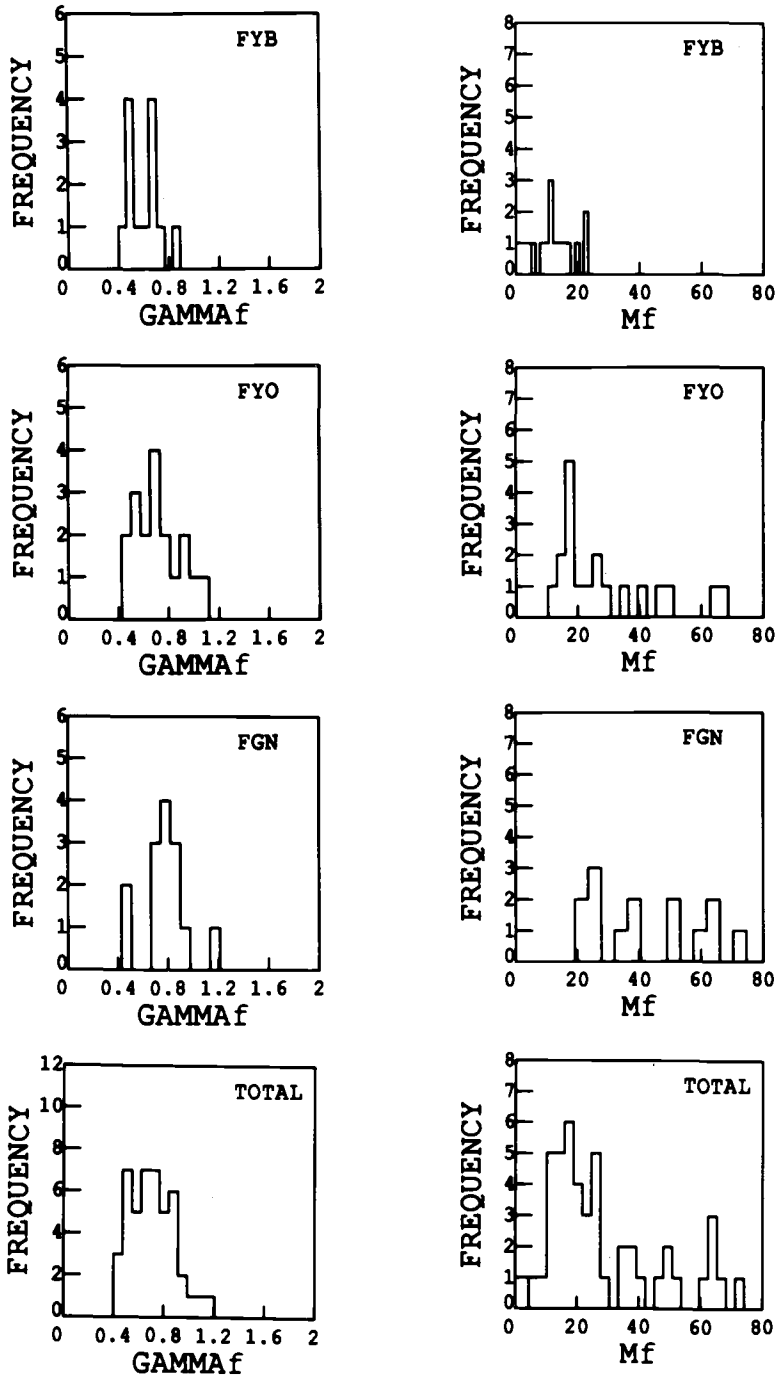

FIG. 7—*Histograms showing a comparison of the* γ_f *and* M_f *parameter distributions for each material and for the full data set.*

0.3 and 0.5, which is much larger than the value of 0.1 presently allowed in ASTM E 1152-87. The major shortcoming of Parameters γ_o and γ_f, is that they would be difficult to define in applications where relatively short cracks were present in thick walls, or where irregular crack shapes were present. The M or ω parameters are much more applicable to structural integrity and tearing instability analyses, but as shown earlier, the M parameters and the ω parameters based on total J appear to be material or specimen size dependent, or both.

The remaining parameter appears to be ω_{PLo}, which ranked third in material insensitivity, and is shown in the histograms of Fig. 8. This quantity is used in the next section to establish an ω criterion to define the expected region of J control with respect to both the applied J and the amount of crack extension.

Development of an ω Criterion

The size limits set on J and J-R curves by ASTM standards are often used by engineers to set limits for the use of J for engineering applications. As just described, recent experimental work has shown that the limits presently in these ASTM standards seem to have little experimental justification. Extension of this work has led to the definition of an experimental J-control limit that has the positive feature that a meaningful and clearly definable limit can be observed by direct experimental methodology. The object here is to reestablish an analytical relationship for the limit to J control that is based on these new results and can be applied to engineering applications.

The observation made in the previous section, that an ω quantity based on the plastic J component seems to be the parameter most directly related to the limit of J-controlled crack growth, gives a way to define an analytic definition of the regime of J-controlled growth.

As presented earlier, the definition of ω based on the plastic J component is

$$\omega_{PL} = \frac{b}{J_{PL}} \frac{dJ_{PL}}{da} \tag{16}$$

Starting with a key-curve load displacement relationship of the form

$$\frac{PW}{Bb^2} = F_1 = k[\Delta_{PL}/W]^n \tag{17}$$

where

P = load,
W = specimen width,
Δ_{PL} = plastic component of the load line displacement,
B = specimen thickness,
b = the uncracked ligament, and
k and n = material parameters.

Using the basic definition of J that

$$J_{PL} = -\int_0^{\Delta_{PL}} \frac{\partial P}{\partial a} d\,\Delta_{PL} \tag{18}$$

gives

$$J_{PL} = \frac{2b_o k}{n+1} \left[\frac{\Delta_{PL}}{W}\right]^{n+1} \tag{19}$$

with b_o = the initial uncracked ligament.

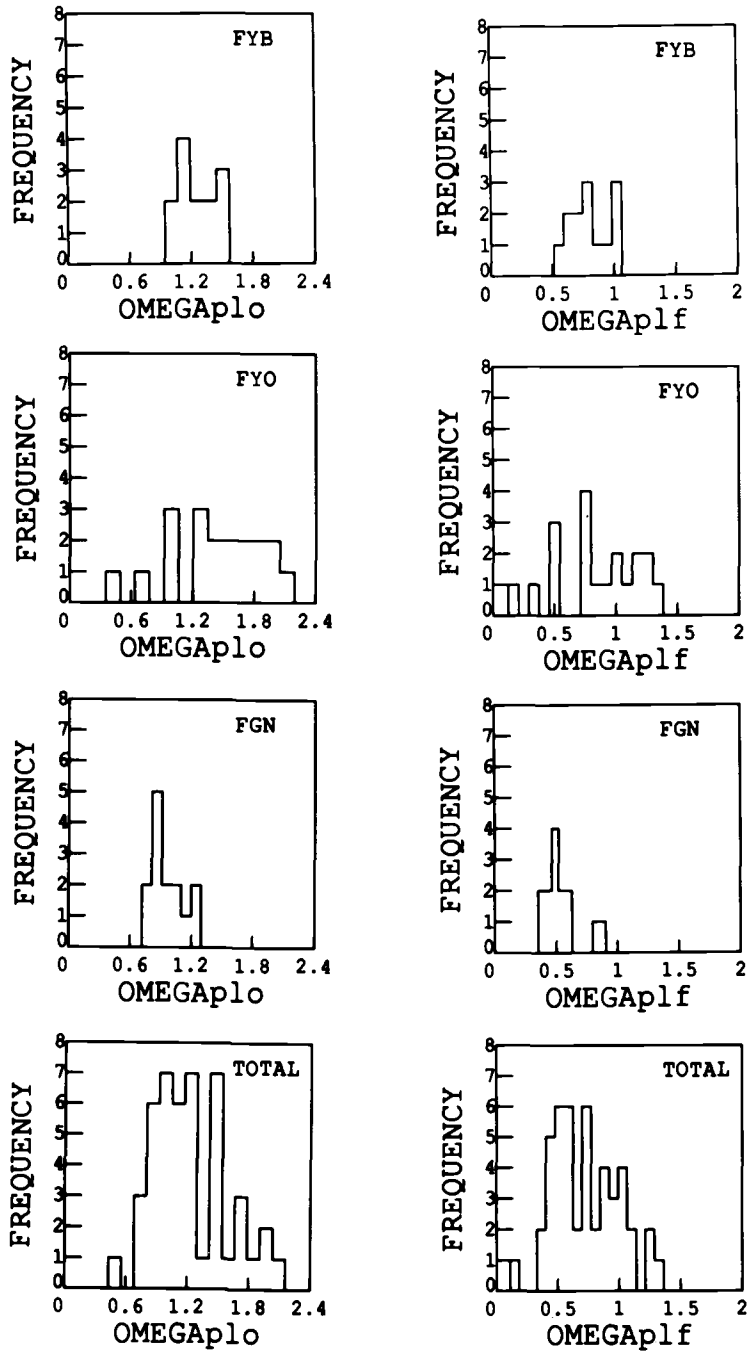

FIG. 8—*Histograms showing distribution of the* ω_{PLo} *and* ω_{PLf} *parameters for each material and for the full data set.*

Using a linear form to relate Δ_{PL} and Δa in the J-control zone of Fig. 3, that is

$$\frac{\Delta_{PL}}{W} = k_4 \frac{\Delta a}{W} + k_3 \tag{20}$$

gives an equation for J_{PL} that

$$J_{PL} = \frac{2\,kW}{n+1}\left[\frac{b_o}{W} - \frac{\Delta a}{W}\right]\left[k_4 \frac{\Delta a}{W} + k_3\right]^{n+1} \tag{21}$$

Finally, ω_{PL} can be calculated from Eqs 16 and 21 as

$$\omega_{PL} = \frac{\dfrac{k_4 b}{W}\left[k_4 \dfrac{\Delta a}{W} + k_3\right]^{n} - \dfrac{1}{n+1}\left[k_4 \dfrac{\Delta a}{W} + k_3\right]^{n+1}}{\dfrac{J_{PL}}{2bk}} \tag{22}$$

Fits of the key-curve form of Eq 18 to data for structural steels has shown that

$$2k \approx \sigma_f = \frac{\sigma_y + \sigma_{uts}}{2} \tag{23}$$

and also using

$$\frac{b}{W} = \frac{b_o}{W} - \frac{\Delta a}{W}$$

gives

$$\omega_{PL} = \frac{k_4\left[\dfrac{b_o}{W} - \dfrac{\Delta a}{W}\right]^2\left[k_4 \dfrac{\Delta a}{W} + k_3\right]^{n} - \dfrac{1}{n+1}\left[k_4 \dfrac{\Delta a}{W} + k_3\right]^{n+1}}{\dfrac{J_{PL}}{W\sigma_f}} \tag{24}$$

Determination of ω_{PL} using the J-control limit analysis presented earlier allows evaluation of Eq 24 and the development of a combined J_{PL}, $\Delta a/W$ criterion for the applicability of the J-integral method as shown in Fig. 9 for an FYB alloy specimen. The fitting coefficients used for this case and several others are presented in Table 9. A normalized J_{PL} resistance curve is also shown in Fig. 9 and the singularity limit point is marked by the change from hollow to solid data symbols.

Similar ω criteria boundaries can be developed in other ways. For example, starting with a power law model of a J_{PL} resistance curve of the form

$$J_{PL} = A\left[\frac{\Delta a}{W}\right]^m \tag{25}$$

gives

$$\frac{dJ_{PL}}{da} = \frac{mA}{W}\left[\frac{\Delta a}{W}\right]^{m-1} \tag{26}$$

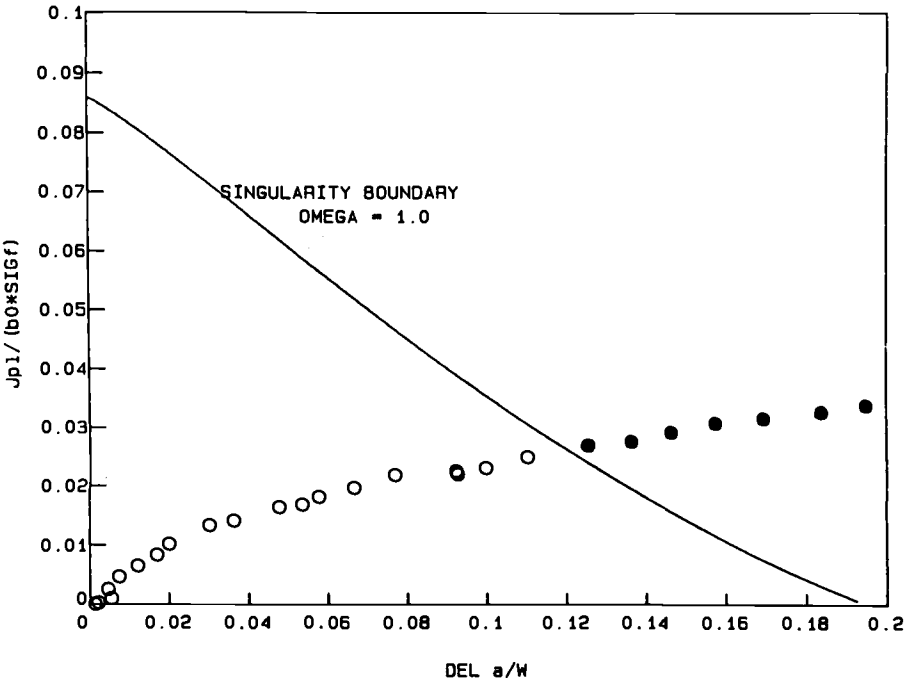

FIG. 9—*Region of J-controlled growth defined by an* ω_{PLo} *criteria.*

and

$$\omega_{\mathrm{PL}} = \frac{mA}{J_{PL}} \frac{[b_{\mathrm{o}} - \Delta a]}{W} \left[\frac{\Delta a}{W}\right]^{m-1} \tag{27}$$

or, if ω_{PL} is taken as 1.0

$$\frac{J_{\mathrm{PL}}}{b_{\mathrm{o}}\sigma_f} = \frac{mA}{b_{\mathrm{o}}\sigma_f} \left[\frac{b_{\mathrm{o}}}{W} - \frac{\Delta a}{W}\right] \left[\frac{\Delta a}{W}\right]^{m-1} \tag{28}$$

Alternatively, starting with an exponential model of a J_{PL} resistance curve of the form

$$J_{\mathrm{PL}} = J_F - C_1 \exp\left[\frac{C_2 \Delta a}{W}\right] \tag{29}$$

TABLE 9—*FYB alloy fit coefficients—analysis model.*

Specimen Identification	W, mm	a_{o}, mm	n	k, MPa	k_3	k_4	σ_f, MPa
FYB A1	50.8	30.7	0.064	383	0.005	0.263	630
FYB A2	50.8	30.9	0.061	377	0.002	0.255	630
FYB S1	25.4	15.4	0.056	362	0.010	0.328	630
FYB S2	25.4	15.4	0.059	364	0.003	0.423	630

gives

$$\frac{dJ_{PL}}{da} = \frac{-C_1C_2}{W} \exp\left[\frac{C_2\Delta a}{W}\right] \tag{30}$$

and

$$\omega_{PL} = \frac{-C_1C_2}{J_{PL}}\left[\frac{b_o}{W} - \frac{\Delta a}{W}\right] \exp\left[\frac{C_2\Delta a}{W}\right] \tag{31}$$

Taking $\omega_{PL} = 1$ gives

$$\frac{J_{PL}}{b_o\sigma_f} = \frac{-C_1C_2}{b_o\sigma_f}\left[\frac{b_o}{W} - \frac{\Delta a}{W}\right] \exp\left[C_2\frac{\Delta a}{W}\right] \tag{32}$$

Equations 28 and 32 are compared with the previous form, Eq 24, in Fig. 10 and, except for the extreme limits of $\Delta a/W$, the comparison is good. Coefficients used to evaluate Eqs 28 and 32 were fitted to the FYB data using applicable techniques and are shown in Table 10.

For completeness, the full set of FYB J-control limits based on J deformation, is plotted in Fig. 11 and compared with the analysis model limit of Eq 24 with $\omega_{PL} = 1.0$. Clearly, smaller ω_{PL} values could be used, shifting the J-control boundary outward, except for one specimen. The exact value of ω_{PL} to use for a general form of Eq 24, which would be

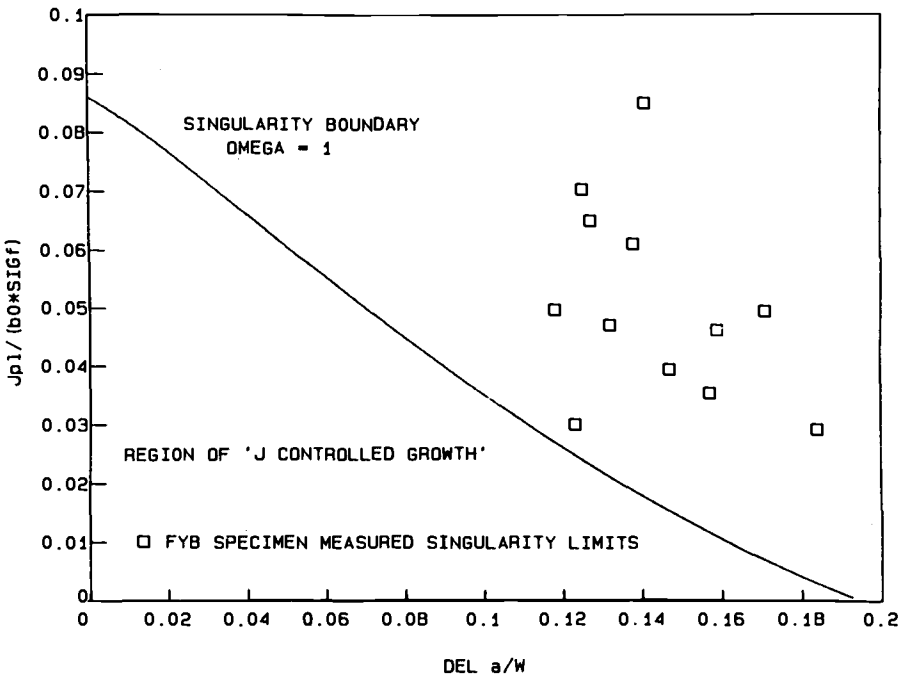

FIG. 10—*Region of J-controlled growth compared with measured data for the FYB code material.*

TABLE 10—*FYB alloy fit coefficients.*

Specimen Identification	Power Law Model		Exponential Model		
	A, kJ/m^2	m	J_E, kJ/m^2	C_1, kJ/m^2	C_2
FYB A1	883	0.509	408	347	−10.8
FYB A2	922	0.579	628	547	−3.70
FYB S1	532	0.436	236	178	−17.78
FYB S2	746	0.574	393	340	−6.45

applicable to a wide range of materials, is presently the object of study, but seems to be very close to 1.0.

Conclusions

This work proposes that the ω criterion of Hutchinson and Paris provides a useful limit to the applicability of the J-integral. A further result is that the ω criterion provides a combined limit on crack extension and the J value reached during the fracture process. Tabulated results on a considerable set of data show that valid J-controlled crack growth can exist with ω as low as 1, far smaller than the 5 to 10 suggested in the original work by Hutchinson and Paris.

Other criteria proposed on $J/(b_o\sigma_f)$ and $\Delta a/b_o$ were also investigated. Setting a multiple on $J/(b_o\sigma_f)$ does not seem to have any support in the data set analyzed, with critical values varying according to specimen size and material type. The use of the plastic J component

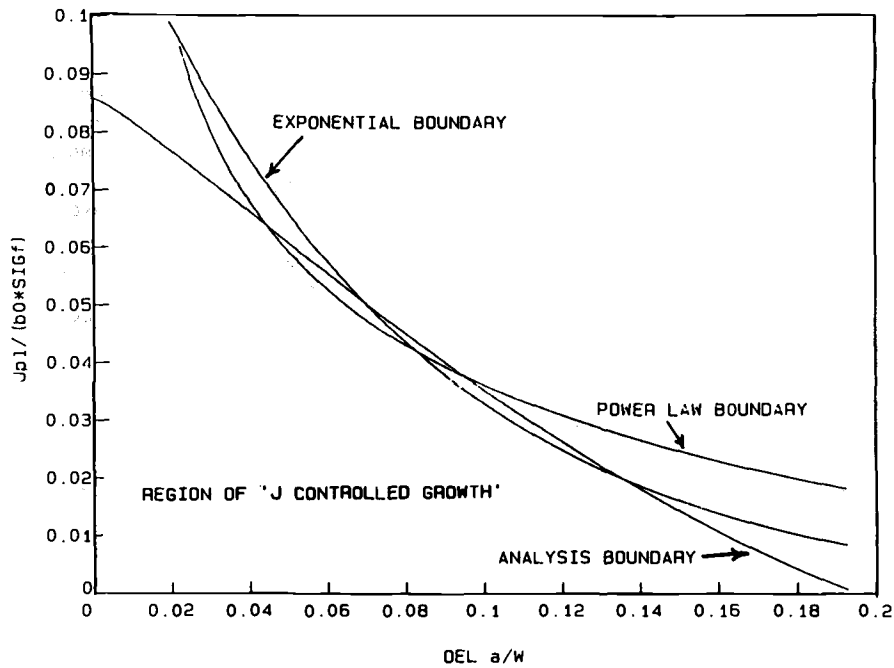

FIG. 11—*Comparison of alternative methods used to define a region of J-controlled crack growth.*

did not change this conclusion, nor did the use of the Ernst modified J or even the plastic component of modified J.

A criterion on $\Delta a/b_o$ finds good support in the data set with critical values being between 0.3 and 0.5. The ω criterion was preferred here, however, since it is felt that limits on a J-integral value are essential and should not be eliminated. While the criterion shows more variability than one based on $\Delta a/b_o$, it is felt that the variability of ω results from the need to fit and evaluate dJ/da, and it is not necessarily a sign that the ω criterion is not applicable. Indeed the simple models presented show how an ω criterion represents a limit on both $\Delta a/b_o$ and on the plastic J level generating a zone of J-controlled growth. The ω parameter based on the plastic component of J is distinctly better than an ω parameter based on the total J, and a limiting value of 1.0 appears applicable. However, this value should be checked with data from additional materials and specimen geometries before incorporation in test standards.

References

[1] Joyce, J. A. and Gudas, J. P., "Computer Interactive J_{Ic} Testing on Navy Alloys," *Elastic-Plastic Fracture, ASTM STP 668*, J. D. Landes, J. A. Begley, and G. A. Clarke, Eds., American Society for Testing and Materials, Philadelphia, 1979, pp. 451–468.

[2] Johnson, R., "Resolution of the Reactor Vessel Materials Toughess Safety Issue," NUREG-0744, U.S. Nuclear Regulatory Commission, Washington, DC, Sept. 1981.

[3] Joyce, J. A. and Hackett, E. M., "Development of an Engineering Definition of the Extent of J Singularity Controlled Crack Growth," NUREG/CR-5238, U.S. Nuclear Regulatory Commission, Washington, DC, March 1989.

[4] Hutchinson, J. W., *Journal of the Mechanics and Physics of Solids*, Vol. 16, 1968, pp. 13–31.

[5] Rice, J. R. and Rosengren, G. F., *Journal of the Mechanics and Physics of Solids*, Vol. 16, 1968, pp. 1–12.

[6] Hutchinson, J. W. and Paris, P. C., "Stability Analysis of J Controlled Growth," *Elastic Plastic Fracture, ASTM STP 668*, American Society for Testing and Materials, Philadelphia, 1979, pp. 37–64.

[7] Paris, P. C., discussion to J. A Begley and J. D. Landes in *Fracture Mechanics, ASTM STP 514*, American Society for Testing and Materials, Philadelphia, 1972, pp. 21–22.

[8] Landes, J. D. and Begley, J. A. in *Fracture Toughness, ASTM STP 514*, American Society for Testing and Materials, Philadelphia, 1972, pp. 1–20.

[9] McMeeking, R. M. and Parks, D. M., "On Criteria for J-Dominance of Crack-Tip Fields in Large-Scale Yielding," *Elastic-Plastic Fracture, ASTM STP 668*, J. D. Landes, J. A. Begley, and G. A. Clarke, Eds., American Society for Testing and Materials, Philadelphia, 1979, pp. 175–194.

[10] Davis, D. A., Vassilaros, M. G., and Gudas, J. P., "Specimen Geometry and Extended Crack Growth Effects on J-R Curve Characteristics for HY-130 and ASTM A533 Steels," *Elastic-Plastic Fracture: Second Symposium, Volume II: Fracture Curves and Engineering Applications, ASTM STP 803*, C. F. Shih and J. P. Gudas, Eds., American Society for Testing and Materials, Philadelphia, 1983, pp. II–582–II–610.

[11] McCabe, D. E., Landes, J. D., and Ernst, H. T., "An Evaluation of the J_R-Curve Method for Fracture Toughness Characterization," *Elastic-Plastic Fracture: Second Symposium, Volume II: Fracture Curves and Engineering Applications, ASTM STP 803*, C. F. Shih and J. P. Gudas, Eds., American Society for Testing and Materials, Philadelphia, 1983, pp. II–562–II–581.

[12] Shih, C. F. and German, M. D., *International Journal of Fracture*, Vol. 17, No. 1, 1981.

[13] Newman, J. C., Booth, B. C., and Shivakurman, K. N., "An Elastic-Plastic Finite-Element Analysis of the J-Resistance Curve Using a CTOD Criterion," *Fracture Mechanics: Eighteenth Symposium, ASTM STP 945*, D. T. Read and R. P. Reed, Eds., American Society for Testing and Materials, Philadelphia, 1988, pp. 665–685.

[14] Joyce, J. A., Davis, D. A., Hackett, E. M., and Hays, R. A., "Application of the J Integral and Modified J Integral to Cases of Large Crack Extension" presented at the 21st National Symposium on Fracture, American Society for Testing and Materials, Annapolis, MD, 28–30 June 1988.

[15] Ernst, H. A., "Material Resistance and Instability Beyond J-Controlled Crack Growth," *Elastic-Plastic Fracture: Second Symposium, Volume I: Inelastic Crack Analysis, ASTM STP 803*, C. F. Shih and J. P. Gudas, Eds., American Society for Testing and Materials, Philadelphia, 1983, pp. I–191–I–213.

J. Robin Gordon[1] *and Richard L. Jones*[2]

Specimen Size Requirements for Elastic-Plastic Crack Growth Resistance Curves

REFERENCE: Gordon, J. R. and Jones, R. L., **"Specimen Size Requirements for Elastic-Plastic Crack Growth Resistance Curves,"** *Elastic-Plastic Fracture Test Methods: The User's Experience (Second Volume), ASTM STP 1114*, J. A. Joyce, Ed., American Society for Testing and Materials, Philadelphia, 1991, pp. 81–101.

ABSTRACT: This paper presents the results of an experimental program to study size and geometry effects in CTOD *R*-curves. The results were obtained from room temperature unloading compliance *R*-curve tests on different sized single-edge-notch bend (SENB) specimens made from HY100 steel. The crack growth resistance was measured in terms of conventional CTOD, δ_o, (that is, as defined in BS 5762), CTOD corrected for crack growth, δ_R, and CTOD derived using a double clip gage arrangement δ_{dc}. It was found that all the CTOD *R*-curves exhibited upswings after crack extensions corresponding to approximately 17% of the initial uncracked ligament. Moreover, the slope of the CTOD *R*-curve increased dramatically after crack extensions corresponding to approximately 45% of the initial ligament. Apart from the *R*-curves obtained from the smaller specimens, normalizing the crack growth axis by dividing the crack extension by the initial ligament resulted in normalized CTOD *R*-curves which were in reasonable agreement over the entire crack growth range studied (that is, 60% of the initial uncracked ligament).

KEY WORDS: fracture mechanics, fracture toughness, ductile fracture, CTOD, *R*-curves, *J*-controlled crack growth, HY 100 steel, normalized *R*-curves

Nomenclature

a = Crack length
a_o = Initial crack length
Δa = Crack extension
B = Specimen thickness
B_n = Net thickness
W = Specimen width
b = Uncracked ligament
b_o = Initial uncracked ligament
E = Young's modulus
K = Stress intensity factory
V = Crack mouth opening displacement
V_e = Elastic component of V

[1]Manager, Engineering Department, Edison Welding Institute, 1100 Kinnear Road, Columbus, OH 43212.
[2]Head, Marine Structural and Engineering Metallurgy Section, U.K. Admiralty Research Establishment, Holton Heath, Poole, United Kingdom.

V_p = Plastic component of V
z = Knife edge height
J = Fracture resistance J
δ_o = Conventional crack tip opening displacement (CTOD)
δ_R = CTOD corrected for crack growth
δ_{dc} = CTOD calculated using double clip gage arrangement
ν = Poisson's ratio
ρ, α, and ω = Parameters for specifying the limits of J or CTOD controlled crack growth
σ_{ys} = Yield strength
σ_{flow} = Flow strength

Subscripts

k, $k-1$ = unloading number
o = initial
u = upper
l = lower
e, el = elastic
p, pl = plastic

When a material exhibits fully ductile behavior its resistance to crack extension is usually presented in the form of an elastic-plastic crack growth resistance curve (R-curve). In essence the R-curve is a plot of the variation in crack growth resistance, generally expressed in terms of CTOD or J, during the process of stable crack extension.

Over the last few years recommended test procedures have been published [*1–5*] which cover the measurement of J and CTOD R-curves using the multiple specimen method or the single specimen unloading compliance technique. Provided certain restrictions are satisfied the resulting R-curves can be regarded as material properties. The purpose of the limitations is to ensure that J and CTOD remain valid characterizing parameters during the process of stable crack extension. If these conditions are satisfied the crack growth process if frequently referred to as being either J or CTOD controlled, whichever is applicable.

It is generally accepted that the following conditions must be satisfied to ensure J-controlled crack growth [*6–8*]

$$B, b > \frac{\rho J}{\sigma_{flow}} \qquad \rho > 20\text{–}25 \text{ for bend specimens} \tag{1}$$

$$\Delta a \leq \alpha(W - a_o) \qquad \alpha = 0.06\text{–}0.1 \text{ for bend specimens} \tag{2}$$

$$\omega = \frac{b}{J}\frac{dJ}{da} \qquad \omega > 2.5\text{–}10.0 \text{ for bend specimens} \tag{3}$$

where

b, b_o = current and initial uncracked ligaments,
a, a_o = current and initial crack length,
a = crack growth, and
σ_{flow} = material flow strength.

Work conducted by Hellman and Schwalbe [*9*] on thin sheet material indicates that similar limits exist for CTOD but that the restrictions are less severe than those for J. It should be

stressed, however, that this program was primarily concerned with establishing plane stress R-curve limits rather than plane strain limits.

Nevertheless, based on the work by Hellman and Schwalbe, the following restrictions have been included in the draft European Group on Fracture (EGF) ductile fracture test procedure [*4*] for CTOD controlled crack growth under plane strain conditions

$$B, b > \rho\delta \qquad \rho = 50 \text{ for bend and compact specimens} \tag{4}$$

$$\Delta a \leq \alpha(W - a_o) \qquad \alpha = 0.1 \text{ for bend and compact specimens} \tag{5}$$

where δ = CTOD.

This paper presents results from a large experimental program to study geometry and size effects in elastic-plastic crack growth resistance curves and in particular the limits of CTOD controlled crack growth. The proposed test program includes low, medium, and high toughness materials. The results obtained from the low toughness material (Ti-3Al-2V alloy) have been published previously [*10,11*]. This paper presents the results for the medium toughness material (HY 100 steel).

The crack growth resistance of the HY 100 steel was measured in terms of the following fracture parameters:

1. Standard CTOD (δ_o) based on the original crack tip location, that is, as defined in BS 5762.
2. CTOD corrected for crack growth (δ_R).
3. CTOD derived from double clip gage measurements (δ_{dc}).

Material

The material selected for this investigation was HY 100 grade steel supplied in the form of a 75-mm-thick plate. This medium tearing resistance alloy has a nominal yield strength of 875 N/mm^2 and a tensile strength of 910 N/mm^2.

Test Program

General

The test program consisted of 27 room temperature unloading compliance R-curve tests on single-edge-notch bend (SENB) specimens of different sizes. The SENB specimens, which were all L-T orientation with respect to the rolling direction of the plate, were sidegrooved by 20% after being fatigue precracked to provide initial crack length to specimen width ratios (a_o/W) of approximately 0.6. All the SENB specimens were tested with a loading span to specimen width ratio (S/W) of 4.0.

The fracture toughness test program was developed to enable independent studies of size and geometry effects. Details of the overall test matrix are given in Table 1.

Size Effects Program

Five SENB specimen sizes were studied in this program corresponding to nominal thicknesses of 15, 30, 45, 60, and 90 mm. All the specimens had a width equal to twice the thickness (B by $2B$). For each specimen size, three room temperature unloading compliance tests were performed.

TABLE 1—*Details of SENB specimens.*

Specimen Numbers	Specimen Dimensions		
	Thickness, B (mm)	Width, W (mm)	Net Thickness, B_n (mm)
	(*a*) Size Effects Program		
1 to 3	15	30	12
4 to 6	30	60	24
7 to 9	45	90	36
10 to 12	60	120	48
13 to 15	75	150	60
	(*b*) Geometry Effects Program		
16 to 18	30	15	24
19 to 21	30	30	24
4 to 6	30	60	24
22 to 24	30	90	24
25 to 27	30	120	24

Geometry Effects Program

Five SENB specimen geometries were studied in this program corresponding to B by $1/2B$, B by B, B by $2B$, B by $3B$, and B by $4B$. All the specimens had a nominal thickness (B) of 30 mm. For each specimen geometry three room temperature unloading compliance tests were performed.

Test Details

The unloading compliance tests were conducted in broad agreement with the draft EGF R-curve test procedure [*4*]. Each test was terminated after the crack had grown by approximately 60% of the original uncracked ligament. At each unloading the appropriate values of δ_o, δ_R, and δ_{dc} were calculated. All the SENB specimens were fitted with double clip gage arrangements to permit the calculation of δ_{dc}.

Standard CTOD (δ_o)—The standard formula in BS 5762 [*12*] for calculating CTOD from an SENB specimen is given by

$$\delta = \frac{K^2(1 - \nu^2)}{2E\sigma_{ys}} + \frac{0.4(W - a_o)}{0.4W + 0.6a_o + z} V_p \tag{6}$$

where

K = stress intensity factor,
σ_{ys} = yield strength,
ν = Poisson's ratio,
z = knife edge height,
V = mouth opening displacement, and
V_p = plastic component of mouth opening displacement ($V - V_e$) where the elastic component (V_e), is based on the initial slope of the load displacement record.

The first term in Eq 6 represents the small scale yielding component of CTOD, which is expressed as a function of the stress intensity factor. As the fracture toughness specimens tested in this investigation were sidegrooved, the stress intensity factors were determined

using the following expression

$$K = \frac{P}{(BB_n)^{1/2} W^{1/2}} F(a_o/W) \tag{7}$$

where $F(a_o/W)$ = the stress intensity function given in BS 5762.

The second term in Eq 6 is the plastic component of CTOD, which is calculated from the plastic component of mouth opening displacement (V_p). This calculation assumes that a plastic hinge forms at a point of 0.4 ($W - a_o$) ahead of the initial crack tip. No account, therefore, is taken of the fact that the center of rotation of the plastic hinge may move as the crack extends. The general method of determining V_p involves measuring the slope of the load versus mouth opening displacement test record in the elastic regime, so that the elastic component of the mouth opening displacement at the point of interest can be subtracted from the total displacement. Note, since the construction procedure uses the slope of the initial elastic portion of the test record, which is a function of a_o, the calculation of V_p does not take crack growth into consideration.

CTOD Corrected for Crack Growth (δ_R)—The draft EGF ductile fracture test procedure [*4*] includes an expression for calculating CTOD which takes crack growth into account. The formula, which is applicable to both compact and SENB specimens, was originally proposed by Hellman and Schwalbe [*8*] and is given by

$$\delta_R = \frac{K^2(1 - \nu^2)}{2E\,\sigma_{ys}} + \frac{[0.6\Delta a + 0.4(W - a_o)]}{[0.6(a_o + \Delta a) + 0.4W + z]} V_p \tag{8}$$

where Δa = ductile crack extension.

Hellman and Schwalbe have shown that this correction for crack growth has to be applied to ensure agreement with the CTOD measured at the original crack tip. The principle behind this correction is that the plastic hinge forms $0.4[W - (a_o + \Delta a)]$ ahead of the final crack tip. Equation 8, therefore, does not take into account the fact that the plastic hinge position changes with increasing crack growth. This problem, however, can be overcome if the plastic component of δ_R is rewritten in an incremental form. The resulting expression is given by

$$\delta_{RK} = \frac{K_k^2(1 - \nu^2)}{2E\,\sigma_{ys}} + \delta_{plk} \tag{9}$$

where

$$\delta_{plk} = \delta_{plk-1} + \left[\frac{0.6(a_k - a_o) + 0.4(W - a_o)}{0.6a_k + 0.4W + z}\right](V_{pk} - V_{pk-1})$$

δ_{R_k} = δ_R evaluated at crack length a_k,
$[\delta_{pl_k}]$ = plastic component of δ_R evaluated at crack length a_k, and
a_k = crack length at kth unloading.

In this incremental equation it is assumed that the instantaneous center of rotation of the plastic hinge is located 40% of the remaining ligament ahead of the current crack. In addition, the stress intensity factor and the plastic component of mouth opening displacement are based on the current crack length, that is, the slope of the unloading line at the kth unloading is used to evaluate V_{pk}.

CTOD Derived from Double Clip Gage (δ_{dc})—The calculation of δ_R assumes that the instantaneous plastic hinge is located 40% of the remaining ligament ahead of the current crack. Previous work on a titanium alloy [*11*] has shown that this assumption is not always valid. In the case of the titanium alloy it was found that the instantaneous plastic rotational factor increased from approximately 0.3 to 0.7 over 10 mm of crack growth in a 20 by 40-mm SENB specimen.

The problems associated with the assumption of a constant plastic rotational factor can, to some extent, be avoided by fitting a double clip gage arrangement to the fracture toughness specimens. In such cases an estimate of the total CTOD (δ_{dc}) can be obtained using the following relationship

$$\delta_{dc} = \frac{K^2(1 - \nu^2)}{2E\,\sigma_{ys}} + \delta_{pl} \tag{10}$$

where

$$\delta_{pl} = V_p^u - \left[\frac{(V_p^u - V_p^l)\,(z_u + a_o)}{(z_u - z_l)}\right]$$

V_p^l = plastic mouth opening displacement associated with lower clip gage,
V_p^u = plastic mouth opening displacement associated with upper clip gage,
z_l = lower knife edge height, and
z_u = upper knife edge height.

In this expression the plastic component of δ_{dc} is calculated directly from the measured V_p's obtained from the two clip gages. The calculation assumes that δ_{pl} is given by a linear extrapolation of the upper and lower V_p's as illustrated in Fig. 1.

If necesssary, Eq 10 can be reformulated to give the following incremental expression

$$\delta_{dck} = \frac{K_k^2(1 - \nu^2)}{2E\,\sigma_{ys}} + \delta_{plk} \tag{11}$$

where

$$\delta_{plk} = \delta_{plk-1} + (V_{pk}^1 - V_{pk-1}) - \left[\frac{(V_{pk}^u - V_{pk-1}^u) - (V_{pk}^l - V_{pk-1}^l)\,(z_l + a_o)}{(z_u - z_l)}\right]$$

Results

General

All the unloading compliance CTOD *R*-curves satisfied the requirement that the difference between the measured and predicted crack growth should not exceed 10% [*1*]. Indeed, in the majority of tests the difference was less than 5%.

To give an indication of the variability of the CTOD *R*-curve data the δ_o *R*-curves obtained for the 15 by 30-mm SENB specimens are compared in Fig. 2.

The unloading compliance test data were also analyzed to determine the amount of stable crack growth that preceded the maximum applied load in each test. The average values of crack extension up to maximum load, Δa_m, are presented in Table 2 for each specimen size studied.

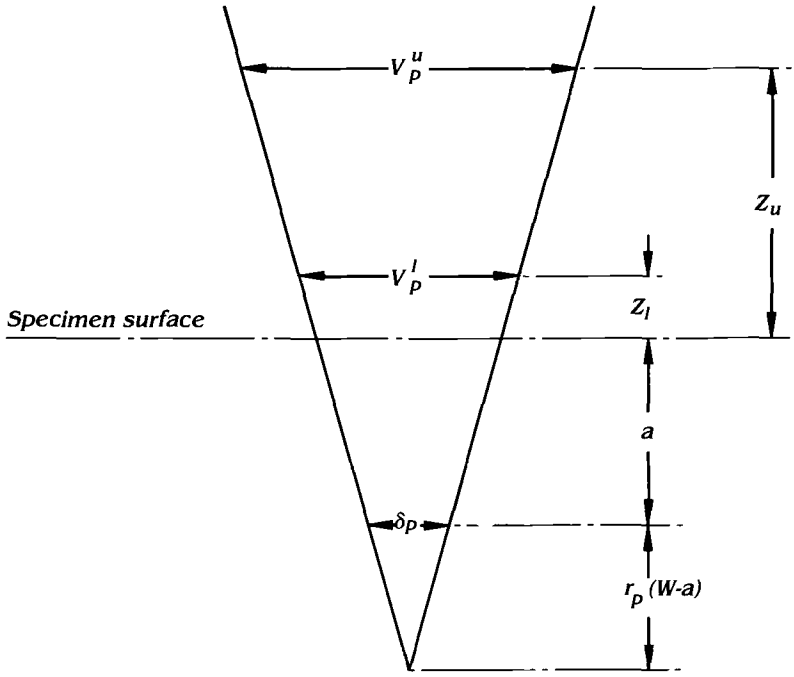

FIG. 1—*Measurement of plastic component of CTOD using double clip gage arrangement.*

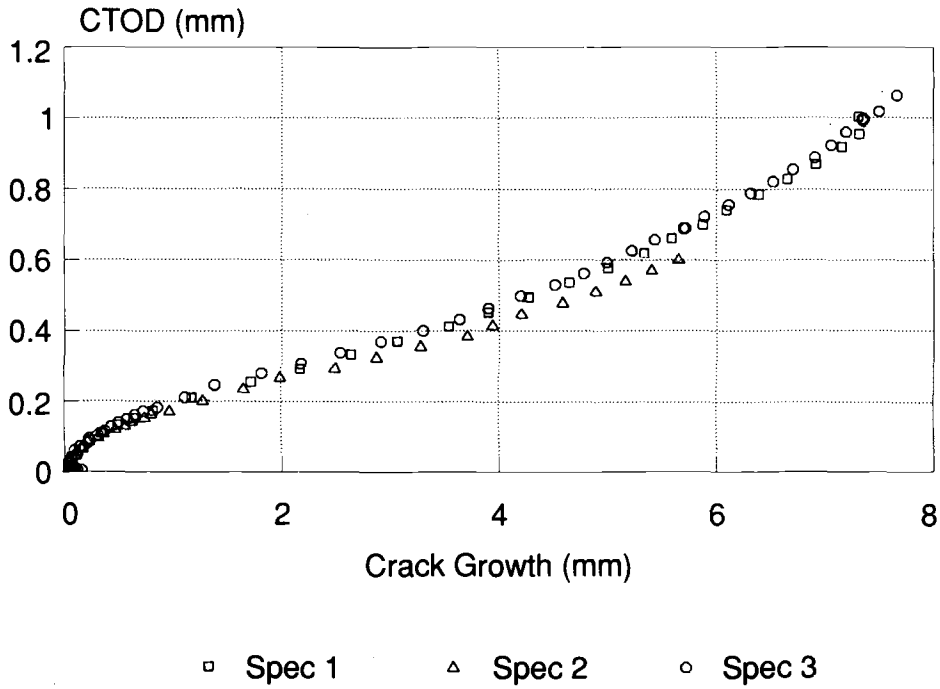

FIG. 2—*Comparison of* δ_0 *R-curves obtained from 15 by 30 mm SENB specimens.*

TABLE 2—*Average amount of stable crack extension (Δa_m) which occurred prior to maximum load.*

Specimen Size, mm (B by W)	Δa_m, mm
(*a*) SIZE EFFECTS PROGRAM	
15 by 30	0.53
30 by 60	1.03
45 by 90	1.63
60 by 120	2.25
75 by 150	3.33
(*b*) GEOMETRY EFFECTS PROGRAM	
30 by 15	0.28
30 by 30	0.40
30 by 60	1.03
30 by 90	1.84
30 by 120	2.21

Size Effects Program

The CTOD R-curves obtained in the size effects program are presented in Figs. 3 to 5. In each case the CTOD R-curve presented for each specimen size represents the mean CTOD R-curve behavior obtained from a set of three specimens.

It is evident from Figs. 3 to 5 that all three sets of R-curves (δ_o, δ_R, and δ_{dc}) display broadly similar trends. Initially the R-curves obtained from the small specimens exhibit

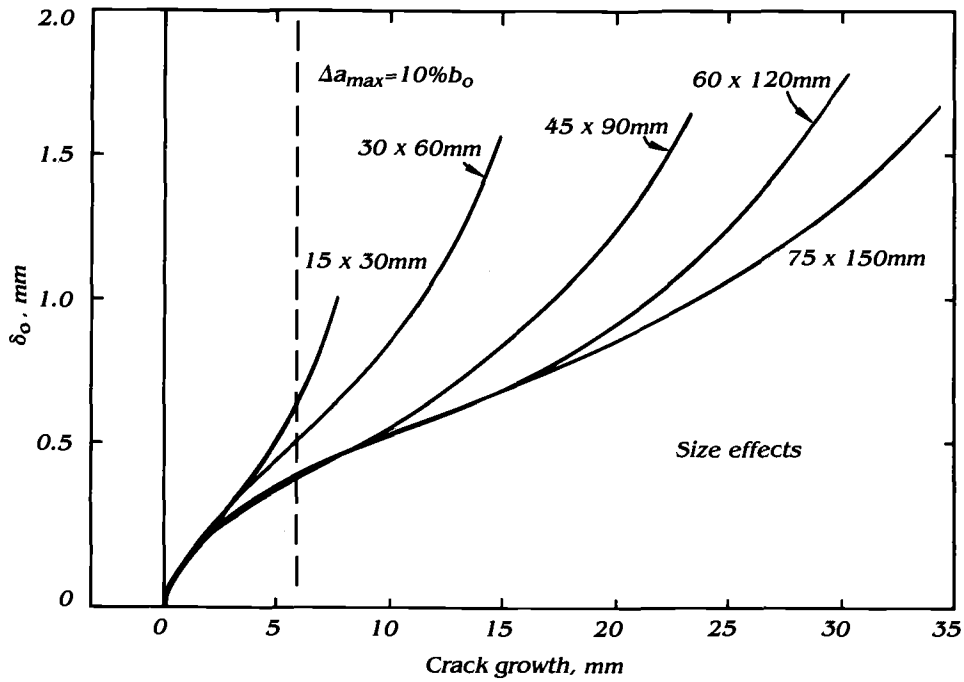

FIG. 3—*Comparison of* δ_o R-*curves (size effects program).*

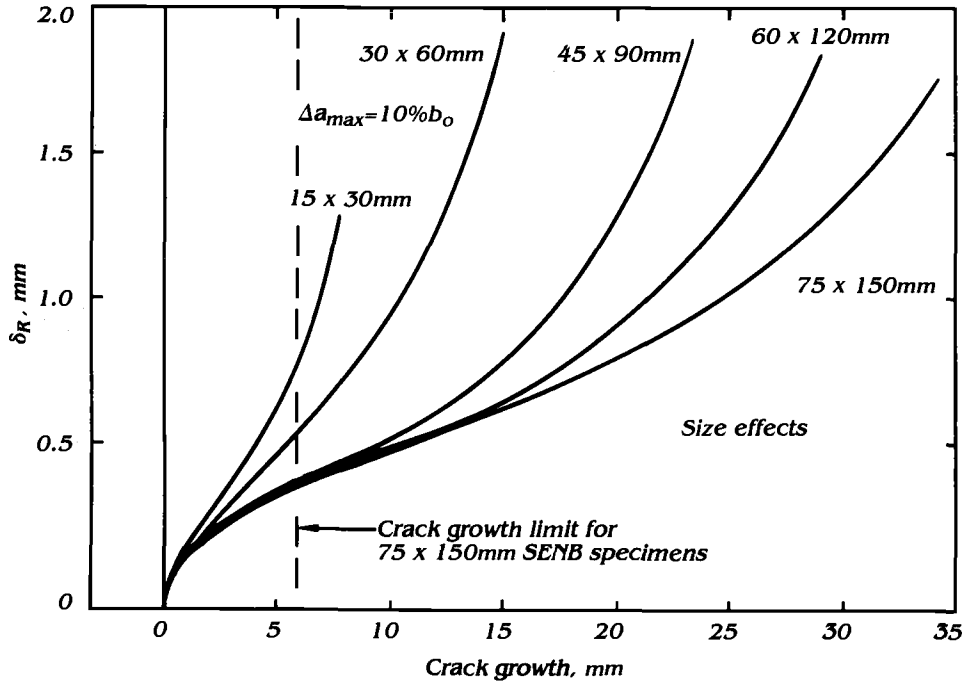

FIG. 4—*Comparison of* δ_R *R-curves (size effects program).*

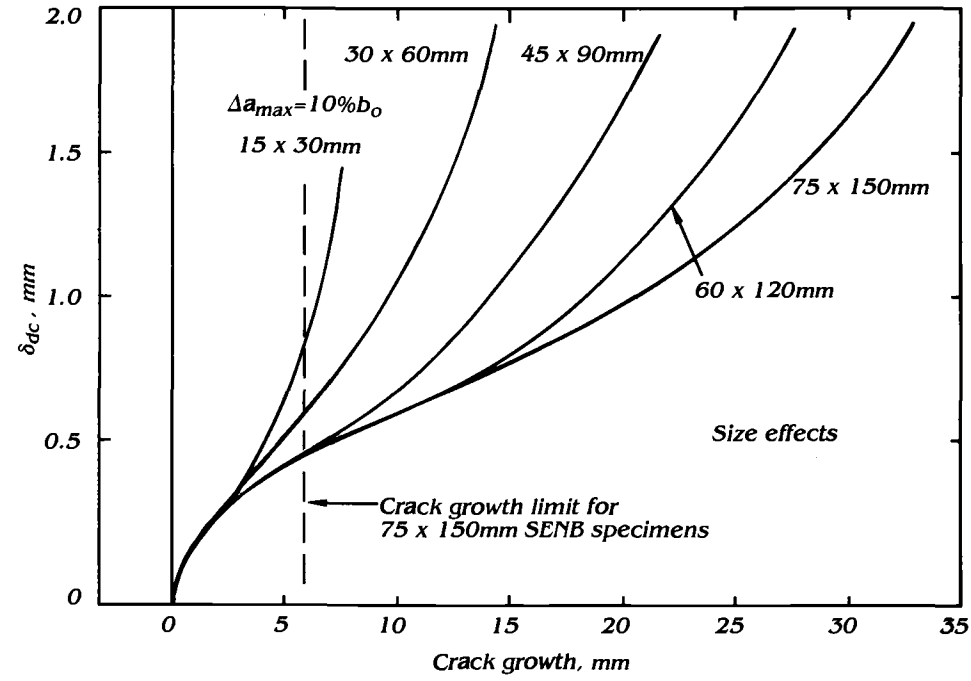

FIG. 5—*Comparison of* δ_{dc} *R-curves (size effects program).*

nominally identical behavior to the large specimen R-curves, but as crack growth continues the small specimen R-curves exhibit upswings. Moreover the points at which the R-curves exhibit the upswings appears to be dependent on specimen size; the smaller specimens displaying upswings at smaller values of crack extension.

Geometry Effects Program

The mean CTOD R-curves obtained in the geometry effects program are presented in Figs. 6 to 8. Also included in Figs. 6 to 8 are the corresponding CTOD R-curves obtained from the 75 by 150-mm SENB specimens as these were the largest specimens tested in this project and hence should exhibit the largest amount of stable-crack growth under which CTOD controlled crack growth occurred.

The CTOD R-curve trends presented in Figs. 6 to 8 are similar to those obtained in the size effects program, that is, initially the small specimen R-curves are in excellent agreement with the R-curves obtained from the larger specimens but as crack growth continues the small specimen R-curves exhibit upswings. It is also evident from Figs. 6 to 8 that although the R-curves obtained from the specimens of constant thickness (that is, 30 mm) all tend to follow a standard R-curve up to the point of separation, the corresponding CTOD R-curves obtained from the 75 by 150-mm specimens exhibit significantly different behavior separating from the 30-mm-thick specimen R-curves at relatively small values of crack extension.

Discussion of Results

At the outset of this project it was hoped that it would be possible to estimate the limits of CTOD controlled crack growth from the CTOD R-curves by identifying the point at

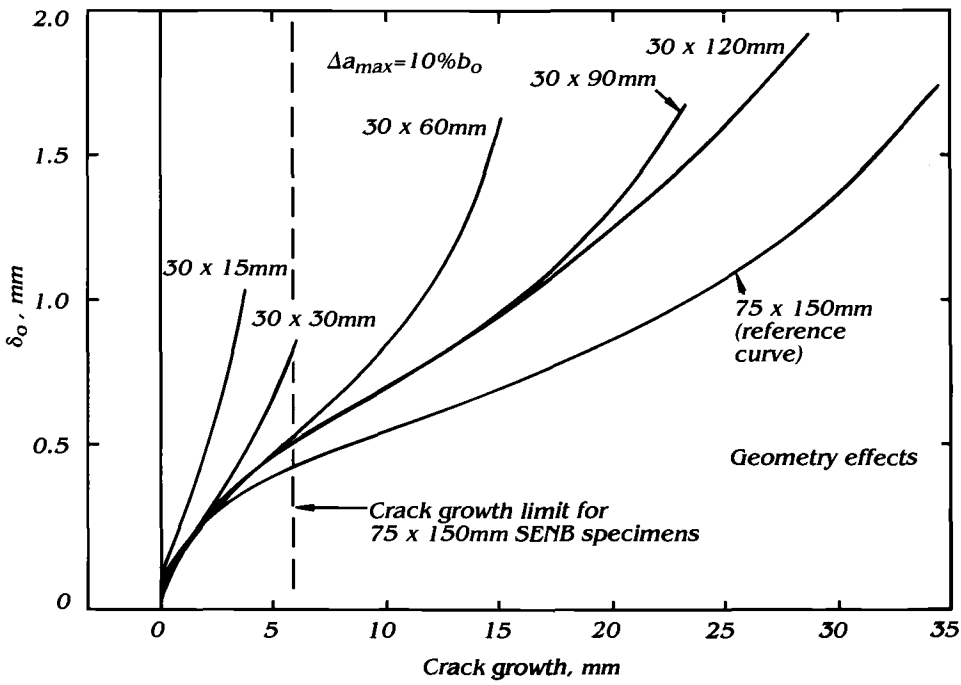

FIG. 6—*Comparison of* δ_o R-*curves (geometry effects program).*

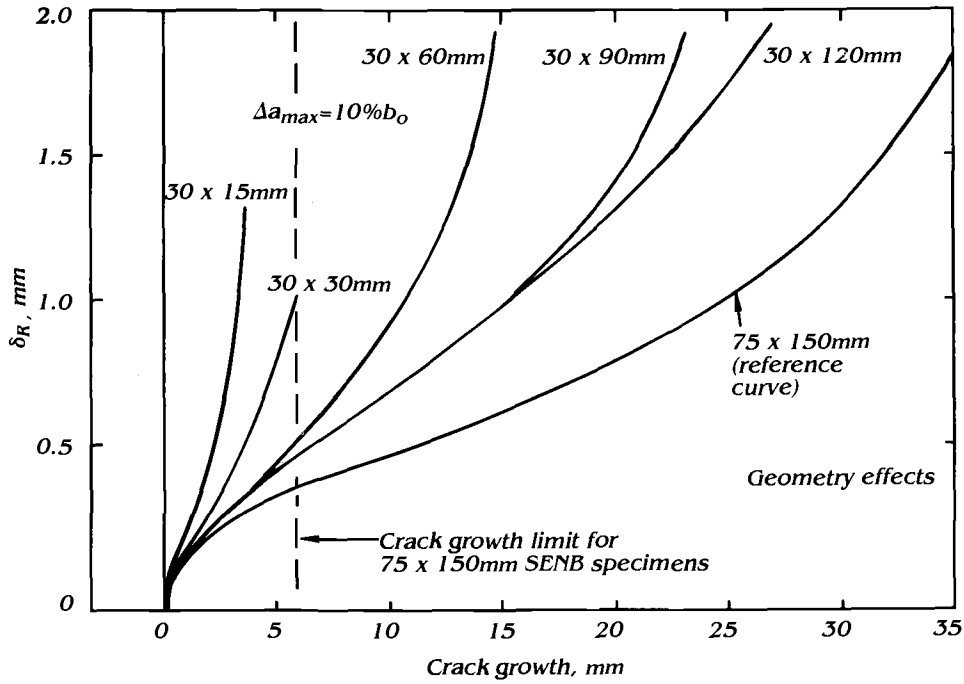

FIG. 7—*Comparison of* δ_R R-*curves (geometry effects program).*

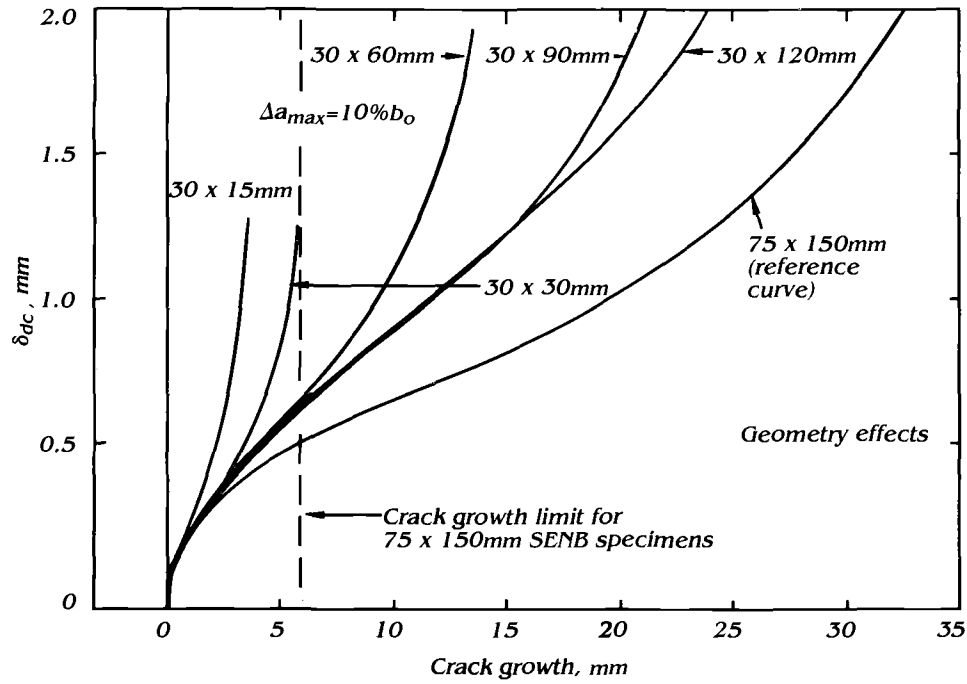

FIG. 8—*Comparison of* δ_{dc} R-*curves (geometry effects program).*

which the small specimen R-curves separate from the large specimen R-curves and evaluating the limiting values of ρ, α, and ω using the following expressions

$$\alpha = \frac{\Delta a_s}{b_o} \tag{12}$$

$$\rho = \frac{B}{\delta_s}, \frac{b}{\delta_s} \tag{13}$$

$$\omega = \frac{b}{\delta_s}, \frac{d\delta}{da} \tag{14}$$

where

Δa_s = crack growth at separation, and
δ_s = CTOD at separation.

However, as demonstrated from the previous work on a titanium alloy the breakdown of J and CTOD controlled crack growth is a gradual process and consequently the R-curves do not always exhibit well defined separation points. Nevertheless, in order to provide information on the limits of CTOD controlled crack growth values of ρ, α, and ω were estimated directly from the CTOD R-curves presented in Figs. 3 to 8. The limiting values of ρ, α, and ω were calculated based on the conditions corresponding to the commencement of the upswing in the CTOD R-curves. The limiting values of ρ, α, and ω are presented in Tables 3 and 4 for the size and geometry effects programs, respectively. Note in the case of the geometry effects program the limiting values of ρ, α, and ω presented in Table 4, were determined for the conditions corresponding to the separation of the small specimen R-curves from the CTOD R-curves obtained from the 30 by 120-mm specimens. Also since the ρ criterion is related to both ligament and specimen thickness and ρ results have been

TABLE 3—*Estimated values of* ρ, α, *and* ω *for CTOD* R-*curves in size effects program.*

Specimen size, mm (B by W)	δ_s, mm	Δa_s, mm	α	ρ_B	ρ_b	ρ_{bo}	ω
			δ_o *R*-CURVES				
15 by 30	0.28	2.0	0.17	53.6	35.7	42.9	2.81
30 by 60	0.32	2.4	0.10	93.7	67.5	75.0	6.18
45 by 90	0.56	8.5	0.24	80.4	49.1	64.3	2.21
60 by 120	0.82	16.5	0.34	73.2	38.4	38.4	1.38
			δ_R *R*-CURVES				
15 by 30	0.19	1.16	0.097	78.9	57.1	63.2	5.32
30 by 60	0.25	2.24	0.094	120.0	87.0	96.0	11.06
45 by 90	0.47	8.0	0.22	95.7	59.6	95.7	2.38
60 by 120	0.59	12.5	0.26	101.6	60.5	81.4	2.02
			δ_{dc} *R*-CURVES				
15 by 30	0.33	2.2	0.18	45.5	29.7	36.4	3.30
30 by 60	0.40	2.9	0.12	75.0	52.8	60.0	5.09
45 by 90	0.56	7.1	0.20	80.4	51.6	64.3	2.72
60 by 120	0.81	14.1	0.29	74.1	41.9	59.3	1.80

NOTES—δ_s = value of CTOD at point of separation.
Δa_s = amount of crack growth before separation.

TABLE 4—*Estimated values of* ρ, α, *and* ω *for CTOD* R-*curves in geometry effects program.*

Specimen size (B by W) mm	δ_s, mm	Δa_s, mm	α	ρ_B	ρ_b	ρ_{bo}	ω
			δ_o *R*-CURVES				
30 by 15	0.123	0.31	0.052	244.0	46.3	48.7	7.82
30 by 30	0.307	2.26	0.19	97.7	31.7	39.1	2.60
30 by 60	0.54	5.36	0.22	55.6	34.5	44.4	1.89
30 by 90	1.15	17.3	0.48	26.1	16.3	31.3	0.87
			δ_R *R*-CURVES				
30 by 15	0.154	0.31	0.052	195.0	36.9	39.0	4.69
30 by 30	0.246	1.28	0.11	122.0	48.8	48.8	3.89
30 by 60	0.408	3.7	0.15	73.5	49.8	58.8	2.92
30 by 90	1.05	15.5	0.43	28.7	20.0	34.3	1.03
			δ_{dc} *R*-CURVES				
30 by 15	0.254	0.82	0.14	118.0	20.5	23.6	3.59
30 by 30	0.43	2.80	0.23	69.6	21.6	27.8	2.06
30 by 60	0.66	6.1	0.25	45.8	27.7	36.7	1.69
30 by 90	1.14	13.5	0.37	26.3	20.1	31.6	1.04

NOTES—δ_s = value of CTOD at point of separation.
Δa_s = amount of crack growth before separation.

further broken down to denote the specimen dimension used in the calculation (that is, ρ_b = ρ based on current ligament, ρ_{b_o} = ρ based on initial ligament, etc.).

As mentioned previously although the CTOD *R*-curves obtained from the specimens of constant thickness follow a standard *R*-curve up to the point of separation the corresponding CTOD *R*-curves obtained from the 75 by 150-mm specimens exhibited significantly different behavior. The limiting values of ρ, α, and ω corresponding to the point of separation between the geometry effects CTOD *R*-curves and the corresponding CTOD *R*-curves obtained from the 75 by 150-mm specimens are presented in Table 5.

It is evident from Tables 3, 4, and 5 that the limiting values of ρ, α, and ω obtained from the various CTOD *R*-curves do not exhibit a consistent trend. This is perhaps indicative of the problems associated with identifying the separation points. Nevertheless, based on the information presented in Tables 3, 4, and 5 it is possible to draw the following conclusions:

1. The δ and δ_R *R*-curves exhibited size and geometry independence over approximately the same ranges of crack extension.
2. In general the δ_{dc} *R*-curves exhibited size and geometry independence over slightly larger ranges of crack extension than the corresponding δ_o or δ_R *R*-curves.
3. For specimens of a given thickness, increasing the specimen width appears to increase the crack growth range over which the CTOD *R*-curves are in agreement.

In order to produce more accurate estimates of the limiting values of ρ, α, and ω, fifth order polynomials were fitted to the various CTOD *R*-curves by the method of least squares. For each specimen size three fifth order polynomial fits were determined corresponding to δ_o, δ_R, and δ_{dc} *R*-curve behavior. In all cases the fifth order polynomial expressions produced excellent fits. The subsequent polynomial expressions were then differentiated to produce plots of $d\delta/da$ versus Δa. A typical plot is presented in Fig. 9. It is clear that there are two

TABLE 5—*Estimated values of* ρ, α, *and* ω *for CTOD* R*-curves in geometry effects program based on the separation from the CTOD* R*-curve obtained from the 75 by 150 mm SENB specimen.*

Specimen size (B by W) mm	δ_s, mm	Δa_s, mm	α	ρ_B	ρ_b	ρ_{bo}	ω
			δ_o *R*-CURVES				
30 by 15	0.123	0.31	0.052	244	46.3	48.7	7.82
30 by 30	0.307	2.26	0.19	97.7	31.7	39.1	2.60
30 by 60	0.32	2.40	0.10	93.7	67.5	75.0	6.18
30 by 90	0.32	2.40	0.047	93.7	105.0	112.5	9.27
30 by 120	0.32	2.40	0.05	93.7	142.5	150.0	12.36
			δ_R *R*-CURVES				
30 by 15	0.154	0.31	0.052	195	36.9	39.0	4.69
30 by 30	0.246	1.28	0.11	122	43.6	48.8	3.89
30 by 60	0.25	2.24	0.094	120	87.0	96.0	11.06
30 by 90	0.25	2.24	0.062	120	135.0	144.0	16.6
30 by 120	0.25	2.24	0.047	120	183.0	192.0	22.1
			δ_{dc} *R*-CURVES				
30 by 15	0.254	0.82	0.14	118	20.5	23.6	3.59
30 by 30	0.43	2.80	0.23	69.6	21.6	27.8	2.06
30 by 60	0.40	2.90	0.12	75.0	52.8	60.0	5.09
30 by 90	0.40	2.90	0.08	75.0	82.8	90.0	7.64
30 by 120	0.40	2.90	0.06	75.0	112.8	120.0	10.2

NOTES—δ_s = value of CTOD at point of separation.
Δa_s = amount of crack growth before separation.

critical points in the plot of $d\delta/da$ versus Δa either of which could possibly be used to define the point of separation. The first critical point (Point A) is the point of minimum gradient whereas the second critical point (Point B) corresponds to the position where the slope of the CTOD *R*-curve rises dramatically.

To study this behavior in more detail, graphs of $d\delta/da$ versus $\Delta a/b_o$ were produced for all the CTOD *R*-curves obtained in both the geometry and size effects programs. The results obtained from the δ_{dc} *R*-curves in the size and geometry effects programs are presented in Fig. 10.

The CTOD and Δa values corresponding to Points A and B together with the associated values of ρ, α, and ω are presented in Tables 6 and 7 for the δ_{dc} *R*-curves obtained in the size and geometry effects program, respectively. The corresponding information for the δ_o *R*-curves is presented in Tables 8 and 9. It is clear from Tables 6 to 9 that in general the mean α values corresponding to Points A and B remain fixed at 0.17 and 0.44 regardless of specimen size or CTOD parameter. This trend was also exhibited by the δ_R *R*-curves.

Based on the previously aforementioned trends it is postulated that the limiting value of α for HY100 steel CTOD *R*-curve data is 0.17. Beyond this limit the CTOD *R*-curves exhibit upswings which in the opinion of the authors is due to loss of crack tip constraint. Indeed, since a reduction in constraint is likely to result in large amounts of additional information being required to produce small amounts of crack extension, it is not unreasonable to expect an upswing in CTOD *R*-curves. Although a limiting α value of 0.17 appears to apply to all the CTOD *R*-curves obtained in this project it does not necessarily guarantee size independent *R*-curve behavior. Indeed, if the CTOD *R*-curves obtained in the geometry effects

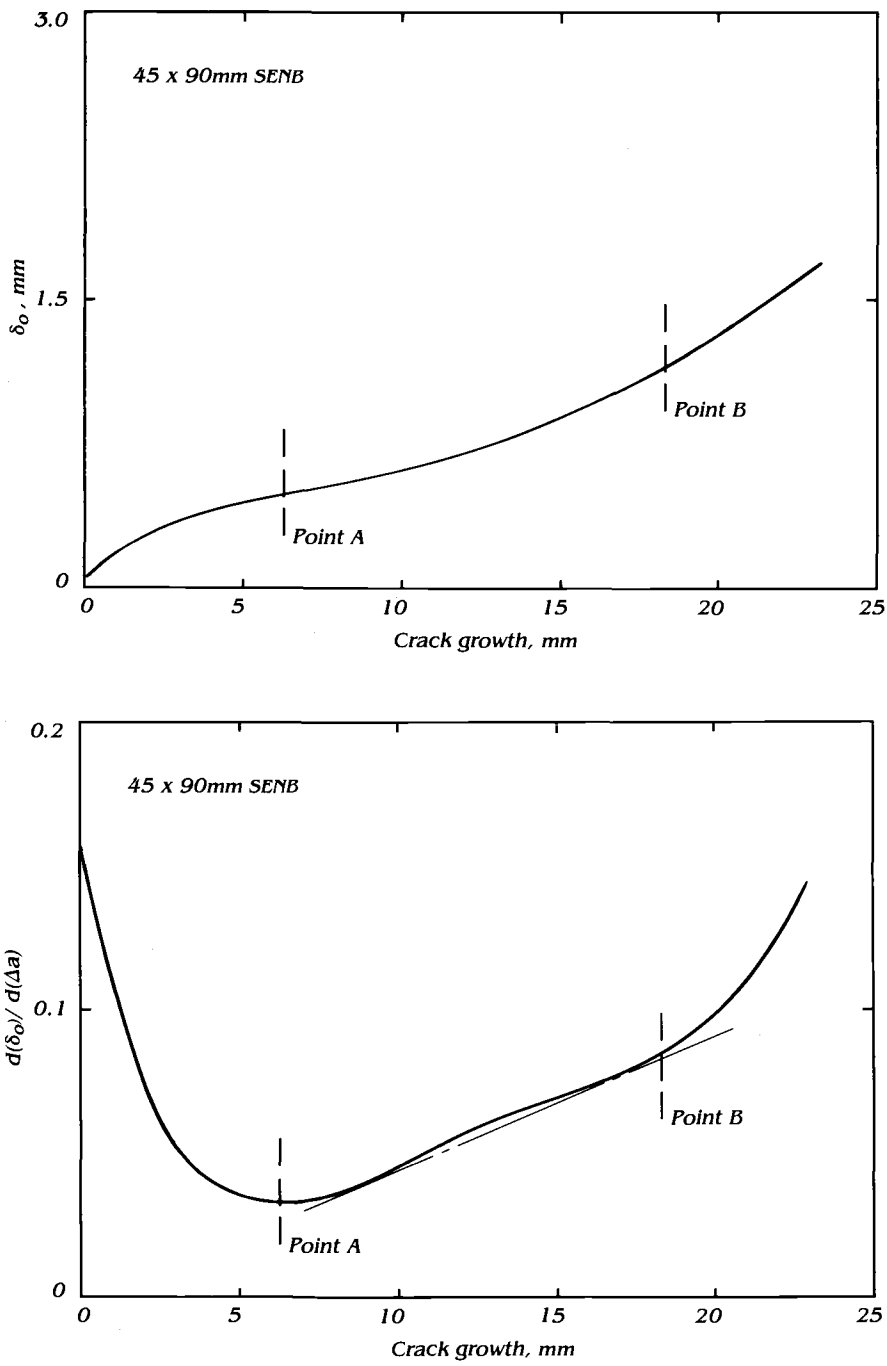

FIG. 9—*Plot of* $d\delta_o/d(\Delta a)$ *for 45 by 90-mm SENB specimen.*

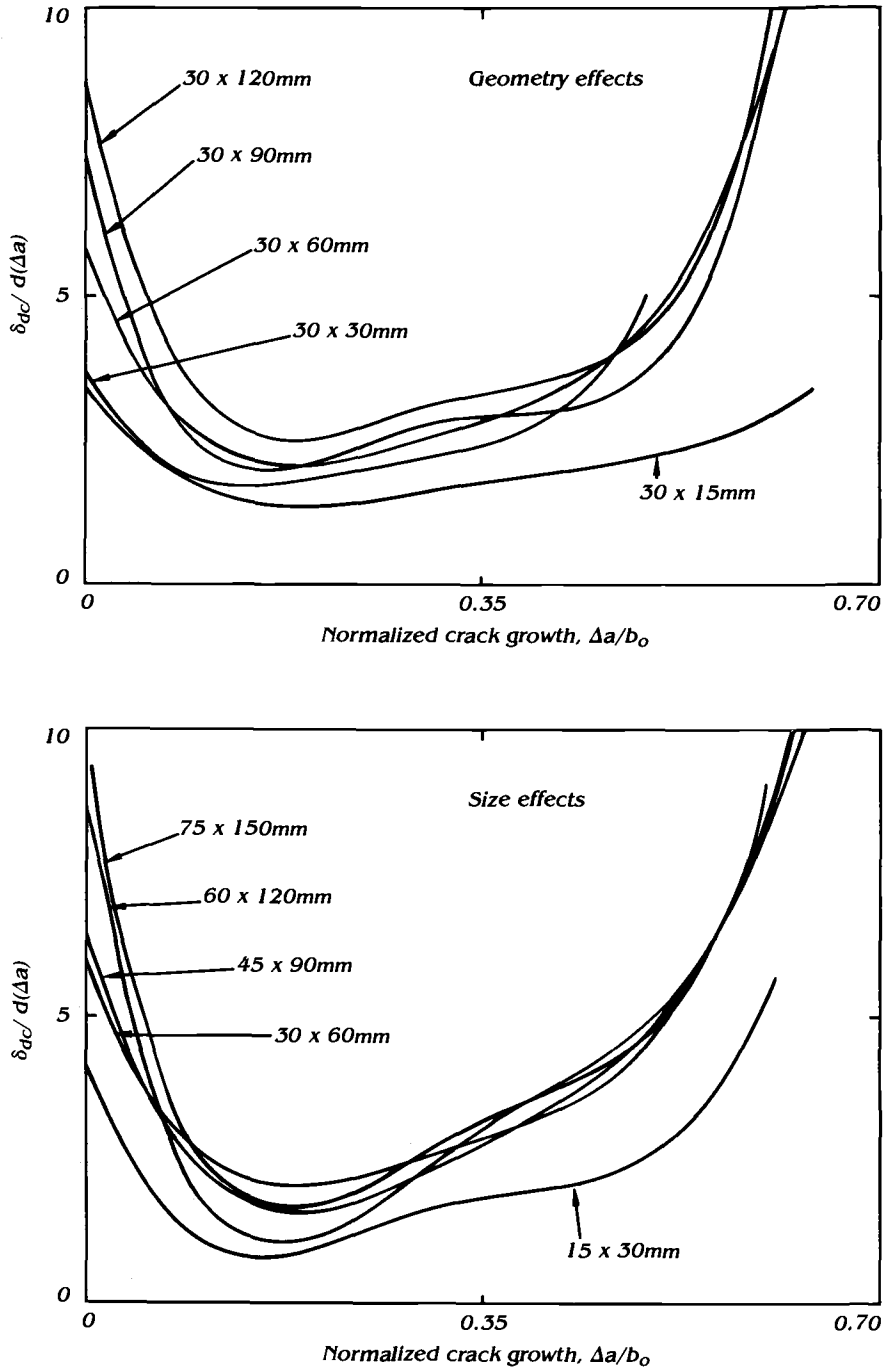

FIG. 10—*Comparison of* $d\delta_{dc}/d(\Delta a)$ *versus* $\Delta a/b_o$ *plots for geometry and size effects* δ_{dc} R-*curve data.*

TABLE 6—*Estimated values of* ρ, α, *and* ω *for* δ_{dc} *R-curve data in size effects program calculated for polynomial fits.*

Specimen size, mm	δ_{dc} Separation, mm	Δa at Separation, mm	ρ_B	ρ_b	α	ω
		POINT A DATA				
15 by 30	0.26	1.7	57.7	39.62	0.142	2.294
30 by 60	0.58	4.3	51.7	33.97	0.179	2.955
45 by 90	0.58	6.6	77.6	50.69	0.183	2.129
60 by 120	0.57	8.0	105.2	70.18	0.167	1.263
75 by 150	0.68	10.2	110.3	73.24	0.170	1.831
		POINT B DATA				
15 by 30	0.75	5.5	20.0	8.7	0.458	1.621
60 by 60	1.11	9.3	27.0	13.2	0.388	1.748
45 by 90	1.23	16.1	36.6	16.2	0.447	1.796
60 by 120	1.45	23.3	41.4	17.0	0.485	1.703
75 by 150	1.50	27.7	50.0	21.3	0.462	1.507

TABLE 7—*Estimated values of* ρ, α, *and* ω *for* δ_{dc} *R-curve data in geometry effects program calculated for polynomial fits.*

Specimen size, mm	δ_{dc} Separation, mm	Δa at Separation, mm	ρ_B	ρ_b	α	ω
		POINT A DATA				
30 by 15	0.37	1.11	81.1	13.2	0.185	2.855
30 by 30	0.34	1.68	88.2	30.4	0.140	4.310
30 by 60	0.58	4.3	51.7	30.0	0.179	2.955
30 by 90	0.58	5.6	51.7	52.4	0.156	2.621
30 by 120	0.79	8.5	38.0	50.0	0.177	2.500
		POINT B DATA				
30 by 15	0.87	2.92	34.5	3.5	0.487	1.257
30 by 30	0.73	4.06	41.1	10.9	0.338	2.121
30 by 60	1.11	9.3	27.0	13.2	0.388	1.748
30 by 90	1.39	16.4	21.6	14.1	0.456	1.227
30 by 120	1.69	22.0	17.8	15.4	0.458	1.215

TABLE 8—*Estimated values of* ρ, α, *and* ω *for* δ_o *R-curve data in size effects program calculated for polynomial fits.*

Specimen Size, mm	δ_o at Separation, kJ/m^2	Δa Separation, mm	ρ_B	ρ_b	α	ω
		POINT A DATA				
15 by 30	0.27	1.9	55.6	37.4	0.158	2.469
30 by 60	0.46	4.0	65.2	43.5	0.167	2.517
45 by 90	0.47	6.4	95.7	63.0	0.178	2.015
60 by 120	0.52	8.0	115.4	76.92	0.167	1.462
75 by 150	0.62	10.2	121.0	80.32	0.170	1.687
		POINT B DATA				
15 by 30	0.71	5.9	21.1	8.6	0.492	1.220
30 by 60	0.99	11.0	30.3	13.1	0.458	1.379
45 by 90	1.17	18.3	38.5	15.1	0.508	1.316
60 by 120	1.34	24.6	44.8	17.5	0.513	1.292
75 by 150	1.37	29.5	54.7	22.3	0.492	1.224

TABLE 9—*Estimated values of* ρ, α, *and* ω *for* δ_o R-*curve data in geometry effects program calculated for polynomial fits.*

Specimen Size, mm	δ_o at Separation, mm	Δa Separation, mm	ρ_B	ρ_b	α	ω
		POINT A DATA				
30 by 15	0.33	1.14	90.9	14.7	0.190	2.563
30 by 30	0.31	1.78	96.8	33.0	0.148	3.396
30 by 60	0.46	4.0	65.2	43.5	0.167	2.517
30 by 90	0.54	5.8	55.5	55.9	0.161	2.181
30 by 120	0.65	8.2	46.2	61.2	0.171	2.021
		POINT B DATA				
30 by 15	0.75	3.06	40.0	3.9	0.510	1.043
30 by 30	0.65	4.55	46.2	11.5	0.379	1.661
30 by 60	0.99	11.00	30.3	13.1	0.458	1.379
30 by 90	1.20	17.40	25.0	15.5	0.483	1.054
30 by 120	1.36	23.30	22.1	18.2	0.485	1.017

program are compared to the corresponding CTOD *R*-curves obtained from the 75 by 150-mm SENB specimen it is clear that most of the large specimen CTOD *R*-curves in the geometry effects program separate from the 75 by 150-mm SENB CTOD *R*-curve long before the $\alpha = 0.17$ limit. This implies that the 30-mm-thick specimens used in the geometry effects program are not sufficiently thick to produce plane strain conditions beyond CTOD levels of approximately 0.3 mm and crack extensions of 2.5 mm. This corresponds to a limiting ρ_B value of 100.

Having noted the fact that the CTOD *R*-curves obtained in this program tend to exhibit upswings after crack extensions corresponding to approximately 17% of the initial uncracked ligament, it was decided to replot the data with the crack growth axis normalized by initial ligament. The subsequent normalized δ_{dc} *R*-curves are presented in Figs. 11 and 12. It is clear from Fig. 11 that in the case of the size effects program the normalization technique has produced a common curve with the exception of the *R*-curve corresponding to the 15 by 30-mm specimens. In comparison, the normalized δ_{dc} *R*-curves obtained in the geometry effects program are not in particularly good agreement. Nevertheless, comparing the normalized *R*-curves in Figs. 11 and 12 indicates that with the exception of the *R*-curves obtained from the three smallest specimen sizes (that is, 15 by 30 mm, 30 by 15 mm, and 30 by 30 mm) the remaining normalized δ_{dc} *R*-curves are in reasonably good agreement.

Conclusions

A series of unloading compliance *R*-curves tests have been performed on SENB specimens of different sizes made from HY100 steel to study the CTOD *R*-curve behavior at large crack extensions. The crack growth resistance was measured in terms of conventional CTOD, δ_o (as defined in BS 5762), CTOD corrected for crack growth, δ_R, and CTOD derived using a double clip gage arrangement, δ_{dc}. It was found that:

1. The δ_o and δ_R *R*-curves exhibited size and geometry independence over approximately the same ranges of crack extension.
2. In general, the δ_{dc} *R*-curves exhibited size and geometry independence over slightly larger ranges of crack extension than the corresponding δ_o and δ_R *R*-curves. For this

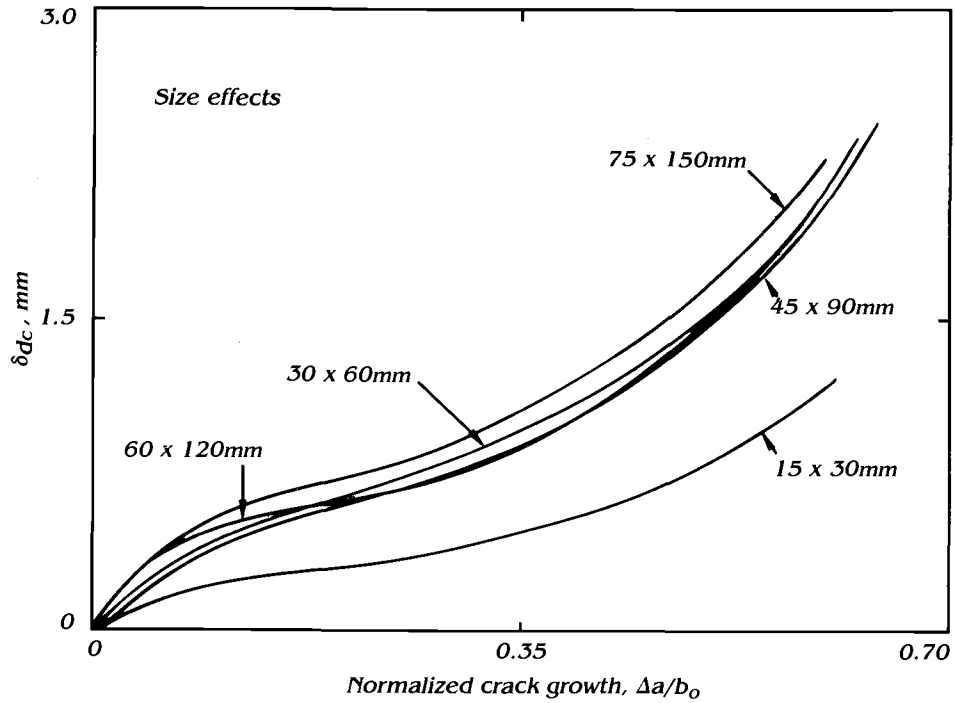

FIG. 11—*Comparison of normalized* δ_{dc} *R-curves (size effects program).*

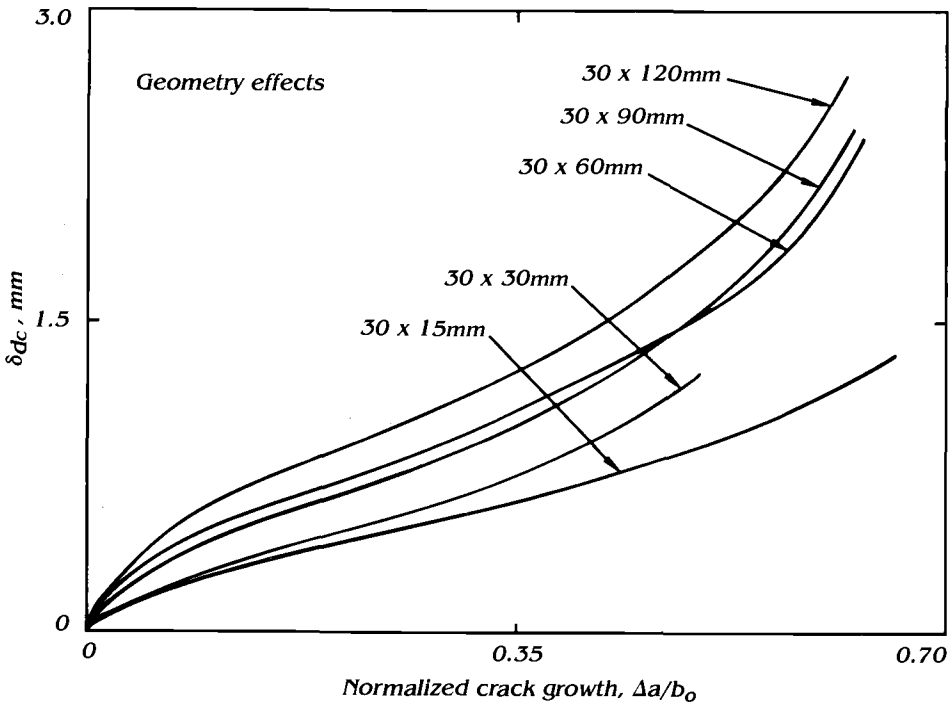

FIG. 12—*Comparison of normalized* δ_{dc} *R-curves (geometry effects program).*

reason it is recommended that CTOD R-curves should be based on the δ_{dc} parameter. This parameter also has the advantage that the calculation procedure does not assume a fixed value of 0.4 for the plastic rotational factor.

3. For specimens of a given thickness increasing the specimen width appears to increase the crack growth range over which the CTOD R-curves are in agreement. Nevertheless, this does not guarantee that the subsequent CTOD R-curves behavior exhibited over this crack growth range is size independent, that is, it may be dependent on specimen thickness.
4. All the CTOD R-curves obtained in this study exhibited upswings. The upswings, in general, started at crack extensions corresponding to 17% of the initial uncracked ligament. At crack extensions corresponding to approximately 45% of the initial uncracked ligament the slope of the CTOD R-curves increased dramatically.
5. Based on these observations it is postulated that the crack growth limit for CTOD controlled crack growth in R-curves obtained from HY100 steel is 17% of the initial uncracked ligament. This condition alone however, is not sufficient to guarantee size/geometry independent results. It is also necessary to have the same level of specimen constraint. The following values of ρ are proposed to ensure plane strain constraint in HY100 steel

$$\rho_B = 100$$

$$\rho_b = 50$$

6. With the exception of the CTOD R-curves obtained from specimens with widths less than or equal to 30 mm, normalizing the crack growth axis by dividing crack extension by the initial uncracked ligament, resulted in normalized CTOD R-curves which were in reasonably good agreement over the entire crack growth range studied in this investigation (that is, 60% of the initial uncracked ligament).

References

[1] Gordon J. R., "The Welding Institute Procedure for the Determination of the Fracture Resistance of Fully Ductile Metals," Welding Institute Report 275, 1985, June 1985.
[2] Neale B. K., Curry, D. A., Greene, G., Haigh, J. R., and Akhurst K. N., "A Procedure for the Determination of the Fracture Resistance of Ductile Steels," *International Journal of Pressure Vessels and Piping*, Vol. 20, 1984, pp. 155–179.
[3] ASTM E 1152 Standard Method of Determining J R-curves, 1987.
[4] European Group on Fracture (EGF) Recommendations for Determining the Fracture Resistance of Ductile Materials, 1st Draft, 1987.
[5] ASTM E 1290 Standard Test Method for Crack Tip Opening Displacement (CTOD) Fracture Toughness Measurement, 1989.
[6] Shih, C. F. and German, M. D., "Requirements for a One Parameter Characterization of Crack Tip Fields by the HRR-Singularity," *International Journal of Fracture*, Vol. 17, 1981, pp. 27–43.
[7] Hutchinson, J. W., "Fundamentals of the Phenomenological Theory of Non-Linear Fracture Mechanics," *Journal of Applied Mechanics*, Vol. 50, 1983, pp. 1042–1051.
[8] Landes, J. D., "Size and Geometry Effects on Elastic-Plastic Characterization," *CNSI Specialists Meeting on Plastic Tearing Instability*, NUREG/CP-0010, Nuclear Regulatory Commission, Washington, DC, 1979, pp. 194–225.
[9] Hellman, D. and Schwalbe, K. H., "On the Experimental Determination of CTOD Based R-Curves," Workshop on the CTOD Methodology, GKSS, Geesthact, 1985.

[*10*] Gordon, J. R. and Jones, R. L., "The Effect of Specimen Size on the *J-R*-Curve Behavior of a Titanium Alloy," *Fatigue and Fracture of Engineering Materials and Structures*, Vol. 12, 1989, pp. 295–308.

[*11*] Gordon, J. R. and Jones, R. L., "The Effect of Specimen Size on the CTOD *R*-Curve Behavior of a Titanium Alloy," *Fatigue and Fracture of Engineering Materials and Structures*, Vol. 12, 1989, pp. 309–321.

[*12*] BS 5762 Methods for Crack Opening Displacement (COD) Testing, British Standards Institution, 1979.

Bruce D. Macdonald,[1] *R. H. Oberdick,*[1] *and A. L. Hiser, Jr.*[2]

A Fracture Instability Data Qualification Limit

REFERENCE: Macdonald, B. D., Oberdick, R. H., and Hiser, A. L., Jr., **"A Fracture Instability Data Qualification Limit,"** *Elastic-Plastic Fracture Test Methods: The User's Experience (Second Volume), ASTM STP 1114*, J. A. Joyce, Ed., American Society for Testing and Materials, Philadelphia, 1991, pp. 102–113.

ABSTRACT: The purpose of this work was to identify a fracture instability data qualification limit. Transition regime fracture data were sorted to disqualify those higher J_{max} valued fracture instability data which had exhibited significant prior stable crack extension. Qualified data were identified as having J_{max} values below the J_{Ic} scatterband. Disqualified data had more than double the average prior stable crack extension of qualified data and had J_{max} values in or above the J_{Ic} scatterband. The higher J_{max} values and significant crack extension of disqualified data appeared to have been associated with a loss of constraint. The data indicated that a specimen size requirement may be needed for elastic-plastic fracture instability data that is different from those for elastic fracture instability or elastic-plastic tearing onset data. However, the value of J_{max} relative to the J_{Ic} scatterband seems more to the point of identifying data that undergo fracture instability prior to significant crack extension.

KEY WORDS: transition regime, elastic-plastic fracture

The *J*-integral (*J*) provides a means for characterizing elastic-plastic fracture instability and tearing resistance of structural steel in all three principal temperature-dependent response regimes: lower shelf, transition, and upper shelf. Therefore, *J* test results can be used to define two types of fracture toughness curves:

1. Fracture toughness at the onset of significant crack extension versus temperature (all three regimes).
2. Stable tearing resistance versus post-onset crack extension (upper shelf).

Test methods and associated data for establishing upper shelf tearing resistance curves already exist, as do test methods and data that support definition of fracture toughness at the onset of significant crack extension on the lower and upper shelf. On the lower shelf, fracture instability at a fracture toughness value of K_{Ic} may be thought of as synonymous with onset of significant crack extension and ASTM Test Method for Plane-Strain Fracture Toughness of Metallic Materials (E 399) is applicable. On the upper shelf, ASTM Test Method for J_{Ic}, a Measure of Fracture Toughness (E 813) provides a consensus definition of tearing onset as occurring at a fraction toughness value of J_{Ic}. If the E 813 formula for *J* is applied to qualified E 399 data, then a fracture instability value of *J* results. This paper addresses data qualification issues associated with defining a *J*-based fracture toughness

[1]Principal engineer and lead engineer, respectively, General Electric Company, Box 1072, Schenectady, NY 12301.

[2]Materials engineer, U.S. Nuclear Regulatory Commission, Washington, DC 20555; formerly, mechanical engineer, Materials Engineering Associates, Lanham, MD 20706.

curve in the transition regime, that is, a J_{max} versus temperature curve below which the effect of crack extension is insignificant.

Defining a transition regime J-test method turns mainly on achieving a consensus on test data qualification rules. The main issues that have been dealt with in existing fracture mechanics test methods and cited in numerous previous publications are: (1) defining insignificant crack extension prior to fracture, that is, limiting prior stable crack extension; (2) demonstrating size effect insensitivity or dealing somehow with the constraint issue; and (3) accounting for (or disallowing) the influence of plasticity. Once these issues have been satisfactorily addressed, the remaining data scatter should be due only to material inhomogeneity. In this paper, prior stable crack extension was considered insignificant if it had no identifiable influence on J at fracture.

Specimen Constraint

The single-edge-notched bend, SEN(B), and compact tension, C(T), formulas for J found in E 813 are considered applicable, provided that the specimen size requirements are met. Landes and Begley [*1*] noted that the basis for these requirements is that crack length, ligament length, and thickness must be large compared to crack-tip opening displacement. If a further thickness effect were active, then apparent fracture toughness would be related inversely to specimen thickness due to loss of through-thickness constraint, as discussed by Srawley and Brown [*2*]. In the event that such an inverse relationship does not exist, then thickness constraint would appear not to be a factor in the J-based interpretation of fracture instability data.

Plasticity

Acceptability of the current ASTM J-based test method E 813 to characterize upper shelf fracture toughness at tearing onset was predicated, in part, on the capacity of the J-integral to account for the influence of plasticity on the crack front neighborhood. That capacity is not diminished when one applies the test method to transition regime testing, since the presence of plasticity is no more prevalent in the transition regime than on the upper shelf. Furthermore, a J-based interpretation of fracture toughness test results assures their applicability to assessing flaw tolerance of structures in the presence of significant plasticity.

Prior Stable Crack Extension

Current upper shelf test methods indicate that fracture toughness increases with significant stable crack extension. The objective of this paper is to identify some threshold below which J, at fracture instability, is not influenced by prior stable crack extension. Due to the fact that this threshold value of crack extension may be of the same order as its variability through the specimen thickness, a threshold based on prior stable crack extension may be unsuitable. Since the value of J at fracture instability is relatively certain, a J-based threshold would be desirable. In particular, J_{Ic} might serve to define the threshold below which prior stable crack extension could be considered insignificant since it occurs near the beginning of slow, stable crack extension.

Fracture Toughness Test Results

Figure 1 shows A508-C12 transition regime test data for C-R orientation compact, C(T), and bend, SEN(B), specimens taken from a single ring forging at midthickness. Various

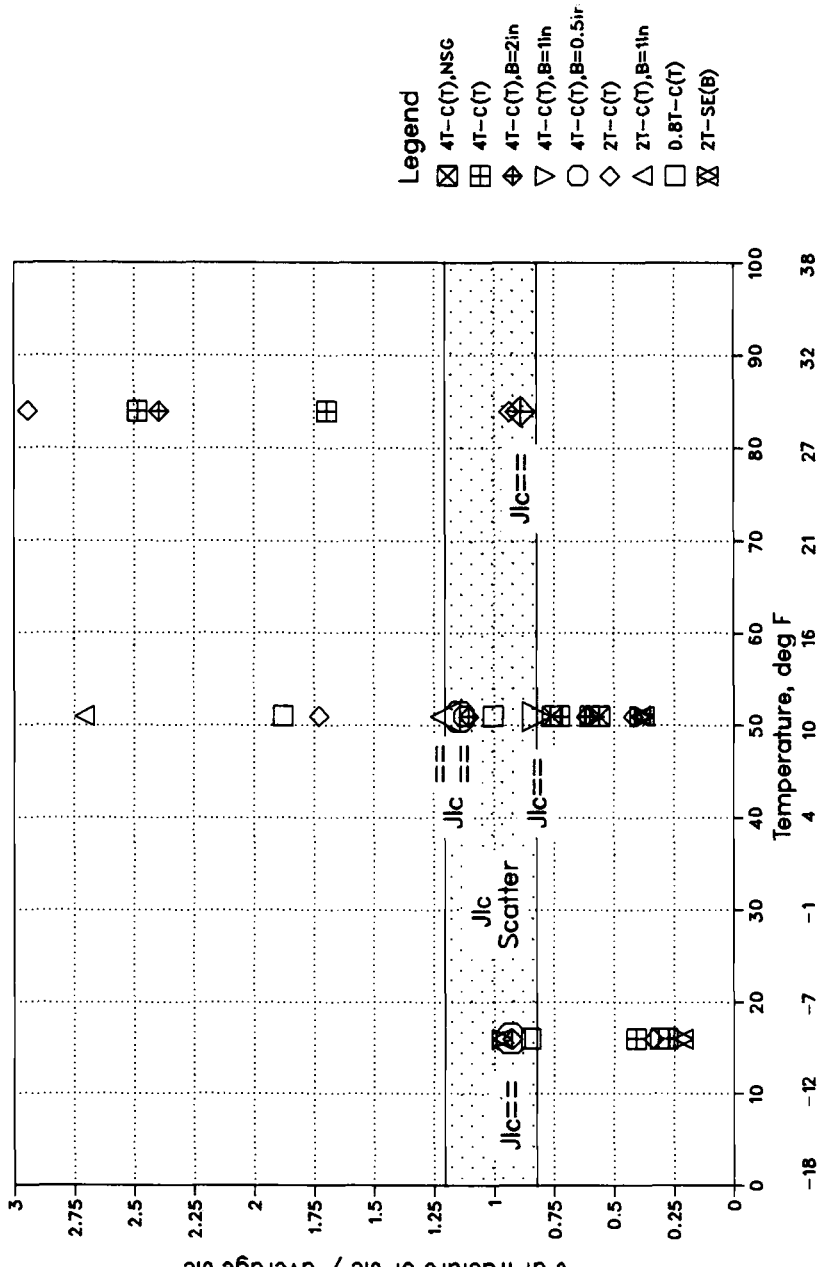

FIG. 1—*A508-C12* J_{Ic} *and* J_{max} *versus temperature.*

specimen types, sizes, and thicknesses, all with initial aspects ratios, a/W, of 0.5, were tested at three temperatures. All specimens were 20% side-grooved except two 4T-C(T) labeled NSG which had no side grooves. Specimen instrumentation supported the needs of the ASTM E 813 single specimen technique employing unloading compliance to infer crack extension. J_{Ic} data were obtained at all test temperatures and were thought to have given an indication of the expected scatter due to material inhomogeneity. At −8.9°C, fracture instability occurred below and within the J_{Ic} scatterband. At 10.6°C, fracture instability occurred below, within, and above the J_{Ic} scatterband. At 28.9°C, fracture instability occurred within and above the J_{Ic} scatterband. The tendency of increasing toughness with temperature was as expected for these transition regime data. The comparable J_{max} values of the smooth and side-grooved 4T-C(T)'s tested at 10.6°C indicated that side groove effects were properly accounted for by the E 813 J formula. Figures 2, 3, and 4 show the 10.6°C, −8.9°C, and 28.9°C data, respectively, in a J versus crack extension (delta a) format. The sloped dashed line is the 0.15 mm exclusion line of ASTM E 813. The slope solid line is that cited in ASTM E 813 for use in identifying J_{Ic}. The small symbols represent qualified E 813 J-integral single-specimen tearing resistance (J-R) data from specimens which provided valid J_{Ic} data. The large symbols represent J-max and prior stable crack extension at fracture instability from specimen tests that did not satisfy the requirements of ASTM E 813.

The seven fracture instability data above the J_{Ic} scatterband in Fig. 1 were to the right of the E 813 0.15 mm exclusion line as shown in Figs. 2 and 4. J-R data in this region are considered suitable for constructing J versus crack extension curves in ASTM E 813. Hence, the crack extension for these seven data was considered significant. Therefore, these seven fracture instability data were disqualified as inapplicable to the task of defining a J_{max} versus temperature curve for which the effect of crack extension is insignificant.

At the highest test temperature, 28.9°C, it was noted that all data achieved at least the minimum J_{Ic} value prior to fracture instability. Hence, J_{Ic} was considered a candidate lower bound value for fracture toughness which would preclude both fracture instability and significant crack extension at that temperature.

At the middle (10.6°C) and lowest (−8.9°C) test temperatures the remaining fracture instability data for consideration were in and below the J_{Ic} scatterband, Fig. 5. Prior stable crack extension, shown in ( ), was fairly small in that all the fracture instability data lay to the left of the 0.15 mm E 813 exclusion line also shown in Figs. 2 and 3. At both −8.9°C and 10.6°C the average prior stable crack extension of the higher J-max data (within the J_{Ic} scatterband) was more than double that of the lower J-max data (below the J_{Ic} scatterband): 0.18 versus 0.08 mm at −8.9°C and 0.31 versus 0.12 mm at 10.6°C.

Clearly, the prior stable crack extension of the higher J-max data was significant when compared with that of the lower J_{max} data because greater prior stable crack extension gave rise to higher J_{max} values. Therefore, fracture instability of these higher J_{max} data was thought to have occurred after the onset of significant crack extension as defined in the introduction. Consequently, all data for which fracture instability occurred at or before the onset of significant crack extension lay below the J_{Ic} scatterband, Fig. 5.

Effect of Specimen Size on Fracture Response

The fracture instability data (small symbols) and J_{Ic} data (large symbols) of Fig. 5 are repeated in Fig. 6 showing the thickness in ( ). For the data below the J_{Ic} scatterband, no trend relating the thickness and fracture toughness was evident. In other words, all those specimens apparently provided sufficient constraint because no specimen size sensitivity was observed. Conversely, the specimens for which fracture instability data were within the J_{Ic} scatterband appeared to have been less constrained, as discussed next.

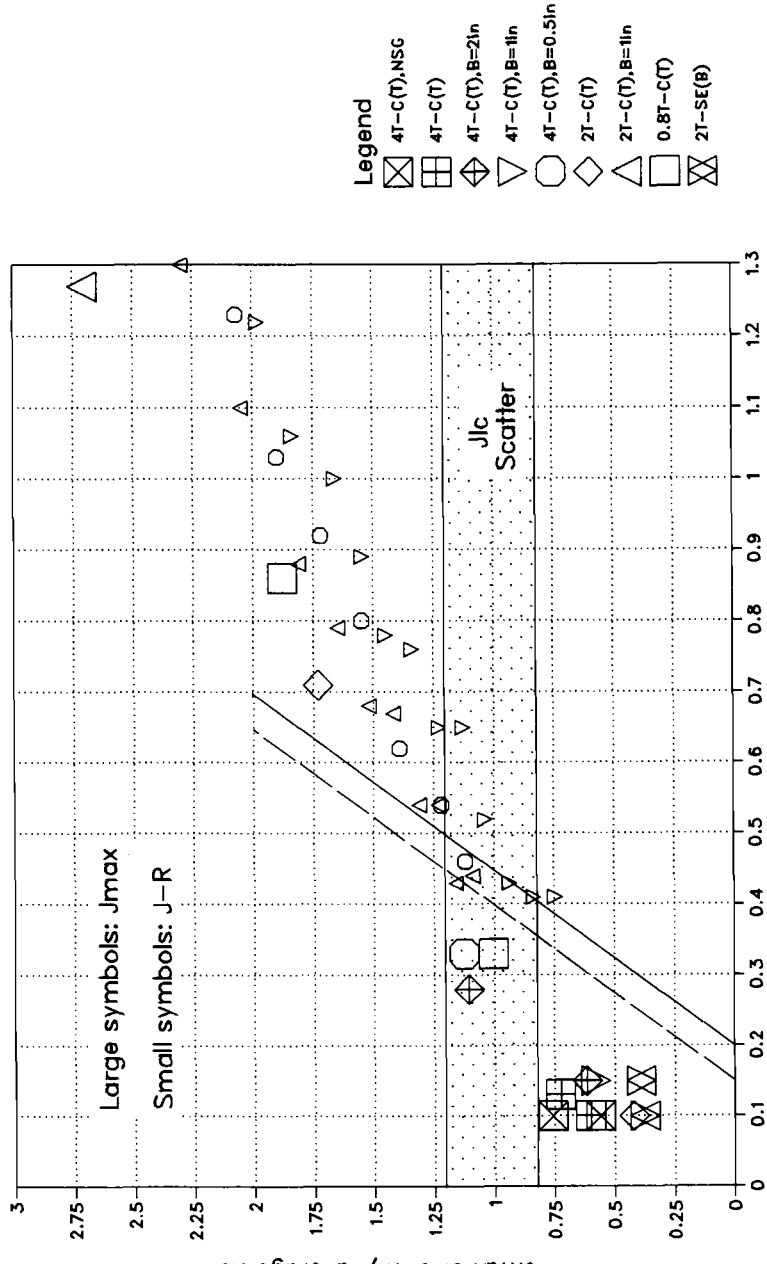

FIG. 2—*A508-C12* J-R *and* J_{max} *versus delta a at 10.6°C.*

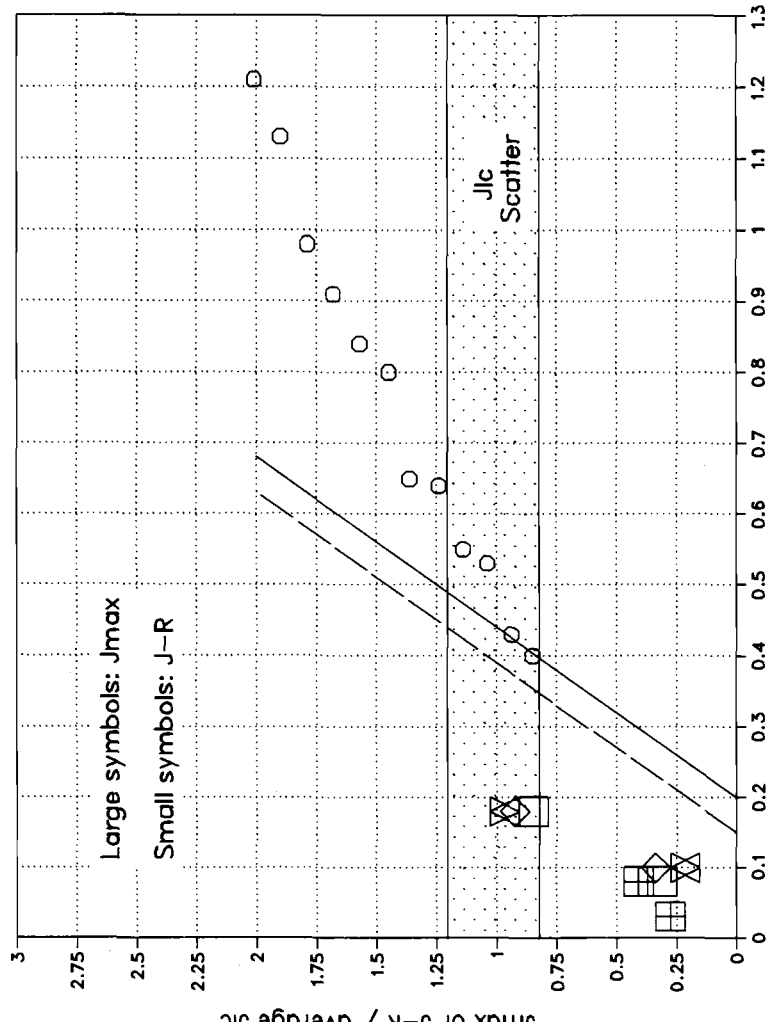

FIG. 3—*A508-C12* J-R *and* J_{max} *versus delta a at* $-8.9°C$.

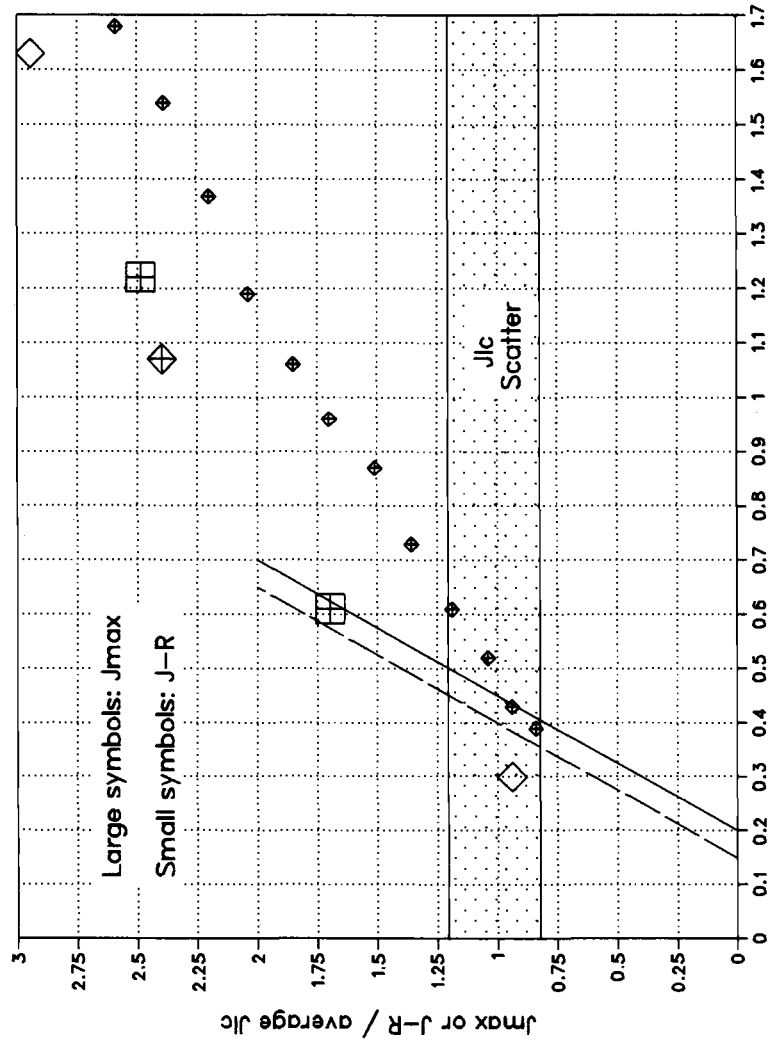

FIG. 4—*A508-Cl2* J-R *and* J_{max} *versus delta a at 28.9°C.*

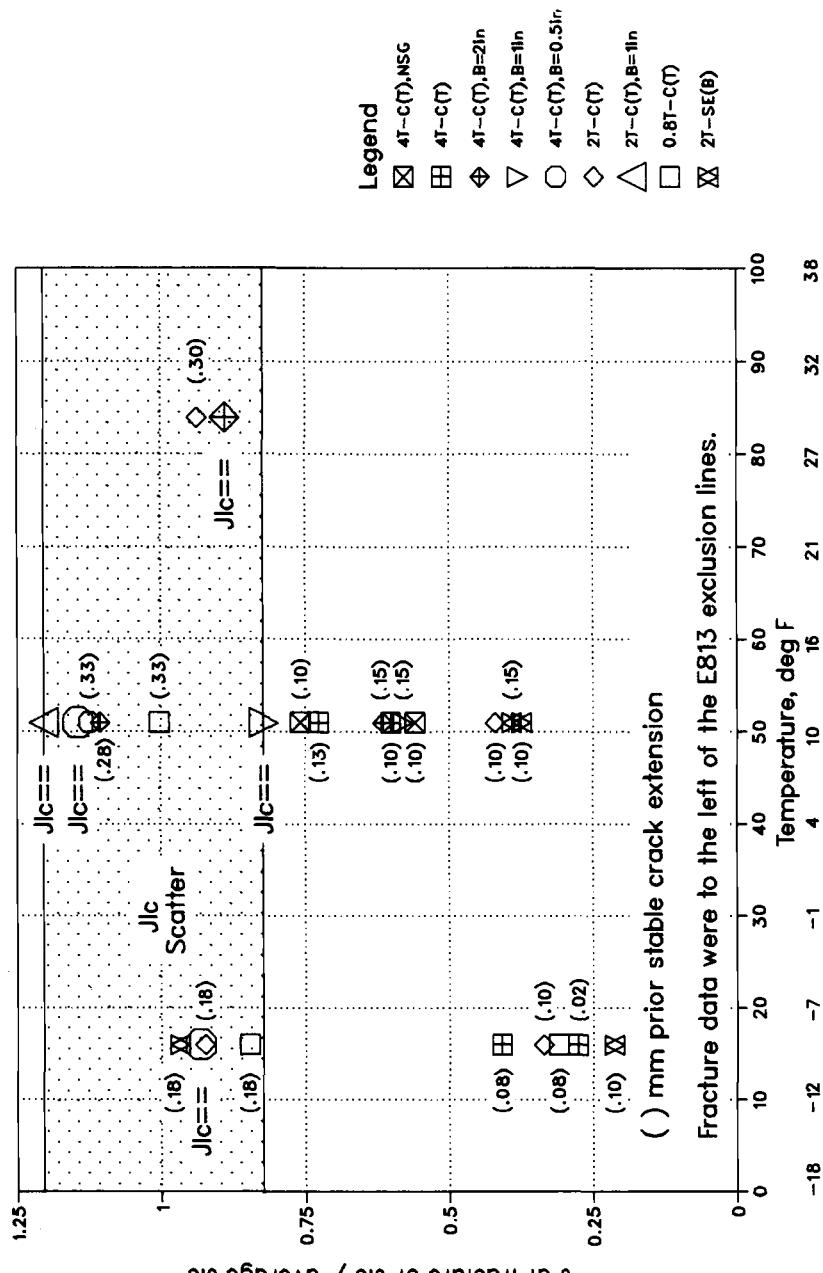

FIG. 5—*A508-C12 J_{max} up to J_{lcmax} versus temperature.*

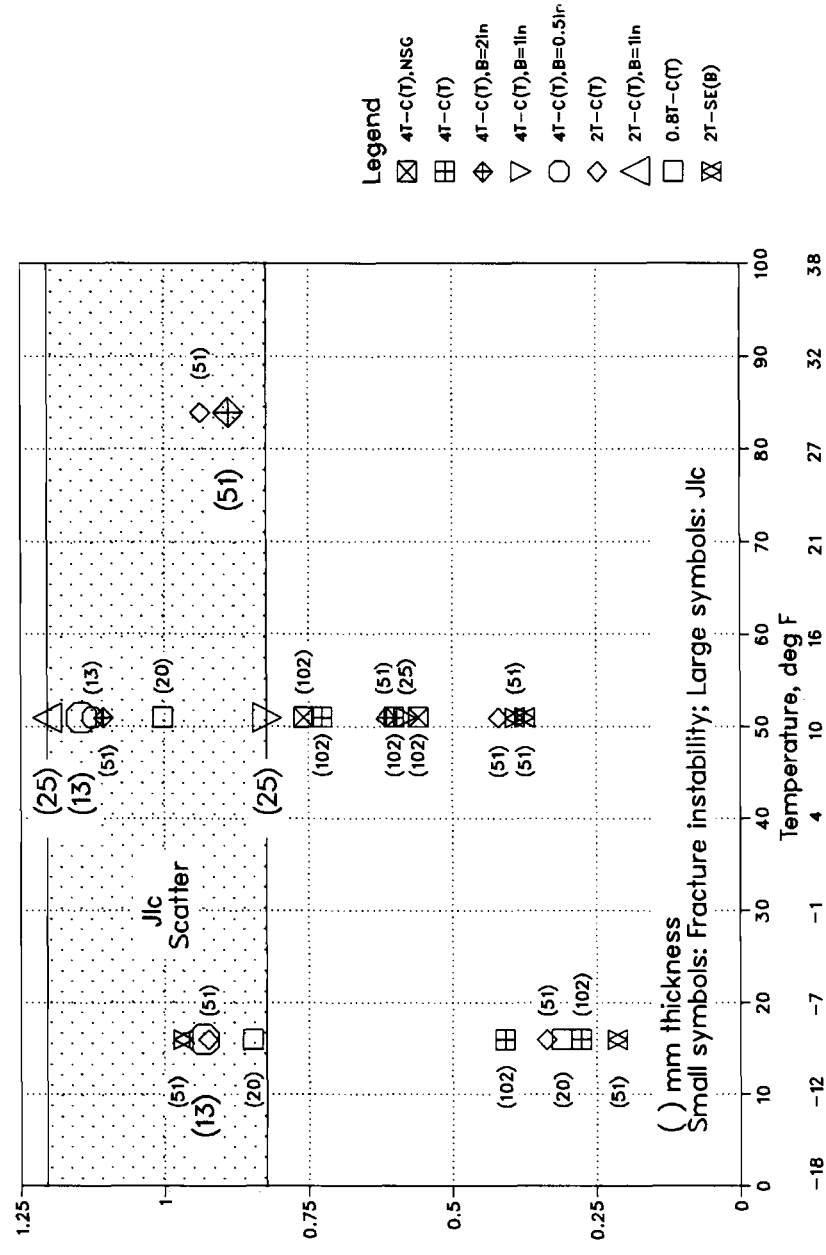

FIG. 6—*Effect of specimen size on fracture response.*

The average thickness of the seven fracture instability specimens within the J_{Ic} scatterband was 37 mm or roughly half that of the 14 specimens below the scatterband, 69 mm. By way of explaining how this affected response, the average thickness of the J_{Ic} specimens was 25 mm. Based on Srawley's and Brown's [2] remarks on thickness effects, the smaller thickness of the J_{Ic} specimens appears to have enhanced plastic flow (or decreased constraint) along the crack front, which decreased the tendency toward fracture instability and encouraged stable crack extension to dissipate the energy applied. For the generally thicker fracture instability specimen data below the J_{Ic} scatterband, the opposite appears to have been true, that is, fracture instability rather than stable crack extension was the preferred means of energy release. The in-between thickness of the fracture instability specimen data within the J_{Ic} scatterband appears to have promoted a response somewhere in between stable tearing and fracture instability prior to the onset of significant crack extension, that is, decreased thickness enhanced plastic flow, which supported increased prior stable crack extension and higher apparent toughness as was noted by Landes and McCabe [3].

Ligament Size Requirements

Based on test data, statistics, and elastic-plastic finite element analysis, Anderson and Dodds [4] concluded that the ligament size requirement of ASTM E 813 should be increased by a factor of eight to assure proper constraint (lack of size effect) in elastic-plastic fracture instability data. That is, ligament size, b, times flow stress, σ_y, divided by J, should exceed 200 rather than 25 as required by the ASTM E 813 test method at J_{max} but should be less than about 900 as required by ASTM E 399 for this material. That quantity, $b \times \sigma_y/J$, is shown in ( ) in Fig. 7 next to the data symbols for all the J_{max} fracture instability values within and below the J_{Ic} scatterband. All $b \times \sigma_y/J$ values met the E 813 requirement. All data within the J_{Ic} scatterband failed the $b \times \sigma_y/J > 200$ requirement, while all data, except one, below the scatterband satisfied that requirement. The exceptional value below the scatterband was 136 for the smallest specimen, 0.8T-C(T), tested at -10.8°C. Its J value was surrounded by those of larger specimens all of which satisfied $b \times \sigma_y > 200$. Its $b \times \sigma_y/J$ value was similar to those of the data within the J_{Ic} scatterband. Again, the aspect ratio for these data was nominally 0.5 so that the proximity effect, if any, of all free surfaces of the crack front should have been about the same. As noted earlier, no thickness, plan size, or ligament size effects were detectable for data below the J_{Ic} scatterband. Hence, in this instance, the J value relative to the J_{Ic} scatterband was a more discriminating means of identifying properly constrained data than the $b \times \sigma_y/J$ value. The J_{max} data above the J_{Ic} scatterband, Fig. 1, had $b \times \sigma_y/J$ values between 22 (0.8T-C(T)) and 119 (4T-C(T)). The 0.8T-C(T) specimen was the only one to fail the ASTM E 813 ligament size requirement, $b \times \sigma_y/J > 25$. The response of the data below the J_{Ic} scatterband was neither that addressed by ASTM E 399 nor E 813. Perhaps a specimen size requirement is needed for elastic-plastic fracture instability data that is different from those for elastic fracture instability or elastic-plastic stable tearing data. However, the value of J_{max} relative to the J_{Ic} scatterband seems more to the point of identifying data that undergo fracture instability prior to significant crack extension.

Summary and Conclusions

The purpose of this work was to identify a fracture instability data qualification limit. Transition regime fracture data were sorted to disqualify those higher J_{max} valued fracture instability data which had exhibited significant prior stable crack extension. Qualified data were identified as having J_{max} values below the J_{Ic} scatterband. Disqualified data had more

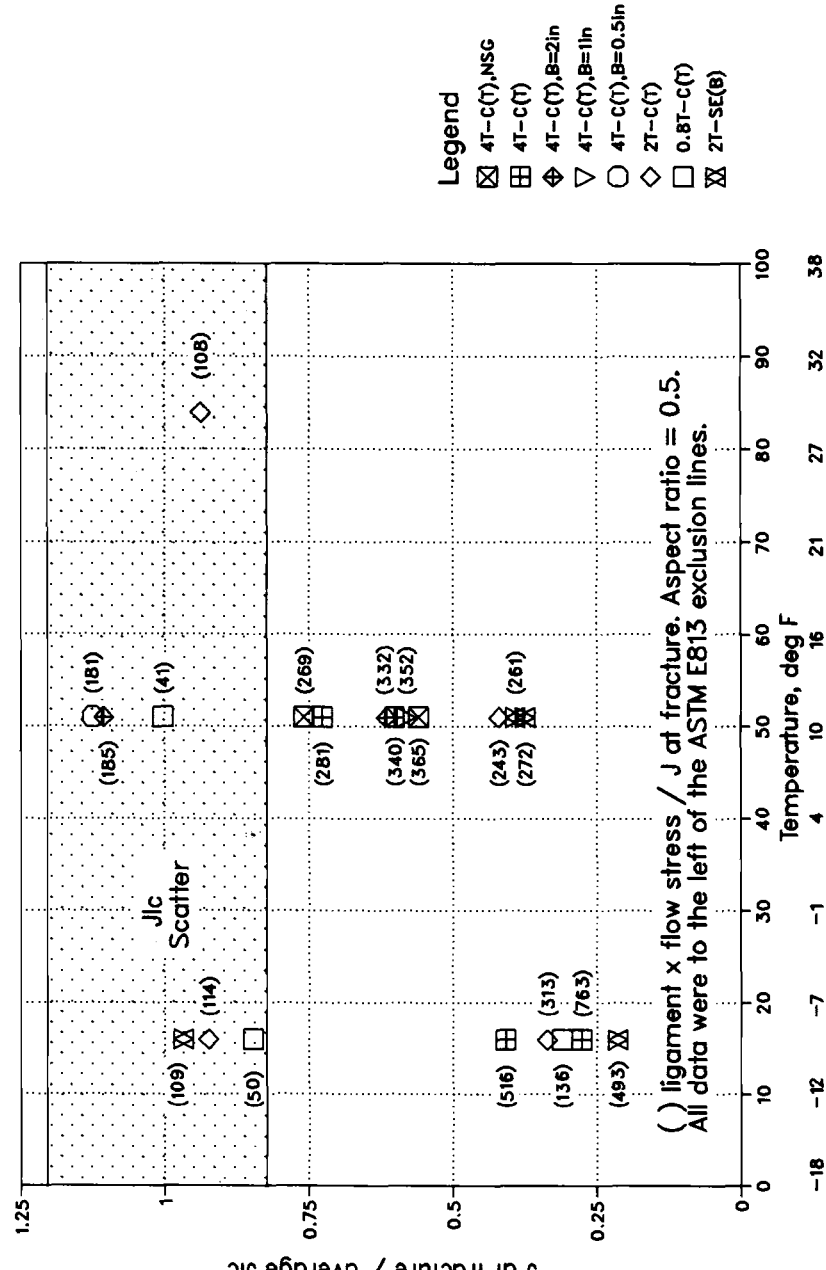

FIG. 7—*Effect of ligament size on fracture response.*

than double the average prior stable crack extension of qualified data and had J_{max} values in or above the J_{Ic} scatterband. The higher J_{max} values and significant crack extension of disqualified data appeared to have been associated with a loss of constraint. The data indicated that a specimen size requirement may be needed for elastic-plastic fracture instability data that is different from those for elastic fracture instability or elastic-plastic tearing onset data. However, the value of J_{max} relative to the J_{Ic} scatterband seems more to the point of identifying data that undergo fracture instability prior to significant crack extension.

Acknowledgments

The authors are indebted to B. A. Myers for rendering the manuscript.

References

[*1*] Landes, J. D. and Begley, J. A. in *Fracture Analysis, ASTM STP 560*, American Society for Testing and Materials, Philadelphia, 1974, pp. 170–186.

[*2*] Srawley, J. E. and Brown, W. F., Jr. in *Fracture Toughness Testing and Its Applications, ASTM STP 381*, American Society for Testing and Materials, Philadelphia, 1965, pp. 133–195.

[*3*] Landes, J. D. and McCabe D. E. in *Fracture Mechanics: Fifteenth Symposium, ASTM STP 833*, American Society for Testing and Materials, Philadelphia, 1984, pp. 378–392.

[*4*] Anderson, T. L. and Dodds, R. H., Jr., private communication and presentation at 2nd Users' Symposium on *J*-Integral Test Methods, Orlando, Florida, 8–9 Nov. 1989.

Monir H. Sharobeam,[1] *John D. Landes,*[1] *and Ruben Herrera*[1]

Development of Eta Factors in Elastic-Plastic Fracture Testing Using a Load Separation Technique

REFERENCE: Sharobeam, M. H., Landes, J. D., and Herrera, R., **"Development of Eta Factors in Elastic-Plastic Fracture Testing Using a Load Separation Technique,"** *Elastic-Plastic Fracture Test Methods: The User's Experience (Second Volume), ASTM STP 1114*, J. A. Joyce, Ed., American Society for Testing and Materials, Philadelphia, 1991, pp. 114–132.

ABSTRACT: A method for experimentally determining the eta (η) factor based on separation constants has been recently proposed. This method has two important implications for elastic-plastic fracture toughness testing. First, the method can be used to determine the η factors for any new test specimen geometry which might be added to existing test standards. Such specimens as disk compact, arc bend, and arc tension are used in the K_{Ic} test standard. They can be added to the J based standards if the specimen calibrations are known, one being the η factor calibration. In this paper a step by step procedure is given describing η factor calibration for an arbitrary specimen geometry based on a series of blunt notched specimens.

The procedure proposed in this paper was then applied to existing blunt notch data for the traditional test specimen geometries, the compact, and single edge notched bend specimens. The results of the study show different values for η from these in the existing standards both in magnitude and trend with a/W. In addition they show a slight material sensitivity. The consequences of having incorrect η factors in the test standards are explored in a sensitivity study. These results are used to evaluate the importance of having correct η factors and recommendations are made.

KEY WORDS: ductile fracture, eta factor, load separation, blunt notch testing, standard test method, J-integral

In late 1960s, Rice [*1,2*] proposed the J-integral as a new parameter that characterizes crack tip singularity in elastic-plastic fracture behavior of metals. Since then, one concern is the development of successful experimental technique to evaluate J. The early approach, introducted by Landes and Begley [*3,4*] based on the energy rate interpretation of J, requires the testing of many identical blunt notched specimens of different crack lengths in order to establish the energy-crack length relationship, from which J is evaluated. Despite the reliability and the theoretical basis of this technique, it was not very successful because of the high cost and time required for specimen preparation and testing. A new technique that requires the testing of only one specimen succeeded the old technique and was widely accepted. It is based on the assumption that the load can be represented as the multiplication of two separate functions; a crack geometry function and a material deformation function. This separable form, which was first proposed by Rice et al. [*5*], brought a new definition of J as a factor, defined later as η, times the area under the load-displacement record per unit uncracked ligament area. Hence, J can be evaluated by testing one specimen if this factor is known for the specimen configuration. This concept is important in the development

[1]Graduate assistant, professor, and research associate, respectively, University of Tennessee, Knoxville, TN 37996. Mr. Herrera is presently professor at National University of Mar Del Plata, Argentina.

of standard test methods where all calculations of J are made using area under a load versus displacement record. However, the values of η used in current test methods do not have a well established basis in analysis or experimental work. Rather present values of η evolved through a series of approximate analyses and experimental results. When a test standard was written, the best available values of η at that time were incorporated. No further development work was done on η until recently. The next section follows the evolution of the η value development from the early work of Rice until the present.

Historical η Development

Historically, the first value for the η was 2. It was derived by Rice et al. [5] for deeply cracked bend specimen. This was not completely accurate for specimens that were not purely loaded in bending. Merkle and Corten [6] developed an analysis that accounts for the small tension component in the compact specimen. They concluded that J for a specimen of unit thickness can be represented as

$$J = \left[\frac{2(1 + \alpha)}{1 + \alpha^2}\right]\left[\frac{A}{b}\right] \tag{1}$$

where

$$\alpha = \left[\left(\frac{2a}{b}\right)^2 + 2\left(\frac{2a}{b}\right) + 2\right]^{1/2} - \left(\frac{2a}{b} + 1\right) \tag{2}$$

A = area under the load displacement record,
a = crack length, and
b = uncracked ligament.

Equation 1 implies that the η factor for the compact specimen is $[2(1 + \alpha)/(1 + \alpha^2)]$.

Landes et al. [7] conducted an experimental evaluation of η in which they tested blunt notched specimens of different crack lengths. Their analysis used the energy rate interpretation to infer values of η. The goal was to determine which of the values of η proposed at that time best fit their experimental results. No value of η fit over the entire range of crack lengths; however, the Merkle-Corten equation best approximated their results. Rather than suggesting a new equation for η, they recommended the Merkle-Corten value and this then became widely accepted.

Following this work Clarke and Landes [8] concluded that using a single η ($\eta = \eta_{el} = \eta_{pl}$) for the compact specimen yielded J values that agree well with the multispecimen technique with η closely approximated by the following equation

$$\eta = 2 + 0.522\,\frac{b}{W} \tag{3}$$

where, W is the specimen width. The value of η in Eq 3 comes from a linear fit to the Merkle-Corten expression in Eqs 1 and 2.

Rice et al. [5] proposed splitting J into elastic and plastic portions; J_{el} and J_{pl}. This was later generalized by Sumpter and Turner [9], into a new form that agrees with the single specimen technique as

$$J = \eta_{el}\frac{A_{el}}{b} + \eta_{pl}\frac{A_{pl}}{b} \tag{4}$$

where A_{el} and A_{pl} are the elastic and plastic parts of the area under the load-displacement record. This was the first time that separate multiplication factors and J components were used. This approach later became accepted in all of the test standards.

Ernst and Paris [*10*] proved that η exists only if the load is represented by a separable form. This is true by definition in the elastic behavior because of the linearity of the load-displacement record. η_{el} is shown to be

$$\eta_{el} = \frac{b}{C}\frac{dC}{da} \tag{5}$$

where C is the compliance which is a function only of the crack length. For the plastic region, they suggested using the η value of Clarke and Landes because this was the most reasonable estimate at that time.

Using the η of Eq 3 for η_{pl}, the corresponding separable form for the load in the plastic region for the compact specimen will be

$$P = B\left\{\frac{b^2}{W}\cdot \exp\left(0.522\,\frac{b}{W}\right)\right\}\left\{H\left(v_{pl}\right)\right\} \tag{6}$$

where

P = load,
B = thickness,
v_{pl} = plastic displacement, and
$H(v_{pl})$ = deformation function.

This form can be rewritten for unit thickness as

$$P = G\left(\frac{a}{W}\right)H(v_{pl}) \tag{7}$$

where $G(a/W)$ is the crack geometry function.

The ASTM Standard Test Methods for J_{Ic}, a Measure of Fracture Toughness (E 813) and for Determining J-R Curves (E 1152) require the estimation of J as the sum of J_{el} and J_{pl} with J_{pl} represented as

$$J_{pl} = \frac{\eta_{pl}}{Bb}A_{pl} \tag{8}$$

where

$$\eta_{pl} = 2$$

for bend specimen

$$= 2 + 0.522\,\frac{b}{W}$$

for compact specimen.

These values were taken from the best available values at the time these test standards were written and no additional development work was done.

Briefly, the assumption of the load separation introduced the new J definition and the associated η factor. The assumption did not evolve as an exact theoretical solution, but mainly from the need to develop a single specimen technique to evaluate J. The agreement between both techniques provided the only basis to use the new J form.

Recently, Sharobeam and Landes [*11–12*] studied the load-displacement records of previously tested specimens of four different geometries and six different materials. For both plane strain and plane stress constraint, they demonstrated the load separation in the plastic region except for a small region at the beginning of the plastic behavior. This established a more solid experimental basis for the single specimen form and its associated η factor.

η-Calculation

The η factor can be evaluated only by comparing the single specimen form

$$J = \frac{\eta}{bB} \int P dv \tag{9}$$

with one of the other two forms; the contour line integral form

$$J = \int_\Gamma \left(W dy - T_i \frac{\partial u_i}{\partial x} dS \right) \tag{10}$$

or the energy rate interpretation form

$$J = \frac{-1}{B} \frac{dU}{da} \tag{11}$$

where U is the potential energy. This can be implemented analytically, numerically, or experimentally with one exception that the contour integral form cannot be evaluated experimentally for standard specimens. For all solutions, the load displacement records have to be defined. Also, either the strain energy and stress vector variations over a certain contour, or the change of the load-displacement record with the crack length have to be provided. This can be as lengthy and approximate as an analytical solution. Numerical methods, such as finite elements, can give better results but may not match the experimental results because the assumptions used in the numerical solution may not accurately model the real specimen behavior. However, the main objective of this paper is to evaluate η from the experimental data. This can be done [*7*] by comparing the single specimen form of Eq 9 with the energy rate interpretation form of Eq 11, which yields

$$\eta = b \cdot \left(- \frac{dU}{da} \right) \Big/ \left(\int P dv \right) \tag{12a}$$

This requires the testing of many identical specimens with different crack lengths, evaluating the area under the load displacement records at different displacements, constructing the area-crack length fit for different displacements, then calculating the slopes of the constructed curves for different displacement at different crack lengths, and finally substituting the slope and corresponding area values in Eq 12*a*. This is the classical method for evaluating η from experimental data. In case of η_{pl} evaluation, only the plastic areas under the test records have to be included. Equation 12*a* can be modified for the plastic region as

$$\eta_{pl} = b \left(- dU_{pl}/da \right) / \left(\int P dv_{pl} \right) \tag{12b}$$

where U_{pl} is the plastic potential energy. In the classical method, the successive estimation of the area under the load-displacement record usually accumulates errors. Then fitting the data to evaluate the slope and dividing again by the area may add additional errors to the process. Also it is proved experimentally that there is a limited nonseparable region in the beginning of the plastic behavior. This may result in a significant error in η_{pl} value because the single specimen form is based on the assumption that the load is completely separable.

Sharobeam and Landes [*11*] have introduced a new method to evaluate η_{pl} from the experimental data using the separation criterion. This method avoids most of the mentioned sources of errors and gives consistent η_{pl} values. Figure 1 illustrates the separation criterion for two test records of different stationary crack lengths; a_i and a_j. The ratio $P(a_i)/P(a_j)$ maintains a constant value over all of the domain of the plastic displacement if the load is separable. Mathematically, this can be explained as

$$S_{ij} = \left.\frac{P(a_i)}{P(a_j)}\right|_{\upsilon_{pl}} = \left.\frac{G(a_i/W) \cdot H(\upsilon_{pl}/W)}{G(a_j/W) \cdot H(\upsilon_{pl}/W)}\right|_{\upsilon_{pl}}$$

$$= \frac{G(a_i/W)}{G(a_j/W)} \tag{13}$$

$$= \text{constant}$$

for stationary cracks.

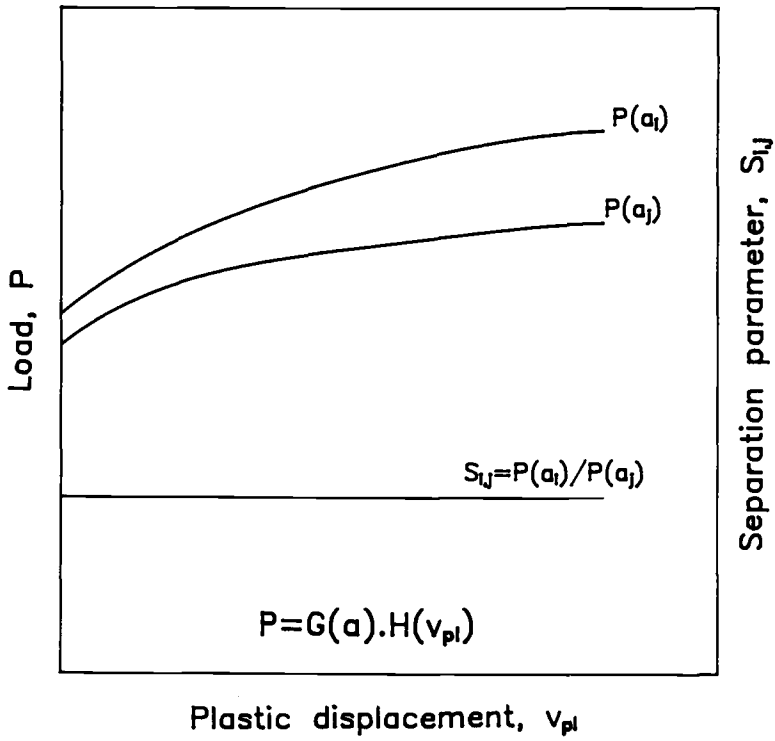

FIG. 1—*Load separation in the plastic region.*

As mentioned before, this has been investigated for wide combinations of materials, configurations, and constraints. As examples, Figs. 2 and 3 show the test records and separation parameters for blunt notched specimens of two geometries compact and center cracked tension respectively. The test records were originally reported in Ref 7. The specimens are machined from HY130 steel with 2.29 cm (0.9 in.) thickness and 5.08 cm (2 in.) width, and they are blunt notched with crack to width ratio varying from 0.4 to 0.85. A test record of intermediate crack length can be chosen as a reference record (a_j/W) to demonstrate the load separation, as shown in Eq 13.

As mentioned before, η_{pl} can be evaluated from experimental data by comparing the single specimen form with the energy rate form. Substituting Eq 7 into Eq 12*b* results

$$\eta_{pl} = -\frac{G'(a/W)}{G(a/W)} \cdot \frac{b}{W} \tag{14}$$

where

$$G'(a/W) = \frac{dG'(a/W)}{d(a/W)} = -\frac{dG'(b/W)}{d(b/W)}$$

Equation 14 can be also written as

$$\eta_{pl} = \frac{dG(b/W)/d(b/W)}{G(b/W)} \cdot \frac{b}{W} \tag{15}$$

The separation parameter $S_{i,j}$ has been defined as the ratio of the geometry functions of two stationary crack lengths; a_i and a_j, Eq 13. Then, for the same reference crack length a_j, and different a_i, Eq 13 will be a proportional relationship between the separation parameter $S_{i,j}$ and the geometry function $G(a_i/W)$

$$S_{i,j} = A \cdot G(a_i/W) \tag{16}$$

where A is a constant.

This means that constructing the $S_{i,j}$ versus a_i/W (or b_i/W) fit will establish the $G(b_i/W)$ versus b_i/W relationship. Then η_{pl} can be evaluated using Eq 15. The $S_{i,j}$ versus b_i/W fit is very likely to be a power law. Figures 4*a* and *b* show the relationship between the separation parameter $S_{i,j}$ and the uncracked ligament b_i/W for the previously mentioned test records on logarithmic coordinates. It is clear that the power law fit is a good candidate for this relationship. Figures 4*c* and *d* show how close the power law fits these data. Also, Table 1 shows a survey of the different materials, configurations, constraints, and crack length ranges that have been studied in Ref *11* and *12*. All the studied cases, except the A106 steel set, showed a power law fit. Therefore, the geometry function is a power law function and can be represented as

$$G(b/W) = C \cdot (b/W)^m \tag{17}$$

where C is a constant. Hence, Eq 15 yields

$$\eta_{pl} = m$$

The new η_{pl} method is simple, especially when $G(b/W)$ is well represented by a power law function. Figure 5 shows a schematic of the new η_{pl} method. This method avoids the ac-

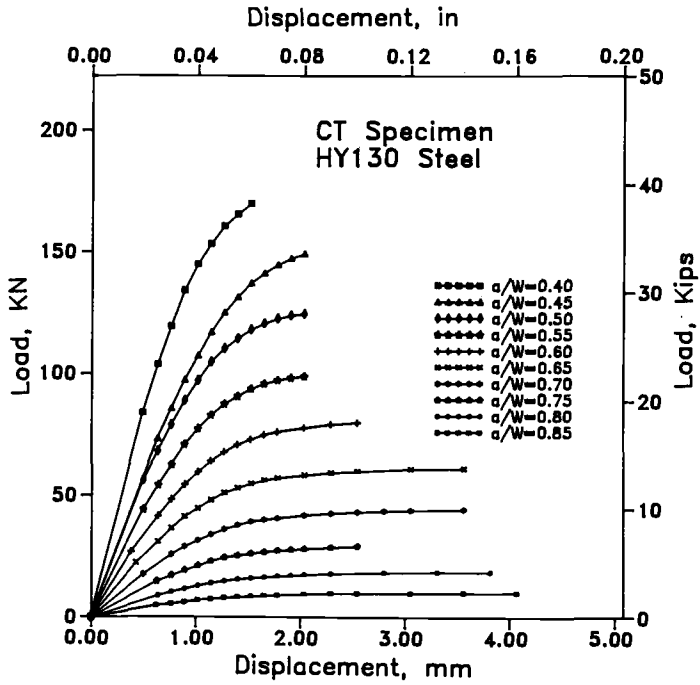

FIG. 2a—*Test records of blunt notched compact specimens.*

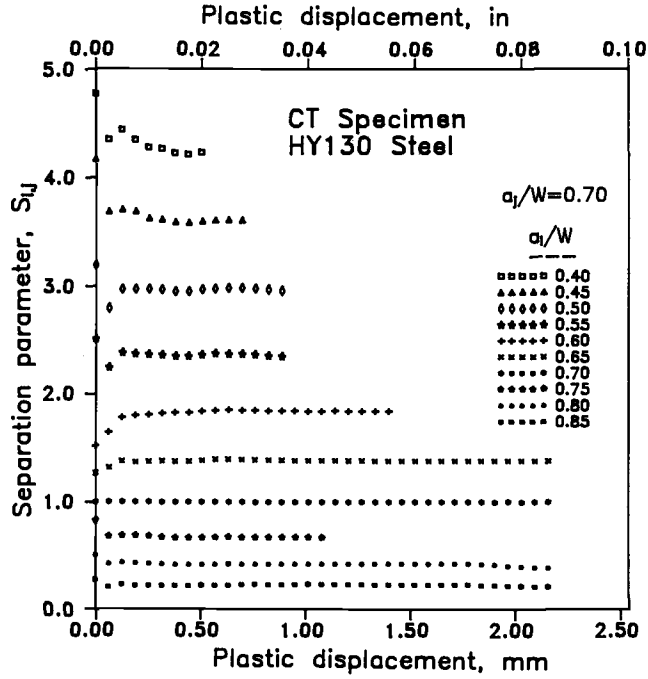

FIG. 2b—*Separation of the compact specimens test records in the plastic region.*

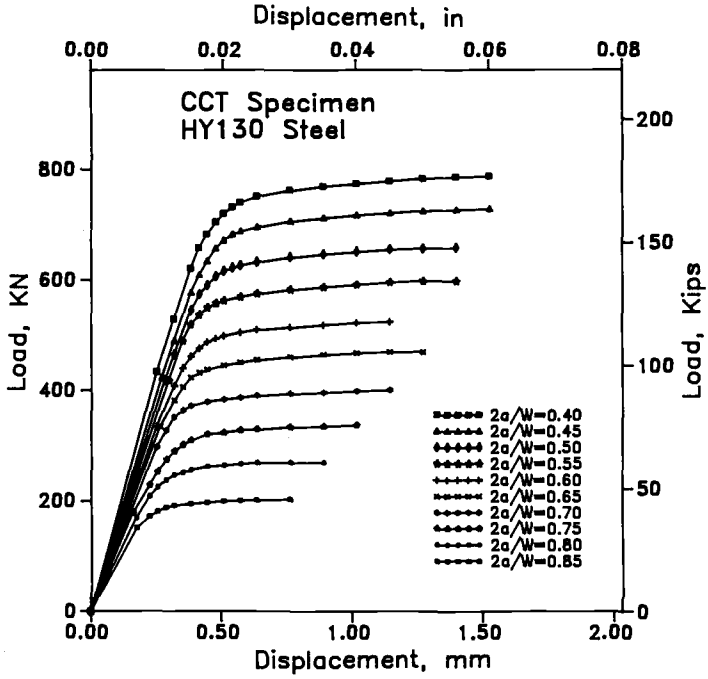

FIG. 3*a*—*Test records of center cracked tension specimens—blunt notched.*

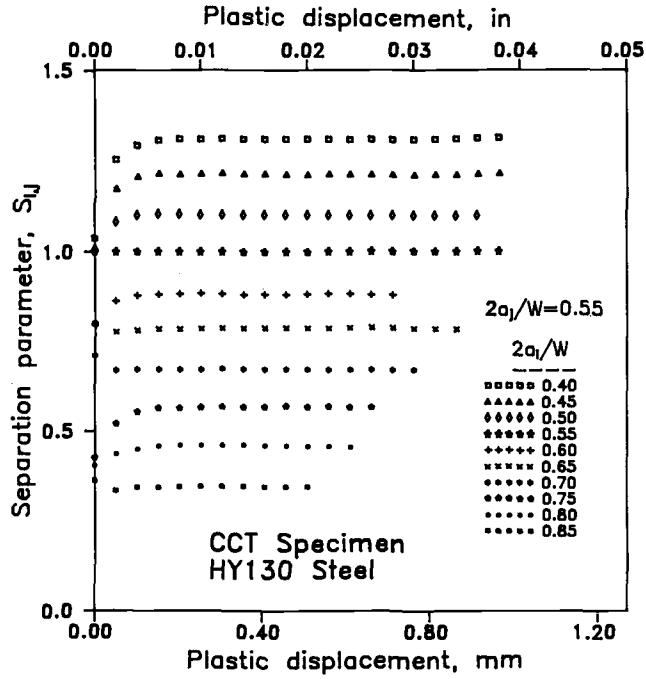

FIG. 3*b*—*Separation of the center cracked tension specimens test records in the plastic region.*

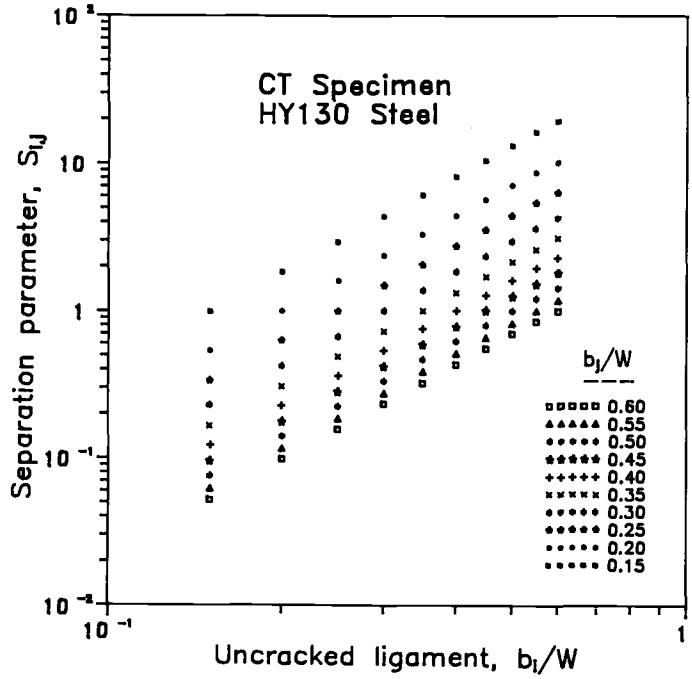

FIG. 4*a*—*Separation constants versus the uncracked ligament on logarithmic coordinates.*

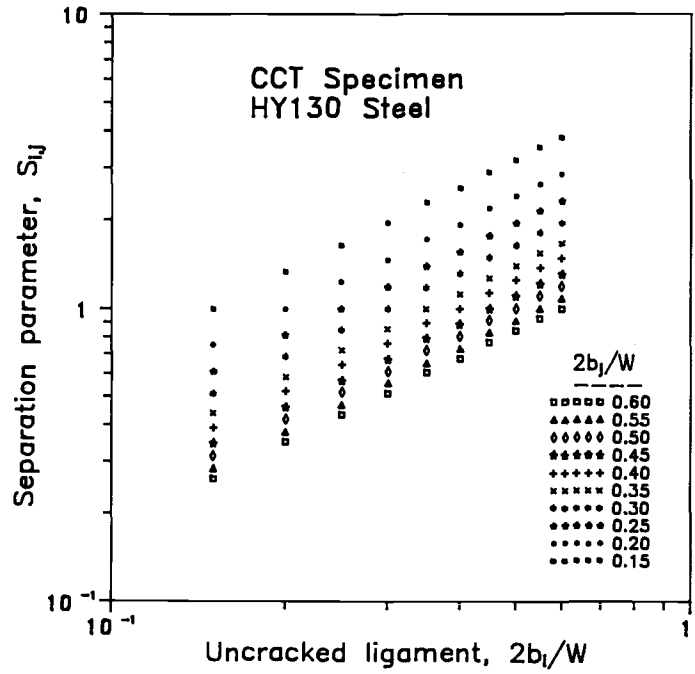

FIG. 4*b*—*Separation constants versus the uncracked ligament on logarithmic coordinates.*

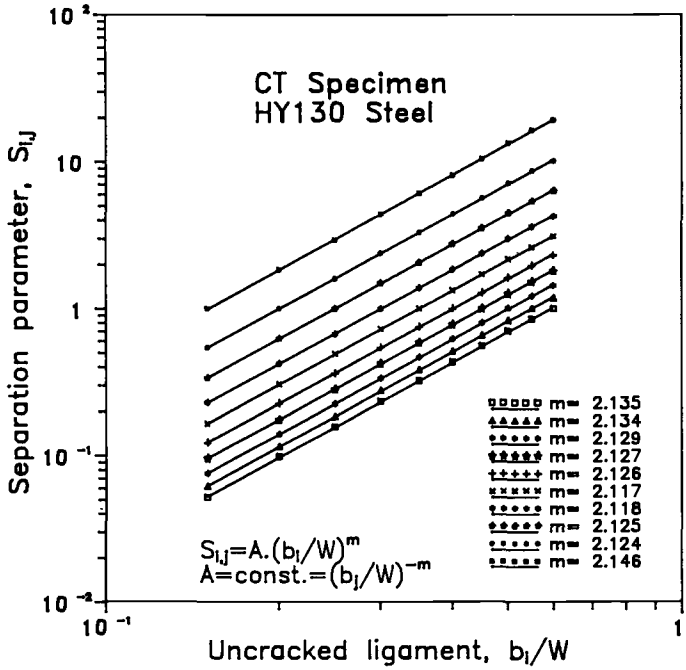

FIG. 4*c*—$S_{i,j}$-b_i/W *power law fit with respect to different* b_j/W *values.*

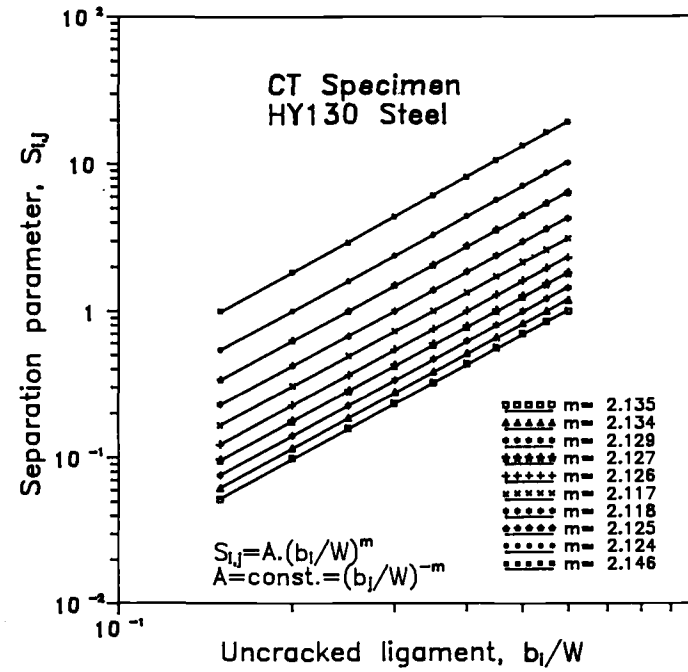

FIG. 4*d*—$S_{i,j}$-b_i/W *power law fit with respect to different* b_j/W *values.*

TABLE 1—*Survey of different stationary crack sets studied in Ref* 12 *and* 13.

Geometry	Material	Dimensions and Constraints	Crack length range	Power law index	Source of data
1. Compact	HY130	W = 50 mm B = 22.9 mm no side groove	a/W = 0.4 to 0.85 (10 specimens)	2.13	Westinghouse, Ref *7*
2. Center cracked tension	HY130	W = 50 mm B = 22.9 mm no side groove	a/W = 0.4 to 0.85 (10 specimens)	0.963	Westinghouse, Ref *7*
3. Single edge notched bend	HY130	W = 50 mm B = 22.9 mm span = 4 W no side groove	a/W = 0.4 to 0.85 (10 specimens)	1.94	Westinghouse, Ref *7*
4. Compact	HSLA80	W = 51 mm B = W/2 20% side groove	a/W = 0.65 to 0.758 (3 specimens)	2.32	Hackett and Joyce, Ref *13*
5. Compact	HY80	W = 51 mm B = W/2 20% side groove	a/W = 0.603 to 0.756 (3 specimens)	2.25	Hackett and Joyce, Ref *13*
6. Compact	A533B	W = 51 B = W/2 20% side groove	a/W = 0.608 to 0.729 (3 specimens)	2.17	Hackett and Joyce, Ref *13*
7. Compact	A106	W = 51 B = W/2 20% side groove	a/W = 0.703 to 0.806 (3 specimens)	2.11 (bad fit)	Hackett and Joyce, Ref *13*
8. Single edge notched tension	A533B	W = 76 mm B = 2.5 mm no side groove	a/W = 0.2 to 0.8 (7 specimens)	2.44	Westinghouse, Ref *14*
9. Single edge notched tension	A710	W = 152 mm B = 2.5 mm no side groove	a/W = 0.2 to 0.7 (6 specimens)	2.37	Westinghouse, Ref *15*
10. Single edge notched tension	A710	W = 152 mm B = 25.4 mm no side groove	a/W = 0.5 to 0.7 (3 specimens)	2.33	Westinghouse, Ref *15*
11. Single edge notched tension	A710	W = 152 mm B = 25.4 mm 20% side groove	a/W = 0.4 to 0.7 (3 specimens)	2.32	Westinghouse, Ref *15*
12. Single edge notched tension	A710	W = 152 mm B = 25.4 mm 50% side groove	a/W = 0.3 to 0.7 (3 specimens)	2.42	Westinghouse, Ref *15*

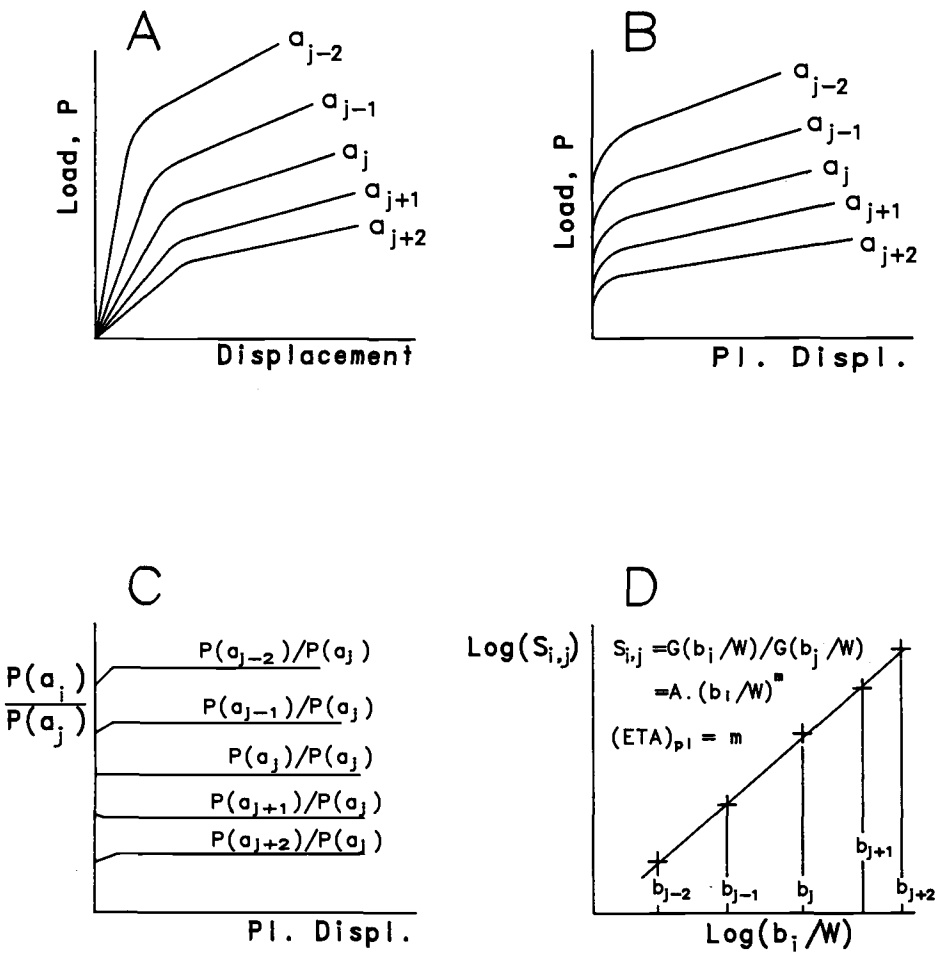

FIG. 5—*Flow chart of the new* η_{pl} *method.*

cumulation and amplification of approximation errors in the classical method. Also it does not gain any error from the nonseparable region. The portion of the area that exists in the nonseparable region causes a significant error in the classical method η_{pl} values, especially for low plastic displacement values. These errors converge slowly after the separation starts. Figures 6*a* and *b* show how long it takes the classical η_{pl} values to converge after the separation starts, for the previously mentioned geometries.

Generally, the new method η_{pl} values are more accurate and consistent. Table 2 shows the η_{pl} values of each method for the mentioned compact and center cracked tension specimen sets and also a single edge notched bend specimens set. The bend specimens were machined from the same material with the same width and thickness and with a span to width ratio of 4.0. The classical η_{pl} values have been chosen after they had reasonably converged.

Many geometries such as; single edge notched tension, disk compact, arc bend, arc tension, and others, have been excluded from the *J*-integral based standard test methods because of the absence of an effective method to evaluate η. But because of the simplicity and con-

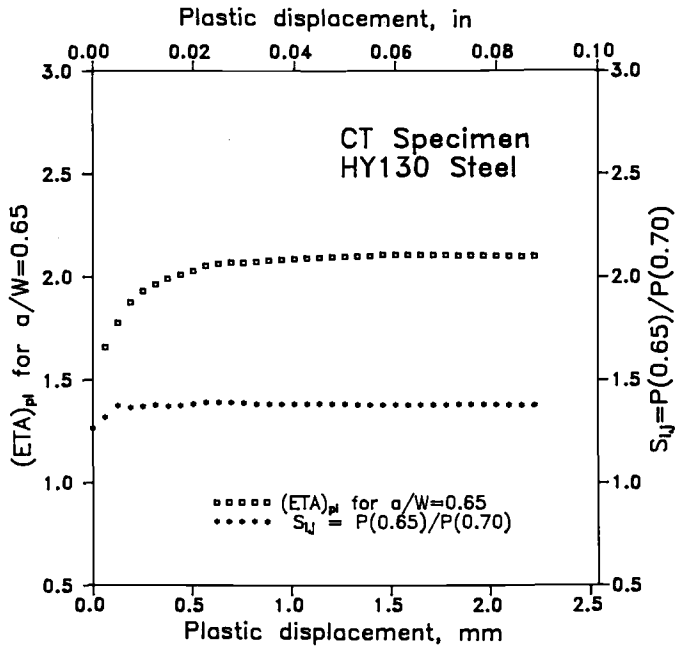

FIG. 6*a*—*Effect of the unseparable region on* η_{pl} *in compact specimen.*

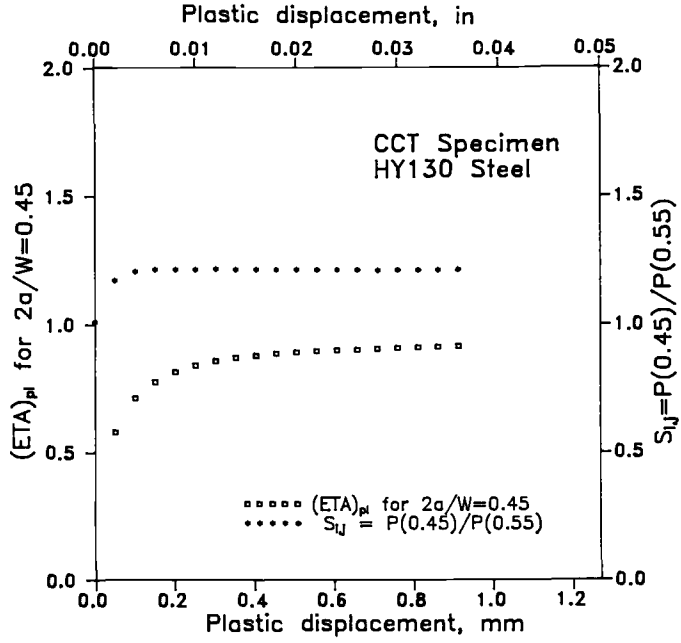

FIG. 6*b*—*Effect of the nonseparable region on* η_{pl} *in center cracked tension specimens.*

TABLE 2—*Comparison of* η_{pl} *values using both methods.*

	Compact		Center Cracked		Bend	
a/W[a]	Classical[b]	New[c]	Classical	New	Classical	New
0.45	2.11	2.13	0.90	0.963	1.85	1.94
0.55	2.20	2.13	0.95	0.963	1.97	1.94
0.65	2.08	2.13	0.91	0.963	1.92	1.94
0.75	2.14	2.13	1.00	0.963	1.89	1.94

[a] $2a/W$ for center cracked tension specimens.
[b] Using Eq 11.
[c] Using the load separation technique.

sistency of the new method, many of these geometries can be included. For example, Table 1 shows five different sets of single edge notched tension specimens have been studied as a new geometry candidate. These data have been reported in Refs *14* and *15*. The step by step evaluation of η_{pl} for one of these sets is shown in Figs. 7*a*, *b*, and *c*. The specimens are 7.62 cm (3 in.) wide and 0.25 cm (0.1 in.) thick and they are machined from A533B steel. They were prepared with blunt notch crack with length to width ratio varying from $a/W = 0.2$ to $a/W = 0.8$. The power law fit results are shown on Fig. 7*d*.

The other four sets were machined from the A710 steel with 15.24 cm (6 in.) width but with different thickness constraints. η_{pl} value did not show much change between the 0.25 cm (0.1 in.) thickness set which is a pure plane stress case and the 2.54 cm (1.0 in.) thickness set even with a 20 or 50% side grooving which intensifies the plane strain constraint. This may suggest that η_{pl} does not change considerably with the change of the constraint in the single edge notched tension configuration.

J-Calculations

The η_{pl} formulas for J_{pl} used in the standard test method are given with Eq 8. These were based on the best available solutions at the time the standard was written. The results of the blunt notched experiments analyzed by load separation suggests that these formulas may not be correct. The importance of this difference can best be evaluated by how it influences *J*-calculations. This will be done for the compact geometry.

The formula for η_{pl} used in the standard test method for η_{pl} shows a function which decreases gradually with increasing a/W, reaching a value of 2.0 as a/W approaches 1.0. The value of η_{pl} from the load separation suggests that η_{pl} is nearly constant, and not a function of a/W. For the comparisons made in this paper a value of $\eta_{pl} = 2.15$ was used for the load separation. The η_{pl} from the test method $\eta_{pl} = 2 + 0.522\ b/W$ ranges from about 2.26 to 2.10 in the typical range of a/W used for testing ($0.5 < a/W < 0.8$). The two different values are nearly identical and the effect on *J*-calculations would be expected to be minimal.

An example of *J-R* curves calculated by the two different η_{pl} values is shown in Fig. 8 for an A106 steel and in Fig. 9 for an A508 steel. Neither calculation shows much of a difference in the *J-R* curves. The A508 steel shows a greater difference, presumably because it is more ductile and has a higher J_{pl} component. In contrast to the difference in *J-R* curve caused by a different η_{pl}, the error caused in the *J-R* curve evaluation by an incorrect measure of crack length is illustrated in Fig. 10. Here the crack length measured by elastic compliance did not match the physically measured crack length. This shows a much greater difference in *R* curve. The point illustrated in Fig. 10 is that other factors in the *J-R* curve evaluation can influence its value much more than the choice of η_{pl}, at least for the compact specimen. For

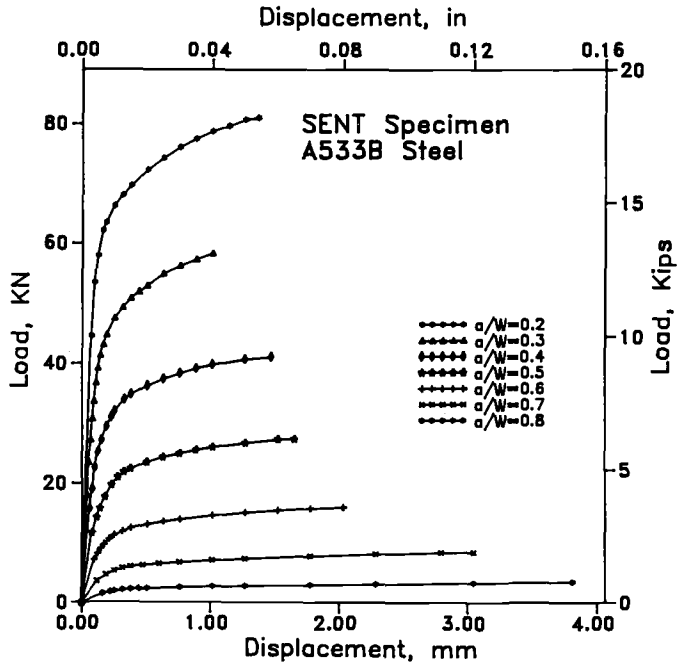

FIG. 7a—*Test records of single edge tension specimens—blunt notched.*

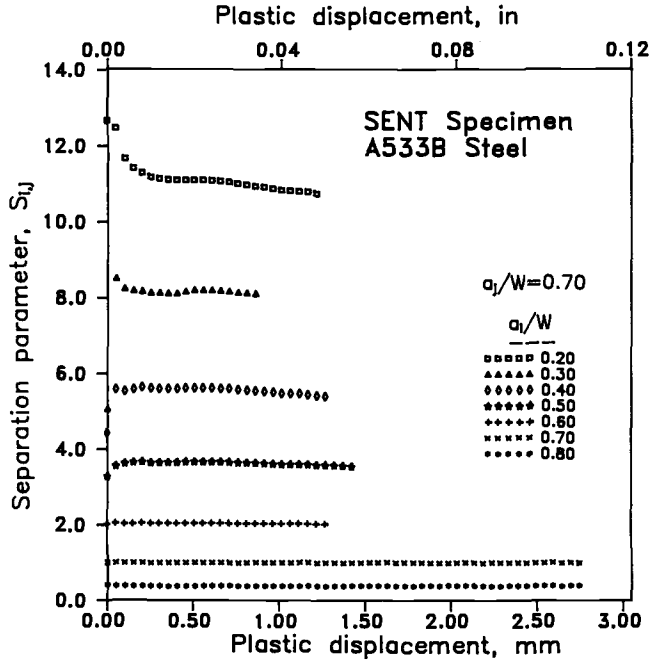

FIG. 7b—*Separation of single edge notched tension specimens test records in the plastic region.*

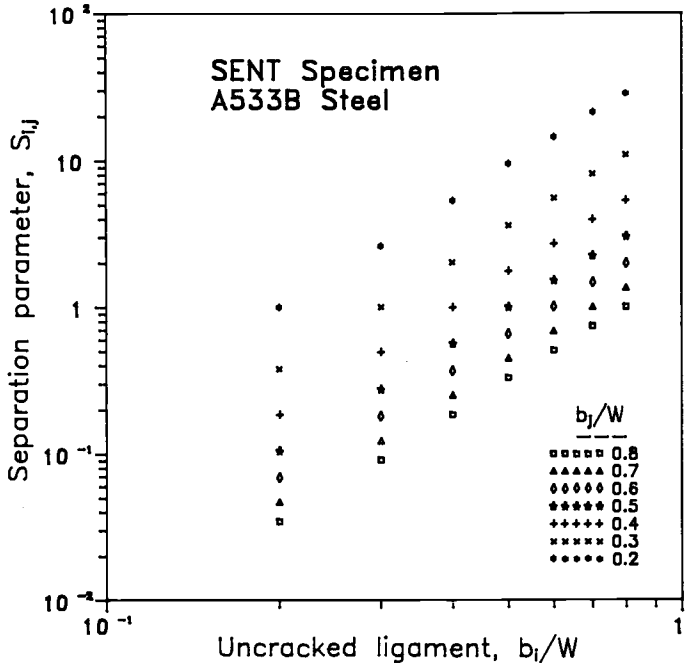

FIG. 7c—*Separation constants versus the uncracked ligament on logarithmic coordinates.*

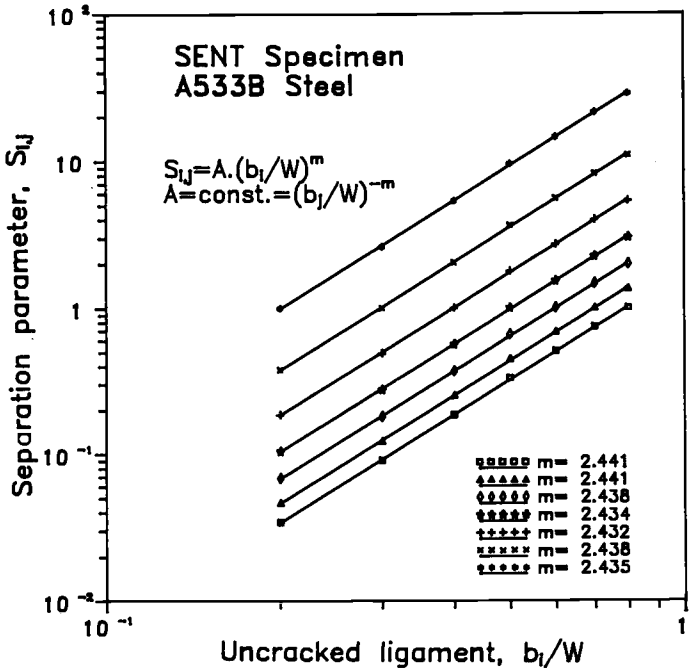

FIG. 7d—$S_{i,j}$-b_i/W *power law fit with respect to different* b_j/W *values.*

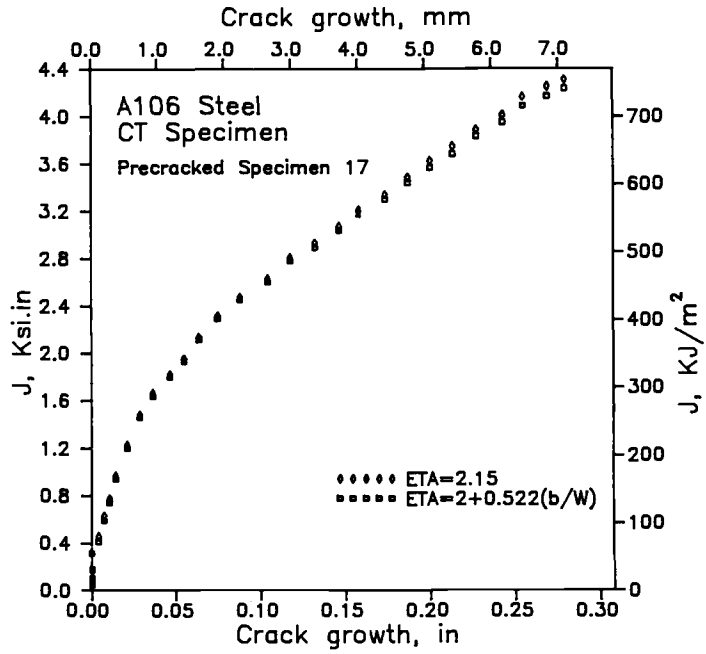

FIG. 8—*Effect of different* η_{pl} *values on A106* J-R *curve.*

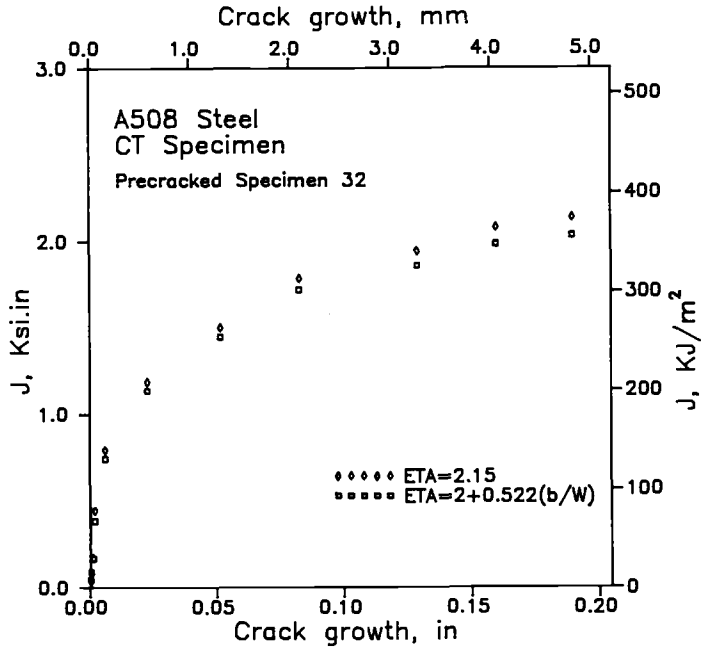

FIG. 9—*Effect of different* η_{pl} *values on A508* J-R *curve.*

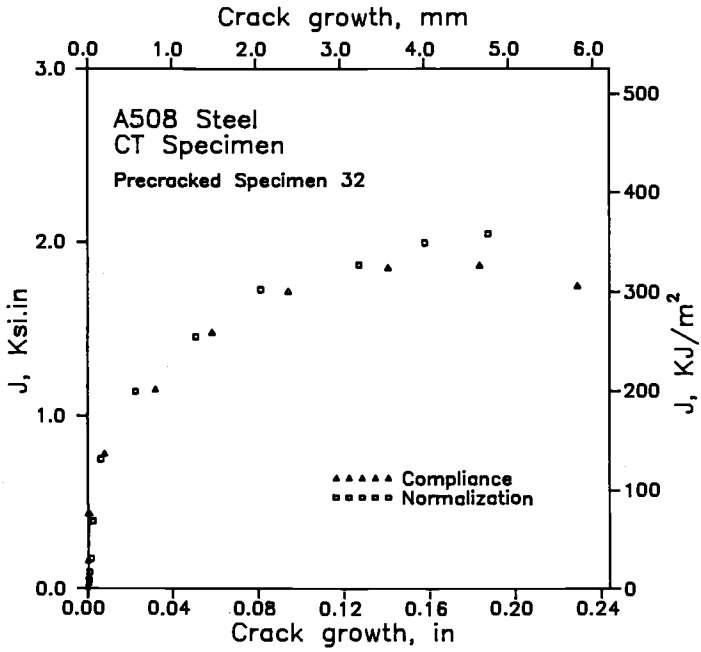

FIG. 10—*Effect of incorrect crack length predicted by compliance on* J-R *curve.*

this case an error in crack length estimate accompanies an error in elastic compliance which in turn gives the incorrect evaluation of the plastic area used in the J_{pl} calculation.

The effect of errors in η_{pl} on J_{pl} calculation may be relative to the particular specimen being evaluated. However for the two standard specimens used in *J-R* curve testing, the compact specimen and the three-point loaded single edge notched bend, the differences between the η_{pl} used in the standard test method and a new, possibly more appropriate value of η_{pl}, is not enough to cause concern and no change in η_{pl} is warranted.

Summary and Recommendations

The new method for developing η values for *J*-calculation, that of using the load separation principle, raises two important issues for the elastic plastic test methods. First, the present values of η_{pl} may not be entirely correct. The error in η_{pl} however is not large enough to warrant a change at this time. Considering the problems that might be caused by a change in η_{pl} such as need to change software, concern about data analyzed with the original η_{pl} and others, a change in η_{pl} should be only made when there is clear evidence that the present value is not appropriate. Since that has not been demonstrated, our recommendation is to keep the present η_{pl} values for both three-point bend and compact specimens.

The second important issue is that of calibrating new specimens for use in elastic-plastic fracture testing. The load separation method is recommended as the best method to use. It can be used with experimental studies, the best is blunt notched specimens of varying *a/W*, and with numerical studies of a similar nature. With the ease of the load separation method and its avoidance of calibration inaccuracies, the new specimens can be more easily cali-

brated. It is recommended that new specimens then be added, when appropriate to the elastic plastic test methods.

A third issue, indirectly related to the test methods, is that of the nonseparable region in J analysis. Certainly over this region η_{pl} is not well defined; hence, J_{pl} values may be in error. In many cases this region is so small that it is not significant. However, further studies of this problem are recommended.

References

[1] Rice, J. R., "A Path Independent Integral and the Approximate Analysis of Strain Concentration by Notches and Cracks," *Journal of Applied Mechanics*, 1968, pp. 379–386.

[2] Rice, J. R., "Mathematical Analysis in the Mechanics Fracture," Vol. 2 of *Fracture*, an Advanced Treatise, Liebowitz, H., Ed., Academic Press, New York, 1968.

[3] Begley, J. A. and Landes, J. D., "The J-Integral as a Fracture Criterion," *Fracture Toughness, ASTM STP 514*, American Society for Testing and Materials, Philadelphia, 1972, pp. 1–23.

[4] Landes, J. D. and Begley, J. A., "The Effect of Specimen Geometry on J_{Ic}, *Fracture Toughness, ASTM STP 514*, American Society for Testing and Materials, Philadelphia, 1972, pp. 24–39.

[5] Rice, J. R., Paris, P. C., and Merkle, J. G., "Some Further Results of J-Integral Analysis and Estimates," *Progress in Flaw Growth and Fracture Toughness Testing, ASTM STP 536*, American Society for Testing and Materials, Philadelphia, 1973, pp. 231–245.

[6] Merkle, J. G. and Corten, H. T., "A J-Integral Analysis for the Compact Specimen, Considering Axial Force as Well as Bending Effects," Paper No. 74-PVP-33, American Society of Mechanical Engineers, 1974.

[7] Landes, J. D., Walker, H., and Clarke, G. A., "Evaluation of Estimation Procedures Used in J-Integral Testing," *Elastic-Plastic Fracture, ASTM STP 668*, American Society for Testing and Materials, Philadelphia, 1979, pp. 266–287.

[8] Clarke, G. A. and Landes, J. D., "Evaluation of the J-Integral for the Compact Specimen," *Journal of Testing and Evaluation*, Vol. 7, No. 5, Sept. 1979, pp. 264–269.

[9] Sumpter, J. D. G. and Turner, C. E., "Method for Laboratory Determination of J_{Ic}," *Cracks and Fracture, ASTM STP 601*, American Society for Testing and Materials, Philadelphia, 1976, pp. 3–18.

[10] Ernst, H. A. and Paris, P. C., "Techniques of Analysis of Load-Displacement Records by J-Integral Methods," NUREG/CR-1222, Nuclear Regulatory Commission, Washington, DC, Jan. 1980.

[11] Sharobeam, M. H. and Landes, J. D., "The Separation Criterion and Methodology in Ductile Fracture Mechanics," *International Journal of Fracture*, Vol. 47, 1991, pp. 81–104.

[12] Sharobeam, M. H., "The Role of Geometry and Deformation in Ductile Fracture Methodology," Ph.D. dissertation, University of Tennessee, Knoxville, TN, in progress.

[13] Joyce, J. A., Davis, D. A., Hackett, E. M., and Hayes, R. A., "Application of the J-Integral and the Modified J-Integral to Cases of Large Crack Extension," NUREG CR-5143, Nuclear Regulatory Commission, Washington, DC, Feb. 1989.

[14] Landes, J. D., McCabe, D. E., and Ernst, H. A., "Fracture Testing of Ductile Steels," NP 5014, Final Report of Research Project 1238-2, Electric Power Research Institute, Palo Alto, CA, Jan. 1987.

[15] McCabe, D. E., Ernst, H. A., and Landes, J. D., "Development of an Elastic-Plastic Methodology to Assess Structural Reliability and Material Selection for Navy Applications," Annual Report, Contract No. N00 167-83-C-0121, Westinghouse R&D Center, Pittsburgh, PA, March 1985.

Sabu J. John[1]

Obtaining *J*-Resistance Curves Using the Key-Curve and Elastic Unloading Compliance Methods: An Integrity Assessment Study

REFERENCE: John, S. J., **"Obtaining *J*-Resistance Curves Using the Key-Curve and Elastic Unloading Compliance Methods: An Integrity Assessment Study,"** *Elastic-Plastic Fracture Test Methods: The User's Experience (Second Volume), ASTM STP 1114*, J. A. Joyce, Ed., American Society for Testing and Materials, Philadelphia, 1991, pp. 133–149.

ABSTRACT: The increasing use of *J*-resistance curves in design and ductile instability has inspired the need for a detailed and, indeed, reliable determination scheme for such curves. The basis for this paper emerged as part of a study of size effects on *J*-resistance curves. The three-part presentation includes descriptive sections for both the elastic unloading compliance and the key-curve methods, with the third part forming a comparative study of both procedures. Three-point bend specimens were used for testing the unloading compliance method using the crack mouth opening displacements for crack extension predictions. Using this specimen type, an empirically-based crack extension curvature correction procedure is introduced to correct crack length predictions for curved fronts. The load-line displacements were used for the crack tip energy evaluations with appropriate on-line corrections for indentation. The implementation of the key-curve method is reported and using compact tension specimens throughout, the results are compared to that of the elastic unloading compliance and the multiple specimen method. Finally, the virtues and drawbacks of both methods are compared and recommendations made. While the continuous nature of the key-curve method might be desirable for certain critical instability analyses, the justification of the experimental and numerical effort required is questioned.

KEY WORDS: normalized load, key curves, unloading compliance, fracture, three-point bend, compact tension, compliance, calibration, computer interaction, *J*-resistance, elastic-plastic fracture, test methods

Nomenclature

a, a_o, a_7	Crack length, initial, seven-point average
a_9, a_{max}, a_f	Nine-point average crack length, maximum crack length of a curved crack front, final crack length
B, B_n, B_g	Thickness, net, gross
b, b_o, b_i	Ligament, original, current
C	Compliance
E, E'	Young's modulus, effective
F_1	Normalized load used in the key-curve analysis
J	*J* contour integral

[1]Post doctoral research assistant, Department of Mechanical Engineering, Imperial College of Science, Technology and Medicine, London, SW7 2BX, United Kingdom.

P, P_L Load, limit
q, q_{pl}, q_{el} Load point displacement, plastic component, elastic component
S Three-point bend specimen span
U Total energy plus fracture energy, evaluated under a load-displacement trace
U_{pl}, U_{el} Plastic work done, elastic work done
W Specimen width
Δ Displacement
ν Poisson's ratio

The concept of J-resistance curves for characterizing post yield fracture behavior has provided the impetus for determining such curves using various methods. Naturally, this choice would depend primarily on the ease of application and accuracy of the procedure. This report attempts to point up the difficulties and virtues of both methods. One version of the key-curve technique, developed by Ernst et al. [*1*], is utilized and incorporated in an on-line computer program that is described here. This procedure, which uses compact tension specimens, is compared with the elastic unloading compliance method and multiple specimen procedures using identical specimen types. A crack front curvature correction procedure is introduced. Although the introduction of the procedure is made with three-point bend specimens, the results can be applied to compact tension samples to produce similar correction results. The limitations of the procedure are however clearly stated in this paper.

Theory

Key-Curve or Calibration Method

The key-curve method described here is an experimental technique for developing a continuous J-R curve from load-displacement records alone. Ernst et al. [*1*], who developed this technique, realized that for simple test specimen geometries, the load-displacement relationship must have the form

$$PW/Bb^2 = F_1\ (\Delta, a \text{ and material properties}) \tag{1}$$

Using deformation plasticity theory

$$J = -1/W \int^{\Delta} \partial P/\partial(a/W)\,|_{\Delta}\, d\Delta = 1/W \int^{P} \partial P/\partial(a/W)|_P\, dP \tag{2}$$

Also, assuming J and P to be a function of displacement, Δ, and crack length, a, and that total derivatives of J and P exist, then

$$\begin{aligned} dJ &= \partial J/\partial\Delta(d\Delta) + \partial J/\partial a(da) \\ dP &= \partial P/\partial\Delta(d\Delta) + \partial P/\partial a(da) \end{aligned} \tag{3}$$

Combining Eqs 1, 2, and 3, it can be shown that

$$\begin{aligned} dJ = [(2b/W)F_1 - (b/W)^2(\partial F_1/\partial(a/W))]d\Delta + \Bigg[-\int^{\Delta} 2/WF_1 d\Delta \\ + \int^{\Delta} 4b/W^2(\partial F_1/\partial(a/W)) - \int^{\Delta} (b^2/W^3)(\partial^2 F_1/\partial(a/W)^2 \Bigg] da \end{aligned} \tag{4}$$

and

$$da = \frac{[dP - (b/W)^2\, \partial F_1/\partial(\Delta/W)\, d\Delta]\, W}{(b^2/W)(\partial F_1/\partial(a/W)) - 2bF_1} \tag{5}$$

Therefore, if values for $\partial F_1/\partial(\Delta/W)$ and $\partial F_1/\partial(a/W)$ are available, then dJ and da values can be evaluated from Eqs 4 and 5, respectively. J and Δa values can then be found by the following operation

$$\begin{aligned} J &= \sum_1^n dJ \\ \Delta a &= \sum_1^n da \end{aligned} \tag{6}$$

Elastic Unloading Compliance Method

The concept of this method provides the ground work for its application in obtaining a J-resistance (J-R) curve with a single specimen. This is done by obtaining crack growth estimates from successive partial unloadings during the loading history of the test specimen [2]. By integrating up to the point of unloading, the work done, U, can be obtained, from which J values can be calculated, hence a J-R curve is produced.

Equipment

A 530-kN-capacity screw-driven testing machine was used for the unloading compliance method using three-point bend samples. A 250-kN servohydraulic machine was used for all fatigue precracking and the key curve testing. The instrumentation system consisted of the following units: a clip gage supplied, an analog plotter, and a variable setting signal filter. Data logging and on-line processing were performed on a simple personal computer. This was connected, through a IEEE 488 interface, to the various peripherals.

All tests were performed on a titanium alloy, Ti-6Al-2Cb-1Mo-1Ta [Ti(6-2-1-1)]. The mechanical properties for titanium alloy (6-2-1-1) are: 0.2% proof stress = 728 MPa, tensile strength = 828 MPa, Young's modulus = 123 200 MPa, and percentage elongation = 12%. The flow stress, σ_{fl}, is taken to be the average of the proof stress and the tensile strength, that is, 778 MPa.

General Experimental and Computational Details

Key-Curve Method

Experiments—Small (B = 17.5 mm) compact tension specimens proportions, described by ASTM Test Method for J_{Ic}, a Measure of Fracture Toughness (E 813-81), were used so that load-displacement values of higher Δ/W could be achieved without proportionately more crack growth. A total of seven specimens were fatigue pre-cracked to crack depth ratios of between a/W = 0.62 and 0.92.

The instrumentation used was the same as the elastic unloading compliance method (Fig. 1) but a different software package was developed for this method; an explicit description of this package is given later. The schematic of the key-curve's numerical processing path is shown in Fig. 2.

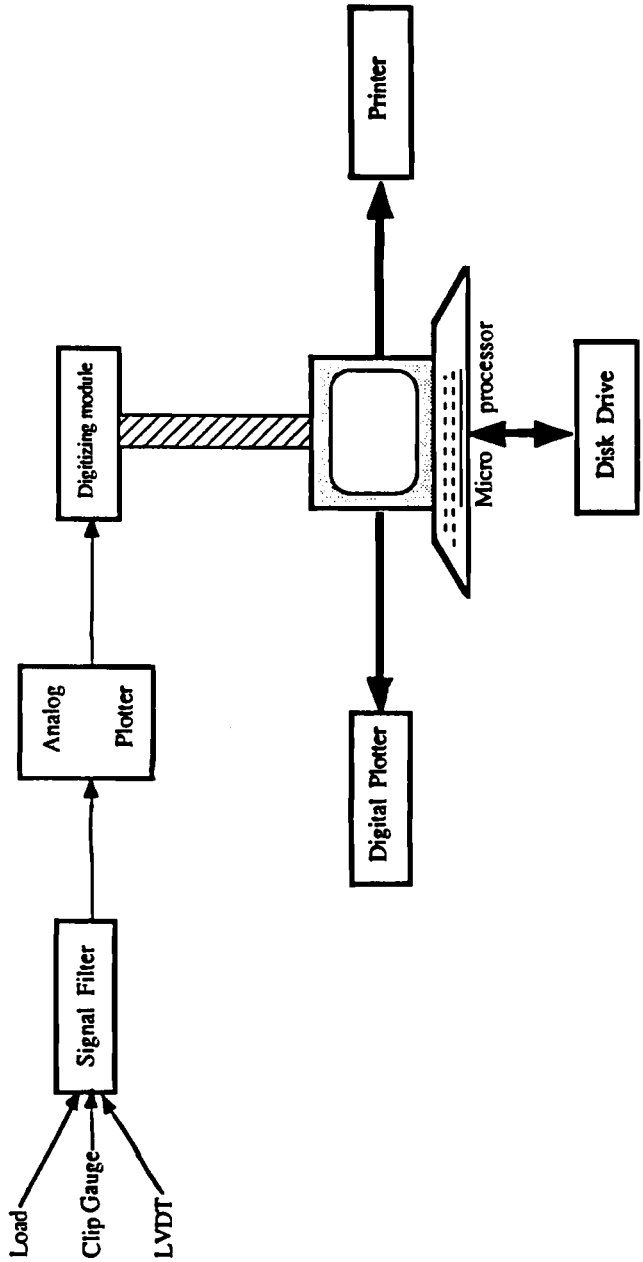

FIG. 1—*Schematic of the instrumentation system.*

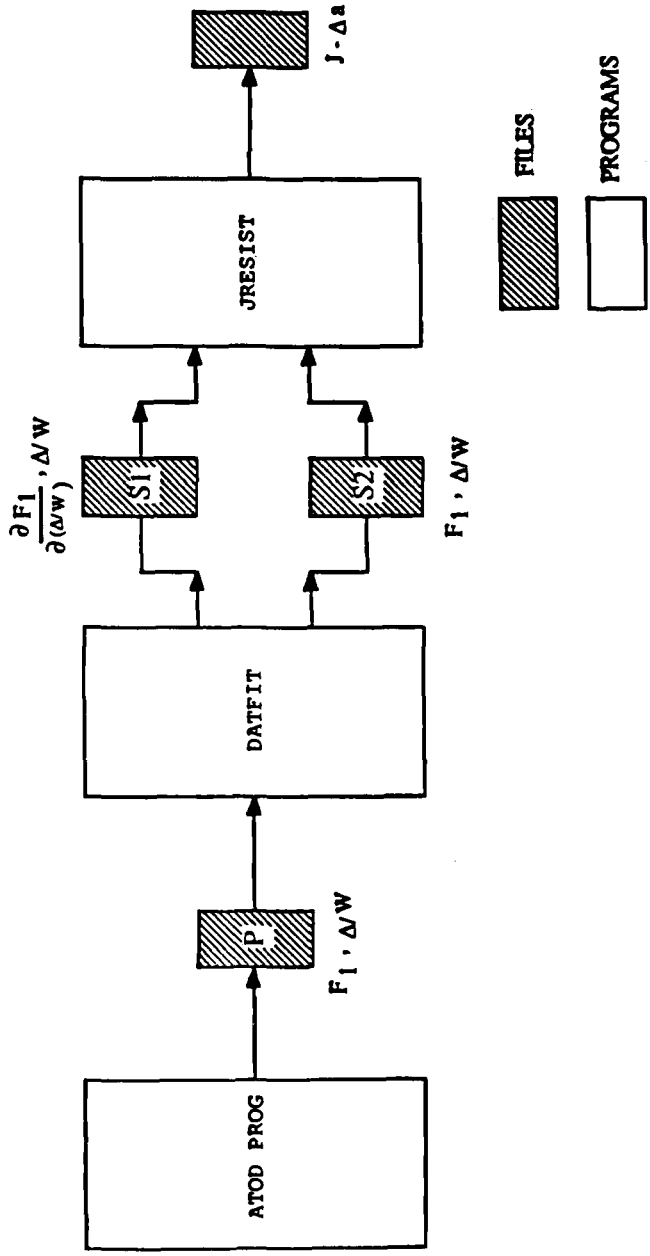

FIG. 2—*Program datafile linkup system designed for microcomputer processing of the key curve analysis.*

Each of the seven specimens was loaded to its limit and the data points were collected by the computer at the rate of 145 data pairs/min. A uniform cross-head, speed of 0.25 mm/min was maintained throughout the loading period. An analog plot was obtained for all the specimens.

The specimens were then broken by high energy impact, after heat tinting at 400°C for 15 min. The fatigue crack length was measured by averaging lengths across the crack face, as described in ASTM E 813-81. Ductile crack growth of not more than 2% of the ligament was observed on the crack face of almost all the specimens tested.

Computation and the Program-Datafile-Link-Up System—The load and displacement values are normalized as PW/Bb^2 and Δ/W, respectively. These normalized load and displacement functions are then passed through a curve-fitting program, DATFIT (see Fig. 2), to facilitate numerical differentiation for the $\partial F_1/\partial(\Delta/W)$ values in Eq 4 and 5. The $\partial F_1/\partial(a/W)$ values are obtained from a plot of F_1 against a/W levels as shown in Fig. 3. From this figure, it is seen that F_1 is a weak function of a/W, therefore, $\partial^2 F_1/\partial(a/W)^2$ was set to zero. Similar trends have also been reported by Joyce et al. [*3*]. A plot of all the F_1 functions against Δ/W after curve fitting is showed in Fig. 4.

DATFIT fits a fifth order polynomial to the plots shown in Fig. 5 after normalization to F_1 and Δ/W. It differentiates the F_1 function numerically with respect to Δ/W and stores all the F_1 function values and its derivatives, $\partial F_1/\partial(\Delta/W)$. So from primary files created by ATOD PROG, secondary files are created by DATFIT.

To obtain the J-resistance curves, discrete versions are written for Eqs 4 and 5, namely

$$dJ_n = [(2b/W)F_{1n} - (b/W)^2 (\partial F_1/\partial(a/W))_n]\, d\Delta_n + \left[-2/W \sum_{i=1} F_{1i} d\Delta_i + 4b/W^2 \sum_{i=1}^{n} (\partial F_1/\partial(a/W))_i d\Delta\right] da_n \tag{7}$$

and

$$da_n = \frac{[dP_n - (b^2/W^2)\partial F_1/\partial(\Delta/W) d\Delta_n]W}{(b^2/W)(\partial F_1/\partial(a/W)) - 2bF_1} \tag{8}$$

Therefore, (as in Eq 6)

$$J = \sum_{i=1}^{n} dJ_n \tag{9}$$

and

$$\Delta a = \sum_{i=1}^{n} da_n \tag{10}$$

The final processing program, JRESIST, utilizes Eqs 7 through 10 for computing J and Δa values.

Elastic Unloading Compliance

The method described here is for the three-point bend specimen and is not strictly according to the ASTM E 813-87.

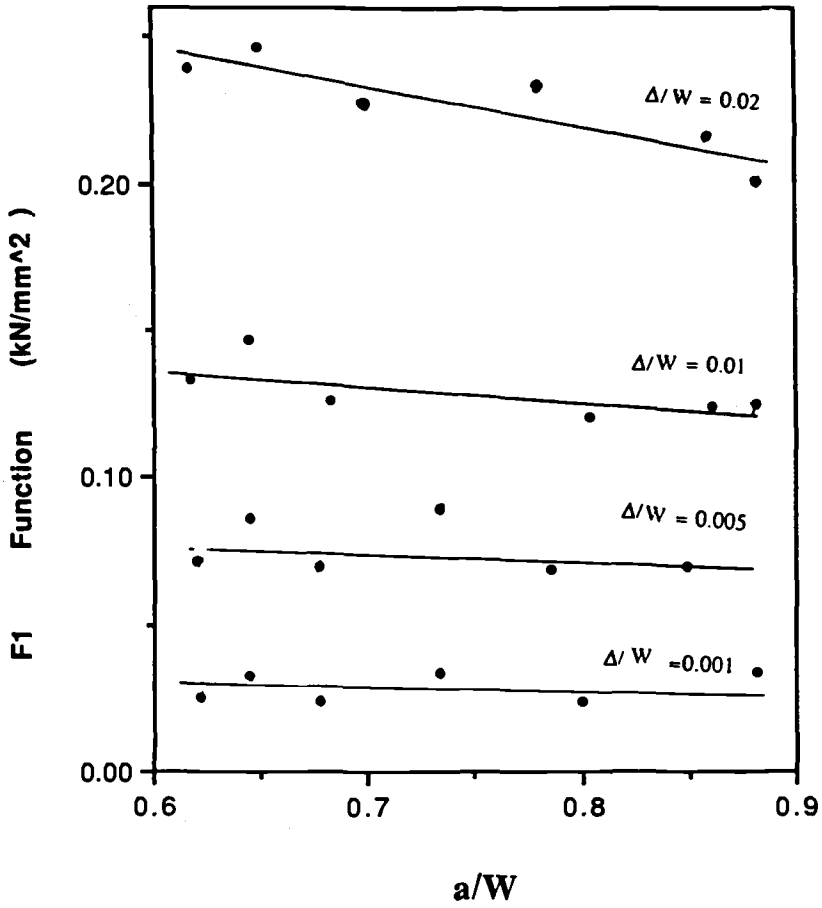

FIG. 3—F_1 *variation with* (a/W) *for different displacement levels used in the key curve analysis.*

The details of the procedure, highlight the accuracy of the compliance factor of Kapp et al. [*4*] for the three-point bend specimen, see Fig. 6. Also included in this paper, are computer-interactive procedures that correct for specimen indentation and crack front curvature. However, for strict comparative purposes, see Fig. 7, the compact tension specimen was used throughout, be it for the key curve, elastic unloading compliance (using the calibration functions of Saxena and Hudak [*5*]), or the multiple specimen method.

Roller Indentation

To correct for roller indentation in the three-point bend tests, a roller indentation test was set up with a broken half of a test specimen. The inverse slope of the load-displacement plot is obtained and used in correcting for extraneous displacements as shown later. If C_I is the inverse slope of the indentation trace (I = indentation), the correction, in terms of work done, is

$$U_I = (1/2)C_I P^2$$

(from work done under linear elasticity (1/2 P_q, where $q = C_I P$)).

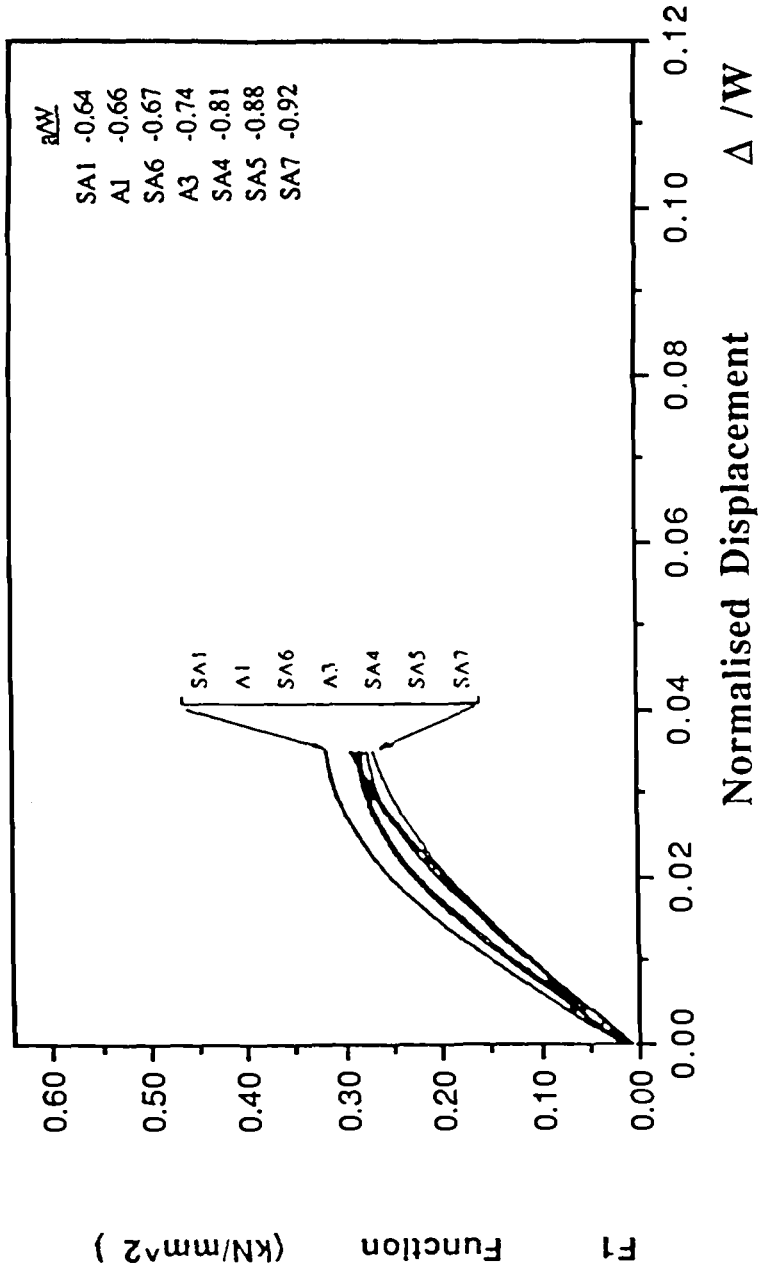

FIG. 4—F_1 *variation with normalized displacements used in the key curve analysis.*

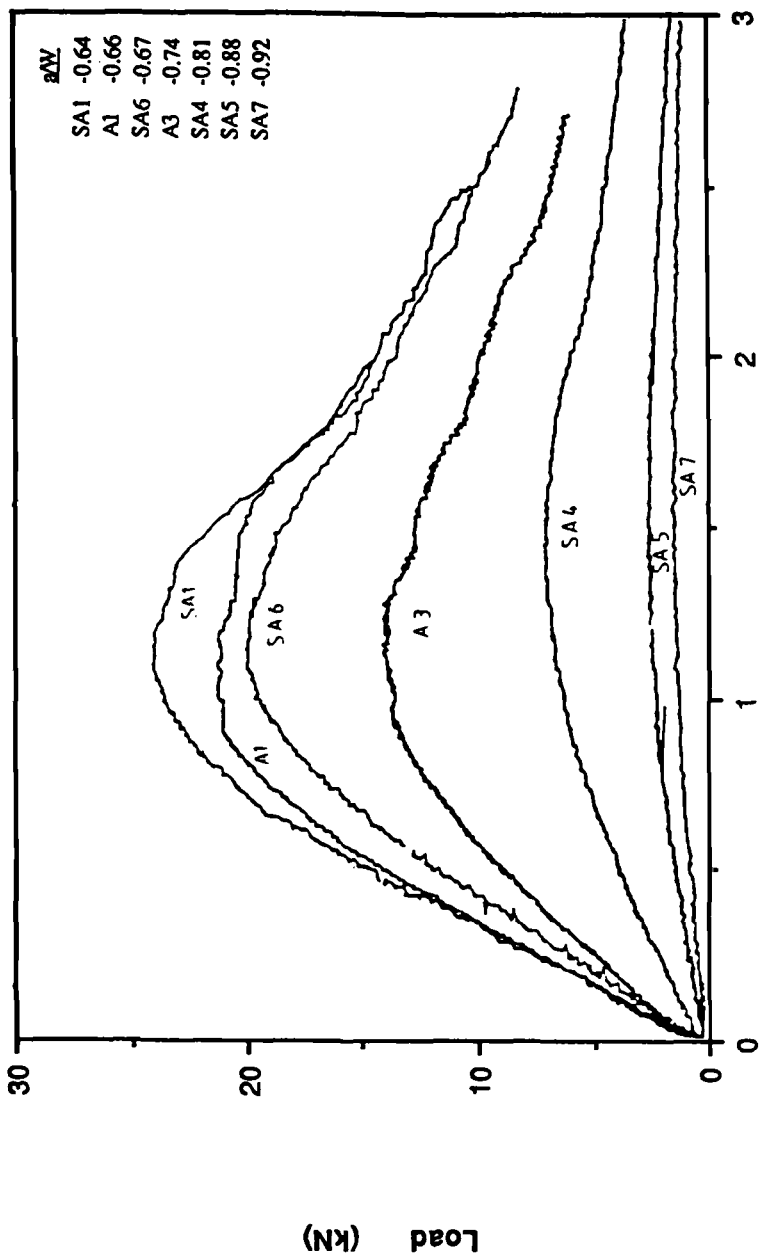

FIG. 5—*Load-displacement plots for the key curve analysis.*

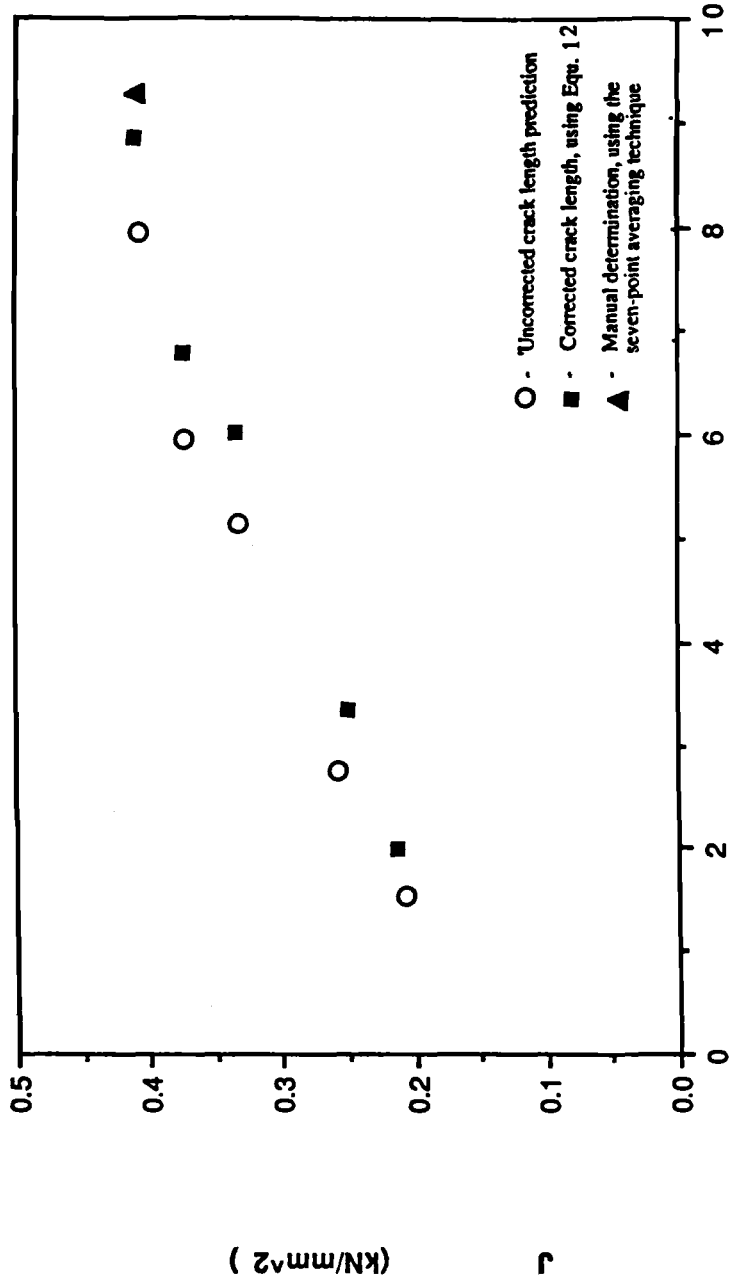

FIG. 6—*Comparison of crack extension predictions with the three-point bend specimen.*

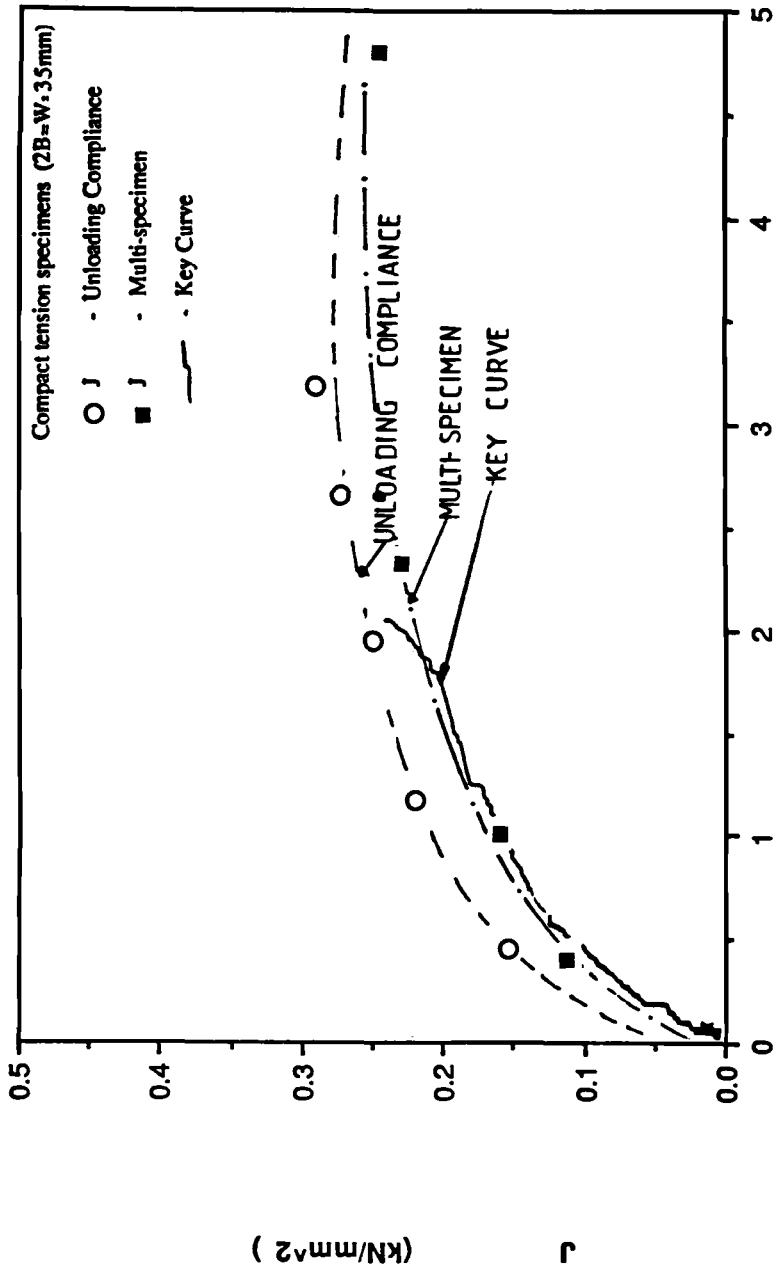

FIG. 7—*Comparison of testing methods using the compact tension specimen.*

TABLE 1—*Crack length measurements across the crack face of the three-point bend specimens* (B = *17.5 mm*, W = *2B*) *with different levels of ductile crack growth after unloading compliance tests.*

	$a_{f,\text{comp}}$, mm	$a_{f,7}$, mm	$a_{f,9}$, mm	$a_{o,7}$, mm	$a_{o,9}$, mm	$a_{f,\max}$, mm	$a_{f,\min}$, mm	$a_{o,\max}$, mm	$a_{o,\min}$, mm	[(1) − (2)]/(2),	Δa_7, mm	$\Delta a_7/b_0$, mm	$\Delta a_7/W$, mm	Δa_9, mm	$\Delta a_9/b_0$, mm	$\Delta a_9/W$, mm	Δa_{comp}, mm	$\Delta a_{\text{comp}}/b_0$, mm	$\Delta a_{\text{comp}}/W$, mm	$\Delta a_{\max}$, mm
B_9	27.47	28.68	28.07	20.00	19.76	29.42	26.00	20.03	19.05	0.132	8.67	0.578	0.247	8.31	0.545	0.237	7.54	0.500	0.215	9.39
B_{10}	21.08	21.66	21.05	20.03	20.01	22.67	18.30	20.53	18.22	0.239	1.35	0.092	0.038	1.04	0.069	0.029	1.02	0.068	0.029	2.10
B_2	20.48	20.89	20.45	19.75	19.58	21.28	19.10	19.8	19.05	0.114	1.14	0.074	0.033	0.87	0.056	0.025	0.76	0.050	0.021	1.40
B_7	21.26	22.19	21.39	18.64	18.54	25.30	18.50	18.87	18.05	0.367	3.55	0.215	0.104	2.85	0.173	0.08	2.66	0.161	0.761	6.43

TABLE 2—*Number of crack-length-measurement-based compliance values for Ti(6-2-1-1) three-point bend specimens.*

	$C_{f,\text{comp}}$ mm/kN	$C_{f,7}$ mm/kN	$C_{f,\max}$ mm/kN	$C_{f,9}$ mm/kN	C_7/C_{comp}	$C_{\max}/C_{\text{comp}}$	C_9/C_{comp}
B_9	0.1366	0.1999	0.2706	0.1656	1.46	1.98	1.92
B_{10}	0.0301	0.0333	0.0412	0.0299	1.16	1.37	0.98
B_2	0.0269	0.0289	0.0314	0.0267	1.07	1.16	0.99
B_7	0.0309	0.0373	0.0761	0.0319	1.2	2.45	1.03

C_I is determined to be 3.59×10^{-3} kN/mm for Ti(6-2-1-1) with the three-point bend rig on the Tinius Olsen testing machine. This corrective process is incorporated in the computer software described in Ref *6*. This linear form is described and shown explicitly in Ref *6*, where the initial nonlinear "slack" of the setup quickly becomes quite linear, particularly within the nominal testing loads of the specimens.

Crack Front Curvature Correction

In this section, crack front curvature is studied and an empirically-based solution is presented to account for this phenomenon in Ti(6-2-1-1). The final objective is the inclusion in interactive numerical processing of data for on-line, reliable crack length predictions.

Procedure

Three-point bend Ti(6-2-1-1) test specimens of standard (ASTM E 813-81) dimensions were used throughout this study. The steps taken were as follows:

1. Four test specimens of fatigue precracked depth ratio, $a/W = 0.55$, were used to obtain *J-R* curves for different levels of crack growth. After the test, the four specimens were heat tinted and broken to two halves. Seven-point and nine-point measurements were taken across the crack face for both the original ($a_{o,7,9}$) and final crack lengths ($a_{f,7,9}$). Subscripts 7 and 9 represent the seven- and nine-point average measuring techniques for the crack length across the crack face. Crack length averages of these measurements were evaluated. A comprehensive table of these measurements is shown in Table 1.
2. Based on these measurements, inverse compliance equations by Kapp et al. [*4*] were used to evaluate what the compliance measurement would have been if $a_{f,7}$, $a_{f,9}$, and $a_{f,\max}$ were measured. The inverse mouth-opening compliance equation used was

$$E'B\,\Delta(1 - a/W)^2/[3.95\,P(S/W)(a/W)] = f_{3PBMC}\,(a/W) \tag{11}$$

   where $f_{3PBMC}(a/W) = 2.21 - 6.57\,(a/W) + 17.9\,(a/W)^2 - 26.6\,(a/W)^3 + 19.9\,(a/W)^4$.
3. These "would be" compliances, $a_{f,7}$, $a_{f,9}$ and $a_{f,\max}$, are then normalized with the actual measured compliance, $C_{f,\text{comp}}$. Table 2 displays these "would be" compliances and their respective ratios. A plot of this ratio against $\Delta a/b_o$ is shown in Fig. 8.
4. The values of these curves were then used as data for the curve fitting routine (developed for the key curve analysis) described in Ref *6*.

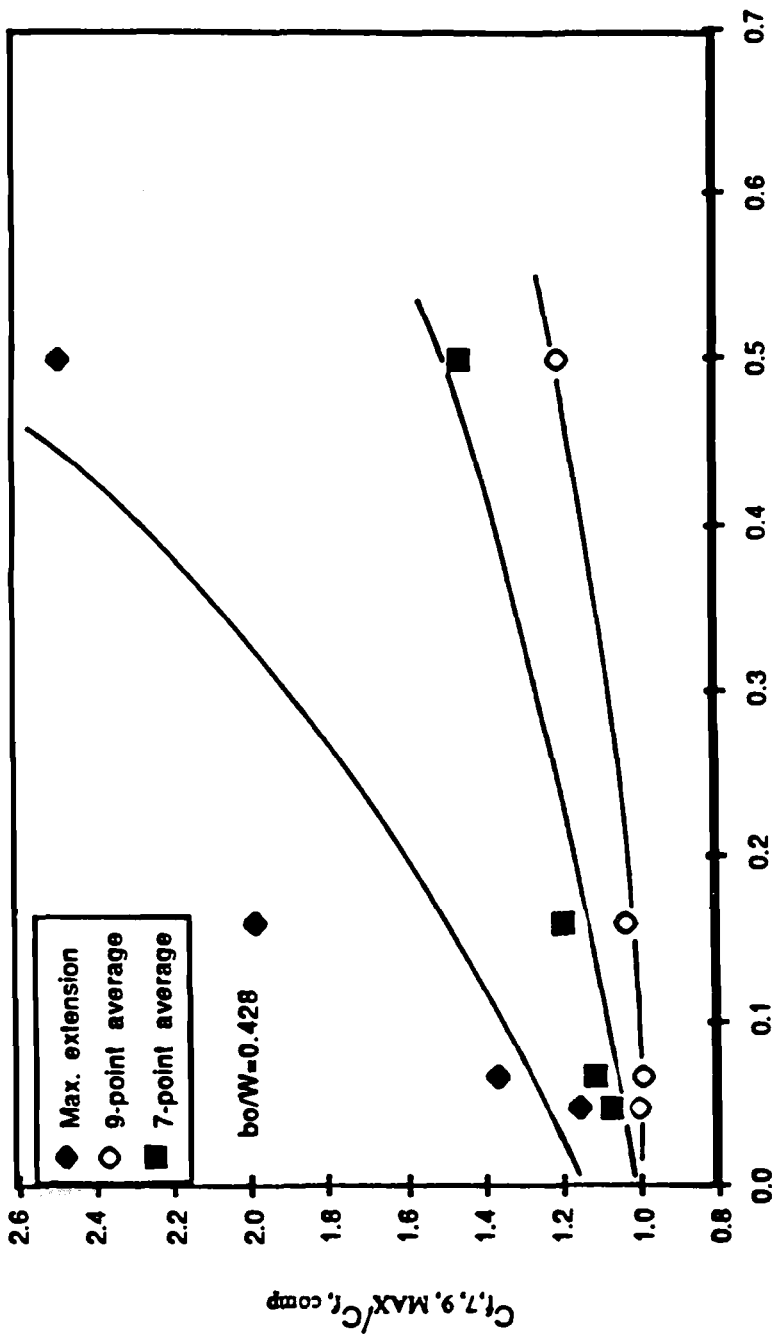

FIG. 8—*Compliance ratio plot against normalized crack extension for Ti(6-2-1-1).*

The result of the computation yielded fifth order polynomials as

$$C_7/C_{comp} = 1.002 + 3.497\,(\Delta a/W) - 53.163\,(\Delta a/W)^2 + 512.9\,(\Delta a/W)^3 - 1948.8\,(\Delta a/W)^4 + 2568.8\,(\Delta a/W)^5 \quad (12)$$

$$C_{max}/C_{comp} = 1.003 + 3.456\,(\Delta a/W) + 23.32\,(\Delta a/W)^2 - 351.52\,(\Delta a/W)^3 + 1717.05\,(\Delta a/W)^4 - 2682.3\,(\Delta a/W)^5 \quad (13)$$

$$C_9/C_{comp} = 1.000 - 0.2335\,(\Delta a/W) + 8.49\,(\Delta a/W)^2 - 38.71\,(\Delta a/W)^3 + 123.72\,(\Delta a/W)^4 - 136.7\,(\Delta a/W)^5 \quad (14)$$

These equations are valid only for titanium alloy Ti(6-2-1-1) and for cases where a_o/W is about 0.56 and $0 < \Delta a/W < 0.3$.

Therefore, for similar degrees of shearlip formation, corrective equations such as Eqs 12 through 14 can be used to "correct" for curvature by evaluating the chosen (seven- or nine-point) "would be" compliance from crack extensions (Δa) obtained from the measured (uncorrected) compliance.

The new compliance is then evaluated using Eqs 12, 13, or 14 that are used for evaluating the "corrected" crack length by the usual compliance calibration equations. The form of the "corrective" Eqs 12 to 14 was considered convenient for the interactive unloading compliance computer program SULCO, described in Ref *6*. Equation 12 is included in SULCO, and it is used in the calculation routine just described.

A typical crack length-corrected *J-R* curve for the three-point bend specimen is shown in Fig. 6. All the versions of *J* shown in Figs. 6 and 7 are from J_{i+1} as defined by ASTM E 813-81.

Results and Discussion

The Key-Curve Technique

Computation—The entire computational processing was confined to the 32-K microcomputer. This capability was made possible by the program datafile linkup system, see Fig. 2, which essentially discretized the numerical processing. Unlike the single-specimen, completely computer processed, unloading compliance procedure discussed later, the key-curve method is a multi-specimen technique and the numerical work is only partially computer processed.

Recalling Eqs 4 and 5 for the *n*th step

$$dJ_n = [(2b/W)F_{1n} - (b/W)^2(\partial F_1/\partial(a/W))_n]\,d\Delta_n + \left[-2/W \sum_{i=1}^{n} F_{1i}d\Delta_i + 4b/W^2 \sum_{i=1}^{n} (\partial F_1/\partial(a/W))_i d\Delta\right] da_n$$

and

$$da_n = \frac{[dP_n - (b^2/W^2)\,\partial F_1/\partial(\Delta/W)\,d\Delta_n]\,W}{(b^2/W)\,(\partial F_1/\partial(a/W)) - 2bF_1}$$

Attention here is directed towards the function, $\partial F_1/\partial(a/W)$, values of which are obtained from Fig. 3. From this figure, it can clearly be seen that F_1 is a weak function of a/W. This is however not surprising as seen when F_1 is plotted against normalized displacement for various crack depth ratios in Fig. 4. The strong dependence of the load, P, on displacement and crack length, as shown in Fig. 5, is weakened, especially for crack length when F_1 is introduced, since F_1 is PW/Bb^2; the b^2 playing a strong normalizing role.

Also, for limited crack extension up to about maximum load, F_1 is a particularly weak function of a/W. The weak function of F_1 against a/W, coupled with the extensive scatter shown in Fig. 3 provides suspect values of $\partial F_1/\partial(a/W)$. Also inherent in the analysis is the assumption that $\Delta a = 0$ for all the specimens that could be questioned since crack extension is known to initiate before maximum load in Ti(6-2-1-1). Therefore, the b values in Eqs 4 and 5 might not entirely be correct, particularly close to maximum load. In light of this discussion, the repeatability of the continuous key-curve-generated J-R curve shown in Fig. 7 was difficult to obtain when applied to other a/W ratios. Herrera and Landers [*7,8*] have recently reported a similar conclusion where a non-growing crack is needed for this type of analysis in order to justify the initial assumptions of the method. They proposed an individual calibration curve rather than a "universal" one attempted by the F_1 function, used here. They suggest a procedure that makes use of experimental results and finite element analyses to choose a functional form of the calibration curve that is based on separable multiplicative functions of load, crack length, and displacement.

The comparison shown in Fig. 7 is between compact tension specimens. Both the compliance calibration function of Saxena and Hudak [*5*] and the curvature correction equation (Eq 12) were applied to these test specimens. The multiple specimen procedure was performed according to ASTM E 813-81. Finally, as seen in the description of ASTM E 813-81, the key-curve procedure is significantly more difficult to apply than the unloading compliance method.

The Unloading Compliance Technique as Applied to the Three-Point Bend Specimen

Experimentation—This method was considered the most suitable and was consequently used for the geometry effect study of the J-R curves discussed here. The procedure uses a single specimen and thus results in considerable savings in material and time when compared with the multispecimen and key-curve methods. Also, this procedure is wholly computer interactive, while the other methods are not.

Computation—The integration under the load-displacement plot is fairly accurate to within 5%, if the proper limits for the integration are obtained, that is, data sample pairs between successive unloadings. Extraneous displacements are corrected for by subtracting the indentation work from the actual work done as described earlier. The nonlinearity of the unloading lines are limited by the extent of unloading and hence the number of data pairs acquired during unloading. A 10 to 15% unloading is usually sufficient to cause substantial linearity of the unloading slope. Also, included in the software are steps aimed at processing the central portion of the unloading line (SULCO, described in Ref *6*). These include a small delay in data acquisition when unloading commences, and the first and last data pairs are ignored in the least-squares analysis.

Since practical difficulties were envisaged in measuring specimen load-line compliance, the mouth-opening compliance calibration by Kapp et al. [*4*] was used and subsequently incorporated in SULCO, the unloading compliance interactive program.

Crack predictions (using the mouth-opening compliance calibrations by Kapp et al. [*4*], and provided the crack front is relatively straight) were generally accurate to within 0.5 mm. This is usually the case for sidegrooved specimens. For nonsidegrooved specimens, where crack tunneling occurs, the empirical correction Eqs 12, 13, and 14 appear to correct the

predicted (effective) crack length to the optically measured crack length. Figure 6 shows a comparison of predicted, corrected, and measured final crack length (based on the seven-point average). This seven-point-average correction equation (Eq 12) has also been incorporated into SULCO. Therefore, even with nonsidegrooved test specimens, the crack length predictions could be fairly close to the actual measured crack length if the curvature correction equations are adopted.

Although the methodology of the procedure described here highlights (see Fig. 6) the validity of the three-point bend calibration equations of Kapp et al. [*4*] and other corrections for crack front curvature and indentation, a similar procedure can be applied to compact tension specimens. Figure 7 compares the various test methods and the unloading compliance method using the crack front curvature correction procedure on the compact tension specimens.

Figure 7 shows results on compact tension specimens even though a study of the elastic unloading compliance method applied to compact tension and three-point bend specimens showed only a 3 to 7% difference in the *J-R* curves [*6*].

Conclusions

The cost, in both time and material terms, will need to be assessed in order to enable the key-curve method to compete against the unloading compliance method for the generation of *J-R* curves. Though the continuous nature of the *J-R* curve obtained from the key-curve method is desirable for some critical instability analyses [*6*], the unloading compliance procedure is much better suited for most circumstances. Also, the repeatability of these curves from the key-curve analyses described here was difficult to obtain. Perhaps the similar "single-specimen-calibration-curve" method described by Herrera and Landes [*7,8*] will be developed further in order to increase the confidence of applying the key-curve method to *J-R* curve testing.

For the elastic unloading compliance method, once the calibration function is reliable and corrections for specimen indentation and crack front curvature are made, it is fairly easy to implement and repeatability is good.

References

[*1*] Ernst, H. A., Paris, P. C., Rossow, M., and Hutchinson, J. W. in *Fracture Mechanics (11th Conference), ASTM STP 677*, C. Smith, Ed., American Society for Testing and Materials, Philadelphia, pp. 581–599.

[*2*] Joyce, J. A. and Gudas, J. P., "Computer Interactive J_{Ic} Testing of Navy Alloys," *Elastic-Plastic Fracture, ASTM STP 668*, J. D. Landers, J. A. Begley, and G. A. Clarke, Eds., 1979, pp. 451–468.

[*3*] Joyce, J. A., Ernst, H., and Paris, P. C., Direct Evaluation of *J*-resistance Curves from Load-Displacement Records," *Fracture Mechanics (12th Conference), ASTM STP 700*, American Society for Testing and Materials, Philadelphia, 1980, pp. 222–236.

[*4*] Kapp, J. A., Leger, G. S., and Gross, B., Wide-Range Displacement Expressions for Standard Fracture Mechanics Specimens," *Fracture Mechanics: Sixteenth Symposium, ASTM STP 868*, Kanninen and Hooper, Eds., American Society for Testing and Materials, Philadelphia, 1985, pp. 27–44.

[*5*] Saxena, A. and Hudak, S. J., "Review and Extension of Compliance Information for Common Crack Growth Specimens," *International Journal of Fracture*, Vol. 14, 1978, pp. 453–468.

[*6*] John, S. J., "Tearing Toughness and Unstable Ductile Behaviour of a Titanium Alloy, PhD thesis, University of London, 1986.

[*7*] Herrera, R. and Landes, J. D., "A Direct J-R Curve Analysis of Fracture Toughness Tests," *Journal of Testing and Evaluation*, Vol. 16, No. 5, Sept. 1988, pp. 453–468.

[*8*] Landes, J. D. and Herrera, R., "A New Look at J-R Curve Analysis," *International Journal of Fracture*, Vol. 36, 1988, pp. R9–R14.

Naotake Ohtsuka[1]

Nonincremental Evaluation of Modified *J-R* Curve

REFERENCE: Ohtsuka, N., **"Nonincremental Evaluation of Modified *J-R* Curve,"** *Elastic-Plastic Fracture Test Methods: The User's Experience (Second Volume), ASTM STP 1114*, J. A. Joyce, Ed., American Society for Testing and Materials, Philadelphia, 1991, pp. 150–162.

ABSTRACT: A method to calculate the deformation theory J, J_D, which takes into account the influence of crack growth on J, and a modified version of the J-integral, J_M, to allow a large relaxation of restrictions on the amount of crack extension and specimen configuration were proposed by Ernst et al. In this work, simple and nonincremental formulas for J_D, J_M, and crack extension, based on the single-specimen key-curve method using blunt U-notched specimens are proposed. The methods are applied to the determination of J-R curve for three-point bend type and compact tension type specimens. The accuracy of the methods in the determination of the J-R curves is discussed, emphasizing the differences between J-R curves for J_D and J_M.

KEY WORDS: J-integral, fracture toughness, J-resistance curve, modified J-integral, key curve, J_{Ic} test, crack extension, elastic-plastic fracture, test methods

The potential of the J-integral [*1*] has been demonstrated as a fracture-initiation criterion in the large-scale plastic yielding range [*2*]. The J-R curve concept was introduced later to characterize the stable crack growth resistance of materials in the regime of small amounts of crack extension [*3*]. Ernst et al. have proposed a generalized method [*4*] and a formula [*5*] to calculate deformation theory J, J_D, which takes into account the influence of crack growth on J. Because the deformation theory J-R curve is dependent on size and type of specimens with large amounts of crack extension, a modified version of the J-integral, J_M, has been introduced by Ernst [*6*]. However, evaluation of the deformation theory, J_D, and the modified version, J_M, requires incremental calculations. The procedure to calculate the value of J_D is shown in ASTM Test Method for Determining J-R Curves (E 1152-87). Joyce et al. [*7*] developed the key-curve method to generate the J-R curve from load-displacement records of a full-size specimen and multiple subsize specimens, following the work of Ernst et al. [*4*]. In this work, nonincremental simple formulas for the two types of J-integral, J_D and J_M, and for crack extension, Δa, are proposed and are applied to the determination of the J-R curve of three-point bending and compact tension (CT) specimens by the simplified single-specimen key-curve method.

Theoretical Considerations

Evaluation of Crack Extension

Let us consider the case that the plasticity of a specimen is confined to the uncracked ligament region and the J-integral of the specimen from a load-displacement record, such

[1]Associate professor, Department of Mechanical and System Engineering, Faculty of Science and Technology, Ryukoku University, 1-5 Yokotani, Oe-cho Seta, Ohtsu 520-21, Japan.

as Path 1 as shown in Fig. 1, is obtained as [*5,8*]

$$J = \frac{\eta}{b}\int_0^{\delta} P d\delta \tag{1}$$

where

P = load per unit net thickness,
δ = displacement,
η = function of a/W or b/W only,
a = crack length,
W = specimen width, and
b = remaining uncracked ligament ($= W - a$).

In this case, the load-displacement relationship for the simple specimen can be expressed by the following equation [*5*]

$$\frac{P}{W} = \left(\frac{b}{W}\right)^2 \cdot F\left(\frac{a}{W}, \frac{\delta}{W}\right) = \left(\frac{b}{W}\right)^2 \cdot g\left(\frac{b}{W}\right) \cdot H\left(\frac{\delta}{W}\right) \tag{2}$$

where F, g, and H are functions of parameters in the parentheses.

The η and g functions for the three-point bend (3PB) specimens with small remaining ligament are given as [*5*]

$$\eta = 2 \text{ and } g = 1 \tag{3}$$

Considering paths like Path 2 and Path 3 in Fig. 1, where crack length is constant at the final value, a, and the initial value, a_0, up to the final δ, respectively, physical crack extension for 3PB is derived as

$$\Delta a = b_0 (1 - \sqrt{(P/P_0)}) + J/(4\sigma_f) \tag{4}$$

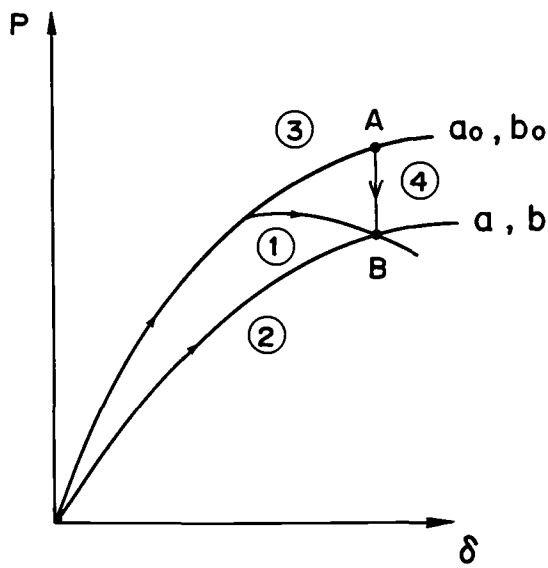

FIG. 1—*Schematic* P-δ *curves.*

where the subscript, 0, denotes being on the Path 3, which has an ability to develop the H function in Eq 2 [7]. The first term in the right-hand side of Eq 4 corresponding to stable crack tearing is derived from the ratio of Eq 2 for Path 2 to Path 3 in Fig. 1 by putting $g = 1$ [9]. The second term in the right-hand side of Eq 4 corresponding to pseudocrack advance is derived from the equation for crack tip blunting [10] where σ_f is flow stress, that is, the average of ultimate tensile strength and yield stress.

Then for the compact tension (CT) specimen [5]

$$\eta = 2 + 0.522(b/W) = 2 + 0.522(1 - \alpha_0)(1 - \Delta a/b_0), \text{ and}$$

$$g(b/W) = \exp(0.522b/W)$$

$$= \exp\{0.522(1 - \alpha_0)(1 - \Delta a/b_0)\} \tag{5}$$

where $\alpha_0 = a_0/W$ and Δa are the crack extension from Point A to Point B on Path 4 in Fig. 1. Substituting Eq 5 to Eq 2, and taking the ratio of this equation for Path 2 to Path 3 in Fig. 1

$$\left(1 - \frac{\Delta a}{b_0}\right)^2 = \left(\frac{P}{P_0}\right) \cdot \exp\{0.522(1 - \alpha_0)\Delta a/b_0\} \tag{6}$$

From Eq 6 and the equation for crack tip blunting, the approximate equation of Δa for CT specimens is derived as

$$\Delta a = b_0 \frac{(1 - \sqrt{P/P_0})}{1 + 0.261(1 - \alpha_0)\sqrt{P/P_0}} + J/(4\sigma_f) \tag{7}$$

The foregoing equations are different from the incremental formulas, $J = \Sigma\, dJ_n$ and $\Delta a = \Sigma da_n$, in the originally proposed key-curve method by Joyce et al. [7], where dJ_n and da_n are evaluated using the F function in Eq 2 from the analysis of multiple subsize specimens.

Equation for J_D

The deformation theory J-integral for paths like Path 3 to Path 4, where δ is constant and crack length grows from a_0 to current value a, is expressed as [5]

$$J_D = J_0 - \int_{a_0}^{a} \frac{\gamma J}{b}\, da \tag{8}$$

where J_0 is J at Point A expressed by Eq 1 with a constant initial crack length, a_0. The function, γ, is defined as

$$\gamma = \{\eta - 1 - (b\eta')/(W\eta)\} \tag{9}$$

Using Eqs 3 and 5, γ is equal to 1 for 3PB specimens and can be approximated for CT specimens as [5]

$$\gamma = 1 + 0.76b/W \tag{10}$$

Equation 8 is approximated in the incremental form as [5]

$$J_{D,i+1} = \{J_{D,i} + (\eta/b)_i\, A_{i,i+1}\}\{1 - (\gamma/b)_i\,(a_{i+1} - a_i)\} \tag{11}$$

where Subscript i indicates functions evaluated at that step. The term $A_{i,i+1}$ refers to the area enclosed by the actual $P - \delta$ test record and lines of constant displacement, δ_i and δ_{i+1}. Equation 11 is used for the evaluation of plastic components of J_D in ASTM E 1152–87.

Considering the crack extension, Δa, on Path 4 (from Path 3 to Path 2), the following inequality is obtained.

$$\frac{\gamma J_0 \Delta a}{b} > \int_{a_0}^{a} \left(\frac{\gamma J}{b}\right) da > \frac{\gamma_0 J_D \Delta a}{b} \tag{12}$$

Substituting Eq 12 into Eq 8, the upper and lower bounds of Eq 8 are given as

$$\frac{J_0}{(1 + \gamma_0 \Delta a/b)} > J_D > J_0 \left\{1 - \frac{\gamma \Delta a}{b}\right\} \tag{13}$$

The average of the two boundary values thus gives an approximate value of J_D as

$$J_D \simeq \frac{J_0}{2} \left\{1 + \frac{1}{1 + \gamma_0 \Delta a/b_0} - \frac{\gamma \Delta a}{b}\right\} \tag{14}$$

In the case that

$$\zeta \equiv b_0/(\gamma_0 \Delta a) >> 1 \tag{15}$$

a simple and approximate formula of Eq 14 for the deformation theory, J_D, is rewritten as

$$J_D \simeq J_0 \left\{1 - \left(\frac{\Delta a}{2}\right)\left(\frac{\gamma_0}{b_0} + \frac{\gamma}{b}\right)\right\} \tag{16}$$

Although this is an approximate equation for J_D, it does not require an incremental calculation as in Eq 11.

Equation for J_M

Although Eq 8 correctly evaluates J for crack growth, the value of the deformation theory, J_D, depends solely on size and type of specimen in the presence of enough crack growth. Therefore, Ernst proposed a new J-like parameter, the modified J, J_M, that characterizes the material resistance to crack growth in a way that is independent of specimen size. A generalized expression for modified J_M is given as [6]

$$J_M = J_D + \int_{a_0}^{a} (mJ_{pl}/b) da \tag{17}$$

where J_D is the deformation theory J-integral; J_{pl} is a plastic part of the deformation theory, J_D; and m is generally equal to γ in Eq 9. Although J_M has advantages over J_D, the evaluation of the J-R curve using J_M requires numerical integrations.

Similar to Eq 12, the upper and lower bounds of J_M in Eq 17 are given as

$$J_M < J_D + \int_{a_0}^{a} \left(\frac{mJ_D}{b}\right) da < J_D \left\{1 + \left(\frac{m\Delta a}{b}\right)\right\} \tag{18}$$

and

$$J_M > J_D \left(1 + \frac{m_0 \Delta a}{2b_0}\right) \tag{19}$$

By equating m to γ and averaging the two boundary values of Eqs 18 and 19, J_M is approximated as

$$J_M \simeq J_D \left\{1 + \left(\frac{\Delta a}{2}\right)\left(\frac{\gamma_0}{2b_0} + \frac{\gamma}{b}\right)\right\} \tag{20}$$

Substituting Eq 16 into Eq 20, the following simpler and approximate equation without numerical integration is introduced.

$$J_M \simeq J_0 \left(1 - \frac{\gamma_0 \Delta a}{2b_0}\right) \tag{21}$$

J_{Ic} *and Tearing Modulus,* T_M

J_{Ic} is an engineering estimate of fracture toughness near the onset of slow stable crack growth, and is defined as the J value at the intersection of a blunting line and the J-R curve [*2*]. Referring to the second term of the right-hand side in Eqs 4 and 7 [*10*], the blunting line, approximating the crack tip stretch effects, is drawn by the equation that

$$J = 4\sigma_f \Delta a \tag{22}$$

where σ_f is the flow stress.

In order to demonstrate the characteristics of crack growth whether in a stable or unstable manner, Paris et al. [*11*] introduced a nondimensional quantity called the tearing modulus, T_M, that has the form

$$T_M = \frac{E}{\sigma_f^2} \frac{dJ}{da} \tag{23}$$

where E is the elastic modulus. The value of T_M is evaluated using the J-R curve of the material for the previously mentioned J_0, J_D, or J_M.

Experimental Procedure

In order to compare the approximate formulas for the deformation theory, J_D, and the modified J_M with the original ones, static fracture toughness tests were conducted.

Test for Bending Specimens

The test material was ASTM A508-Cl.3 steel. The chemical compositions and the mechanical properties are listed in Tables 1 and 2. The test specimens were blunt U-notched or fatigue precracked Charpy type and 3PB type with 40% side grooves, as are shown in Fig. 2. The maximum stress intensity factor of the fatigue cycle was less than 18.6 MPa $\sqrt{\text{m}}$.

TABLE 1—*Chemical compositions of materials.*

Material	C	Si	Mn	P	S	Cu	Ni	Cr	Mo
A508	0.17	0.32	1.37	0.003	0.002	0.02	0.67	0.16	0.54
A533B	0.20	0.28	1.46	0.020	0.013	0.16	0.61	0.14	0.51

TABLE 2—*Mechanical properties of materials.*

Material	Yield Strength, MPa	Tensile Strength, MPa	Flow Stress, MPa	Elongation, %	Reduction of Area, %
A508	464	616	540	24.5	71.9
A533B	480	632	556	27.7	65.2

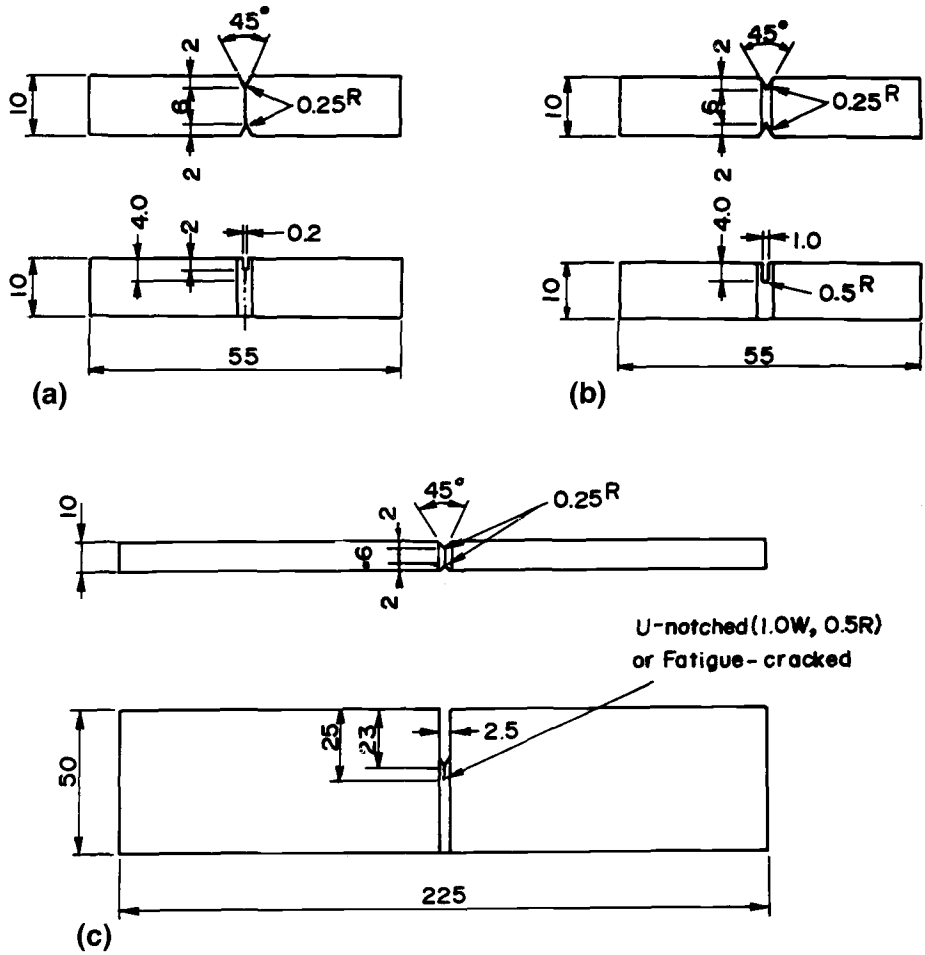

(*a*) Fatigue precracked Charpy specimen.
(*b*) U-notched Charpy specimen.
(*c*) Fatigue precracked or U-notched three-point bend specimen.

FIG. 2—*Geometry of test specimens for A508 steel. (Dimensions in mm.)*

The J_{Ic} test, using a multiple-specimen method, was conducted at 100°C, referring to ASTM Test Method for J_{Ic}, a Measure of Fracture Toughness (E 813-86) and JSME Test (S 001-1981) [*10*]. The loading spans of the Charpy and 3PB specimens were 40 and 200 mm, respectively. The load and crosshead displacement were recorded during the test.

The *J-R* curves by the multiple-specimen fractography method [*10*] were obtained from the relationship between the *J*-integrals, calculated by Eq 1, and crack extension, Δa. The crack extension was measured by scanning electron microscopic observation of the fracture surface as the average value at nine equally spaced points through the specimen thickness.

On the other hand, the *J-R* curve was obtained by the single-specimen key-curve method. The procedure is as follows. Denoting subscripts f and u as being fatigue precracked and U-notched specimens, respectively, the *P*-δ curves of the two specimens are then superimposed. When the dimension of the two specimens does not coincide with each other, the latter curve, which is assumed to be Path 3 in Fig. 1, is converted from Eq 2 by

$$\delta = \delta_u W_f/W_u \tag{24}$$

$$P = \left(\frac{P_u W_f}{W_u}\right)\left(\frac{1 - \alpha_f}{1 - \alpha_u}\right)^2 \tag{25}$$

where $\alpha_u = a_u/W_u$ and $\alpha_f = a_f/W_f$. The *J*-integrals at any displacement level of the fatigue-cracked specimen are calculated by the corresponding equations, using the $P_f - \delta_f$ relationship on Path 1 and the $P_u - \delta_u$ relationship on Path 3 in Fig. 1. Namely, the *H* function in Eq 2 is evaluated by the $P_u - \delta_u$ record of a single blunt U-notched specimen. Then the J_0 is obtained by Eq 1, and the J_D by Eqs 11 or 16, the J_M by Eqs 17, 20, or 21. The corresponding crack extension, Δa, is calculated by Eq 4.

Test for CT Specimens

The material tested was ASTM A533B-Cl.1 steel and the chemical compositions and the mechanical properties are listed in Tables 1 and 2. Some of the material were subjected to thermal aging by heating for 36 days at 400 or 500°C. The blunt U-notched or fatigue precracked CT specimens with 20% side grooves, shown in Fig. 3, were used. The maximum stress intensity factor of the fatigue cycle was less than 18.6 MPa $\sqrt{m}$.

The single-specimen key-curve test, followed by the previously mentioned procedure, was conducted at room temperature for the CT specimens. The *J-R* curves were determined from the relationship between the *J*-integral, calculated by Eqs 1, 11, 16, 20, or 21, and the corresponding crack extension Δa by Eq 7.

For comparison, the unloading compliance J_{Ic} test using single specimen was conducted at room temperature. The test procedure was referred to ASTM E 1152-87 except for the calculation of the *J*-integral in accordance to ASTM E 813-86.

Experimental Results and Discussion

Results of Bending Specimens

Figure 4 compares *J-R* curves of 3PB specimens of A508 steel at 100°C that were determined from the multiple-specimen fractography method and the single-specimen key-curve method. The values of the *J*-integral in the figure are calculated by Eq 1. The comparison of the Charpy-type and 3PB specimens is also shown in the same figure.

The fatigue cracked specimens in Fig. 4 were loaded beyond the maximum load of the U-notched specimen, where the key-curve method cannot be applied due to the occurrence

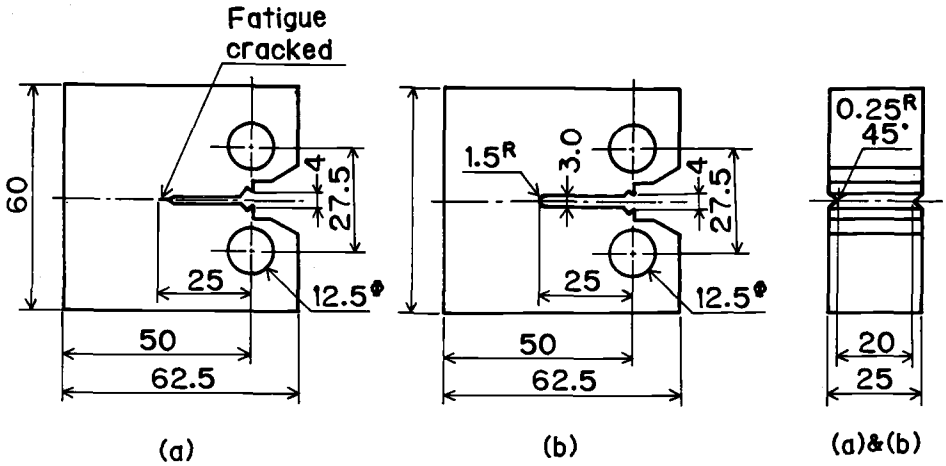

(*a*) Fatigue precracked compact tension specimen.
(*b*) U-notched compact tension specimen.

FIG. 3—*Geometry of test specimens for A533B steel. (Dimensions in mm.)*

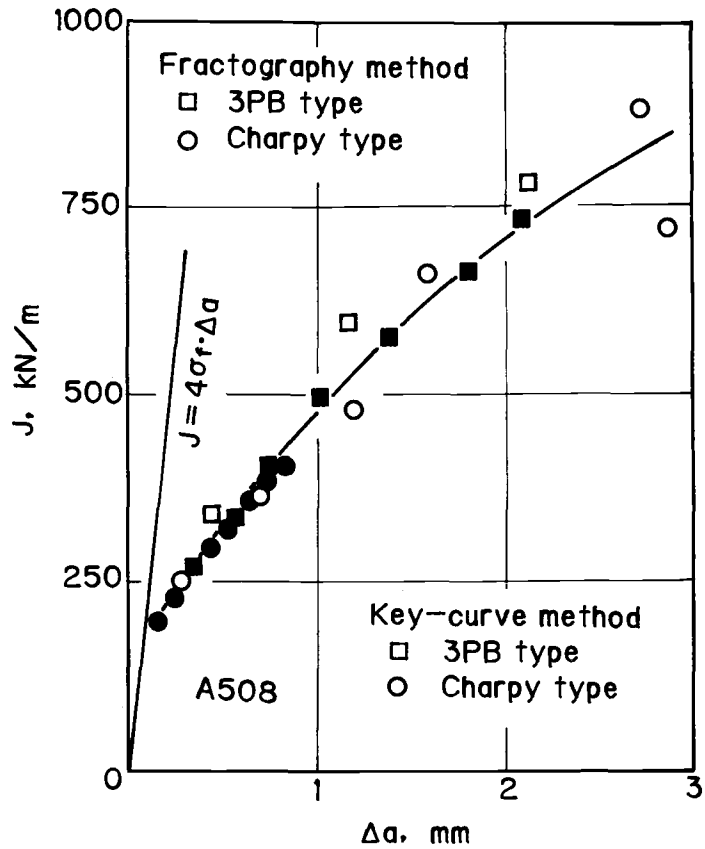

FIG. 4—*Comparison of* J_0-R *curves, obtained by the multiple-specimen fractography method and the single-specimen key-curve method, for the 3PB specimen and the Charpy specimen of A508 steel, tested at 100°C.*

of crack extension in the U-notched specimen. Therefore, the direct comparison of Eq 4 with the final measured Δa done optically could not be made for A508 steel. However, as there is little difference between the results of the multiple-specimen fractography method and the single-specimen key-curve method in Fig. 4, the key-curve method, using a U-notched specimen and nonincremental Eq 4 for Δa, is considered to be effective regardless of specimen geometry.

Results of CT Specimens

Figures 5 through 7 compare *J-R* curves of CT specimens of as-received and thermal-aged materials, respectively, of A533B steel at room temperature. In these figures, the circles indicate the *J-R* curve determined from the unloading compliance method, while the triangles and squares are from the key-curve method corresponding to crack extension, calculated by Eqs 4 and 7, respectively. The values of *J*-integral in the figures are calculated by Eq 1.

Solid symbols in Figs. 6 and 7 indicate the optically measured final crack extension. It is seen in Figs. 6 and 7 that the estimated final Δa by Eq 7 in the key-curve method has smaller error than by the unloading compliance method. The fatigue cracked specimen in Fig. 5 was loaded beyond the maximum load of the U-notched specimen, where the key-curve method cannot be applied due to the occurrence of crack extension in the U-notched specimen. Therefore, the direct comparison of Eq 7 with optically measured Δa could not be made for the case of Fig. 5.

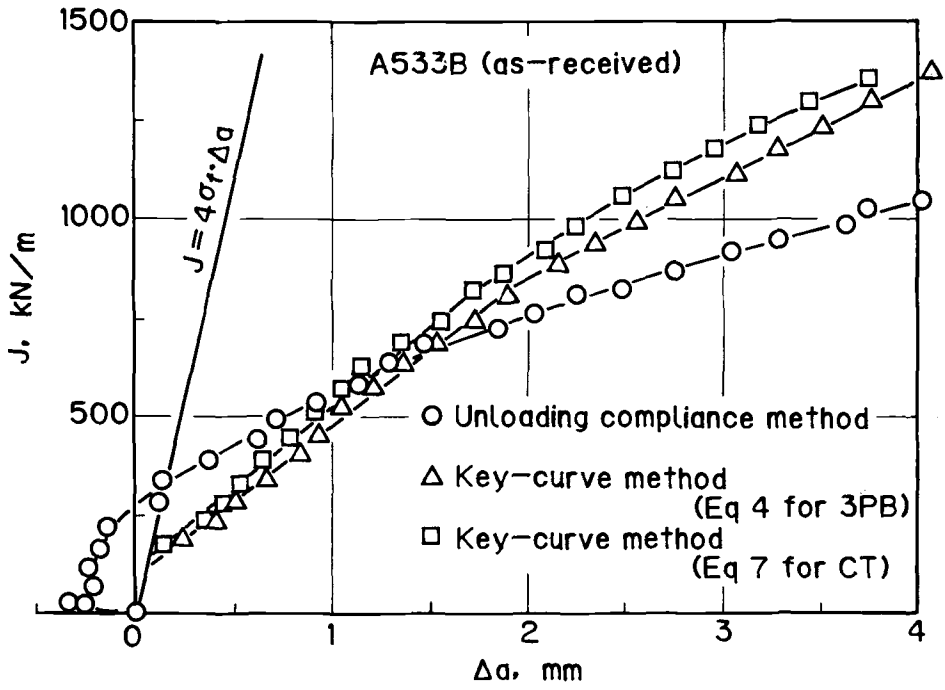

FIG. 5—*Comparison of* J_0-R *curves, obtained by the single-specimen unloading compliance method and the single-specimen key-curve method, tested at room temperature. The specimen is CT type of as-received A533B steel.*

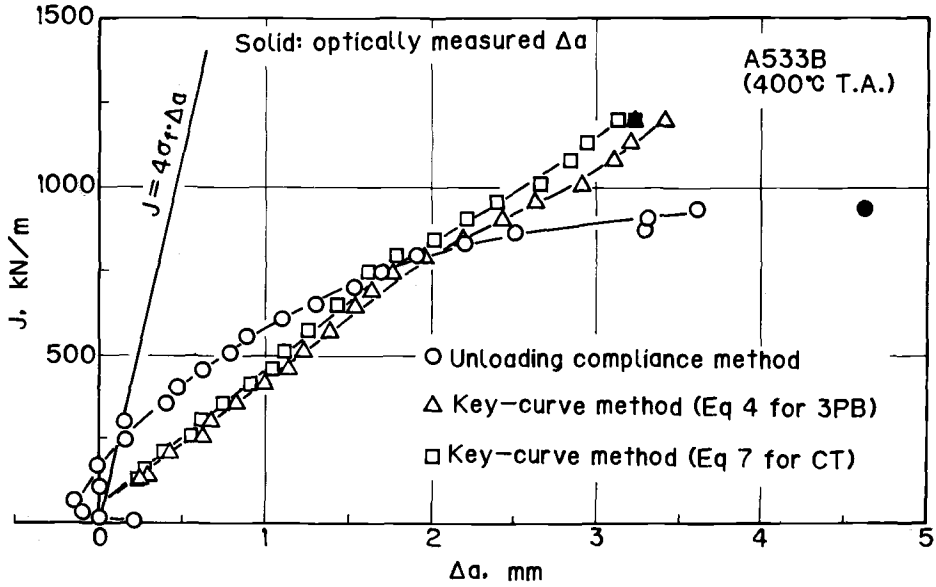

FIG. 6—*Comparison of* J_0-R *curves, obtained by the single-specimen unloading compliance method and the single-specimen key-curve method, tested at room temperature. The specimen is CT type of A533B steel, thermal aged at 400°C for 36 days.*

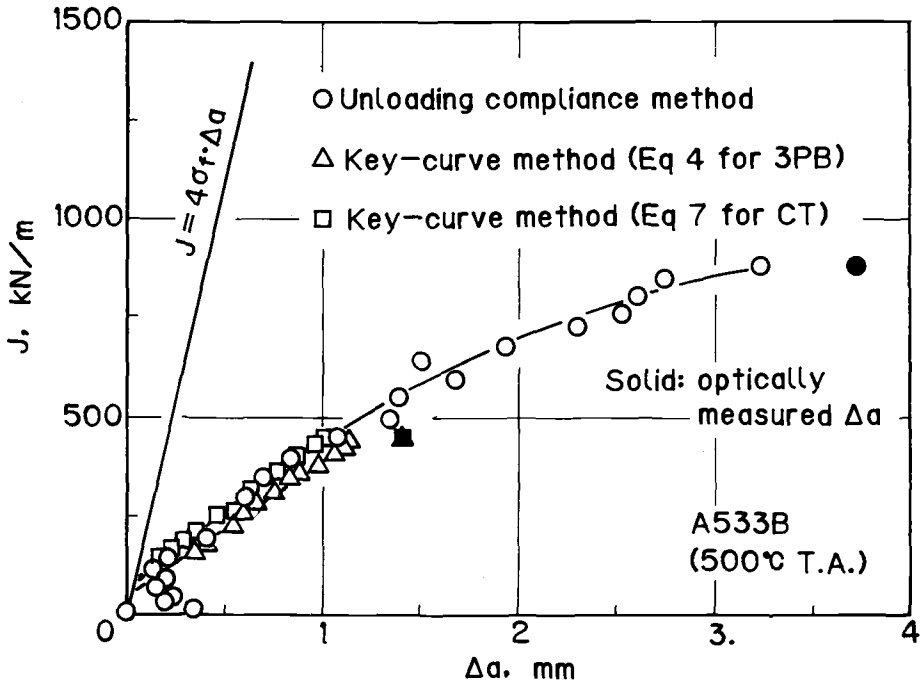

FIG. 7—*Comparison of* J_0-R *curves, obtained by the single-specimen unloading compliance method and the single-specimen key-curve method, tested at room temperature. The specimen is CT type of A533B steel, thermal aged at 500°C for 36 days.*

TABLE 3—*Comparison of* J_{Ic} *and* T_M *of A533B steel.*

Material	Reference Fig. No.	Method	J_{Ic}, kN/m	T_M
As-received	5	UC[a]	320	185
		KC[b]	150	263
Thermal aged at 400°C	6	UC	220	301
		KC	90	251
Thermal aged at 500°C	7	UC	70	254
		KC	75	254

[a]UC = unloading compliance method, [b]KC = key-curve method.

Figures 5 and 6 show some differences between the *J-R* curves determined from the unloading compliance method and the key-curve method, where little difference is seen between them in Fig. 7. Due to the limited number of specimens, the comparison with the *J-R* curves, determined from the multiple-specimen method, has not been conducted for the material.

Equation 7 for the calculation of crack extension of CT specimens resulted in slightly higher gradient of *J-R* curves in Figs. 5 through 7 than that by the simpler Eq 5 for 3PB

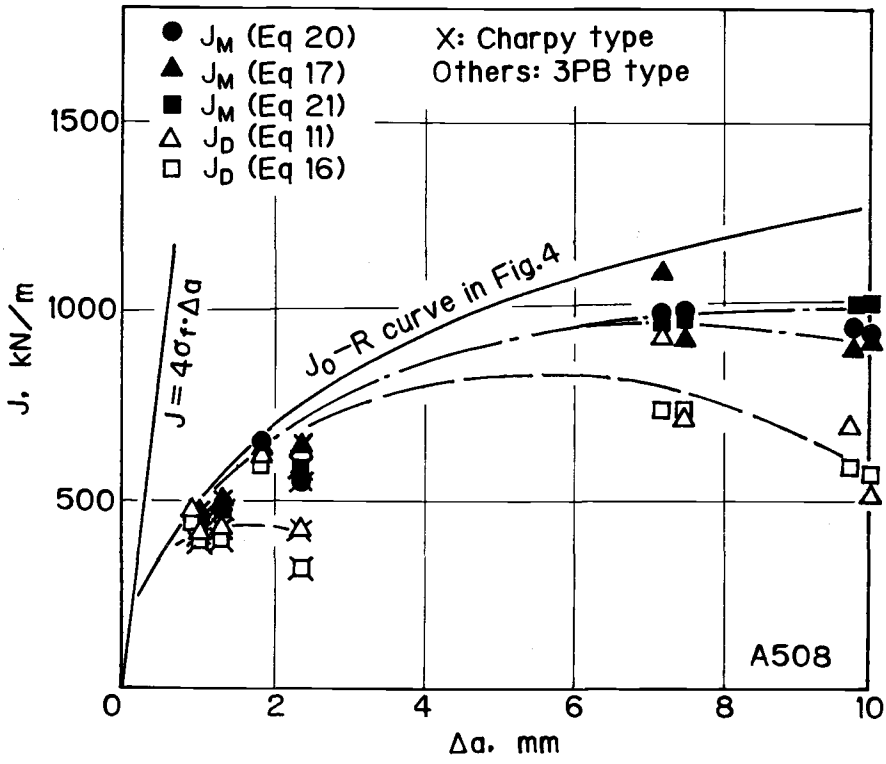

FIG. 8—*Comparison of* J-R *curves, obtained by different formulas on the deformation theory,* J_D, *and the modified* J_M. *The material is A508 steel and the test was conducted by the single-specimen key-curve method at 100°C. The* X *marks denote the result of the Charpy specimens, and the others the 3PB specimens.*

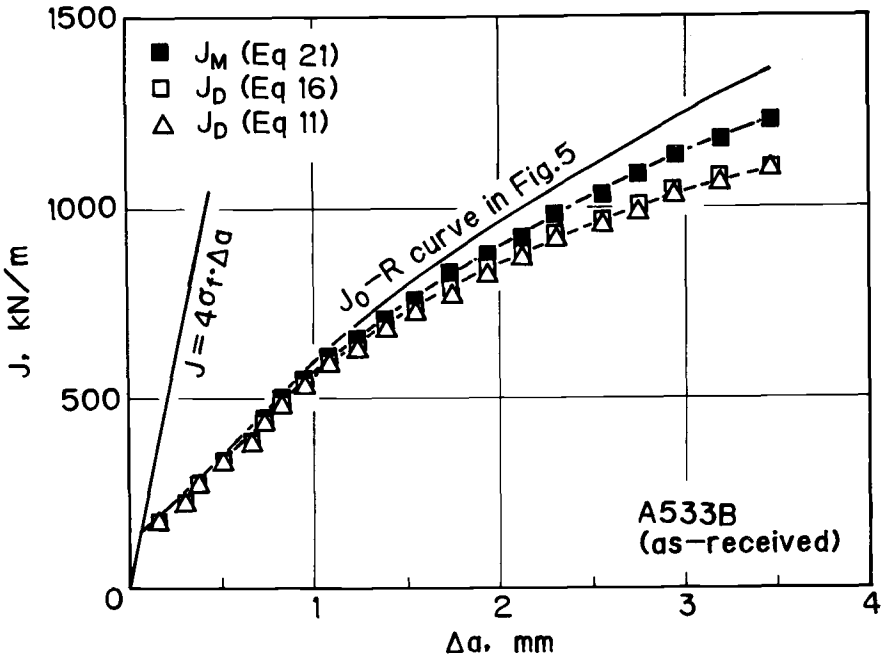

FIG. 9—*Comparison of* J-R *curves, obtained by different formulas on the deformation theory,* J_D, *and the modified* J_M. *The material is as-received A533B steel and the test was conducted by the single-specimen key-curve method at room temperature.*

specimens. The comparison of the values of J_{Ic} and the tearing modulus T_M in Eq 23 at the initial part of *J-R* curves is summarized in Table 3. It is seen in Table 3 that the results of the key-curve method indicate more clearly the decrease of J_{Ic} and T_M due to the thermal aging than the unloading compliance method.

J_D-R *and* J_M-R *Curves*

Figures 8 and 9 compare the deformation theory J_D-R curves, calculated by the ASTM incremental formula of Eq 11, with those, calculated by the simple approximate formula, of Eq 16. Since little difference is seen in the results obtained by the two equations, it is found that if J_0 on Path 3 in Fig. 1 with the absence of crack growth is estimated using the U-notched specimen, then the deformation theory *J*-integral is directly evaluated by Eq 16, instead of making incremental calculations shown in the ASTM E 1152–87.

Also, Figs. 8 and 9 indicate the comparison of the modified J_M-R curves, calculated by Eq 21 in the same test conditions, with those calculated by Eq 17, into which the value of the deformation theory, J_D, from Eq 11 is substituted. These two curves in the two figures coincide well with each other. Therefore, it is shown that the modified *J*-integral, J_M, for the determination of *J-R* curve can be evaluated simply and accurately by Eq 21, and without incremental calculations of Eq 11 and numerical integration of Eq 17. When Δa is large and Eq 15 is not satisfied, substitution of Eq 14 to J_D in Eq 20 improves the accuracy of J_M, as is shown in Fig. 8.

The limiting condition of Eq 15 for the approximate J_D Eq 16 is evaluated from the deviation point of J_D-R curves from J_M-R curves in Figs. 8 and 9 as $\zeta \geqq 10 \sim 15$. In the

same way, the limiting condition of Eq 15 for the approximate J_M Eq 21 is evaluated from the deviation point of different J_M-R curves in Fig. 8 as $\zeta \geqq 4$.

Figures 8 and 9 indicate that the deformation theory J_D-R curve tends to have a maximum value, while the modified J_M-R curve has a tendency to be saturated as Δa increases. This suggests the importance of the modified J-integral in the presence of a significant amount of crack extension.

Conclusions

Simple and nonincremental formulas for the evaluation of the J-R curve based on the deformation theory J-integral, J_D, and the modified version of J-integral, J_M, and the simplified key-curve method using a pair of blunt U-notched and fatigue cracked specimens have been proposed. The J-R curves, determined from the key-curve method, have shown sufficient accuracy of the proposed formulas and methods well beyond the J-controlled crack growth regime, regardless of size and type of specimens and materials. The decrease of J_{Ic} and the tearing modulus, T_M, due to thermal aging was more obvious in the key-curve method than in the unloading compliance method. The difference of the J-R curves between J_D and J_M indicates the importance of the modified J-integral in the presence of a significant crack extension.

References

[1] Rice, J. R., "A Path Independent Integral and the Approximate Analysis of Strain Concentration by Notches and Cracks," *Transactions*, American Society of Mechanical Engineers, *Journal of Applied Mechanics*, Vol. 35, 1968, pp. 379–386.

[2] Begley, J. A. and Landes, J. D., "The J Integral as a Fracture Criterion," *Fracture Toughness, ASTM STP 514*, American Society for Testing and Materials, Philadelphia, 1972, pp. 1–23.

[3] Hutchinson, J. W. and Paris, P. C., "Stability Analysis of J-Controlled Crack Growth," *Elastic-Plastic Fracture, ASTM STP 668*, J. D. Landes, J. A. Begley, and G. A. Clarke, Eds., American Society for Testing and Materials, Philadelphia, 1979, pp. 37–64.

[4] Ernst, H. A., Paris, P. C., Rossow, M., and Hutchinson, J. W., "Analysis of Load-Displacement Relationship to Determine J-R Curve and Tearing Instability Material Properties," *Fracture Mechanics (Eleventh Conference), ASTM STP 677*, C. Smith, Ed., American Society for Testing and Materials, Philadelphia, 1979, pp. 581–599.

[5] Ernst, H. A., Paris, P. C., and Landes, J. D., "Estimations on J-Integral and Tearing Modulus from a Single Specimen Test Record," *Fracture Mechanics (Thirteenth Conference), ASTM STP 743*, Richard Roberts, Ed., American Society for Testing and Materials, Philadelphia, 1981, pp. 476–502.

[6] Ernst, H. A., "Material Resistance and Instability Beyond J-Controlled Crack Growth," *Elastic-Plastic Fracture: Second Symposium, Vol. I: Inelastic Crack Analysis, ASTM STP 803*, C. F. Shih and J. P. Gudas, Eds., American Society for Testing and Materials, Philadelphia, 1983, pp. I-191–I-213.

[7] Joyce, J. A., Ernst, H. A., and Paris, P. C., "Direct Evaluation of J-Resistance Curves from Load Displacement Records," *Fracture Mechanics (Twelfth Conference), ASTM STP 700*, American Society for Testing and Materials, Philadelphia, 1980, pp. 222–236.

[8] Landes, J. D., Walker, H., and Clarke, G. A., "Evaluation of Estimation Procedures Used in J-Integral Testing," *Elastic-Plastic Fracture, ASTM STP 668*, J. D. Landes, J. A. Begley, and G. A. Clarke, Eds., American Society for Testing and Materials, Philadelphia, 1979, pp. 266–287.

[9] Ohtsuka, N., "Evaluation of Tearing Instability from a Load-Displacement Relationship," *Transactions*, Japan Society of Mechanical Engineers, Series A, Vol. 54, No. 497, 1988, pp. 72–77 (in Japanese).

[10] "Standard Method of Test for Elastic-Plastic Fracture Toughness J_{Ic}," JSME S 001-1981, Japan Society of Mechanical Engineers, 1981 (in Japanese).

[11] Paris, P. C., Tada, H., Zahoor, A., and Ernst, H. A., "The Theory of the Tearing Mode of Elastic-Plastic Crack Growth," *Elastic-Plastic Fracture, ASTM STP 668*, J. D. Landes, J. A. Begley, and G. A. Clarke, Eds., American Society for Testing and Materials, Philadelphia, 1979, pp. 5–36.

Mark P. Landow[1] *and Charles W. Marschall*[1]

Experience in Using Direct Current Electric Potential to Monitor Crack Growth in Ductile Metals

REFERENCE: Landow, M. P. and Marschall, C. W., **Experience in Using Direct Current Electric Potential to Monitor Crack Growth in Ductile Metals,"** *Elastic-Plastic Fracture Test Methods: The User's Experience (Second Volume), ASTM STP 1114*, J. A. Joyce, Ed., American Society for Testing and Materials, Philadelphia, 1991, pp. 163–177.

ABSTRACT: The direct-current electric potential (d-c EP) method is receiving increasing attention as an alternative to the unloading compliance method for monitoring crack initiation and growth during fracture toughness testing of ductile metals. Advantages of the d-c EP method include uninterrupted tests, continuous monitoring of crack extension, ability to accurately measure relatively large amounts of crack growth, and ability to be used at high displacement rates in many materials. The principal shortcoming of the d-c EP method (as with most other methods) is the uncertainty in defining the point of crack initiation in some tests.

This paper describes Battelle's experience in using the d-c EP method to monitor crack initiation and growth in compact (tension) specimens machined from various pipes used in cooling systems of nuclear reactors. Among the materials investigated are carbon steel pipes (base metal and weld metal) and extremely ductile austenitic stainless steel pipes (base metal and weld metal). Discussed in the paper are: (1) estimation of the crack-initiation point from d-c EP data, (2) ability of the d-c EP method to accurately predict large amounts of crack growth in highly ductile metals, (3) modification of the Johnson equation to improve the accuracy of the d-c EP method for large crack growth, and (4) use of the d-c EP method at high displacement rates.

KEY WORDS: electric potential method, crack initiation, crack growth

Background

Ever since the introduction of the *J*-integral into fracture mechanics terminology in the 1970s, there has been a strong need to be able to monitor crack extension in fracture-mechanics specimens. Such a need did not exist for measurement of K_{Ic}, the plane-strain fracture toughness, because K_{Ic} is strictly a crack-initiation parameter which is derived from the interpretation of a simple load-displacement record. J_{Ic} while also a crack-initiation parameter, require that crack growth data be obtained and extrapolated back to a small amount of growth to determine the crack-initiation point. Finally, *J*-resistance curves, which show how *J* changes with changing crack length, obviously require that crack-growth data be obtained.

The very first *J*-testing standard [Standard Method for J_{Ic}, A Measure of Fracture Toughness (ASTM E 813-81)] recommended that crack growth be determined by testing a number

[1]Research scientist and senior research scientist, respectively, Battelle, Columbus, OH 43201-2693.

of specimens to different amount of displacement, marking the final crack front by heat tinting or fatigue, breaking the specimen open to reveal the fracture surface, and measuring the crack growth directly from the fracture surface with a traveling microscope. Clearly, this is a nearly fool-proof method for determining crack extension at a specific point in a test and one that is still used in some laboratories. It required a minimum of sophistication in either equipment or procedures. However, because the method, usually called the multiple-specimen method, was slow and laborious, interest quickly developed in other methods that would permit obtaining J versus crack extension data from a test on a single specimen. The single-specimen method that has become most popular is referred to as the unloading compliance method [*1*]. In that method a compact or bend specimen is partially unloaded at frequent intervals during a test, and the crack length at each unloading point is computed from the known compliance relation for the particular specimen type.

Another single-specimen method that is receiving increasing attention for monitoring stable crack extension in fracture-mechanics testing measures the electric potential at the crack mouth as a constant electric current is passed through the specimen [*2–15*]. The method is referred to as the electric potential method or the potential drop method. When the appropriate calibration is applied to the data, the change in potential can be used to indicate the change in crack length.

The electric potential method has several obvious advantages over the unloading compliance method. It permits tests to be conducted without interrupting for unloadings. It permits continuous, rather than intermittent, monitoring of crack extension, and it permits use of high displacement rates. In spite of these advantages, however, no standard method has yet been developed for incorporating the electric potential method in J_{Ic} or J-R curve testing.

In a recently completed program conducted for the United States Nuclear Regulatory Commission, Battelle employed the direct-current electric potential (d-c EP) method for determining crack extension during tests using compact specimens machined from coolant pipes of the type used in nuclear reactor systems. The impetus for using that method came largely from work reported by Johnson [*3*] and Schwalbe and Hellman [*7*]. Of particular importance to the Battelle study was the demonstration in Ref *7* that a single calibration equation, the so-called Johnson equation, could be used in tests on all compact specimens, independent of specimen material, specimen dimensions, test temperature, or current. The calibration formula is, from Ref *7*

$$a = (2w/\pi) \cos^{-1} \frac{\cosh (\pi y/2w)}{\cosh \{(U/U_o) \cosh^{-1} [\cosh (\pi y/2w)/\cos(\pi a_o/2w)]\}} \tag{1}$$

where

a = crack length,
a_o = original crack length,
w = specimen width,
$2y$ = the spacing of the potential probes (Fig. 1), and
U/U_o = the ratio of electric potential at a particular point in the test to that at the start of stable crack growth.

An added advantage of this formula is that precise placement of the potential probes is not necessary, so long as the actual value of $2y$ is included in Eq 1.

This paper describes Battelle's experience in using the d-c EP method and Eq 1 to monitor crack initiation and growth in C(T) specimens machined from nuclear-grade pipes of both

carbon steels and austenitic stainless steels, and including both base metals and weld metals. The data generated in these tests were used in the analysis of the experimental pipe rupture tests, where large amounts of stable crack growth can be obtained. For this reason many of the compact-specimen tests were extended beyond the limits covered by ASTM E 813, so that the displacement of the potential probes had to be taken into account when evaluating Eq 1.

Experimental Procedures

The experimental setup used at Battelle for monitoring crack extension in C(T) tests is shown in Fig. 1. The attachment points for the current leads at Locations A and B have been shown by Schwalbe and Hellman [7] to give results that are in good agreement with the Johnson Eq 1.

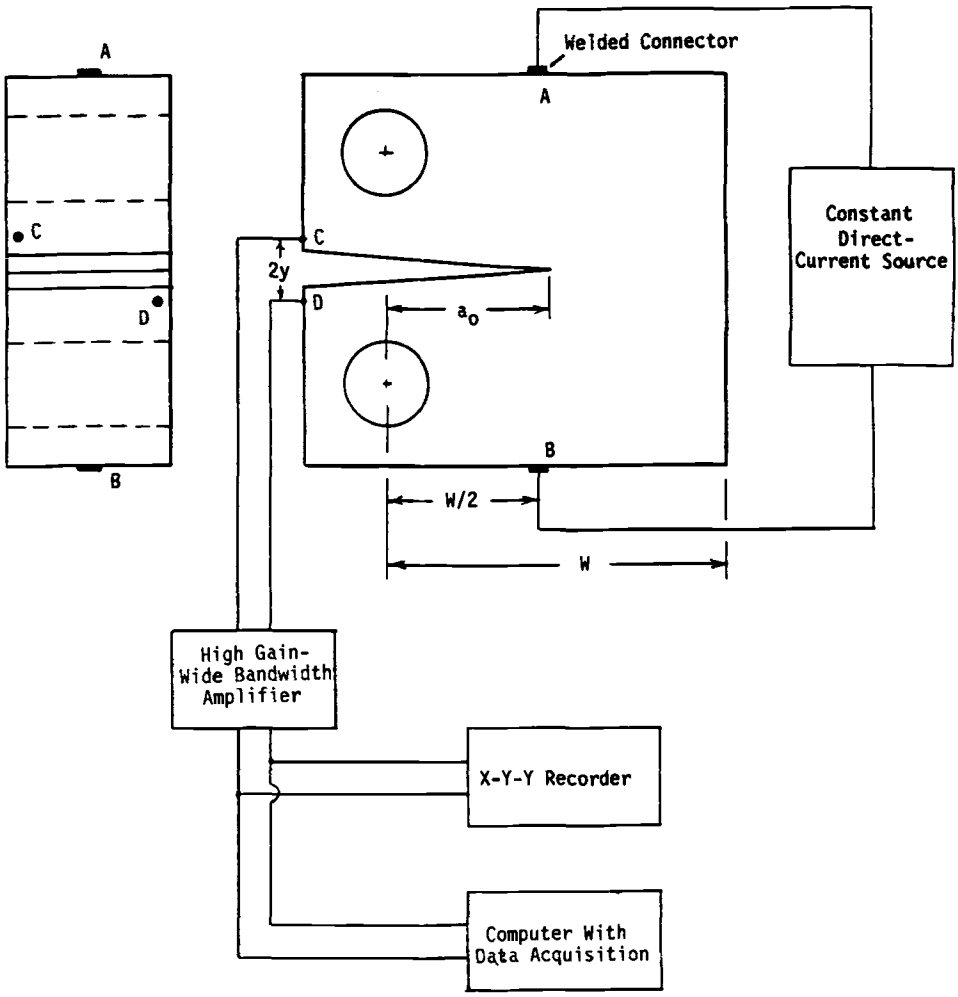

FIG. 1—*Schematic illustration of direct-current electric potential method used at Battelle to monitor crack extension.*

The potential leads were spark-welded to the specimens across the notch mouth at Locations C and D. These leads were iron wires in the case of carbon steel specimens, and Type 304 stainless steel wires in the case of stainless steel specimens, to minimize thermal electromotive force voltage that can arise when dissimilar metals are in contact. As can be seen in the edge-on-view in Fig. 1, Location C was near one side of the specimen and Location D near the other side, in an attempt to detect average crack length in those cases where the crack front was not straight.

At the start of a test, the current was adjusted to provide a potential of approximately 400 to 500 μV across the potential leads. That level of potential was achieved readily with available power supplies and gave a reasonable ratio of signal to noise. The magnitude of the direct current required to achieve that potential depended on the specimen material, specimen size, and test temperature. The gain setting used in the Ectron amplifier was 1000 with no filtering of the signal through the amplifer.

Several different testing machines were used in the program because of the variety of compact-specimen sizes tested. Sizes ranged from 0.4 T planform dimensions by 5 mm (0.2 in.) thick to 10 T by 25.4 mm (1 in.) thick. In each testing machine, a current path through the load train was prevented by insulating the load cell from the machine. This insulation was accomplished by placing a thin, nonconducting ring between the load cell and the stationary crosshead of the machine and securing the load cell with nylon bolts.

During a *J-R* curve test on a C(T) specimen, the electric potential, U, was monitored in two ways. A continuous record of U versus load-line displacement, V_{LL}, was obtained on an X-Y-Y recorder, and U versus V_{LL} readings were recorded every 4 s using a computer equipped with an acquisition board. The test was terminated when the crack had grown to a length of approximately 50 to 70% of the original ligament.

Analysis of d-c EP Data to Estimate the Point of Crack Initiation

In analyzing d-c EP data to estimate the point at which a crack initiates from the original fatigue precrack, we first examine the curve of U versus V_{LL}, in the manner suggested many years ago by Lowes and Fearnehough [*4*], and subsequently confirmed by Wilkowski et al. [*9,13*] and Vassilaros and Hackett [*10*]. Those investigators reported that the U versus V_{LL} curve showed an initial portion in which U rose linearly with V_{LL}, after which U began to rise more steeply. The point at which the curve departed from a straight line was shown to be a good approximation of the point of crack initiation. An example of such a graph is shown in the middle diagram of Fig. 2, which is an actual test record for a C(T) specimen tested in the Degraded Piping Program. Notice that the estimated crack initiation Point, I, lies at a reasonable location on the upper diagram in Fig. 2, that is, beyond the point of departure from linear-elastic behavior and below the maximum-load point. At Battelle, in addition to examining the U versus V_{LL} graph, we examine also a graph of load versus U (bottom diagram in Fig. 2) to look for a distinct slope change that will confirm the selection of Point I as a good estimate of the crack initiation point [*11*].

Another example of actual test data from a C(T) specimen in the Degraded Piping Program is shown in Fig. 3. In that test, the U versus V_{LL} graph (middle diagram) does not show as distinct a deviation from linearity as in Fig. 2. In fact, three different points—A, B, and C—appear about equally credible as crack initiation points. In cases like this, we examine the load versus U graph (lower diagram) for points of slope change and use engineering judgment to select the most probable point of crack initiation, making certain that it lies at a reasonable location on the load-displacement curve (upper diagram), that is, beyond the linear elastic part of the curve and prior to maximum load. For the data shown in Fig. 3, Point B was selected as the most probable point of crack initiation. As discussed in Ref *14*,

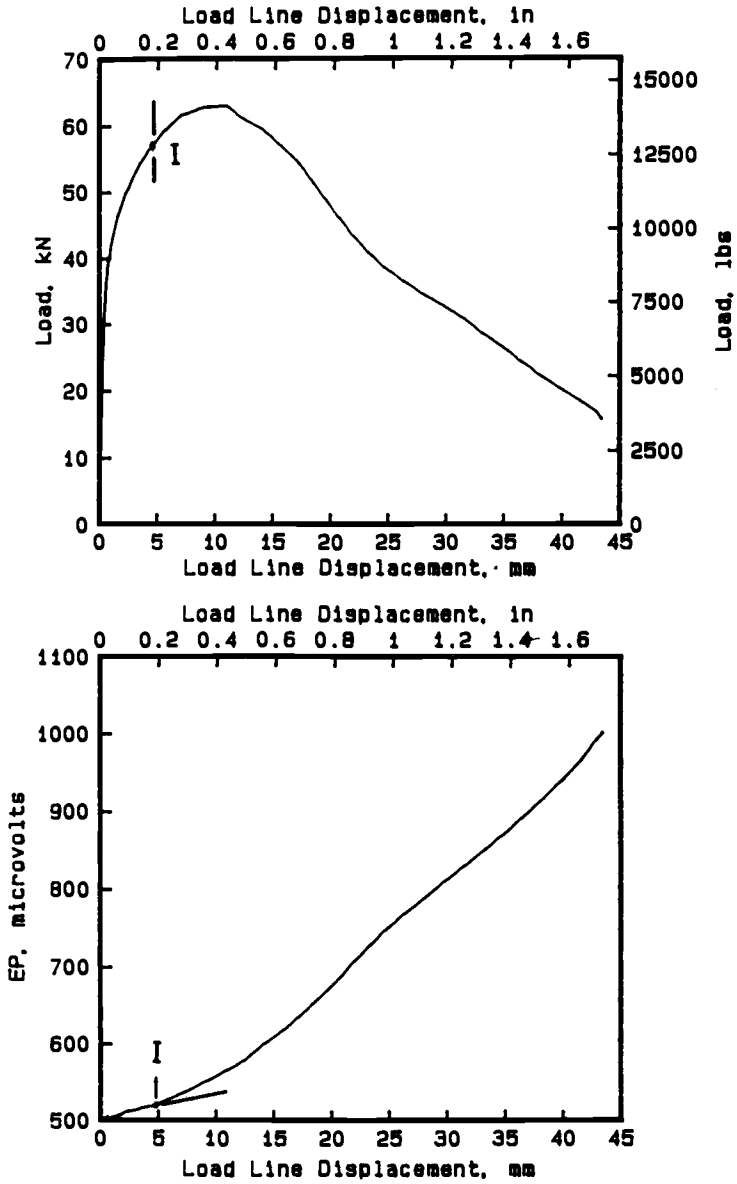

FIG. 2—*Load/displacement/d-c EP data for ASTM A351, Grade CF8M stainless steel C(T) specimen to illustrate determination of crack initiation Point, I. Specimen was 1.5 T planform size; thickness was 23.9 mm (0.94 in.).*

the J at initiation is very sensitive to the selection of the crack initiation point on the load-displacement curve.

The overall accuracy with which the point of crack initiation was determined from d-c EP data in the C(T) tests conducted at Battelle was not established. A few tests conducted early in the program were terminated at displacements on either side of the anticipated

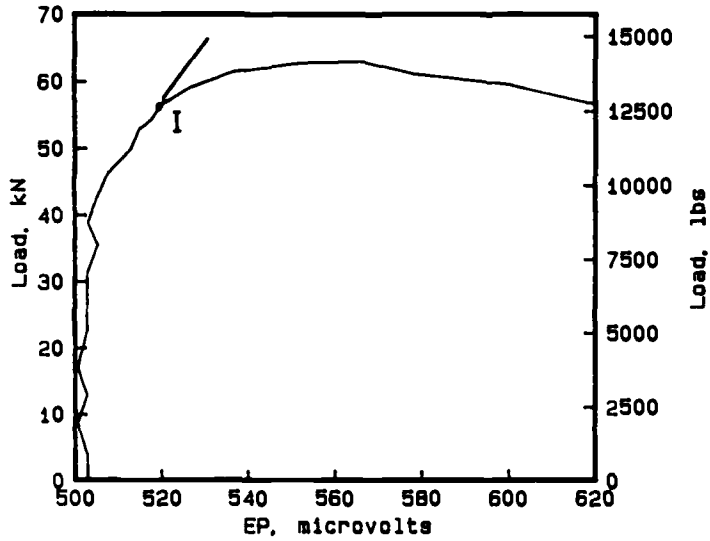

FIG. 2—*Continued*

crack initiation point, as estimated from d-c EP measurements. When the specimens were heat tinted and broken open, the results confirmed the findings of Refs *4*, *9*, *10*, and *13*, namely, that the point of departure from linearity of the U versus V_{LL} curve provides a good estimate of crack initiation.

Analysis of d-c EP Data to Estimate Crack Extension

The method employed at Battelle to estimate the amount of crack extension uses the d-c EP data in conjunction with the Johnson equation (Eq 1). After we have estimated the point of crack initiation (see previous section), we set the value of d-c EP at that point equal to U_o. We calculate values of crack length beyond initiation by inserting appropriate values for U, a_o, y, and w in Eq 1. Rather than using a constant value for y (half the potential-probe spacing) in Eq 1, we allow the value of y to increase in proportion to the displacement because our work has shown that this slight modification to Eq 1 provides a more accurate estimate of the actual crack extension [*15*]. In Ref *15*, the intermediate crack lengths were marked by unloading the specimen by approximately 90% during the testing of the specimen, and post-test crack measurements were made after the specimen was broken open. Figure 4 shows the excellent agreement obtained between calculated and actual crack extensions when that modification was employed in a highly ductile Type 304 stainless steel C(T) specimen. Without that modification, Eq 1 seriously underestimated the actual crack growth, as is shown in Fig. 4.

Other methods that have been employed to determine crack extension from d-c electric potential data include: (1) empirically derived equations from experimental specimens using saw cut notches of different depths and (2) linear interpolation methods. The weakness of the empirical, saw-cut method is that a new calibration is required whenever specimen dimensions or specimen configuration are changed. Also, for specimens that exhibit extensive plastic deformation during testing, the method using empirical equations from saw-cut specimens does not adequately account for the increase in the measured potential from plastic deformation.

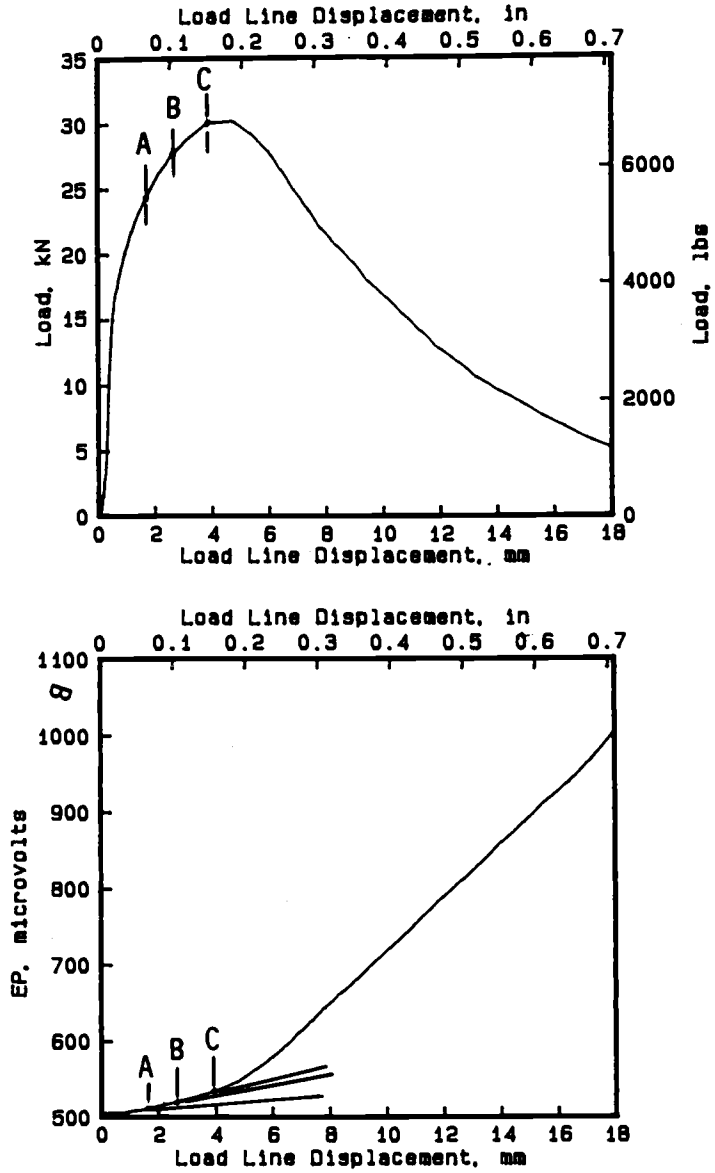

FIG. 3—*Load/displacement/d-c EP data for an ASTM A333 Grade 6 C(T) specimen to illustrate several possible indications of crack initiation at Points A, B, and C. Specimen was 1 T planform size; thickness was 12.2 mm (0.48 in.); 20% side grooved.*

Linear interpolation methods would appear to be well suited to accurate estimation of crack extension because they are forced to provide correct answers at the beginning and end of crack growth and they are self-calibrating for each specimen. A linear interpolation method, described by Hollstein et al. [*16*], is shown schematically in Fig. 5. To calculate the amount of crack extension, Δa, at any point in the test, simply multiply $\Delta U/U_T$ by the

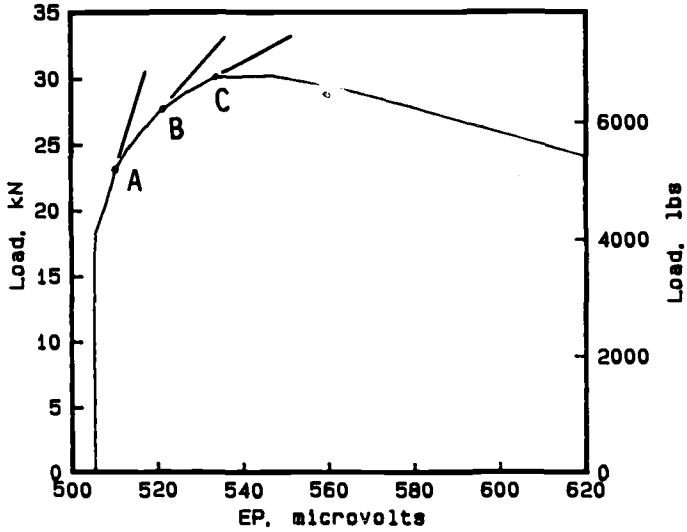

FIG. 3—*Continued*

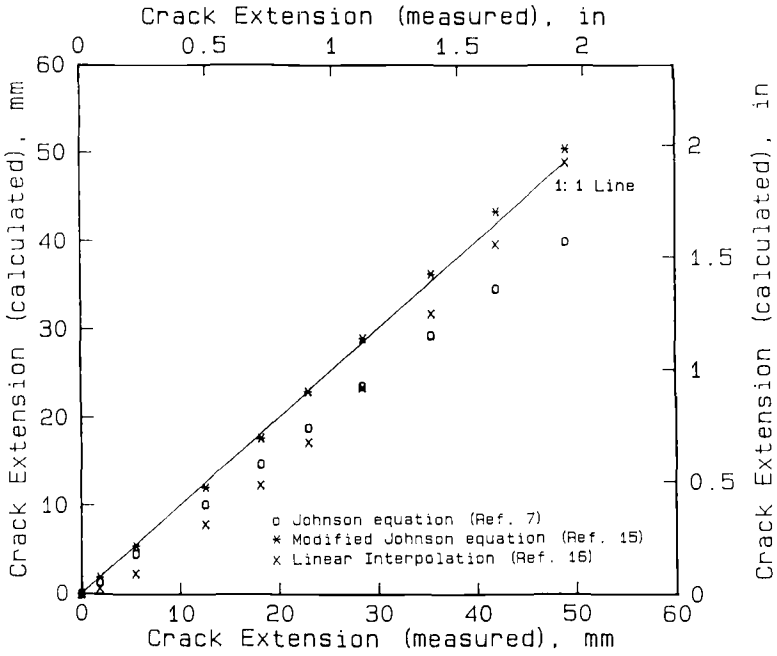

FIG. 4—*Comparison of calculated crack extension with measured crack extension.*

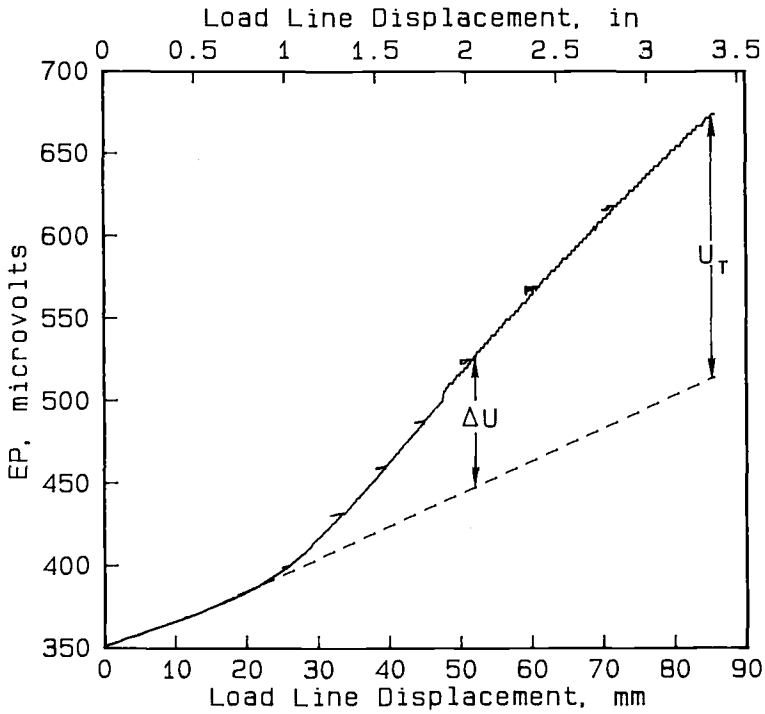

FIG. 5—*Illustration showing how the linear interpolation method in Ref* 16 *was used. Note: curve shown is EP/displacement record of test used in comparison shown in Fig. 4.*

actual total crack extension, Δa_T, measured at the end of the test

$$\Delta a = (\Delta U/U_T)\, \Delta a_T \tag{2}$$

When we applied this method to the d-c EP data from Ref *15*, we found that the agreement between calculated and actual crack growth was relatively poor, except at the end points of the test (see Fig. 4 and Table 1). At all intermediate points in the test, the linear interpolation method underestimated the actual crack extension. It is possible that the agreement would have been significantly better if the total crack extension had been smaller, say 10% of the original ligament rather than about 65% because of the nonlinearity of the a versus U relationship.

Battelle Experience in Estimating Crack Extension

In tests at Battelle, the modified Johnson equation has been used in determining crack extension for several different sizes and thicknesses of C(T) specimens and for crack growth during the test of about 50 to 70% of the initial ligament. Figure 6 and Table 2 illustrate the degree of agreement between predicted and actual crack growth at the end of a test for both ferritic steels and austenitic stainless steels, the majority of which were tested at 288°C (550°F). In over 40% of the tests the calculated crack extension was within ±5% of the measured crack extensions, and in 88% of the tests, calculated crack extensions were within ±15% of the measured crack extensions. The average difference between calculated and

TABLE 1—*Comparison of measured crack extensions with crack extensions calculated from Johnson equation.*

Material: Type 304 stainless steel.
Temperature: 22°C (72°F).
Specimen type: 3T Planform-size compact specimen, B = 25.4 mm (1 in.), W = 152.4 mm (6 in.), and a_0 = 80.11 mm (3.154) in.).
Potential probe location: C-D in Fig. 1.

Unloading Number	Measured Extension, mm (in.)	Calculated Crack Extension, mm (in.), and Percentage Error		
		Johnson Equation	Modified Johnson Equation	Linear Interpolation (Ref *16*)
1	0.000 (0.000)	0.00 (0.000) 0.0%	0.00 (0.000) 0.0%	0.00 (0.000) 0.0%
2	1.88 (0.074)	1.42 (0.056) −24.3%	1.83 (0.072) −2.7%	0.69 (0.0271) −63.4%
3	5.54 (0.218)	4.60 (0.181) −17.0%	5.33 (0.210) −3.7%	2.41 (0.095) −56.4%
4	12.60 (0.496)	10.19 (0.401) −19.2%	11.96 (0.471) −5.0%	7.95 (0.313) −36.9%
5	18.16 (0.715)	14.73 (0.580) −18.9%	17.58 (0.692) −3.2%	12.34 (0.486) −32.0%
6	22.99 (0.905)	18.92 (0.745) −17.7%	22.91 (0.902) −0.3%	17.27 (0.680) −24.9%
7	28.50 (1.122)	23.67 (0.932) −16.9%	28.91 (1.138) +1.4%	23.47 (0.924) −17.7%
8	35.41 (1.394)	29.39 (1.157) −17.0%	36.17 (1.424) +2.2%	31.08 (1.252) −10.2%
9	41.94 (1.651)	34.70 (1.366) −17.6%	43.33 (1.706) +3.3%	39.73 (1.564) −5.3%
10	48.97 (1.928)	40.01 (1.575) −18.3%	50.37 (1.983) +2.9%	48.97 (1.928) 0.0%

actual final crack extension was 7.7%, with a standard deviation of 6.3%. Austenitic steel specimens, which exhibited greater crack-opening displacements and greater lateral contraction ahead of the crack than did ferritic specimens, showed performance results that were approximately the same as those for ferritic steel specimens.

Figure 6 also shows that the calculated crack length was generally slightly less than the measured crack length, especially for the ferritic steels. That result was unexpected; it had been anticipated that d-c EP values might overestimate crack extension because both plastic deformation and ligament contraction ahead of the crack would cause d-c EP values to be raised beyond those due to increased crack length. Also not clear is the reason for the relatively poor agreement (>15% error) between calculated and actual crack extension in about 12% of the tests. The tests in which poor agreement was observed were nominally identical to those in which agreement was good, and nothing unusual was observed in the d-c EP data.

In another group of tests conducted at Battelle as part of a U.S. Nuclear Regulatory Commission (NRC) sponsored round-robin program, excellent agreement between calculated and measured crack extension was obtained using the modified Johnson equation. Tests on three A106 Grade B steels and three aluminum-alloy 1 T C(T) specimens showed average errors of 2.7% with a standard deviation of 1.9%. Crack growth in those tests ranged from 36 to 50% of the original ligament.

Use of d-c Electric Potential in Rapid Rate Loading Tests

Another advantage of the d-c electric potential technique over the unloading compliance technique is that for many materials stable crack extension can be monitored during rapid-rate-loading (high-displacement-rate) tests. Tests have been performed at Battelle on both ferritic steels and austenitic stainless steel C(T) specimens at displacement rates that were

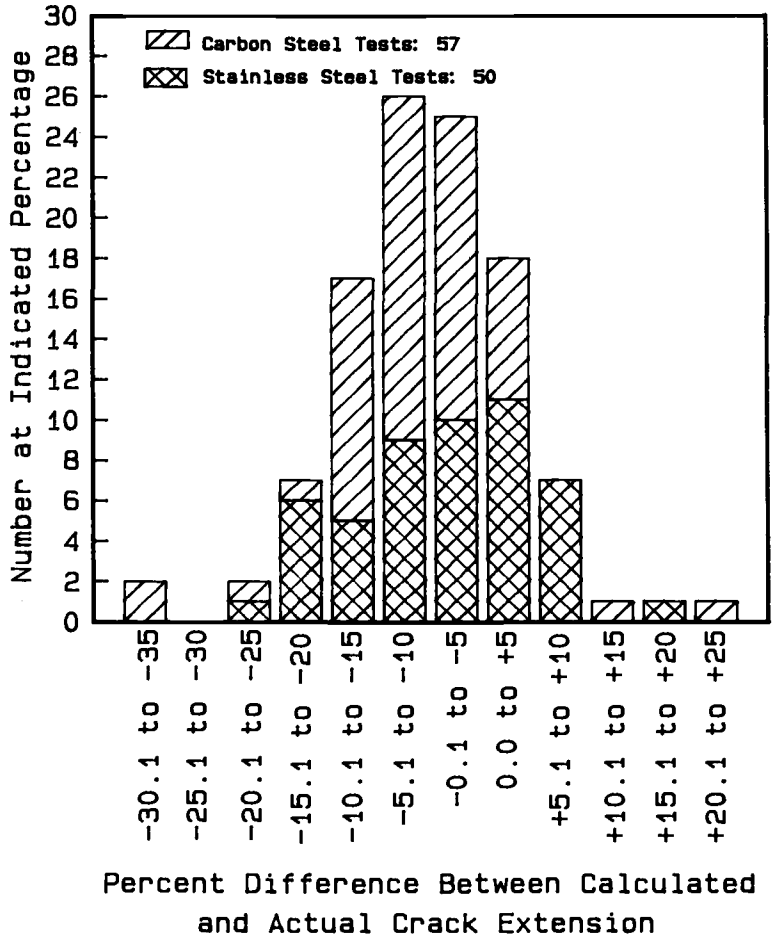

FIG. 6—*Frequency distribution of error in final crack length calculation using d-c electric potential and the modified Johnson equation.*

TABLE 2—*Ability of d-c EP method to estimate total crack extension in* J-R *curve tests of compact specimens.*
(Number of results examined: 60 carbon steel and 47 stainless steel)

Material	Percentage of Results Showing Indicated Difference Between Calculated and Actual Crack Extension		
	±5% max	±10% max	±15% max
Carbon steel	37	70	92
Stainless steel	45	72	83
Combined carbon steel and stainless steel	40	71	88

selected to reach crack initiation in approximately 0.2 s. No problems were encountered in using the d-c EP method in rapid loading tests on the austenitic stainless steel specimens. However, we did encounter problems with the d-c electric potential technique in the determination of crack initiation for the ferritic steels specimens. The major problem encountered was that of a rapid-loading voltage pulse superimposed on the d-c electric potential signal. The problem is illustrated by the test data shown in Fig. 7 for a specimen in which the d-c EP value at the start of the test was approximately 400 μV, a value that we typically use in quasi-static (low-displacement-rate) tests. Notice that the voltage pulse makes it virtually impossible to use the d-c EP data for detecting crack initiation and the early stages of crack growth.

Several rapid-loading tests were performed on a 0.5 T C(T) carbon-steel specimen to determine the source of the voltage pulse. The tests were performed on notched specimens with no applied current through the specimen. Figure 8 shows the electric potential signal recorded in a test specimen that was loaded rapidly to produce a relatively large amount of stable crack extension. This result suggests that the voltage pulse can be attributed to the ferromagnetic properties of the ferritic steel, probably due to the sudden reorientation of ferromagnetic domains when stress is applied rapidly. In a number of tests where the electric potential signal was measured with no applied current through the specimen, the maximum level of the voltage pulse varied among tests, but in some cases exceeded 150 μV for the 0.5 T C(T) specimens being tested. Recall that in our usual static-test procedure, the current was initially set so that the starting potential was 400 to 500 μV; hence, a 150 μV pulse is highly significant.

Several schemes for reducing the magnitude of the pulse were attempted without success. One approach that provided some help in minimizing the effect of the pulse without changing the pulse magnitude was to increase the current through the specimen to produce a signif-

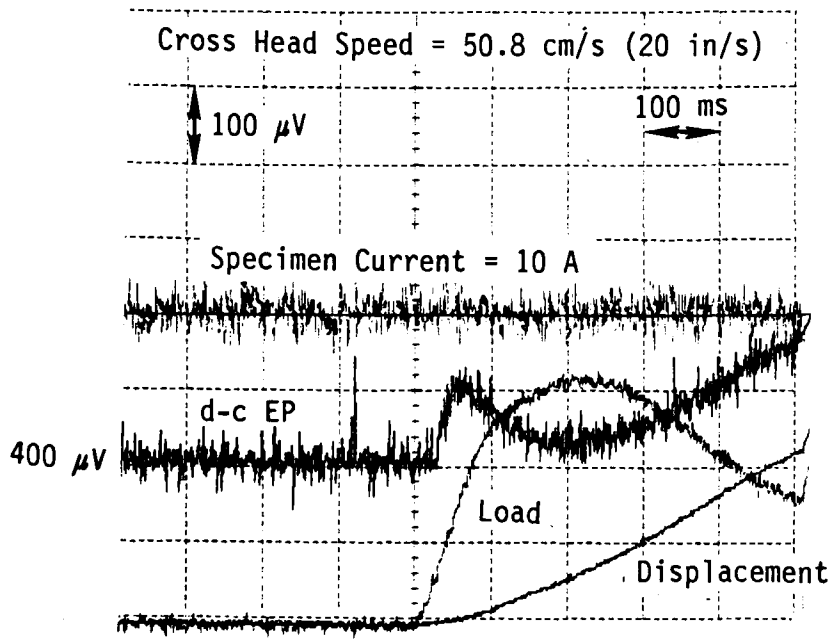

FIG. 7—*Appearance of a voltage pulse in the d-c electric potential signal during testing of a ferritic steel C(T) specimen at a high displacement rate.*

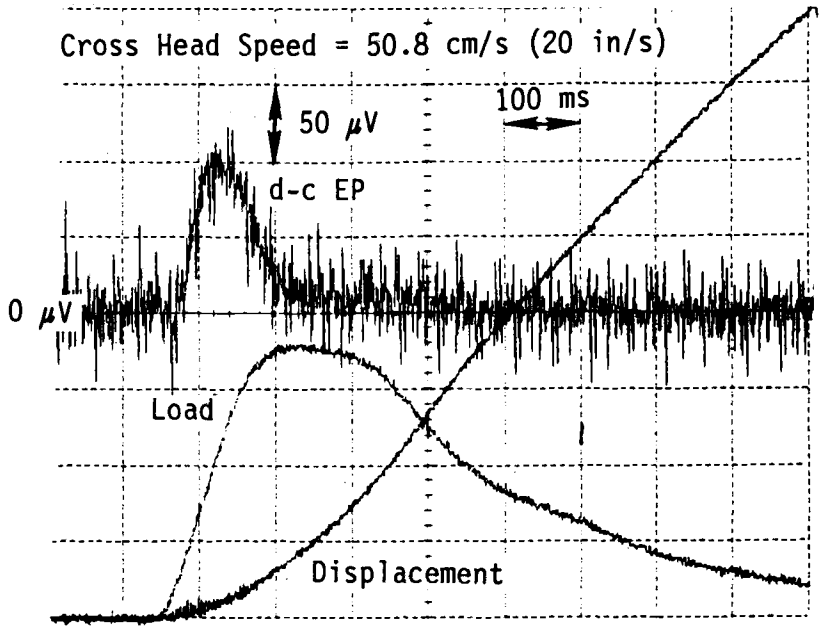

FIG. 8—*Voltage pulse in electric potential signal in a 1/2 T C(T) ferritic steel specimen that was tested with no applied current.*

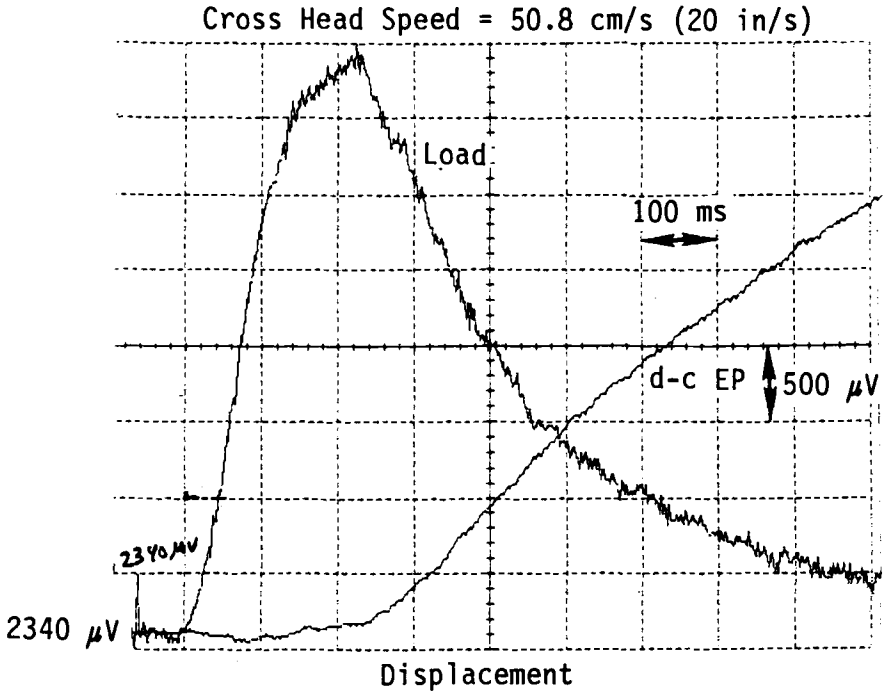

FIG. 9—*Load/displacement and electric-potential-signal/displacement traces for a 1/2 T C(T) ferritic steel specimen tested with initial electric potential of 2340 μV and no voltage pulse in loading regions.*

icantly higher starting value of d-c EP. Figure 8 shows the test record of a 0.5 T C(T) specimen in which the potential at the start of the test was 2340 μV rather than the usual 400 μV. Notice the almost complete absence of a voltage pulse at the start of loading. Based on this result, it would appear that use of a sufficiently high applied current through the ferromagnetic test specimen will minimize the effect of the rapid-loading pulse. This solution is not foolproof, however. For example, if larger specimens or higher rates of loading are used, the voltage pulse could be much more pronounced. If its effect on the electric potential data is to be minimized by the procedure described here, the applied current may have to be so large as to be impractical.

Discussion

The findings reported here confirm that the direct-current electric potential method is a sound, practical procedure for single-specimen *J-R* curve testing. In most cases, it provides a reasonable estimate of the crack initiation point and a good estimate of the amount of crack extension. For nonferromagnetic materials, it can be used in rapid-rate loading as well as in slow-rate loading tests. Under certain, limited conditions, it also can be used for testing ferromagnetic materials at high displacement rates.

Of the two parameters estimated from d-c EP data, the crack initiation point remains more difficult to determine with confidence than does the amount of crack growth. Even the amount of crack growth, however, is not always determined with the degree of accuracy desired, for reasons that are not known but which may be related to specimen lateral contraction ahead of the crack, specimen lateral expansion at the back edge, and general yielding.

An ongoing need exists to develop appropriate standards for using the electric potential procedure, both with respect to conducting the tests and interpreting the data. An effort to develop such standards is underway within the ASTM.

Acknowledgments

The authors are grateful to P. R. Held and P. N. Mincer for their careful experimental work and to A. R. Rosenfield and T. P. Groveneveld for reviewing the manuscript. We express our thanks also to Battelle for supporting a study of the voltage pulse produced in ferromagnetic materials under rapid loading. Finally, we acknowledge the U.S. Nuclear Regulatory Commission's sponsorship of the Degraded Piping Program.

References

[1] Clarke, G. A., Andrews, W. R., Paris, P. C., and Schmidt, D. W., "Single Specimen Tests for J_{Ic} Determination," *Mechanics of Crack Growth, ASTM STP 590*, American Society for Testing and Materials, Philadelphia, 1976, pp. 27–42.

[2] Anctil, A. A., Kula, E. B., and DiCesare, E., "Electric Potential Technique for Determining Slow Crack Growth," *Proceedings*, American Society for Testing and Materials, Philadelphia, Vol. 63, 1963, p. 799.

[3] Johnson, H. H., "Calibrating the Electric Potential Method for Studying Slow Crack Growth," *Materials Research and Standards*, Vol. 5, No. 9, Sept. 1965, pp. 442–445.

[4] Lowes, J. M. and Fearnehough, G. D., "The Detection of Slow Crack Growth in Crack Opening Displacement Specimens Using an Electrical Potential Method," *Engineering Fracture Mechanics*, Vol. 3, 1971, pp. 103–108.

[5] Aronson, G. H. and Ritchie, R. O., "Optimization of the Electrical Potential Technique for Crack Growth Monitoring in Compact Test Pieces Using Finite Element Analysis," *Journal of Testing and Evaluation*, Vol. 7, No. 4, July 1979, pp. 208–215.

[6] Ritchie, R. O. and Bathe, K. J., "On the Calibration of Electrical Potential Technique for Mon-

itoring Crack Growth Using Finite Element Methods," *International Journal of Fracture*, Vol. 15, No. 1, 1979, pp. 46–55.

[7] Schwalbe, K.-H. and Hellmann, D., "Application of the Electrical Potential Method to Crack Length Measurements Using Johnson's Formula," *Journal of Testing and Evaluation*, Vol. 9, No. 3, May 1981, pp. 218–221.

[8] Schwalbe, K.-H., "Test Techniques," *Advances in Fracture Research, Proceedings of the Fifth International Conference on Fracture*, Vol. 4, 1981, pp. 1421–1446.

[9] Wilkowski, G. M., Wambaugh, J. O., and Prabhat, K., "Single Specimen *J*-Resistance Curve Evaluations Using the Direct-Current Electric Potential Method and a Computerized Data Acquisition System," *Fracture Mechanics: Fifteenth Symposium, ASTM STP 833*, R. J. Sanford, Ed., American Society for Testing and Materials, Philadelphia, 1984, pp. 553–576.

[10] Vassilaros, M. G. and Hackett, E. M., "*J*-Integral *R*-Curve Testing of High Strength Steels Utilizing the Direct Current Potential Drop Method," *Fracture Mechanics: 15th Symposium, ASTM STP 833*, R. J. Sanford, Ed., American Society for Testing and Materials, Philadelphia, 1984, pp. 535–552.

[11] Schwalbe, K.-H., Hellmann, D., Heerens, J., Knaack, J., and Muller-Roos, J., "Measurement of Stable Crack Growth Including Detection of Initiation of Growth Using the D-C Potential Drop and the Partial Unloading Methods," *Elastic-Plastic Fracture Test Methods: The User's Experience, ASTM STP 856*, E. T. Wessel and F. J. Loss, Eds., American Society for Testing and Materials, Philadelphia, 1985, pp. 338–362.

[12] Hackett, E. M., Kirk, M. T., and Hays, R. A., "An Evaluation of *J-R* Curve Testing of Nuclear Piping Materials Using the Direct Current Potential Drop Technique," David Taylor Naval Ship R & D Center, NUREG/CR-4540, August 1986.

[13] Wilkowski, G. M. and Maxey, W. A., "Review and Applications of the Electric Potential Method for Measuring Crack Growth in Specimens, Flawed Pipes, and Pressure Vessels," *Fracture Mechanics: Fourteenth Symposium-Volume II: Testing and Applications, ASTM STP 791*, J. C. Lewis and G. Sines, Eds., American Society for Testing and Materials, Philadelphia, 1983, pp. II–266–II–294.

[14] Marschall, C. W. and Landow, M. P., this publication, pp. 238–259.

[15] Marschall, C. W., Held, P. R., Landow, M. P., and Mincer, P. N., "Use of Direct-Current Electric Potential Method to Monitor Large Amounts of Crack Growth in Highly Ductile Metals," *Fracture Mechanics: Twenty-First Symposium, ASTM STP 1074*, J. P. Gudas, J. A. Joyce, and E. M. Hackett, Eds., American Society for Testing and Materials, Philadelphia, 1990, pp. 581–593.

[16] Hollstein, T., Blauel, J. G., and Voss, B., "On the Determination of Elastic-Plastic Fracture Material Parameters: A Comparison of Different Test Methods," *Elastic-Plastic Fracture Test Methods: The User's Experience, ASTM STP 856*, E. T. Wessel and F. J. Loss, Eds., American Society for Testing and Materials, Philadelphia, 1985, pp. 104–116.

Jun Ming Hu[1] *and Pedro Albrecht*[1]

Analysis of Deformation Behavior During Plastic Fracture

REFERENCE: Hu, J. M. and Albrecht, P., "**Analysis of Deformation Behavior During Plastic Fracture,**" *Elastic-Plastic Fracture Test Methods: The User's Experience (Second Volume), ASTM STP 1114*, J. A. Joyce, Ed., American Society for Testing and Materials, Philadelphia, 1991, pp. 178–196.

ABSTRACT: The authors have previously shown that the cracks in compact tension specimen fabricated from A533B steel, HY80 steel, A710 steel, and CS19 aluminum extended at limit load. The present study examines the deformation behavior of C(T) specimens. The approach consists of deriving an equation for the plastic rotation factor, proposing an empirical equation for the plastic CTOD *R*-curve, and presenting the procedures for predicting the load versus load-line displacement curve with the plastic CTOD *R*-curve and limit load solution. The results obtained in this study lead to three important observations. First, many specimens that were reported by previous investigators to have failed in elastic-plastic fracture actually failed in plastic fracture. Second, a parameter based on plastic deformations at the crack tip, such as plastic CTOD, may better characterize the resistance to crack extension in plastic fracture. Third, for the fully plastic range of fracture behavior, the curve of load versus load-line displacement can be predicted knowing two material properties, the flow stress and the plastic CTOD *R*-curve.

KEY WORDS: plastic fracture, limit load, compact tension specimen, crack tip opening displacement, plastic rotation factor, CTOD *R*-curve

The fracture of a cracked body can be broadly characterized as being elastic, elastic-plastic, or plastic. In elastic fracture the size of the plastic zone at the crack tip is much smaller than the crack length or the dimensions of the body, the remote strains are smaller than the yield strain, and the work of plastic flow at the crack tip is negligible. The onset of crack extension in elastic fracture is characterized by the crack tip singularity parameters, G or K, of linear-elastic fracture mechanics (LEFM).

In elastic-plastic fracture the plastic zone is large but still surrounded by an elastic stress field, the remote strains may approach the yield strain, and the work of plastic flow near the crack tip is small in comparison with the reversible elastic strain energy and of the same order of magnitude as the irreversible work of fracture. The onset of crack extension in elastic-plastic fracture is controlled by the crack-tip singularity parameter, J, of elastic-plastic fracture mechanics (EPFM).

In plastic fracture the plastic zone is spread out along the entire length of the net ligament from the crack tip to the back face of the specimen, the remote strains exceed the yield strain, and the work of remote plastic flow is larger than the reversible elastic strain energy and the irreversible work of fracture. The writers believe that under these conditions of plastic fracture the load-carrying capacity of the specimen can be determined from a limit

[1]Research associate and professor, respectively, Department of Civil Engineering, University of Maryland, College Park, MD 20742.

load calculation. The two specimen halves rotate about the plastic hinge. The degree of hinge rotation is related to crack extension and depends on the ductility of the material. Crack extension is likely governed by a crack tip deformation parameter such as the local strain, displacement, or rotation angle.

Plastic fracture analysis has been largely ignored in previous work. Yet, the plastic limit load of a test specimen should be calculated and compared with the applied load to determine whether the fracture is elastic-plastic or plastic. In a first step towards determining whether a specimen fails in plastic fracture, Hu et al. [*1*] reviewed limit load solutions reported in the literature for compact tension [C(T)] specimen, modified these solutions as needed, and then compared them with measured load versus crack extension behavior for different specimen sizes, initial crack lengths, and types of metals. It was found that load carrying capacities of these spcimens are determined by limit load. This paper extends the load analysis to the investigation of deformation behavior. For A533B and HY80 steels, the load-line displacement (LLD) as a measure of global deformation will be investigated, the plastic crack tip opening displacement, $CTOD_p$, versus crack extension (plastic CTOD R-curve) as a local characterization parameter will be calculated, and a procedure to predict the load versus load-line displacement curves based on the plastic CTOD R-curve and limit load solution will be presented. The plastic CTOD R-curves for various other metals will be investigated also in this paper. The paper will first review the work on limit load analysis, derive plastic rotation factor, then calculate plastic CTOD R-curve, and use it to predict load versus load-line displacement curve.

Limit Load

Green [*2*], and Green and Hundy [*3*] derived the limit moment for a bending bar with a wedge-like notch. The limit moment was calculated from the equations of equilibrium between the applied external moment and the resisting internal moment produced by the shear and normal stresses acting along circular-linear slip lines.

Beginning with Green's solution for a wedge angle approaching zero and assuming the circular-linear slip lines shown in Fig. 1, Hu et al. [*1*] derived the limit load for the compact tension C(T) specimen subjected to the combined effects of tension and bending on the uncracked ligament. The equations of force and moment equilibrium yielded expressions for the limit load

$$P_L = \frac{2}{\sqrt{3}} WB\sigma_0 \left(2.572 \frac{R}{W-a} - 1\right)\left(1 - \frac{a}{W}\right) \tag{1}$$

and the radius of the circular segment of the slip line (Fig. 1)

$$R = W[\sqrt{0.6977(a/W)^2 + 0.4090} - 1.0520(a/W)] \tag{2}$$

where

W = specimen width,
B = specimen thickness,
σ_0 = flow stress, and
a = crack length.

Green [*2*] showed that for a wedge angle approaching zero, as is the case for a cracked body, $\alpha + \beta = 117.02$ deg. Since the linear segment of the slip line is assumed to intersect

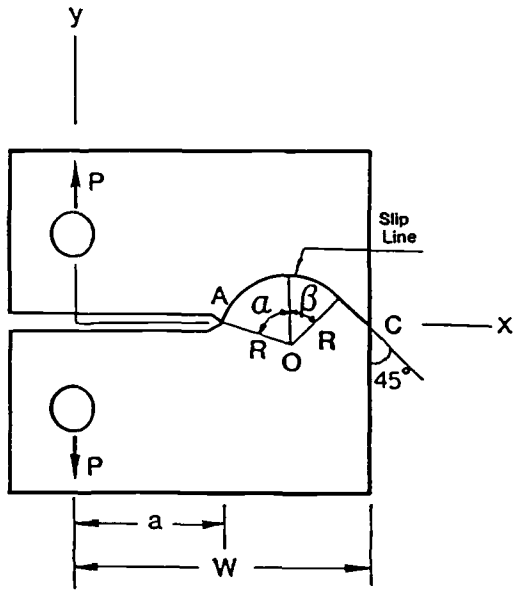

FIG. 1—*Circular-linear slip line in compact tension specimen* (only upper slip line is shown).

the back face of the specimen at an angle of 45 deg, it follows that $\beta = 45$ deg and thus $\alpha = 72.02$ deg.

Hu et al. [*1*] then predicted with Eq 1 the curves of load versus crack extension in C(T) specimens fabricated from A710 steel, A533B steel, HY80 steel, and CS19 aluminum. The unloading compliance data needed to perform the calculations came from the work reported in Refs 4, 5, 6, and 7, respectively. The value of the flow stress in Eq 1 was $\sigma_0 = 0.5(\sigma_{ys} + \sigma_u)$, where σ_{ys} = yield stress and σ_u = tensile strength; and the net specimen thickness was $B = B_n$ for side-grooved specimens. The properties and chemical compositions of the materials are given in Tables 1 and 2.

The predicted load versus crack extension curves agreed well with the corresponding measured curves for all four metals despite differences in specimen size (0.5T and 1T), initial crack length ($a_0/W = 0.55$ to 0.81), and fracture toughness ($J_{Ic} = 183$ to 435 kJ/m^2 for steel and $J_{Ic} = 25$ kJ/m^2 for aluminum as listed in Table 1).

TABLE 1—*Material properties.*

Source	Material	Yield Strength, σ_{ys} (MPa)	Tensile Strength, σ_u (MPa)	Flow Stress, σ_o (MPa)	Elongation, %	Fracture Toughness, J_{Ic} (kJ/m^2)	Test Temperature, T (°C)
4	A710	517	605	561	31	435	RT[a]
6	A533B-H13	462	621	542	26	244	88
5	A533B-02	448	621	534	19	240	150
8	A508	280	550	465	30	187	205
4	HY80	614	731	672	23	183	RT
9	A302B	459	585	522	19	109	82
7	CS19	251	408	329	24	25	RT

[a]RT = room temperature.

TABLE 2—*Chemical composition.*

Source	Material	Alloy Content, %										
		C	Mn	P	S	Cu	Si	Ni	Cr	Mo	V	Ti
4	A710[a]	0.04	0.59	0.005	0.004	1.17	0.25	0.90	0.70	0.19	0.003	0.06
6	A533B-H13	0.19	1.28	0.012	0.013	. . .	0.21	0.64	. . .	. . .	. . .	. . .
5	A533B-02	0.22	1.48	0.012	0.018	. . .	0.25	0.68	. . .	. . .	. . .	. . .
8	A508	0.21	0.72	0.01	0.008	0.04	0.03	0.73	0.33	0.60	0.03	. . .
4	HY80	0.15	0.33	0.012	0.013	0.033	0.18	2.55	1.66	0.37	0.003	0.001
9	A302B[b]	0.21	1.46	0.010	0.021	0.059	0.24	0.23	0.06	0.54	0.012	0.008
7	CS19[c]	. . .	0.33	. . .	. . .	. . .	0.08	. . .	0.10	. . .	. . .	. . .

[a]Including 0.03% Cb.
[b]Including 0.007% Cb.
[c]Including 8.42% Mg, 0.07% Fe, and 0.001% Be.

As an example of the previous analysis [*1*], Fig. 2 shows the measured load versus crack length data for 20% side grooved 1T C(T) specimens of A710 steel, A533B-H13 steel, HY80 steel, and CS19 aluminum. For ease of comparing the data, the load was normalized with respect to the flow stress, net specimen thickness, and specimen width. The correlation with the limit load predicted with Eq 1 was best for the A533B and HY80 steels. The very tough A710 steel specimen had higher than predicted limit load, and the CS19 aluminum specimen approached the limit load only after some crack extension. The relative positions of these four materials in Fig. 2 corresponded directly to the degree of plastic deformation and the relative toughness defined by the value of J_{Ic} (Table 1) measured in accordance with the

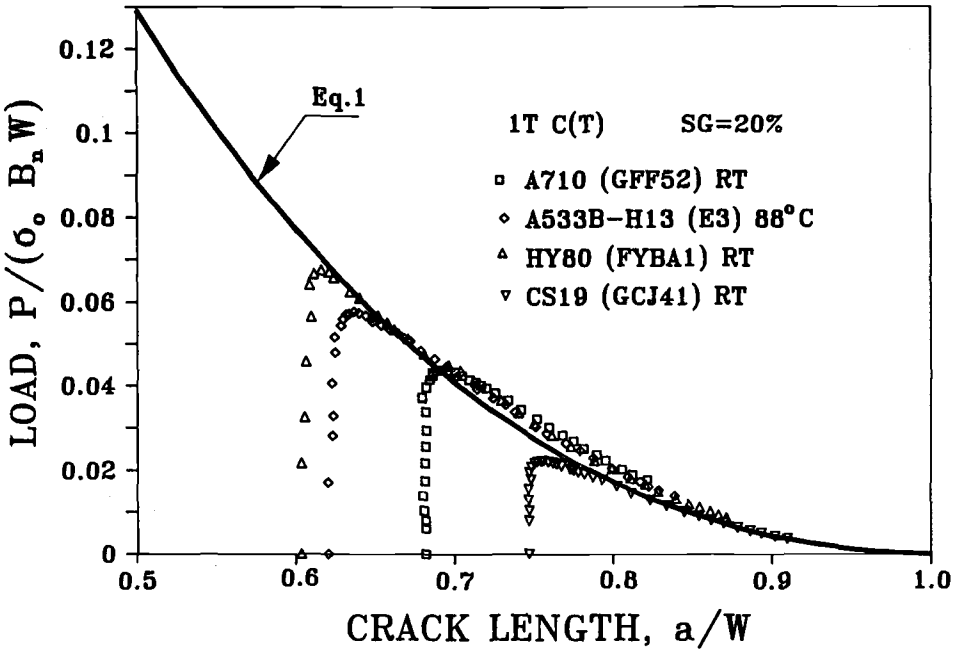

FIG. 2—*Effect of type of material on crack extension in 1T C(T) specimens.*

ASTM Test Method for J_{Ic}, a Measure of Fracture Toughness (E 813). The high-toughness A710 steel specimen deformed so much that the specimen expanded laterally and the side grooves closed at the back face. This increase in thickness elevated the limit load as the test progressed.

The ASTM standard test methods for determining K_{Ic} [Test Method for Plane Strain Fracture Toughness of Metallic Materials (E 399)], J_{Ic} (E 813), *J-R* curve [Test Methods for Determining *J-R* Curves (E 1152)], and CTOD [Test Method for Crack-Tip Opening Displacement (CTOD) Fracture Toughness Measurements (E 1290)] specify an upper limit on the fatigue precracking load for the C(T) specimen, which is 40% of the load that was previously thought to be a reasonable approximation of the limit load. Since the accurate limit load solution given by Eq 1 is 30% higher than the previous estimate, it is recommended that the ASTM precracking load be raised by 30%.

Since the publication of Ref *1*, the authors analyzed data for C(T) specimens greater than 1T. The required unloading compliance data came from the work reported in Refs *8* and *9*. Figure 3 shows the effect of specimen size on the crack extension behavior of 1T, 2T, 4T, and 10T C(T) specimens of A508 steel [*8*]. The data points for the 1T and 2T specimens rose nearly vertically until they reached or exceeded the predicted limit load and then curved downwards. The data points for the 4T and 10T specimens began to curve downwards before reaching the predicted limit load. However, even in the 10T specimen the data points eventually exceeded the limit load curve as the crack extended. This behavior is indicative of plastic fracture.

Figure 4 compares the measured load versus crack extension data for 0.5T, 1T, 2T, 4T, and 6T C(T) specimens fabricated from A302B steel [*9*]. The data points for the 0.5T and 1T specimens approached the predicted limit load curve after some crack extension, while

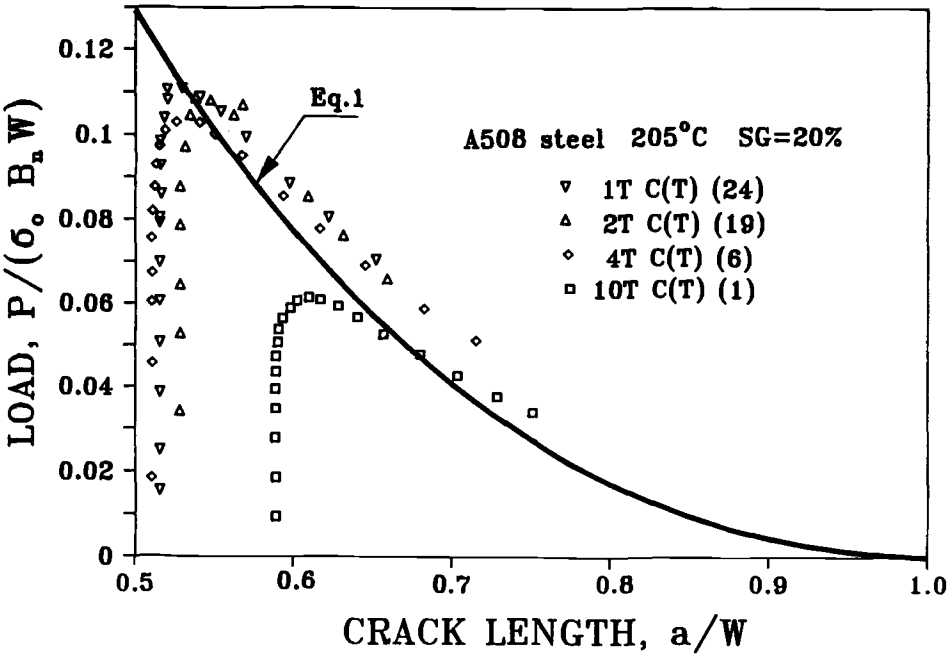

FIG. 3—*Effect of specimen size on crack extension in C(T) specimens of A508B steel.*

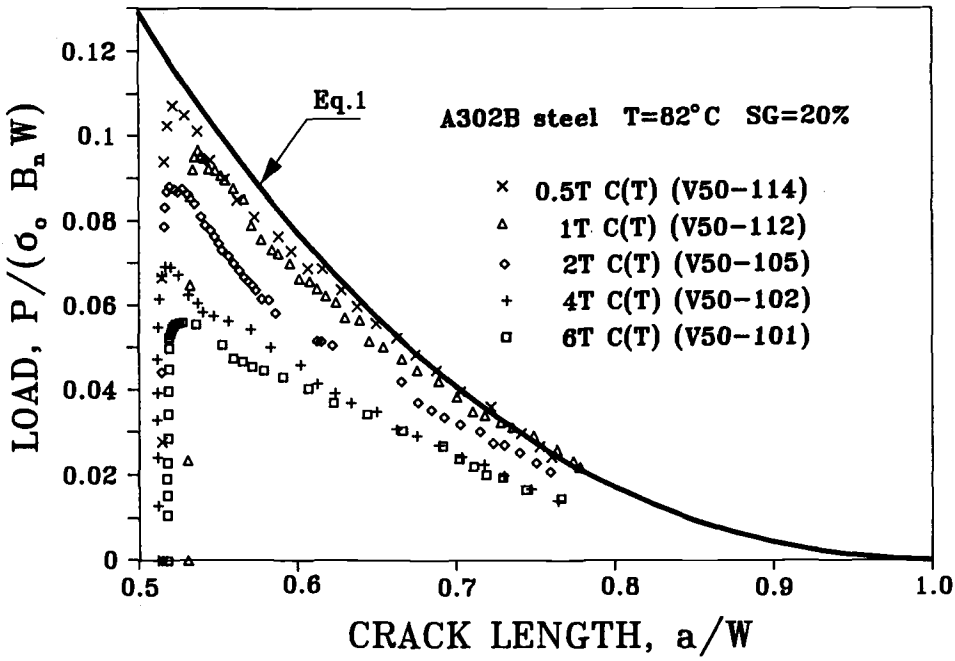

FIG. 4—*Effect of specimen size on crack extension in C(T) specimens of A302B steel.*

those for the 2T, 4T, and 6T specimens failed to reach the predicted limit load curve. The smaller specimens likely failed in plastic fracture, but the larger specimens certainly did not.

The following analysis of deformation is limited to fully ductile C(T) specimens with cracks extending at limit load.

Plastic Rotation Factor

Of the many ways of analyzing ductile fracture in test specimens and structures, the driving force for crack extension in terms of the CTOD is the common approach for which the following equation is given in the ASTM E 1290

$$\delta = \delta_e + \delta_p = \frac{K^2(1 - \nu^2)}{2\sigma_{ys}E} + \frac{r_p(W - a)}{a + r_p(W - a)}v_p \tag{3}$$

where

r_p = plastic rotation factor,
v_p = plastic load-line displacement,
K = stress intensity factor,
E = modulus of elasticity, and
ν = Poisson's ratio.

The two terms in Eq 3 represent the elastic and plastic parts of CTOD. The plastic CTOD is calculated from the plastic load-line displacement (LLD), v_p, assuming rigid-body rotation of the specimen halves around the plastic hinge whose rotation point ahead of the crack tip is defined by the plastic rotation factor. Since the plastic LLD is a measure of the global

plastic deformation, the plastic CTOD should be a measure of the local plastic deformation at the crack tip. The correctness of the so determinned CTOD value depends largely on the accuracy of the expression for the rotation factor.

The modified Green solution [*1*] predicts rigid-plastic rotation of the specimen halves around the two centers of rotation (points 0 in Fig. 1) whose coordinates are given by

$$x_0 = a + R \sin \alpha \tag{4}$$

$$y_0 = \pm R \cos \alpha \tag{5}$$

Substituting the radius, R, of the slip line from Eq 2 and setting $\alpha = 72.02$ deg leads to

$$x_0 = W\sqrt{0.6311(a/W)^2 + 0.3699} \tag{6}$$

$$y_0 = W[\sqrt{0.0667(a/W) + 0.0391} - 0.3251(a/W)] \tag{7}$$

The plastic rotation factor is defined as the horizontal distance from the crack tip to the rotation center as normalized by the uncracked ligament. It is expressed as (Fig. 1)

$$r_p = \frac{x_0 - a}{W - a} \tag{8}$$

Substituting x_0 from Eq 6 into Eq 8 gives the following expression for the plastic rotation factor predicted by the modified Green solution which is used in this study

$$r_p = \frac{1}{1 - a/W}\left[\sqrt{0.6311(a/W)^2 + 0.3699} - a/W\right] \tag{9}$$

In comparison, the ASTM CTOD standard specifies the following values

$$r_p = 0.47 \text{ for } 0.45 \leq a/W \leq 0.50 \tag{10}$$

and

$$r_p = 0.46 \text{ for } 0.50 \leq a/W \leq 0.55 \tag{11}$$

Green's solution [*2*] for pure bending gives a constant value of the plastic rotation factor for all crack sizes

$$r_p = 0.37 \tag{12}$$

And, finally, Merkle and Corten's solution [*10*] for combined tension and bending gives

$$r_p = \left[\left(\frac{a/W}{1 - a/W}\right)^2 + \frac{a/W}{1 - a/W} + \frac{1}{2}\right]^{1/2} - \frac{a/W}{1 - a/W} \tag{13}$$

Figure 5 compares the plastic rotation factor calculated from the modified Green solution (Eq 9) with those of the ASTM CTOD standard (Eqs 10 and 11), Green's pure bending solution (Eq 12), and Merkle-Corten's solution (Eq 13). For $0.45 < a/W < 0.55$, the modified Green solution gives about the same value of r_p as does the CTOD standard. Also, as

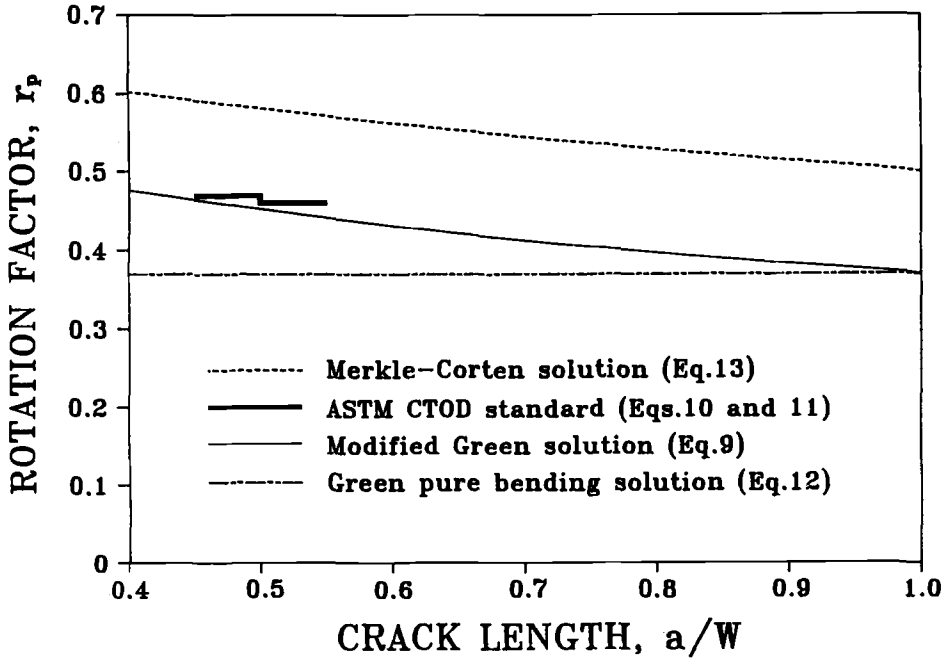

FIG. 5—*Plastic rotation factor.*

expected, the value of r_p gradually approaches the value for pure bending with increasing crack length. The Merkle-Corten solution gives a plastic rotation factor about one-third larger than the modified Green solution.

Plastic CTOD *R*-Curve

It is believed that the *J*-integral approach is no longer valid for crack extension in plastic fracture. An alternative resistance parameter to characterize crack extension such as CTOD needs to be investigated. The ASTM standard test method E 1290 expresses the CTOD as the sum of its elastic and plastic components. In plastic fracture, the meaning of the stress intensity factor in the first term of Eq 3 is lost because crack extension is dominated by plastic deformation at limit load. Also, analysis of available data shows that the first term in Eq 3 is much smaller than the second term. In this study, the resistance to crack extension is expressed in terms of the plastic CTOD, the second term of Eq 3. In the remainder of this paper, the deformation behavior of small-size specimens of A533 and HY80 steel is investigated, the plastic CTOD *R*-curves for seven materials are compared, and the effect of specimen size on the plastic CTOD *R*-curve is shown for A508 and A302B steels. All data came from elastic-compliance tests performed by others [*4–9*]. The data presented hereafter were analyzed by the authors.

Figure 6 shows a typical plot of load versus LLD measured in a single-specimen, elastic-compliance test. The load and LLD data for such plots were recorded digitally in the tests performed in Refs *4–7* and *9*, and graphically in Ref *8*.

Figure 7 shows with square symbols the test data for load versus LLD of 1T C(T) specimens fabricated from A533B-H13 steel. The initial crack sizes were a_0/W = 0.620 and 0.758. Each point corresponds to a location on the measured load versus LLD curve where the

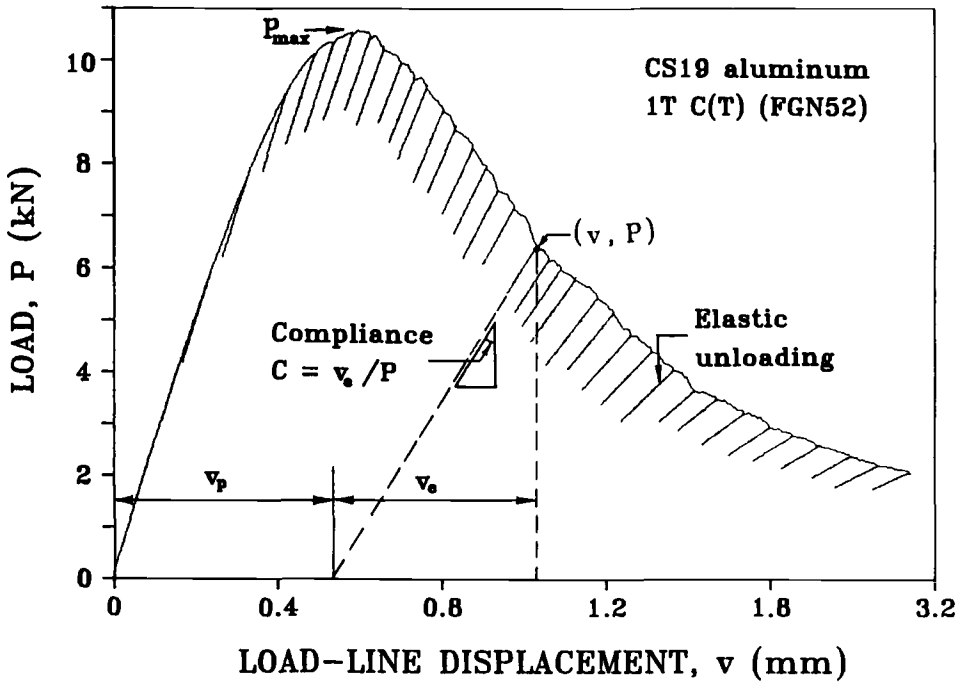

FIG. 6—*Typical load versus load-line displacement plot from single-specimen, unloading-compliance test.*

compliance and crack length were determined from the slope of a 10% unloading line. Similarly, Fig. 8 shows the test data for load versus LLD of 0.5T and 1T C(T) specimens fabricated from HY80 steel. The initial crack lengths were $a_0/W = 0.606$ and 0.603, respectively. The material properties and chemical compositions of the steels are given in Tables 1 and 2.

The inverse slope of the unloading line gives the compliance, C, of the specimen at the corresponding point on the load versus LLD curve. The measured compliance, obtained by fitting a straight-line to the data points for each partial unloading, was substituted in the wide-range, elastic compliance expression for the C(T) specimen [*11*]

$$C = \frac{V_e}{P} = \frac{1}{BE}\left[\frac{1 + a/W}{1 - a/W}\right] f(a/W) \tag{14}$$

where

$$f(a/W) = 2.1630 + 12.219\, a/W - 20.065(a/W)^2 - 0.9925(a/W)^3 + 20.609(a/W)^4 - 9.9314(a/W)^5 \tag{15}$$

Equation 14 was then solved for the crack length at that point. As an example, the data points of load versus crack length plotted in Fig. 2 for the E3 and FYBA1 specimens correspond to the data points of load versus LLD potted in Figs. 7 and 8 for the same specimens.

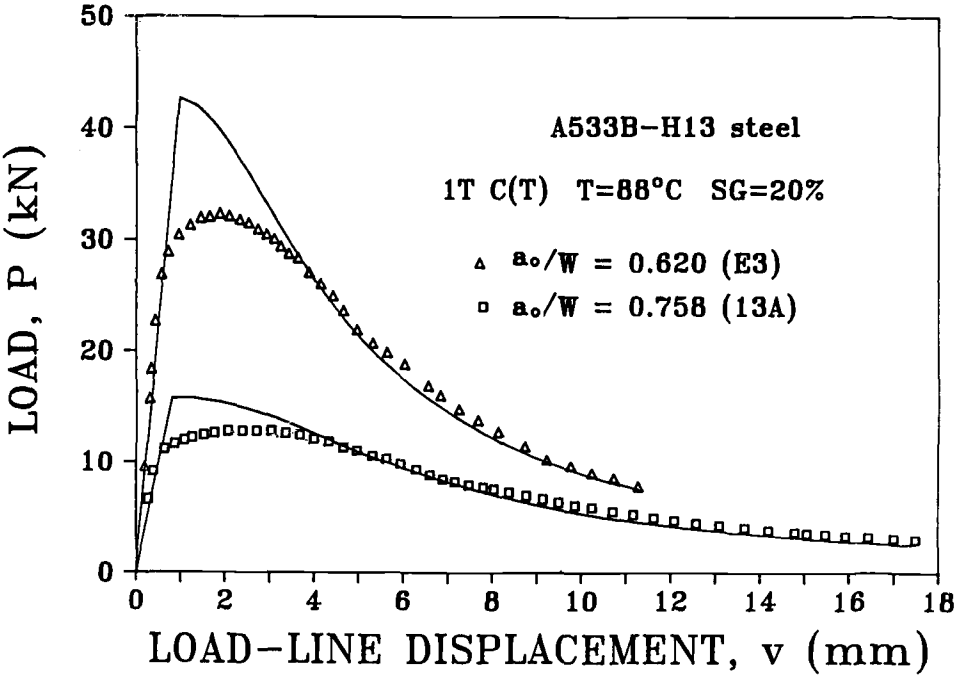

FIG. 7—*Load versus load-line displacement curves for 1T C(T) specimens of A533B steel.*

The measured LLD, v, was separated into its elastic and plastic components as follows. First, the elastic LLD was determined from

$$v_e = CP \tag{16}$$

where

C = measured elastic compliance, and
P = measured load at point of unloading.

Subtracting the elastic LLD from the total LLD then gave the plastic LLD

$$v_p = v - v_e \tag{17}$$

where v = measured LLD at point of unloading.

Figure 9 shows the data points for elastic and plastic LLDs of two 1T C(T) specimens fabricated from A533B steel, whose initial crack lengths were $a_0/W = 0.620$ and 0.758. Again, each data point on this figure corresponds to a point on the load versus LLD curve at which the specimens were partially unloaded, as in Figs. 2 and 7. The elastic LLD remained nearly constant, whereas the plastic LLD greatly increased over the full range of crack extension. Since the crack extension from $P = 0$ to $P = P_{max}$ was only about $\Delta a = 0.015\ W$ (Fig. 2), most of the elastic and plastic LLD curves shown in Fig. 9 were for crack extension after P_{max} had been reached.

Similarly, Fig. 10 shows the elastic and plastic LLDs for two HY80 steel specimens: one for a 0.5T C(T) specimen with an initial crack length of $a_0/W = 0.606$, the other for a 1T C(T) specimen with $a_0/W = 0.603$. The trends of the displacement curves were similar to

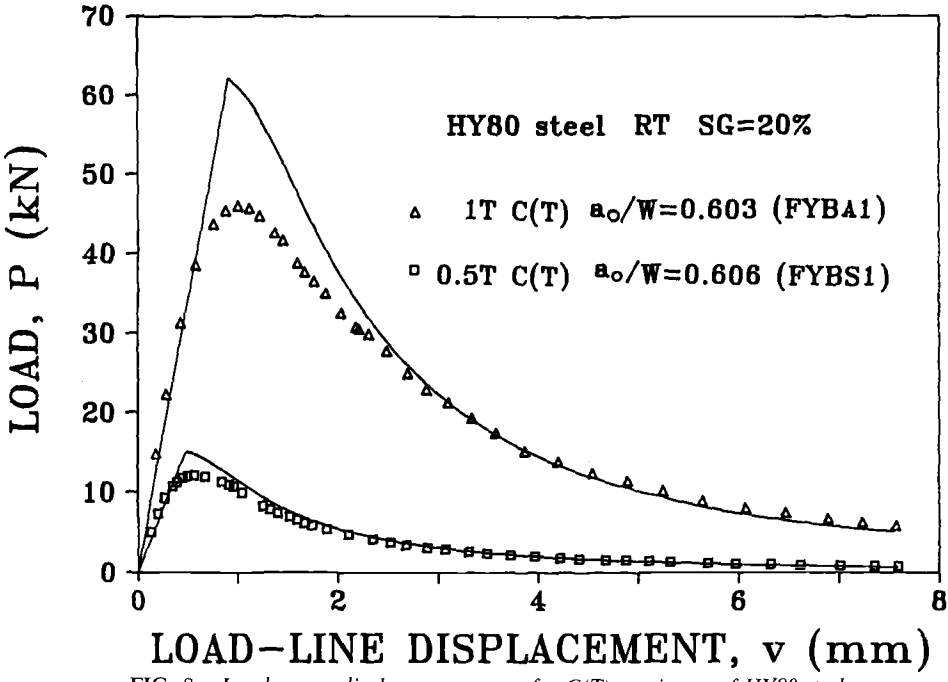

FIG. 8—*Load versus displacement curves for C(T) specimens of HY80 steel.*

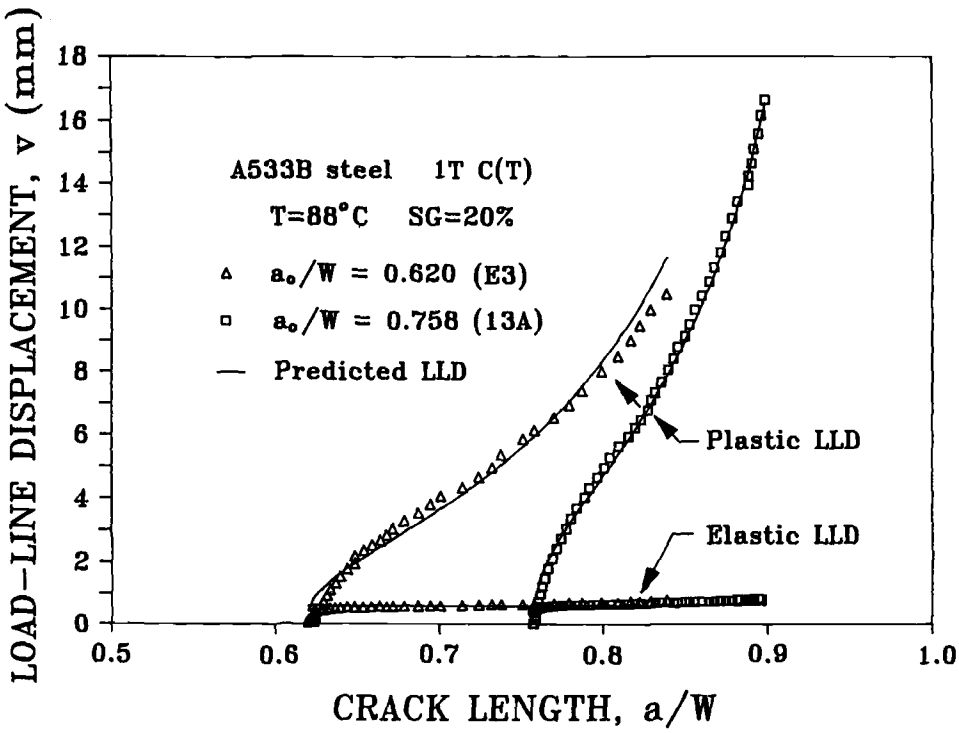

FIG. 9—*Separation of load-line displacement of A533B steel specimens into elastic and plastic components.*

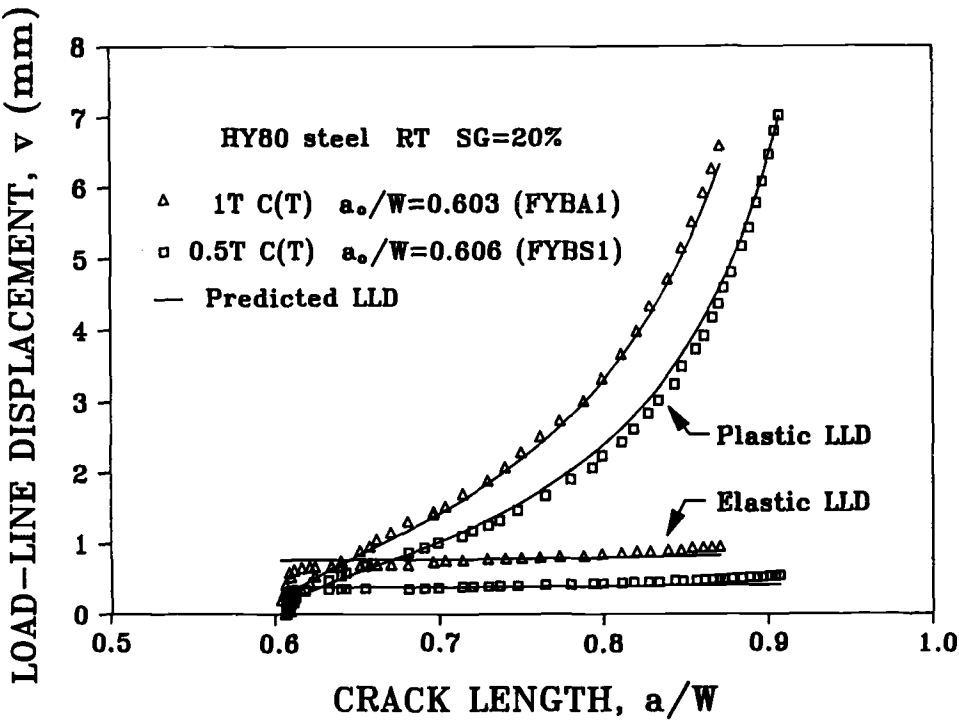

FIG. 10—*Separation of load-line displacement of HY80 steel specimens into elastic and plastic components.*

those for the A533B steel specimens (Fig. 9). But, while the 1T C(T) specimens of both steels had elastic LLDs of comparable values, the tougher A533B steel specimens had larger plastic LLDs than the less tough HY80 specimens.

Under rigid plastic rotation of the two specimen halves at limit load, the ratio of plastic CTOD to plastic LLD is equal to the ratio of the horizontal distances from the crack tip and load line to the rotation centers (Fig. 1). From similar triangles, the plastic CTOD is then given by

$$\delta_p = \frac{x_0 - a}{x_0} v_p \tag{18}$$

where the measured values of x_0, a, and v_p come from Eqs 6, 14, and 17, respectively.

The data points for plastic CTOD versus crack extension, $\Delta a = a - a_0$, were plotted in Fig. 11 for the C(T) specimens of A533B and HY80 steels. Within the limited range of data examined in this figure, the correlation was very good for the A533B steel specimens of same size by different initial crack lengths as well as for the HY80 steel specimens of different sizes but same initial crack length. This held true up to very large crack extensions of $\Delta a = 7.7$ mm, which corresponds to 50% of the initial crack size in the 0.5T specimen and 25% in the 1T specimen.

The plots of plastic CTOD versus crack extension represent R-curves characterizing the transition from elastic-plastic crack extension of a fatigue crack during the rising portion of the load versus LLD curve, over the hump at P_{max}, and down the long plastic tearing during the falling portion of the load versus LLD curve (Figs. 7 and 8).

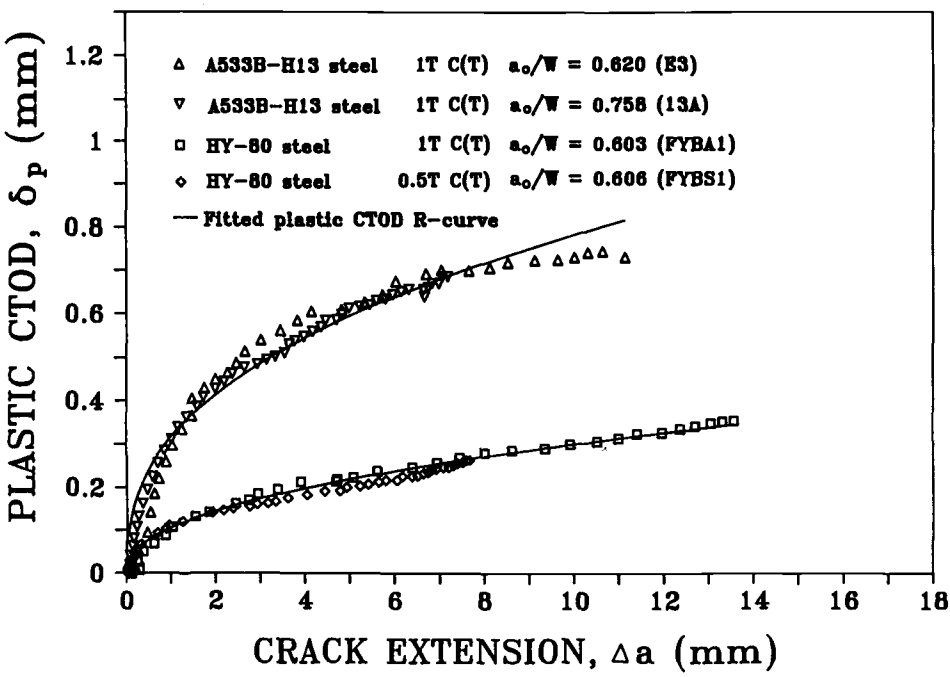

FIG. 11—*Plastic CTOD resistance curves for C(T) specimens of A533B and HY80 steels.*

The plastic CTOD *R*-curve is the basis for predicting the plastic LLD of the C(T) specimens. The data points for plastic CTOD versus crack extension in the A533B and HY80 steel specimens were replotted in the log-log Fig. 12. All points corresponding to crack extensions less than 0.4 mm were deleted so as not to unduly influence the slope of the line with points that are clustered near the origin in the linear plot of Fig. 11 but widely spaced in the logarithmic plot of Fig. 12. The plastic CTOD *R*-curve data were fitted with the power function

$$\delta_p = C_1(\Delta a)^{C_2} \tag{19}$$

Table 3 lists the values of the regression coefficients C_1 and C_2 that were calculated by the least-squares method. Equation 19, drawn in Fig. 12 as straight lines, fitted very well the *R*-curve data for the A533B steel specimen No. 13A and the two HY80 steel specimens, but not quite as well the data for the other A533B steel specimen E3. Equation 19 was replotted in Fig. 11. As was already observed in Fig. 12, it fitted well the *R*-curve data for all but the A533B steel specimen E3. Functions other than Eq 19 may exist that better fit the data.

Based on the limited data analyzed just mentioned, it appears that the plastic CTOD *R*-curve may be independent of initial crack length (A533B) and specimen size (HY80 steel). If this observation were confirmed for specimens of different types of steels, geometries, initial crack lengths, and specimen sizes, the plastic CTOD *R*-curve could be considered a material property.

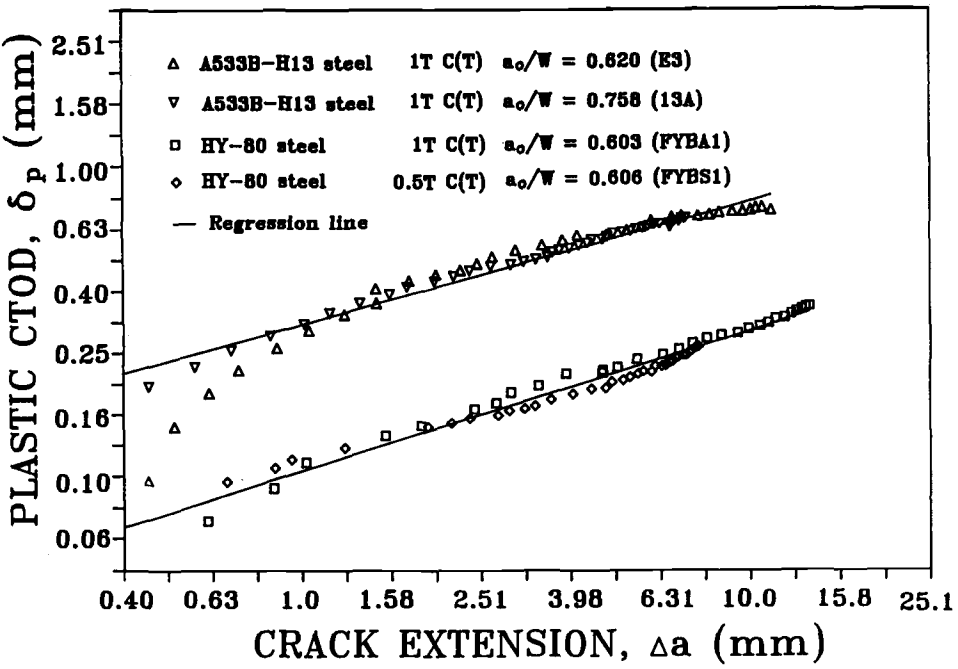

FIG. 12—*Log-log linear plastic CTOD resistance curves.*

Prediction of Load Versus Load-Line Displacement Curve

Given the plastic CTOD *R*-curve and the limit load equation, the load versus load-line displacement curve can be predicted. The required material properties are the two constants in the plastic CTOD *R*-curve and the flow stress.

The elastic LLD was predicted by substituting the limit load from Eq 1 into the wide-range elastic compliance expression of Eq 14 and solving for

$$v_e = \frac{P_L}{BE}\left(\frac{1 + a/W}{1 - a/W}\right) f(a/W) \tag{20}$$

where $f(a/W)$ is given by Eq 15.

TABLE 3—*Regression coefficients of plastic CTOD* R-*curves.*

Material	Specimens Size	Regression Coefficients[a] Intercept, C_1	Slope, C_2
A533B-H13	1T	0.3132	0.3968
HY80	0.5T and 1T	0.1046	0.4555

[a]For a and δ_p in units of mm.

The plastic LLD was predicted by substituting the plastic CTOD, δ_p, from the R-curve Eq 19 into Eq 18 and solving for

$$v_p = \frac{x_0}{x_0 - a} C_1(\Delta a)^{C_2} \tag{21}$$

The elastic and plastic LLDs, predicted with Eqs 20 and 21, are shown as solid curves in Figs. 9 and 10 for the A533B and HY80 steel specimens, respectively. As can be seen, the predicted elastic LLDs are nearly constant between $a/W = 0.6$ to 0.8 and slightly increase when $a/W > 0.8$. At very long crack extensions the data points rise slightly above the predicted values.

Since the plastic CTOD in Fig. 11 was determined by similar triangles from the plastic LLDs in Figs. 9 and 10, an R-curve that fits well the former data should equally well predict the latter data. This was indeed the case. Finally, adding Eqs 20 and 21 gives the total, predicted LLD

$$v = \frac{P_L}{BE}\left(\frac{1 + a/W}{1 - a/W}\right) f(a/W) + \frac{x_0}{x - a} C_1(\Delta a)^{C_2} \tag{22}$$

The predicted curves of load versus LLD for the A533B and HY80 steel specimens are shown in Figs. 7 and 8, respectively. The elastic portion of the curve to the left of P_{max} was obtained from the elastic compliance Eq 14 for initial crack length $a = a_0$ and elastic modulus $E = 200$ GPa. As was expected, the compliance equation predicted well the elastic behavior of the C(T) specimens.

The fully plastic portion of the curve to the right of P_{max} was obtained from the limit load Eq 1 and the displacement Eq 22 for increasing values of crack length, a, and crack extension, $\Delta a = a - a_0$. Equations 1 and 14 predicted well the measured load versus LLD curves for large crack extensions, but they could not predict the transition from the elastic-plastic to the fully plastic behavior, over the hump at P_{max}. In the elastic-plastic region, the shape of the crack tip gradually changed from that of the fatigue precrack to a blunted crack and then to a plastic tear.

The correlation between the predicted and measured curves on the left side of the hump could be improved by adding to the elastic displacement a term that accounts for the yielding that takes place in the growing crack-tip plastic zone, in the absence of crack extension. This could easily be done, for example, if the key curve were known for a given C(T) specimen and material. The correlation on the right side of the hump might be improved by selecting a function that more accurately fits the plastic CTOD R-curve data at very small amounts of crack extension.

Of importance here is the finding that the load versus LLD behavior of the C(T) specimen in the plastic region can be predicted from the theoretical limit load and the CTOD R-curve assuming that the specimen halves rotate around the plastic hinge.

Additional Plastic CTOD *R*-Curve Data

In addition to the data for A533B-H13 and HY80 steels shown in Fig. 11, the plastic CTOD R-curves were also determined from elastic-compliance data for C(T) specimens fabricated from A710, A533B-02, A508, and A302B steels as well as CS19 aluminum.

Figure 13 shows the R-curves for pairs of 0.5T and 1T specimens of all five metals. The initial crack sizes in the 0.5T and 1T specimens were, respectively: $a_0/W = 0.63$ and 0.67 for A710 steel, 0.61 and 0.61 for A533B-02 steel, 0.535 and 0.502 for A508 steel, 0.51 and

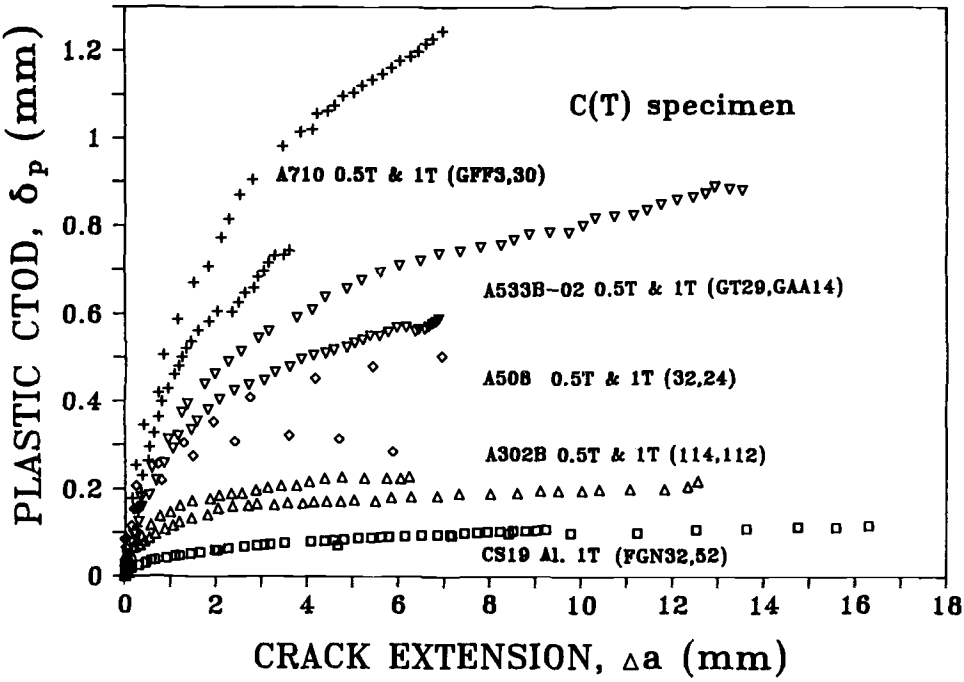

FIG. 13—*Additional plastic CTOD R-curve for small-size C(T) specimens.*

0.53 for A302B steel, and 0.57 and 0.70 for two 1T C(T) specimens of CS19 aluminum. The two *R*-curves for the same material correlated best for CS19 aluminum, and well for A533B-02 and A302B steels. The *R*-curves for the A533B-02 steel specimens fell in the same band as those for the A533B-H13 specimens shown in Fig. 11. For the A710 and A508 steels, the *R*-curve of the 0.5T specimen at long crack extension was significantly lower than that for the 1T specimen. This seemingly abnormal behavior of the 0.5T specimens may have resulted from the closing of the side grooves in the A710 steel specimen at large plastic hinge rotations and perhaps a lack of accuracy in determining the compliance from the graphical output of load versus LLD in the A508 steel specimen. In the latter case, for example, the measured and predicted crack sizes at the end of the test differed by 22% [*8*]. Aside from the 0.5T specimens of A710 and A508 steels, the data support the hypothesis that the plastic CTOD *R*-curve for plastic fracture may be a material property.

The plastic CTOD *R*-curves for 0.5T to 10T C(T) specimens of A508 steel shown in Fig. 14 follow the same general path, with the specimens of smaller size peeling off to the right as the crack becomes longer. All A508 steel specimens reached and even exceeded the limit load (Fig. 3), and their behavior can be therefore characterized as plastic fracture.

In contrast, the plastic CTOD *R*-curves for 0.5T to 6T C(T) specimens of A302B steel shown in Fig. 15 follow about the same path only for a very short crack extension of about 1 mm after which the specimens peel off to the right, with the largest specimen peeling off first. As was discussed earlier, the 0.5T and 1T specimens approached the predicted limit load while the 2T, 4T, and 6T specimens did not. The cracks in the large specimens extended under elastic-plastic fracture conditions. Indeed, the plastic CTODs of the large A302B steel specimens (Fig. 15) were an order of magnitude smaller than those for the large A508 steel

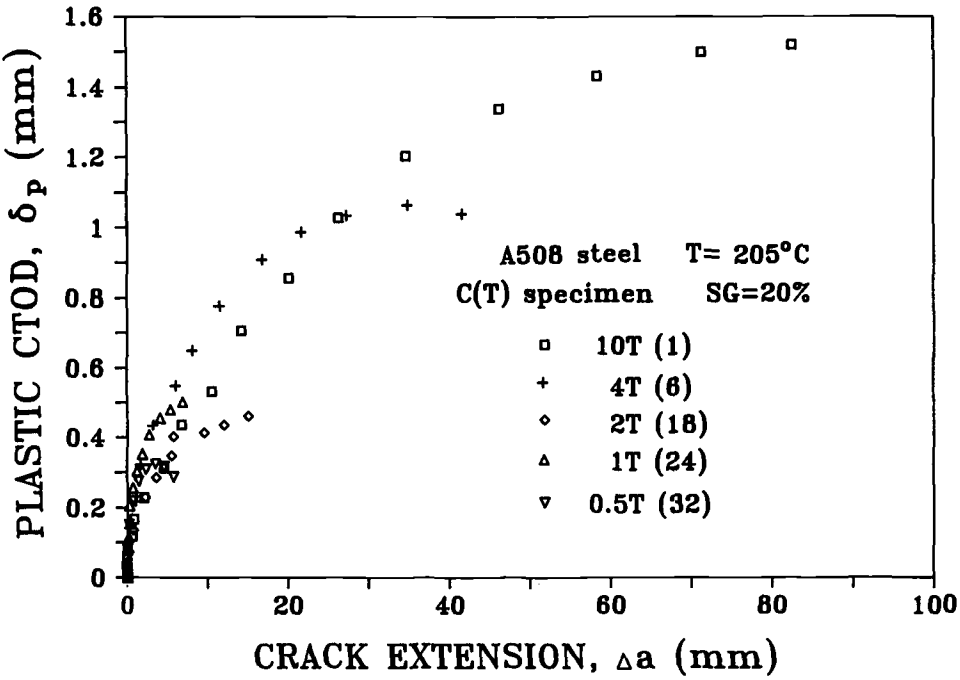

FIG. 14—*Plastic CTOD R-curve for small-size and large-size C(T) specimens of A508 steel.*

specimens (Fig. 14). Since the plastic hinge did not form, the two specimen halves could not have rotated as a mechanism around the plastic hinge. Therefore, the calculation of plastic CTOD with Eq 18 by similar triangles is invalid. New equations are needed to calculate the plastic CTOD in specimens that have a significant plastic zone at the crack tip but do not yield along the full length of the net ligament.

Conclusions

The following conclusions can be drawn from the results of the present study:

1. The modified Green solution, Eq 1, accurately estimates the limit load of the C(T) specimen. The plastic rotation factor, Eq 9, obtained from the modified Green slip line field, accurately estimates the rotation center of the plastic hinge of the C(T) specimen. Equation 1 for the limit load and Eq 9 for the plastic rotation factor are valid for crack lengths ranging from $a/W = 0.4$ to 1.0.

2. It is recommended that the step function for the plastic rotation factor in the ASTM standard test method for determining CTOD (E 1290) should be replaced by Eq 9. Also, the maximum fatigue precracking load specified in the ASTM standard test methods for determining K_{Ic} (E 399), J_{Ic} (E 813), *J-R* curve (E 1152), and CTOD (E 1290) should be increased by 30%.

3. The cracks extended at limit load in the 0.5T and 1T C(T) specimens fabricated from A710 steel, A533B steel, A508 steel, HY80 steel, A302B steel, and CS19 aluminum. They also extended at limit load in the 2T, 4T, and 10T C(T) specimens of A508 steel. But the 2T, 4T, and 6T C(T) specimens of A302B steel failed at loads lower than the predicted limit load. In general, the predictions were best for small-size specimens and long cracks.

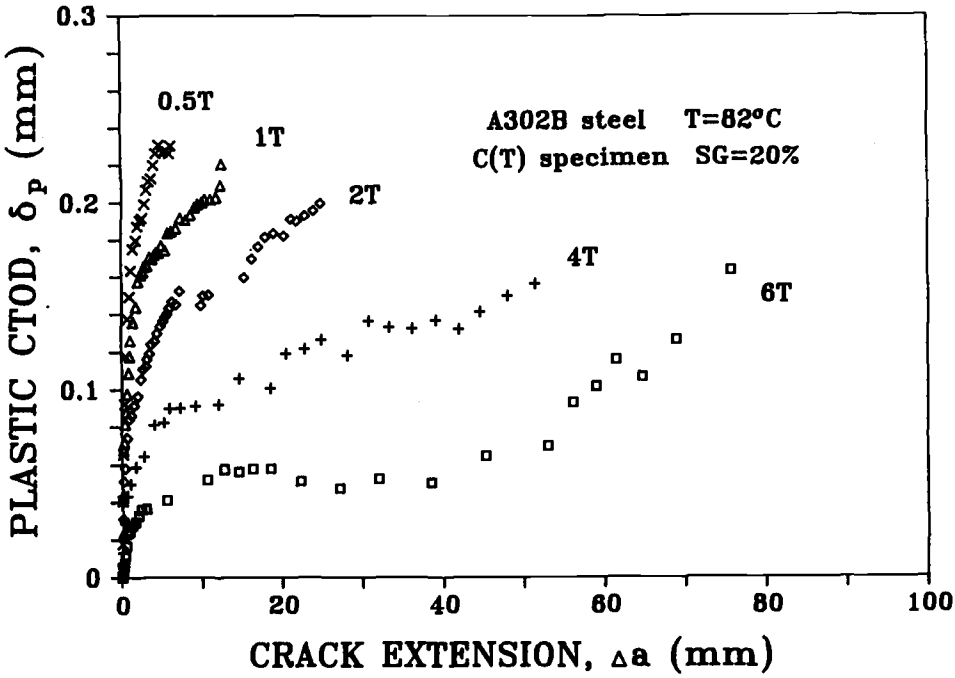

FIG. 15—*Plastic CTOD R-curve for small-size and large-size C(T) specimens of A302B steel.*

4. The mode of failure should be clearly described as being one of elastic, elastic-plastic, or plastic fracture. The specimen fails in elastic fracture when $K = K_c$, in elastic-plastic fracture when $J = J_c$, and in plastic fracture when $P = P_L$. Crack extension in plastic fracture can be characterized by a local crack-tip deformation parameter. The plastic CTOD *R*-curve is a possible choice. The plastic CTOD can be determined from the plastic part of the load-line displacement and the plastic rotation factor. This method of determining the plastic CTOD is only valid for plastic fracture, because the derivation of the plastic rotation factor assumes that the two specimens halves rotate as rigid bodies around the plastic hinge.

5. The plastic CTOD *R*-curves were found to be independent of specimen size and initial crack length for 0.5T and 1T C(T) specimens of A533B steel, HY80 steel, and CS19 aluminum. They were also independent of specimen size for crack extensions of up to $\Delta a/W = 0.1$ in 0.5T to 10T C(T) specimens of A508 steel. However, the plastic CTOD *R*-curves were not the same for the A302 steel specimens, which failed in plastic fracture [0.5T and 1T C(T)] as well as elastic-plastic fracture [2T, 4T, and 6T C(T)]. Whether the plastic CTOD *R*-curve is a material property for plastic fracture needs to be verified with analysis of more data.

6. The load versus load-line displacement behavior of A533B 1T C(T) and HY80 0.5T and 1T C(T) specimens beyond the maximum measured load was well predicted with the theoretical limit load, calculated elastic load-line displacement, and plastic load-line displacement obtained from the plastic CTOD *R*-curve.

Acknowledgment

The authors are grateful to James A. Joyce, U.S. Naval Academy and D. E. McCabe, Oak Ridge National Laboratory for providing the elastic-compliance data for the specimens

analyzed in the present study and for their helpful comments on the fracture behavior of materials.

References

[1] Hu, J. M., Cheng, J., Albrecht, P., and Joyce, J. A., "Ductile Crack Extension in Compact Specimens at Limit Load," *Advances in Fracture Research, Proceedings*, Seventh International Conference on Fracture (ICF7), Vol. 1, Pergamon Press, Oxford, U.K., 1989, pp. 349–358.

[2] Green, A. P., "The Plastic Yielding of Notched Bars due to Bending," *Journal of Mechanics and Applied Mathematics*, Vol. 6, Part 2, 1953, pp. 223–239.

[3] Green, A. P. and Hundy, B. B., "Initial Plastic Yielding in Notch Bend Tests," *Journal of the Mechanics and Physics of Solids*, Vol. 4, 1956, pp. 128–145.

[4] Joyce, J. A., "Development of an Engineering Definition of the Extent of *J* Singularity Controlled Crack Growth," Report No. NUREG/CR-5238, U.S. Nuclear Regulatory Commission, Washington, DC, 1989.

[5] Vassilaros, M. G., Joyce, J. A., and Gudas, J. P., "Effect of Specimen Geometry on the *J-R* Curve for ASTM A533B Steel," *Fracture Mechanics (Twelfth Conference), ASTM STP 700*, American Society for Testing and Materials, Philadelphia, 1980, pp. 251–270.

[6] Joyce, J. A., "Ductile to Brittle Toughness Transition Characterization of A533B Steel," Report No. NUREG/CR-5142, U.S. Nuclear Regulatory Commission, Washington, DC, 1988.

[7] Czyryca, E. J. and Vassilaros, M. G., "Mechanical Fatigue and Fracture Properties of Aluminum-Magnesium Alloy CS-19-H3E19 and Weldments," Report No. DT-NSRDC/SME-80/106, David W. Taylor Naval Ship Research and Development Center, Bethesda, MD, 1981.

[8] Landes, J. D., McCabe, D. E., and Ernst, H. A., "Elastic-Plastic Methodology to Establish R-Curves and Instability Criteria," Final Report No. RP 1238-2, Westinghouse Research and Development Center, Pittsburgh, PA, March, 1983.

[9] Hiser, A. L. and Terrell, J. B., "Size Effect on *J-R* Curves for A302-B Plate," NRC Report NUREG/CR-5265, U.S. Nuclear Regulatory Commission, Washington, DC, 1989.

[10] Merkle, J. G. and Corten, H. T., "A *J*-Integral Analysis for the Compact Specimen, Considering Axial Force as well as Bending Effects," *Journal of Pressure Vessel Technology*, American Society of Mechanical Engineers, 1974, pp. 286–292.

[11] Hudak, S. J., Saxena, A., Bucci, R. J., and Malcolm, R. C., "Development of Standard Methods of Testing and Analyzing Fatigue Crack Growth Rate Data," Report No. AFML-TR-78-40, Air Force Materials Laboratory, Wright-Patterson Air Force Base, OH, 1978.

John H. Underwood,[1] *Richard A. Farrara,*[1] *G. Peter O'Hara,*[1] *John J. Zalinka,*[1] *and John R. Senick*[1]

Fracture Toughness and Fatigue Crack Initiation Tests of Welded Precipitation-Hardening Stainless Steel

REFERENCE: Underwood, J. H., Farrara, R. A., O'Hara, G. P., Zalinka, J. J., and Senick, J. R., **"Fracture Toughness and Fatigue Crack Initiation Tests of Welded Precipitation-Hardening Stainless Steel,"** *Elastic-Plastic Fracture Test Methods: The User's Experience (Second Volume), ASTM STP 1114*, J. A. Joyce, Ed., American Society for Testing and Materials, Philadelphia, 1991, pp. 197–212.

ABSTRACT: An analysis is described of a welded stainless steel box beam that experienced a structural failure during fatigue testing. Cracks initiated at notches caused by partial penetration welds and grew to a length of several centimetres in about 1000 load cycles.

The objective here is to describe the characterization of fracture toughness and fatigue crack initiation for the precipitation-hardening stainless steels used for the welds and parent plate of the beam. Three-point bend specimens were used to measure both fatigue crack initiation life and the *J*-integral fracture toughness of the parent plate and weld metal in various conditions. The notch fatigue analysis method of Barsom and Rolfe was used to analyze the crack initiation test results. The crack was grown further, side notches were added, and J_{Ic} tests were performed using ASTM Test Method for J_{Ic}, a Measure of Fracture Toughness (E 813-87) with a modified load-line-displacement unloading-compliance procedure to measure crack growth.

Conclusions drawn from the work include the following: (*a*) J_{Ic} can be accurately determined with a three-point bend test using load-line displacement to measure crack growth by unloading compliance (An accurate expression for *a/W* in terms of load-line displacement was developed.); and (*b*) fatigue crack initiation life and J_{Ic} fracture toughness of stainless steels in various conditions were characterized. The welded and aged condition, with no intermediate solution treatment, showed unstable, cleavage-type fracture and resulted in a low J_{Ic} value and a short initiation life.

KEY WORDS: elastic-plastic fracture, test methods, fracture toughness, *J*-integral, welds, stainless steels, fatigue initiation, unloading compliance

A welded stainless steel structure recently experienced an unanticipated failure while being subjected to fatigue testing by the U. S. Army. In the Spring of 1988, the primary box beam of a proprietary structure, shown schematically in Fig. 1, failed in the area of the bottom plate. Excessive deformation of the structure during fatigue loading prompted test personnel to reinspect the bottom plate area, where cracks were observed in the vicinity of the welds. Further inspection and investigation revealed that the cracks initiated at notches caused by partial penetration welds of the stiffener plates to the bottom plate. Sharp notches were formed in the gap between the stiffener and the slot in the bottom plate. Cracks

[1]Research engineer, mechanical engineer, mechanical engineer, mechanical engineering technician, and mechanical engineer, respectively, Army Armament RD&E Center, Watervliet, NY 12189.

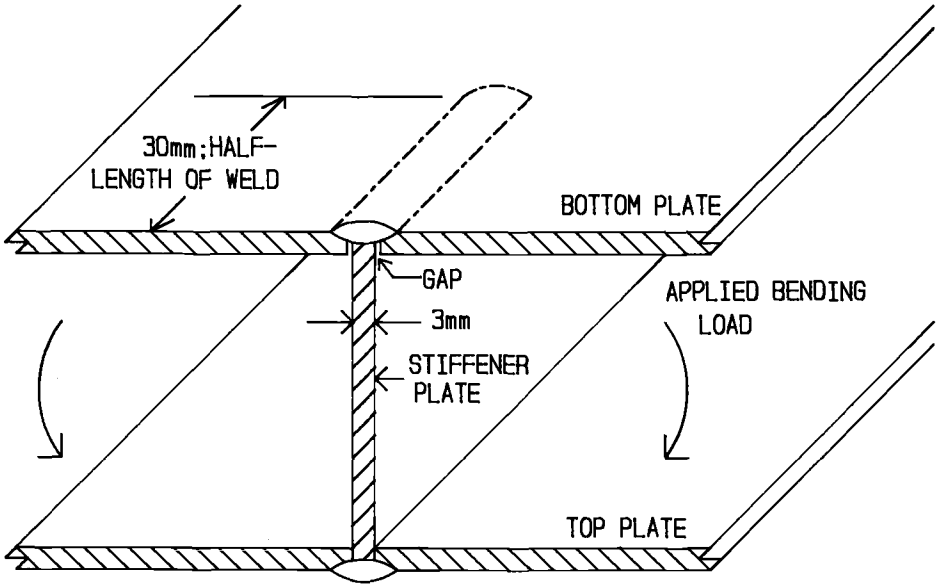

FIG. 1—*Welded box beam configuration.*

initiated at these notches and grew to a length of several centimetres in about 1000 load cycles.

The primary objective here is to describe the fracture toughness and fatigue crack initiation characterization of the type of precipitation-hardening stainless steels used for the welds and parent plate of the structure. This information was required to understand the cause of the failure and implement corrective action. Description of the overall investigation, cause of failure, and correction aspects will be given elsewhere. Material characterization tests are the emphasis here. Although fatigue initiation tests and fracture toughness tests and their analysis are quite different, a common sample was successfully used for both types of test.

A second objective is to describe the development and use of a modified load-line-displacement unloading-compliance procedure to measure crack growth for J_{Ic} tests with bend specimens. The section size available from the component precluded the standard procedure, wherein both load-line and crack-mouth displacement are measured. Results of analyses are described that indicate that measurement of a bottom surface displacement near the load line can be used to determine both of the basic results in a J_{Ic} test, that is, applied J and crack growth.

Methods

General Procedure

Three-point-bend notched specimens were used to measure both fatigue crack initiation life and J-integral fracture toughness of plate and weld metal in various conditions. The nominal specimen configuration shown in Fig. 2 was used for plate specimens and specimens made from full penetration weld samples. The materials and conditions tested are shown in Table 1, along with representative data to show the general nature of the results; details will be discussed later. Fatigue loading was applied to the notched specimen and the number

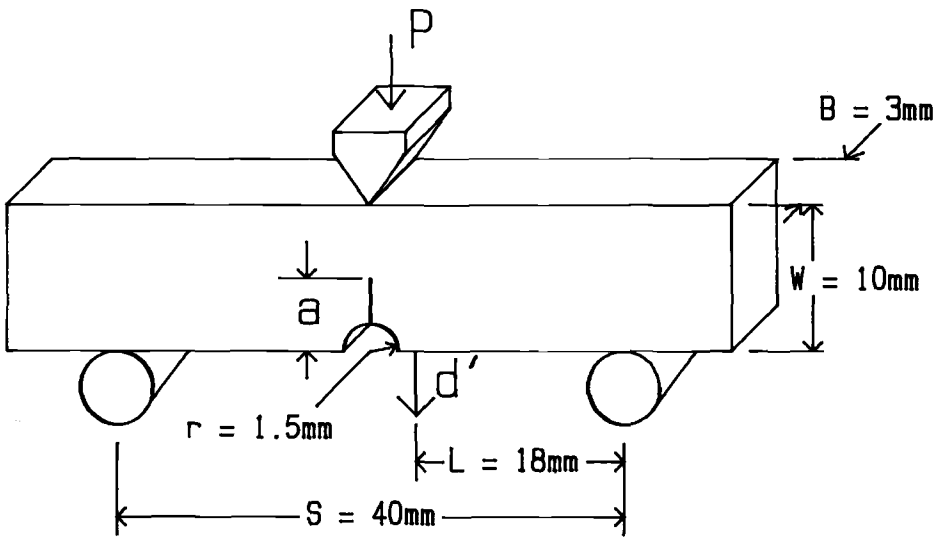

FIG. 2—*Test specimen for fracture toughness and fatigue crack initiation tests.*

of cycles to crack initiation was determined. The notch-fatigue-life analysis method of Barsom and Rolfe [*1*] was used to analyze the test results. The crack was lengthened, side notches were added, and J_{Ic} tests were performed using a modified ASTM Test Method for J_{Ic}, a Measure of Fracture Toughness (E 813–87) procedure.

TABLE 1—*Summary of J_{Ic} and fatigue crack initiation tests performed with stainless steel plate and weld metal.*

Material	Condition	J_{Ic}, typical, kN/m	Initiation, S_n = 1000 MPa cycles
	PLATE		
95–15	treat[a], age at 530°C		
	L-T orientation	180	7 000
	T-L orientation	70	. . .
15–5 PH	treat[b], age at 593°C	200	17 000
	WELD		
95–14	treat[a], age at 530°C	80	. . .
15–500	as welded	120	26 000
	age at 593°C	80–160	15 000
	treat, age at 593°C	160	26 000
17–400	as welded	100	20 000
	age at 593°C	80–150	14 000
	treat, age at 593°C	150	22 000

[a]Heat treatment of 95–15 and 95–14: solution treat at 1050°C (5 min), air cool; condition at 750°C (2h), air cool; cool to below −5°C (2 h); and age at 530°C (2 h), air cool.

[b]Heat treatment of 15–5 PH: solution treat at 1040°C (½ h), air cool; and age at 593°C (4 h), air cool.

Materials

Five precipitation-hardening stainless steels with 15% chromium, 5% nickel nominal composition were tested: plate and weld-filler metal designated 95-15 and 95-14, respectively, from which the structure under investigation was fabricated; plate designated 15-5 PH; weld-filler metals 15-500 and 17-400, as specified in AMS 5826 and 5825, respectively. Chemical compositions of these five steels are given in Table 2, based on measurements from the current work and prior related work [*2*] and on specifications in the case of two or the weld-filler metals. The composition measurements in the current work were made with a direct reading emission spectrometer. There was no indication that the composition of the steel was outside of the appropriate specification.

Instrumentation

The fatigue initiation tests were performed on a servohydraulic test system in load control. A pragmatic definition of crack initiation was adopted for these tests. Initiation was defined as the number of cycles required for a surface crack to initiate and grow across the full 3-mm thickness of the notch root. The point of initiation was determined using a low power microscope and also by carefully noting the change of the displacement range of the test system instrumentation as the fatigue test proceeded.

The J_{Ic} tests were run in displacement control using the ramp-type function generator of the test system. A ramp command signal was used to load the specimen to the first level chosen for performing unloading-compliance crack length measurements. The manual set control was then used to partially unload the specimen, and the unloading slope was recorded at ten times the X and Y gains used for the primary recording of load versus displacement. After each unloading was completed, the ramp loading was resumed to continue the test to the next hold and unload position. Figure 3 shows block diagrams of the equipment and signals necessary to perform the loading and recording.

Two highly stable adjustable power supplies were necessary to obtain suitable $\times 10$ gain unloading-compliance plots. Two X-Y plotters of the high impedance type were used, with inputs capable of accepting a floating signal and common mode voltages of about ± 10 Vdc. This was necessary because the $\times 10$ gain plotter measured the difference between two

TABLE 2—*Compositions of precipitation hardening stainless steel plate and weld metal.*

	Cr	Ni	Mo	Cu	Mn	Si	C	S	P	Nb	Ti
					PLATE						
95–15 (measured; Ref 2)	15.9	5.5	1.8	1.8	1.33	0.36	0.07	0.007	0.020	0.05	0.09
15–5 PH (measured; current)	15.2	4.4	. . .	3.1	0.80	0.75	0.04	0.010	0.018	. . .	. . .
					WELD						
95–14 (measured; Ref 2)	14.2	5.4	1.5	1.8	0.72	0.41	0.04	0.004	0.019	0.24	. . .
15–500	14.4	4.8	0.3	3.0	0.25	0.60	0.025	0.010	0.020	. . .	. . .
(AMS 5826)	15.3	5.5	max	3.5	0.75	max	0.050	max	max	. . .	. . .
17–400	16.0	4.5	. . .	3.25	0.25	0.75	0.050	0.025	0.025	. . .	. . .
(AMS 5825)	16.8	5.0	. . .	4.00	0.75	max	max	max	max	. . .	. . .

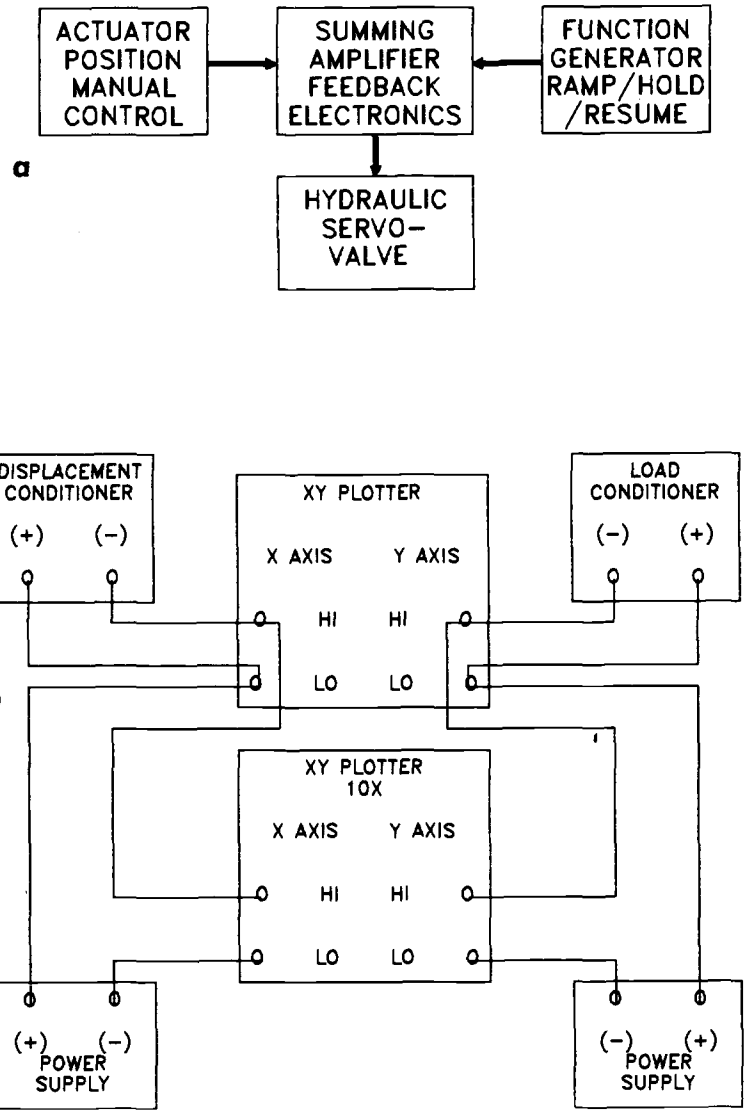

FIG. 3—*Test equipment for unloading-compliance* J_{Ic} *tests; (A) servohydraulic machine control, and (B)* X-Y *plotter arrangement.*

voltage signals, that of the load or displacement transducer and that of the power supply output. Polarities were strictly observed in order to obtain only a difference signal.

Fatigue Crack Initiation

The approach [*1*] for characterizing fatigue crack initiation has been used for ASTM A723 high strength steels with various notch geometries [*3*], so it was applied to the steels of similar strength level in this investigation. The approach is based on the expression for the

maximum notch stress, S_m, normal to the major axis of an elliptical notch with radius, r

$$S_m = 1.12K/(r)^{1/2} \tag{1}$$

where K is the appropriate opening mode stress intensity factor for the notch geometry and applied loading. This relationship is exact only as $r \rightarrow 0$, but it has been found to provide a useful characterization of notch root stress and associated fatigue initiation life at notches with radius of a few millimetres or less [*1,3*].

The $K/(r)^{1/2}$ approach was used here to compare the measured fatigue lives from the three-point bend specimens of the type shown in Fig. 2 with lives from test specimens cut from partial penetration welds in the structure. The only additional information needed was the K solution for the partial penetration weld specimen. This was obtained by finite element analysis, as discussed in the section on results.

J_{Ic} *Test Procedures*

In general, the procedures for performing and analyzing the J_{Ic} tests were those of ASTM E 813-87 with one significant modification, that is, displacement was measured on the bottom surface of the specimen and somewhat off the load-line. This displacement was used for both J calculations and for unloading-compliance crack length measurements, whereas ASTM E 813-87 requires a load-line displacement for J calculations and a crack-mouth-opening displacement for crack length measurements. If the modified simpler approach using bottom surface displacement were shown to be suitable, it would be a considerable advantage, particularly for small bend specimens. The following sections on J calculation and unloading compliance address the modified procedure.

J *Calculation*—The use of a modified displacement for J calculation can be considered in relation to Fig. 2. The displacement on the bottom surface, d', was measured near the load line, and was converted to load-line displacement, d, as follows

$$d = d'(S/2L) \tag{2}$$

Equation 2 would give the same displacement as that measured exactly at the load line if there were ideal rigid body displacements on the bottom surface. Recent analysis [*4*] showed this to be essentially the case. Elastic finite element results of bottom surface dislacements showed, for example, that for $2L/S = 0.9$ and $a/W = 0.6$ the value of displacement calculated from Eq 2 was within 0.8% of the load-line displacement result obtained directly from the finite element analysis. Also, keep in mind that the total load-line displacement in a J_{Ic} test is often controlled by plastic deformation in the ligament ahead of the crack. This causes a rigid-body type rotation of the bottom surface, and this is well described by Eq 2.

The calculation of J included the Eq 2 expression for d, but otherwise followed the procedures of ASTM E 813-87 and ASTM Test Method for Determining J-R Curves (E 1152-87). The calculation is outlined as follows

$$\begin{aligned} J_i = {} & [P_i Sf(a_0/W)/(BB_n)^{1/2}W^{3/2}]^2[(1 - \mu^2)/E] \\ & + \Sigma_i\{[P_i + P_{i-1}][d(p)_i - d(p)_{i-1}]/b_0B_n\} \end{aligned} \tag{3}$$

where P_i and $d(p)_i$ are the load and the increment of plastic displacement for a given unloading (see Fig. 4); a_0 and b_0 are the starting crack length and uncracked ligament, respectively; $f(a_0/W)$ is from the three-point bend K expression of ASTM Test Method for

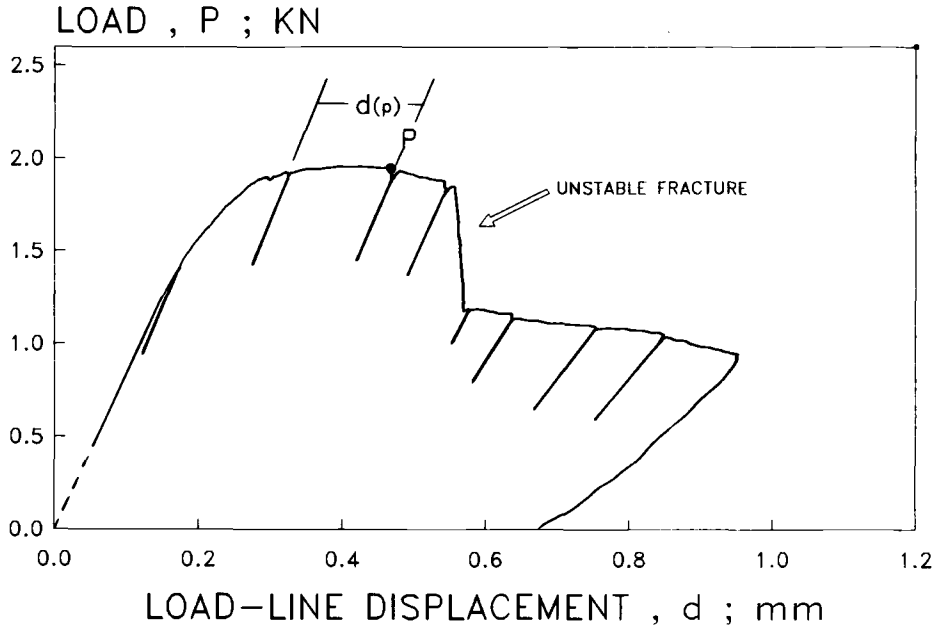

FIG. 4—*Load-displacement behavior for 15–500 weld; welded and aged at 593°C.*

Plane-Strain Fracture Toughness of Metallic Materials (E 399-83); B_n is net specimen thickness after side notching; and μ and E are Poisson's ratio and elastic modulus, taken as 0.3 and 207 000 MPa, respectively. Equation 3 was used as shown to calculate J except on the two occasions of unstable fracture, one of which is shown in Fig. 4. In these cases, an average of the loads at the beginning and end of the unstable growth was used for P_i, rather than using the load at the point of unloading.

Unloading Compliance—Load-line displacement can be used in place of crack-mouth displacement for measurement of unloading-compliance crack growth provided that an expression for a/W in terms of load-line displacement is available. A new expression for a/W in terms of d was developed here, based on the available expression [5] for d in terms of a/W. The new expression is

$$a/W = 1.0005 - 4.1527U + 9.7477U^2 - 214.2U^3 + 1604.3U^4 - 4633.4U^5 \quad (4)$$

where

$U = 1/\{[dE(BB_n)^{1/2}/P]^{1/2} + 1\}$ for the range $0.2 < a/W < 1.0$.

The new inverse expression, Eq 4, represents the earlier expression [5] with an accuracy of 0.0015 a/W. For a narrower range, $0.40 < a/W < 0.85$, the new expression represents the earlier expression with an accuracy of 0.0002 a/W. So it is accurate enough for general use in unloading compliance calculations, including calculations that iterate between the displacement expression and the a/W expression.

Another requirement for the use of load-line displacement in unloading compliance calculations is that this type of displacement is adequately sensitive to crack length changes in the geometry range of intended use. A comparison of crack-mouth and load-line displacements as a function of crack length is shown in Table 3. The dimensionless parameters

TABLE 3—*Calculated elastic crack-mouth-opening displacement,* v, *and load-line displacement,* d, *for a three-point bend specimen.*

a/W	*vEB/P*	*dEB/P*
0.00	0.00	19.09
0.20	7.07	23.58
0.40	20.83	39.01
0.60	64.36	88.28
0.80	323.9	365.0
0.95	6026.	6147.

vEB/P and *dEB/P* were obtained from Refs *6* and *5*, respectively. Note that for *a/W* below about 0.2 *dEB/P* has poor sensitivity to a change in *a/W* and should not be used to measure crack length; *vEB/P* should be used in this range. For *a/W* above 0.2, either displacement can be used.

TABLE 4—J_{Ic} *results for stainless steel plate and weld metal in various conditions.*

Specimen Number	Condition	*J*-Integral Toughness, J_{Ic}, kN/m	Effective Yield, *Sy*, MPa	Validity Ratio, *B Sy*/25 *J*
		95–15 PLATE; L-T		
AP-L1	treat, age (Ref *2*)	185	1000	1.30
AP-L2		173		1.39
DP-L1	treat, age	198	943	0.51
DP-L2		183		0.56
		95–15 PLATE; T-L		
AP-T1	treat, age (Ref *2*)	47	1010	5.16
AP-T2		44		5.51
DP-T1	treat, age	66	998	1.63
DP-T2		70		1.54
		15–5 PH PLATE; T-L		
15-T1	treat, age	192	1100	1.09
15-T2		238		0.88
		95–14 WELD		
UW-1	weld, treat, age	94	1230	1.33
UW-2		79		1.57
		15–500 WELD		
5-3	as welded	124	1050	0.92
5-4		107		1.07
5A-1	weld, age	76	1220	2.05
5A-2		156		1.00
5S-3	weld, treat, age	157	1200	0.82
5S-4		157		0.82
		17–400 WELD		
7-1	as welded	103	1280	1.40
7-3		105		1.38
7A-3	weld, age	147	1280	1.04
7A-4		76		2.03
7S-1	weld, treat, age	167	1140	0.84
7S-2		135		1.04

Results

J_{Ic} *Fracture Toughness*

Table 4 lists the results of 20 J_{1c} tests for the five materials in various conditions, the effective yield strength, *Sy*, and the calculated ratio of specimen thickness, *B*, to the ASTM E 813-87 thickness requirement for a valid J_{1c} test, 25 *J*/*Sy*. For a sample to be of valid size, the ratio [*BSy*/25 *J*] must equal unity or more. Test results for L-T and T-L orientations of the same material from the prior related work [*2*] are listed for comparison. The general trend of the tests here is that the available 3-mm nominal material thickness was adequate for a valid result in most cases. Two of the ten pairs of results gave an average ratio of thickness to valid size below unity, that is, 0.54 and 0.82, but all other pairs had one or both values above unity.

The directional nature of J_{1c} for the 95-15 plate is demonstrated in Fig. 5. This plot of *J* versus crack growth data for the T-L and L-T orientations shows that the longitudinal toughness is about three times the transverse value. This significant difference is due to the existence of delta ferrite that is elongated during the hot rolling operation [*7*]. The 95-15 material is a semi-austenitic stainless steel, with a mixed austenitic and ferritic structure at room temperature after solution treatment. This allows rolling to thin plate or forming to small radii, which are advantages for producing complex structures. A disadvantage of this material is anisotropy of toughness caused by the elongated delta ferrite. Figure 5 also shows good correspondence between the earlier results [*2*], which used a different lot and thickness of material, and the current results.

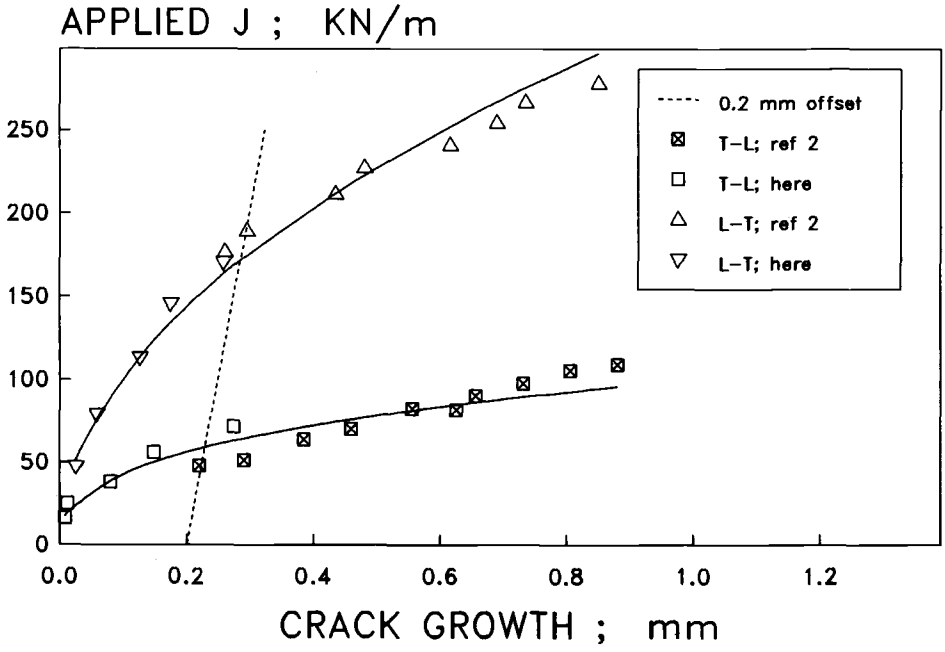

AP-T1; T-L orientation, Ref *2*.
AP-L1; L-T orientation, Ref *2*.
DP-T1; T-L orientation, current work.
DP-L2; L-T orientation, current work.

FIG. 5—J *versus crack growth for 95-15 plate; solution treated, aged at 530°C.*

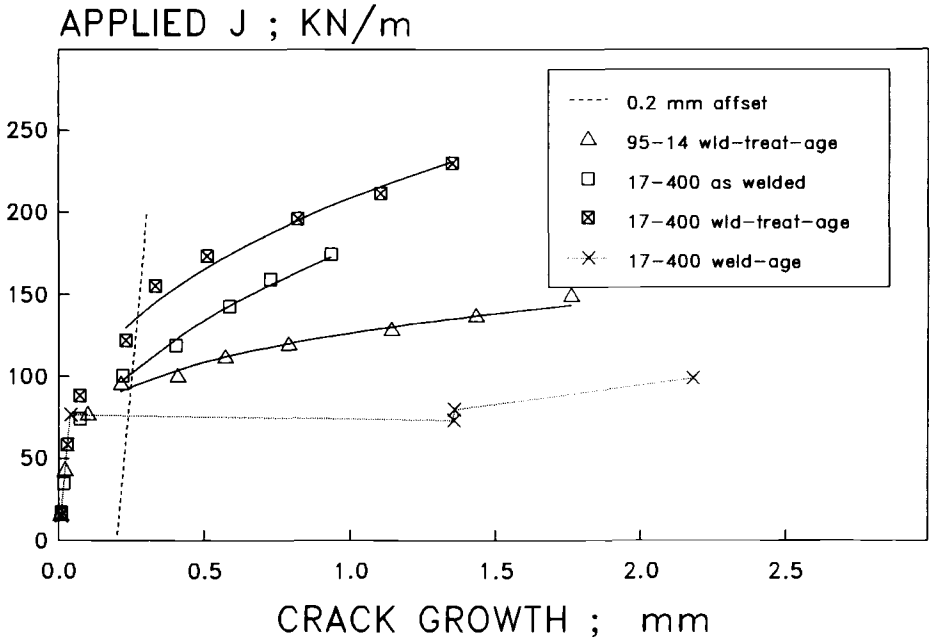

UW-1; 95-14, welded, treated, aged at 530°C.
7-1; 17-400, as welded.
7A-4; 17-400, welded, aged at 593°C.
7S-2; 17-400, welded, treated, aged at 593°C.

FIG. 6—J *versus crack growth for 17-400 and 95-14 welds in various conditions.*

A comparison of key *J*-integral fracture toughness results of the investigation is presented in Fig. 6. It shows *J* versus crack growth results for the 95-14 weld metal in the condition currently used in the structure, along with a prospective future replacement weld material, 17-400, in three heat treat conditions. The highest toughness results were from 17-400 conventionally solution treated and aged, followed by 17-400 as welded, 95-14 conventionally processed, and finally 17-400 aged only. This last, lowest toughness result was from Specimen 7A-4, the second specimen that displayed unstable fracture, in a similar manner to that shown for 15-500 aged only, see Fig. 4. The *J* versus crack growth curve for the unstable fracture in Fig. 6 was not fit with the usual power-law ASTM E 813-87 procedure because of the instability; linear segments were used to connect the unloading data points. However, it is clear from Fig. 6 that both J_{Ic} and the *J*-integral toughness following additional crack growth were significantly reduced for the welded and aged 17-400 material. Table 4 shows this value and the value for the other unstable fracture to be the lowest toughness observed for the 15-500 and 17-400 materials. It is important to note from Fig. 6 that the unstable fracture results in toughness values that are progressively lower than those of the other conditions as crack growth progresses.

Scanning electron microscope fractographs of 17-400 welds in the highest and lowest toughness conditions of Fig. 6 are shown in Fig. 7. The solution treated and aged sample (7A) showed classic dimpled rupture, whereas the aged-only sample (7B) showed evidence of cleavage. Visual examination could also distinguish between the two; the solution treated and aged sample had a uniform region of fast fracture, whereas the aged-only sample contained shiny faceted regions on the fast fracture surface. The occurrence of cleavage in

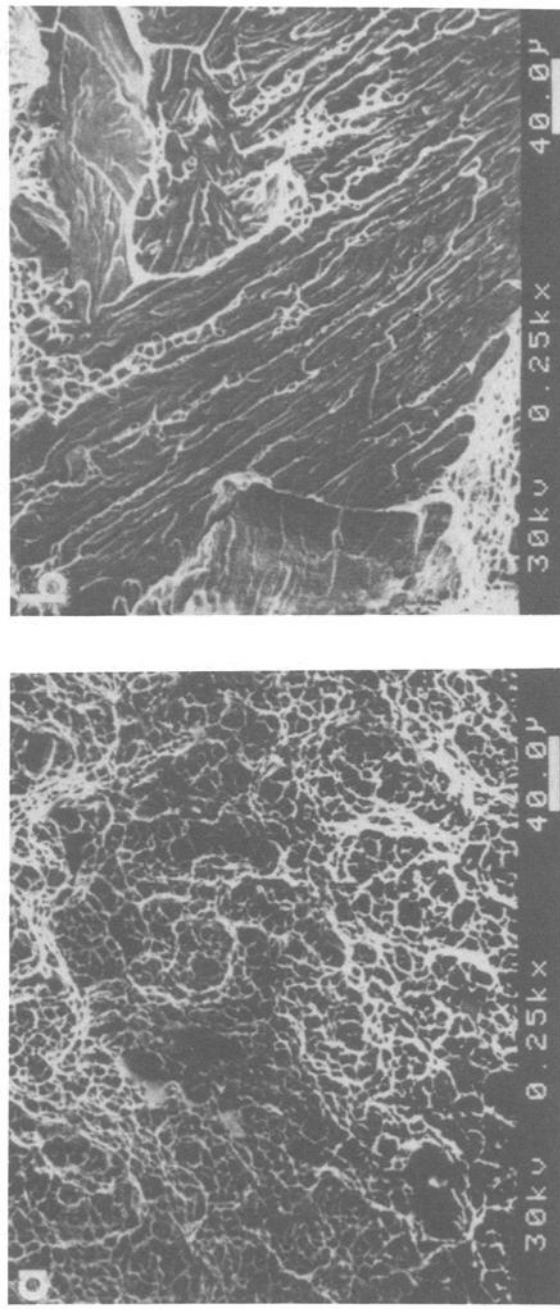

FIG. 7—*Scanning electron microscope fractographs of 15-500 welds; (A) welded, treated, aged, and (B) welded, aged.*

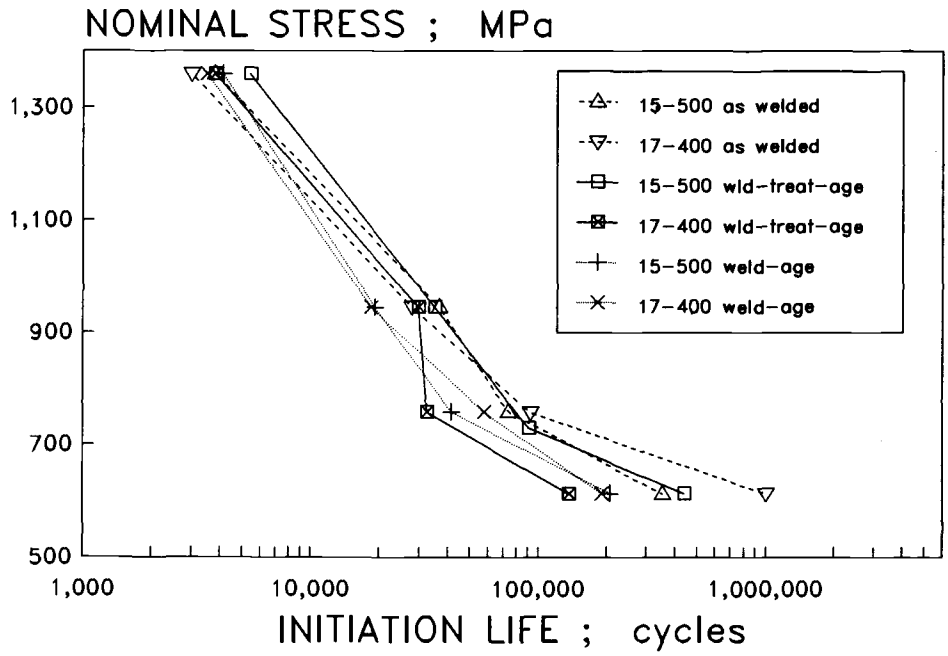

FIG. 8—*Fatigue crack initiation behavior of 15–500 and 17–400 welds in various conditions.*

the aged-only samples is in agreement with other results [*8,9*]. The as-welded microstructure contains islands of ferrite in a matrix of austenite and martensite. When this structure is aged directly after welding, it is susceptible to cleavage of the ferrite and martensite. Bosworth and Zvanut [*8*] found that directly aged 15-500 and 17-400 welds resulted in lower strength and toughness than solution treated and aged welds.

Fatigue Crack Initiation

Fatigue tests were performed with specimens as shown in Fig. 2 for the 15-500 and 17-400 weld materials in three conditions and at four load levels, 24 tests in all. The results are shown in Fig. 8. A nominal bending stress at the ligament ahead of the notch, S_n, was calculated as follows (see Fig. 2 for nomenclature)

$$S_n = 1.5PS/B(W - a)^2 \tag{5}$$

The number of cycles required for initiation across the full width of the specimen varied by less than a factor of two for the different materials at the highest nominal stress and by a larger amount at lower stress, as is expected in fatigue. Generally, the aged-only condition for both materials showed the shortest initiation life.

Fatigue crack initiation at partial penetration welds in the structure is believed to have had a major effect on the life of the structure, so it would be useful to compare the initiation life at partial penetration welds to the results from the test specimens of Fig. 2. The $K/(r)^{1/2}$ approach [*1*] can be used for this comparison. For the test specimen in Fig. 2, the two basic parameters, K and r, are known. For the partial penetration weld in the structure, a finite element solution is required to calculate K. Figure 9 shows the finite element grid; half of

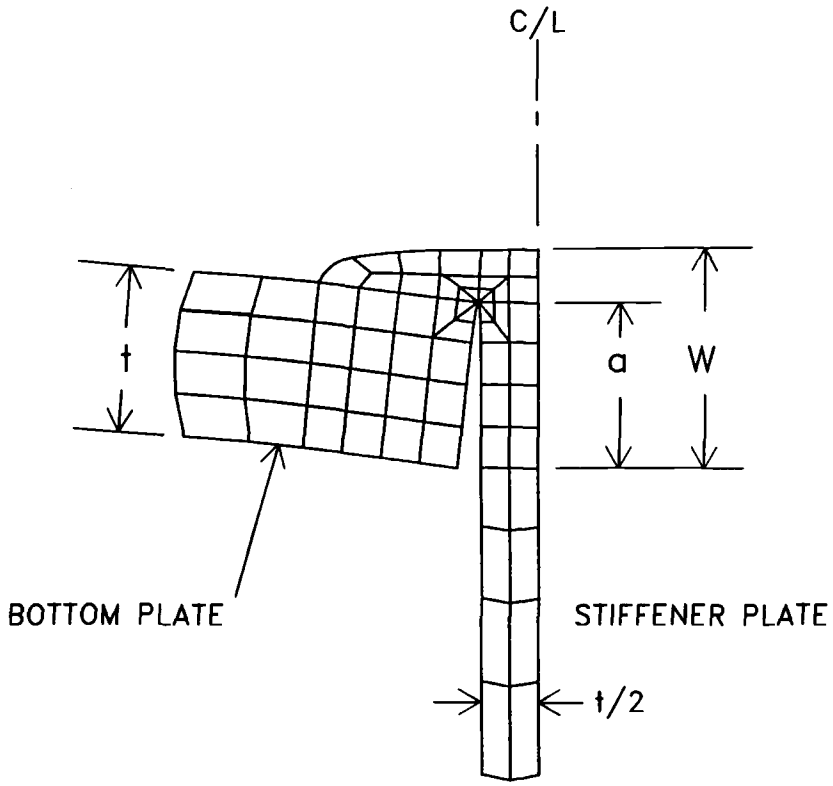

FIG. 9—*Deformed finite element model of stiffener-to-bottom plate weld specimen.*

the weld is shown because of the usual symmetry argument. Two notches formed by the gaps between the stiffener plate and the slot in the bottom plate were modeled. The ratio of total width of weld to the plate thickness, t, is 2.91; the ratio of the total plate plus weld thickness, W, to t is 1.27. The penetration of a typical weld into the bottom plate was up to about 50% penetration, with a minimum of about 0% penetration (that is, no penetration into the thickness of the bottom plate) as shown in Fig. 9. A 0% penetration weld corresponds to a notch completely through the bottom plate, that is, $a = t$, as shown in Fig. 9.

The K results from the finite element model for the double edge notch with $S/W = 11$, corresponding to the tests of partial penetration weld specimens cut from the structure, are shown in Table 5. The results are compared with the standard single-edge-notched bend specimen of ASTM E 399-83. Note that the dimensionless K parameter used in Table 5 includes the specimen span, S; this produces about the same value of the K parameter for quite different values of S/W. Generally, the double-notch weld specimen results are about 10% higher than those of the standard single-notch specimen. We interpret this to be an indication that the reduction in specimen depth, W, away from the center line of the weld causes a significant increase in K for the weld specimen over that of the standard specimen. This increase in K more than makes up for the decrease in K that is expected due to the two cracks.

Fatigue lives from the standard specimen tests are compared directly with lives from weld specimens cut from the structure in Fig. 10. The values of K for the $r = 1.5$ mm tests are from ASTM E 399-87 relationships for the Fig. 2 geometry; for the $r = 0.13$ mm tests, K

TABLE 5—*Calculated stress intensity factor,* K, *for standard single-edge crack specimen and double-edge crack weld specimen loaded in three-point bending.*

a/W	$[KBW^{3/2}/PS]$; standard, $S/W = 4$, one crack	$[KBW^{3/2}/PS]$; weld, $S/W = 11$, two cracks
0.098	0.84	0.93
0.196	1.16	1.28
0.295	1.50	1.64
0.393	1.94	2.11
0.491	2.59	2.81
0.589	3.62	3.94
0.688	5.50	6.03
0.786	9.73	11.44

is from the Table 5 results and r is defined by the gap between the stiffener and the slot in the bottom plate. Note that the ordinate of Fig. 10 includes the effective yield strength to account for the important effect of strength on fatigue initiation life. Including Sy also makes the values dimensionless and thus usable in any set of units. Note also that the data for $r = 1.5$ mm is initiation life, whereas the data for $r = 0.13$ mm is total life. This is a reasonable comparison because the total lives for the $r = 0.13$ mm tests are believed to be predominantly initiation cycles.

The most significant feature of the results in Fig. 10 is that the fatigue lives of four materials are well represented by a single expression. The straight line shown, obtained by power law

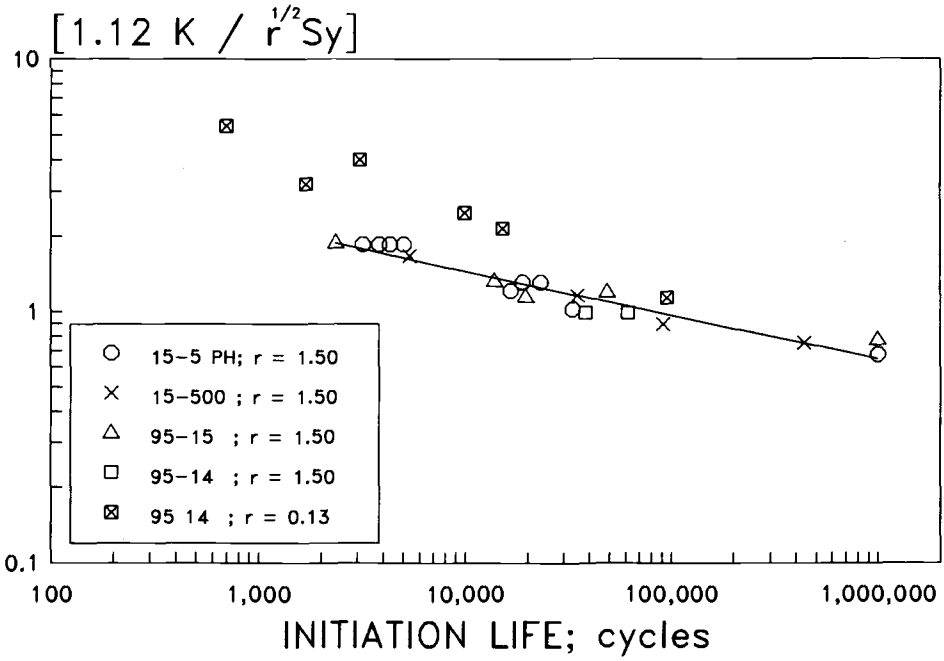

FIG. 10—*Fatigue life described by* $[K/r^{1/2}Sy]$ *parameter for specimens of different material and configuration.*

regression of the $r = 1.5$ mm data, has the formula

$$N = 85\,000[1.12K/r^{1/2}Sy]^{-5.7} \tag{6}$$

and a correlation coefficient of 0.96. This expression can be used to describe (or predict, for a courageous user) a fatigue initiation life for a notch with a radius of about 2 mm or less and for which a solution for K is known. The lives for the weld specimens with $r = 0.13$ mm are typically about twice those from Eq 6, so the equation has some application to the partial penetration welds as well, even though it is somewhat conservative. Of course, higher lives for the $r = 0.13$ mm specimens are expected, considering that these tests include growth as well as initiation cycles.

Summary

1. J_{Ic} test procedures for the three-point bend specimen were developed using a near-load-line bottom surface displacement for unloading compliance measurements of crack growth. A new expression for a/W in terms of load-line displacement was developed.

2. J_{Ic} toughness was measured for two plate and three weld-metal precipitation-hardening stainless steels in various welded and heat treated conditions. Measurements were made from samples that were cut from welds, including some samples that displayed cleavage failure due to an incomplete heat treatment following welding.

3. Fatigue crack initiation life was measured for two plate and three weld-metal steels in various conditions. Lives from 1000 to 1 000 000 cycles were measured using a 1.5 mm radius notch in three-point bend specimens subjected to ligament stresses of about the yield strength level.

4. The ratio of maximum notch-root stress defined by a $K/(r)^{1/2}$ parameter to material yield strength gave a good description of fatigue crack initiation for four steels. The approach also gave an approximate description of initiation for other tests with one of the steels using samples with a significantly different notched configuration.

Acknowledgments

We are pleased to acknowledge the help of E. Troiano with failure analysis, L. A. King with specimen preparation, M. F. Flezar with chemical composition measurements, D. J. Corrigan with graphics presentation, and J. Feneck for guidance throughout the investigation.

References

[1] Barsom, J. M. and Rolfe, S. T., *Fracture and Fatigue Control in Structures*, Prentice-Hall, Englewood Cliffs, NJ, 1987.

[2] Farrara, R. A., "Fatigue—Fracture Properties of a Semi-Austenitic PH Stainless Steel," Report MRL-R-1041, Materials Research Laboratories, Melbourne, Australia, Feb. 1987.

[3] Underwood, J. H., "Fatigue Life Analysis and Tensile Overload Effects with High Strength Steel Notched Specimens," *High Pressure in Science and Technology, Part II*, C. Homan, R. K. MacCrone, and E. Whalley, Eds., Elsevier, New York, 1984, pp. 209–214.

[4] Underwood, J. H. and Witherell, M. D., "Load-Line Displacements for Three-Point-Bend J Tests using Bottom Surface Displacements," *Engineering Fracture Mechanics*, Vol. 37, 1990, pp. 1277–1278.

[5] Underwood, J. H., Kapp, J. A., and Baratta, F. I., "More on Compliance of the Three-Point Bend Specimen," *International Journal of Fracture*, Vol. 28, 1985, pp. R41–R45.

[6] Tada, H., Paris, P. C., and Irwin, G. R., *The Stress Analysis of Cracks Handbook*, Paris Productions Inc., St. Louis, 1985, p. 2.17.

[7] *Metals Handbook Ninth Edition, Vol. 9, Metalography and Microstructures*, ASM, Metals Park, OH, 1985, p. 285.
[8] Bosworth, T. J. and Zvanut, A. J., "Development of a Direct Aging Filler Metal for Welding 15-5 PH/17-4 PH Steel," *Welding Research Supplement,* June 1977, pp. 159s–170s.
[9] Schichtmann, H., "High-Speed Craft Ride on Welded Hydrofoils," *Welding Design and Fabrication*, March 1981, pp. 91–95.

Stephen M. Graham,[1] *W. Randolph Lloyd,*[1] *and Walter G. Reuter*[1]

Experience with *J* Testing of Type 304/308 Stainless Steel Weldment

REFERENCE: Graham, S. M., Lloyd, W. R., and Reuter, W. G., **"Experience with *J* Testing of Type 304/308 Stainless Steel Weldment,"** *Elastic-Plastic Fracture Test Methods: The User's Experience (Second Volume), ASTM STP 1114*, J. A. Joyce, Ed., American Society for Testing and Materials, Philadelphia, 1991, pp. 213–224.

ABSTRACT: Crack initiation toughness tests were conducted using the *J*-integral as a fracture characterizing parameter according to the ASTM Test Method for J_{Ic}, a Measure of Fracture Toughness (E 813-87). The specimens were made from a weldment of Type 304 stainless steel (SS) base metal and Type 308 SS weld metal, and were fabricated such that the crack initiation toughness (J_{Ic}) of the weld metal could be measured. A peculiar feature of all of the tests was that crack growth occurred in an inverse tunneling mode. The provisional initiation toughnesses (J_Q) calculated from the test results were determined to be invalid because the validation requirements on change in crack front curvature and on accuracy of the predicted crack extension were not met. The accuracy of the predicted extensions was improved by applying correction factors to the last measured compliances to account for crack front curvature, plastic deformation, friction, and indentation. The excessive change in crack front curvature was caused by the transition from tunneling growth during fatigue precracking (before the specimens were side grooved) to inverse tunneling during slow stable crack growth. Crack growth by inverse tunneling indicates a constraint condition at the root of the side-grooves that is more severe than in the center. If this is the case, the measured initiation toughness should be a valid indication of the lower bound for high constraint.

KEY WORDS: elastic-plastic fracture, test methods, *J*-integral, austenitic stainless steels, welds, crack extension, unloading compliance, three-point bend test

Fracture toughness tests were conducted on a weldment of Type 304 stainless steel (SS) base metal and Type 308 SS weld metal using the ASTM Test Method for J_{Ic}, a Measure of Fracture Toughness (E 813-87). The purpose of these tests was to determine the crack initiation toughness of the weld metal. The results of these tests are examined in light of developments in the field of fracture toughness testing since the last revision of ASTM E 813 in 1987. The developments considered here are those that specifically affect the calculation of crack length from the compliance data for single-edge bend [SE(B)] specimens, the determination of a provisional initiation toughness (J_Q), and the validation of that initiation toughness.

Experimental Procedure

A weldment was fabricated from two pieces of 50.8-mm-thick Type 304 SS plate using Type 308 SS fillter metal and an auto submerged arc process. The weld was two sided and was formed in 27 successive passes. Tension specimens were removed from the weldment

[1]Engineering specialist, engineering specialist, and principal engineer, respectively, Idaho National Engineering Laboratory, EG&G Idaho, Inc., Idaho Falls, ID 83415-2218.

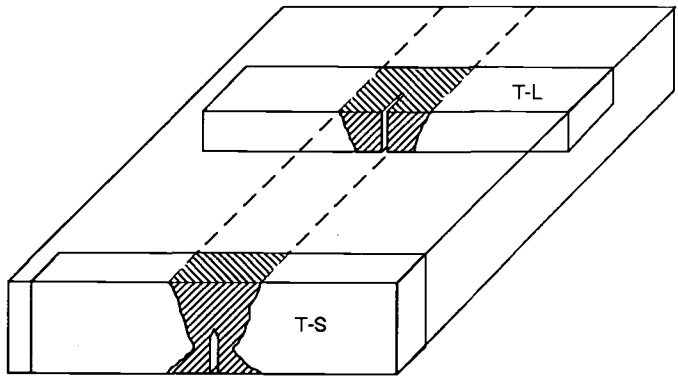

FIG. 1—*Diagram of weldment showing shape of weld zone and placement of specimens in weldment. Letter designation refers to crack plane orientation (crack plane normal–crack growth direction).*

to determine the mechanical properties of the Type 308 SS weld metal; the measured values were: yield strength = 468 MPa, tensile strength = 653 MPa, and elastic modulus = 2.08 $\times$ 10^5 MPa.

Standard SE(B) specimens were prepared from the weldment with the machined notch in the approximate center of the weld, as shown in Fig. 1. The specimen dimensions are shown in Fig. 2. Five specimens were tested in this program, two of T-L orientation and three of T-S orientation.

The three-point bending fixture was made according to the recommendations of ASTM E 813-87 except that hardened steel bearing surfaces were added for the two end support roller pins. Crack mouth opening displacement (COD) was measured with a clip gage, also made basically according to the recommendations in ASTM E 813-87. The design of the

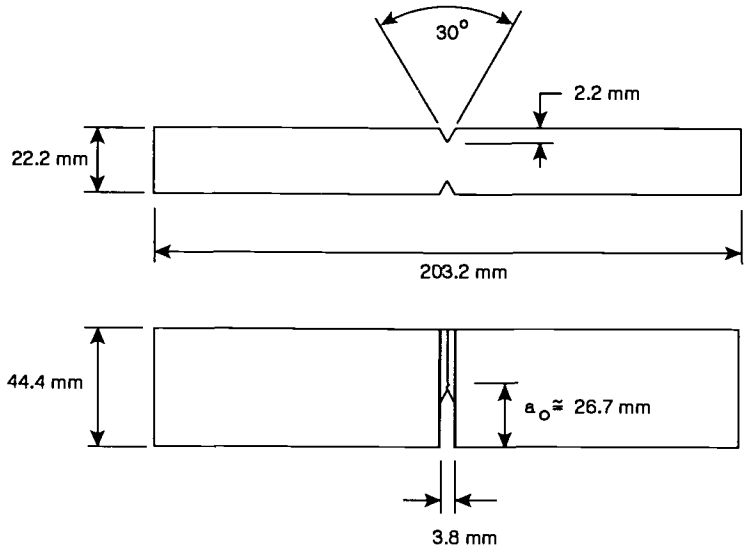

FIG. 2—*Dimensions of SE(B) specimen.*

grooves at the tips of the gage arms was modified to ensure that the knife edge sat in the bottom of the groove, and that there was sufficient clearance to allow for free rotation of the knife edges up to full-scale displacement. These modifications to the bend fixture and clip gage were found to reduce problems with apparent negative crack growth at low J(<17.5 kJ/m^2).

The load point displacement (LPD) was measured with a linear variable differential transformer (LVDT) mounted between the loading roller and the bend fixture. The measured LPD was corrected for load train compliance using the procedure in Section A1.4.4 of ASTM E 813-87.

The tests were conducted using a computer-controlled servohydraulic test machine. Automated J test software was used to calibrate the transducers, run the J test procedure using the single specimen technique, and analyze data. The software followed the guidelines set forth in ASTM E 813-87 for running the test and analyzing the data. Crack lengths were calculated using the crack opening compliance, as measured with the clip gage.

Results

The results presented here are for one particular specimen, however, they are representative of the results obtained for all of the specimens. In the following discussion, analysis of the validity requirements will be presented for all of the specimens.

A typical plot of J versus crack length obtained during testing is indicated by square symbols in Fig. 3. Two observations can be made from the crack lengths calculated using the plane stress elastic modulus: (1) for low J values (<17.5 kJ/m^2), the crack length appears to decrease with increasing J; and (2) the crack lengths calculated by unloading compliance, especially the initial crack length, are larger than the physical crack lengths measured on the fracture surface (the latter being represented by Xs). The problems of apparent negative crack growth and scatter in the crack length data for small amounts of crack growth have

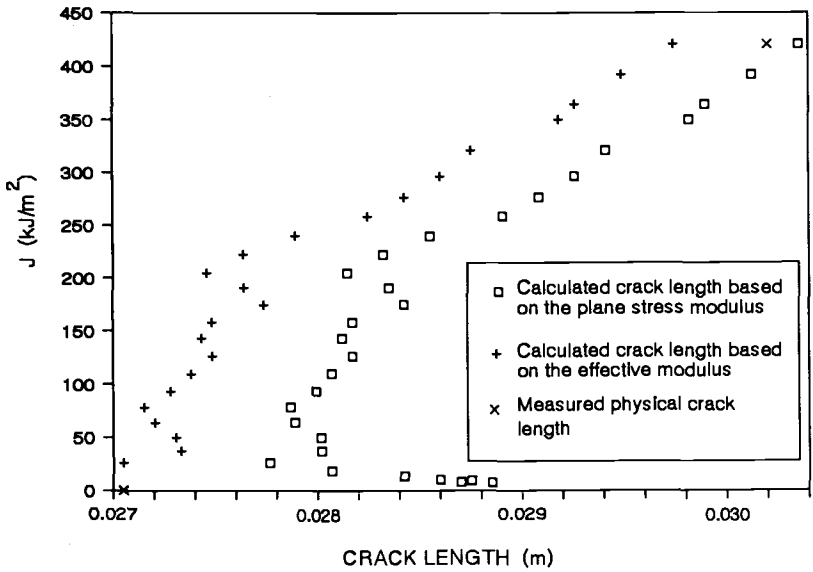

FIG. 3—J *versus crack length for Type 308 SS weld metal SE(B) Specimen WLC-1.*

been observed by other investigators for compact tension, C(T), specimens [*1,2*] and for SE(B) specimens [*3*]. The apparent negative crack growth is believed to be caused by friction and misalignment in the fixtures and, as mentioned previously, was reduced through careful design of the bend fixture and clip gage, and alignment of the bend fixture.

The discrepancy between the calculated and physical crack lengths is due, in part, to the choice of the elastic modulus in the calculation of crack length from compliance. The elastic modulus is a function of the state of stress, or degree of constraint, of the specimen. The automated *J* test software calculated the crack lengths during testing based on the assumption of plane stress. This discrepancy can be reduced by calculating the effective modulus based on the initial compliance and the initial physical crack length, and then using this modulus instead of the plane stress modulus to calculate crack length. Using this approach, it is also possible to correct for calibration errors. Taking the minimum of the measured compliances as the initial compliance, the effective modulus for Specimen WLC-1 is 1.878×10^5 MPa. One of the validity requirements for ASTM E 813-87 is that the difference between the effective modulus and the elastic modulus must be less than 10%. For Type 308 SS weld metal, the plane stress elastic modulus is 2.082×10^5 MPa and the difference is 9.8%, which is just within the required limits. The crack lengths calculated using the effective modulus are also shown in Fig. 3, where the points that exhibited apparent negative crack growth have been omitted. The calculated final crack length is now less than the physical final crack length, and the difference between them is 0.00047 m.

The standard does not specify requirements for accuracy of crack length determination because the data analysis is based on crack shape or extension, not crack length. There are two requirements that pertain to crack extension. One is that the crack front curvature remain within certain limits. A diagram showing the initial and final crack fronts determined from measurements on the fracture surface of a typical specimen is given in Fig. 4. The

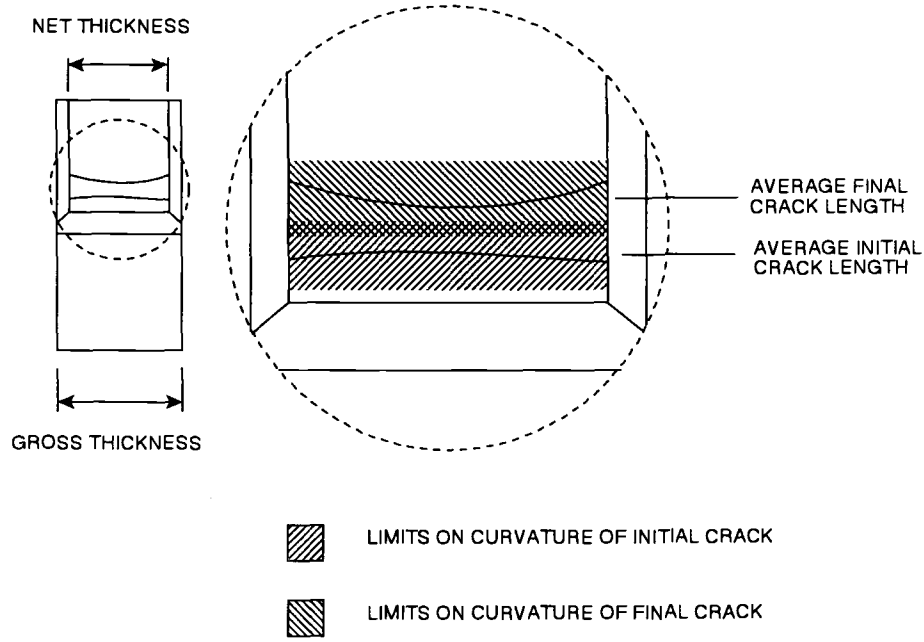

FIG. 4—*Position of the initial and final crack fronts on Type 308 SS weld Specimen WLC-1 and the allowable limits on curvature according to ASTM E 813-87.*

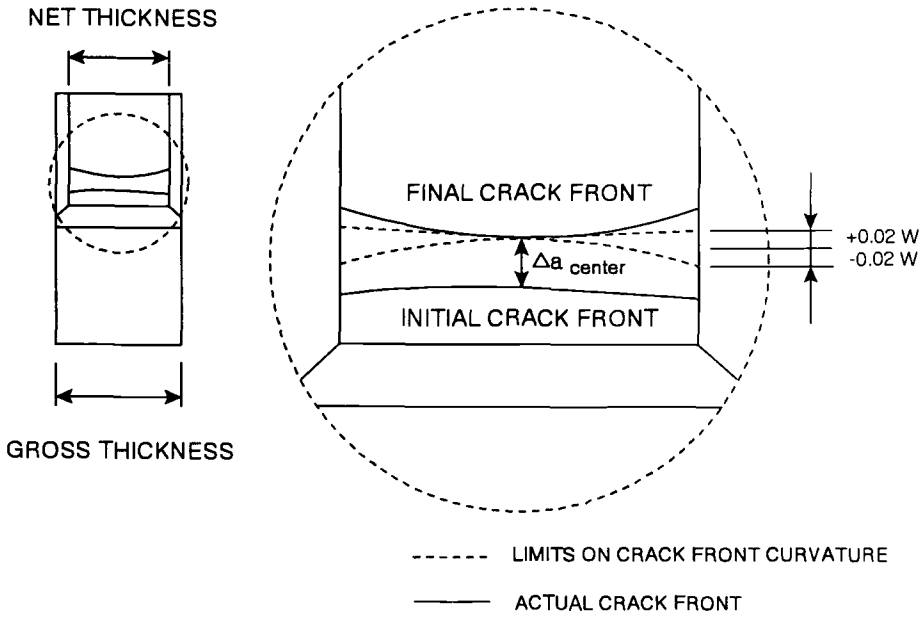

FIG. 5—*Position of initial and final crack fronts on Type 308 SS weld Specimen WLC-1 and the limits on change in crack front curvature according to ASTM E 813-87.*

specimen was fatigue precracked before side-grooving, thereby causing a slight tunneling of the initial crack front. The addition of the side grooves caused the crack growth mode to change from tunneling to inverse tunneling. Section 9.4.1.5 of ASTM E 813-87 requires that the difference between the crack length at any point and the average crack length be less than 7% of the average crack length. The limits for the initial and final cracks are also shown in Fig. 4. It is clear that the initial and final crack fronts are well within these limits. It is also apparent that this requirement is not particularly restrictive, and that the standard allows for considerable crack front curvature.

Section 9.4.1.6 of ASTM E 813-87 requires that the difference in crack extension between the edges and the center be less than $\pm 0.02\ W$. This places a restriction on the change in the crack front curvature between the initial and final crack fronts. The dashed line crack fronts shown in Fig. 5 indicate the limits on the change in crack front curvature. It is apparent that this requirement is quite restrictive since both the initial and final crack fronts are well within the limits on curvature, however, the change in crack growth mode from tunneling to inverse tunneling causes the change in curvature to exceed the limits. This was true for all of the specimens tested, as shown in Fig. 6. The inability to meet this requirement caused all of the provisional crack initiation toughnesses to be invalid.

A typical plot of J versus crack extension is shown in Fig. 7. The negative crack growth is apparent as the crack extension decreases with increasing J for low values of J. The problem with this negative crack growth is that it causes confusion over the true value of the initial crack length. Sections 8.4.3.1 and .2 of ASTM E 813-87 specify that the initial crack length shall be determined by the average of three compliance measurements made at a maximum load of 10 to 40% of the limit load. Using this approach would cause the crack extension in the early part of the test to be negative. The approach used for plotting the data in Fig. 7 was to estimate the initial crack length as the minimum calculated crack length. This choice of initial crack length shifts the crack extension such that all values are

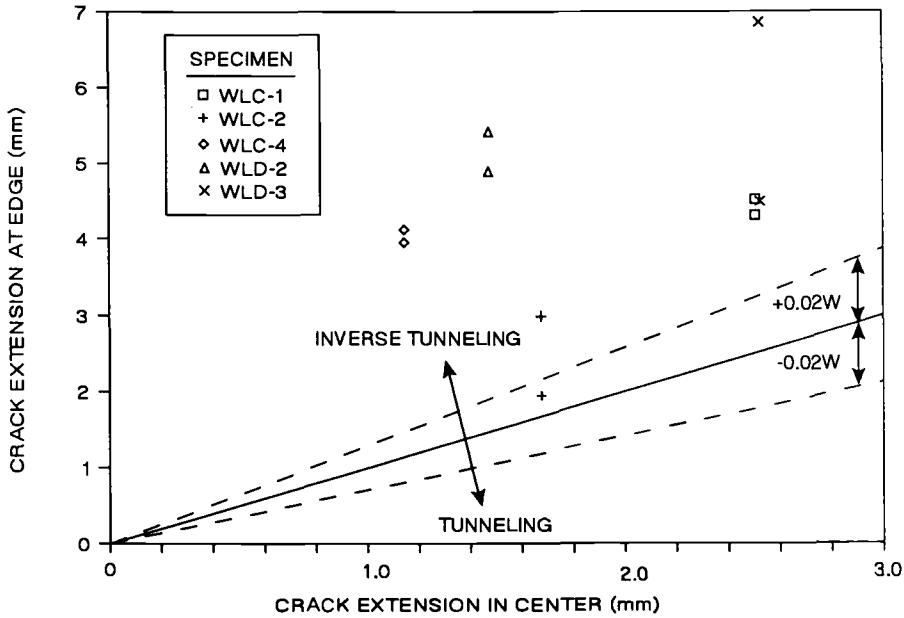

FIG. 6—*Change in crack front curvature during crack extension for Type 308 SS weld metal. The two points shown for each specimen represent the two near-surface edges of the crack.*

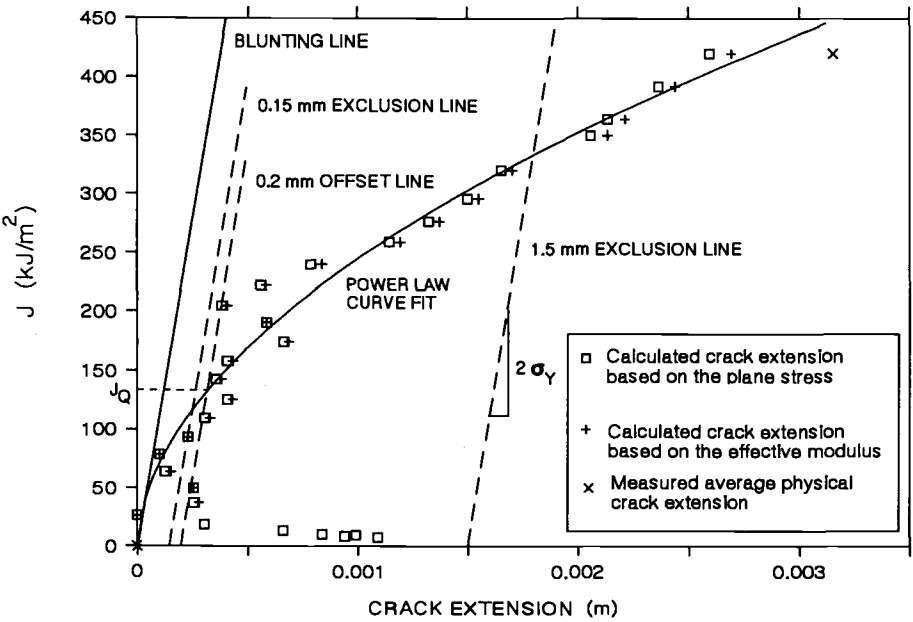

FIG. 7—J *versus crack extension calculated using the plane stress and the effective elastic modulus for Type 308 SS weld metal Specimen WLC-1.*

positive. This minimum crack length generally occurred for J of approximately 20 kJ/m^2. The crack extension due to blunting was considered to be negligible at this low J value, and therefore was neglected. In the analysis of the data to determine the power law growth curve and the provisional initiation toughness, the early points exhibiting apparent negative crack growth were excluded.

The average physical crack extension, as measured on the fracture surface, is also plotted in Fig. 7. Section 9.4.1.7 of ASTM E 813-87 requires that difference between the calculated and physical crack extension be less than ± 0.15 times the physical crack extension for extensions less than the maximum value, and ± 0.15 times the maximum value thereafter. The normalized difference in crack extension is plotted for all of the specimens in Fig. 8. For these tests, the unloading compliance method of determining crack length tends to under-predict the crack extension, and the amount of under-prediction increases with increasing crack extension. Three of the specimens fall within the required limits while the two specimens with the largest crack extension do not. This implies that the accuracy of the calculated crack lengths based on the compliance equations given in ASTM E 813-87 decreases with increasing crack length. The work of Steenkamp [*4*], Prantl [*5*], and Prij [*6*] suggests that the accuracy of the final calculated crack lengths can be improved by correcting the last measured compliance for the effects of crack front curvature, large deformation, indentation, and friction. The corrections of Steenkamp will be presented, and the last measured compliances will be reanalyzed using these corrections, in the next section.

Correction of the Measured Compliances

The equations for calculating crack length from compliance given in ASTM E 813-87 were derived from theoretical relationships for a specimen with a perfectly straight crack front

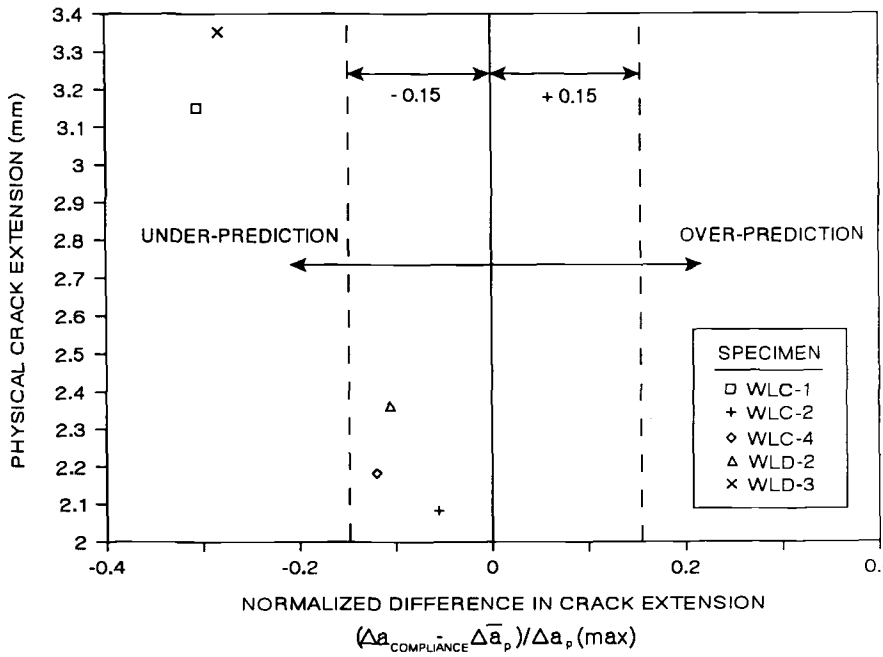

FIG. 8—*Accuracy of unloading compliance technique for crack length determination in SE(B) specimen of Type 308 SS weld metal.*

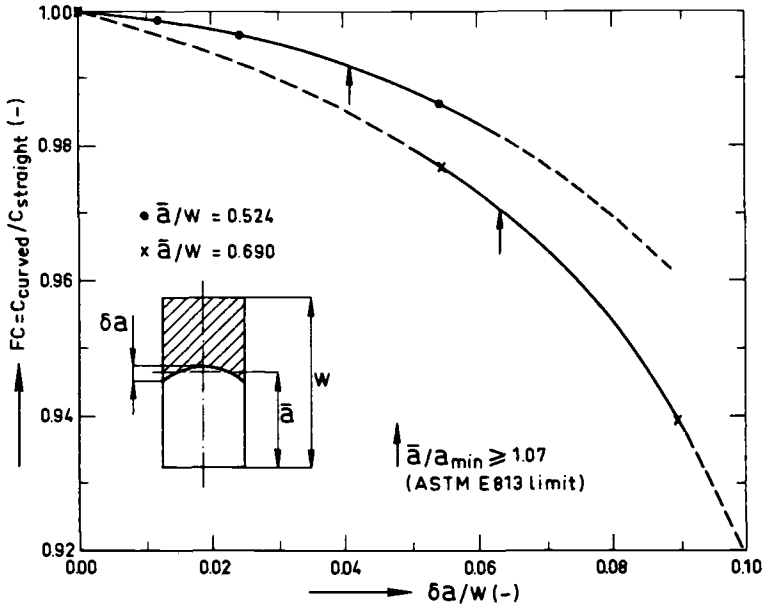

FIG. 9—*The influence of crack front curvature on compliance* [4].

undergoing small deformations under ideal three-point bending. In reality, the crack front is never perfectly straight, the specimen may experience large deformation, and the rollers do not exert point loading. A thorough study was done on the effect of these factors on compliance for SE(B)-type specimens by Steenkamp [*4*]. The correction factors derived by Steenkamp will be used to correct the final calculated crack lengths.

Steenkamp used elastic finite element methods to examine the effect of crack front curvature on compliance. He considered only plane sided specimens, without side grooves, and crack fronts that resulted from tunneling crack growth. The results of his analysis showed that for the same average crack length, the effect of crack front curvature is to decrease the compliance. He defines a compliance correction factor, F_C, which is the ratio of the compliances of a curved and a straight crack, each with the same average crack length. The correction factor is given for various amounts of curvature in Fig. 9. Dividing the measured compliance by this factor will increase the compliance to the value for a straight crack with the same average crack length.

The effect of large deformation on compliance was examined using elastic-plastic finite element analysis [*4*]. Steenkamp found that the deviation of the compliance due to elastic-plastic deformation is solely a function of the angle of rotation of the specimen halves. He defines a correction factor, F_D, that is plotted as a function of rotation angle (in radians) in Fig. 10. The correction factor is always less than one, indicating that the effect of elastic-plastic deformation is to decrease the compliance compared with an elastically deformed specimen.

Friction between the rollers and the specimen will alter the effective bending moment with respect to idealized three-point loading, and thereby affect the compliance. Steenkamp derived analytical expressions for the effective bending moment, and used these to define a compliance correction factor for friction, F_R. The correction factor was found to be a function of the angle of rotation of the specimen halves, α, and the roller diameter, D. It can be seen from the plotted values of F_R in Fig. 10 that the effect of friction is small.

The final correction that Steenkamp derived was for indentation of the specimen at the center roller. The correction factor for indentation, F_I, was found to be a function of the angle of rotation (α), the material properties, and the specimen dimensions. Values of the correction factor for one particular material and specimen size are shown in Fig. 10. It can be seen that the effect of indentation is small compared to the effect of deformation, especially for large rotation angles.

The compliance corrections derived by Steenkamp were used to correct the last measured compliances for the tests of the Type 308 SS SE(B) specimens. The corrections for curvature and indentation are only approximate since the crack front shapes considered by Steenkamp did not include those formed by inverse tunneling, and the material properties used to derive the indentation correction factor are not the same as those for Type 308 SS weld metal. The effect of inverse tunneling on compliance should be examined further; however, the results of Steenkamp will be used to indicate the general trend of the correction. The differences in crack extension between the calculated crack lengths, after correction, and the physical crack lengths are shown in Fig. 11. The calculated crack lengths now overpredict the crack extension for four of the five specimens; however, in all cases the normalized difference in crack extension falls within the limits specified in the standard.

Discussion

The J_Q values obtained from the test results are not valid initiation toughnesses because the data failed the validation requirements on accuracy of the crack extension calculation and on the change in curvature of the crack front. The accuracy of the crack extension calculation was improved by applying compliance correction factors that account for deviations of the actual test from the ideal case of a perfect specimen in pure three-point bending.

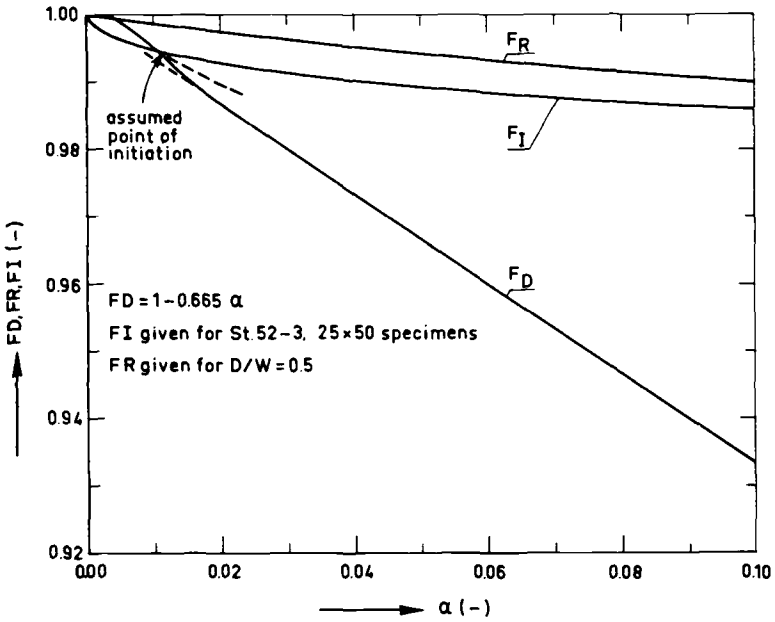

FIG. 10—*Compliance correction factors for deformation (F_D), friction (F_R), and indentation (F_I)* [4].

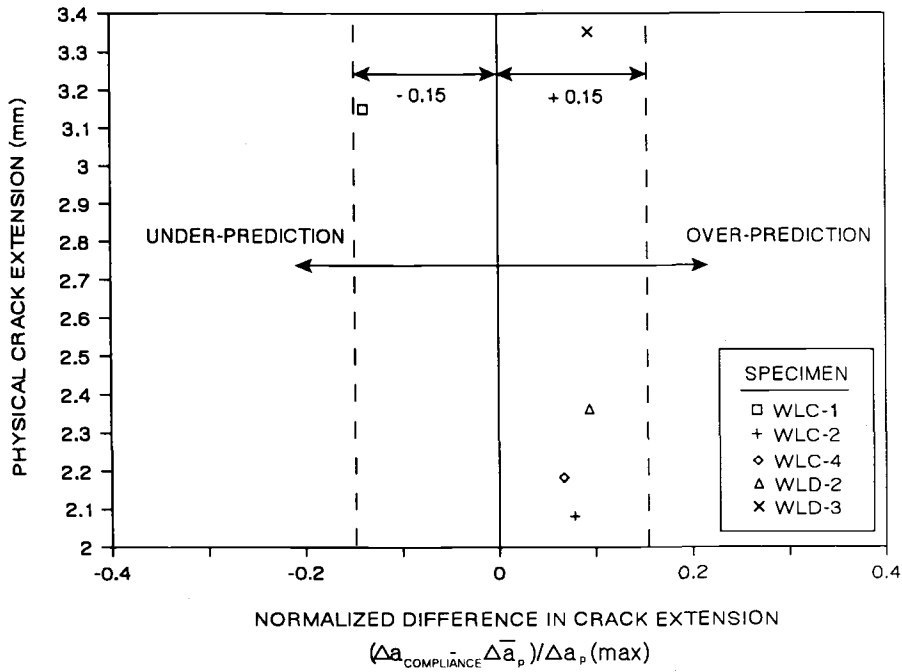

FIG. 11—*Accuracy of unloading compliance technique for calculating crack length in Type 308 SS weld metal SE(B) specimens after incorporating compliance corrections.*

After applying these corrections, the validation requirement for accuracy of the crack extension prediction was satisfied for all of the specimens.

This leaves the limit on change in crack front curvature as the sole validation requirement preventing the measured J_Q values from being considered valid initiation toughnesses. A peculiar feature of these tests was the change in crack growth mode from tunneling to inverse tunneling. This behavior has been observed in other tests on Type 304 SS [*7,8*]. The tunneling growth mode is caused by relief of constraint at the free surfaces. This implies that the presence of the side grooves has increased the constraint at the edges to a level that is greater than the constraint in the center. If this is so, the severity of the stress state in the specimen is such that the measured initiation toughness should represent a lower bound. It seems contradictory that both the initial crack front and the final crack front are well within the limits on curvature, but the change in curvature exceeds the limits. The change in crack growth mode causes the difference in crack extension between the center and the edges to exceed the specified limits. Perhaps reevaluation of the reasoning behind this requirement would allow for reinterpretation under the condition of inverse tunneling crack growth.

Conclusions

A peculiar feature of these tests was that crack growth occurred in an inverse tunneling mode. The transition from tunneling growth during fatigue precracking to inverse tunneling during stable crack growth caused the change in crack curvature to violate the validation requirement on crack extension. Problems were also encountered with discrepencies between

the final physical crack length, as measured on the fracture surface, and the unloading compliance calculation of final crack length. Consequently, the provisional initiation toughnesses (J_Q) calculated from the test results were determined to be invalid measurements of the initiation toughness J_{Ic}.

The accuracy of the unloading compliance calculations of final crack length was improved by applying correction factors to account for crack front curvature, plastic deformation, friction, and indentation to the measured compliances. The corrections brought the difference between the physical and calculated final crack lengths within the limits specified in ASTM E 813-87.

The large change in crack front curvature was caused by the transition from tunneling growth during fatigue precracking (before the specimens were side grooved) to inverse tunneling during slow stable crack growth. The validation requirements on crack curvature and crack extension appear to be inconsistent for this case where the initial and final cracks are well within the limits on curvature; however, the difference in crack extension between the edge and center exceeds the limits by a considerable margin. Presumably, the requirements are intended to ensure that the stress state in the specimen is predominantly two-dimensional plane strain. Excessive curvature of the crack front causes the stress state to become three dimensional. For these tests, the initial crack fronts are within the required limits on curvature, and the transition from tunneling to inverse tunneling indicates that during the early part of stable crack growth, the crack front curvature was decreasing. The curvature of the final crack fronts was also within the required limits, thereby satisfying the intent of maintaining a predominantly two-dimensional plane strain state of stress, although violating the crack extension requirement. The reasoning behind the validation requirement on change in crack front curvature should be reexamined in light of the possibility of crack growth by inverse tunneling.

Acknowledgments

This work was supported by the U.S. Department of Energy, Office of Energy Research, Office of Basic Energy Sciences, under DOE Contract No. DE-AC07-76ID01570.

References

[1] Schwalbe, K. H. et al., "Measurement of Stable Crack Growth Including Detection of Initiation of Growth using the DC Potential Drop and the Partial Unloading Methods," *Ductile Fracture Test Methods, Proceedings*, CSNI Workshop, Paris, France, 1–3 Dec. 1982, pp. 18–53.

[2] Voss, B., "On the Problem of Negative Crack Growth and Load Relaxation in Single Specimen Partial Unloading Compliance Tests," *Ductile Fracture Test Methods, Proceedings*, CSNI Workshop, Paris, France, 1–3 Dec. 1982, pp. 210–219.

[3] Bamford, W. H. and Bush, A. J., "Fracture Behavior of Stainless Steel," *Elastic-Plastic Fracture, ASTM STP 668*, J. D. Landes, J. A. Begley, and G. A. Clarke, Eds., American Society for Testing and Materials, Philadelphia, 1979, pp. 553–577.

[4] Steenkamp, P. A. J. M., *Investigation into the Validity of J-Based Methods for the Prediction of Ductile Tearing and Fracture*, PhD thesis, WTHD No. 180, Department of Mechanical Engineering, Delft University of Technology, The Netherlands, 1986.

[5] Prandtl, G., "Assessment of Crack Extension by Different Methods," *Ductile Fracture Test Methods, Proceedings*, CSNI Workshop, Paris, France, 1–3 Dec. 1982, pp. 115–122.

[6] Prij, J., "Some Finite Element Results of CTS Specimen," *Ductile Fracture Test Methods, Proceedings*, CSNI Workshop, Paris, France, 1–3 Dec. 1982, pp. 169–180.

[7] de Vries, M. I. and Schapp, B., "Experimental Observations of Ductile Crack Growth in Type 304 Stainless Steel," *Elastic-Plastic Test Methods: The User's Experience, ASTM STP 856*, E. T. Wessel and F. J. Loss, Eds., American Society for Testing and Materials, Philadelphia, 1985, pp. 183–195.

[8] Menke, B. H., Loss, F. J., and Gray, R. A., "Effects of Side Grooving on R-Curve Slope and Crack Extension in Small Elastic-Plastic Test Specimens," Report of National Research Laboratory Progress, Sept. 1979, pp. 11–14.

[9] Dawes, M. G., "Elastic-Plastic Fracture Toughness Based on the COD and J-Contour Integral Concepts," *Elastic-Plastic Fracture, ASTM STP 668*, J. D. Landes, J. A. Begley, and G. A. Clarke, Eds., American Society for Testing and Materials, Philadelphia, 1979, pp. 307–333.

Kenneth K. Yoon,[1] *W. Alan Van Der Sluys,*[2] *and Arthur L. Lowe, Jr.*[1]

Key-Curve Analysis of Linde 80 Welds

REFERENCE: Yoon, K. K., Van Der Sluys, W. A., and Lowe, A. L., Jr., **"Key-Curve Analysis of Linde 80 Welds,"** *Elastic-Plastic Fracture Test Methods: The User's Experience (Second Volume), ASTM STP 1114*, J. A. Joyce, Ed., American Society for Testing and Materials, Philadelphia, 1991, pp. 225–237.

ABSTRACT: Some reactor vessel weldments have relatively high copper contents that, when exposed to neutron irradiation, cause reductions in fracture toughness in the Charpy upper-shelf energy temperature region. To address this concern, a large number of both unirradiated and irradiated compact specimens were tested and the resulting *J*-resistance curves were generated. Key curves were developed from the load displacement records of single-specimen unloading compliance test data for magnesium-molybdenum-nickel/Linde 80 submerged-arc weld metals to study various aspects of toughness data behavior. In this paper, only a number of representative compact specimen tests are analyzed using the Herrera and Landes individual specimen key-curve approach to compare specimen size, temperature, and irradiation effects as part of a *J*-resistance model development effort for the Linde 80 class of weld metals.

The results of this study indicate (1) that the key-curve method works when applied to the Linde 80 type weld metals, (2) that a power law representation of the key curve provides a means to extract the Ramberg-Osgood exponent from the key curve if there are no available tensile data for the weld metal, and (3) that the irradiated specimens from both power reactors and a test reactor do not exhibit significant differences in comparable key-curve characteristics.

KEY WORDS: key curves, fracture, calibration, unloading compliance, fracture tests, elastic-plastic fracture, test methods

Before 1972, a number of nuclear power plant reactor vessels were fabricated by the automatic submerged-arc welding process using copper plated manganese-molybdenum-nickel (Mn-Mo-Ni) weld filler wire and Linde 80 weld flux. This wire and flux combination resulted in a relatively high copper content in the weldment. The copper was identified as the primary cause of a reduction in the Charpy upper-shelf fracture toughness properties under continued neutron irradiation. There are a number of reactor vessels containing Mn-Mo-Ni/Linde 80 submerged-arc welds in their beltline region and they are recognized for their susceptibility to reduced fracture toughness and, as a result, are the subject of an ongoing program of fracture toughness data acquisition and analysis to assure the structural integrity for all operating conditions.

For the last 14 years, a systematic fracture toughness acquisition program has been in progress by the Babcock & Wilcox (B&W) Owners Group, which is composed of those utilities with power plants that have reactor vessels with this concern. In this program, a large number of compact specimens fabricated from the same material as used to fabricate the reactor vessels were irradiated in commercial nuclear power plants. In addition, the

[1]Advisory engineers, Engineering and Plant Service Division, B&W Nuclear Service Company, Lynchburg, VA 24506.

[2]Scientist, Alliance Research Center, Babcock & Wilcox, Alliance, OH 44601.

Nuclear Regulatory Commission (NRC) conducted a research program within the Heavy Section Steel Technology (HSST) program where a large number of the compact specimens of the same materials donated by the B&W Owners Grop were irradiated in a test reactor and then tested and evaluated.

As the products from these programs, two large databases for this class of weld metals were established. Based on these databases, a *J*-resistance curve model development effort was undertaken. As a part of this overall effort, a key-curve analysis was performed using a small number of representative compact specimen test records taken from these two databases. The results from this analysis are presented in this paper. The primary interest is to determine if the use of the key-curve method would help in the study of the following issues:

1. specimen size effects,
2. test temperature effects,
3. differences in unirradiated weld metal data versus irradiated weld metal data, and
4. differences in power reactor irradiated weld metal data versus test reactor irradiated weld metal data.

Key-Curve Method

Ernst et al. [*1*] introduced the key-curve concept, which is based on flow properties of ductile material. Joyce and others [*2*] experimentally constructed the key curve for a HY130 steel and demonstrated that *J-R* curves could be developed by the key-curve method. To construct a generic key curve for a specific material and a type of test specimen, testing of multiple specimens with varying initial crack sizes is necessary. Joyce [*3*] applied this approach to dynamic *J*-testing of a A533B low-alloy steel used in reactor vessels and generated dynamic *J-R* curves from the key curve.

Recently, Herrera and Landes [*4*] applied this concept to construct an individual specimen key curve using the flow properties of the specimen instead of using a multispecimen test to construct a generic key curve. The basis for this approach is the assumption that the key curve can be represented by a power law functional form. The two constants in the power law equation are determined from the load-displacement pair at the final crack point, and the Ramberg-Osgood exponent from a matching tension test. Alternatively, the authors demonstrated that the load-displacement pair at the crack-initiation point can be substituted for the Ramberg-Osgood exponent. Consequently, *J-R* curves can be generated from the key curves without the crack extension calculations required by the unloading compliance method.

Following Ernst [*1*] and Joyce [*2*], the testing of a precracked fracture specimen involves three primary continuously changing variables, that is, load, P; displacement, v; and crack length, a. The relationship among these variables can be represented by a function, F, as follows

$$P = F(a/W, v/W) \tag{1}$$

where W is the width of the specimen. In Ref *3*, it was shown that a separation of variable approach can be applied to F resulting in the form

$$P = G(a/W)H(v_{pl}/W)$$

where displacement v is separated into elastic and plastic components

$$v = v_{el} + v_{pl}$$

and from the compliance function, $C(a/W)$, the elastic displacement is given by

$$v_{el} = PC(a/W)$$

For bend-type specimens, $G(a/W)$ can be described in terms of the remaining uncracked ligament, b, in the form

$$P = Bb^2/W\, g(b/W)H(v_{pl}/W) \tag{2}$$

where B is specimen thickness. The function, g, for the compact specimen is given in Ref *5* as

$$g(b/W) = \exp[0.522(b/W)]$$

and for the three-point bend specimen

$$g(b/W) = 1$$

and if a normalized load, P_N, is defined as

$$P_N = PW/[Bb^2g(b/W)]$$

then from Eq 2

$$P_N = H(v_{pl}/W) \tag{3}$$

A plot of P_N versus v_{pl}/W defines a key curve, or a calibration curve, for the material and the specimen type.

Power Law Function, *H*

Following Ref *4*, each key curve is analyzed assuming that the inverse of the H function in Eq 3 is in a power law form as

$$v_{pl}/W = \beta P_N^n \tag{4}$$

where β is a constant and n is the exponent similar to the Ramberg-Osgood exponent.

Taking the logarithm of both sides of Eq 4

$$\log(v_{pl}/W) = \log \beta + n \log P_N$$

and rearranging

$$n = [\log(v_{pl}/W) - \log \beta]/\log P_N \tag{5}$$

The exponent, n, is determined from the slope of a log-log plot of a key curve.

J-Control Limit Assessment

ASTM Test Method for Determining *J-R* Curves (E 1152-87) allows crack growth of only 10% of the initial uncracked ligament in a compact specimen, however, many investigators observed well-behaved *J-R* curves far beyond the 10% limit in actual tests of pressure vessel materials [*6*]. To assess the maximum applicable limit, Joyce [*6*] suggested a plot of the plastic portion of the load-line displacement, v_{pl}/W, and crack extension, $\Delta a/W$, as shown in Fig. 1 for Specimen 21. After the initial blunting phase, there is a linear relationship between these two variables. The crack length where the linear relationship starts to fail is called as the *J*-control limit of this specimen. Joyce suggested that the crack extension validity limit should be where the plastic displacement versus crack extension curve deviated from the straight line by more than 5%. This point signifies the onset of a plastic hinge formation. In the specimen evaluated in Fig. 1, the linear relationship holds until $\Delta a/W$ reaches a value of 0.22. This point corresponds to 44% of the initial uncracked ligament. This concept was found very useful in analyzing key curves as discussed in the following section.

Key Curves for Linde 80 Weld Material

For a selected group of Mn-Mo-Ni/Linde 80 weld metals, key curves were generated using Eq 3 and are plotted in Figs. 2 through 5. Some of the key curves are closely grouped, which suggests the existence of a generic key curve for select groups of data. There are some irregular key curves in these figures as would be expected from any experimentally obtained set of data. These curves include the data from both unirradiated and irradiated specimens.

Figure 2 contains five key curves from one weld metal. There are three different compact specimen sizes and two test temperatures, 249°C (480°F) and 288°C (550°F). The legend in

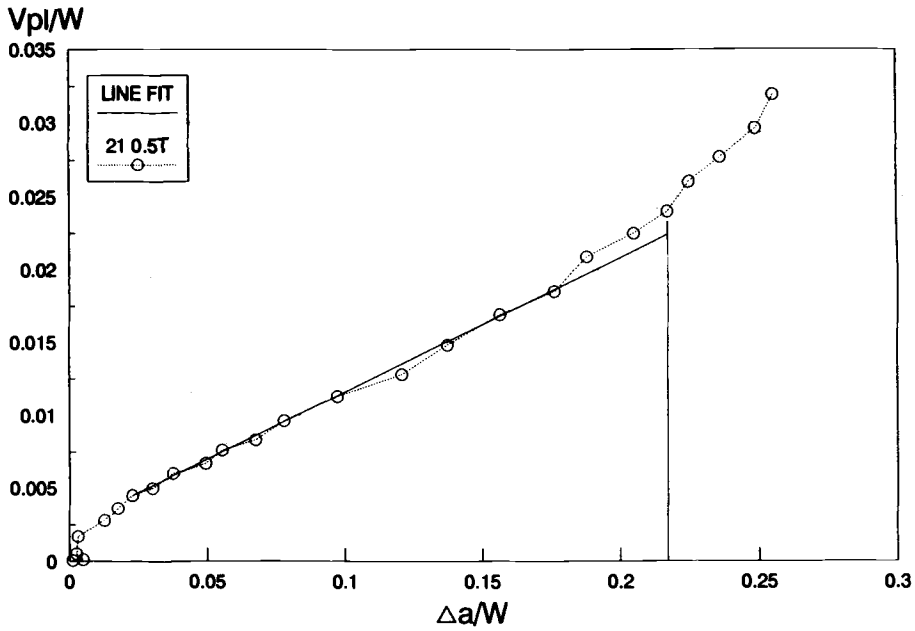

FIG. 1—*Singularity assessment.*

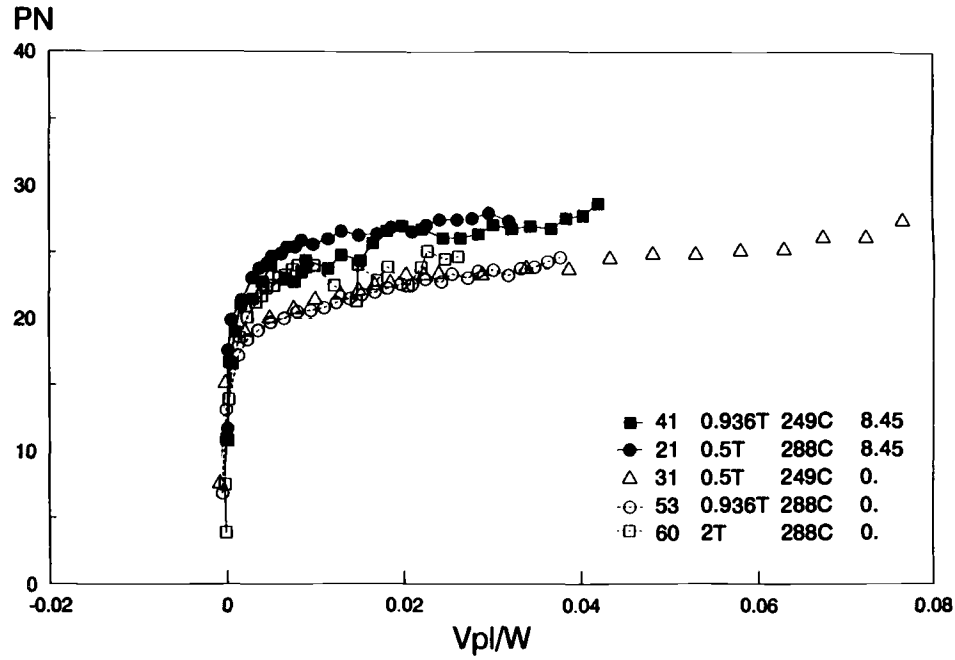

FIG. 2—*Key curves for Group W1.*

the figure indicates the specimen number followed by the specimen size and the test temperature. The last number is neutron fluence, in units of 10^{18} n/cm^2, to which the specimens were exposed prior to testing. Two key curves for irradiated specimens (Specimens 41 and 21) show higher P_N values compared with the rest. This is expected because of the increased strength properties of the irradiated material. The key curves in Fig. 3 are all irradiated data to the same neutron fluence, but tested at different temperatures in the Charpy upper-shelf energy range. These curves are well grouped also, except for the 0.5T compact specimen for which there is no obvious explanation. In contrast, Fig. 4 shows two 0.5T irradiated compact specimens with almost identical key curves despite a difference in test temperatures. One unirradiated 0.936T compact specimen data exhibited a slightly lower key curve but its slope is not as steep as the irradiated key curves, indicating a lower Ramberg-Osgood hardening exponent for the unirradiated material. The irradiated specimen curves shown in Fig. 5 have a narrow scatter band except for the one unirradiated specimen curve. With the exception of Group W2 shown in Fig. 3, the key curves of the irradiated data in Fig. 5 appear to be representative of the other groups as well. These specimens in Group W2 also are characterized by low R-curves.

In Fig. 6, the key curve for Specimen 53 is compared with a normalized load displacement curve without crack growth. This is an unirradiated 0.936T compact specimen tested at 288°C (550°F). According to the first method described in Ref *4*, when the hardening exponent of 8.2 from a tension test record from a Ramberg-Osgood fit is used, the load displacement pair at the last test point yields a β value of 2.95×10^{-14}. The key curve for Specimen 53 and the curve obtained from Eq 4 are in good agreement as shown in Fig. 7. This good agreement means that the power law representation of the inverse H function works well with this type of material. This also suggests that the key-curve method may be used in reverse for obtaining the exponent, n, as illustrated in Fig. 8.

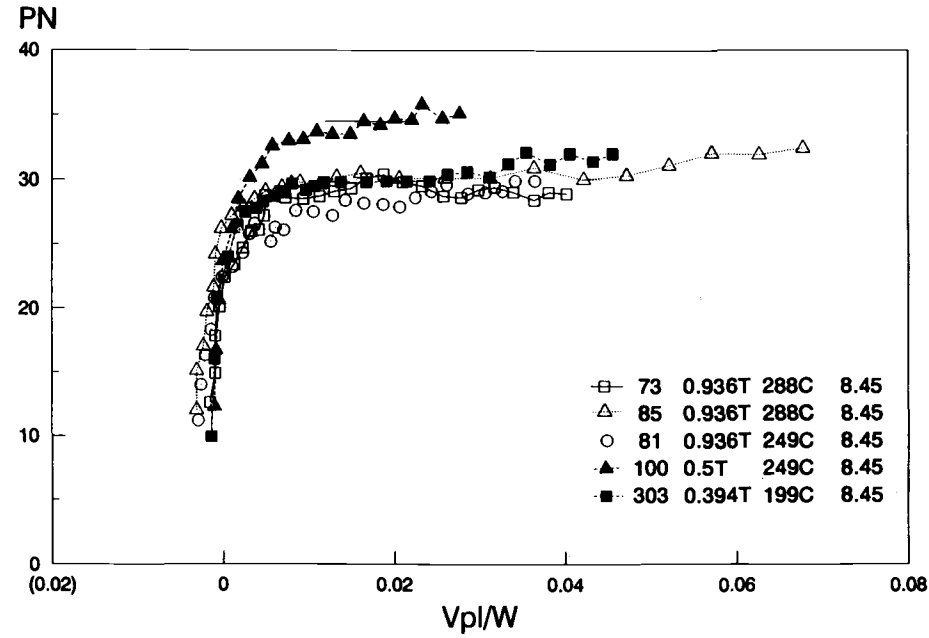

FIG. 3—*Key curves for Group W2.*

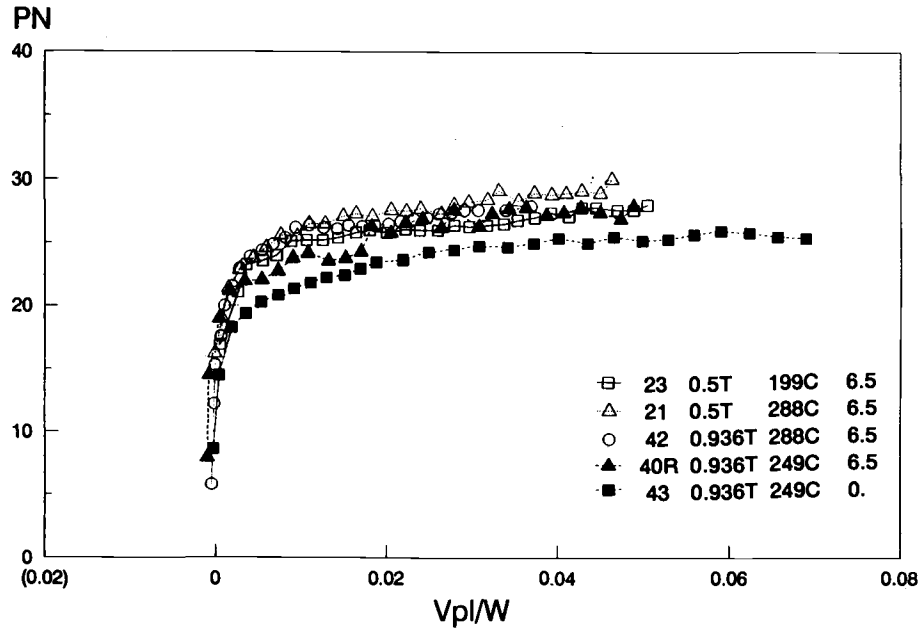

FIG. 4—*Key curves for Group W3.*

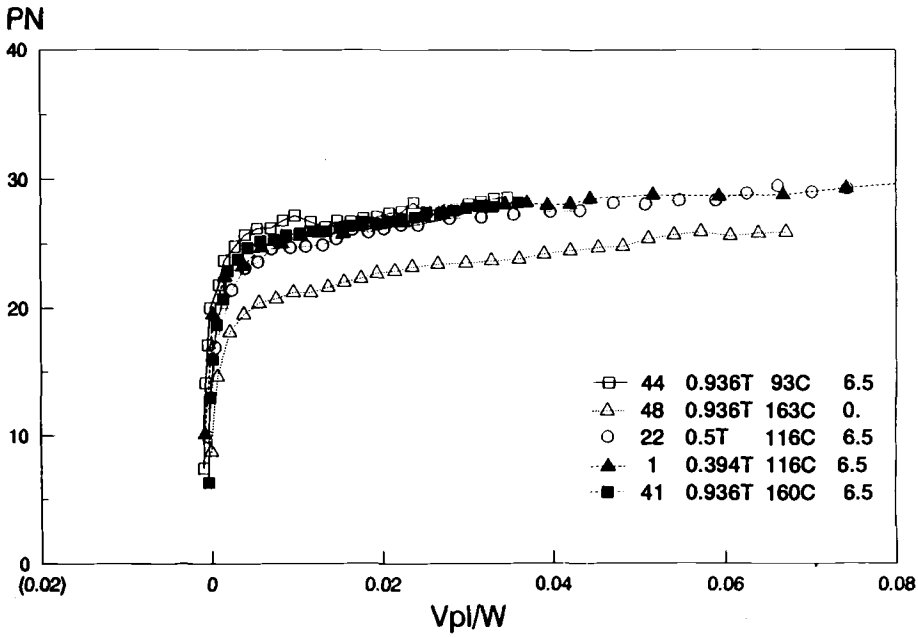

FIG. 5—*Key curves for Group W4.*

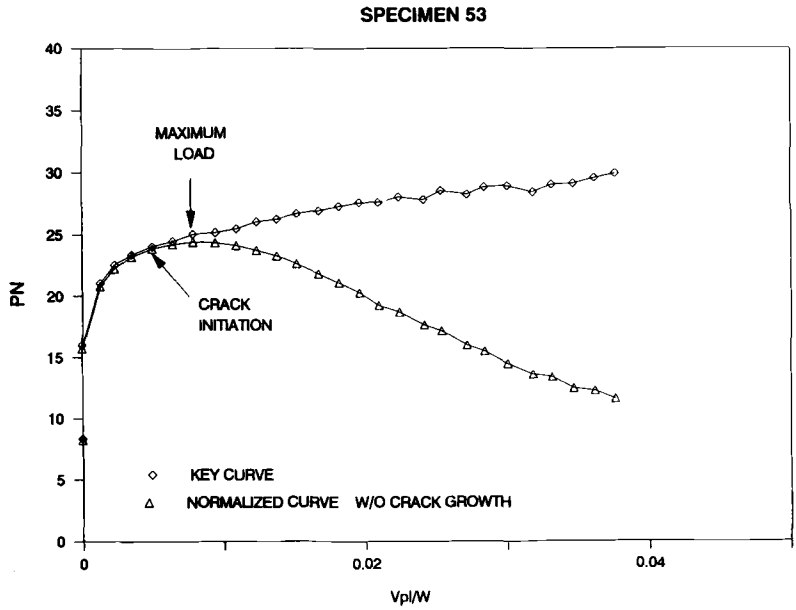

FIG. 6—*Crack initiation point determination.*

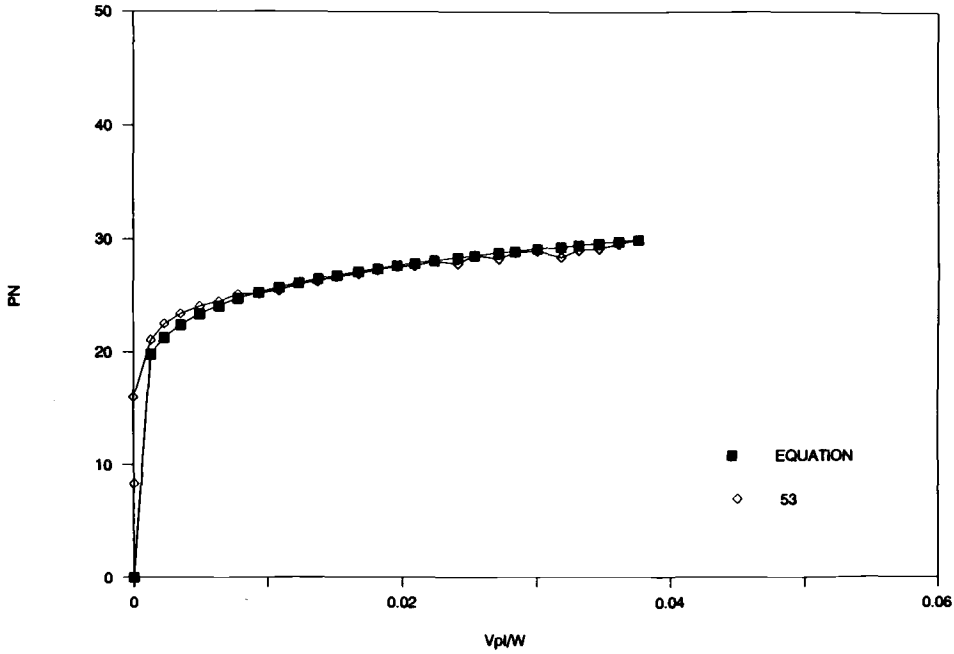

FIG. 7—*Power law function versus key curve.*

The point where the two curves in Fig. 6 start to deviate from each other was used as the crack-initiation point by Herrera and Landes, as a second method for determining the two constants used in Eq 4. In this case, the crack-initiation point becomes two data points prior to the maximum load point. Subsequent evaluation of numerous data revealed that the maximum load point can serve as the lower limit of the valid crack extension range. The upper valid crack extension limit can be determined by Joyce's *J*-control limit as discussed previously.

Figure 8 illustrates a logarithmic scale plot of the key curve for Specimen 53 with the valid data range marked. A linear regression analysis of the valid data points provides a Ramberg-Osgood exponent, n. A value of n of 8.9 was obtained from the key curve, and it is comparable to the 8.2 value obtained from a corresponding tension test result.

Key Curves of Irradiated Weld Metals

Specimen 41 in Fig. 2 is a irradiated 0.936*T* compact specimen exposed to a fluence of 8.5×10^{18} n/cm^2 and tested at 249°C (480°F). Specimen 21 is a 0.5*T* compact specimen exposed to the same fluence and tested at 288°C (550°F). A *J*-control limit assessment produced the upper limits of the valid test data points shown in Fig. 9. The upper valid crack extension limit of Specimen 21 is 43% of the initial ligament size, b_o. The same limit of Specimen 41 is 51% of b_o. The key curves for these specimens are shown in Fig. 10 with their respective validity ranges marked. A linear regression of the valid data points in a logarithmic plot resulted in n values of 10.5 and 15.2, which are reasonable values for an irradiated Mn-Mo-Ni/Linde 80 weld metal. This relationship is presented in Fig. 11.

As a comparison, an irradiated 1.6*T* compact specimen was selected from the HSST database. This specimen had a fluence of 9.44×10^{18} n/cm^2 and was tested at 288°C (550°F).

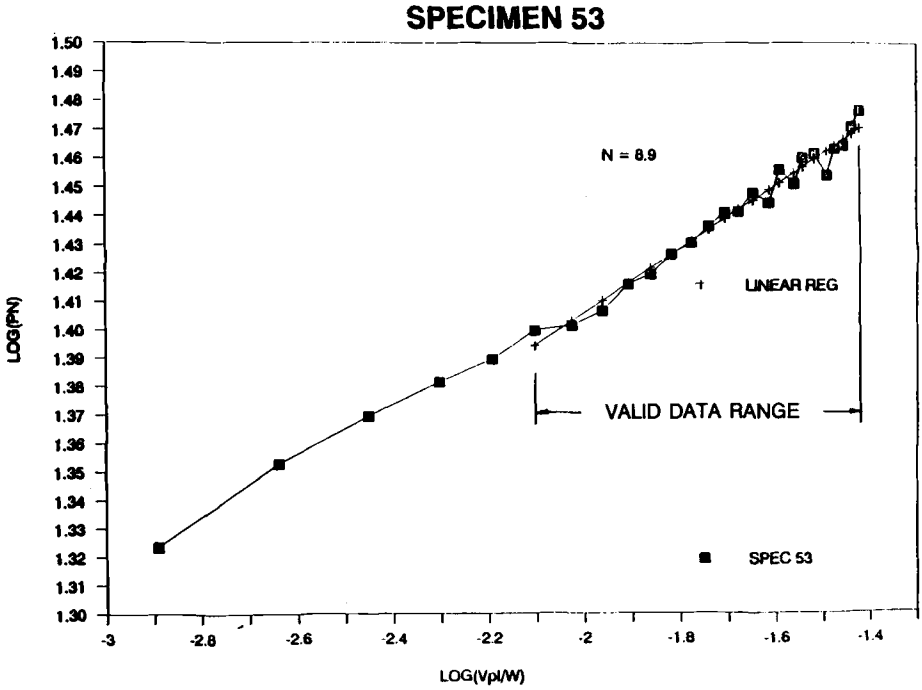

FIG. 8—*Key curve in logarithmic scale.*

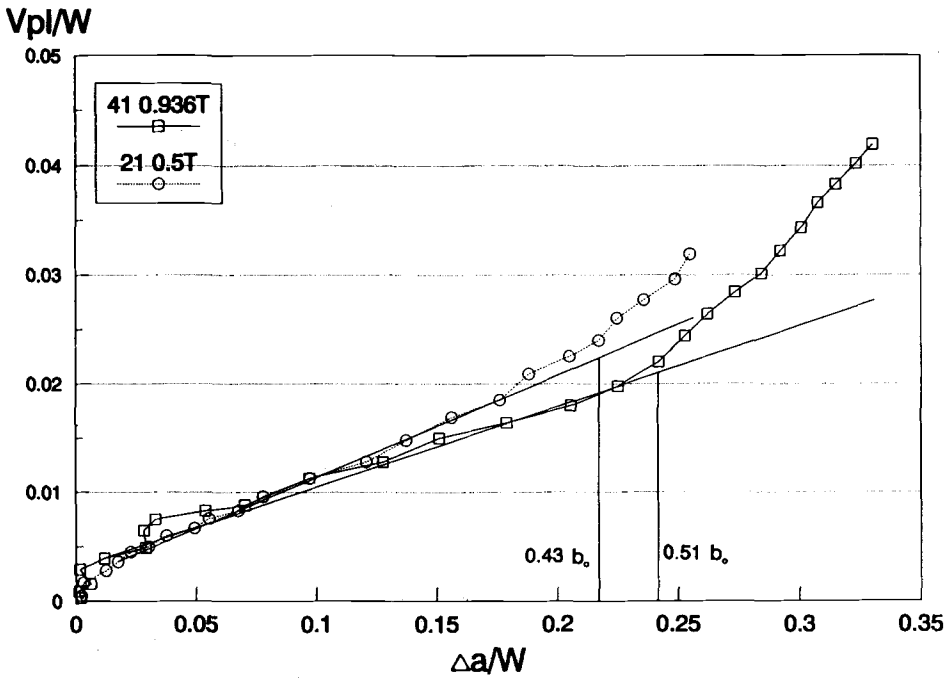

FIG. 9—*Singularity assessment Group W1.*

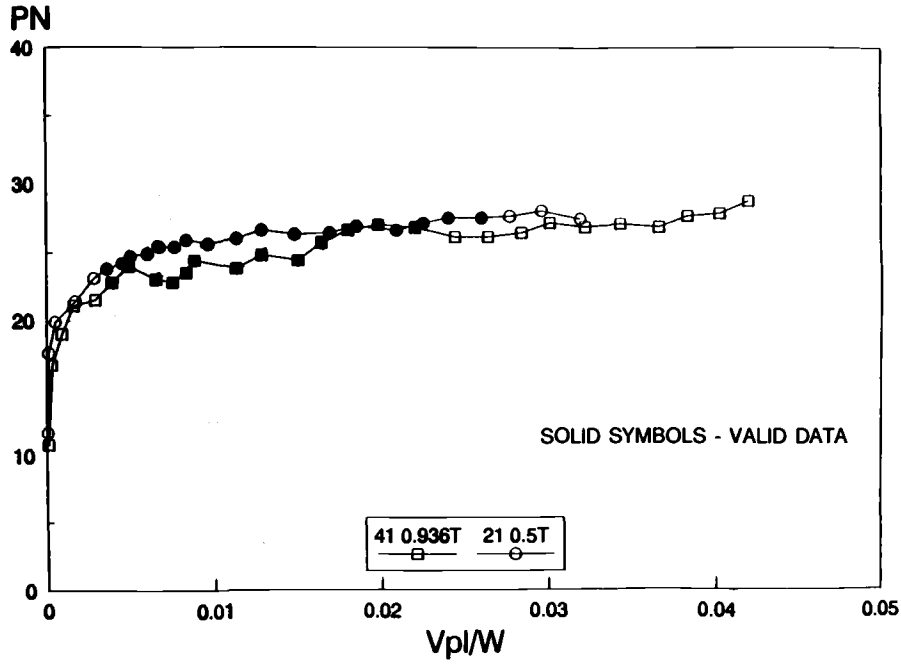

FIG. 10—*Key curves for irradiated data, Group W1.*

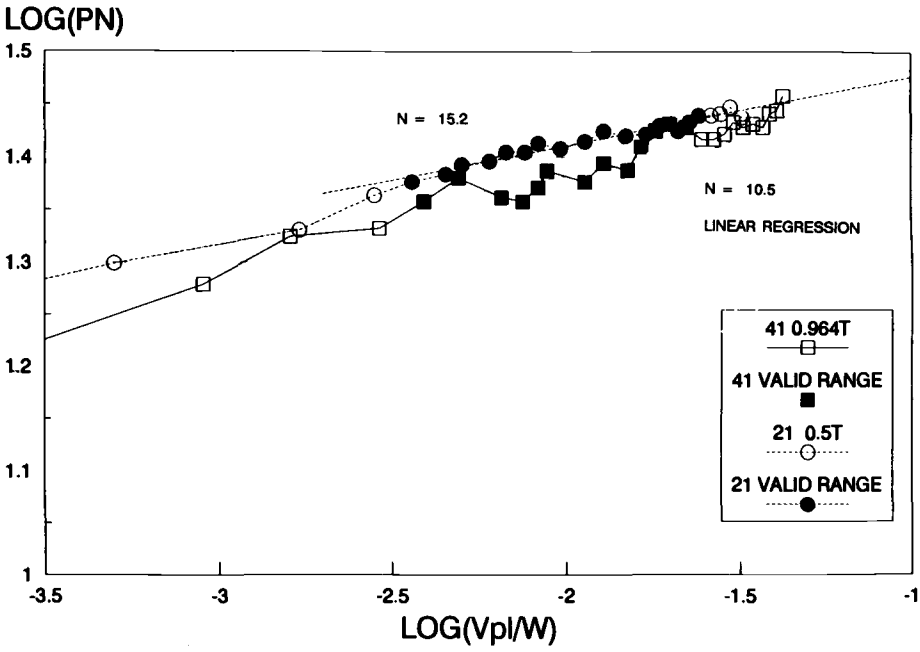

FIG. 11—*Key curves in logarithmic scale.*

In Fig. 12, the key curve for this specimen is compared with those shown in Fig. 10. The fluence values are similar among these specimens but the nominal flux rate for the HSST data was 1.5×10^{12} n/cm^2/s, approximately 20 times higher than the nominal flux rate for the power reactors. A J-control limit assessment revealed that the crack extension is valid up to $\Delta a = 17.3$ mm (0.68 in.), which is 46% of b_o. All specimens of Mn-Mo-Ni/Linde 80 welds consistently exhibit the validity limit of 38 to 51% of the uncracked ligament, b_o. A regression analysis on the valid log-log key-curve data yields n equal to 12.0, as shown in Fig. 13. Since the variation of the hardening exponent, n, is not as sensitive at high n values (considering that the slope of the horizontal line in the log-log plot is infinity), one can conclude that there is no significant difference between the test reactor data and the two power reactor irradiated data as shown in Fig. 12.

Summary and Discussions

In general, the key curves for unirradiated Mn-Mo-Ni/Linde 80 weld materials lie in a very narrow range relative to each other, indicating the homogeneity of the material and suggesting the potential of the existence of a generic key curve for the material.

The Joyce J-control limit assessment method effectively defines the upper limit of the valid data range for key-curve application.

A reverse application of the H function by a linear regression of the log-log key-curve data between the maximum load point and the upper validity limit based on the J control limit assessment consistently yielded good values for the exponent, n. This may be a useful tool for determining the exponent, n, when there is a lack of any companion tensile data for the particular material.

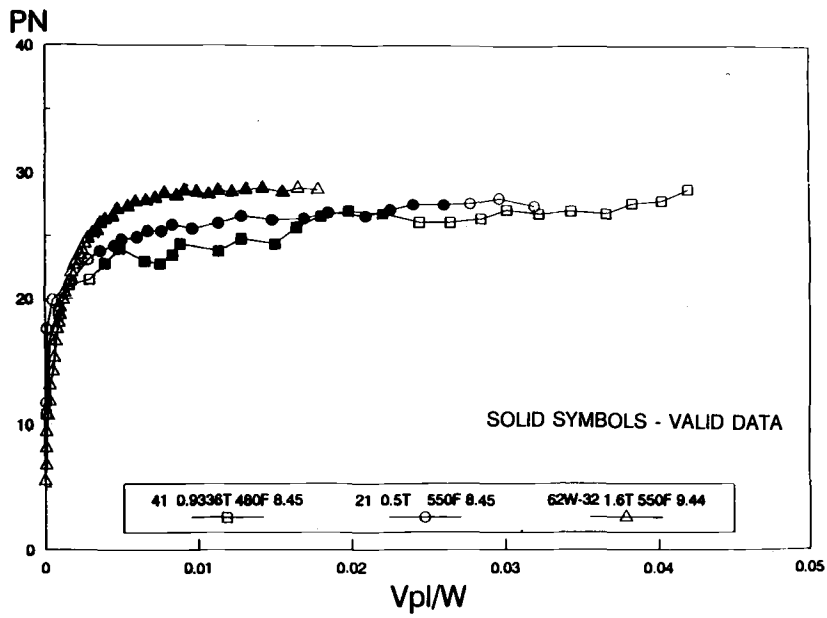

FIG. 12—*Key curves of irradiated specimens.*

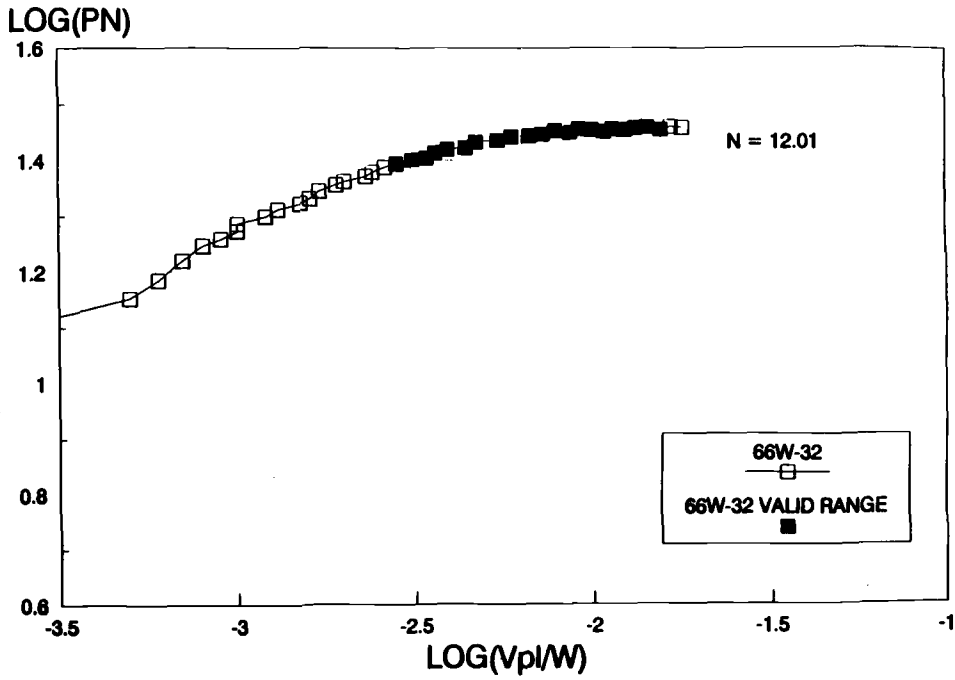

FIG. 13—*Logarithmic plot of key curve.*

The limited study of the key curves for material irradiated in a power reactor versus one for the same material irradiated in a test reactor indicates that there appears to be no visible effect related to flux rate for the range of flux rates available in this database.

To make a meaningful comparison between the post-test crack measurement versus the predicted crack size for the last load-displacement pair, the test should not be conducted much beyond the *J*-control limit.

There was no distinctive difference in the key curves for the groups of material that varied slightly in chemical composition. Specimen size effect does not appear to be important. The effect of test temperature is not evident. The irradiated data showed higher and flatter key curves than the unirradiated data. This trend is expected because of increased strength properties and greater hardening behavior of the irradiated materials compared with unirradiated materials.

References

[*1*] Ernst, H. A., Paris, P. C., Rossow, M., and Hutchinson, J. W., "Analysis of Load Displacement Relationship to Determine *J-R* Curve and Tearing Instability Material Properties," *Fracture Mechanics (11th Conference), ASTM STP 677*, C. Smith, Ed., American Society for Testing and Materials, Philadelphia, 1979, pp. 581–599.

[*2*] Joyce, J. A., Ernst, H. A., and Paris, P. C., "Direct Evaluation of *J*-Resistance Curve from Load Displacement Records," *Fracture Mechanics (12th Conference), ASTM STP 700*, American Society for Testing and Materials, Philadelphia, 1980, pp. 222–236.

[*3*] Joyce, J. A., "Static and Dynamic *J-R* Curve Testing of A533B Steel Using the Key Curve Analysis Technique," *Fracture Mechanics: Fourteenth Symposium, Vol. I: Theory and Analysis, ASTM STP 791*, Lewis and Sines, Eds., American Society for Testing and Materials, Philadelphia, 1983, pp. I-543–I-560.

[4] Herrera, R. and Landes, J. D., "A Direct *J-R* Curve Analysis of Fracture Toughness Tests," *Journal of Testing Evaluation*, Vol. 16, No. 5, Sept. 1988, pp. 427–449.

[5] Ernst, H., Paris, P. C., and Landes, J. D., "Estimation of *J*-Integral and Tearing Modulus T from a Single Specimen Test Record," *Fracture Mechanics (Thirteenth Conference), ASTM STP 743*, Land and Otten, Eds., American Society for Testing and Materials, Philadelphia, 1981, pp. 476–502.

[6] Joyce, J. A. and Hackett, E. M., "Development of an Engineering Definition of the Extent of J Singularity Controlled Crack Growth," NUREG/CR-5238, Nuclear Regulatory Commission, Washington, DC, May 1989.

Charles W. Marschall[1] *and Mark P. Landow*[1]

Observations in Conducting *J-R* Curve Tests on Nuclear Piping Materials

REFERENCE: Marschall, C. W. and Landow, M. P., **"Observations in Conducting *J-R* Curve Tests on Nuclear Piping Materials,"** *Elastic-Plastic Fracture Test Methods: The User's Experience (Second Volume), ASTM STP 1114*, J. A. Joyce, Ed., American Society for Testing and Materials, Philadelphia, 1991, pp. 238–259.

ABSTRACT: This paper describes some of Battelle's experiences in developing *J-R* data for nuclear piping materials. Compact specimens were machined from both carbon steel and stainless steel pipe and subjected to testing at elevated temperatures, similar to temperatures encountered in nuclear reactor coolant piping. In many cases, the specimens displayed toughness levels above those considered valid by ASTM standard methods of testing. Furthermore, cracks were grown by about 50% of the original ligament, well in excess of the 10% limit imposed by ASTM Test Method for Determining *J-R* Curves (E 1152-87).

Topics discussed in the paper include: (1) monitoring crack extension using the direct-current electric potential method, (2) specimen thickness changes ahead of the growing crack, (3) observations of fracture appearance and crack growth direction in ferritic versus austenitic steels, (4) observations of ductile-crack jumps in carbon steels tested at 288°C (550°F), (5) unusual effects of partial unloadings in testing carbon steels at 288°C (550°F), and (6) difficulties with certain ASTM definitions in testing highly ductile materials.

KEY WORDS: elastic-plastic fracture, test methods, *J*-resistance curves, nuclear piping steels, electric potential method, ductile crack growth, crack instabilities, unloading effects

In 1984, the U.S. Nuclear Regulatory Commission (NRC) contracted with Battelle to conduct a research investigation referred to as the Degraded Piping Program—Phase II. The primary objective of the program was to provide the NRC with state-of-the-art fracture-mechanics analysis methods for predicting the behavior of degraded, that is, cracked, piping operating under light-water-reactor conditions. Full-scale pipe fracture experiments were used to validate the analyses. Complementing the analyses and the pipe experiments were material characterization studies, conducted on laboratory specimens machined from pipes from the same heats of steel as those used in the pipe tests. This paper presents a number of observations pertaining to laboratory tests performed to obtain *J*-resistance curves for the various pipe materials.

Status of *J-R* Curve Testing at the Start of the Program

At the start of the program in 1984, no standard method had been formulated for conducting *J-R* curve tests, though work was in progress within ASTM Committee E-24 on Fracture Testing. Guidance for test procedures came principally from ASTM Standard Test Method for J_{1c}, a Measure of Fracture Toughness (E 813-81).

ASTM E 813-81 recommended that a multiple-specimen method be used to construct a graph of J versus crack extension (Δa) for Δa values in the range of 0.15 to 1.5 mm (0.006

[1]Senior research scientist and research scientist, respectively, Battelle, Columbus, OH 43201-269

to 0.060 in.). A value for J_{Ic} was produced by extrapolation of the least-squares straight line through those data to the point of intersection with the blunting line, defined as

$$J = 2\sigma_y \Delta a \tag{1}$$

where σ_y is the average of the 0.2% offset yield strength and the ultimate tensile strength.

While ASTM E 813-81 advocated the multiple-specimen method of testing and dealt only with determination J_{Ic}, it did allow use of single-specimen methods and provided mathematical procedures for accounting for crack growth when calculating J values beyond the crack-initiation event. With respect to single-specimen methods, the unloading-compliance procedure [*1*] was the one most widely used in 1984 for monitoring crack extension. However, extensive interest was being shown also in the direct-current electric potential (d-c EP) method for calculating crack extension without the need for periodic unloadings [*2–6*].

The expression given in ASTM E 813-81 for accounting for crack extension in calculating J values is

$$J_{i+1} = [J_i + \eta_i(A_{i+1} - A_i)/b_i B_N] [1 - \gamma_i(a_{i+1} - a_i)/b_i] \tag{2}$$

The subscripts i and $i + 1$ relate to test record increments, and the parameters η, γ, b, A, and a are updated between each step and defined as:

$\eta = 2 + 0.522\ b/W$,
$\gamma = 1 + 0.76\ b/W$,
$b = [W - (a_o + \Delta a)]$
A = area under load-displacement curve, and
a = crack length.

The value of J so calculated was frequently called Deformation Theory J (J_D). Thus, even though the primary purpose of ASTM E 813-81 was to obtain J_{Ic} values, it also provided methods for developing curves of J versus crack extension, commonly referred to as J-resistance or J-R curves.

During that same time period when the Degraded Piping Program was beginning, work was in progress on developing alternative procedures for computing J values. One procedure, developed by Ernst [*7*] to minimize specimen size effects and to ease restrictions on the amount of crack extension permitted within the framework of J-controlled crack growth, used an expression identical to Eq 2, except that a plasticity term was added. The result was termed modified J (J_M), where

$$J_{M(i+1)} = J_{D(i+1)} + \int_{a_o}^{a_{i+1}} J_{pl}(\gamma/b)\ da \tag{3}$$

where J_{pl} is the plastic component of J. Shortly thereafter, impetus arose for separating the calculation of J into elastic and plastic components, that is

$$J = J_{el} + J_{pl} \tag{4}$$

where

$$J_{el} = K_{el}^2 (1 - \nu^2)/E \tag{5}$$

ν = Poisson's ratio
E = Young's modulus of elasticity, and

$$J_{pl(i)} = [J_{pl(i-1)} + \eta_i(A_{pl(i)} - A_{pl(i-1)})/b_i B_N] [1 - \gamma_i(a_i - a_{i-1})/b_i]. \tag{6}$$

Initially, when J_D or J_M were calculated by separation into elastic and plastic components (Eq 4), the results were termed J_D^* and J_M^*, to distinguish them from values obtained from Eqs 2 and 3. At the present time, however, because of the general acceptance of Eq 4, the terms J_D^* and J_M^* have been replaced by the simpler terms J and J_M, respectively. It should be noted that J values computed by separation into elastic and plastic components (Eq 4) do not differ appreciably from those calculated from Eqs 2 and 3.

Among the guidelines existing in 1984 for conducting J-R curve tests were these:

1. Either compact tension C(T) or single-edge bend SE(B) specimens were recommended.
2. The maximum valid value for J_{Ic} was determined from specimen dimensions (B = thickness, a = crack length, and b = uncracked ligament length) and the material's flow strength (σ_y), using the relationship

$$J_{Ic}\,(\max) = D\sigma_y/25 \tag{7}$$

   where D is the smallest of the three dimensions B, a, and b.
3. The maximum valid value for J beyond the onset of cracking was

$$J(\max) = D\sigma_y/15 \tag{8}$$

4. Crack extension should be limited to a maximum of 10% of the original uncracked ligament.
5. For highly ductile materials, such as austenitic stainless steels, the methods described in ASTM E 813-81 for determining J_{Ic} were not applicable.

Test Procedures Used in the Degraded Piping Program

The approach adopted at Battelle for determining J-R curves for the various pipe materials being investigated in the Degraded Piping Program was as follows. Cracks were grown in laboratory specimens, C(T) or SE(B) machined from pipes, to simulate as closely as possible the growth of cracks in full-scale pipe tests. Relatively little attention was paid to adhering to validity requirements for $J_{Ic}(\max)$, $J(\max)$, or maximum crack extension, $\Delta a(\max)$.

The rationale for testing specimens that, in many cases, did not meet established specimen-size criteria and for permitting large amounts of crack growth can be stated simply. The fracture resistance data that were to be developed were not for the purpose of characterizing a certain material under conditions of plane strain; rather, they were to characterize a pipe material in a thickness approximately equal to its wall thickness. The crack was allowed to grow far in excess of 10% of the original ligament because pipe tests typically have large amounts of crack growth.

In adhering to the preceding approach and rationale, the following guidelines and procedures were adopted:

1. C(T) or SE(B) specimens should be machined from pipe without flattening the pipe, to avoid changing the properties of the material.
2. The specimen thickness should be no less than approximately 0.8 of the pipe-wall thickness (to reasonably simulate the full-thickness pipe) and the lateral dimensions should be as large as possible for that specimen thickness.
3. The notch tip geometry in the laboratory specimens should be the same as that employed in the pipe-fracture experiments; in some cases, this was a sharp-machined notch and in others a fatigue crack.

4. The orientation of the growing crack should be the same as in the pipe-fracture experiments.
5. The test temperature should be the same as in the pipe-fracture experiments.
6. The rate of straining should be similar to that employed in the pipe-fracture experiments.
7. The crack should be allowed to grow to a length of at least 50% of the original ligament.
8. The specimens should be side grooved only if required to grow the crack in the desired direction.
9. A single-specimen method that employs the d-c EP method for monitoring crack initiation and crack growth should be used to obtain *J-R* curves; the value of J at the point of crack initiation, as revealed by the d-c EP data, should be called J_{init}.
10. J_D-R curves should be calculated using the method of ASTM E 813-81 (see Eq 2); in addition, values of J_M, J_D^*, and J_M^*, should be calculated as described previously.

Observations in Conducting *J-R* Curve Tests

Monitoring Crack Extension Using d-c EP

In the majority of tests in this program, Battelle's experience in employing the d-c EP method for monitoring crack growth in C(T) specimens was satisfactory. The procedure adopted was similar to one employed by Schwalbe and Hellmann [*3*,*4*] in which constant-current leads were attached to the top and bottom edges at $W/2$ from the load line, and the potential was measured across the notch mouth (see Fig. 1). The load cell was electrically isolated to prevent a current path through the load train. The point of crack initiation was determined from slope changes in curves of U (electric potential) versus displacement and U versus load, applying engineering judgment. To compute the amount of crack growth at any point in the test after initiation, the ratio of U to U_o (the potential at initiation) was inserted into the Johnson equation [*2*,*3*]. As is noted in Ref *8*, the agreement between calculated and measured crack growth was improved by permitting the value of $2y$ (the potential probe spacing) in the Johnson expression to increase in proportion to the load-line displacement. When that modification was employed, crack extensions of up to about 70% of the original ligament were monitored with an error of no more than 5% in a 25.4-mm (1-in.) thick $3T$-planform-size C(T) specimen of Type 304 stainless steel.

An inclusive summary of the crack-growth comparisons from 107 C(T) tests involving both carbon steels and austenitic stainless steels and a variety of specimen sizes and thicknesses is given in Table 1. The results indicated that the d-c EP method met or exceeded the performance described earlier, that is, maximum error of 5%, in 40% of the tests [*9*]. In 71% of the tests, agreement between calculated and actual crack extension was within 10%, and in 88% of the tests, agreement was within 15%. The average difference between calculated and actual final crack extension was 7.7%, with a standard deviation of 6.3%. Austenitic steel specimens, which exhibited greater crack-opening displacements and greater thinning ahead of the crack than did ferritic specimens, showed performance results that were approximately the same as those for ferritic steel specimens.

In another group of tests conducted at Battelle as part of an NRC-sponsored round-robin program, excellent results were obtained using the d-c EP procedures described in this paper [*8*]. Tests on three A106B steels and three aluminum-alloy 1T C(T) specimens gave excellent agreement between calculated and actual final crack extensions; the average error was 2.7% and the standard deviation was 1.9%. Crack growth in those tests ranged from 36 to 50% of the original ligament.

The reasons for the relatively poor performance of the d-c EP method in 12% of the

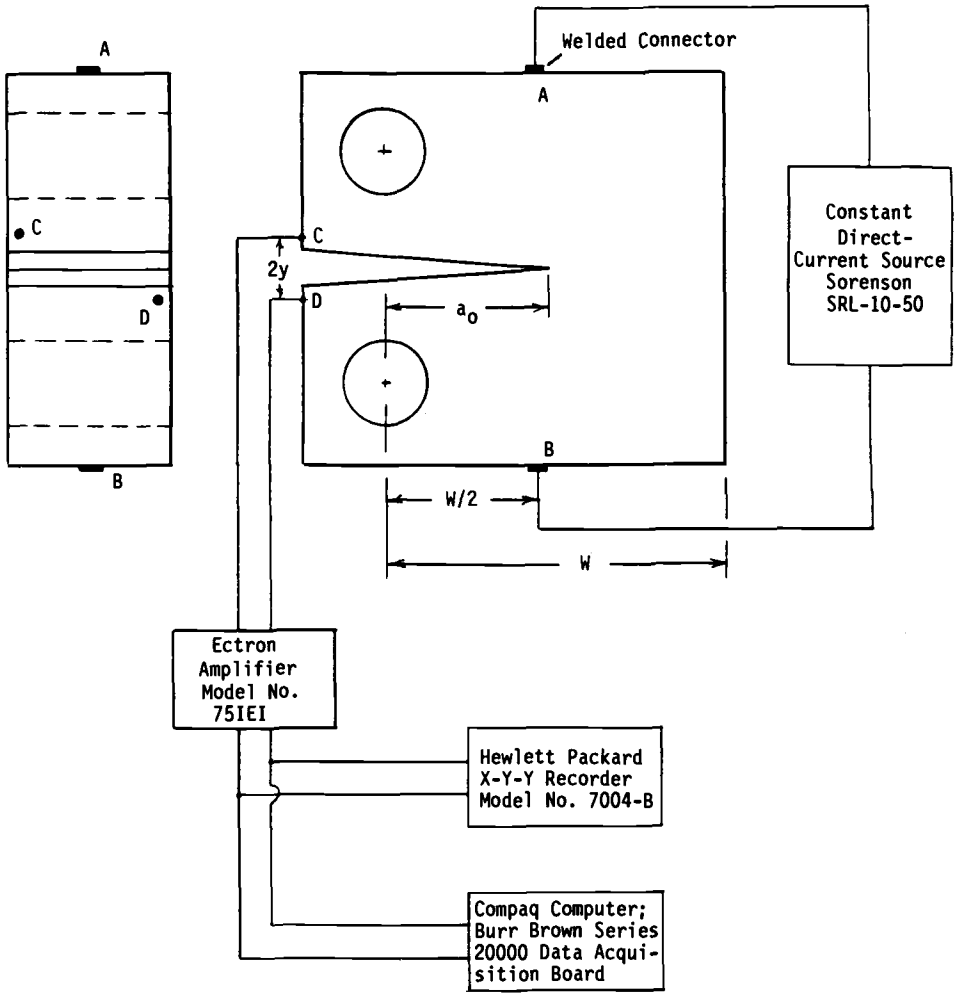

FIG. 1—*Schematic illustration of direct-current electric potential method used at Battelle to monitor crack extension.*

TABLE 1—*Ability of d-c EP method to estimate total crack extension in* J-R-*curve tests of compact specimens (number of results examined: 60 carbon steel and 47 stainless steel).*

	Percentage of Results Showing Indicated Difference Between Calculated and Actual Crack Extension		
Material	±5% (max)	±10% (max)	±15% (max)
Carbon steel	37	70	92
Stainless steel	45	72	83
Combined carbon steel and stainless steel	40	71	88

Degraded Piping Program tests are not known. No obvious procedural faults were apparent in those tests where calculated and actual crack extension were in wide disagreement.

While the extent of crack growth calculated from d-c EP was generally in good agreement with the actual amount, determination of the onset of cracking often included some uncertainties. Figure 2 shows an example of a test in which crack initiation could be defined

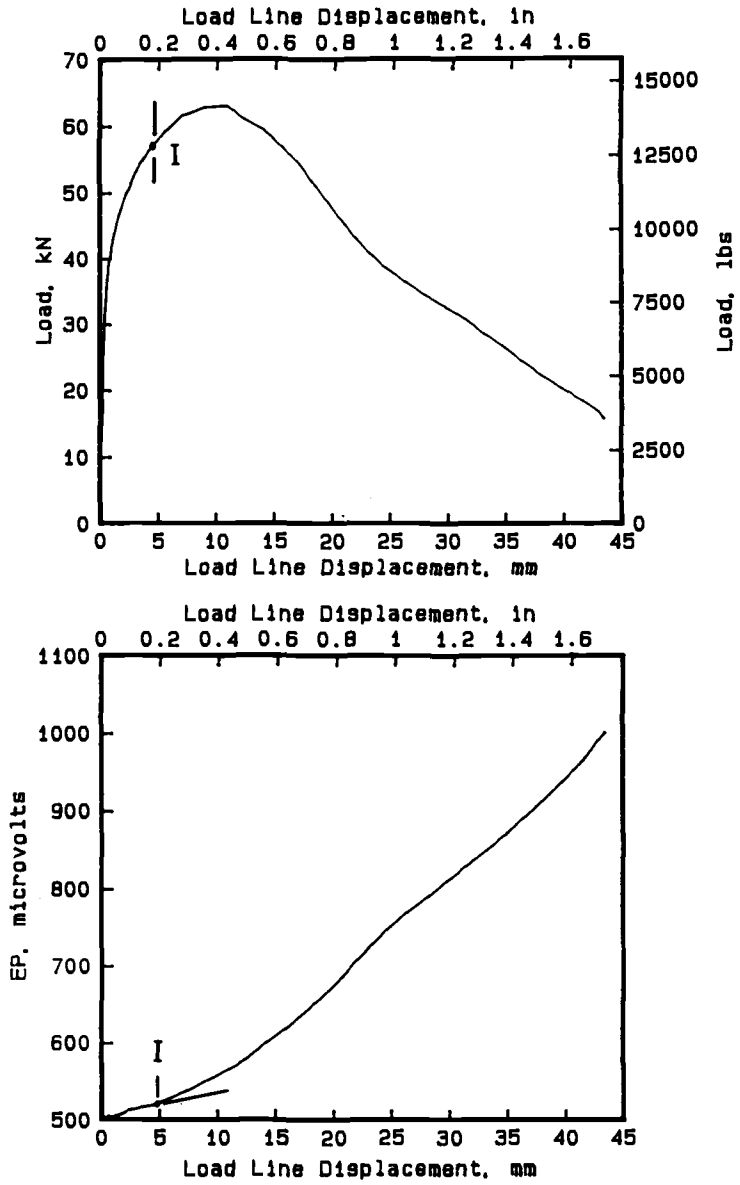

FIG. 2—*Load-displacement-d-c EP data for an ASTM A351, Grade CF8M stainless steel C(T) specimen to illustrate determination of crack initiation point, Point I: Specimen was 1.5* T *planform-size; thickness was 23.9 mm (0.94 in.).*

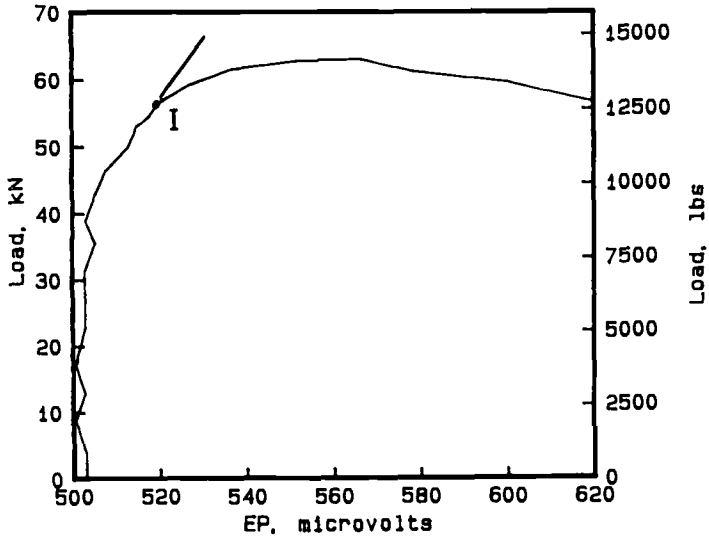

FIG. 2—*Continued.*

without difficulty from the test data. In that figure, determination of the point of crack initiation was based on the point at which the curve of potential (U) versus load-line displacement (v_{LL}) deviated from a straight line (Point I). The slope change at Point I in the curve of load (P) versus U was used merely to corroborate that selection of the crack-initiation point.

Figure 3, on the other hand, is an example of a test in which additional engineering judgment was required in selecting the point of crack initiation. In Figure 3, the graph of

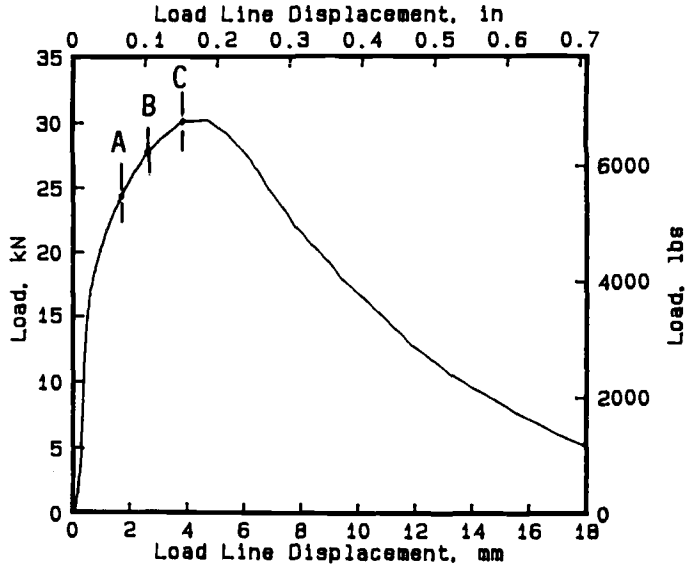

FIG. 3—*Load-displacement-d-c EP data for an ASTM A333 Grade 6 C(T) specimen to illustrate several possible indications of crack initiation at Points A, B, or C: Specimen was 1T planform-size; thickness was 12.2 mm (0.48 in.); 20% side grooved.*

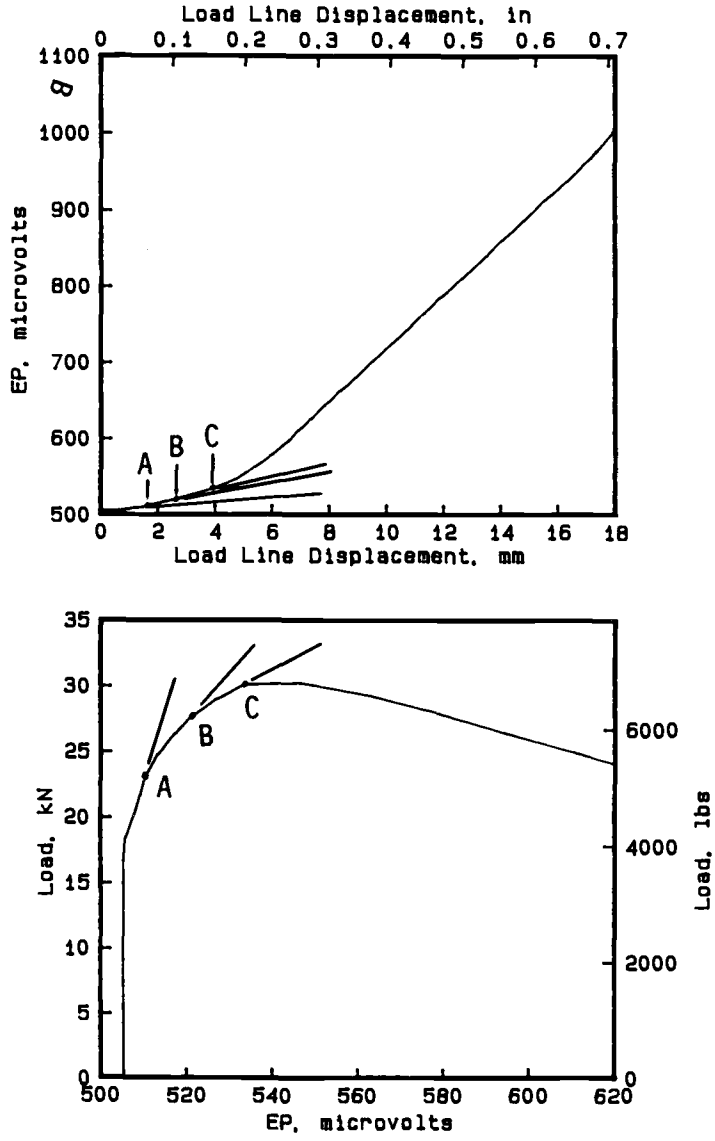

FIG. 3—*Continued.*

U versus v_{LL} did not show as distinct a deviation from linearity as in Fig. 2. In fact, three different points, A, B, and C, appear about equally credible as crack-initiation points from the U-v_{LL} and the P-U plots. In this example, Point B was selected as the most likely point of crack initiation, for reasons that are given in Ref *9*. The value of J at crack initiation, J_{init}, calculated at Points A, B, and C, ranged from approximately 150 to 600 kJ/m^2 (875 to 3400 in · lb/in.^{2}) at Points A and C, respectively, with a most probable value of 325 kJ/m^2 (1860 in. · lb/in.^{2}), calculated at Point B. Clearly, other investigators might have interpreted the data differently and selected a different crack initiation point.

The fact that uncertainties exist in unequivocally detecting the crack initiation point in highly ductile metals from d-c EP data should, perhaps, not be surprising. Microscopic examination of the crack tip region in a Type 304 stainless steel specimen as it was being tested showed that, because of the large blunting that occurred, identifying the precise onset of crack extension was a difficult determination to make, even at a magnification of $\times 30$.

While the example shown in Fig. 3 gave a relatively large uncertainty in the value of J_{init}, the large amounts of crack extension investigated in the Degraded Piping Program render J_{init} a less significant quantity than it might be in certain other J-R curve applications. Nonetheless, positive detection of the crack initiation point remains as one of the major weaknesses of the d-c EP method.

Battelle's experience in using d-c EP for monitoring crack initiation and growth is described in more detail in Ref *9*. It is important that standard procedures are developed soon for this simple and very promising technique. Work towards that development is currently underway within ASTM Committee E-24 on Fracture Testing.

Thickness Changes Ahead of the Growing Crack

It was common in the Degraded Piping Program to observe significant thickness changes ahead of the growing crack in C(T) and SE(B) specimens. Figure 4 illustrates the extensive thinning as well as the back-edge thickening that was observed in a fractured Type 304 stainless steel C(T) specimen. These thickness changes, which vary in magnitude with location in the ligament and with the crack-tip position, are not accounted for in calculating J values in any of the ASTM standard methods; instead, the thickness is assumed to be constant and equal to the original specimen thickness.

In order to obtain data on the magnitude and distribution of the thickness change, measurements were made on a 25.4-mm (1 in.) thick 3T planform C(T) specimen of Type 304 stainless steel as it was being tested at room temperature. Thickness measurements were made along the crack line and at several locations near the crack line at ten different times during the test. Figure 5 shows the load-versus-displacement curve indicates the ten times at which thickness measurements were made. The first measurements were made just prior to crack initiation and the last were made after the crack had extended a distance equal to about 65% of the original ligament. Maximum load in the test occurred between the second and third thickness measurements.

Figure 6 shows the results of the thickness measurements. Notice in Sketch 1 of Fig. 6 (just prior to crack initiation) that significant thinning was already present near the crack tip and measurable thickening was already occurring near the back edge of the specimens;

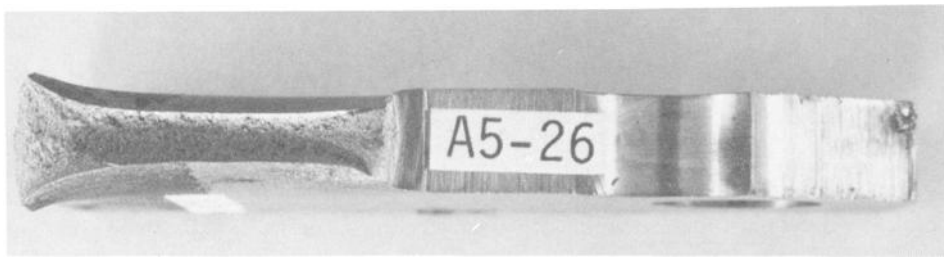

FIG. 4—*Photograph of fracture surface of Type 304 stainless steel compact specimen to illustrate thinning (necking) and back-edge thickening: 1T planform-size specimen; 7.3 mm (0.288 in.) thick; tested at 288°C (550°F)*].

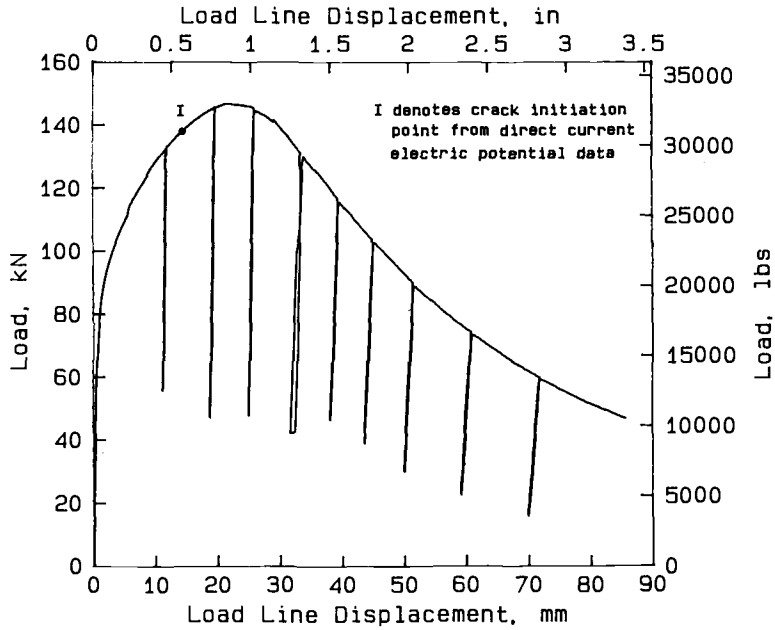

FIG. 5—*Load-versus-displacement record for Type 304 stainless steel compact specimen: 3T planform-size specimen; 25.4 mm (1.0 in.) thick.*

at the crack tip, the thickness was reduced by 13.5%. Proceeding through Sketches 2, 3, 4, and 5, in which the current crack-tip location is indicated by an arrow, the thickness reduction at the current crack-tip location increased steadily until it reached approximately 35% in Sketch 5. Thereafter, it remained essentially constant (Sketches 5 through 10). Thus, the thickness reduction at the crack tip continued to increase for some time beyond the achievement of maximum load in the test, before reaching a steady-state value.

Beyond Sketch 4 in Fig. 6, the thickness-reduction contours above the crack line remained nearly unchanged, except that they spread to the right along with the crack front. This result, too, suggested steady-state crack growth was occurring. Thickening near the back edge increased continuously as the test progressed, as would be expected from the steadily increasing compressive strain in that region.

Clearly, it is incorrect to assume constant specimen thickness in *J-R* curve tests of highly ductile metals, as is done in all ASTM standards that relate to the *J* integral. Examination of the mathematical expressions needed to calculate *J* suggests that accounting for thickness reductions would increase *J* values somewhat. However, the magnitude of the effect is difficult to predict because the thickness change varies with distance from the crack line and distance ahead of the crack tip. Additional experimental data and careful analysis are required before an engineering solution is available that will permit thickness reduction to be accounted for in calculating *J* values.

Observations of Fracture Appearance and Crack Growth Direction

Significant differences in crack growth behavior were noted between tests on austenitic stainless steel and ferritic carbon steel specimens that were not side grooved. In the austenitic steels, the fracture faces were essentially flat, with perhaps a slight cupping, and perpen-

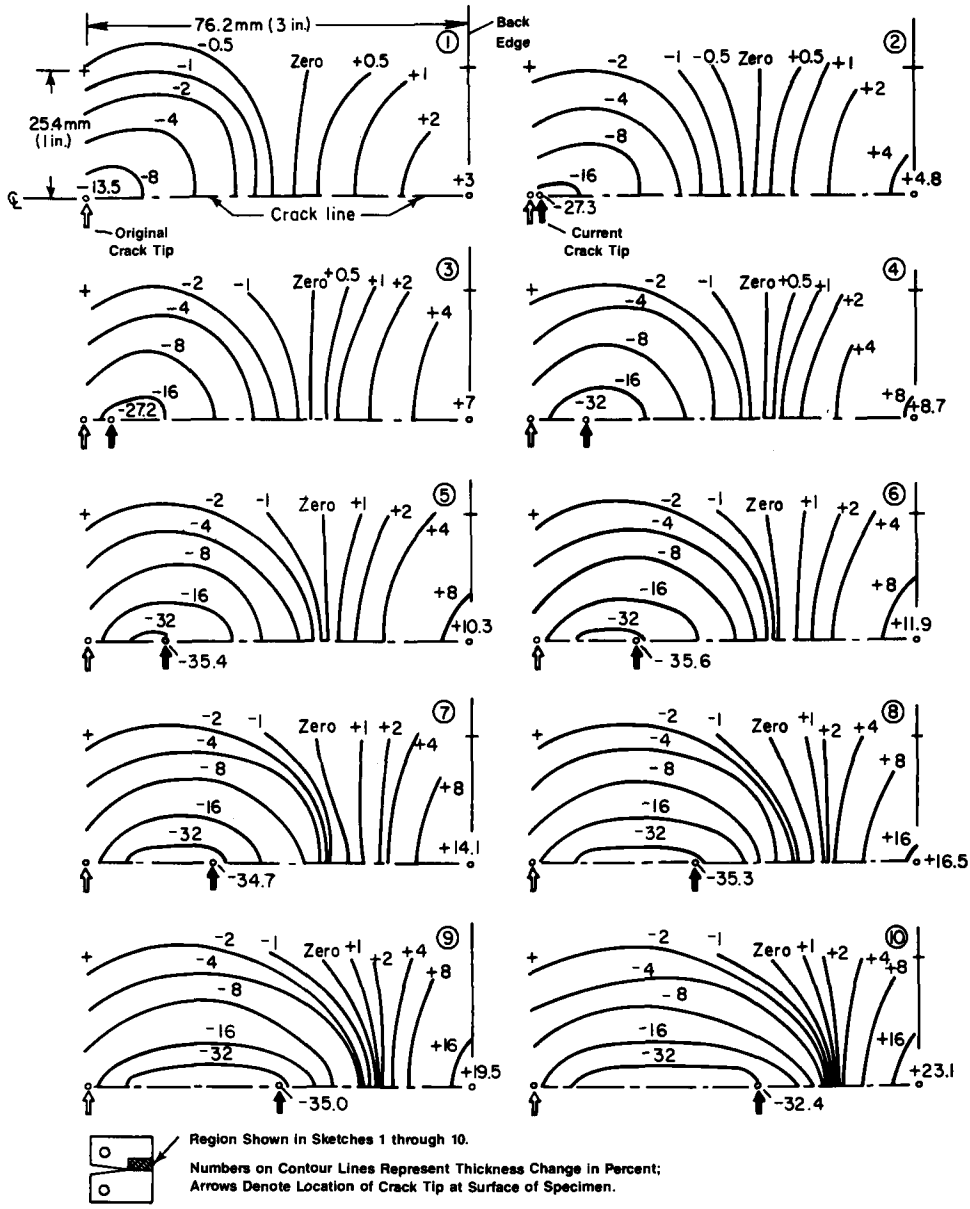

FIG. 6—*Thickness changes in a Type 304 stainless steel 3T planform-size C(T) specimen, 25.4 mm (1 in.) thick, tested at room temperature.*

dicular to the loading direction (see Fig. 7*a*). As was just noted, they displayed extensive thinning (necking) near the crack plane. The crack-growth direction in austenitic specimens was nearly always straight, that is, in the intended direction, both in C(T) tests and full-scale pipe tests that employed the L-C crack orientation.

The ferritic steels, on the other hand, displayed pronounced shear lips, either single shear or double shear (see Fig. 7*b*). Often, the growing crack deviated drastically from the

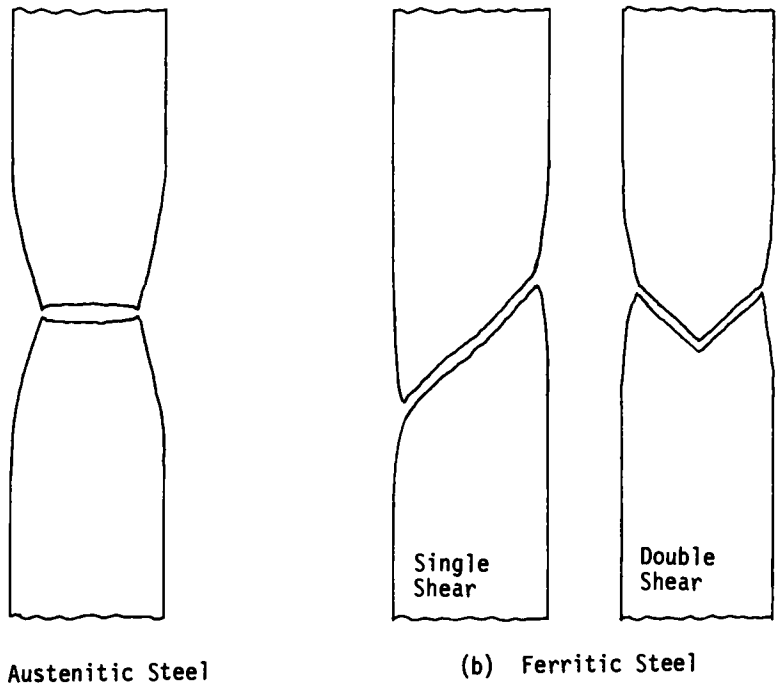

FIG. 7—*Schematic illustration of fracture types observed in compact specimens tested at 288°C (550°F):* (a) *austenitic stainless steel, and* (b) *ferritic carbon steel.*

intended path, both in compact specimens and in full-scale pipe tests in which the intended crack growth direction was circumferential (L-C orientation).

One of the carbon-steel pipes that displayed crack turning was an ASTM A333, Grade 6 steel seamless pipe; it had a diameter of 100 mm (4 in.) and a wall thickness of 8.6 mm (0.34 in.). Metallographic investigation of the outside surface of this pipe revealed the presence of elongated and clustered nonmetallic inclusions, oriented at an angle of 20 to 30 deg to the pipe axis. Since it is the nonmetallic inclusions that are largely responsible for orientation effects in steel products, this observation may help to explain the tendency of cracks to grow away from the circumferential direction both in pipe tests, in which the pipe was subjected to four-point bending, and in compact-specimen tests. The source of the inclusion orientation at an angle to the pipe axis stems from the process used to produce seamless pipe; apparently, it is common for seamless pipe to develop a twist during the hot forming as it is being manufactured [*10*].

Several 0.4*T* planform-size C(T) specimens having a thickness of 6.9 mm (0.27 in.) were machined from the A333 Grade 6 pipe in several different orientations. Testing of those specimens at 288°C (550°F) confirmed the presence of an orientation effect in this pipe. As is shown in Fig. 8, regardless of the initial orientation of the notch plane in the compact specimens, the crack tended to grow on a plane oriented about 20 to 30 deg from the pipe axis, corresponding with the inclusion orientation determined metallographically. The existence of an orientation effect is indicated also by values of J_{init}. As is shown in Table 2, notches oriented in the circumferential direction produced J_{init} values several times those for the other two orientations investigated.

Even if the pipe had not been twisted during manufacture, it is possible that the crack would have turned from the circumferential direction because of inclusions aligned in the

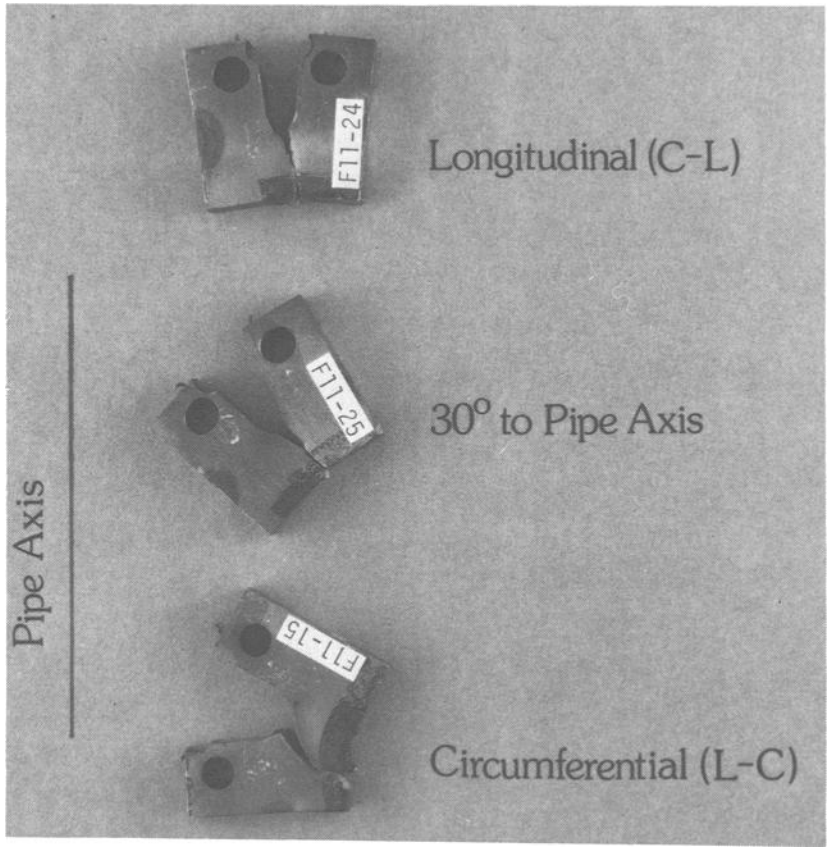

FIG. 8—*Photograph of tested carbon steel compact specimens to illustrate tendency of crack to grow along a plane oriented at 20° to 30° from the pipe axis.*

TABLE 2—*Effect of specimen orientation on J_{init} values for pipe DP2-F11.*[a]

Specimen Identification Number	Notch Orientation	(kJ/m²)	J_{init}[b], in.·lb/in.²
F11-17	circumferential	(294)	1680
F11-18	circumferential	(375)	2140
F11-23	longitudinal	(71)	408
F11-24	longitudinal	(81)	461
F11-25	30° to pipe axis	(75)	430
F11-26	30° to pipe axis	(105)	599

[a]Material: SA333, Grade 6 pipe; 100-mm (4-in.) diameter, Schedule 80. Specimen type: 0.4T plan-form-size compact, thickness 6.9 mm (0.27 in.). Test temperature: 288°C (550°F).

[b]At onset of crack growth, as determined from point of deviation from a straight line in a graph of d-c EP versus displacement.

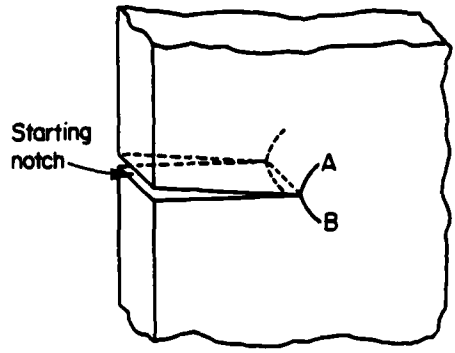

FIG. 9—*Surface crack formation in specimens that develop shear lips.*

axial direction. Axial alignment of inclusions is common in pipes because the axial direction is the principal working direction in manufacturing the pipes. The opportunity for turning arises early in the test when a plastic hinge, associated with the formation of shear lips, forms at the notch tip; the crack initially follows the boundary of the hinge at an angle of about 45 deg from the intended plane of fracture. Once growing at a large angle to the intended plane, the crack may continue growing with relative ease along a plane of lower toughness.

As was noted previously, a plastic hinge forms at the notch tip in the early stages of shear lip development. Crack growth at the specimen surface initially follows the hinge boundary, both above and below the notch, as is shown schematically in Fig. 9. Eventually, either Crack Direction A or Direction B predominates on each surface. If the same crack growth direction is established on both the front and back surfaces, a double-shear crack will form and crack growth will continue at a large angle to the original notch, that is, in a lower toughness direction (Fig. 10*a*). If opposite crack growth directions are established on the two surfaces, a single shear crack will form and the crack will grow in the same direction as the original notch, though the plane of fracture will be tilted (Fig. 10*b*). In compact specimens, the likelihood of double shear appears to be about the same as that for single shear. However, in pipe tests conducted in four-point bending, some as-yet-unknown factor may strongly favor the occurrence of cracks that turn from the circumferential direction.

Additional studies will be required to establish a more certain explanation for crack turning and whether its occurrence can be predicted. Crack turning does not pose a serious problem in compact-specimen testing because it can be prevented by side grooving the specimens. In pipe tests, however, it presents a very real problem because of the mixed-mode nature of the fracture and the difficulty in analyzing the pipe test results.

Additional studies will be required to establish a more certain explanation for crack turning and whether its occurrence can be predicted. Crack turning does not pose a serious problem in compact-specimen testing because it can be prevented by side grooving the specimens. In pipe tests, however, it presents a very real problem because of the mixed-mode nature of the fracture and the difficulty in analyzing the pipe test results.

Observations of Ductile Crack Jumps in Carbon Steels Tested at 288°C (550°F)

Approximately half of the carbon steels tested in the Degraded Piping Program exhibited bursts of rapid fracture during tests of compact specimens at 288°C (550°F). All tests were conducted under displacement control. An example of a load-versus-displacement curve for

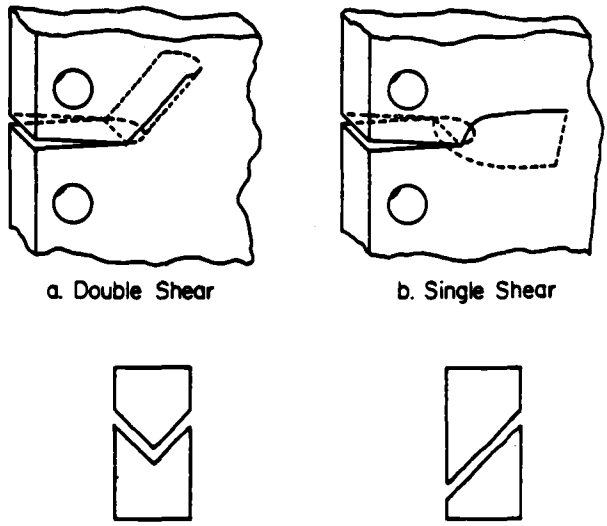

FIG. 10—*Double-shear versus single-shear fractures observed in carbon steel compact specimens.*

a specimen in which several bursts of rapid fracture occurred is shown in Fig. 11. Similar behavior was noted in several full-scale pipe fracture experiments on carbon steels [*11*].

The behavior was not predictable, that is, one specimen from a particular pipe might display crack jumps while a nominally identical specimen might show only stable tearing.

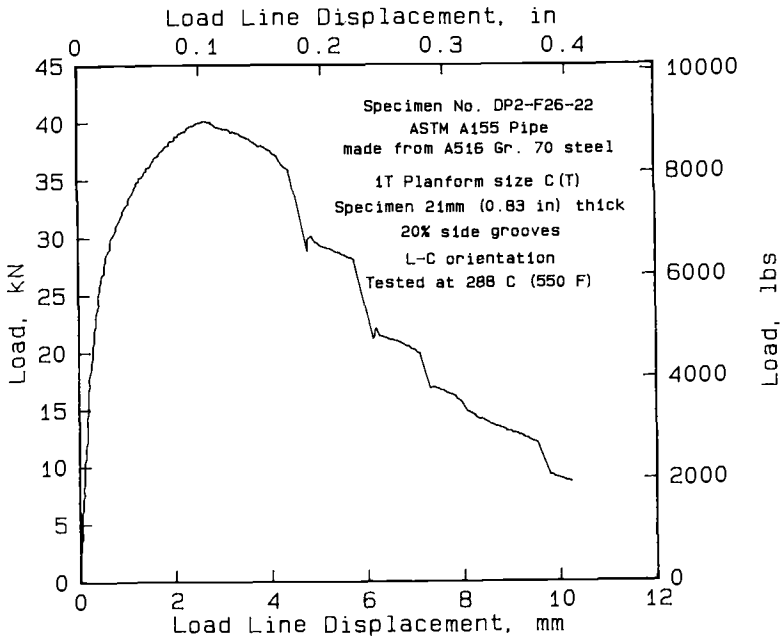

FIG. 11—*Load-displacement record for a carbon steel compact specimen that displayed several bursts of unstable crack growth at 288°C (550°F).*

Likewise, one specimen might undergo numerous small crack jumps and another specimen of the same material might show one large crack jump. Furthermore, there was not a perfect correlation between crack jumps in compact specimen tests and in full-scale pipe tests. No convincing explanation for unstable cracking has yet been advanced. Cursory analysis of the data permits excessive machine compliance to be ruled out as a probable cause. A candidate explanation discussed in Ref *11* is dynamic strain aging (DSA). Tension tests conducted at several different temperatures on the carbon steels investigated in the Degraded Piping Program indicated that all were susceptible to DSA, although some displayed greater susceptibility than others. However, no simple correlation appears to exist between degree of susceptibility to DSA, as revealed by tension tests, and the occurrence of crack jumps in 288°C (550°F) tests of C(T) specimens. Additionally, even if the two phenomena were related, no satisfactory explanation has been offered of how DSA can cause crack jumps.

Aside from the possible undesirable effects of crack instabilities on pipes in reactors, the phenomenon also causes complications for calculating a *J*-resistance curve. From a theoretical basis, it is probably incorrect to calculate *J* beyond the instability point because that basis assumes stable, continuous, ductile tearing in a homogeneous material. Nonetheless, it may be important for engineering purposes that an approximate *J-R* curve be calculated for materials that display unstable crack growth.

As is discussed in Ref *11*, several possible calculation methods might be considered (refer to Fig. 12). In Fig. 12, the solid line, ABC, represents a recorder trace of a single instability

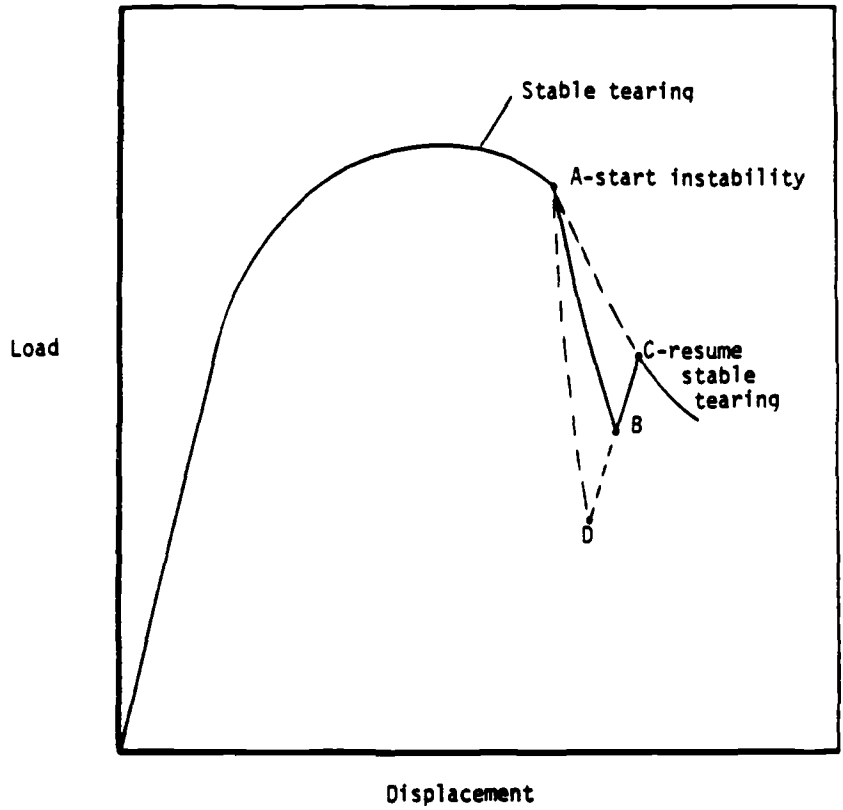

FIG. 12—*Schematic illustration of one burst of unstable crack growth in a fracture toughness test.*

event. Since the event often is faster than the recording equipment used in quasi-static testing, the actual load-displacement relationship might have followed curve ADC. Furthermore, the actual load drop during the instability would depend on load-train compliance; for example, a very stiff load train could result in a near-zero load at Point D. Because of the uncertainty in the actual curve during the crack jump and its dependence on compliance, there might be some justification for simply performing a linear interpolation from Point A to Point C. Curve AC clearly would yield higher J values than would Curves ABC or ADC because of greater area under the curve.

After selecting an appropriate load-versus-displacement curve for the instability event, a second decision relates to the number of points to be used in calculating the J-R curve in that region. Should only the data from the points shown in Fig. 12 (Points A, B, C, and D) be used or should an arbitrary number of intermediate points be added? That decision is important because the displacement interval can have an effect on the calculated J-R curve.

Figure 13 shows J-R curves at 288°C (550°F) calculated by the procedures of ASTM E 1152-87, for an A516 Grade 70 steel whose load-displacement record was shown in Fig. 11. The specimen exhibited four distinct crack jumps, estimated to be 1.96, 1.48, 1.22, and 0.66 mm (0.077, 0.058, 0.048, and 0.026 in.) in length. With reference to Fig. 12, the calculations were performed using Curve ABC, without using any additional data points between Points A and B. Three of the four regions of unstable crack extension are evident on the J-R curve, as is the change in slope of the curves at the first two instabilities.

Two other observations regarding calculation of J-R curves in the presence of crack instabilities appear to be pertinent: (1) when crack jumps are relatively small, any of the calculation methods just discussed will give approximately the same results; and (2) since J by the methods of ASTM E 1152 or E 813 is a cumulative parameter (that is, $J_{i+1} = J_i$ plus a crack-growth term), the J value just past the onset of an instability will be close to the

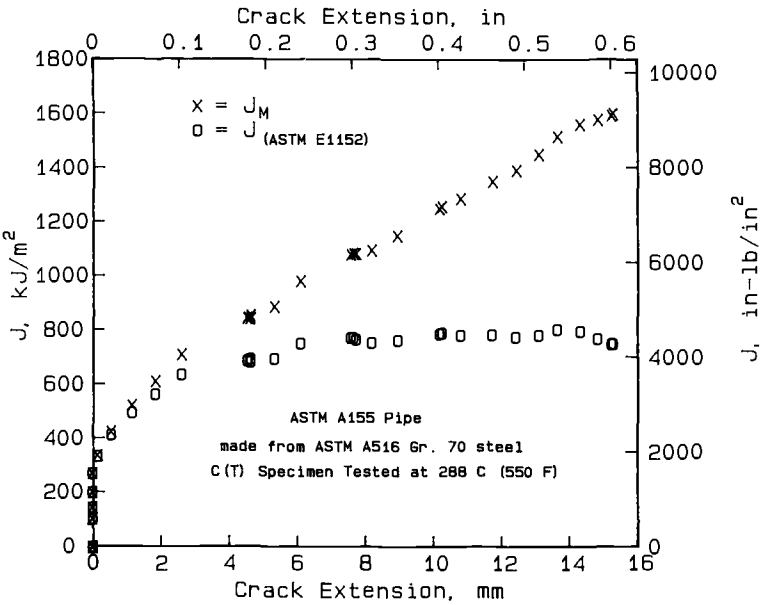

FIG. 13—J-*resistance curves for C(T) test that exhibited several bursts of unstable crack growth, as shown in Fig. 11.*

previous value for stable crack growth, even though there may be a large instantaneous change in the fracture toughness. Thus, the *J-R* curve calculation method may tend to mask local regions of unusually high or low toughness.

Clearly, the findings described here indicate that further work is needed to develop suitable engineering methods for computing *J-R* curves in specimens exhibiting unstable crack extension.

Unusual Effect of Partial Unloadings in Testing Carbon Steel

Work reported in Ref *12* describes an unusual and unexpected effect of periodic, partial unloadings of ASTM A106B carbon steel compact specimens tested at 288°C (550°F). In two specimens that were partially unloaded several times at regular intervals prior to attaining the maximum-load point, the load-displacement curve deviated from a straight line much earlier and the maximum load was 15 to 20% less than in two nominally identical specimens tested under monotonically increasing displacement. Figure 14 illustrates the behavior for one of each of the two types of loading. Also, of interest to the preceding section of this paper, both test procedures resulted in sizable crack jumps at approximately the maximum load point in the tests. However, it should be noted also that C(T) specimens of the same steel tested at Materials Engineering Associates, using the unloading compliance procedure to detect crack growth, experienced only slow stable crack growth.

The cause of the reduced loads in the specimens that were partially unloaded, in the manner of the unloading-compliance method for monitoring crack growth, is not known. To the authors' knowledge, such an effect has not been reported previously. The result is puzzling because extensive testing was conducted on the unloading compliance method prior to its adoption by ASTM as an acceptable method for monitoring crack extension in elastic-plastic fracture-toughness testing [*1*]. That earlier work demonstrated that periodic partial unloadings of approximately 10% of maximum load produced no significant effect on the calculated *J-R* curve. In addition, Sutton and Vassilaros [*13*] observed no significant effect on the *J-R* curve of unloadings as large as 90% of maximum load. Kaiser [*14*] found similar results for 100% unloadings, so long as the number of unloadings was not excessive. However, to the best of the authors' knowledge, all of the demonstration experiments were performed at room temperature. The tests reported here, on the other hand, were conducted at 288°C (550°F) on a carbon steel susceptible to dynamic strain aging. Admittedly, the data are limited but the results were duplicated in repeat tests. Therefore, the authors suggest that it might be prudent for other investigators, who are using unloading compliance to test carbon steels at elevated temperatures, to conduct a few preliminary tests to look for possible effects of periodic unloadings on the load-displacement curve.

If subsequent experiments on other carbon steels at elevated temperatures confirm the existence of unloading effects of the type illustrated in Fig. 14, a second caution should be sounded. If a flawed structure experiences cyclic loading at an elevated temperature, it may be unwise to employ monotonic loading in elevated-temperature compact-tension tests designed to simulate the structure because they might provide an overestimate of the structure's load carrying ability.

Defining Crack Size, Specimen Width, and Load-Line Displacement in Ductile Materials

In highly ductile materials, testing of fracture-toughness specimens to large amounts of crack extension causes problems in some of the fundamental definitions used in fracture mechanics testing, namely, crack size (a), specimen width (W), and load-line displacement (v_{LL}). Each of those quantities requires selection of a reference plane in the specimen.

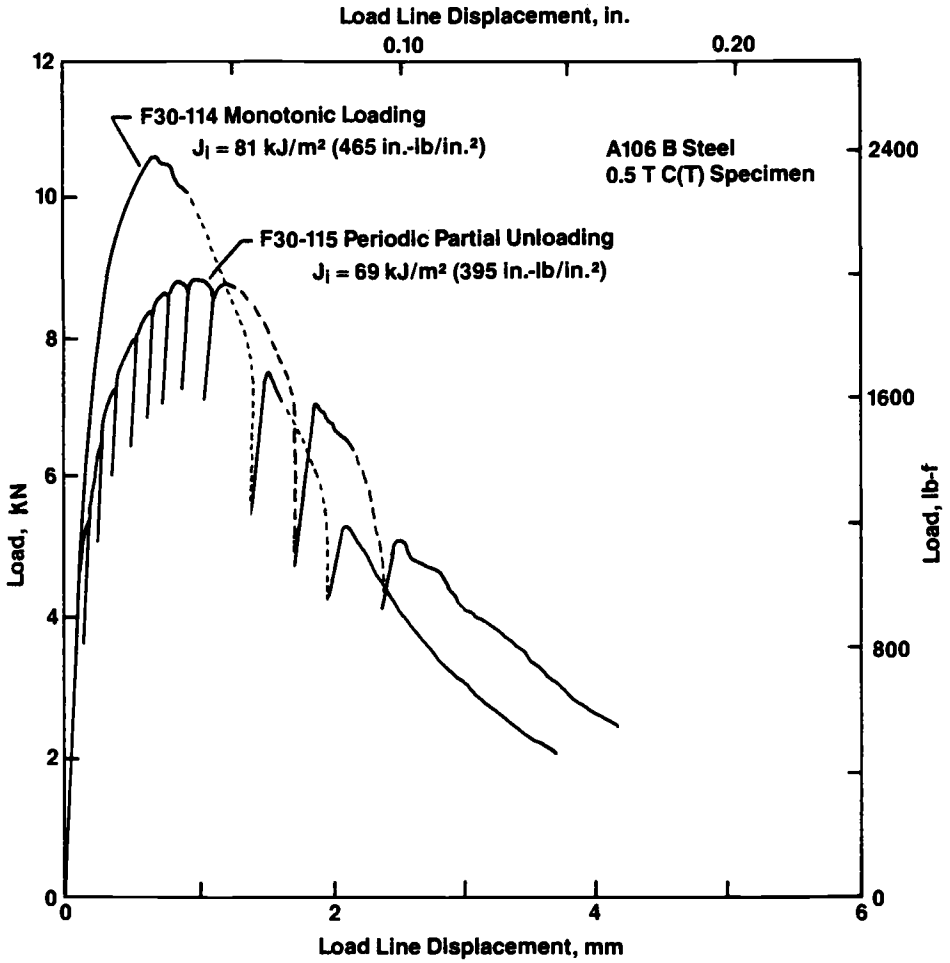

FIG. 14—*Load-displacement curves illustrating effect of periodic partial unloadings of compact specimens tested at 288°C (550°F).*

According to ASTM Terminology Relating to Fracture Testing (E 616-82), ASTM E 813-87, and ASTM E 1152-87, the reference plane in a compact specimen is the one normal to the sides and containing the load line. Figure 15*a* shows that reference plane and dimensions a and W for a compact specimen. Load-line displacement is commonly measured between Points C and D.

Figure 15*b* is a schematic illustration of the appearance of an austenitic stainless steel specimen after it has experienced crack growth of 35 to 40% of the original ligament. Notice that the displacement-measurement points (C and D) no longer lie along the load line, which has now moved to Line GH. Thus, the displacements being measured are not truly v_{LL}. Only if displacements were measured between Points B and E could they correctly be called v_{LL}. Likewise, although it is customary to continue to measure a and W from Line AC or Line DF, both should be measured from Line GH, the shifted reference plane and load line, according to existing definitions.

The authors believe that the current ASTM definition of crack size and specimen width

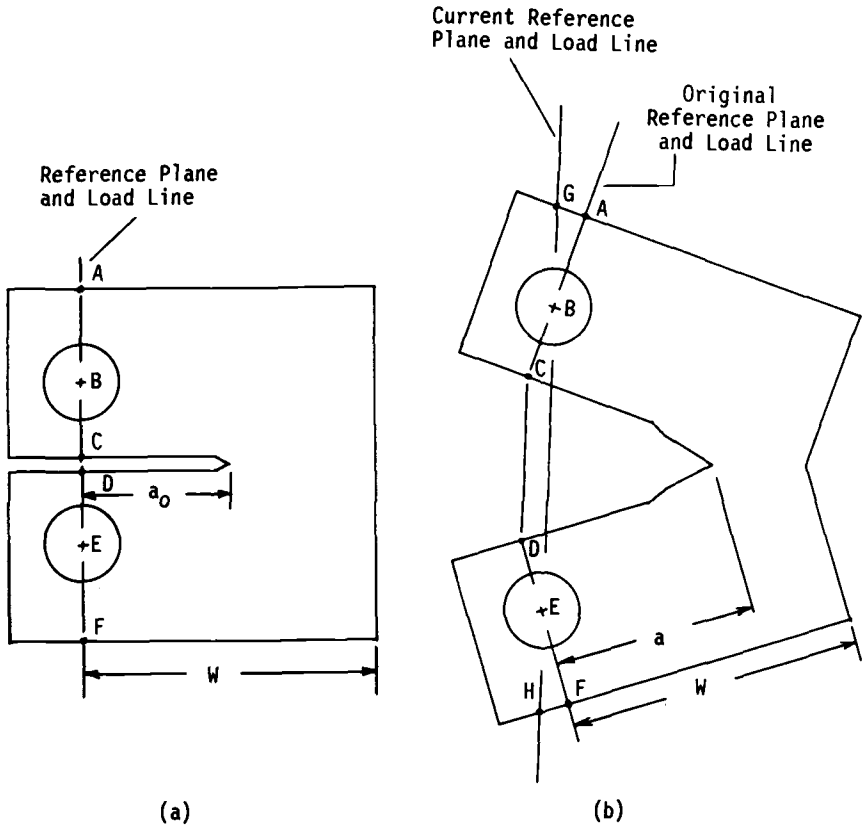

FIG. 15—*Schematic illustration of change in load-line location after large crack growth in a highly ductile C(T) specimen.*

should be changed to refer to a reference plane normal to the sides of the specimen and containing the *original* load line. That change would mean that current usage of the terms a and W in specimens partially or completely tested would match the definition.

Beyond the question of definitions, this discussion casts some doubts about the accuracy of the expressions for calculating J after large amounts of displacement and crack growth, because the true meaning of the quantities a and W becomes cloudy after the specimen exhibits large shape changes. Attempts to deal with this question were beyond the scope of Battelle's investigation.

Discussion

The observations discussed in this paper indicate that needs exist in the following areas of elastic-plastic fracture test methods:

1. Standardized procedures should be developed both for obtaining direct-current electric potential data and for interpreting the data to provide accurate measurements of crack extension.

2. Work is needed to provide guidance in calculating J values when significant thickness reductions occur in advance of the crack.
3. An engineering approach is needed for calculating J-R curves in the presence of rapid crack bursts interspersed with periods of stable tearing, as are sometimes observed in carbon steels tested at 288°C (550°F).
4. When using unloading compliance to test carbon steels at elevated temperatures, it might be prudent to conduct preliminary tests to look for possible effects of periodic unloadings on the load-displacement curve.
5. Consideration should be given to changing the definition of crack size and specimen width in several ASTM standard methods.

In addition, consideration should be given in future versions of the J-R curve standards to experimenters who are trying to measure the crack growth resistance of a material in the same thickness as used in a specific application, especially when those tests produce results that are invalid by ASTM E 1152-87.

Acknowledgments

The authors are grateful to the NRC for their support of most of the work described here. Mr. M. Mayfield served as project officer for that work. We also acknowledge Battelle's support of some of the work on direct-current electrical potential studies and measurement of thickness changes near an advancing crack. Finally, none of this work could have been accomplished without the capable assistance of P. R. Held, P. N. Mincer, and G. Wall.

Thanks are due also to T. P. Groeneveld and A. R. Rosenfield for reviewing the manuscript and to C. Pepper for preparing the manuscript for publication.

References

[1] Clark, G. A., Andrews, W. R., Paris, P. C., and Schmidt, D. W., "Single Specimen Tests for J_{Ic} Determination," *Mechanics of Crack Growth, ASTM STP 590*, American Society for Testing and Materials, Philadelphia, 1976, pp. 27–42.

[2] Johnson, H. H., "Calibrating the Electric Potential Method for Studying Slow Crack Growth," *Materials Research and Standards*, Vol. 5, 1965, pp. 442–445.

[3] Schwalbe, K. H. and Hellmann, D., "Application of the Electrical Potential Method to Crack Length Measurements Using Johnson's Formula," *Journal of Testing and Evaluation*, Vol. 9, No. 3, 1981, pp. 218–221.

[4] Schwalbe, K. H., Hellmann, D., Heerens, J., Knaack, J., and Muller-Roos, J., "Measurement of Stable Crack Growth Including Detection of Initiation of Growth Using the DC Potential Drop and the Partial Unloading Methods," *Ductile Fracture Test Methods, Proceedings*, CSNI Workshop Organization for Economic Cooperation and Development, Paris, 1983, pp. 18–53.

[5] Wilkowski, G. M., Wambaugh, J. O., and Prabhat, K., "Single Specimen J-Resistance Curve Evaluations using the Direct-Current Electric Potential Method and a Computerized Data Acquisition System," *Fracture Mechanics: Fifteenth Symposium, ASTM STP 833*, R. J. Sanford, Ed., American Society for Testing and Materials, Philadelphia, 1984, pp. 553–576.

[6] Vassilaros, M. G. and Hackett, E. M., "J-Integral R-Curve Testing of High Strength Steels Utilizing the Direct Current Potential Drop Method," *Fracture Mechanics: Fifteenth Symposium, ASTM STP 833*, R. J. Sanford, Ed., American Society for Testing and Materials, Philadelphia, 1984, pp. 535–552.

[7] Ernst, H., "Materials Resistance and Instability Beyond J-Controlled Crack Growth," *Elastic-Plastic Fracture: Second Symposium, Vol. I: Inelastic Crack Analysis, ASTM STP 803*, C. F. Shih and J. P. Gudas, Eds., American Society for Testing and Materials, Philadelphia, 1983, pp. I-191–I-213.

[8] Marschall, C. W., Held, P. R., Landow, M. P., and Mincer, P. N., "Use of the Direct-Current Electric Potential Method to Monitor Large Amounts of Crack Growth in Highly Ductile Metals,"

Fracture Mechanics: Twenty-First Symposium, ASTM STP 1074, J. P. Gudas, J. A. Joyce, and E. M. Hackett, Eds., American Society for Testing and Materials, Philadelphia, 1990, pp. 581–593.

[*9*] Landow, M. P. and Marschall, C. W., "Experience In Using Direct Current Electric Potential to Monitor Crack Growth in Ductile Metals," this publication, pp. 163–177.

[*10*] Williams, D. N., private communication, Battelle, June 1987.

[*11*] Marschall, C. W., Landow, M. P., and Wilkowski, G. M., "Effect of Dynamic Strain Aging on Fracture Resistance of Carbon Steels Operating at Light-Water-Reactor Temperatures," *Fracture Mechanics: Twenty-First Symposium, ASTM STP 1074*, J. P. Gudas, J. A. Joyce, and E. M. Hackett, Eds., American Society for Testing and Materials, Philadelphia, 1990, pp. 339–360.

[*12*] Marschall, C. W., Landow, M. P., and Held, P. R., "Unusual Effect of Periodic Unloadings on Behavior of Fracture Toughness Specimens," presented at ASME/JSME Pressure Vessel and Piping Conference, Honolulu, July 1989.

[*13*] Sutton, G. E. and Vassilaros, M. G., "Study of the Effects of Elastic Unloadings on the J-R Curves from Compact Specimens," David W. Taylor Naval Ship R & D Center, NUREG/CR-4283, June 1985.

[*14*] Kaiser, S., "On the Relation Between Stable Crack Growth and Fatigue," *Fatigue of Engineering Materials and Structures*, Vol. 6, No. 1, 1983, pp. 33–49.

Andrea D. Gallant,[1] *Isa Bar-On,*[1] *and Floyd R. Tuler*[1]

Effect of Residual Stress on the *J-R* Curve of HY-100 Steel

REFERENCE: Gallant, A. D., Bar-On, I., and Tuler, F. R., **"Effect of Residual Stress on the *J-R* Curve of HY-100 Steel,"** *Elastic-Plastic Fracture Test Methods: The User's Experience (Second Volume), ASTM STP 1114*, J. A. Joyce, Ed., American Society for Testing and Materials, Philadelphia, 1991, pp. 260–272.

ABSTRACT: Fabrication processes in structural components can result in intended or inadvertent material behavior changes due to plastic deformation and residual stresses. In this study, the effect of a residual stress field caused by prior plastic deformation of a beam in four-point bending on the *J-R* curve of 12.7 mm (0.5 in.) thick specimens of HY-100 steel was investigated. Specimen blanks were deformed in four-point bending to two different levels of deflection prior to machining the starter notch. The resulting residual stress field in a companion test specimen was measured on side surfaces and through-the-thickness by a multiple exposure X-ray diffraction technique. *J*-testing was performed in three-point bending on undeformed specimens and the two deformed specimen sets using a modified multiple-specimen technique. A decrease in J_Q and tearing modulus, T, with increasing specimen deflection was observed. The decrease in J_Q was comparable to that observed previously in uniformly prestrained specimens.

KEY WORDS: elastic-plastic fracture, test methods, *J-R* curve, residual stress, steels, prestrained specimens

The application of fracture mechanics to design and materials testing assumes that the material to be evaluated is macroscopically homogeneous and that the stress fields within the material are a result of the applied loads and the existing cracks. Metal working operations such as rolling and bending, however, can induce considerable strain hardening that is not necessarily homogeneous and can leave the material with nonhomogeneous mechanical properties and residual stresses. Welding can also introduce severe residual stresses of up to yield-stress magnitude. In these cases, the underlying assumptions may not be met by the actual material conditions. Since the *J*-integral is related to the crack tip stress-strain field, any changes in the material or its stress-strain state might be expected to influence the evaluation of J_{Ic} and the *J-R* curve. This possible influence would be of concern to the designer who was designing into the plastic range of the material, a practice that is becoming increasingly more common as sophisticated analytical design methods develop.

This paper evaluates the combined effect of a residual stress field and prestrain caused by four-point bending on the *J-R* curve of HY-100 steel. Using a three-point-bend, chord-supported-arc specimen geometry, *J-R* curves from the deformed specimens are compared to curves from unstressed single-edge-notched bend (SENB) specimens taken from the same plate of material. The multiple exposure method for X-ray diffraction determination of residual stress was used to assess the stress field in two specimens before and after fracture

[1]Research assistant, associate professor, and professor, respectively, Worcester Polytechnic Institute, Worcester, MA 01609. Ms. Gallant is now at General Dynamics Corporation, Electric Boat Division, Groton, CT 06430.

toughness testing. The results are compared to the first stage of this research [*1*], which examined uniaxially prestained material, to assess the effect of the residual stress field. To allow direct comparison to the results of the previous work, specimens of the same nominal dimensions were used and ASTM Test Method for J_{Ic}, a Measure of Fracture Toughness (E 813-81) was followed except where noted.

Background

Recently, work has been published on the fracture characteristics of uniformly prestrained material [*1*]. The effect of uniform tensile prestrain on mechanical properties of HY-80 was investigated by Novak [*2*]. A decrease in K level for overload fracture was observed in precracked cantilever beam tests. Clayton and Knott [*3*] found that compressive prestrain in crack opening displacement (COD) tests on four-point bend specimens decreased the COD necessary to initiate ductile fracture in HY-80 steel. Fracture mechanism studies indicated that differences in shear decohesion behavior occurred as a function of strain. Mullican [*4*] correlated the decrease in J_{Ic} of prestrained HY-100 steel with a decrease in fracture strain at the crack tip. Sanford [*5*] in a later report from the same program confirmed this finding by noting that increased prestrain resulted in smaller stretch zone widths. Werchniak [*6*] evaluated the effects of compressive and tensile prestrains on low cycle fatigue life of HY-80 steel notched cantilever beam specimens. Compressive prestrain was detrimental to the fatigue life, while tensile prestrain increased the fatigue life when the stress cycling was below the yield strength. For stress cycling above the yield strength, tensile prestrain had little effect.

Thompson and Knott [*7*] found that 20% tensile prestrain in free-cutting mild steel decreased the COD for crack initiation. More macroscopic path deflections were noted in the prestrained material with the paths corresponding to the predicted direction of maximum shear. Bar-On and coworkers [*1*] found a decrease in J_{Ic} and tearing modulus for increasing tensile prestrain in HY-100 steel three-point bend specimens. Secondary cracking and crack path deflections were noted in the prestrained material and correlated with J-R curve anomalies.

Many studies have observed crack path deflections or crack meandering in ductile fracture. Chipperfield and Knott [*8*] and Beachem and Yoder [*9*] found zig-zag crack paths occurring in the ductile fracture of steel. You and Knott [*10*] conducted a study on HY-80 and HY-130 steels. The ductile fracture of HY-130 steel was dominated by shearing with distinct shear steps on the fracture surface, while HY-80 steel exhibited shearing to a lesser extent.

Material

A 50.8-mm (2-in.)-thick plate of HY-100 steel was supplied in the normalized condition. The compositional analysis provided by the manufacturer is summarized in Table 1. The plate was flame cut into sections and stress relieved at 552°C for 2 h. The mechanical properties, as reported in the work by Bar-On et al. [*1*], are given in Table 2.

Three-point bend blanks with a nominal size of 11.4 by 50.7 by 254 mm were machined from the stress relieved plate with an L-S orientation. The blanks were separated into three

TABLE 1—*Chemical analysis of the HY-100 steel as provided by the manufacturer.*

C	Mn	P	S	Cu	Si	Ni	Cr	Mo	V	Ti
0.17	0.30	0.007	0.012	0.19	0.28	3.16	1.74	0.48	0.003	0.003

TABLE 2—*Tensile properties of HY-100.*

	σ_y		Ultimate Tensile Strength		σ_f^a		
	MPa	ksi	MPa	ksi	MPa	ksi	Δe_f^b
Longitudinal	762.6	110.6	842.6	122.2	1670	242.2	0.24
Transverse	772.2	112.0	842.6	122.2	1621	235.1	0.21

[a] $\sigma_f = \frac{P_f}{A_f}$; P_f = final load, A_f = final area.

[b] $\Delta e_f = \frac{l_f - l_o}{l_o}$; l_o, l_f = initial and final length, respectively.

sets: one set was deformed in four-point bending to a nominal deflection of 6.2 mm; the second set was deformed to a nominal deflection of 9.5 mm; and the remaining specimens were reserved for non-deformed control specimens. All three sets were prepared as SENB specimens, with modifications applying to the two deformed sets. The deformed specimens were notched on the compressive side of the specimen and a chord support, fulfilling the recommendations outlined in Ref [*11*], was machined to allow three-point bend testing. Figure 1 shows the geometry of the deformed specimen sets.

Experimental Procedure

The fracture toughness tests were conducted under displacement control on a 250 kN servohydraulic test machine. Originally, single specimen tests were performed, but severe negative crack growth obscured trends to such an extent that a modified multiple-specimen J test procedure was used, in which additional crack length information was obtained by the introduction of marking inks [*12*]. These inks were forced into the crack by air pressure.

J-values were determined following ASTM experimental procedures for J_{Ic} testing. J_Q and tearing modulus were calculated by two procedures: (1) the linear best fit to valid data

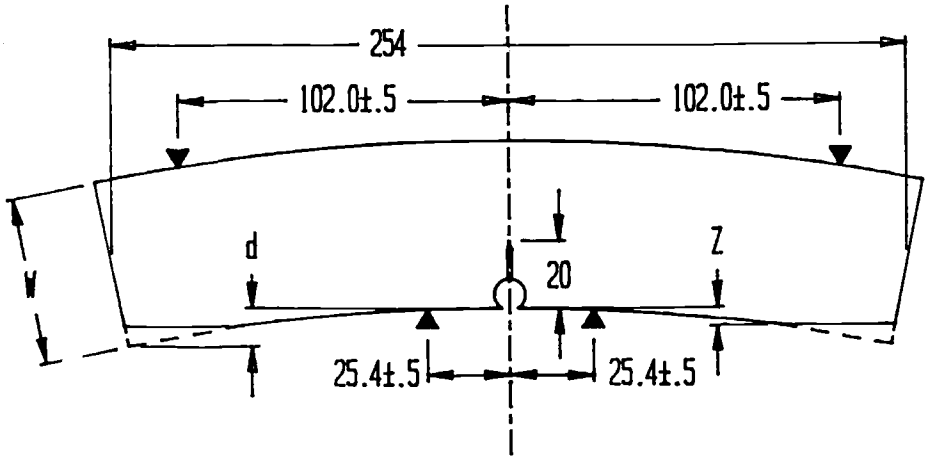

FIG. 1—*Specimen geometry of deformed specimen, including four-point bend loading points;* Z ≤ *0.1*W *and* ▲ = *load points for deformation. (See Table 3 for individual* d *and* W *specimens. All dimensions are in millimetres.)*

points as recommended in ASTM E 813–81, and (2) using the polynomial expression $J = A\,a^B$ of ASTM E 813–87.

Residual stress was measured by an X-ray diffraction technique on a diffractometer with a chromium radiation source tube and a nickel filter. Data were collected using a personal computer interfaced with a microprocessor-based controller. Peak positions were determined by least squares parabolic fit to seven intensity points spaced at an 0.2° interval, after background and Lorentz-Polarization and adsorption effects were corrected. A $\sin^2(\psi)$ method with parafocusing was used for residual stress determination because of expected oscillations in the interplanar spacing versus ψ angle data [*13*]. This is common in plastically strained material and is believed to be related to the micro-stress system in the material [*14–16*]. A two-exposure method is inadequate for characterizing residual stress in plastically deformed material.

The residual stress component acting on the crack plane in Mode I was measured for two states using comparison samples. The dimensions of these specimens are given in Table 3. An original stress state of a specimen from the 9.5-mm nominal deflection set before crack propagation was measured on specimen R03. The stress component was measured along both sides and through the thickness of the material in front of the crack plane. The location and size of typical X-ray beam spots are shown in Fig. 2. The procedure in the SAE report on X-ray determination of residual stress [*13*] was used to correct the stress relaxation due to material removal for through-the-thickness measurements. Specimen R10 represents the final residual stress state of a specimen from the 9.5-mm nominal deflection set after crack propagation. Only the internal stress component was measured in Specimen R10 because of the side groove.

Results

The side and internal through-the-thickness residual stress fields in a comparison specimen from the 9.5-mm nominal deflection set prior to crack extension by tearing are shown in Fig. 3. It is important to acknowledge that an X-ray determined stress value represents an average stress value incorporating both micro- and macro-stresses over a finite volume of material. The volume of material sampled is delineated by the beam size and the depth of

TABLE 3—*Individual specimen information.*

Specimen Identification	Permanent Deflection, mm	Width, W, mm	Thickness, B, mm	Net Thickness, B_n, mm
R03	9.88	50.88	11.48	11.48
R08	9.26	50.83	11.63	9.07
R09	9.32	50.83	11.20	9.04
R10	9.48	50.75	11.30	9.25
R14	9.60	50.52	11.28	8.99
R15	9.53	50.55	11.30	8.79
R16	9.53	50.50	11.10	8.92
R22	6.21	50.88	11.41	8.71
R23	6.11	50.95	11.35	9.02
R24	6.15	50.83	11.10	7.90
R06	6.08	50.67	11.33	8.84
R18	0.00	50.62	11.33	10.47
R19	0.00	50.75	11.51	9.22
M34	0.00	49.43	11.48	9.14

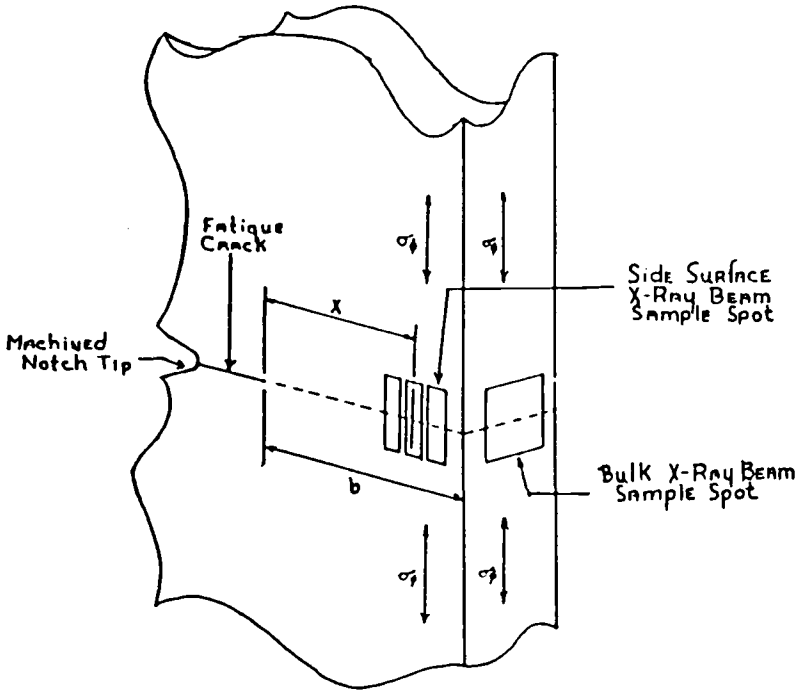

FIG. 2—*Illustration of X-ray beam sample spots.*

X-ray penetration, with the depth of penetration being on the order of 10 to 50 μm. Figure 3 shows a difference in the quantitative and qualitative aspects of the surface and internal residual stress fields. The differences between surface and internal yield and flow stresses has been proposed as the origin for these differences.

The internal residual stress in a 9.5-mm nominal deflection representative sample after crack propagation is compared to the internal stress field from Fig. 3 in Fig. 4. The sample positions have been normalized with respect to the remaining ligament. Figure 5 summarizes the results of propagating a crack into a residual stress field. All positions are normalized with respect to the remaining ligament.

The results of the modified multiple-specimen fracture toughness tests from the non-deformed baseline specimen set are compared to the noncrack-growth-corrected single-specimen data from Bar-On and coworkers [*1*] for unprestrained specimens of identical size and composition in Fig. 6. The data fall low on the curve, but their own comparison of visual crack lengths to their single-specimen curves demonstrated that the single-specimen technique tended to report a shorter crack length.

Figures 7 and 8 summarize the *J*-test results for the 6.2- and 9.5-mm nominal deflection specimen sets, respectively. There is considerable scatter in the data, which is not surprising since there are several possible contributing factors. The complex geometry of the deformed specimens may have contributed to curve scatter. The difficulty of testing identical specimens for the curve generation is compounded by the additional requirement of producing an identical crack length that terminates in material that is prestrained to some exact percent. Table 4 documents the variability in crack length and specimen deflection. Inspection of the fracture surface after testing showed evidence of secondary cracking, irregular fracture surfaces, and uneven crack front advance. In the work of Bar-On and coworkers [*1*], these

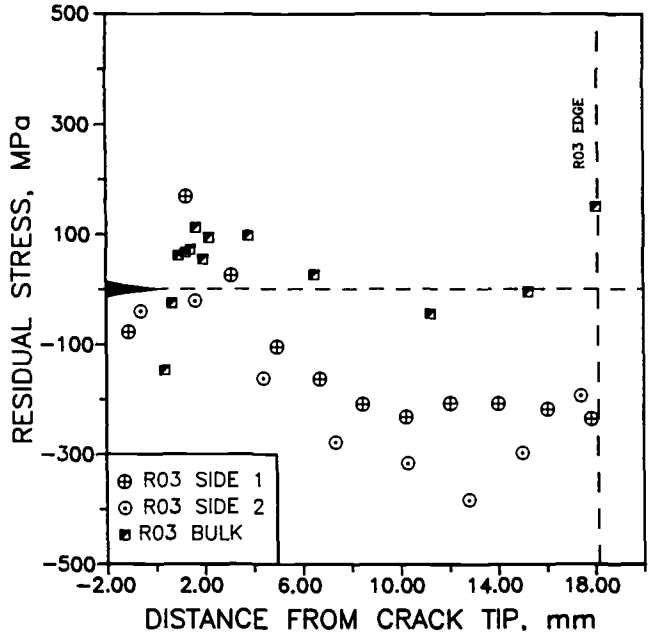

FIG. 3—*Residual stresses in Specimen R03, both side surfaces and bulk measurements (9.5-mm nominal deflection).*

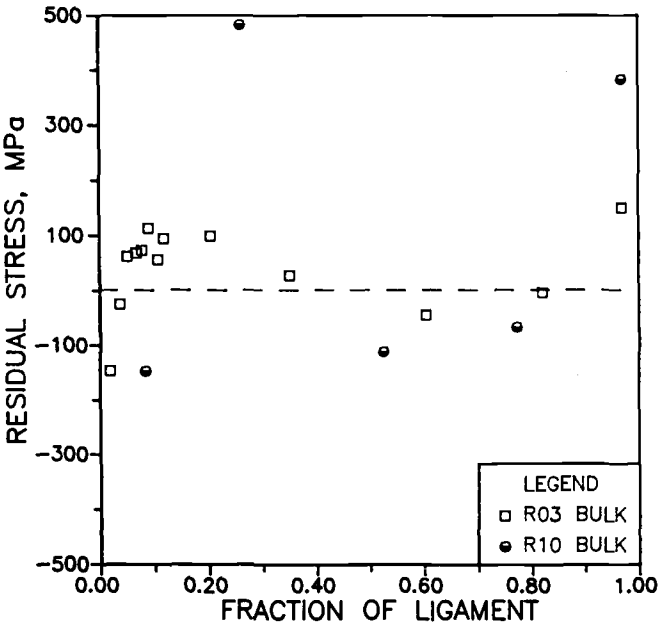

FIG. 4—*Comparison of bulk residual stress for specimens, before and after tearing (R03, R10) versus fraction of remaining ligament.*

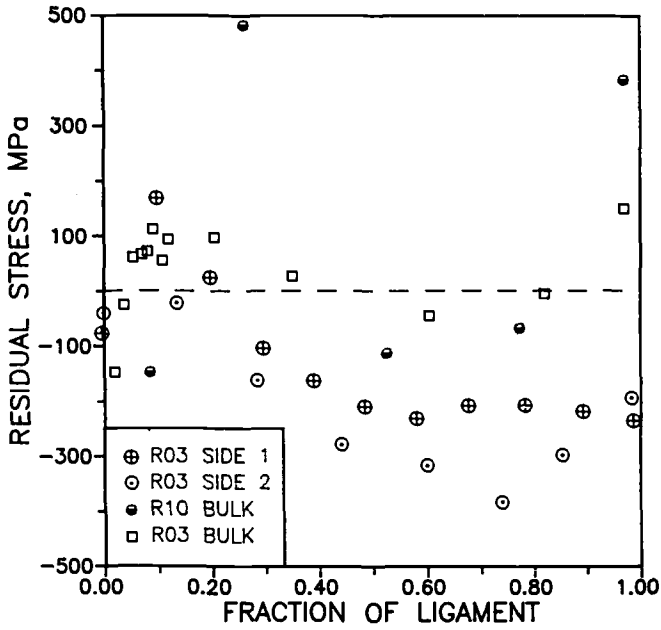

FIG. 5—*Comparison of side surfaces and bulk residual stresses as a function of remaining ligament.*

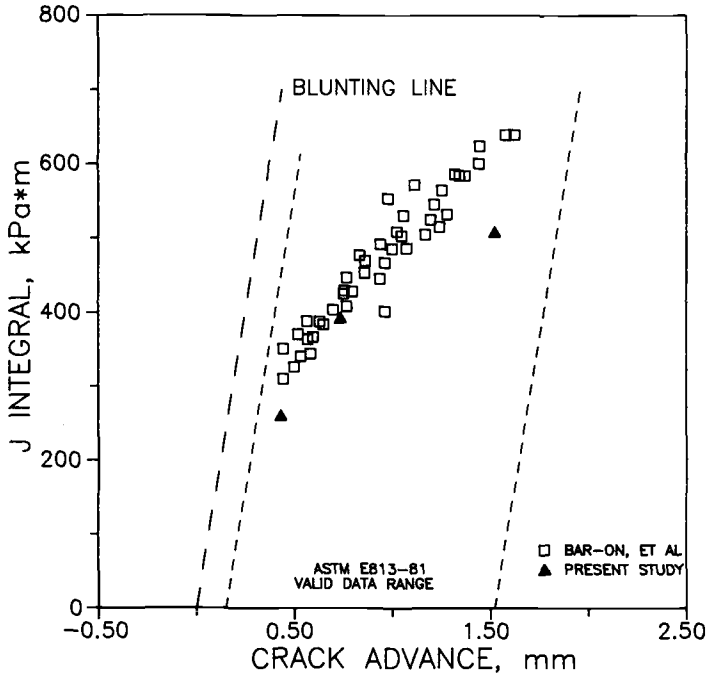

FIG. 6—*Zero percent prestrained* J-R *curve from Bar-On et al.* [1] *with data from 0-mm nominal deflection specimens.*

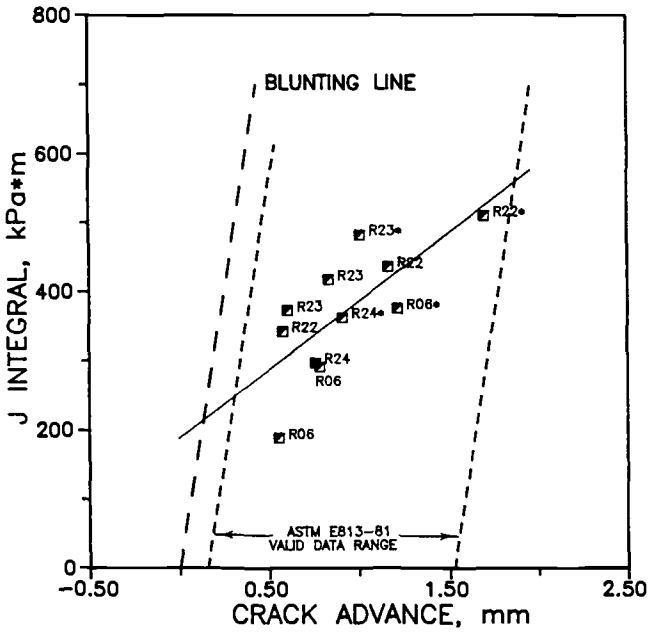

FIG. 7—J-R *curve for 6.2-mm nominal deflection HY-100 steel specimens (11.5-mm nominal thickness).*

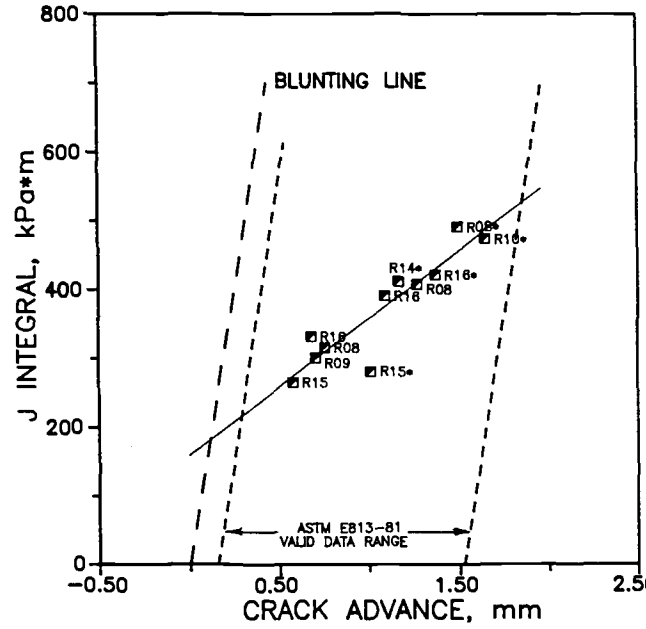

FIG. 8—J-R *curve for 9.5-mm nominal deflection HY-100 steel specimens (11.5-mm nominal thickness).*

TABLE 4—*Precracking information for individual specimens.*

Specimen Identification	Starter Crack Length, a_o, mm	Final Crack Extention, a, mm	Testing Procedure	Delta Load for Final K, kN
R03	32.21	0.00	X-ray	5.95
R08	32.62	1.50	single J	7.33
R09	32.75	3.10	single J	7.33
R10	32.75	1.65	single J, X-ray	7.37
R14	32.16	1.17	multi-specimen J	7.06
R15	31.79	1.02	multi-specimen J	7.15
R16	32.60	1.37	multi-specimen J	6.84
R22	32.11	1.70	multi-specimen J	7.19
R23	32.00	1.02	multi-specimen J	7.15
R24	32.09	0.91	multi-specimen J	6.97
R06	31.86	1.22	multi-specimen J	7.06
R18	31.63	0.73	single J	7.81
R19	32.72	2.08	single J	7.55
M34	30.78	2.31	single J	7.41

NOTE—Precracking was at 10 Hz, load ratio of 0.1.

features were also observed and correlated with discrepancies in the J-R curve. Microstructural effects related to the specimen orientation to the parent plate may affect J-R curves. Irregular features and secondary branching of the crack can be seen in Fig. 9 and 10. Many such features were evident on the specimens of this study.

Figures 11 and 12 summarize the results of the J test for the three deflection sets. The requirements of ASTM E 813–81 were applied within reason, the main exceptions being the 0.5 T thickness, the chord-supported arc geometry, and the use of crack front inks. A small but distinct drop in calculated J_Q value with increasing specimen deflection can be seen in Fig. 11. Figure 12 reports the relationship between tearing modulus, J value, and nominal specimen deflection for the power law curve.

The possible conditions impacting the fracture resistance are the plastically strained material at the crack tip, the residual stress field, the inhomogeneous character of the full

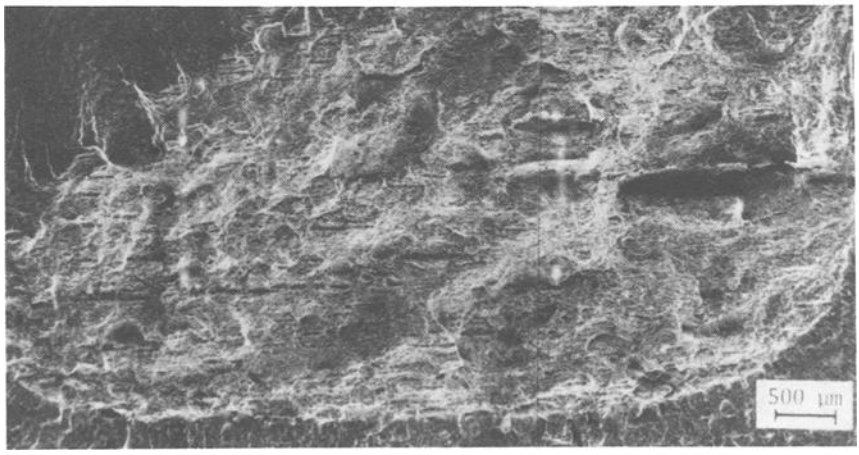

FIG. 9—*Fracture surface of Specimen R09 showing local out-of-plane crack propagation.*

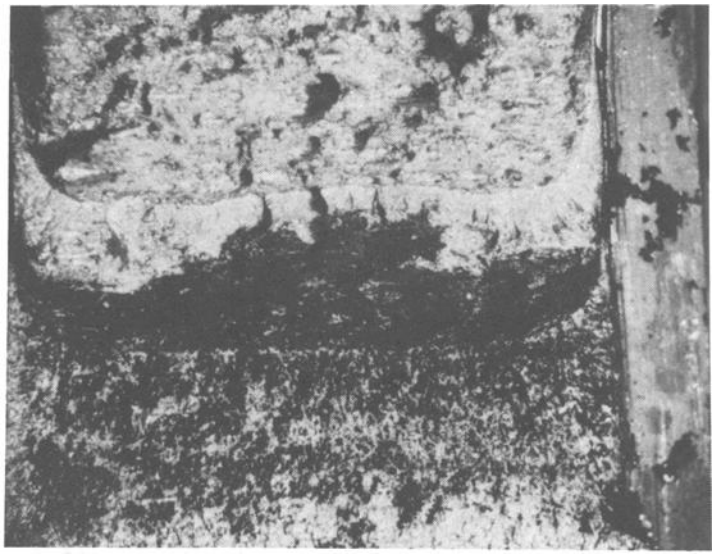

FIG. 10—*Fracture surface of Specimen R14 showing irregular crack front.*

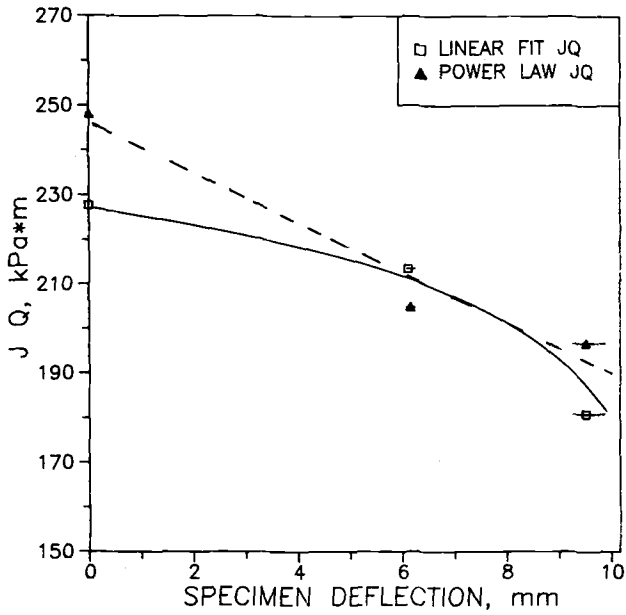

FIG. 11—J_Q *versus nominal specimen deflection (HY-100 steel, 11.5-mm nominal thickness).*

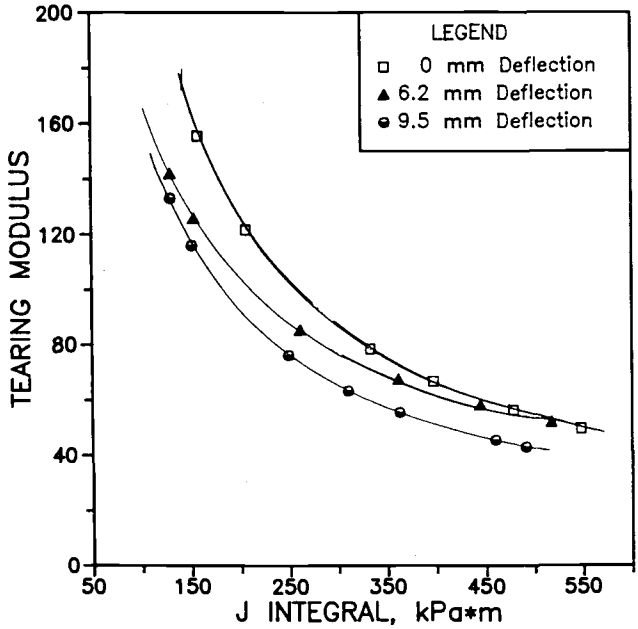

FIG. 12—*Tearing modulus as a function of* J*-integral (HY-100 steel, 11.5-mm nominal thickness).*

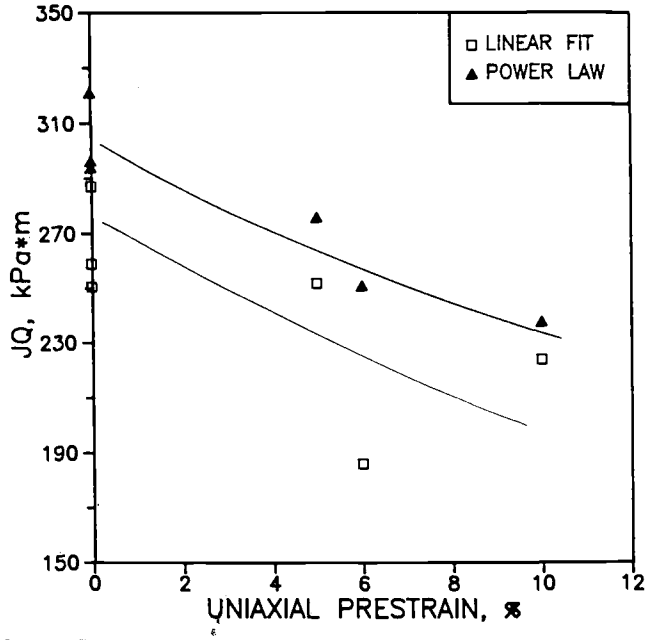

FIG. 13—J_Q *versus percent uniaxial tensile strain from Bar-On et al.* [1].

specimen material, and the geometry. The geometry should have little effect as long as the specimen curvature is small. The deflections used are smaller than the empirically determined limits from Ref [*11*].

The plastic strain generated during four-point bending of the specimen was estimated using the following assumptions: the material behavior is linear elastic—perfectly plastic; the specimen is curved uniformly from end to end; the rotation of the specimen ends, with respect to the perpendicular due to elastic deformation, is very small; and the plastic strain distribution from the elastic core to the outer fiber is linear. This estimate predicts that only 1.2 to 1.7% plastic strain exists at the crack tip with a strain gradient of about 0.04% per millimetre. Comparing this with the uniaxially prestrained specimens from the Bar-On and coworkers study [*1*], a uniaxial prestrain of 10% was necessary to realize the same drop in J value (see Fig. 13). It is an interesting observation, however, that the maximum prestrain in the 9.5 mm nominal deflection specimens, that is, the strain in the extreme fibers, was estimated to be approximately 8 to 10%. This is possible evidence that the far-field inhomogeneous character of the specimen may effect the fracture behavior of the specimen. The presence of the approximately 100 MPa compressive stress should, based on intuition, increase the tearing resistance of a material, but the possibility that it could have a net detrimental effect cannot be ruled out. X-ray diffraction is believed to account for the micro-stress system in an average, global way. The exact nature of the theorized micro-stress system is not understood, but could conceivably impact a micromechanical event such as fracture initiation. Also, only one component of the residual stress field was measured. The possibility that a three-dimensional stress state with severe conditions exists at the crack tip cannot be eliminated on the basis of this work.

The results indicate, however, that the effect of the plastic deformation in the specimen has a larger influence on the J-R curve than the residual stress at the crack tip. This is especially interesting, since it could have been argued that the compressive stress at the crack tip should increase the fracture resistance, whereas this work found an overall decrease in the resistance to fracture.

Conclusions

J-R curves were determined for three sets of bars of HY-100 steel with the nominal dimensions of 51 by 11 by 254 mm. Two of the three sets had been permanently deformed in four-point bending. One set had an average maximum permanent deflection of 6.152 mm; the other set had an average maximum permanent deflection of 9.512 mm. All three sets of specimens were notched and then precracked to a nominal starter crack length-to-width ratio (a_o/W) of 0.64. The permanently deformed specimen sets were tested as three-point bend, chord supported arc specimens; the non-deformed set was tested as single-edge-notched three-point bend bars. A modified multiple-specimen technique, using inks to mark several crack fronts for the Δa information, and either computer-monitored load-displacement data or autographically recorded load-versus-displacement curves for the J values, were used. This technique yielded data that were in good agreement with previous noncrack growth corrected single-specimen curves from specimens with the same dimensions taken from the same plate of material.

The residual stress field in a sample from the 9.5-mm deflection set before testing was measured on both sides and through the uncracked ligament. There were significant differences between side and through-the-thickness residual stress fields, particularly for the portion of the ligament further than 2 mm from the crack tip.

The residual stress field through the thickness of a 9.5-mm deflection specimen that had been torn 1.64 mm during J testing was measured. Compared to the untorn specimen on a

fraction of remaining ligament scale, the fields qualitatively appear the same. The magnitudes of the extreme stresses, however, were approximately double for the torn specimen, indicating that crack extension does not result in residual stress relief.

A decrease in J_Q with increasing deflection was observed. J_Q dropped 47 to 50 MPa, depending on the type of curve fit, for a nominal permanent deflection of 9.5 mm. The magnitude of the decrease in J_Q from no deflection to 9.5-mm deflection was about the same as observed in specimens that had been uniaxially prestrained 5 to 10% in the work by Bar-On and co-workers. The plastic strain in the area of the crack tip had been estimated to be only 1.5%. The maximum prestrain in the 9.5-mm nominal deflection specimens, the strain in the extreme fibers, was estimated to be 8 to 10%. This is possible evidence that the far field inhomogeneous character of the specimen may affect the fracture behavior of the specimen of a larger extent than the plastic strain or the residual stress at the crack tip.

Acknowledgments

This work was supported by General Dynamics, Electric Boat Division, Groton, Connecticut.

References

[1] Bar-On, I., Tuler, F. R., and Howerton, W. M., "Effect of Prestrain on the *J*-Resistance Curve of HY-100 Steel," *Nonlinear Fracture Mechanics: Volume II-Elastic-Plastic Fracture, ASTM STP 995*, J. D. Landes, A. Saxena, and J. G. Merkle, Eds., American Society for Testing and Materials, Philadelphia, 1989, pp. 244–258.

[2] Novak, S. R., *Engineering Fracture Mechanics*, Vol. 5, 1973.

[3] Clayton, J. Q. and Knott, J. F., *Metal Science*, Vol. 10, 1972.

[4] Mullican, J. N., "Fracture Toughness Degradation in HY-80 and HY-100 after Prestrain," M. S. thesis, Naval Postgraduate School, Monterey, CA, 1983.

[5] Sanford, G. B., "Degradation of Fracture Toughness in Steels Due to Prior Strain: A Predictive Model," M. S. thesis, Naval Postgraduate School, Monterey, CA, 1983.

[6] Werchniak, W., *Engineering Fracture Mechanics*, Vol. 4, 1972.

[7] Thompson, H. E. and Knott, J. F., "Effects of Crack Length and Pre-strain on Ductile Fracture," *Proceedings, The Fracture Control of Engineering Structures*, Vol. 3, Amsterdam, 1986.

[8] Chipperfield, C. G. and Knott, J. F., *Metals Technology*, Vol. 2, 1975.

[9] Beachem, C. D. and Yoder, G. R., *Metallurgical Transactions*, Vol. 4, 1973.

[10] You, C. P. and Knott, J. F., "Fracture and the Role of Microstructure," Vol. 1, Engineering Materials Advisory Services Ltd., U.K., 1982.

[11] Underwood, J. H., Kapp, J. A., and Witherell, M. D. in *Fracture Mechanics: Seventeenth Volume, ASTM STP 905*, J. H. Underwood, R. Chait, C. W. Smith, D. P. Wilhem, W. A. Andrews, and J. C. Newman, Eds., American Society for Testing and Materials, Philadelphia, 1986.

[12] Steenkamp, P. A. J. M. and Hartevelt, M., "Crack Front Marking by Dye Penetrants," Report MMPP-232, Delft University of Technology, The Netherlands, 1984.

[13] "Residual Stress Measurement by X-Ray Diffraction—SAE J784a," Society of Automotive Engineering, Inc., New York, 1971.

[14] Marion, R. H. and Cohen, J. B., "Anomalies in Measurement of Residual Stress by X-Ray Diffraction," *Advances in X-Ray Analysis*, Vol. 18, 1975.

[15] Cullity, B. D., "Some Problems in X-Ray Stress Measurement," *Advances in X-Ray Analysis*, Vol. 20, 1977.

[16] Dölle, H. and Cohen, J. B., "Evaluation of (Residual) Stresses in Textured Cubic Metals," *Metallurgical Transactions*, Vol. 11a, No. 5, 1980.

Marie T. Miglin,[1] *C. Scott Wade,*[1] *James A. Joyce,*[2] *and W. Alan Van Der Sluys*[1]

Dynamic Fracture Toughness of Modified SA508C12 in the Ductile-to-Brittle Transition Region

REFERENCE: Miglin, M. T., Wade, C. S., Joyce, J. A., and Van Der Sluys, W. A., **"Dynamic Fracture Toughness of Modified SA508C12 in the Ductile-to-Brittle Transition Region,"** *Elastic-Plastic Fracture Test Methods: The User's Experience (Second Volume), ASTM STP 1114*, J. A. Joyce, Ed., American Society for Testing and Materials, Philadelphia, 1991, pp. 273–288.

ABSTRACT: Fracture toughness testing of steels in the ductile-to-brittle transition region is complicated by a high degree of data scatter. Variations in the amount of ductile tearing prior to cleavage initiation often accompany the data scatter. Dynamic toughness testing is shown to be experimentally successful at reducing the incidence of prior ductile tearing. For the displacement rates tested, dynamic toughness values are at or above the lower-bound static toughness. Analysis of transition region toughness data using Weibull statistics, available energy analysis, and a constraint correction procedure is discussed.

KEY WORDS: elastic-plastic fracture, test methods, fracture, cleavage, steels, pressure vessel steels, low-alloy steels, toughness, fracture toughness, ductile-brittle transition, ductile tearing

There is a great deal of scatter in fracture toughness data for ferrous materials tested in the ductile-to-brittle transition region. Data scatter for pressure vessel steels typically covers half an order of magnitude. Some scatter resulting from experimental error and specimen-to-specimen differences in metallurgical structure and specimen geometry is inherent to fracture testing. In addition, cleavage fracture data is scattered because cleavage nucleation sites have statistical spatial and strength distributions.

Pressure vessel steels tested in the transition region fail by cleavage or tearing alone, or by ductile tearing followed by cleavage failure. Variations in the amount of ductile tearing prior to cleavage failure contribute to the data scatter. Various analytical methods have been devised for dealing with data scatter [*1–8*]. No experimental methods for suppressing ductile tearing have been developed. This work represents the beginning of an investigation into the use of dynamic loading to promote cleavage initiation without prior ductile tearing.

It is important to suppress ductile tearing prior to cleavage in laboratory specimens. The structure to which the data are applied may not tear prior to cleavage because plasticity is constrained by material thickness or geometry. Thus, laboratory experiments may predict unrealistically high toughness values if tearing prior to cleavage cannot be suppressed.

Increasing the strain rate in fracture toughness tests of steels in the transition region decreases the measured toughness, as shown in Fig. 1 [*9*]. The dynamic toughness versus temperature curve is similar to the static toughness versus temperature curve, except that the dynamic curve is shifted to higher temperatures. The mechanisms underlying this shift

[1]Research specialist, group leader, and scientist, Babcock & Wilcox, Alliance, OH 44601.
[2]Professor of Mechanical Engineering, U.S. Naval Academy, Annapolis, MD 21402.

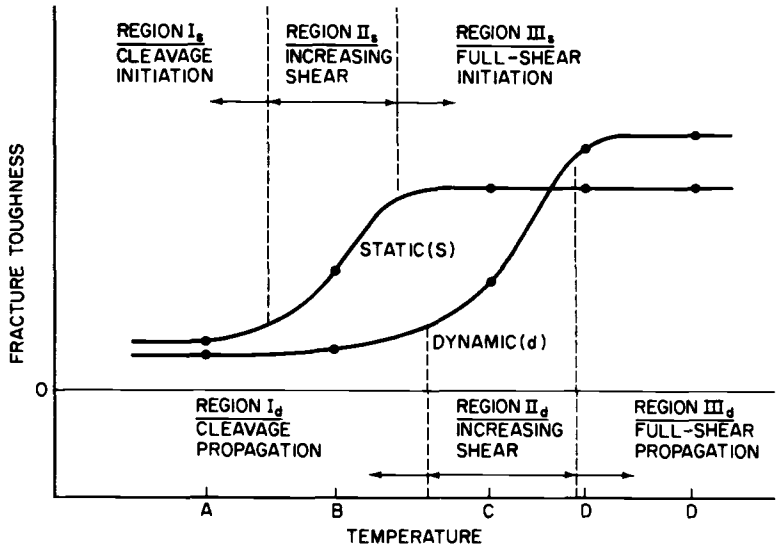

FIG. 1—*Schematic showing the relationship between static and dynamic fracture toughness* [9].

are not fully understood, although it is thought to result from an elevation of the flow properties by the increased strain rate. Various theoretical explanations of the role of strain rate in cleavage fracture have been presented in the literature [*10–14*]. Experimentally, elevation of applied strain rate in otherwise conventional toughness tests conducted in the transition region suppresses ductile tearing and promotes pure cleavage fracture [*12*].

Experimental Procedures

Test material was taken from a 20.3-cm-thick forged hollow cylinder of SA508C12 (Bethlehem Steel Heat No. 121S163) given a special heat treatment to produce mechanical properties typical of radiation-damaged material for the Pressurized Thermal Shock project of the Heavy-Section Steel Technology Program [*15*]. The static fracture toughness as a function of temperature for this material is shown in Fig. 2 [*16,17*]. Most of the data in Fig. 2 were collected for the Pressurized Thermal Shock project using 25.4-mm-thick (1*T*) compact specimens without side grooves. Ten of the 1*T* data points at 80°C (175°F) and the two 102-mm (4*T*) data points were obtained from static tests of side-grooved compact specimens in a program examining transition region data scatter [*17*]. All specimens were in the *C-R* orientation as described in ASTM Test Method for Plane-Strain Fracture Toughness of Metallic Materials (E 399-83), and were taken from the parent forging at various depths.

Dynamic fracture toughness tests were conducted at 80°C in a servohydraulic loading system capable of displacement rates up to 0.32 m/s. Compact fracture specimens in the *C-R* orientation, as described in ASTM E 399-83 or ASTM Test for J_{Ic}, a Measure of Fracture Toughness (E 813-87), were loaded using a slip grip fixture. The slip grip fixture allows the ram to move several centimetres before engaging to load the test specimen. In this way, the ram is traveling at its maximum attainable speed when specimen loading initiates. Eleven 1*T* and ten 12.5-mm-thick (1/2*T*) fatigue-precracked compact specimens were tested in this manner. The 1*T* specimens were precracked to a slightly greater depth than the 1/2*T* specimens because of concerns about exceeding the load capacity of the test machine. All specimens were side grooved to a depth of 10% of total thickness on each

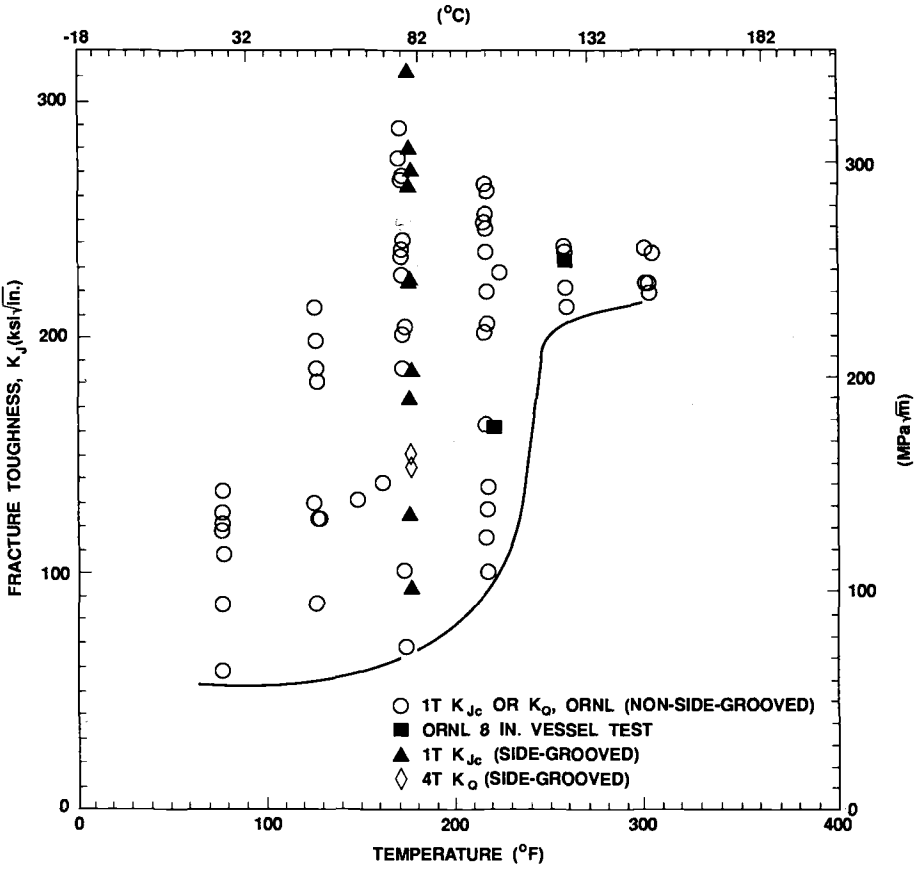

FIG. 2—*Static fracture toughness as a function of temperature for the modified SA508C12 steel used in this program* [16]. *Solid triangles indicate side-grooved* 1T *compact results from a previous program investigating data scatter* [17]. *Upper-shelf values are* K *calculated from* J_{Ic}.

side. Load and displacement data were recorded during testing using a digital transient recorder. Load was monitored using an in-line 89 KN load cell. Load-line displacement was monitored using a dual-beam displacement transducer mounted on knife edges in the crack mouth. The dynamic response of the system was checked to ensure that accurate load and displacement values were recorded.

Five dynamic tension tests were conducted at 80°C using the same test machine as for the compact fracture specimens. Round bar specimens with a 12.5-mm gage length and 2.8-mm diameter were tested according to ASTM Test Methods of Tension Testing of Metallic Materials (E 8-86). Specimens were oriented such that the fracture surface of the tensile bar is parallel to the crack plane of the compact fracture specimen. The displacement rate between the specimen grips was monitored using a single-beam displacement transducer and a digital transient recorder.

Additional dynamic fracture toughness tests were conducted at 80°C in a drop tower with a striker velocity of 2.5 m/s. Three-point bend specimens in the *C-R* orientation as described in ASTM E 399-83 or E 813-87 were tested in the facility shown in Fig. 3. The specimen is supported by flat-hardened anvils. Crossed wedge-shaped absorbers of annealed 5086 alu-

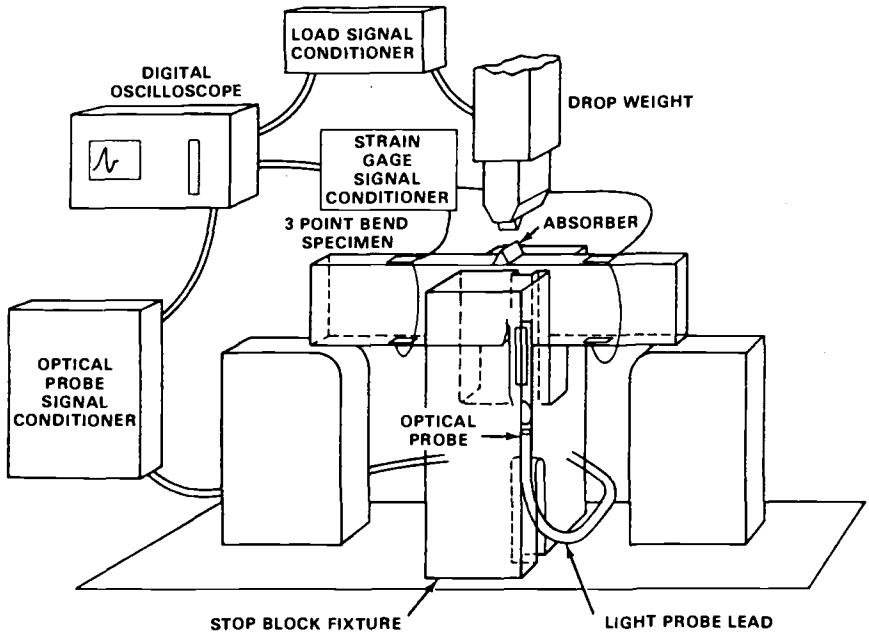

FIG. 3—*Experimental setup for drop tower tests* [18].

minum are used to eliminate surface contact shock, which produces oscillations in the load-versus-time record. Load is measured by a full bridge of strain gages mounted at the quarter-span positions on the specimen. Load-line displacement is measured using an optical probe. A detailed description of the test apparatus is provided in Ref *18*. Nine 1*T* three-point bend bars, fatigue precracked and side grooved by 10% of total thickness on each side, were tested in the drop tower facility.

Test Results

Tension Tests

Results of the dynamic tension tests are presented in Table 1. In all tests, the displacement rate was approximately 0.23 m/s up to the yield point. All specimens fractured by ductile void growth. At 80°C, the static yield strength is 590 MPa and the static ultimate strength is 756 MPa [*16*]. The dynamic values reported in Table 1 do not differ significantly from the static values.

Fracture Toughness Tests

Dynamic fracture toughness test results are given in Table 2 and shown graphically in Figs. 4 through 6. Figures 4 and 5 show typical load-displacement traces for dynamic tests performed in the servohydraulic and drop tower facilities, respectively.

Dynamic fracture toughness values were determined by calculating the fracture energy required to produce cleavage, J_c, and converting it to a critical stress intensity for cleavage, K_{Jc}, according to

$$K_{Jc} = (J_c E/(1 - \nu^2))^{1/2}$$

TABLE 1—*Results of dynamic tension tests at 80°C.*

Specimen Number	Yield Strength, MPa	Ultimate Strength, MPa	Reduction of Area, %
1	621	824	52
2	634	761	61
3	592	756	56
4	551	797	55
5	597	754	62

Fracture energy, J_c, was calculated according to ASTM Test Method for Determining *J-R* Curves (E 1152–87), except that it was not possible to calculate J incrementally because crack growth was not monitored during testing.

From Fig. 2, the lowest static toughness value for this material at 80°C is 75 MPa $\sqrt{m}$. Because 75 MPa $\sqrt{m}$ is the lowest of 24 1T toughness values and two 4T toughness values,

TABLE 2—*Results of dynamic fracture toughness tests at 80°C.*

Specimen Number	Initial a/W	K^a_{Jc}, MPa $\sqrt{m}$	Displacement Rate at Cleavage, m/s	$\dot{K}$, MPa $\sqrt{m}$/s	K_{AE}, MPa $\sqrt{m}$
			1T COMPACT SPECIMENS		
1	0.64	118	0.12	1.8×10^4	109
2	0.64	225	0.11	1.9×10^4	146
3	0.63	75	0.06	1.9×10^4	75
4	0.63	273	0.14	2.0×10^4	149
5	0.63	258	0.14	1.9×10^4	149
6	0.64	88	0.06	1.7×10^4	88
7	0.63	101	0.11	1.7×10^4	101
8	0.63	101	0.09	1.9×10^4	97
9	0.62	296	0.14	1.9×10^4	150
10	0.62	157	0.09	1.8×10^4	128
11	0.62	189	0.11	2.0×10^4	137
			1/2T COMPACT SPECIMENS		
1	0.54	96	0.10	2.3×10^4	93
2	0.55	288	0.23	5.0×10^4	90
3	0.55	266	0.16	5.3×10^4	98
4	0.52	167	0.11	3.0×10^4	120
5	0.55	242	0.27	4.8×10^4	129
6	0.52	348	0.25	3.5×10^4	131
7	0.52	317	0.23	3.6×10^4	130
8	0.53	98	0.08	2.8×10^4	86
9	0.56	363	0.32	3.4×10^4	127
10	0.54	168	0.12	3.1×10^4	111
			1T THREE-POINT BEND SPECIMENS		
1	0.58	133	0.49	7.27×10^4	110
2	0.58	201	0.51	6.88×10^4	160
3	0.59	138	0.44	6.76×10^4	124
4	0.58	189	0.60	7.56×10^4	152
5	0.58	214	0.59	6.92×10^4	158
6	0.59	231	0.66	7.70×10^4	173
7	0.58	143	0.61	5.84×10^4	129
8	0.59	276	0.79	7.95×10^4	175

[a] K calculated from J at cleavage.

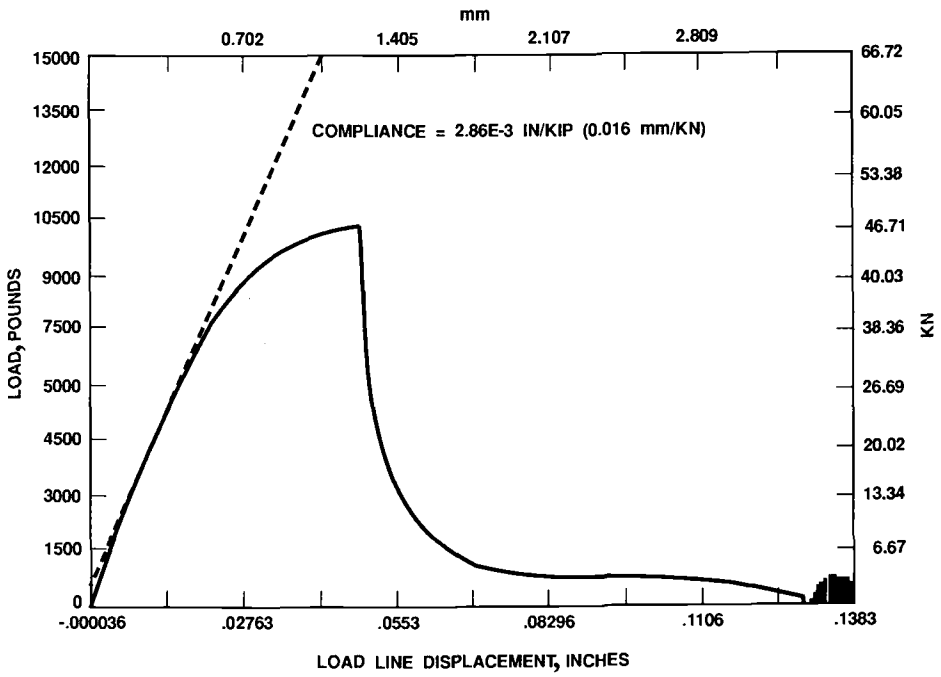

FIG. 4—*Load versus load-line displacement for a typical dynamic* 1T*CT test. The dashed line represents the theoretical compliance of the specimen.*

it is a good estimate of the lower-bound static toughness of this material at 80°C, and is indicated by the horizontal line in Fig. 6. Also shown in Fig. 6 are static data from Fig. 2 obtained with side-grooved 1*T* compact specimens, and additional dynamic three-point bend data [*19*], which are discussed later.

Also shown in Table 2 are testing rate data presented as the load-line displacement rate at cleavage and $\dot{K}$, the time rate of change in applied stress intensity. The displacement rate at cleavage is determined by measuring the slope of the displacement versus time plot in the latter half of the test, where the slope is usually constant. The value of $\dot{K}$ is determined according to ASTM E 399-83, Appendix 7.

From Fig. 6, it is apparent that the effects of increasing displacement rate are sensitive to specimen size and geometry. Data for 1*T* compact specimens show that increasing displacement rate from 2×10^{-5} to 0.11 m/s increases the fraction of specimens that cleave with no prior ductile tearing from 20 to 45%. There is only a slight reduction in data scatter.

Comparison of the 1*T* and 1/2*T* compact specimen data shows higher measured toughness and more data scatter for the 1/2*T* specimens, although the average displacement rate for the 1/2*T* specimens, at 0.19 m/s, is almost twice the average displacement rate for the 1*T* specimens.

Comparison of the dynamic 1*T* three-point bend results and the compact specimen results shows less data scatter for the three-point bend specimens, and a greater percentage (88%) of specimens that cleaved with no prior ductile tearing. The average displacement rate for the three-point bend specimens is 0.59 m/s. Unexpectedly, the three-point bend specimens also produced a higher mean toughness value than the 1*T* compact specimens, although the compact specimens were tested at a lower displacement rate.

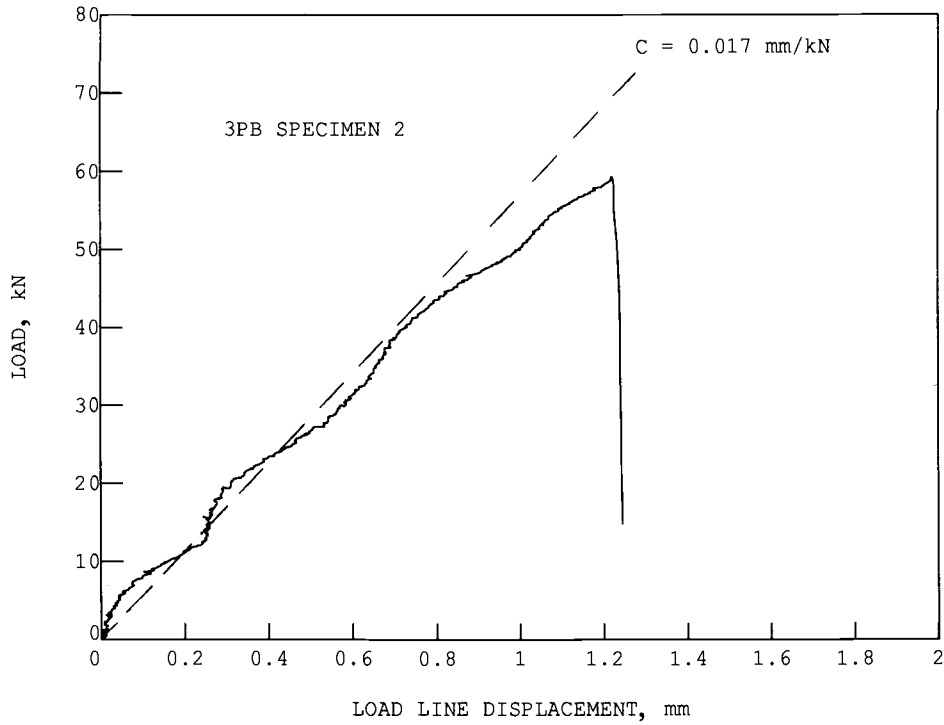

FIG. 5—*Load versus load-line displacement for a typical* 1T *three-point bend test. The dashed line represents the theoretical compliance of the specimen.*

Also shown in Fig. 6 are data for 19 1*T* three-point bend specimens without side grooves tested in another drop tower facility [*19*] at 1.7 m/s. All but one of these specimens (95%) cleaved with no prior ductile tearing. The K_{Jc} values for these specimens are higher than for the side-grooved three-point bend specimens tested at 0.59 m/s. The absence of side grooves may delay the onset of crack initiation, resulting in higher toughness values.

Data Analysis

Available Energy Analysis

The available energy method developed by Rosenfield and Shetty [*4*] is based on Seidl's [*20*] assumption that a cleavage crack is driven by the elastic energy stored in the specimen. The available energy method uses the load and crack length at the onset of cleavage fracture to calculate a K_{Ic} value, in a manner identical to the calculation of K_{el} in ASTM E 1152-87. The energy expended in crack tip blunting and ductile tearing is not included in the fracture toughness calculation; only the elastic energy expended in cleavage fracture contributes to K_{Ic}. Figure 7 presents fracture toughness values for the specimens listed in Table 2 calculated according to the available energy method, designated K_{AE}. Also illustrated are the corresponding ranges in K_{Jc} values. It is apparent that the scatter in K_{AE} values is less than the scatter in K_{Jc} values. Calculating toughness as K_{AE} does not change the lowest toughness value for the two data sets obtained with 1*T* compact specimens. However, calculating toughness by the available energy method reduces the lowest toughness value for the data sets obtained with 1/2*T* compact and 1*T* three-point bend specimens.

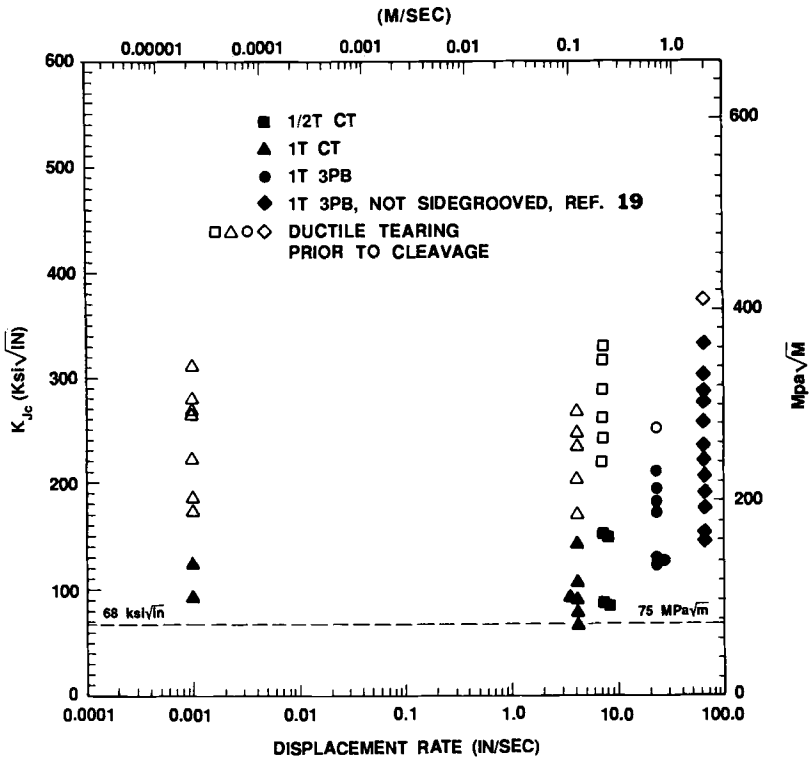

FIG. 6—*Results of dynamic fracture toughness tests plus 10 static side-grooved* 1T *compact results from Fig. 2 (data at left). The dashed line indicates the lowest measured static toughness value at 80°C for this material from Fig. 2.*

Weibull Analysis

Weibull statistics are used for modeling processes governed by a weakest link phenomenon. Landes and Shaffer [*1*] proposed the use of Weibull statistics to model cleavage behavior, assuming that cleavage initiates at a weak point in the material lying ahead of the fatigue precrack. Wallin et al. [*21*] developed a theoretical argument predicting a Weibull slope of four for large cleavage fracture data sets, but demonstrated that data sets with approximately 10 data points could have slopes ranging from 2 to 9.

The results of Weibull analysis of fracture toughness data are given in Table 3 and Fig. 8. Comparison of the Weibull results in Table 3 shows that the static 1*T* compact data and dynamic 1*T* three-point bend (3PB) data provide the best Weibull fits, with R^2 (goodness of fit) values of 95 and 94%, respectively. Both of these data sets have Weibull slopes of approximately 4, the theoretically predicted value [*21*]. The dynamic 1*T* and 1/2*T* compact data do not fit the Weibull distribution as well, with R^2 values of 91 and 92%, respectively, and Weibull slopes of 2.4 and 2.9.

The results of Weibull analysis of the K_{AE} data are shown in Table 3. For all four K_{AE} data sets, the values of R^2 are lower than for the corresponding K_{Jc} data sets, and the slopes are steeper than the theoretically predicted value of 4.

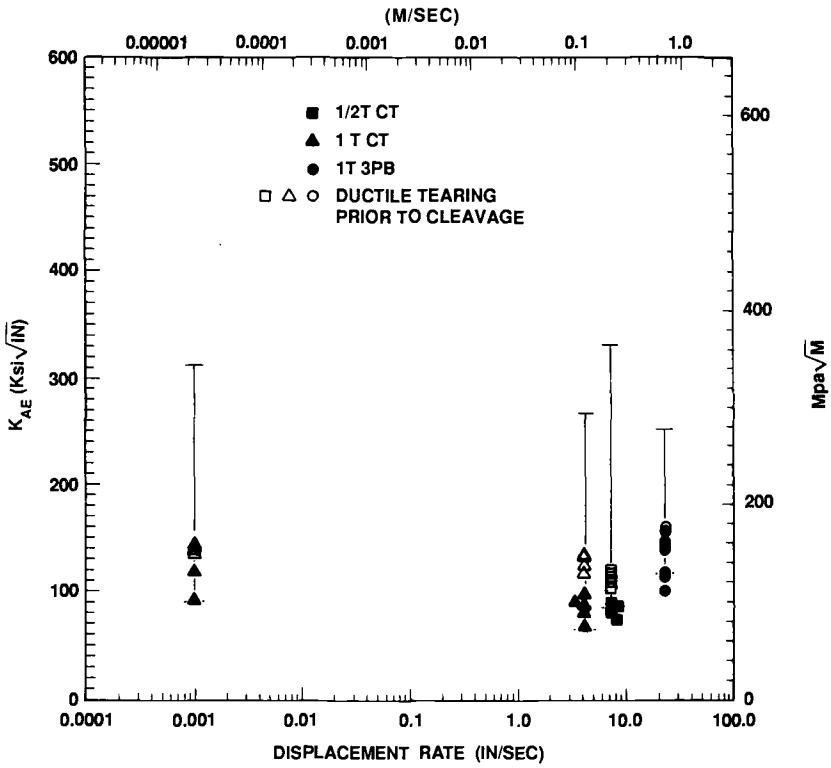

FIG. 7—*Available energy calculations for fracture toughness data shown in Fig. 6. Solid lines indicate range of* K_{Jc} *data from Fig. 6.*

Discussion

The preceding work was designed to test the effectiveness of using dynamic toughness testing to suppress ductile tearing, reduce data scatter, and predict the lower-bound static toughness in the transition region. In the process, several interesting observations were made regarding specimen geometry and data analysis techniques.

Dynamic Toughness Data Scatter

While some of the data scatter observed in the transition region results from ductile tearing prior to cleavage initiation, the present data set also includes some scatter because the test material was taken at various depths within the parent forging. Static fracture toughness varies by approximately 47 MPa $\sqrt{m}$ from the outside diameter (OD) to the inside diameter (ID) of the cylinder [*16*]. Given that the static fracture toughness values at 80°C exhibit a range of 270 MPa $\sqrt{m}$, forging inhomogeneities are a secondary cause of data scatter.

Increasing testing speed appears to be an effective means of suppressing ductile tearing. Comparison of the static and dynamic compact results shown in Fig. 6 shows only a slight decrease in data scatter at the higher rates, which is not surprising because the dynamic tensile results are so close to static results. However, the fraction of specimens that cleave

without prior tearing is more than doubled. Also, the lower bound for the dynamic tests approaches, but does not go below, the lower bound for static data. This is important if dynamic testing is to be used as a means of predicting the static lower bound.

In the transition region, increasing test speed is more effective at suppressing ductile tearing prior to cleavage than decreasing data scatter. It appears that increasing test speed suppresses tearing by raising the resistance to tearing initiation, J_{Ic}; Fig. 1 shows that dynamic testing raises upper-shelf fracture toughness. Suppressing tearing may be useful, however, because existing analytical methods for dealing with data scatter are largely limited to specimens that do not exhibit ductile tearing prior to cleavage [*17*].

The data in Fig. 6 show an apparent increase in toughness with increasing test speed. For the 1/2*T* compact specimens, this may be a result of decreased crack tip constraint in the thinner specimen. Also, the 1/2*T*CT specimens had a slightly smaller *a*/*W* ratio than the dynamic 1*T*CT and three-point bend specimens. The reason for the higher toughness in the 1*T* three-point bend specimens is unclear. Figures 4 and 5 show that the measured and theoretical compliance are in good agreement for both geometries, and no other experimental reasons for the higher toughness of the three-point bends is apparent. It is possible that it is related to the differences observed between bends and compacts when performing J_{IR} tests on the upper shelf of the toughness-temperature curve.

Available Energy Analysis

It is apparent from Fig. 7 that the available energy method is very effective in reducing data scatter. It brings the dynamic toughness values closer to the static lower bound without depressing them below this value.

Calculating toughness as K_{AE} (or K_{el}) eliminates plasticity contributions to the fracture toughness. However, the K_{AE} values obtained with compact and bend specimens are not directly comparable. For a bend specimen and a compact specimen with identical K_{Jc} values, the compact specimen will have a lower K_{el} value. This was observed for three pairs of compact and bend specimens with nearly identical K_{Jc} values taken from Table 2. This same conclusion can be reached analytically using the expressions in ASTM E 1152-87.

Weibull Analysis

While dynamic testing increases the fraction of specimens that cleave with no prior tearing, the data for specimens with no tearing vary widely, from 75 to 231 MPa $\sqrt{m}$. Therefore, some type of statistical data analysis may be necessary to characterize transition region toughness, even if only cleaved specimens are included.

TABLE 3—*Results of two-parameter Weibull analysis for* K_{Jc} *and* K_{AE} *data.*

	Sample Size	Slope	R^2
	K_{Jc}		
Static 1*T*CT	10	3.8	95%
Dynamic 1*T*CT	11	2.4	91%
Dynamic 1/2*T*CT	10	2.9	92%
Dynamic 3PB	8	4.4	94%
	K_{AE}		
Static 1*T*CT	10	15.3	76%
Dynamic 1*T*CT	11	5.6	87%
Dynamic 1/2*T*CT	10	7.9	84%
Dynamic 3PB	8	8.2	90%

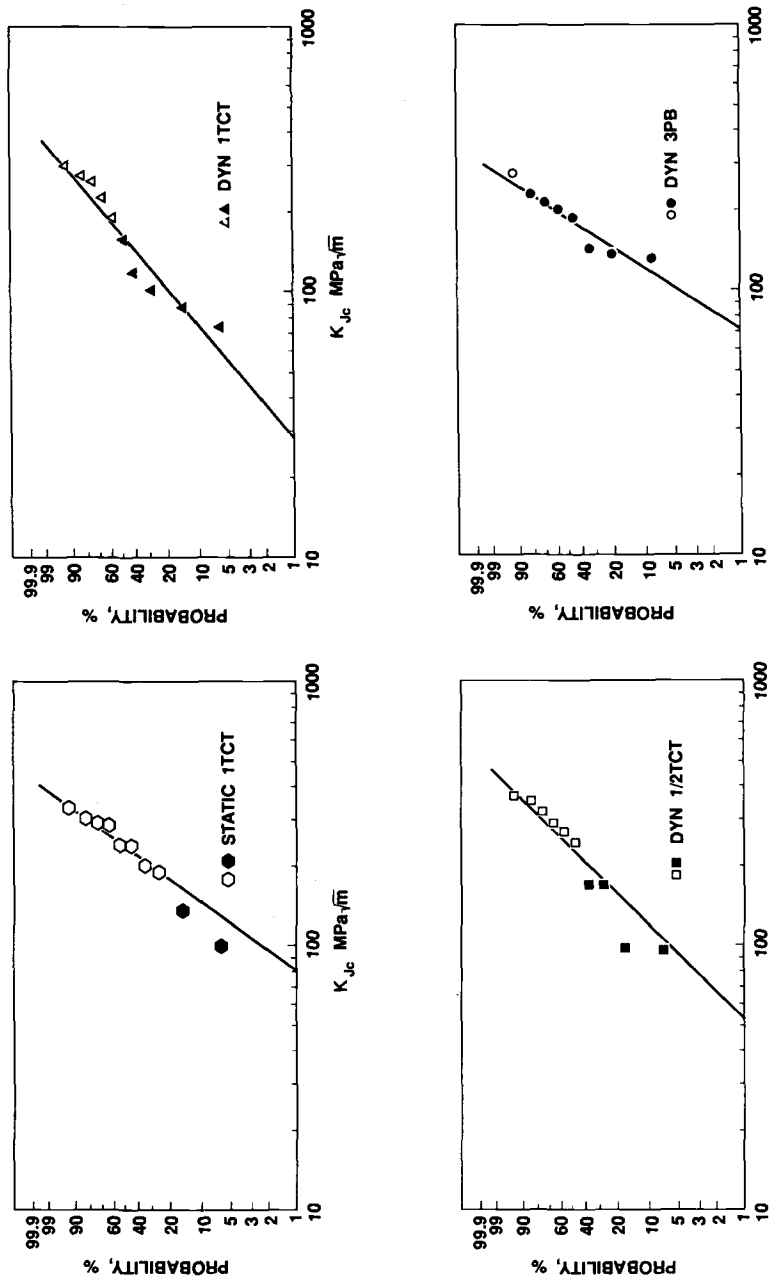

FIG. 8—*Weibull probability plots of fracture toughness for* (a) *static* 1T*CT specimens,* (b) *dynamic* 1T*CT specimens,* (c) *dynamic* 1/2T*CT specimens, and* (d) *dynamic three-point bend specimens. Open symbols indicate specimens that tore prior to cleavage initiation.*

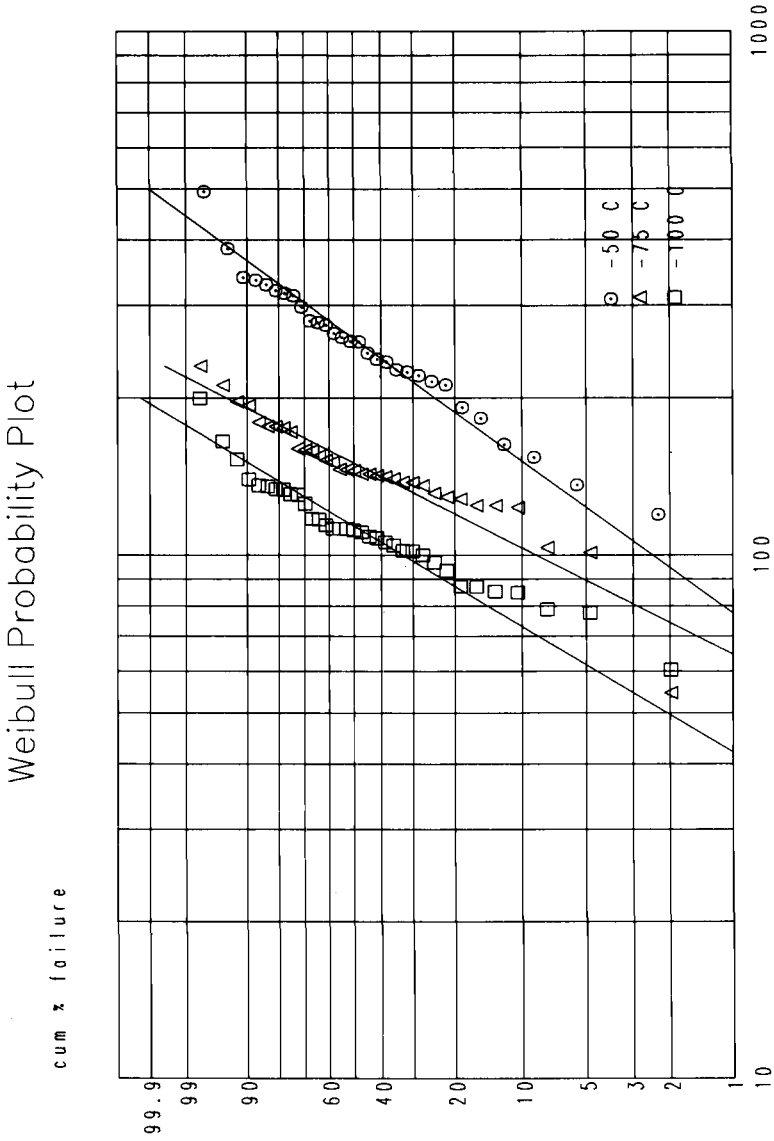

FIG. 9—*Weibull probability plot of K_{Jc} data from a round-robin test program using SA508C13* [22].

Weibull analysis has been used widely for analyzing static cleavage fracture toughness data. However, the Weibull distribution tends to fit fracture data poorly at the low-toughness end of the distribution, as shown for three large data sets in Fig. 9 [*22*]. The data in Fig. 9 are preliminary results of a round-robin testing program using SA508C13. All of the specimens tested at −100 and −75°C had no ductile tearing, yet the Weibull plot is not linear. Wallin [*23*] attributes the nonlinearity to the use of the two-parameter Weibull distribution, which assumes that the minimum possible toughness is zero, a physical impossibility. Wallin begins with a three-parameter Weibull distribution, defines the minimum toughness as 20 MPa $\sqrt{m}$, and sets the slope equal to 4. This improves the linearity, as shown in Fig. 10.

As a descriptor of weakest-link phenomena, one would expect the Weibull distribution to fit dynamic data better than static data, because complications due to plasticity have been minimized. Using the two-parameter Weibull distribution, this is not the case. Using the three-parameter Weibull distribution with slope equal to 4 and minimum toughness equal to 20 MPa$\sqrt{m}$ improves the fit for both the static and dynamic data (see Table 4). The R^2 values for the two-parameter Weibull fit range from 91 to 95%, while the R^2 values for the modified three-parameter Weibull fit range from 94 to 99%.

The applicability of Weibull analysis to K_{AE} data is questionable. The R^2 values are lower than for static or dynamic K_{Jc} data, and the slopes are steeper than the theoretically predicted value of 4, ranging from 5.6 to 15.3.

Constraint Correction

Another means of addressing transition region data scatter has been proposed by Dodds and Anderson [*24*]. Limited to specimens with no tearing prior to cleavage, it corrects the

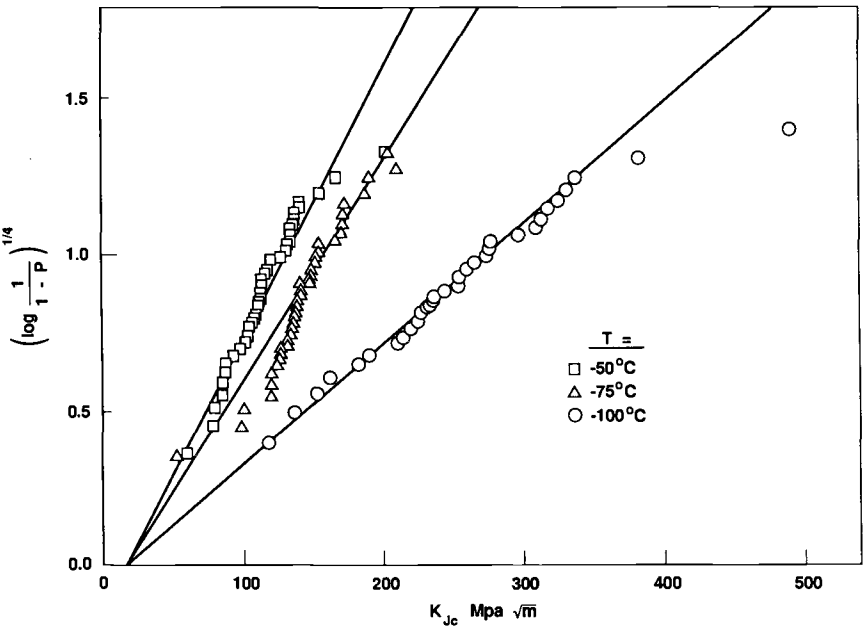

FIG. 10—*Round-robin test data from Fig. 9 analyzed using a three-parameter Weibull function with the slope defined as 4 and the minimum toughness defined as 20 MPa* $\sqrt{m}$. *The* y*-axis is a linearization of the Weibull probability,* P.

TABLE 4—*Results of three-parameter Weibull analysis.*[a]

K_{Jc}	Sample Size	Slope[a]	R^2
Static 1*T*CT	10	4	99%
Dynamic 1*T*CT	11	4	94%
Dynamic 1/2*T*CT	10	4	97%
Dynamic 3PB	8	4	99%

[a]The value of the slope is defined as 4 and the minimum toughness as 20 MPa $\sqrt{m}$.

measured toughness for large-scale yielding by comparing the stress distribution ahead of the crack tip for elastic and elastic-plastic cases. High resolution two-dimensional plane-strain finite element models scale the applied loading to give matching contours of S_{yy}, the stress normal to the crack plane, between small-scale yielding and large-scale yielding. The large-scale yielding J is plotted versus the equivalent J for small-scale yielding for several values of work-hardening exponent, n, and a/W, crack length-to-width ratio. These plots are used to convert experimental values of J to equivalent small-scale yielding values. The constraint-corrected data are shown in Fig. 11. The reduction in data scatter is greater for the 1/2*T* compact and 1*T* three-point bend specimens than for the 1*T* compact specimens.

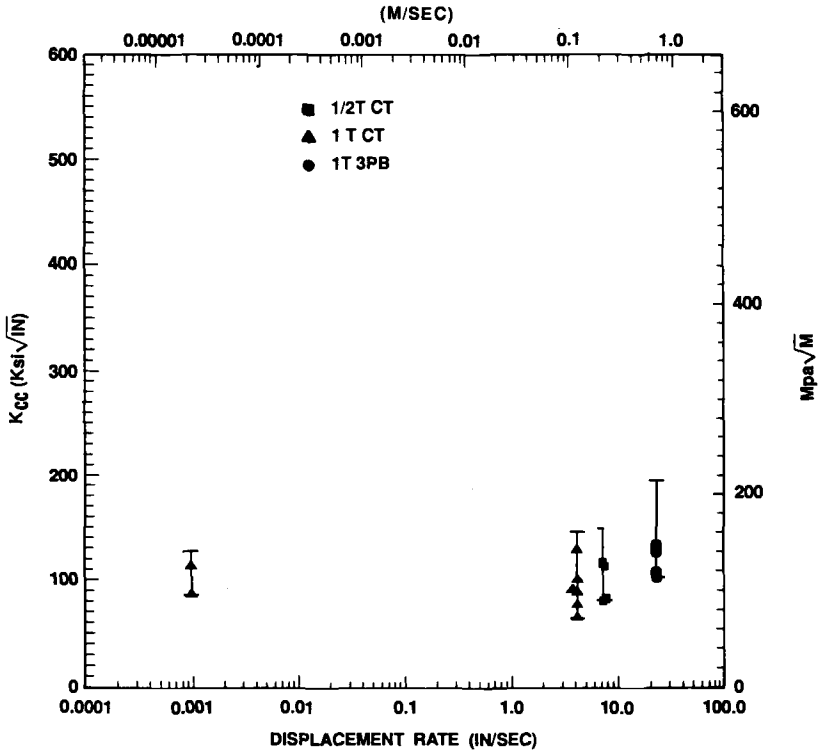

FIG. 11—*Constraint-corrected toughness values for fracture toughness data indicated by solid symbols in Fig. 6.*

The constraint-correction procedure does not depress any of the data below the static lower-bound value of 75 MPa $\sqrt{m}$.

In addition to available energy analysis, Weibull analysis, and constraint correction, there are other methods of treating transition region data scatter [*17*]. Most of these methods are recommended only for specimens that do not tear prior to cleavage. Recently, Wallin [*23*] developed a method for correcting for tearing prior to cleavage. Anderson and Stienstra [*25*] have proposed the use of order statistics, which allows data from specimens with tearing to be censored but included in the analysis. The objective of the present work is to develop the alternative of conducting dynamic tests to suppress ductile tearing, and applying one of the analysis methods that does not permit tearing. Further work in this area will be directed toward increasing testing speed using compact specimens, and selection of an analytical method for reducing data scatter that is applicable to dynamic fracture data. Additionally, fractographic examination will be performed to determine the influence of increased strain rates on the microdeformation and microfailure mechanisms.

Conclusions

Based on the findings in this report, the following conclusions can be drawn.

1. Increasing strain rate in transition-region fracture toughness tests of modified SA508C12 increases the fraction of specimens that cleave with no prior ductile tearing.
2. Dynamic toughness values are equal to or greater than the lower bound static toughness value for modified SA508C12 tested at 80°C at displacement rates up to 0.59 m/s.
3. Calculating dynamic toughness by the available energy method did not reduce dynamic toughness values below the lower bound for static data.
4. The two-parameter Weibull distribution provides a good fit for static compact data with a Weibull slope close to the theoretical value of 4. Dynamic compact data do not fit the distribution as well, and available energy corrected data fit worse than dynamic data. Using a three-parameter Weibull distribution with the slope set equal to four and the minimum toughness equal to 20 MPa$\sqrt{m}$ improves the goodness of fit for both static and dynamic data.
5. A recently-developed constraint correction procedure reduces data scatter for specimens with no prior tearing, which exceed the limitations of small-scale yielding. Constraint correction of static and dynamic data did not depress the values below the lower bound for uncorrected static data.

Acknowledgments

The authors would like to acknowledge the assistance of Mr. B. A. James with data analysis, and Ms. L. A. Oberjohn with statistical analysis. Helpful discussions with Prof. T. L. Anderson and Dr. K. Wallin are greatly appreciated. This work was performed under the sponsorship of the Nuclear Power Division and Nuclear Equipment Division of Babcock & Wilcox, a McDermott company.

References

[*1*] Landes, J. D. and Shaffer, G. H., "Statistical Characterization of Fracture in the Transition Region," *Fracture Mechanics (Twelfth Conference), ASTM STP 700*, American Society for Testing and Materials, Philadelphia, 1980, pp. 368–382.

[*2*] Iwadate, T., Tanaka, Y., Ono, S., and Watanabe, J., "An Analysis of Elastic-Plastic Fracture Toughness Behavior for J_{Ic} Measurement in the Transition Region," *Elastic-Plastic Fracture: Sec-*

ond Symposium, Volume II: Fracture Curves and Engineering Applications, ASTM STP 803, C. F. Shih and J. P. Gudas, Eds., American Society for Testing and Materials, Philadelphia, 1983, pp. II–531–561.

[3] Merkle, J. G., "Evaluations of the Irwin $Beta_{I_c}$ Adjustment for Small Specimen Fracture Toughness Data," *Nuclear Engineering and Design*, Vol. 86, No. 1, April 1985, pp. 111–117.

[4] Rosenfield, A. R. and Shetty, D. K., "Cleavage Fracture of Steel in the Upper Ductile-Brittle Transition Region," *Engineering Fracture Mechanics*, Vol. 17, No. 5, 1983, pp. 461–470.

[5] Watanabe, J., Iwadate, T., Tanaka, Y., Yokobori, T., and Ando, K., "Fracture Toughness in the Transition Region," *Engineering Fracture Mechanics*, Vol. 23, No. 5/6, 1987, pp. 589–600.

[6] Anderson, T. L., "A Combined Statistical/Constraint Model for the Ductile-Brittle Transition Region," *Proceedings*, Third National Symposium on Nonlinear Fracture Mechanics, 6–8 Oct. Knoxville, TN.

[7] Doig, P., "Evaluation of Lower-Bound Fracture Toughness Values using Weibull Analysis of Single Specimen Data," *Engineering Fracture Mechanics*, Vol. 21, No. 5, 1985, pp. 963–987.

[8] Macdonald, B. D., Oberdick, R. H., and Hiser, A. L., Jr., this publication, pp. 102–113.

[9] Barsom, J. M. and Rolfe, S. T., *Fracture and Fatigue Control in Structures: Applications of Fracture Mechanics*, 2nd ed., Prentice-Hall, Inc., Englewood Cliffs, NJ, 1987, p. 133.

[10] Freund, L. B. and Hutchinson, J. W., "High Strain-Rate Crack Growth in Rate Dependent Plastic Solids," *Journal of Mechanics and Physics of Solids*, Vol. 33, No. 2, 1985, pp. 169–191.

[11] Argon, A. S., "Brittle-to-Ductile Transition in Cleavage Fracture," *Acta Metallurgica*, Vol. 35, No. 1, 1987, pp. 185–196.

[12] Irwin, G. R., "Brittle-Ductile Transition Behavior in Reactor Vessel Steels," Report No. NUREG/CP-0082-Vol. 2; CONF-8610135-Vol. 2, Nuclear Regulatory Commission, Washington, DC, Feb. 1987, pp. 251–272.

[13] Kameda, J., "A Kinetic Model for Ductile-Brittle Fracture Mode Transition Behavior," *Acta Metallurgica*, Vol. 34, No. 12, 1986, pp. 2391–2398.

[14] Jokl, M. L., Vitek, V., and McMahon, C. J., Jr., "On the Micromechanics of Brittle Fracture: Existing vs. Injected Cracks," *Acta Metallurgica*, Vol. 37, No. 1, 1989, pp. 87–97.

[15] Bryan, R. H., et al. "Pressurized-Thermal-Shock Test of 6-in.-Thick Pressure Vessels. PTSE-1: Investigation of Warm Prestressing and Upper-Shelf Arrest," ORNL Report No. 6135, NUREG CR-4106, Nuclear Regulatory Commission, 1985.

[16] Domian, H. A., "Vessel V-7 and V-8 Repair and Characterization of Insert Material," ORNL Report No. 82- 52845-1, NUREG CR-3771, Nuclear Regulatory Commission, 1984.

[17] Miglin, M. T., Wade, C. S., and Van Der Sluys, W. A., "Analysis of Fracture Toughness Data for Modified SA508C12 in the Ductile-to-Brittle Transition Region," *Fracture Mechanics: Twenty-First Symposium, ASTM STP 1074*, J. P. Gudas, J. A. Joyce, and E. M. Hackett, Eds., American Society for Testing and Materials, Philadelphia, 1990, pp. 238–263.

[18] Joyce, J. A. and Hackett, E. M., "An Advanced Procedure for *J-R* Curve Testing Using a Drop Tower," *Nonlinear Fracture Mechanics, Volume I: Time Dependent Fracture, ASTM STP 995*, A. Saxena, J. D. Landes, and J. L. Bassani, Eds., American Society for Testing and Materials, Philadelphia, 1989, pp. 298–317.

[19] Hahn, M. T., Report No. CR-88-1026, General Research Corp., 18 April 1988.

[20] Seidl, W., "Specimen Size Effects on the Determination of K_{IC} Values in the Range of Elastic-Plastic Material Behavior," *Engineering Fracture Mechanics*, Vol. 12, 1979, pp. 581–597.

[21] Walllin, K., Saario, T., and Torronen, K., "Theoretical Scatter in Brittle Fracture Toughness Results Described by the Weibull Distribution," *Application of Fracture Mechanics to Materials and Structures*, Martinus Nijhoff, Netherlands, 1984, pp. 511–518.

[22] Data obtained through a round-robin testing program organized by the Japan Society for the Promotion of Science and the Metals Property Council (MPC), courtesy of Dr. M. Praeger of the MPC.

[23] Wallin, K., "Statistical Modelling of Fracture in the Ductile to Brittle Transition Region," *Proceedings*, European Symposium on Elastic-Plastic Fracture Mechanics: Elements of Defect Assessment, 9–12 Oct. 1989, Freiburg, Germany (in press).

[24] Anderson, T. L. and Dodds, R. H., Jr., "Specimen Size Requirements for Fracture Toughness Testing in the Transition Region," *Journal of Testing and Evaluation*, Vol. 19, No. 2, March 1991, pp. 123–124.

[25] Anderson, T. L. and Stienstra, D., "A Model to Predict the Sources and Magnitude of Scatter in Toughness Data in the Transition Region," *Journal of Testing and Evaluation*, Vol. 17, No. 1, Jan. 1989, pp. 46–53.

DISCUSSION

B. Mukherjee[1] *(written discussion)*—What was the reason for choosing J at failure load as the fracture parameter for examining data scatter in the transition region?

If a specimen fails in the rising part of the load displacement curve, then it can be argued that J at that load is material dependent. However, if a specimen fails beyond the maximum load, then J at failure load may be dependent on the specimen geometry as well. In view of this, will the authors comment on the scatter of their data if only results for those specimens that failed before reaching maximum load were considered.

Similarly, if J at crack initiation was selected as the fracture parameter for examining data scatter in the transition region, will it alter some of the observations presented in this paper? Perhaps it is necessary to examine both J at crack initiation and at maximum load to get a complete picture of scatter in this region.

M. T. Miglin, C. S. Wade, W. A. Van Der Sluys, and J. A. Joyce (authors' closure)—J at failure load was chosen as the parameter to describe transition-region data scatter because it corresponds to J at the onset of cleavage fracture. The objective of this work is to achieve a means of conservatively estimating the lower-bound toughness in the transition region, and the fracture mechanism for specimens that fail near the lower bound is cleavage. Therefore, a measure of cleavage resistance is required.

All of the dynamic three-point bend specimens failed before reaching the maximum load. Four of the dynamic compact specimens, one $1T$ and three $1/2T$ specimens, failed by cleavage slightly beyond maximum load. Cleavage occurred so soon after maximum load that the associated loss of constraint and effect on measured J is assumed to be slight. Four of the static $1T$ specimens failed by cleavage well beyond maximum load. For these four specimens, the measured J value is probably elevated to some extent because of the associated reduction in constraint.

A previous paper examined J at crack initiation.[2] Crack initiation occurs by ductile tearing in most of these specimens. At present, there is no known relationship between tearing resistance and cleavage resistance, and it is our objective to determine a conservative method for measuring cleavage resistance. Therefore, J at crack initiation is not relevant. J at maximum load is the J value when the plastic zone is first influenced by the back free surface of the specimen. This also bears no relationship to cleavage resistance and was hence disregarded in the current work.

[1]Ontario Hydro Research, Toronto, Ontario, Canada M8Z 5S4.

[2]Miglin, M. T., Wade, C. S., and Van Der Sluys, W. A., "Analysis of Fracture Toughness Data for SA508C12 in the Ductile-to-Brittle Transition Region," *Fracture Mechanics: Twenty-First Symposium, ASTM STP 1074*, J. P. Gudas, J. A. Joyce, and E. M. Hackett, Eds., American Society for Testing and Materials, Philadelphia, 1990, pp. 238–263.

Donald D. Huang[1]

The Application of the Multispecimen *J*-Integral Technique to Toughened Polymers

REFERENCE: Huang, D. D., **"The Application of the Multispecimen *J*-Integral Technique to Toughened Polymers,"** *Elastic-Plastic Fracture Test Methods: The User's Experience (Second Volume), ASTM STP 1114*, J. A. Joyce, Ed., American Society for Testing and Materials, Philadelphia, 1991, pp. 290–305.

ABSTRACT: The multispecimen *J*-integral technique ASTM Test Method for J_{Ic}, a Measure of Fracture Toughness (E 813–87) has been applied to a series of rubber-toughened polymers to determine the generality of the method for polymeric materials. The experimental procedures produce results that are similar in form with those found in the metals and ceramics literature. However, many of the procedures involving data analysis require reexamination.

In this study, the effects of side grooves, ligament depths, and the relationship between critical initiation *J* and *G* values are examined. The use of side-grooved specimens for *J* testing is a viable way of experimentally verifying plane strain conditions. The ASTM E 813–87 recommendation for the allowable range of ligament depths appears to be inappropriate for toughened polymers. However, the recommendation of $W/B = 2$ as an experimental starting point is sensible. Finally, the J_{Ic} to G_c relationship was explored. In separate, nonstandard *K* tests involving large specimens, the initiation point, G_c, was defined at 2.5% crack growth. J_{Ic}, as calculated by the ASTM E 813–87 construction, was as much as 50% lower than this G_c value. However, when comparing critical *J* and *G* values for specific crack growths, good agreement between the two tests was obtained, provided the crack growth was small. Although the current J_{Ic} construction provides a conservative estimate of the G_c value, it is an open question whether the J_{Ic} value is appropriate for polymer design.

KEY WORDS: multiple specimens, *J*-integral, toughened polymers, ligament depth, elastic-plastic fracture, test methods

Although linear elastic fracture mechanics (LEFM) techniques have been successfully applied to many neat and reinforced polymers [*1*], they are often inadequate for fracture toughness characterization of toughened polymers. These polymer systems are typically multiphase systems in which the optimal toughener particle size is on the order of microns or less. During fabrication of large parts, the toughener can agglomerate, leading to a morphology that is not representative of smaller parts. Consequently, the *J*-integral as proposed by Rice [*2*] is finding increasing use as a characterization parameter for fracture toughness of these materials since significantly smaller specimens may be used. The *J*-integral technique has been applied to a variety of tough polymers including rubber-toughened polymers [*3–10*] and untoughened polymers [*11,12*].

Because there is no current standard for *J*-integral testing of polymers, much of the earlier work has followed some form of ASTM Test Method for J_{Ic}, a Measure of Fracture Toughness (E 813). For example, Refs *3*, and *8* through *10* followed the ASTM E 813–81 method

[1]Group leader, Polymer Products Department, E. I. du Pont de Nemours, Inc., Wilmington, DE 19880-0323.

while Refs 5 through 7, 11, and 12 have applied the ASTM E 813–87 method. While the form of the results in these studies have been consistent with results found in the metals literature, it is still unclear whether the technique can be directly applied to obtain meaningful fracture toughness values in polymers.

The primary differences between ASTM E 813–81 and E 813–87 lie in the data analysis and selection of the initiation value, J_{Ic}. In ASTM E 813–81, the experimental data in the form of a resistance (*J-R*) curve is approximated as a bilinear function. The first line describes the blunting behavior of the material. It is defined as

$$J = 2\,\sigma_y \Delta a$$

where σ_y is determined in a separate tension test on Δa is crack growth. The second line is experimentally determined during the *J* test. The intersection of the two lines represents J_c.

In ASTM E 813–87, the *J-R* curve is experimentally determined and fitted with a power law, $J = C_1\,\Delta a^{C_2}$ where C_1 and C_2 are fitting parameters. J_c has been redefined to be equal to the *J* value at which 0.2 mm of crack growth has occurred. Consequently, J_c is determined by the intersection of the power law fit to the experimental data and a line of Slope $2\sigma_y$ that intersects the abcissa at 0.2 mm.

Both versions of the multispecimen methods of ASTM E 813 have been applied to two rubber-toughened nylons [3–7]. In Ref 3, a modified form of ASTM E 813–81 was used to characterize these polymers using small single-edge-notched bend (SENB) specimens that were 12.7 mm thick. The values of J_c were reported as plane strain values because the specimen sizes either met or were slightly larger than the ASTM recommendation. Additional tests on side-grooved specimens and on ungrooved specimens tested at slightly lower temperatures, produced similar J_c values, thus supporting the notion of a plane strain value [4].

The plane strain assumption was further tested using smaller ungrooved specimens [5] of the two rubber-toughened nylons. *J* tests were conducted on geometrically similar SENB specimens down to thicknesses of 3.2 mm using the ASTM E 813–81 technique. However, a surprising trend of decreasing J_c versus decreasing thickness was found for both materials [5].

By plotting the data for all the specimen sizes on a composite plot, the power law relationship described in ASTM E 813–87 was found. Furthermore, for each material, within experimental scatter, the J_c values obtained by fitting the individual data for each specimen size to its own power law relationship were similar to the J_c value obtained using the composite power law curve [6]. Since a unique *J-R* curve could be generated by a range of specimen sizes, the composite curve was considered a plane strain resistance curve because it described *J-R* behavior that was independent of the in-plane bend bar geometry. (This is especially important since most applications involve thicknesses in this range of sizes.) Based on these findings, the ASTM E 813–87 thickness recommendation for plane strain conditions was found to be too conservative [6].

One explanation for the trend of decreasing J_c values with decreasing thickness was proposed in Ref 7. In order to stay within the *J*-controlled region of crack growth, crack growths were limited to 6% of the ligament as recommended in ASTM E 813. Thus, the amount of allowable crack growth was smaller with smaller specimen sizes. Since the power law fits of the crack growth behaviors of all the specimen sizes were identical, the linear fit proposed in ASTM E 813–81 actually described different portions of the power law *J-R* curve. The bilinear fit for the smaller specimens described the early portion while the larger specimens described the later portion. Since the slopes are steeper in the beginning, the intersections of the *J-R* curves with the blunting line gave lower J_c values.

In this study, the data analysis scheme of ASTM E 813–87 is used to further consider the applicability of the J-integral method to toughened polymers. The effect of side grooves, the effects of different ligament lengths, and the relationships between critical initiation J and G values are investigated for a variety of toughened polymers.

Experimental Details

Materials

The materials used in this study were rubber-toughened nylon 6/6 (RTN66, Zytel ST801), rubber-toughened amorphous nylon (RTAN, Zytel ST901), acrylonitrile-butadiene-styrene (ABS, Cycolac ABS, Grade GSE), and a toughened-polyphenylene oxide (TPPO, Noryl EN265). Both rubber-toughened nylons were injection molded into plaques that were either 100 by 250 by 12.7 mm or 100 by 250 by 3.2 mm. The ABS and TPPO were obtained in both 25- and 50-mm-thick extruded sheets from Westlake Plastics (Lanni, Pennsylvania). The materials were tested dry as molded at 23°C and 50% relative humidity.

Specimen Geometries

Single-edged notched bend (SENB) specimens were machined from either the plaques or the sheets. The specimens were deeply notched to half of the depth, W. Unless stated otherwise, W was maintained at twice the thickness, B. The span-to-depth ratio was held at 4 except as noted later. For the nylons, specimen thicknesses ranged from 12.7 mm to 3.2 mm. The thinner specimens (down to 6.4 mm) were made by milling equal amounts from the outer surfaces of the 12.7-mm-thick injection molded plaques. In addition, 3.2-mm-thick specimens were cut from the 3.2-mm-thick plaques. For the ABS and TPPO, 25-mm-thick specimens were made from the 25-mm-thick sheet. Thinner specimens (down to 7.5 mm) were made by sawing the 50-mm sheet through the thickness. The sawn surface was smoothed by milling. The specimens showed no curvature, so it was assumed that residual stresses were minimal. In all cases, the thickness direction of the plaques or sheets was maintained as the thickness direction of the SENB specimens. In addition, K_c tests were performed on 50-mm-thick SENB specimens.

For both RTN66 and RTAN, additional experiments were conducted using SENB specimens that were side grooved with a blunt cutter (radius of curvature of 250 μm). The total depth of the grooves was 20% of the original thickness. ASTM recommends a total groove depth of 20 to 25%. Additional information on specimen geometries are given in Ref *4*.

Modifications to the Multispecimen J-Integral Method

The J-integral method that is under investigation is a multiple-specimen technique, similar to ASTM E 813. It was originally proposed by Landes and Begley [*13*]. The first specimen is completely fractured to determine the ultimate displacement. Subsequent specimens are loaded to different subcritical displacements to obtain different levels of crack growth. From the area under the loading curve of each test, a value of J is calculated. Crack growth is marked and measured on the fracture surface. Resistance (J-Δa) curves are then constructed. The test is considered a valid test if the specimen thickness meets the requirement that

$$B > 25\ (J_c/\sigma_y)$$

The depth, W, should also be greater than twice the minimum B determined by this equation. There is some flexibility allowed in the depth dimension, as discussed in a later section.

In the current investigation, ASTM E 813 recommendations have not been strictly followed. The following modifications are noted.

1. The crack growth (Δa) was marked by freezing the test specimens in liquid nitrogen and then breaking them at 260 mm/s. An example of the crack growth region is shown in Fig. 1. The crack front is bowed and the Δa value is measured at the center of the specimen. The region next to the initial notch (between Lines A and B) is the crack growth region for this specimen. In J testing of polyethylene, it was shown that a stretch zone next to the initial notch formed first, followed by crack growth [*14*]. This was also observed on a variety of single-phase polymers [*11*]. However, this was not observed in the materials in this investigation. Region AB continuously grew with increasing J levels. If it were the stretch zone due to blunting, it would increase with increasing J and then remain constant at J values greater than J_{Ic}. The reason for the second texture (BC) before the fast fracture region is unclear. Its texture resembled that of the stretch zone found in the specimens that were loaded to sub-J_{Ic} levels. In these specimens, only blunting occurs and only one texture was seen.

   Crack growth was measured at the center of the fracture surface with a traveling microscope. Since the crack fronts were thumbnail shaped, this corresponded to the maximum crack growth. This is the original proposal by Landes and Begley [*13*]. ASTM E 813 recommends making nine equally spaced measurements and averaging them in a prescribed manner. This recommendation was made because the average value would more accurately map the crack front when significant bowing had occurred. The single-point technique that was used here is more convenient and leads to a more conservative J_c value since it overestimates the crack growth.

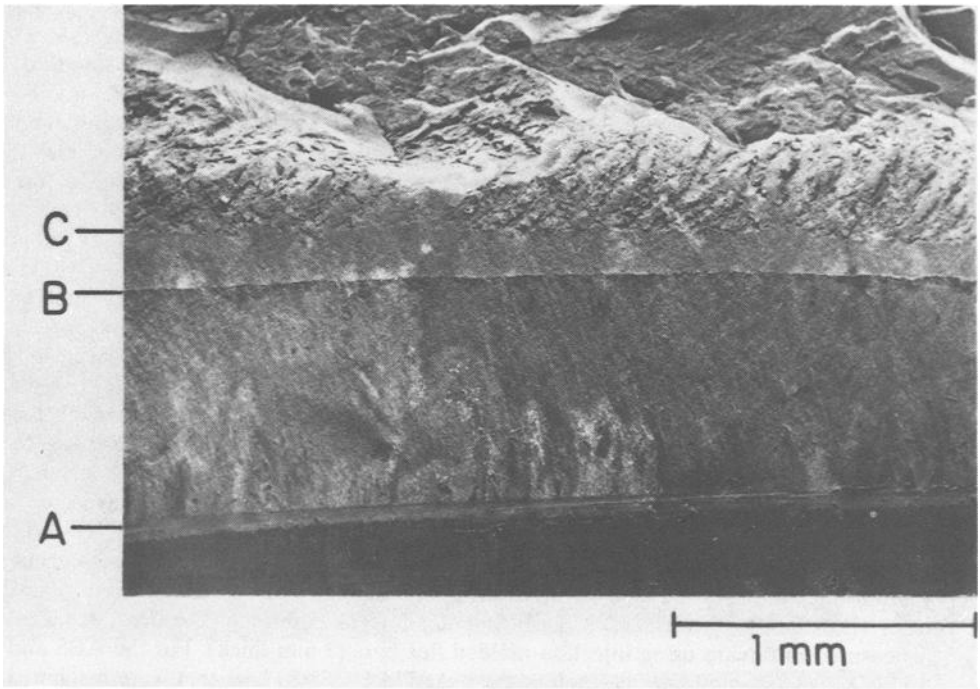

FIG. 1—*Fracture surface of RTAN.*

2. The span-to-depth (S/W) ratio was 3.5 for the 12.7-mm-thick specimens of RTN66 and RTAN. ASTM E 813 recommends a ratio of 4. The span-to-depth ratio is important in the calculation of J. J can be expressed as [*15*]

$$J = J_e + J_p$$

$$= (\eta_e U_e + \eta_p U_p)/Bb$$

where J_e and J_p are the elastic and plastic contributions to J; η_e and η_p are the elastic and plastic work factors; U_e and U_p are the elastic and plastic components of the total energy, U_T; B is the thickness; and b is the ligament. For bend specimens, the η_p factor is independent of S/W ratio. However, η_e has an S/W dependence. When the S/W ratio is 4 and the specimen is deeply notched (greater than 0.4), η_e and η_p are both equal to 2. Therefore, for J calculations, the total energy does not have to be partitioned into its elastic and plastic portions. For this geometry

$$J = 2 U_T/Bb$$

When the S/W ratio is 3.5, η_e equals 2.2 and η_p equals 2. This leads to a maximum error of 10% when the load-deflection curve is completely elastic. The error decreases as the ratio of elastic to plastic energy decreases.

3. The resistance curve was fitted using data points where crack growth was between two offset lines drawn parallel to the blunting line. The minimum offset was 0.6% of the ligament and the maximum offset was 6% of the ligament. ASTM E 813 recommends using parallel lines that are offset by 0.15 and 1.5 mm. Shih [*16*] has shown that the value of J is accurately predicted by these estimation procedures if the crack extension is less than 6% of the remaining ligament. This is a source of confusion in the standard. ASTM E 813 recommends that the test specimens should be a minimum size, that is, $B,b > 25\ (J_{Ic}/\sigma_y)$. It also recommends fixed offsets for the maximum and minimum crack growths. Since the ligaments can be of any size, the fixed offsets will not always guarantee that the crack growths will be less than 6% of the ligament. However, the 6% criterion should not be considered definitive. In ASTM Test Method for Determining J-R Curves (E 1152-87), the allowable amount of J-controlled crack growth is 10%.
4. The loading rates varied from 0.26 to 26 mm/s. This led to loading times as small as 0.05 s at the fastest speed. ASTM E 813 recommends that the loading time be greater than 6 s. ASTM made this recommendation to avoid the complexity of measuring a dynamic fracture toughness.
5. The specimens were notched either with razor blades that were drawn through the specimens or with cutters that were lapped to a radius between 5 and 12 μm. ASTM E 813 recommends a fatigue crack. In the current study, J_{Ic} is independent of notch root radius in the 5 to 12 μm range. Earlier toughness studies of polymers have shown that notching with either razor blades or sharp cutters can be acceptable [*8,17*].
6. For the rubber-toughened nylons, yield strengths were measured in tension using 3-mm-thick injection-molded bars (ASTM Test Method for Tensile Properties of Plastics (D 638-89), Type I). The elastic moduli for the room-temperature tests were measured in flexure using injection-molded flex bars (3 mm thick). For the ABS and TPPO, yield strengths were obtained from ASTM D 638-89 bars that were machined from the extruded sheets. The moduli were calculated from the measured specimen

compliance using the method of Haggag and Underwood [*18*]. Poisson's ratios were assumed to be equal to 0.41.

7. The reported yield strengths were measured at 26 mm/s according to D 638-89. ASTM E 813 recommends using an effective yield strength that is an average between the ultimate tensile strength and the 0.2% offset tensile yield strength.

Data Analysis

A computer controlled servohydraulic system was used for all mechanical testing. Software was developed to run the machine, acquire data in the form of load-displacement curves, and numerically integrate the curves to calculate energy values. After the specimen dimensions and ligament length have been measured using the traveling microscope, a J value for each specimen is calculated.

Because these J values are calculated from the total energy measured from the area under the load-load point displacement curve, an indentation energy correction was also made. This accounts for local deformation at the loading and support points. A fully supported unnotched specimen of the same thickness and depth as the J test specimen is indented with the load point. This test is conducted at the same rate as the J test. Again, a load-load point displacement curve was recorded. The contact stiffness, S, was found to be linear up to the maximum load, P_{max}, in the individual J tests. The energy due to indentation is then

$$U_{in} = 0.75\ (P^2_{max}/S)$$

where U_{in} = total indentation energy.

For an SENB specimen, the total J, $J_T = 2\ (U_T)/Bb$, where U_T is the total energy, B is the specimen thickness, and b is the ligament. The indentation J, J_{in}, can similarly be calculated from U_{in}. The real J value for each test specimen is equal to $J_T - J_{in}$. Depending on the size of the specimen and the amount of crack growth, this correction was as high as 14% of J_T.

Results and Discussion

Mechanical Properties

The mechanical properties of the four materials are listed in Table 1. The parameters, C_1 and C_2, are the power law parameters defined by the J-R equation

$$J = C_1\ \Delta a^{C_2}$$

The J_c values are determined by the ASTM E 813-87 construction. Figure 2 shows the J-R curves for the materials.

The data for the J-R curves were obtained using a range of specimen sizes. Because of this geometry independence, they are all considered unique plane strain curves. Throughout

TABLE 1—*Mechanical properties.*

Material	E, GPa	σ_y, MPa	C_1	C_2	J_{Ic}, kJ/m^2
RTN66	2.0	50	48.2	0.70	29.2
RTAN	2.0	69	35.7	0.68	16.3
ABS	2.3	48	15.5	0.70	6.1
TPPO	2.5	59	12.3	0.58	5.4

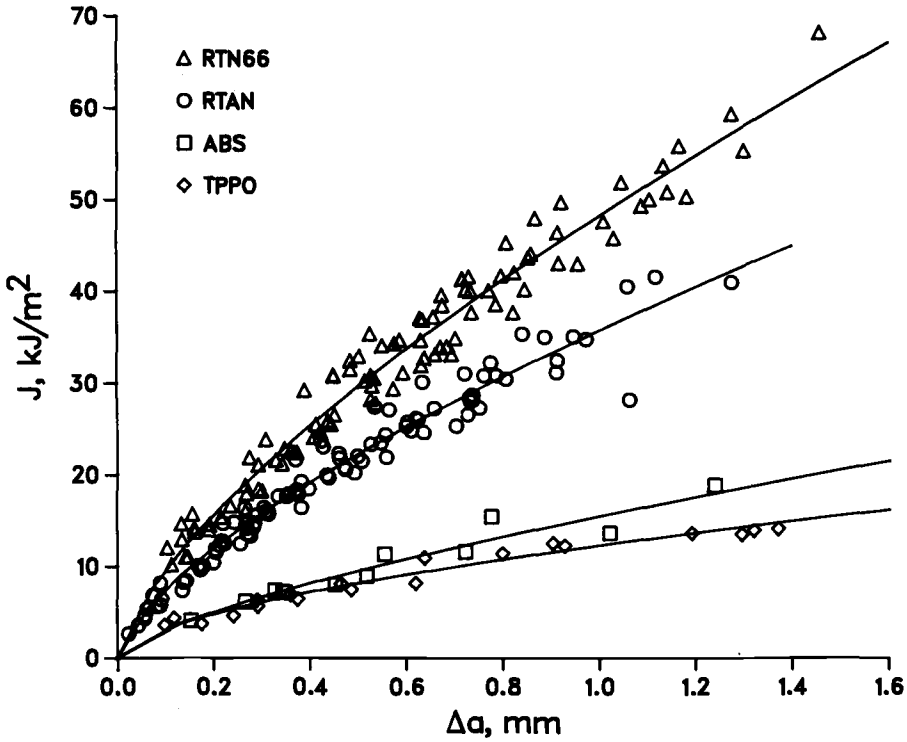

FIG. 2—J-R *data and curve fits for RTN66, RTAN, ABS, and TPPO.*

this paper, the *J-R* curves that are obtained for the various test conditions will be compared to these curves to determine their validity.

Effect of Side Grooves

According to the ASTM size recommendation, RTN66 was the only material that should not have been in plane strain as the largest specimen size. However, the specimens were only 2 mm too small. For the rubber-toughened nylons, 12.7 mm is the practical limit in thickness for injection molded plaques. Ideally, larger specimens should be used to test for geometry independence and plane strain conditions. In larger specimens, proportionately more of the crack front is placed under plane strain conditions leading to lower crack growth resistance and lower fracture toughness values. One technique that also accomplishes this goal is to side groove the specimens.

Results for 20% side-grooved specimens are given in Figs. 3 and 4 for the rubber-toughened nylons. The *J-R* curves for the side-grooved specimens are in excellent agreement with those obtained from the ungrooved specimens. The *J-R* curve for RTAN (Fig. 3) is virtually identical to the unique curve shown in Fig. 2. The *J-R* curve for RTN66 (Fig. 4) is slightly lower at larger crack growths, but is well within the experimental scatter of data shown in Fig. 2. These findings reinforce the notion that a unique plane strain curve has been determined.

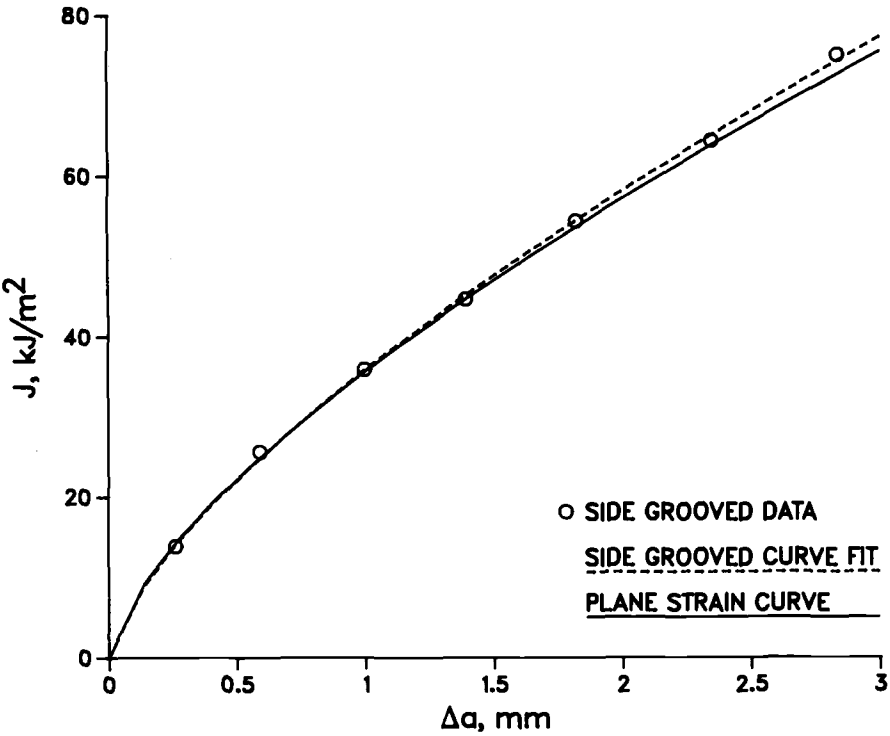

FIG. 3—J *data for RTAN side-grooved (20% B) specimens.*

Effect of Ligament Size

As mentioned earlier, ASTM E 813 does not clearly address the issue of the maximum allowable crack growth when sub-sized (less than 25.4-mm-thick) specimens are used. Crack growths between 0.15 and 1.5 mm are recommended for data selection. However, as described earlier, Shih [*16*] has suggested that crack growth should be restricted to 6% of the ligament in order to keep under *J*-controlled conditions. For small specimens with depths equal to twice the thickness, it is not possible to satisfy both conditions.

Three different specimen sets of RTN66 and RTAN with different *B*/*W* ratios were tested. Figures 5 and 6 show the results of 12.7-mm-thick SENB specimens that had *W*/*B* ratios of 1, 2, and 4 for RTN66 and RTAN, respectively. For comparison purposes, the plane strain curves given in Table 1 are also plotted.

In Fig. 5, there seems to be little effect on the *J*-*R* curve due to changes in the ligament. For the cases of $W/B = 2$ and 4, the data fit the plane strain curve within experimental scatter. Interestingly, although the *J*-*R* data for the $W/B = 1$ set are consistent with the plane strain curve, the data appear to be on the low end of the scatter of the other sets. At small crack growths (three smallest crack growths corresponding to 6% of the ligament), the data fit fairly well. At intermediate crack growths (middle data point at 1.06 mm, 9% of the ligament), the *J* value is low but still acceptable. At large crack growths (greater than 17%), the *J* values are significantly lower.

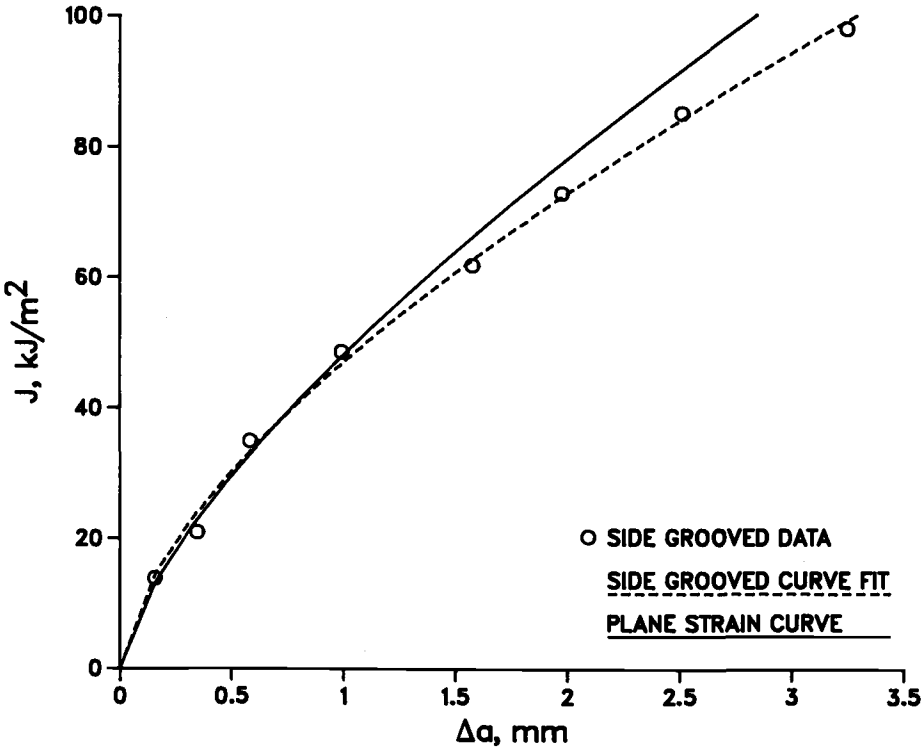

FIG. 4—J *data for RTN66 side-grooved (20% B) specimens.*

These data are consistent with the findings of McCabe et al. [*19*] who tested specimens of A508, Class 2A tube plate material with short ligaments. In that study, it was suggested that the short ligament is not large enough to sustain crack growths for the full *J-R* curve. Therefore, at small growths, the data fit well, but at high crack growths, the *J* values are low. Because of the scatter in the data, more tests are needed to verify this finding.

The *J-R* data for the same specimen geometries for RTAN are given in Fig. 6. In this data set, the data for $W/B = 1$ and 2 are reasonably consistent with each other and the plane strain curve. However, the *J-R* data for the $W/B = 4$ specimen set produce a significantly lower *J-R* curve.

In order to explain these results, the minimum depth for plane strain *J* tests must be considered. Since there are no general recommendations for polymers, the ASTM E 813 standard was used as a first approximation. ASTM E 813 recommends using SENB specimens with $1 < W/B_{min} < 4$ where B_{min} is the minimum plane strain thickness ($B_{min} = 25\ (J_{Ic}/\sigma_y)$). Using the J_{Ic} and σ_y values given in Table 1, B_{min} for RTN66 is 14.6 mm and for RTAN, it is 5.9 mm. For RTN66, it is interesting that acceptable results were obtained on specimens with $W/B_{min} = 0.87$ and 1.7 while the low *J* results were obtained on specimens of $W/B_{min} = 0.44$. Similarly, for RTAN, acceptable results were obtained on specimens with $W/B_{min} = 1.1$ and 2.2 while low results were obtained when $W/B_{min} = 4.2$.

Based on these W/B_{min} ratios, it would appear that W/B_{min} ratios of slightly less than 1 to slightly less than 4 may be appropriate for polymers if the full *J-R* curve is needed. If only the beginning of the *J-R* curve is needed, lower W/B_{min} ratios may be appropriate. The

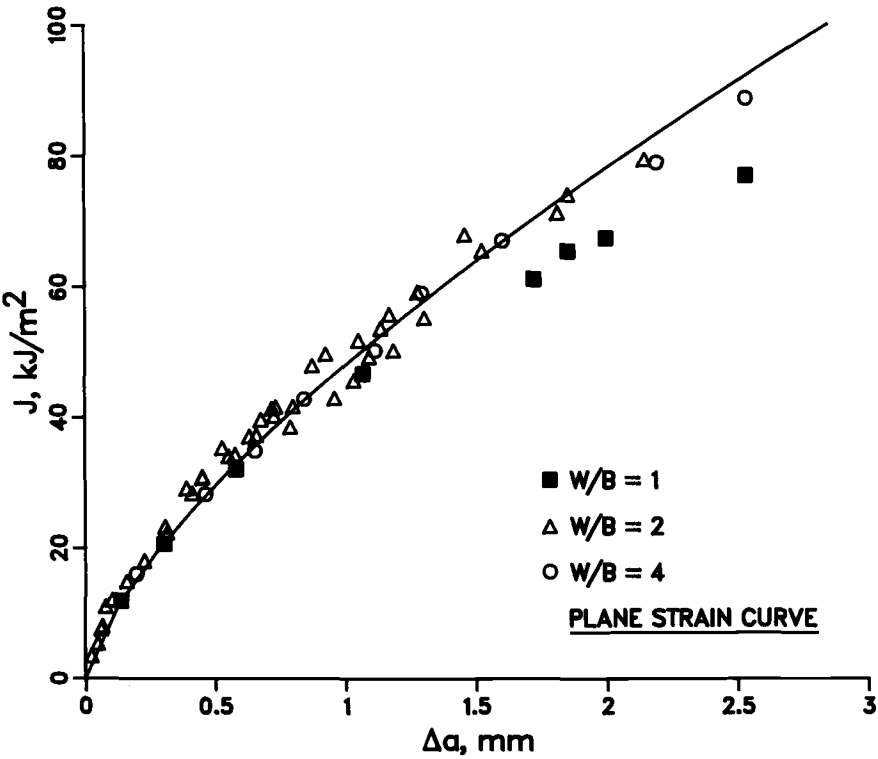

FIG. 5—J *data for RTN66 specimens with varying ligament depths.*

ASTM recommendation of $W/B_{min} = 2$ as a starting point appears to be sensible considering the data. Also, longer ligament depths are preferable to shorter ligament depths within the limits already described. Currently, it is premature to suggest that this specific calculation should be adopted for *J* testing of polymers, because it is unclear whether the selection of J_{Ic}, the ASTM E 813 recommended W/B_{min} ratios, or the B_{min} calculation are valid for these materials. However, this calculation does suggest that the limits to the ligament size should be a function of a fundamental size parameter. Much more data on a variety of polymers are needed to confirm this recommendation.

Initiation J_c, G_c *Relationships*

Begley and Landes [*20*] have shown that the J_{Ic} value determined in the *J*-integral test and the G_{Ic} measured in a standard fracture toughness (*K*) test are equal, if both tests are conducted under plane strain conditions. This relationship was demonstrated using two different steels.

K tests were conducted on 50-mm-thick SENB specimens made from the extruded sheets of ABS and TPPO. The *K* tests were based on the ASTM Test Method for Plane-Strain Fracture Toughness of Metallic Materials (E 399-83) procedures with important differences as noted later. The depths were 100 mm, and *S/W* was maintained at 4. The *K* tests were conducted at the same rate as the *J* tests (25 mm/s). The notches were made by drawing a fresh razor blade through a sawn prenotch. The nominal notch depth-to-specimen depth (*a/*

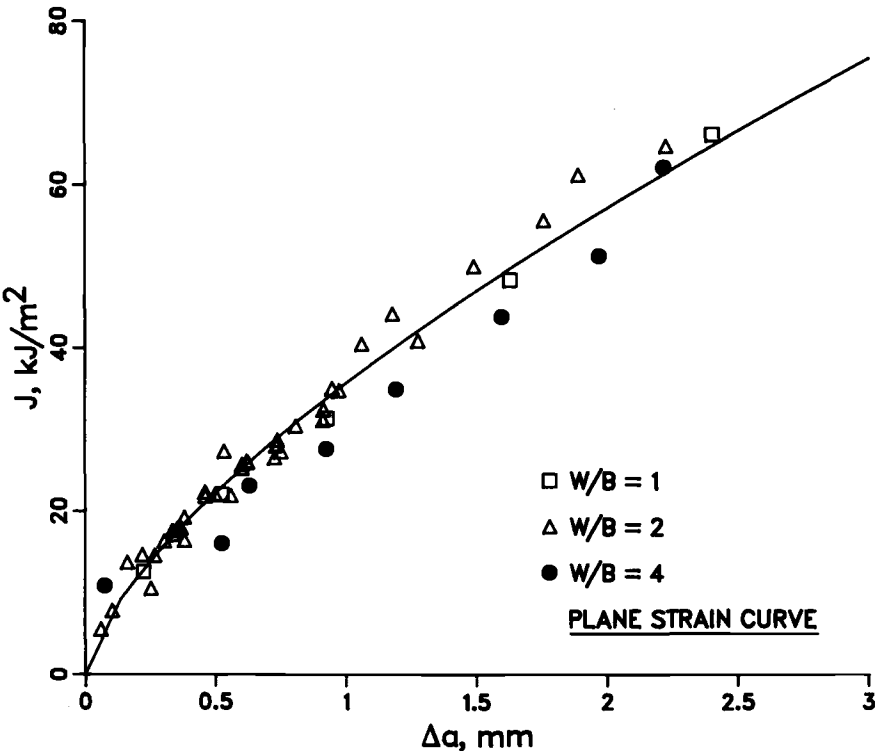

FIG. 6—J *data for RTAN specimens with varying ligament depths.*

W) ratios were 0.25 and 0.40. The load displacement curves were slightly nonlinear. As an indication of the degree of nonlinearity, the ratios of the maximum load, P_{max}, to P_5, the load determined by the intersection of the curve and the secant line representing 95% of the initial stiffness, were less than 1.1 except for one test where the ratio was 1.14.

Because of the difficulties associated with defining initiation when the load displacement curves are nonlinear, ASTM E 399 recommends using P_5 to approximate the initiation point and is used in the K calculation. If the specimen is nominally notched to 50% of its depth, P_5 corrresponds to the load at which the crack has grown 2.5% (maximum) [*21*]. Since the notches in these K tests were not in the range of $0.45 < a/W < 0.55$ as ASTM E 399 recommends, this construction is now inappropriate because P_5 corresponds to crack growths significantly larger than 2.5%.

In order to identify initiation for these specimens, different constructions were necessary. As in ASTM E 399, the initiation point was selected as the point at which 2.5% crack growth occurred. The load at initiation, P_i, was determined by a secant line construction similar to that of ASTM E 399. However, instead of using a 5% offset, a different offset value was used. These offsets were calculated from the expression.

$$\Delta a/a = (\phi/(a/W))(\Delta C/C)$$

where a is crack length, ϕ is the energy calibration factor given in Ref *1* and tabulated in Ref *21*, W is specimen depth, and C is compliance. Thus, the initiation points were deter-

TABLE 2—K *test results.*

a/W	K_c, MPa $\sqrt{m}$	G_c, kJ/m^2	P_{max}/P_i^a
	ABS		
0.25	5.65	11.7	1.25
0.25	5.23	10.0	1.33
0.40	5.59	11.4	1.19
0.40	6.01	13.2	1.18
0.40	5.77	11.7	1.28
	TPPO		
0.25	5.40	10.6	1.20
0.25	5.80	12.2	1.10
0.38	5.44	10.8	1.18
0.38	5.62	11.5	1.11
0.38	5.89	12.7	1.03

[a] P_i corresponds to the load at which 2.5% crack growth has occurred.

mined using offsets of 1.2 and 3.2% for the specimens with a/W of 0.25 and 0.40, respectively. The results are presented in Table 2. The ratio, P_{max}/P_i is also tabulated as an indication of the degree of nonlinearity. Note that, for TPPO, some of the tests meet the P_{max}/P_i requirement even though these offset constructions are more severe.

Using this procedure to define initiation, the average K_c values for ABS were 5.44 MPa $\sqrt{m}$ for $a/W = 0.25$ and 5.79 MPA $\sqrt{m}$ for $a/W = 0.40$. Assuming a Poisson's ratio of 0.40 and a modulus of 2.3 GPa, the average (calculated) G_c values are 10.9 kJ/m^2 and 12.1 kJ/m^2, respectively. For TPPO, the average K_c values were 5.60 MPa $\sqrt{m}$ ($a/W = 0.25$) and 5.65 MPa $\sqrt{m}$ ($a/W = 0.38$). Again, assuming a Poisson's ratio of 0.41 and a modulus of 2.3 GPa, the corresponding G_c values are 11.4 and 11.7 kJ/m^2, respectively. According to the ASTM E 399 size criteria, the specimens would be in plane strain. However, since nonstandard methods were used to determine initiation, it is not clear whether the size recommendations are valid for these tests.

The G_c values for both ABS and TPPO are more than twice as large as their respective J_{Ic} values listed in Table 1. Thus, J_{Ic} may have potential as a design criterion since it is a conservative estimate of the G_c values. However, it is unclear whether the J_{Ic} values determined in this manner are too restrictive for polymer design.

For these materials, the discrepancy between G_c (for 2.5% crack growth) and J_{Ic} may be due to either the definition of J_{Ic} as the J value required to extend the notch by 0.2 mm, the arbitrary selection of initiation in the K test, or both. For a more valid comparison of these measurements, it is necessary to consider the amount of crack growth, Δa, that has occurred in the K tests. As a first approximation, a G_c value should be equal to the J value required for the specific amount of crack growth that corresponds to that G_c. J can be calculated using the plane strain J-R curve.

The results for ABS are presented in Table 3. The crack growths were determined by the offset secant methods described earlier. The crack growths of 0.65 mm and 2.73 mm corresponded to offset secants of 1.2 and 5.0%, respectively, for the specimens with nominal a/W of 0.25. Crack growths of 1.02 and 1.59 mm corresponded to offsets of 3.2 and 5.0%, respectively, for the specimens with nominal a/W of 0.40. The calculated J_c values for these crack growths were obtained by substituting the appropriate Δa value directly into the plane strain equation of Table 1. While there is good agreement between the G_c and J_c values at

TABLE 3—J_c, G_c *comparisons for ABS.*

a/W	Δa, mm	G_c, kJ/m^2	J_c[a], kJ/m^2
0.25	0.65	11.7	11.5
	0.65	10.0	11.5
0.40	1.02	11.4	15.7
	1.02	11.7	15.7
	1.02	13.4	15.7
0.40	1.59	12.3	21.4
	1.59	12.7	21.4
	1.59	12.9	21.4
0.25	2.73	14.3	31.3
	2.73	15.4	31.3

[a]Calculated from plane strain *J-R* curve.

the smallest crack growth, the G_c values increase at a slower rate than the J_c values. At 2.73 mm, the G_c values are approximately 50% of the J_c values. These results are plotted in Fig. 7.

Similar results are given in Table 4 and Fig. 8 for TPPO. The crack growths of 0.65 mm (offset secant of 1.2%) and 2.73 mm (offset secant of 5.0%) were obtained on the specimens with a/W = 0.25. The crack growths of 0.93 (offset secant of 2.9%) and 1.60 mm (offset

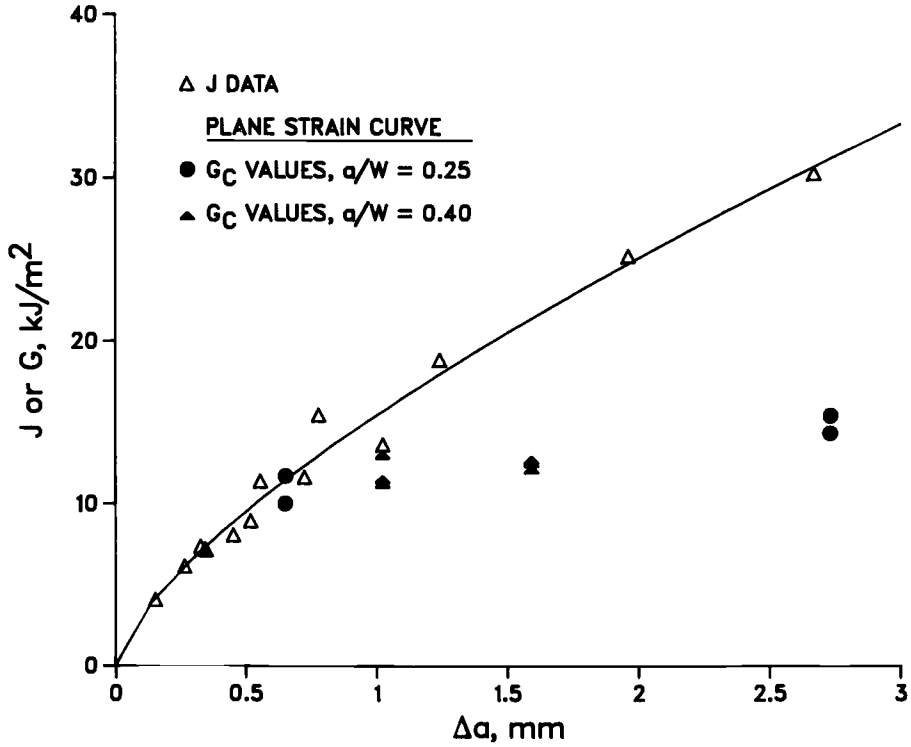

FIG. 7—*Comparison of ABS* G_c *data to* J-R *curve using crack growths calculated from compliance change.*

TABLE 4—J_c, G_c *comparisons for TPPO.*

a/W	Δ*a*, mm	G_c, kJ/m²	J_c[a], kJ/m²
0.25	0.65	10.6	11.5
	0.65	12.2	11.5
0.38	0.93	10.8	11.8
	0.93	11.5	11.8
	0.93	12.7	11.9
0.38	1.60	13.2	16.2
	1.60	13.6	16.2
	1.60	14.1	16.2
0.25	2.73	14.5	22.0
	2.73	12.1	22.0

[a]Calculated from plane strain *J-R* curve.

secant of 5.0%) were obtained with specimens with *a/W* of 0.38. In this case, the agreement between G_c and J_c is good up to crack growths of 1.60 mm. At 2.73 mm, the G_c values are approximately 60% of the J_c values.

These results suggest that the plane strain resistance curve may be used to calculate critical *G* values if initiation is defined at a specific amount of crack growth and if that amount of

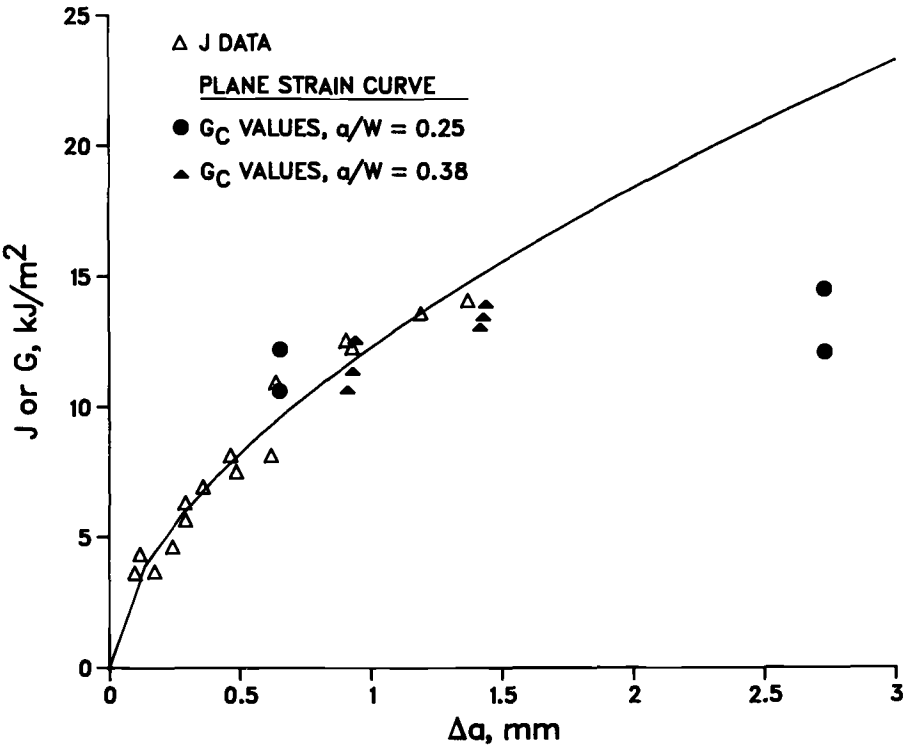

FIG. 8—*Comparison of TPPO* G_c *data to* J-R *curve using crack growths calculated from compliance change.*

crack growth is small. For these two materials, the best agreement between J_c and G_c occurred when Δa was nominally 0.65 mm. In TPPO, the agreement was good over a larger range of Δa. One possibility for this behavior is that the 50-mm-thick specimen size used in the K test was closer to linear elastic plane strain conditions for TPPO than for ABS. Further investigation is required to clarify this point.

While the discrepancies at large crack growths are significant, it is important to note that they may be exaggerated by the different methods used to determine crack growth. The crack growths in the J tests are measured from the fracture surfaces. The G analyses used the offset secant method to calculate the crack growths. This method assumes that crack growth alone is responsible for the change in compliance. Therefore, the calculated crack growths are upper limits to the actual crack growth. A more comprehensive study of the compliance-crack growth relationship in these polymeric systems is needed.

Conclusions

The multispecimen J-Integral method of ASTM E 813-87 was investigated to determine its suitability to measure the fracture toughness of toughened polymers in a way that would be useful for both characterization and design. Many of the procedural details appear to provide results that are consistent in form with J results for metals. For example, the use of side grooves for test specimens appears to be a satisfactory way of getting closer to plane strain conditions.

However, some of the recommendations should be reexamined for use with polymers. In particular, the minimum specimen thickness for plane strain conditions is conservative and the allowable range of ligament depths requires a better definition. Finally, while J_{Ic} can be used for ranking purposes and conservative estimates of G_c, it is yet to be determined whether the selection of 0.2 mm of crack growth as a design definition is appropriate for polymer applications.

As an alternative to using a predetermined critical J value for design, there appears to be potential in using the resistance curves to calculate application-dependent critical J values after determining allowable crack growths. In this study, this calculation was most successful when the crack growths are small. More extensive investigations are needed in this area.

References

[1] Williams, J. G., *Fracture Mechanics of Polymers*, Ellis Horwood, Ltd., Chichester, U.K., 1984.
[2] Rice, J. R., *Journal of Applied Mechanics*, Vol. 35, 1968, p. 379.
[3] Huang, D. D. and Williams, J. G., *Journal of Materials Science*, Vol. 22, 1987, p. 2503.
[4] Huang, D. D. in *Rubber Toughened Plastics, Advances in Chemistry Series*, Vol. 222, C. K. Riew, Ed., American Chemical Society, Washington, DC, 1989, p. 119.
[5] Huang, D. D. in *Proceedings*, Seventh International Conference on Deformation, Yield and Fracture of Polymers, Paper 46, The Plastics and Rubber Institute, London, 1988.
[6] Huang, D. D., *Polymer Preprints*, Vol. 29, No. 2, 1988, p. 159.
[7] Huang, D. D. in *Advances in Fracture Research*, K. Salama et al., Eds., Pergamon Press, New York, 1989, p. 2725.
[8] Hashemi, S. and Williams, J. G., *Polymer Engineering and Science*, Vol. 26, No. 11, 1985, p. 760.
[9] Takemori, M. T. and Narisawa, I. in *Advances in Fracture Research*, K. Salama et al., Eds., Pergamon Press, New York, 1989, p. 2733.
[10] Carling, M. J., "Fracture Mechanics of Short Fibre Composites," PhD thesis, University of London, 1988.
[11] Theuer, T., Cornec, A., Krey, J., and Friedrich, K. in *Proceedings*, Seventh International Conference on Deformation, Yield and Fracture of Polymers, Paper 97, The Plastics and Rubber Institute, London, 1988.
[12] Rimnac, C. M., Wright, T. M., and Klein, R. W., *Polymer Engineering and Science*, Vol. 28, No. 24, 1988, p. 1586.

[13] Landes, J. D. and Begley, J. A. in *Fracture Analysis (8th Conference), ASTM STP 560*, American Society for Testing and Materials, Philadelphia, 1974, pp. 170–186.
[14] Chan, M. K. V. and Williams, J. G., *International Journal of Fracture*, Vol. 19, 1983, p. 145.
[15] Sumpter, J. D. and Turner, C. E., *International Journal of Fracture*, Vol. 9, 1973, p. 320.
[16] Shih, C. F., Andrews, W. R., de Lorenzi, H. G., et al., "Crack Initiation and Growth Under Fully Plastic Conditions: A Methodology for Plastic Fracture," Report NP-701-SR, Electric Power Research Institute, Palo Alto, CA, Feb. 1978, pp. 6.1–6.63.
[17] Hashemi, S. and Williams, J. G., *Plastics and Rubber Processing and Applications*, Vol. 6, 1986, p. 363.
[18] Haggag, F. M. and Underwood, J. H., *International Journal of Fracture*, Vol. 26, 1984, pp. R63–R65.
[19] McCabe, D. E., Landes, J. D., and Ernst, H. A. in *Elastic-Plastic Fracture: Second Symposium, Volume II: Fracture Curves and Engineering Applications, ASTM STP 803*, C. F. Shih and J. P. Gudas, Eds., American Society for Testing and Materials, Philadelphia, 1983, pp. II–562–II–581.
[20] Begley, J. A. and Landes, J. D. in *Fracture Toughness, ASTM STP 514*, American Society for Testing and Materials, Philadelphia, 1972, pp. 1–20.
[21] Williams, J. G., "A Linear Elastic Fracture Mechanics (LEFM) Standard for Determining K_c and G_c for Plastics," EGF Task Group on Polymers and Composites Proposed Testing Protocol, July, 1989.

Henry L. Bernstein[1]

Fracture Toughness of Polycarbonate as Characterized by the *J*-Integral

REFERENCE: Bernstein, H. L., "**Fracture Toughness of Polycarbonate as Characterized by the *J*-Integral,**" *Elastic-Plastic Fracture Test Methods: The User's Experience (Second Volume), ASTM STP 1114*, J. A. Joyce, Ed., American Society for Testing and Materials, Philadelphia, 1991, pp. 306–319.

ABSTRACT: Fracture tests have been conducted on polycarbonate in the elasto-plastic and fully plastic regimes. The fracture behavior was well characterized by the *J*-integral. The value of the *J*-integral at the initiation of crack growth, corresponding to J_{Ic}, was 2.1 kN/m (12.2 psi·in.) for the 1981 ASTM Test Method for J_{Ic}, a Measure of Fracture Toughness (E 813-81), and 3.3 kN/m (19 psi·in.) for the 1987 ASTM (E 813-87). It was found that the value of the *J*-integral at 2% crack growth, 4.4 kN/m (25 psi·in.), corresponded well with values of K_{Ic} in the literature. It is suggested that the value of *J* at 2% crack growth may be a better parameter to characterize fracture than *J* at initiation. The value of the *J*-integral at popin or unstable fracture, 7.3 kN/m (41 psi·in.), was consistent for all the experiments. No effect of crack length or thickness was observed for any of these values of *J*. Two difficulties with the use of the 1987 standard were found. The first was that the data did not coincide with the blunting line. More crack growth was measured than predicted by the blunting line. The second was that a valid data point between the 1 and 1.5-mm offset lines could not be experimentally obtained because of the nature of crack growth in polycarbonate.

KEY WORDS: elastic-plastic fracture, test methods, polycarbonate, *J*-integral, fracture toughness

The purpose of this investigation was to study the fracture of polycarbonate (PC) in the elasto-plastic and fully plastic regimes. Since linear-elastic fracture mechanics is invalid in these regimes, nonlinear fracture-mechanics (NLFM) concepts must be used. The *J*-integral was studied because it is the most widely used NLFM parameter. It has been used to characterize the fracture of a number of materials [*1–14*].

Fracture in the elasto-plastic and fully plastic regimes is an important engineering problem. Some materials, such as PC, are tough and can withstand large amounts of plastic deformation prior to fracture.

The *J*-integral, which was proposed by Rice [*15*], is a two-dimensional, path-independent integral around a crack tip for a nonlinear elastic material. The integral, derived earlier by Eshelby [*16*], is defined for a crack parallel to the *x*-axis as

$$J = \int_{\Gamma} \left(W \, dy - \boldsymbol{T} \cdot \frac{\partial \boldsymbol{u}}{\partial x} \, ds \right) \tag{1}$$

where Γ is a path starting at the lower crack surface and extending in a counterclockwise direction around the crack tip to the upper crack surface; W is the strain-energy density; $\boldsymbol{T}$ is the traction vector along the path; and $\boldsymbol{u}$ is the displacement vector along this path. The

[1]Principal engineer, Southwest Research Institute, San Antonio, TX 78238.

J-integral has been shown by McClintock [*17*], Hutchinson [*18,19*], and Rice and Rosengren [*20*] to characterize the stress and strain field about the crack tip for a power-law hardening material.

The J-integral is related to the stress intensity factor, K, by [*15*]

$$J E' = K^2 \tag{2}$$

where for plane stress, E' is the elastic modulus, E; and for plane strain, E' is $E/(1 - \nu^2)$ where ν is Poisson's ratio.

Experimental methods for measuring the J-integral and determining the beginning of crack growth, called J_{Ic}, have been developed by Begley and Landes [*1,2*]. The ASTM Test Method for J_{Ic}, a Measure of Fracture Toughness (E 813), covers the measurement of J_{Ic} in metals. The original 1981 version determined J_{Ic} by extrapolating a linear fit of the crack growth data to the intersection with the blunting line. The current 1987 version determines J_{Ic} from the intersection of a logarithmic fit of the crack growth data with a 0.2-mm offset blunting line, ASTM E 813 is applicable to metals. There is no corresponding standard for polymers.

Crack growth in PC occurs by the formation of a crazed zone ahead of the crack tip, followed by the rupture of the craze. As the craze breaks, the crack grows and a new craze forms. Reviews on the subject of crazing have been made by Kambour [*21*], Brown [*22*], and Kinloch [*23*] as well as others. Crazing in PC has been studied by Fraser and Ward [*24*] and by Mills [*25*].

Previous studies of the fracture and crack growth behavior of PC have been made by Parvin and Williams [*26,27*], Brinson [*28*], Mills [*25*], Fraser and Ward [*24*], and Key, Katz, and Parker [*29*]. A brief review of these papers can be found in Ref *30*.

Experimental Method

Material

The polycarbonate used was a standard-grade, unshrunk, 25.4-mm (1-in.)-thick sheet of Lexan made by laminating two 12.7-mm (0.5-in.)-thick sheets together. The fracture tests were conducted such that crack growth was always in the same section of the laminate.

The tensile properties of the PC are given as a function of the displacement rate in Table 1. As the displacement rate increased, the strength increased but the elastic modulus was essentially constant. During the test, a neck formed and traveled along the gage length until fracture. Fracture was caused by the formation of a diamond-shaped surface flaw. This flaw grew until it intersected a corner of the "dogbone" specimen, at which point unstable fracture occurred. This same failure mechanism has been observed by Cornes et al. [*31*]. A detailed description of the tensile behavior can be found in Ref *30*.

Test Procedure

Three-point bend specimens, 108 mm (4.25 in.) long by 25.7 mm (1.01 in.) wide with 12.7-mm (0.5-in.) machined notches, were used. (Two of the specimens had notch lengths of 6.35 mm (0.25 in.) rather than 12.7 mm (0.5 in.), but no influence upon the fracture behavior was observed.) Crack lengths ranged from 13.7 to 20.6 mm (0.54 to 0.81 in.) and the thicknesses were 3.18, 6.35, 12.7, and 25.4 mm (0.125, 0.25, 0.5, and 1 in.), as shown in Table 2. Fatigue precracking was used to grow the crack from the notch. All specimens

TABLE 1—*Tensile properties of polycarbonate.*

Displacement Rate, mm/min (in./min)	Elastic Modulus, MPa (psi)	0.2% Offset Yield Stress, MPa (psi)	Ultimate Stress, MPa (psi)	True Stress at Fracture, MPa (psi)	Reduction in Area, %
50.8 (2.0)	2158 (313 000)	41.78 (6060)	66.81 (9690)	79.36 (11 510)	38.6
5.08 (0.2)	2165 (314 000)	39.65 (5750)	64.4 (9340)	71.56 (10 380)	35.4
1.27 (0.05)	2241 (325 000)	39.58 (5740)	65.5 (9500)	84.71 (12 290)	40
0.508 (0.02)	2310 (335 000)	35.92 (5210)	62.06 (9000)	76.51 (11 100)	36.3
Average	2220 (322 000)	39.23 (5690)	64.68 (9380)	78.05 (11 320)	37.6

had the same orientation within the plate, and the crack was grown in the thickness direction, T-S. Thus, the surfaces of the plate and the lamination in the middle of the plate were avoided.

The *J*-integral tests were conducted in a screw-driven Instron machine under displacement control. Two linear variable differential transducers (LVDTs), one on each side of the specimen, measured the load-point displacement between the center tup and the rollers. All tests were conducted at a displacement rate of 0.5 cm/min (0.02 in./min). (It should be noted that Parvin and Williams [*26,27*] found no difference in the fracture properties of PC for rates of 5.0 and 0.5 cm/min (0.2 and 0.02 in./min)).

The value of the *J*-integral was calculated using the equation for a three-point bend specimen

$$J = \frac{2A}{Bb} \tag{3}$$

TABLE 2—*Load-displacement behavior.*

Specimen	*B*, mm (in.)	*a/W*	Load-Displacement Curve	Maximum Load, N (lb)	Ratio of Maximum Load to G&H LL[a]
3	25.76 (1.014)	0.54	A	1303 (293)	0.64
2	5.35 (0.998)	0.70	A	632 (142)	0.73
4	12.70 (0.500)	0.69	A	334 (75)	0.75
6	12.65 (0.498)	0.69	B	338 (76)	0.73
24	12.57 (0.495)	0.80	A	173 (39)	0.89
12	6.30 (0.248)	0.58	B	274 (61.5)	0.67
13	6.35 (0.250)	0.68	B	176 (39.5)	0.73
10	6.35 (0.250)	0.78	D	89 (20)	0.80
15	3.18 (0.125)	0.59	C	153 (34.5)	0.77
20	3.12 (0.123)	0.70	C	81 (18.1)	0.75
21	3.10 (0.122)	0.81	D	38 (8.6)	0.86

[a]G&H LL in Green and Hundley Limit Load (see Eq 4).

where A is the area under the load-displacement curve, B is the thickness; and b is the remaining ligament.

A full description of the test method can be found in Ref *30*.

Crack Length Measurement

Since PC is transparent, an entire J-resistance curve could be obtained from a single specimen. During the test, the crack was photographed using a 35-mm camera with a telephoto lens and a bellows extension. This gave a magnification of approximately one. Then the film was mounted into slide holders and projected onto a wall that magnified the crack about 17 times. The crack length was the average length at the three-quarter points. The surface crack length was not used because it usually could not be seen in the photographs.

Two methods of photographing the crack were used. In the first method, the crack was photographed through the length of the specimen, with white light shining from the opposite end of the specimen. This method was used for all but four of the tests—specimens 10, 12, 15, and 21. For these specimens, the crack was photographed from the side of the specimen, which was illuminated by two light sources on each side of the crack. This second method produced a sharper image of the crack front than the first method.

A photograph taken using the second method is shown in Fig. 1. There are three distinct regions: the fatigue precrack, the crack growth, and a bright featureless region. This bright region was identified as a craze for reasons discussed later. Figure 2 is a photograph taken through the thickness of the specimen using the first method. The bright region at the tip of the crack contains both cracked and crazed material. The division between these regions was obscured by the photographic method.

Results and Discussion

Load-Displacement Behavior

Four types of load-displacement curves were observed, as shown in Fig. 3, and are given in Table 2 for each specimen. They are: unstable fracture, Curve A; popin at maximum load and thereafter stable, Curve B; popin before maximum load and thereafter stable, Curve C; and stable with no popin, Curve D. Unstable fracture (Curve A) was exhibited by the 25.4-mm (1-in.) thick specimens and two of the three 12.7-mm (0.5-in.) thick specimens. Popin at maximum load and thereafter stable (Curve B) appears to be the same process as unstable fracture except that crack arrest takes place. Once the crack arrests, further crack growth is stable. This type of behavior occurred in one of the 12.7-mm (0.5-in.) specimens and the 6.35-mm (0.25-in.) thick specimens with the shorter crack lengths. For popin before the maximum load (Curve C), the load rises smoothly after popin, through the maximum load. This behavior occurred in the 3.18-mm (0.125-in.)-thick specimens having the shorter crack lengths. The 6.35 and 3.18-mm (0.25 and 0.125-in.)-thick specimens having the longest cracks exhibited stable behavior with no popin (Curve D), similar to metals with high toughness.

Key and Katz [*32*] reported similar popin behavior of PC as a function of the thickness. However, it can be seen that popin also depends upon the crack length.

The maximum load and the ratio of the maximum load to the Green and Hundy limit load are given in Table 2 for each specimen. The Green and Hundy limit load [*33*], P_L, is

$$P_L = 0.364\ \sigma_y B b^2 \tag{4}$$

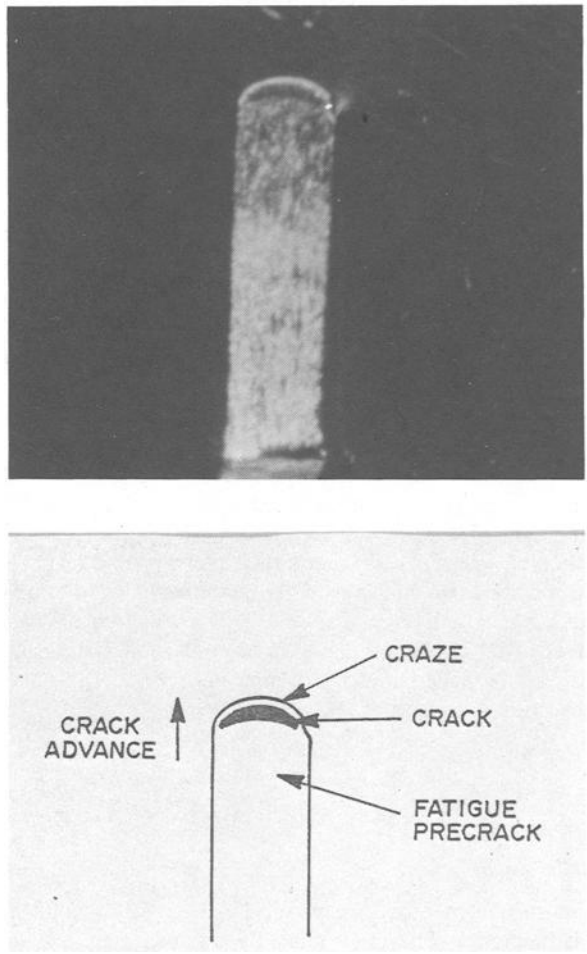

FIG. 1—*Photograph of the crack taken from the side of the specimen.*

where σ_y is the yield stress. The maximum load was always less than the Green and Hundy limit load because crack growth takes place before the maximum load is reached and prevents this limit load from being reached. This was confirmed for all the specimens since the crack was observed to grow before the maximum load was reached.

Crack Growth Behavior

A composite of all the crack growth data as a function of J is shown in Fig. 4. There was no trend in the data with respect to crack length or thickness. The crack growth behaved in a reasonably linear manner with respect to J, except at low values of J. The data were also plotted on logarithmic coordinates since others have observed that logarithmic coordinates linearize crack growth data in steels [*10–12*]. The logarithmic coordinates provided a better fit to the PC data [*30*].

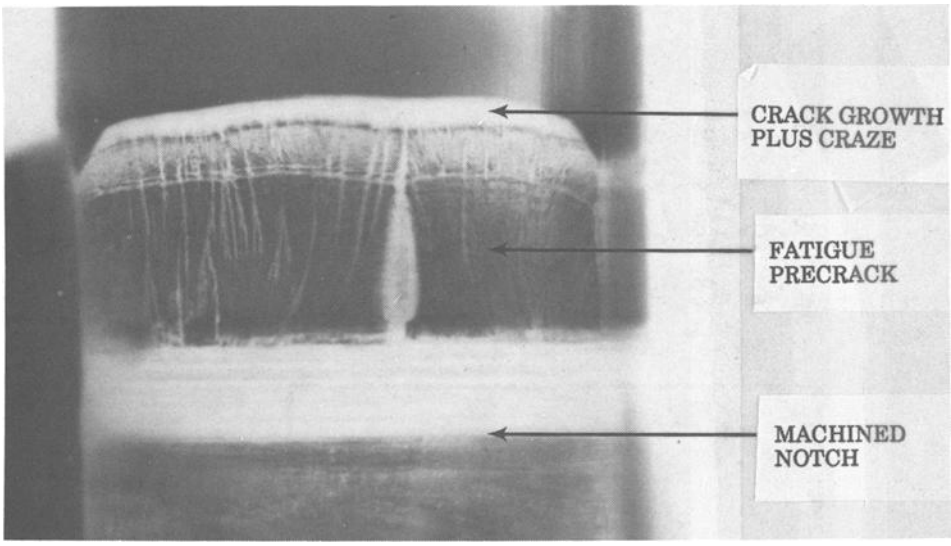

FIG. 2—*Photograph of the crack taken through the length of Specimen 6.*

Experimental data were not observed to follow the blunting line

$$J = 2\Delta a_b \sigma_f \tag{5}$$

where Δa_b is the crack growth due to blunting and σ_f is the flow stress, defined as the average of the yield and tensile stresses. More crack growth was observed than was predicted by the blunting line. This was due to a craze ahead of the crack tip. The craze should open up as the load is applied, reducing the amount of blunting and allowing crack growth within

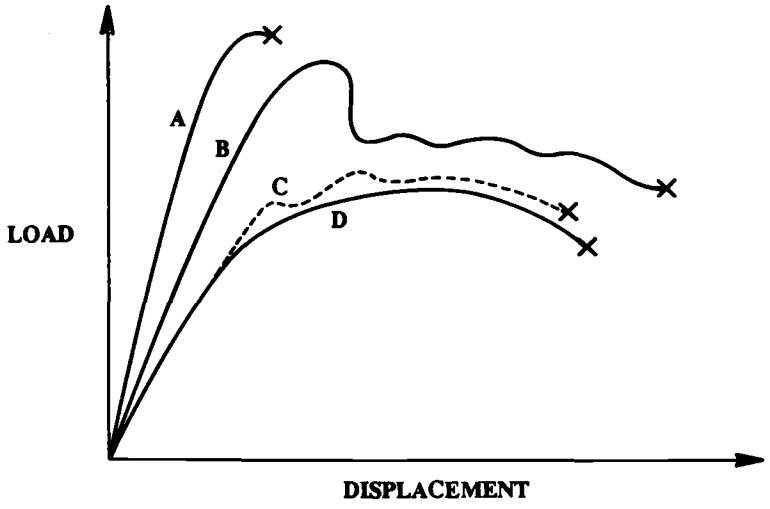

FIG. 3—*Types of load-displacement curves: Curve A is unstable fracture; Curve B is popin at maximum load and thereafter stable; Curve C is popin before maximum load and thereafter stable; and Curve D is stable with no popin.*

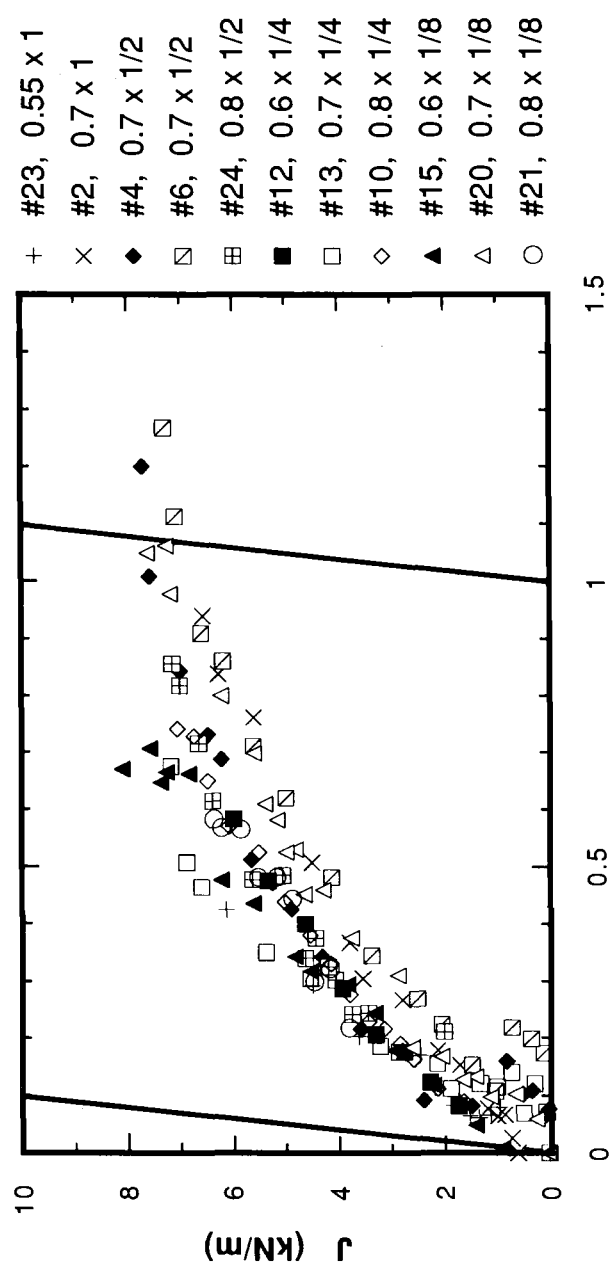

FIG. 4—*J-integral resistance curves. The legend is* #W, Y x Z, *where* W *is the specimen number,* Y *is the nominal* a/w, *and* Z *is the nominal* B *in inches.*

the craze. The craze was present due to the fatigue precracking, which forms a craze ahead of the crack tip [*34–36*].

As the specimen was being loaded in the fracture tests, the craze from the fatigue precracking opened and gave the appearance of crack growth. This behavior was probably responsible for the small amounts of crack growth recorded at low values of J. The maximum values of the craze length were about 0.18 mm (0.007 in.). This value is almost twice the craze length of 0.10 mm (0.004 in.) reported by Fraser and Ward [*24*], but it is of the correct order of magnitude. (These small amounts of crack growth at low values of J were not used in the calculation of J_{Ic}, nor was the crack growth data shifted by these amounts of crack growth. Sometimes this crack growth decreased in magnitude due to small measurement errors, including lighting effects.)

The Dugdale Model [*37*] was used to predict the craze length. Using the true stress at fracture of 78.1 kPa (11 320 psi) for the yield stress, the craze length is predicted to be 0.18 mm (0.007 in.) at a J of 1.07 kN/m (6.1 psi·in.). (The true stress at fracture is approximately equal to the stress in the necked region in the tension test.) This agrees with the maximum craze length observed. Above this value of J, a longer craze length is predicted than observed. Near this value of J, crack growth begins, and it is questionable whether the model is still applicable.

The crack growth initiated and the crack grew a small amount when the specimen was nominally elastic. Some, but not all, of this growth is due to craze formation. The majority of crack growth took place when the specimen was in the elasto-plastic regime. This is shown by measurements of the crack growth during the test, of which Fig. 5 is an example.

During crack growth, the crack would grow more in the center than at the edges, producing a bowed crack front. The edges would separate, leaving a shear lip. In the 3.18-mm (0.125-in.)-thick specimens, the crack front became a "V" shape due to the shear lips.

Fracture Criteria

In this section, criteria for characterizing the fracture behavior of PC are developed and discussed. These criteria are based upon finding a single value for J that describes the fracture toughness of PC. Three values of J were examined: J at the initiation of crack growth, J at 2% crack growth, and J at popin.

J at the initiation of crack growth, J_{init}, was determined by the calculation procedure given in ASTM E 813-81 and E 813-87 for the measurement of J_{Ic}. For the 1981 standard, a linear regression of the data between the 0.15 and 1.5-mm crack growth offsets was made, and the intersection of this line with the blunting line gave the value of $J_{Ic}(81)$. Table 3 contains this value for each specimen. $J_{Ic}(81)$ ranges from 1.6 to 2.9 kN/m (9 to 16 psi·in.), with an average of 2.13 kN/m (12.2 psi·in.) and a standard deviation of 0.43 kN/m (2.45 psi·in.). No influence of the thickness or crack length on $J_{Ic}(81)$ was observed.

For the 1987 standard, a logarithmic fit of the data was made, and the intersection of this curve with the 0.2-mm offset blunting line determined the values of $J_{Ic}(87)$. Table 3 shows $J_{Ic}(87)$, which ranges from 2.3 to 4.0 kN/m (13.0 to 22.8 psi·in.). The average $J_{Ic}(87)$ was 3.33 kN/m (19.04 psi·in.) with a standard deviation of 0.55 kN/m (3.16 psi·in.). No influence of thickness or crack length on $J_{Ic}(87)$ were observed.

In addition, J_{init} was estimated by examining the crack growth data to identify when crack initiation began. These values are given in Table 3 under the column J_{init}-visual. The average value of J_{init} determined by this method was 1.37 kN/m (8.0 psi·in.) with a standard deviation of 0.63 kN/m (3.5 psi·in.), which is lower than the value from the 1981 standard. The $J_{Ic}(81)$ and "visual" values of J_{init} were compared for each specimen, and $J_{Ic}(81)$ was on the average 0.71 kN/m (4.1 psi·in.) higher than the visual value.

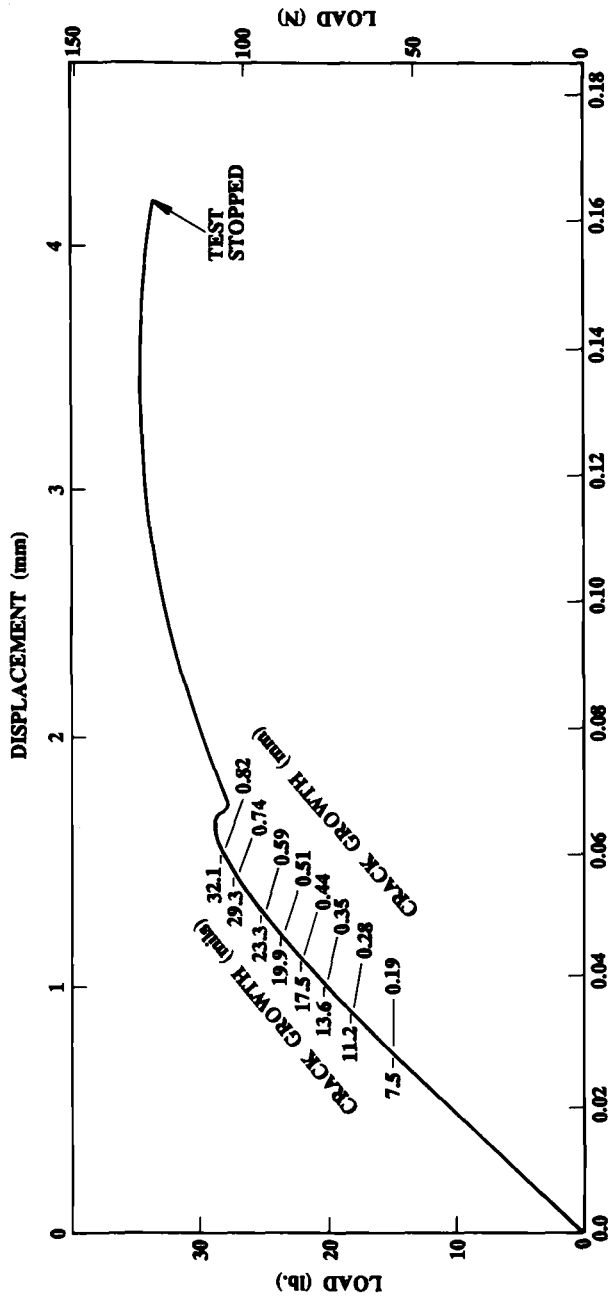

FIG. 5—*Load-displacement curve showing amount of crack growth (Specimen 15,* a/W = *0.6,* B = *3.2 mm).*

TABLE 3—*J-integral fracture criteria.*

Specimen	*B*, mm (in.)	*a*/*W*	*J* at Initiation			*J* at 2% Crack Growth, kN/m (psi·in.)	*J* at Popin, kN/m (psi·in.)
			Visual, kN/m (psi·in.)	E 813-81, kN/m (psi·in.)	E 813-87, kN/m (psi·in.)		
23	25.76 (1.014)	0.54	1.23 (7)	[b]	[b]	4.47 (25.5)	7.36 (42)
2	25.35 (0.998)	0.70	0.70 (4)	1.61 (9.2)	2.66 (15.2)	3.80 (21.7)	7.18 (41)
4	12.70 (0.500)	0.69	2.63 (15)	2.88 (16.4)	3.73 (21.3)	4.47 (25.5)	7.53 (43)
6	12.65 (0.498)	0.69	0.88 (5)	1.56 (8.9)	2.28 (13.0)	3.40 (19.4)	7.36 (42)
24	12.57 (0.495)	0.80	2.10 (12)	2.49 (14.2)	3.59 (20.5)	4.90 (28.0)	7.36 (42)
12	6.30 (0.248)	0.58	0.88 (5)	2.00 (11.4)	3.55 (20.3)	4.03 (23.0)	7.88 (45)
13	6.35 (0.250)	0.68	1.75 (10)	2.31 (13.2)	3.99 (22.8)	5.43 (31.0)	7.18 (41)
10	6.35 (0.250)	0.78	1.05 (6)	2.08 (11.9)	3.78 (19.3)	4.78 (27.3)	[a]
15	3.18 (0.125)	0.59	0.88 (5)	1.67 (9.5)	3.45 (19.7)	4.29 (24.5)	7.36 (42)
20	3.12 (0.123)	0.70	1.58 (9)	2.32 (13.2)	2.87 (16.4)	3.64 (20.8)	6.65 (38)
21	3.10 (0.122)	0.81	1.75 (10)	2.38 (13.6)	3.83 (21.9)	4.76 (27.2)	[a]
Average			1.37 (8.0)	2.13 (12.2)	3.33 (19.0)	4.36 (25.0)	7.3 (41.0)
Standard Deviation			0.63 (3.5)	0.43 (2.5)	0.55 (3.2)	0.61 (3.5)	0.33 (2.2)

[a]No popin.
[b]Insufficient data.

$J_{Ic}(87)$ was larger than $J_{Ic}(81)$ by 1.20 kN/m (6.9 psi·in). This is not surprising since the 1987 standard allows a finite amount of crack growth.

The values of $J_{Ic}(81)$ are in agreement with Parvin and Williams [*26,27*], who measured a J_{init} of 1.94 kN/m (11.1 psi·in.). However, Fraser and Ward [*24*] reported a value of 0.37 kN/m (2.11 psi·in.). This small value may be due to their very sensitive crack measurement technique.

The second fracture criterion was J at 2% crack growth. The value of J was measured at a value of Δa corresponding to 2% of the original crack length. (No secant offset line was used because the blunting line is very steep, resulting in similar values of J with and without an offset line. In addition, no offset value was added to the 2% crack growth, such as 0.2%.) This has the advantages of determining J at a measurable amount of crack growth, and of allowing more of the toughness of the material to be used. A value of 2% crack growth was chosen because this is the amount of crack growth allowed in ASTM Test Method for Plane-Strain Fracture Toughness of Metallic Materials (E 399-83) for K_{Ic}.

The values of J at 2% crack growth, $J(2\%)$, ranged from 3.3 to 5.4 kN/m (19 to 31 psi·in.), with an average of 4.36 kN/m (25.0 psi·in.) and a standard deviation of 0.61 kN/m (3.5 psi·in.). They are given in Table 3. No effect of crack length or thickness upon $J(2\%)$ could be ascertained.

$J_{Ic}(81)$ is equivalent to a K of 2360 kPa $\sqrt{m}$ (2140 psi $\sqrt{in.}$); $J_{Ic}(87)$ is equivalent to a K of 2950 kPa $\sqrt{m}$ (2680 psi $\sqrt{in.}$); and $J(2\%)$ is equivalent to a K of 3370 kPa $\sqrt{m}$ (3070 psi $\sqrt{in.}$). Values of K_{Ic} reported in the literature are 3630 kPa $\sqrt{m}$ (3300 psi $\sqrt{in.}$), by Banasiak [*38,39*] for the same sheet of PC as used in the present study (but in the T-L orientation); 3620 kPa $\sqrt{m}$ (3290 psi $\sqrt{in.}$) by Key and Katz [*32*]; and 3460 kPa $\sqrt{m}$ (3150 psi $\sqrt{in.}$) by Fraser and Ward [*24*]. (The slightly lower value of K corresponding to $J(2\%)$ may be due to the difference in crack growth direction in the present study. It was not possible to obtain a valid K_{Ic} because the specimens were not large enough in the W dimensions.) Thus, $J(2\%)$ appears to be a better measure of K_{Ic} for PC than $J_{Ic}(81)$ or $J_{Ic}(87)$. This should not be surprising since the standard for K_{Ic} allows for 2% crack growth.[2]

The third fracture criterion considered was the value of J at popin. The motivation for this is that PC has much more resistance to fracture than that given by either J_{Ic} or $J(2\%)$. It is desirable to use this additional toughness in design.

The value of J at popin is given in Table 3. When unstable fracture occurred, the value of J at the fracture point was used as the popin value. The average value of J at popin was 7.32 kN/m (41.0 psi·in.) with a standard deviation of 0.33 kN/m (2.2 psi·in.). Specimen thickness and crack length had no effect upon this value. This value is in agreement with a value of 6.16 kN/m (35.2 psi·in.), measured by Parvin and Williams [*27*]. For those specimens in which popin did not occur, the value of J at maximum load closely corresponded to the value of J at popin.

J at popin may be due to the type of specimen geometry employed. Tests need to be made with other geometries before J at popin is used to chracterize the fracture toughness of PC.

[2]A definitive comparison of J_{Ic} with K_{Ic} values requires that the crack growth be measured in the same orientation, which is not the present case. However, little orientation dependence is expected in a 1-in. sheet of polycarbonate because the processing conditions do not impart a texture. This lack of orientation dependence is confirmed by experimental measurements in the literature. Parvin and Williams [*26*] measured the fracture behavior of polycarbonate for single-edge-notched specimens (T-L orientation) and surface-notched specimens (T-S orientation). They found similar values for K_c in both cases, and did not report any orientation effects. Unpublished data by Buisson and Ravi-Chandar on polycarbonate tested in the T-L orientation for J_{Ic} (81) are 2.0 kN/m, which agree with the T-S values in the present paper.

Applicability of ASTM E 813-87 to Polycarbonate

Two aspects of ASTM E 813-87 are unsuitable for polycarbonate. These are the blunting line and the 1-mm offset line. The lack of agreement of the blunting line and the experimental data was discussed earlier in the subsection of crack growth behavior, and was attributed to the formation of a craze ahead of the crack tip. Metals do not encounter this difficulty since they do not craze.

The second aspect of ASTM E 813-87 that is unsuitable for polycarbonate is the requirement of at least one data point between the 1 and 1.5-mm offset lines. For almost all of the experimental data, 1 mm of stable crack growth could not be sustained. Unstable fracture occurred in the thicker specimens, and popin occurred for the intermediate thickness specimens. Popin caused a discontinuous increase in crack growth, which made fitting a smooth curve through the data impossible. For the thinner specimens, a highly nonuniform crack front formed prior to 1 mm of crack growth. Despite the lack of data between the 1 and 1.5-mm offset lines, excellent logarithmic fits to the data were obtained that clearly defined the intersection with the 0.2-mm offset line.

Both of these difficulties with ASTM E 813-87 could be avoided if J_{Ic} was defined at a fixed amount of crack growth that included crazing and blunting. This amount of crack growth should be large enough to allow the value of J_{Ic} to be bracketed by experimental data both greater and lesser than this amount. Then, J_{Ic} could be determined by a linear or logarithmic interpolation between this data, instead of an extrapolation. One such criterion is the use of J at 2% crack growth.

Conclusions

The conclusions from this experimental study of the use of the J-integral to determine the fracture toughness of polycarbonate are as follows:

1. The fracture behavior was well characterized by the J-integral. The values of J_{Ic} are 2.13 kN/m (12.2 psi·in.) by ASTM E 813-81 and 3.3 kN/m (19.0 psi·in.) by ASTM E 813-87.
2. The value of J at 2% crack growth was 4.4 kN/m (25 psi·in.) and corresponded well with values of K_{Ic} in the literature. J_{Ic} as determined by the ASTM standards was lower than K_{Ic}.
3. The value of J at popin or unstable fracture, 7.3 kN/m (41 psi·in.), was consistent for all the experiments.
4. No effect of crack length or thickness was observed for any of these values of J.
5. The experimental data showed more crack extension than predicted by the blunting line.
6. Valid crack growth data between the 1 and 1.5-mm offset lines could not be obtained.
7. It is suggested that J_{Ic} be determined at a finite amount of crack growth plus crazing and blunting, such as 2% crack growth. A sufficient amount of crack growth should be allowed so that an interpolation can be made between data on either side of the measurement point.

Acknowledgments

The author would like to thank the support of the Air Force Wright Aeronautical Laboratories under Contracts F33616-76-C-5191 and F33615-79-C-5025 and for the discussions with Drs. N. Ashbaugh and T. Nicholas.

References

[1] Begley, J. A. and Landes, J. D. in *Fracture Toughness, ASTM STP 514*, American Society for Testing and Materials, Philadelphia, 1972, pp. 1–20.

[2] Landes, J. D. and Begley, J. A. in *Fracture Analysis, (Eighth Conference), ASTM STP 560*, American Society for Testing and Materials, Philadelphia, 1974, pp. 170–186.

[3] Griffis, C. A. and Yoder, G. R., *Journal of Engineering Materials and Technology*, 1976, p. 152.

[4] Clarke, G. A., *Journal of Testing and Evaluation*, Vol. 8, 1980, p. 213.

[5] Clarke, G. A., Landes, J. D., and Begley, J. A., *Journal of Testing and Evaluation*, Vol. 8, 1980, p. 221.

[6] Argy, G., Paris, P. C., and Shaw, F. in *Properties of Materials for Liquefied Natural Gas Tankage, ASTM STP 579*, American Society for Testing and Materials, Philadelphia, 1975, pp. 96–137.

[7] Shih, C. F., deLorenzi, H. G., and Andrews, W. R. in *Elastic-Plastic Fracture, ASTM STP 668*, J. D. Landes, J. A. Begley, and G. A. Clarke, Eds., American Society for Testing and Materials, Philadelphia, 1979, pp. 65–120.

[8] Berger, C., Keller, H. P., and Munz, D. in *Elastic-Plastic Fracture, ASTM STP 668*, J. D. Landes, J. A. Begley, and G. A. Clarke, Eds., American Society for Testing and Materials, Philadelphia, 1979, pp. 378–405.

[9] Joyce, J. A. and Gudas, J. P. in *Elastic-Plastic Fracture, ASTM STP 668*, J. D. Landes, J. A. Begley, and G. A. Clarke, Eds., American Society for Testing and Materials, Philadelphia, 1979, pp. 458–468.

[10] Takahashi, H., Khan, M. A., and Suzuki, M., *Journal of Testing and Evaluation*, Vol. 8, 1980, p. 63.

[11] Takahashi, H., Khan, M. A., and Suzuki, M., *Journal of Testing and Evaluation*, Vol. 9, 1981, p. 14.

[12] Carlson, K. W. and Williams, J. A. in *Fracture Mechanics (Thirteenth Conference), ASTM STP 743*, Lane and Otten, Eds., American Society for Testing and Materials, Philadelphia, 1981, pp. 503–524.

[13] Landes, J. D. and Begley, J. A., "Recent Development in J_{Ic} Testing," Westinghouse Research Labs Scientific Paper 76-1E7-JINTF-P3, Westinghouse Research Labs., Pittsburgh, May 1976.

[14] Zaverl, F., Jr., "The Influence of Specimen Dimensions on a *J*-Fracture Toughness Test," T. & A. M. Report No. 394, Dept. of Theoretical and Applied Mechanics, University of Illinois, Urbana, IL, Sept. 1974.

[15] Rice, J. R., *Journal of Applied Mechanics*, Vol. 35, 1968, p. 379.

[16] Eshelby, J. D. in *Solid State Physics*, F. Seitz and D. Turnbull, Eds., Vol. 3, Academic Press, New York, 1956, pp. 79–144.

[17] McClintock, F. A. in *Fracture*, H. Liebowitz, Ed., Vol. 3, Academic Press, New York, 1971, pp. 47–225.

[18] Hilton, P. D. and Hutchinson, J. W., *Engineering Fracture Mechanics*, Vol. 3, 1971, p. 435.

[19] Hutchinson, J. W., *Journal of the Mechanics and Physics of Solids*, Vol. 16, 1968, p. 13.

[20] Rice, J. R. and Rosengren, G. F., *Journal of Mechanics and Physics of Solids*, Vol. 16, 1968, p. 1.

[21] Kambour, R. P., *Journal of Polymer Science.: Macromolecular Reviews*, Vol. 7, 1973, p. 1.

[22] Brown, N., "Methods of Studying Crazing," *Methods of Experimental Physics*, Vol. 16C, Academic Press, New York, 1980, pp. 233–273.

[23] Kinloch, A. J., *Metal Science*, Vol. 14, 1980, p. 305.

[24] Fraser, R. A. W. and Ward, I. M., *Polymers*, Vol. 19, 1978, p. 220.

[25] Mills, N. J., *Engineering Fracture Mechanics*, Vol. 6, 1974, p. 537.

[26] Parvin, M. and Williams, J. G., *International Journal of Fracture*, Vol. 11, 1975, p. 963.

[27] Parvin, M. and Williams, J. G., *Journal of Materials Science*, Vol. 10, 1975, p. 1883.

[28] Brinson, H. F., *Experimental Mechanics*, Vol. 10, 1970, p. 72.

[29] Key, P. L., Katz, Y., and Parker, E. R., "An Application of Fracture Mechanics to Glassy Plastics," UCRL-17911, University of California Radiation Laboratory, Livermore, CA, Feb. 1968.

[30] Bernstein, H. L., "A Study of the *J*-integral Method Using Polycarbonate," AFWAL-TR-82-4080, Air Force Wright Aeronautical Laboratories, Wright-Patterson Air Force Base, OH, 1982.

[31] Cornes, P. L., Smith, K., and Haward, R. N., *Journal of Polymer Science*, Vol. 15, 1977, p. 955.

[32] Key, P. L. and Katz, Y., *International Journal of Fracture Mechanics*, Vol. 5, 1969, p. 63.

[33] Green, A. P. and Hundy, B. B., *Journal of Mechanics and Physics of Solids*, Vol. 4, 1956, p. 128.

[34] Manson, J. A. and Hertzberg, R. W., "Fatigue Failure in Polymers," *CRC Critical Reviews in Macromolecular Science*, Chemical Rubber Co., Cleveland, Aug. 1973, pp. 433–500.

[35] Hertzberg, R. W., Manson, J. A., and Wu, W. C. in *Progress in Flaw Growth and Fracture*

Toughness Testing, ASTM STP 536, American Society for Testing and Materials, Philadelphia, 1973, pp. 391–403.

[*36*] Hertzberg, R. W. and Manson, J. A., *Fatigue of Engineering Plastics*, Academic Press, New York, 1980.

[*37*] Dugdale, D. S., *Journal of Mechanics and Physics of Solids*, Vol. 8, 1960, p. 100.

[*38*] Banasiak, D. H., "Fatigue Crack Growth and Retardation Using Transparent Polycarbonate," Master's thesis, Air Force Institute of Technology, Wright-Patterson Air Force Base, OH, June 1973.

[*39*] Banasiak, D. H., Grandt, A. F., Jr., and Montulli, L. T., *Journal of Applied Polymer Science*, Vol. 21, 1977, p. 1297.

Wai N. Chung[1] *and James G. Williams*

Determination of J_{Ic} for Polymers Using the Single Specimen Method

REFERENCE: Chung, W. N. and Williams, J. G., **"Determination of J_{Ic} for Polymers Using the Single Specimen Method,"** *Elastic-Plastic Fracture Test Methods: The User's Experience (Second Volume), ASTM STP 1114*, J. A. Joyce, Ed., American Society for Testing and Materials, Philadelphia, 1991, pp. 320–339.

ABSTRACT: The fracture toughness of several polymes is characterized using the *J*-integral method. The single specimen method has been applied, and the tests were conducted on three-point bend specimens of polyvinylidine difluoride, medium and high density polyethylene. The results are compared with the *J-R* curves obtained from the multiple specimen method, which is often used for polymers and has proved to be successful. This has enabled a good degree of confidence be attached to the single specimen method. For each type of polymer, the *J-R* curves obtained from both methods are in good agreement. Hysteresis loops are observed during unloading and reloading because of the viscoelastic nature of the polymers, and the shape of the loops was affected by the friction at the support rollers. The distinction of J_{Ic} values determined according to the ASTM Standards E 813-81 and E 813-87 is shown. The E 813-87 procedure predicts a more consistent J_{Ic} value than the E 813-81, but the adoption of the 0.2 mm offset blunting line does not reflect the actual initiation point and the advantages and drawbacks of each method are discussed. The blunting line suggested in the E 813 protocols is found to be inappropriate for describing the blunting mechanisms of polymers. Some tests were performed at different loading rates to determine the rate sensitivity of both the J_{Ic} values and *J-R* curves. It is suggested that the maximum allowable crack extension recommended for the *J* controlled growth condition is too conservative for polymers, and it is noted that the crack growth is difficult to measure accurately. A maximum allowable crack extension of 10% of the uncracked ligament is considered to be appropriate.

KEY WORDS: *J*-Integral, fracture toughness, single specimen *J* test, multiple specimen *J* test, ASTM E 813, blunting line, polyvinylidine difluoride, polyethylene

The *J*-integral approach has been applied to characterize the fracture toughness of toughened polymers by various investigators [*1–9*]. The method provides a reduction of specimen size required for obtaining valid plane strain fracture toughness when compared to K_{Ic} tests because the plastic plane strain condition is sufficient to achieve a valid fracture toughness value. Thus the specimen size required is much smaller for *J* testing. This gives an advantage for testing polymers since there are considerable difficulties in manufacturing thick sections.

The use of the *J*-integral method is still in its infancy for polymers, but the multiple specimen method described in the ASTM Standard Test Method for J_{Ic} E 813-81, or the updated version of it E 813-87, has been adopted in all the previous studies. However the standard was not strictly followed, and various modifications on the protocol were made by workers in order to accommodate polymers. This method is simple and effective, but a large number of specimens are needed to determine the J_{Ic} value, that is, the value of *J* at the

[1]Research student and professor of Polymer Engineering, respectively, Department of Mechanical Engineering, Imperial College of Science, Technology, and Medicine, London, SW7 2BX, England, U.K.

onset of crack initiation. Included in the E 813-87 is the single specimen method, also known as the unloading compliance method, which needs only one specimen to acquire the entire *J-R* curve and which provides an alternative to the multiple specimen technique. The single specimen method was first developed for metals, the technique is now well established but has rarely been applied to polymers, and the validity of the method is still uncertain. In this study, an attempt is made to determine the J_{Ic} values of several polymers using the single specimen method, and in order to enable a level of confidence to be attached to the method, the results are compared with those obtained by the multiple specimen technique which has been demonstrated to be successful for polymers. The effect of loading rate on J_{Ic} is also investigated since the properties of these materials are strain rate sensitive.

Construction of the *J-R* Curve

For three-point bend specimens having a span to width ratio of 4 and a crack to width ratio greater than 0.5, the parameter J can be determined experimentally using the equation

$$J = \frac{2U}{Bb} \tag{1}$$

where

U = total energy input,
B = specimen thickness, and
b = uncracked ligament.

This provides the basis for determining the J_{Ic} values using the crack growth resistance, or the R-curve. The R-curve is constructed by plotting the J values against the crack extension Δa from which the intersection of the blunting line, and the R-curve is defined as the J_{Ic} value. The blunting line accounts for the apparent increase in crack length Δa_b due to crack tip blunting prior to material separation. Based on the assumption of smooth blunting at the crack tip, the equation of the blunting line is given as

$$J = 2\sigma_y \Delta a \tag{2}$$

where σ_y = yield stress.

This experimental value of J_{Ic} is considered to be valid only if it satisfies the size criteria stated in the ASTM E 813 which ensures that the crack growth occurs under plane strain conditions with the appropriate degree of constraint.

$$B, b > 25\left(\frac{J_c}{\sigma_y}\right) \tag{3}$$

where J_c = measured value of J_{Ic}.

The R-curve can be determined according to the old E 813-81 or the new equivalent of it, E 813-87. The R-curve is represented by a linear regression line in the former case and the point where the regression line meets the blunting line is regarded as the J_{Ic} value. Most of the J work in the past has been based on this method. A power law curve fitting to the data is proposed in the new standard, and the J_{Ic} value is defined as the intersection of the power law fitted R-curve and a 0.2 mm offset blunting line.

Crack Length Prediction

For the unloading compliance method, the crack length is estimated from successive partial unloading during the loading of the test specimen. Crack length can be predicted from the crack mouth opening compliance and the various expressions relating the compliance and crack length for the three-point bend specimen which can be found in the literature [*10–12*]. The one developed by Bakker [*12*], rather than that suggested in the ASTM E 813-87, has been used for crack length estimation since the accuracy is better [*12*]. The transfer function δ_{cm} of the inverse crack mouth opening compliance function developed by Kapp et al. [*11*] is used by Bakker to calculate the first estimate of crack to width ratio, a/W, as shown in Eqs 4*a* and 4*b*

$$\delta_{cm} = \frac{1}{1 + \sqrt{\dfrac{3.95S/W}{E'BC_{cm}\,(\text{exp})}}} \tag{4a}$$

$$\frac{a}{W} = 9.56 \times 10^{-4} + 5.504 \times 10^{-2}\delta_{cm} - 1.0968\,\delta_{cm}^2 + 9.9706\,\delta_{cm}^3 - 13.096\,\delta_{cm}^4 + 5.1707\,\delta_{cm}^5 \tag{4b}$$

where

S = span,
W = width,
a = crack length,
C_{cm} (exp) = measured crack mouth opening compliance,
B = specimen thickness, and
E' = effective modulus (see Eq 6).

A correction on the first estimate was given by Bakker [*12*], shown in Eq 5 to improve the accuracy of the crack length prediction.

$$\left(\frac{a}{W}\right)_{\text{corrected}} = \frac{a}{W} + \frac{C_{cm}(\text{exp}) - C_{cm}(a/W)}{\dfrac{dC_{cm}(a/W)}{d(a/W)}} \tag{5}$$

where $C_{cm}(a/W)$ is the value of compliance calculated from the first estimate of a/W using the following equation

$$E'BC_{cm}(a/W) = \frac{S}{W}\frac{a/W}{(1 - a/W)^2}\left[8.737 - 8.681(a/W)^{0.5} + 3.321(a/W) + 0.573(a/W)^{1.5}\right] \tag{6}$$

In order to account for various uncertainties in testing, an effective modulus E' is evaluated using Eq 6 by measuring the compliance of the first few unloadings where no crack extension occurs. The value of E' should not differ from the elastic modulus E by more than 10%.

Materials

High density polyethylene (HDPE), polyvinylidine difluoride (PVDF), and medium density polyethylene (MDPE) were tested and were supplied in the form of compression moulded

TABLE 1—*Material properties.*

Supplier	Designation	Material	E, GPa	σ_y, MPa
DSM	8621	HDPE	1.7	26
Solvay & Cie	1010	PVDF	2.5	53
BP Chemicals	Rigidex 002-50	MDPE	0.8	17

sheets. Dumbell specimens were used to measure the yield stress σ_y and the elastic modulus E. The maximum load and original cross section area were used to calculate the yield stress. The properties are shown in Table 1.

Experimental Procedure

Specimen Preparation

Specimens were fabricated from the sheets and were notched to a crack to width ratio of 0.6 or 0.55 using a single point flycutter. The tip radius of the flycutter was measured using an optical shadowgraph and were found to be approximately 16 μm. Notches prepared by this method should provide sufficient sharpness at the crack tip [*4*,*9*]. For the MDPE, side grooves of 1.5 mm were machined on both sides of the specimens after the notch had been introduced. All the specimens were loaded in three-point bending with a span to width ratio of 4, and the tests were performed on an Instron testing machine at room temperature. The dimensions of the specimens are given in Table 2.

Multiple Specimen J *Tests*

Nine specimens for each material were prepared and loaded to different predetermined displacements. The load line displacement was measured using the transducer which was built into the machine. The load and displacement were registered by a personal computer connecting to the testing machine, and the area under the load-displacement curve was evaluated. The specimens were then broken open to reveal the crack extension by impact after dipping into liquid nitrogen. The crack size was measured at nine equally spaced points as suggested by E 813-87. The corresponding value of J was calculated using Eq 1.

Single Specimen J *Tests*

For the single specimen J tests, crack length was estimated from the crack mouth opening compliance. The load line displacement and the crack mouth displacement were monitored by a linear variable displacement transducer (LVDT) and a clip gage, respectively. The load and displacements were recorded and plotted on Hewlett Packard X-Y plotters. Knife edges were used to mount the clip gage in order to obtain friction free seating of the gage. The

TABLE 2—*Specimen dimensions for* J *tests.*

Material	W, mm	B, mm	S, mm	Side Groove, Each Side, mm	a/W
HDPE	30	10	120	. . .	0.6
PVDF	22	10	88	. . .	0.55
MDPE	50	25	200	1.5	0.6

layout of the apparatus is shown in Fig. 1. The energy for computation of J in Eq 1 was obtained up to the point of unloading from the load-load line displacement graph, and the crack mouth compliance was measured graphically from the load-clip gage displacement plot. Equations 4*a*, 4*b*, 5, and 6 were used to evaluate the crack length at the point of unloading. During the tests, each specimen was unloaded 12 to 18 times by 20 to 30% of the current load. Loading and reloading were carried out continuously at the same cross head speed. The effective modulus was estimated from the compliance measured between 10 to 30% of the maximum load. The change of morphology, not whitening, on the fracture surface was taken as the extent of crack extension when direct measures of crack length were made. At least two replicates were tested for each material or at each loading rate.

Energy Correction for Indentations

Energy corrections were made for elastic and plastic indentations of the specimen by the loading pin and support rollers. This could be done by use of the actual test fixture and the tested specimen with the arrangement as shown in Fig. 2. The support rollers were butted together and a broken undeformed half specimen was placed on the rollers with the same orientation as during the test. The specimen was loaded to approximately 1.25 times the actual test limit load. The area under this load displacement curve at each load was then subtracted from the one obtained during the fracture test.

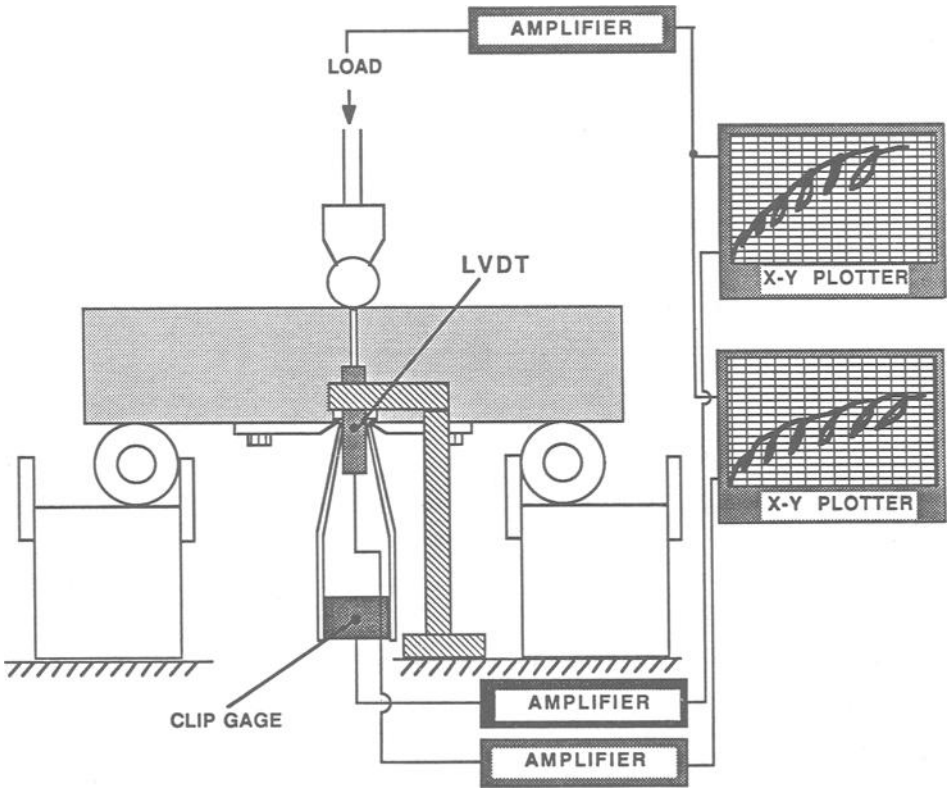

FIG. 1—*The layout of the apparatus for single specimen* J *tests.*

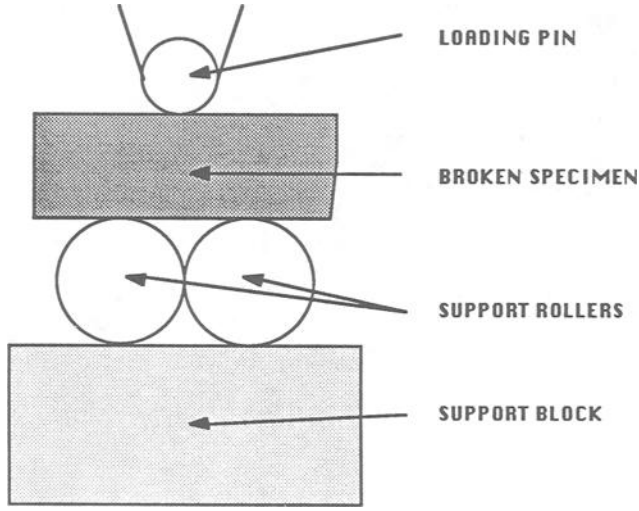

FIG. 2—*The test fixture for the indentation correction.*

Results

Multiple Specimen J *Tests*

The *J-R* curves obtained from the multiple specimen *J* tests are shown in Figs. 3, 4, and 5 for HDPE, PVDF, and MDPE, respectively. It was found that the J_{Ic} values determined according to the new E 813-87 procedures tended to be higher than the ones obtained from

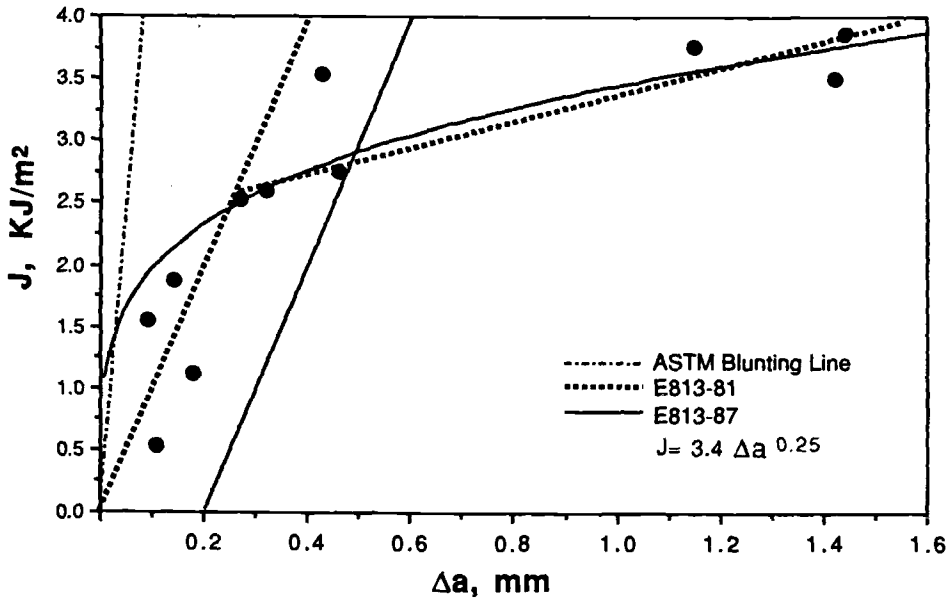

FIG. 3—J-R *curve for HDPE from multiple specimen* J *tests with loading rate of 1 mm/min.*

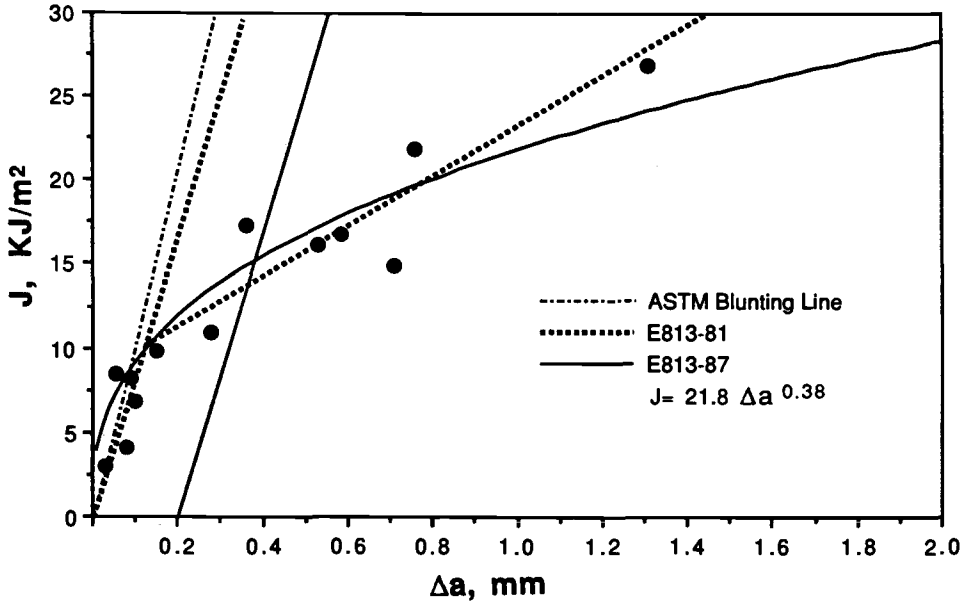

FIG. 4—J-R *curve for PVDF from multiple specimen* J *tests.*

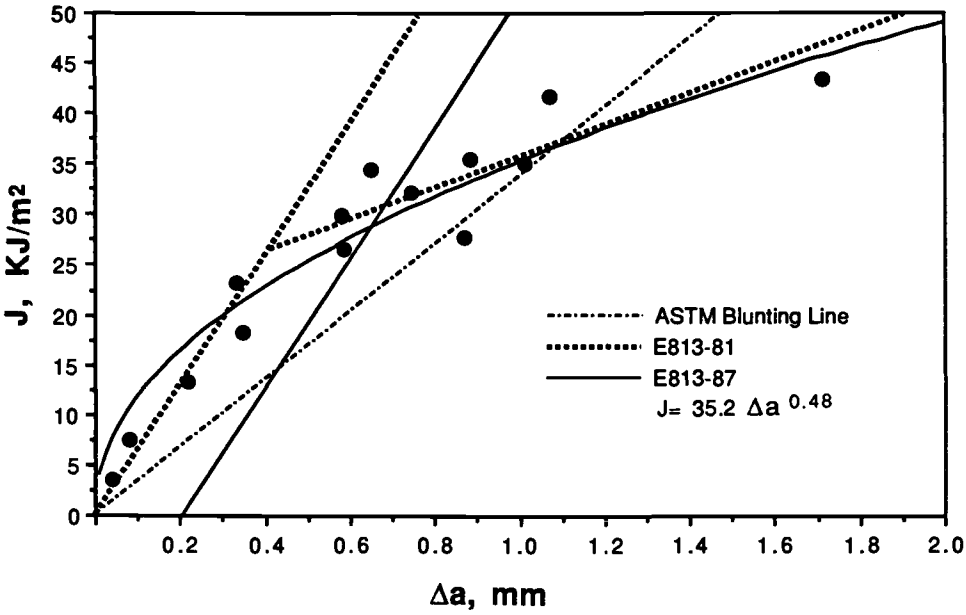

FIG. 5—J-R *curve for MDPE from multiple specimen* J *tests.*

the old standard. From the figures it is also apparent that the conventional blunting line given in Eq 2 does not describe the blunting mechanisms adequately for all the materials. As a result, a best straight line through the data near the blunting region was drawn and taken as the blunting line. All the tests, except for those of MDPE, satisfied the size requirements stated in Eq 3. For the specimens without side grooves, severe crack front curvature was found on the fracture surfaces, and the crack extension at the center was normally larger than the near surface one by more than 0.02 W (where W is the specimen width). The effect of loading rate on the J-R curves for HDPE is illustrated in Fig. 6 (the construction of the blunting line and R-curve is not shown in the graph for clarity). It can be seen that the J_{Ic} values do not vary strongly with the loading rate, but the R-curves tend to flatten slightly as the loading rate increases. However, due to the scatter of the data, additional tests would be needed in order to better define the effect of the loading rate on the R-curve.

Compliance Measurements

Typical load and clip gage displacement curves are shown in Fig. 7. Hysteresis loops resulting from unloading were observed in both the load-clip gage displacement and load-load line displacement plots for all materials. If fixed support rollers were used, rhomboid shaped hysteresis loops resulted as shown in Fig. 8 and they appeared in both the load line and crack mouth compliance. This shows that the friction at the rollers has an effect on the specimen compliance for polymers, and the sharp corners indicate where the friction effect reverses. Thus free rollers must be used in order to minimize error in compliance measurements.

In Fig. 7 it can be seen that the main difficulty in crack length prediction is to determine the correct part of the unloading loop for the compliance measurement. Since an elastic model was adopted to predict the viscoelastic behavior of the materials, certain assumptions

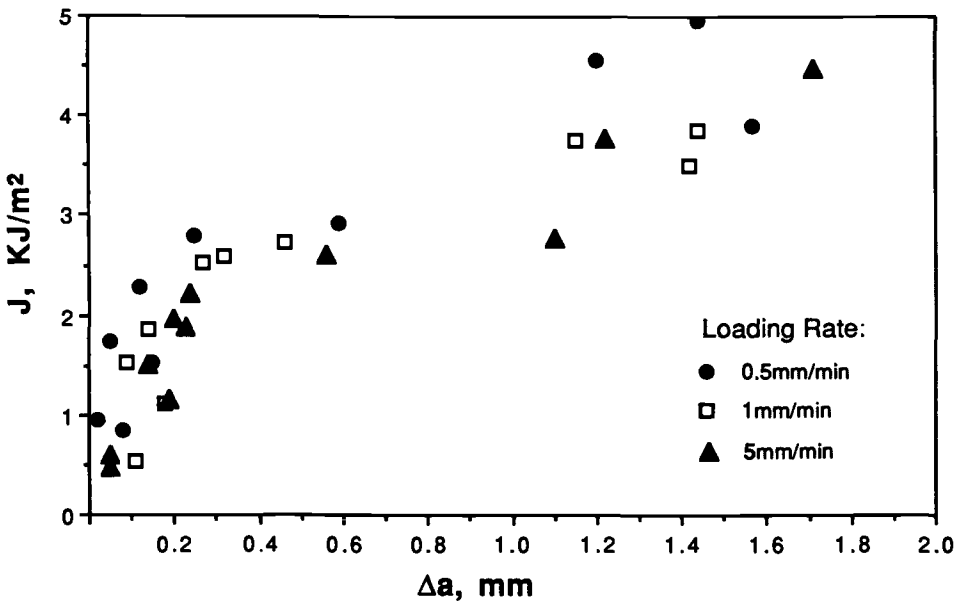

FIG. 6—J-R *curves for HDPE from multiple specimen* J *tests at various loading rates.*

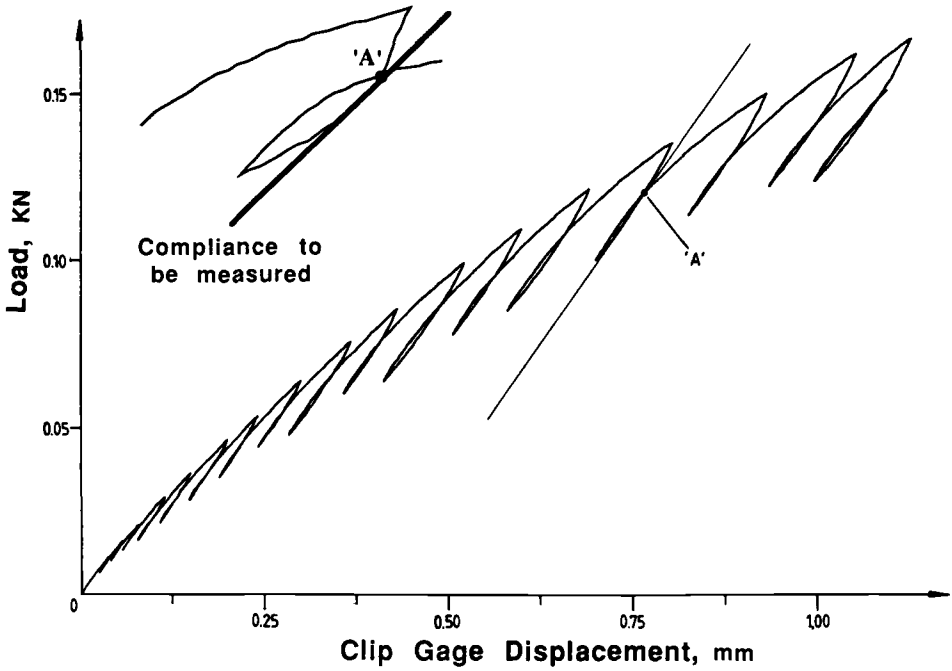

FIG. 7—*Typical load-clip gage displacement curve for HDPE with free support rollers.*

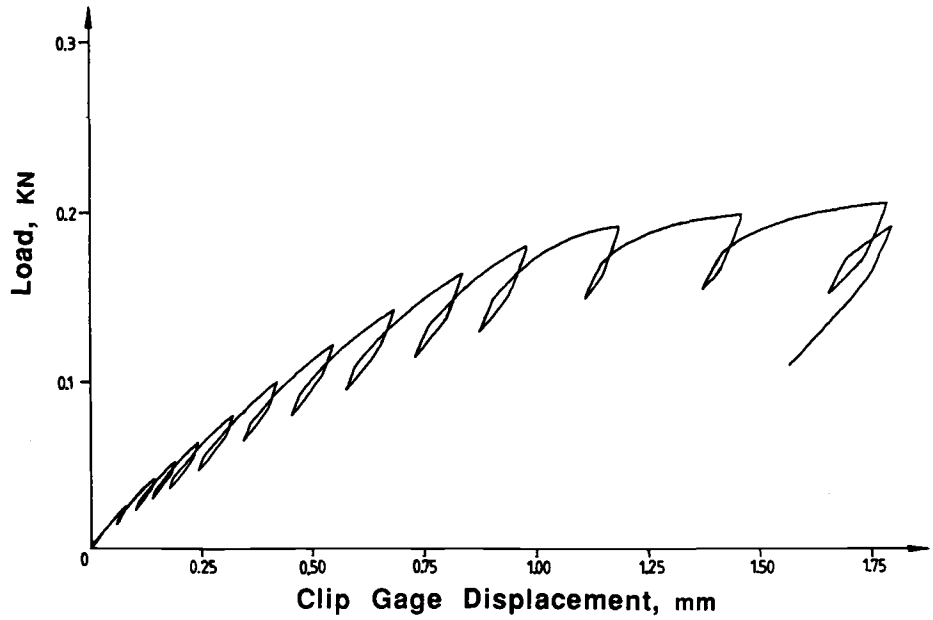

FIG. 8—*Typical load-clip gage displacement curve for HDPE with fixed support rollers.*

were made. Firstly, the material was assumed to behave elastically when it was subjected to sudden changes of loading conditions or rate, and thus the slope taken for calculating the crack length should be close to the point of unloading. Secondly, the region immediately after the unloading point should not be included since pronounced curvature at that region was caused by the redistribution of stress in the system after unloading. The position of the intersection point of the loading and unloading curves, marked as Point A in Fig. 7, was found to be fairly consistent and independent of the amount of unloading which had taken place; hence, Point A could be considered as the end of the stress redistribution in the system. The first linear region starting from Point A was used for crack length estimation as shown in Fig. 7. The change of the slope along the unloading loops for the HDPE and MDPE specimens is shown in Figs. 9 and 10, respectively, where both axes are plotted on arbitrary scales. Despite the scatter in the data, it can be seen that the slope attains a fairly constant value after the Point A, where the material was assumed to commence behaving in an elastic manner; hence, the compliance measurements were taken in this region. The estimated final crack extensions using this procedure were compared with the measured ones, and the results are shown in Fig. 11. The ASTM E 813 standard suggested that the accuracy of the predicted crack extension should be within ±15% of the real value. However, for small amounts of crack extension, this requirement is difficult to achieve. It has been proposed [*13*] that a margin of ±0.1 mm or ±15% in crack extension, whichever is greater, can be regarded as an appropriate requirement for crack length measurement accuracy. Based on these criteria, it can be seen from Fig. 11 that most of the data satisfy this requirement and those which do not are only marginally outside.

Single Specimen J *Tests*

Figures 12, 13, and 14 shows the *J-R* curves obtained from the single specimen *J* tests for HDPE, PVDF, and MDPE, respectively. The experimental blunting lines acquired from

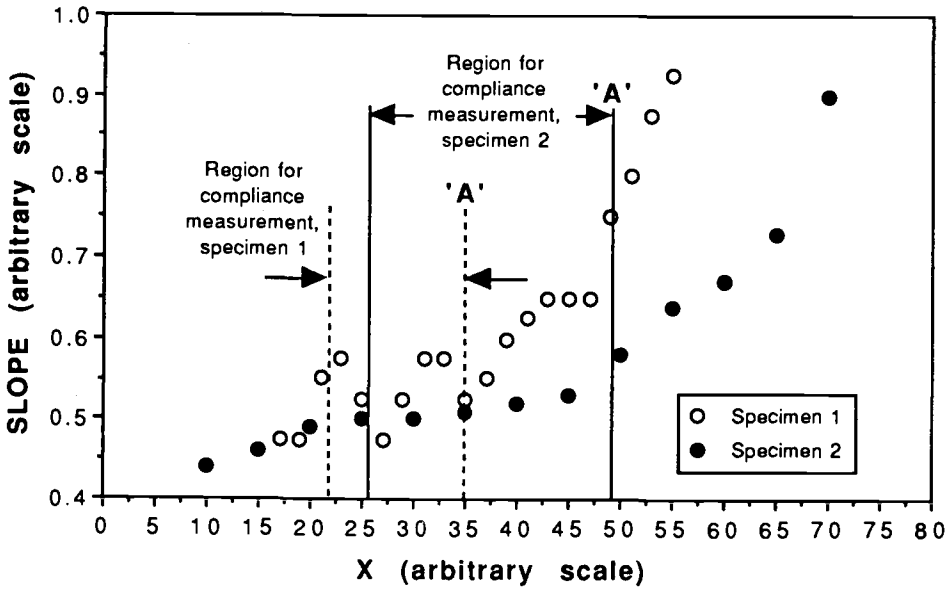

FIG. 9—*The change of slope along the unloading loop for HDPE.*

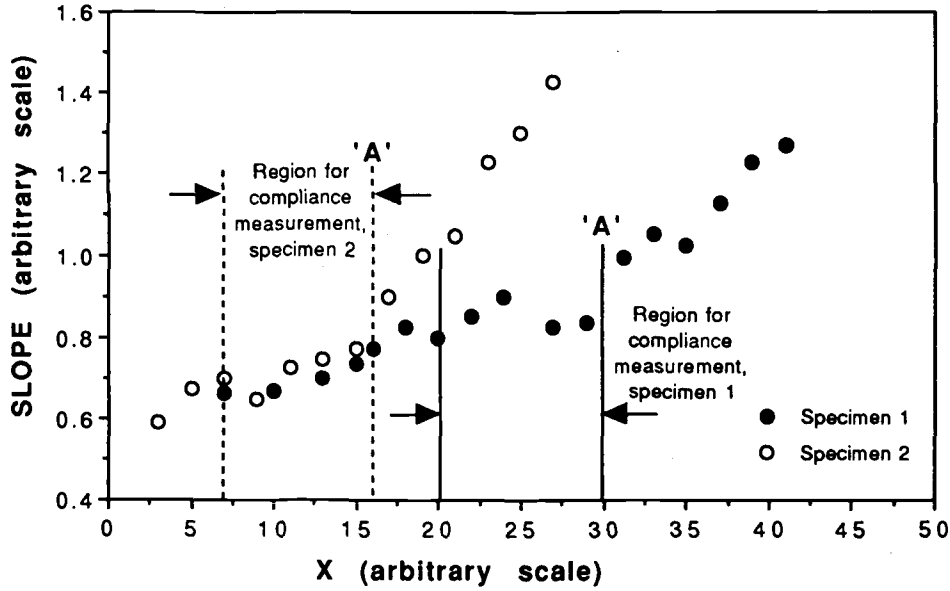

FIG. 10—*The change of slope along the unloading loop for MDPE.*

the multiple specimen J tests were used for evaluating the J_{Ic} values. The new E 813 protocol again predicts higher J_{Ic} values than the old one. The J-R curves for the HDPE at various loading rates are given in Fig. 15, and the effect of the flattening of the R-curve for high loading rates can be also observed. It can be seen that the scatter in the data is more

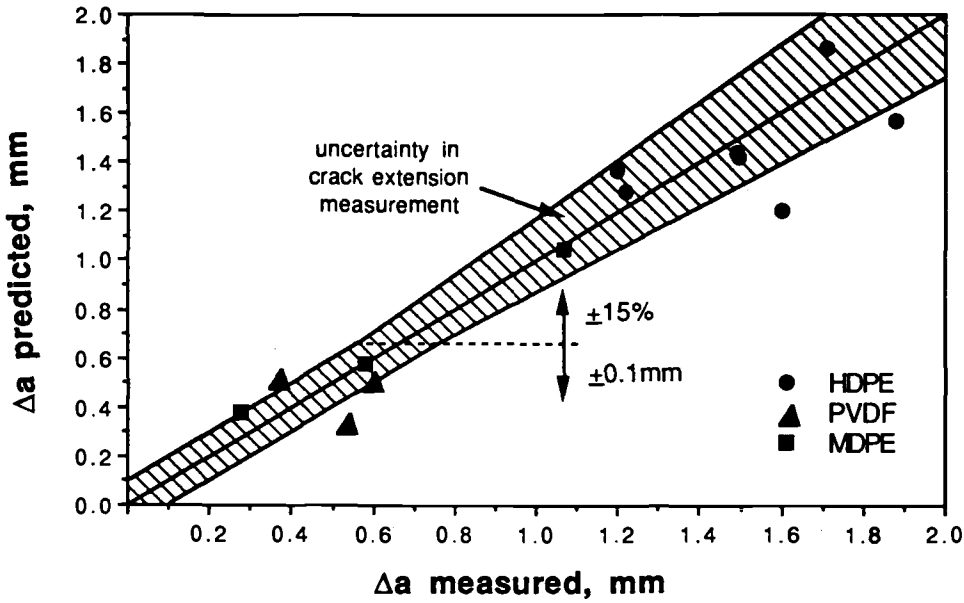

FIG. 11—*Comparison of measured and predicted* Δa.

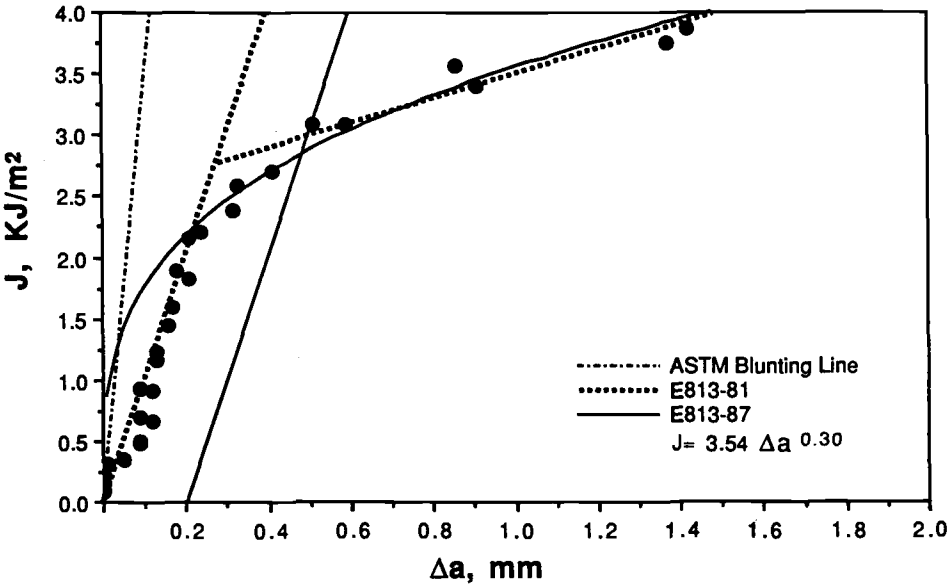

FIG. 12—J-R *curve for HDPE from single specimen* J *tests with loading rate of 1 mm/min.*

pronounced in the blunting region. The *J-R* curves obtained from the two methods are compared and shown in Figs. 16 to 19. Despite the scatter of the data, the *R*-curves acquired from both methods show good agreement. All the numerical results are summarized in Table 3.

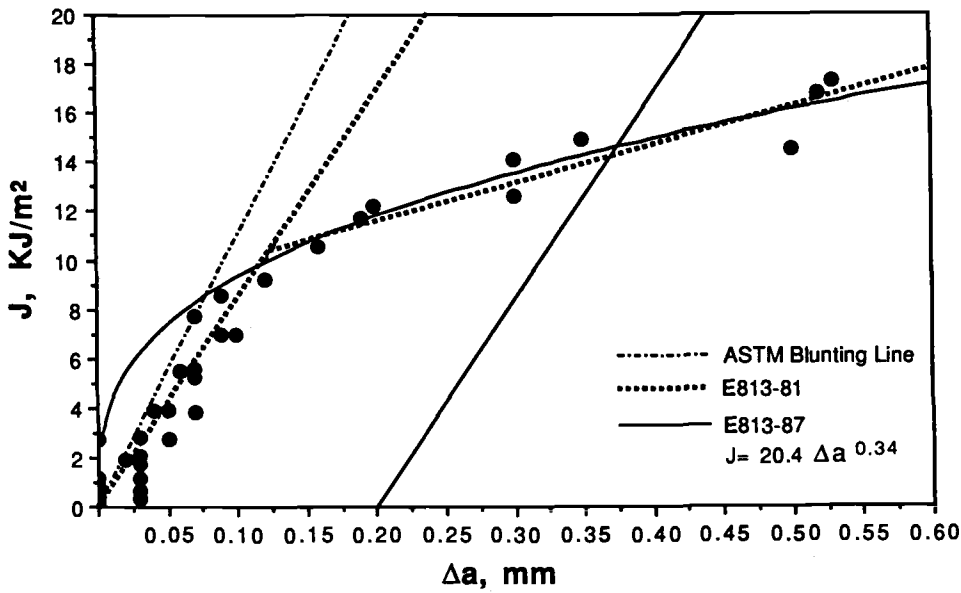

FIG. 13—J-R *curve for PVDF from single specimen* J *tests.*

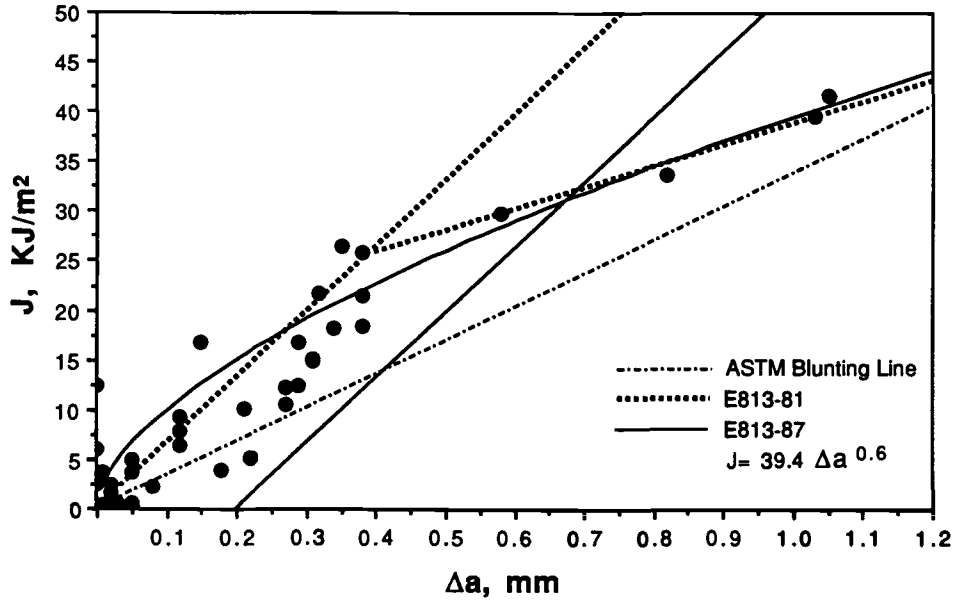

FIG. 14—J-R *curve for MDPE from single speciment* J *tests.*

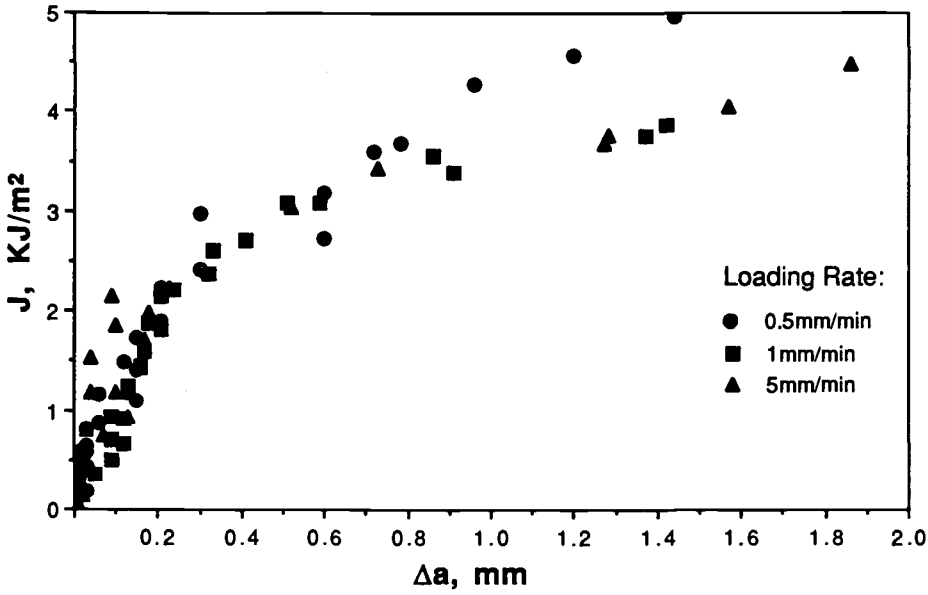

FIG. 15—J-R *curves for HDPE from single specimen* J *tests at various loading rates.*

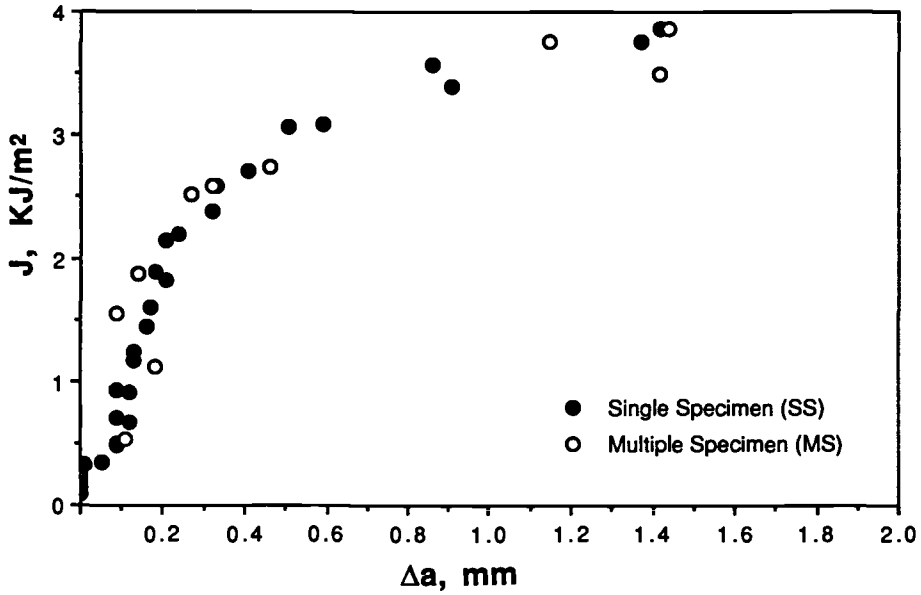

FIG. 16—*Comparison of* J-R *curves from multiple and single specimen* J *tests for HDPE.*

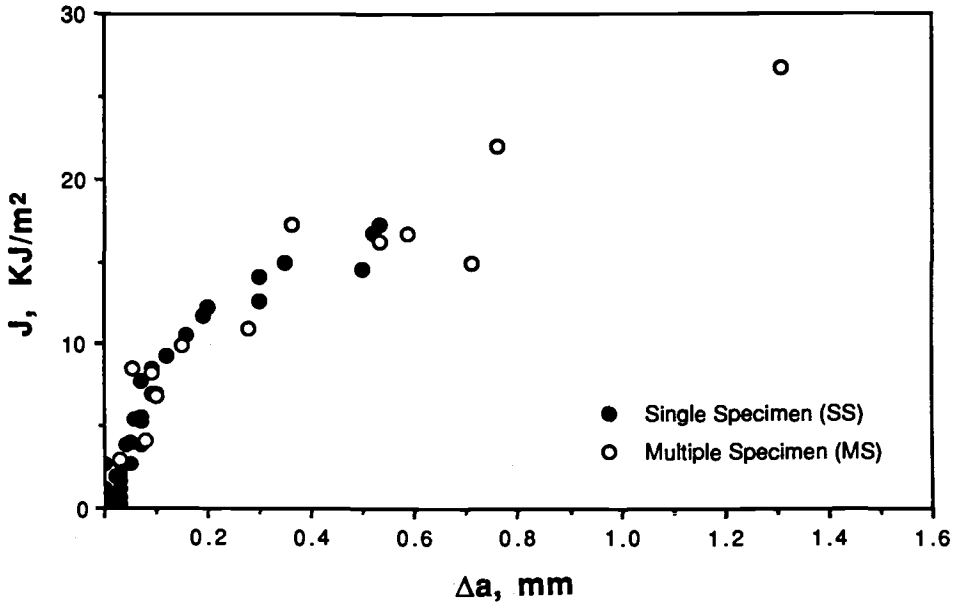

FIG. 17—*Comparison of* J-R *curves from multiple and single specimen* J *tests for PVDF.*

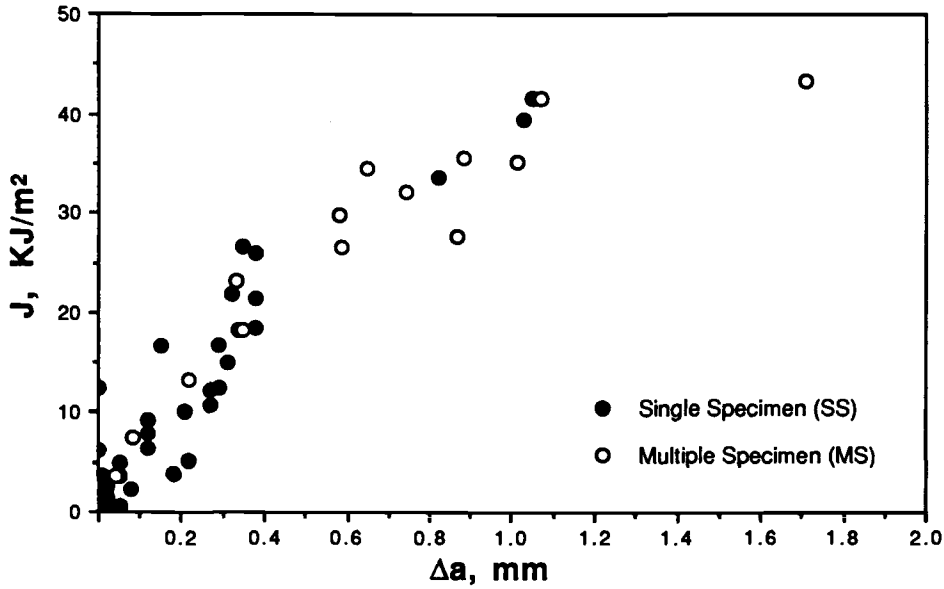

FIG. 18—*Comparison of* J-R *curves from multiple and single specimen* J *tests for MDPE.*

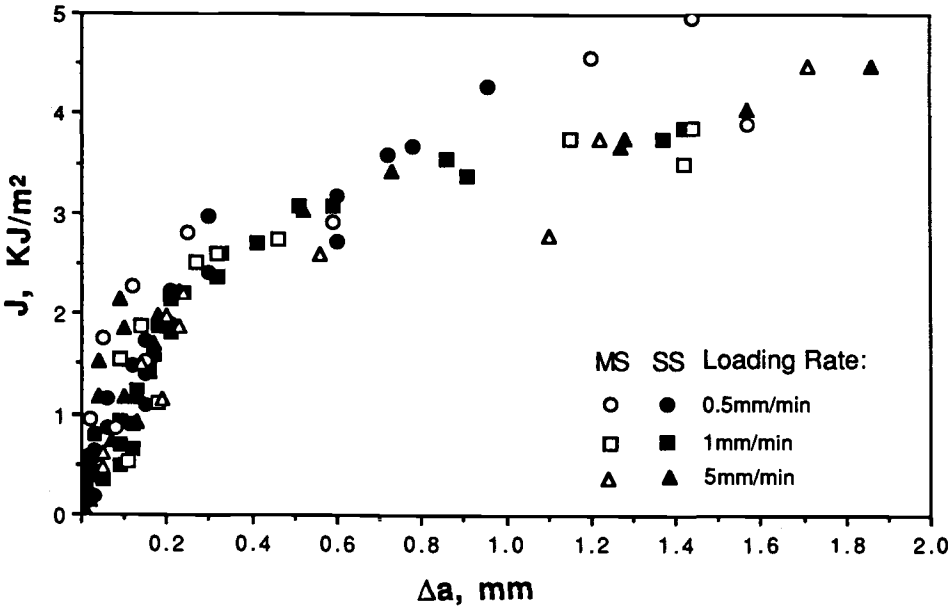

FIG. 19—*Comparison of* J-R *curves from multiple and single specimen* J *tests for HDPE at various loading rates.*

TABLE 3—*Main results.*

Material	Loading Rate, mm/min	J_{Ic}, kJ/m²			
		Multiple Specimen		Single Specimen	
		E 813-81	E 813-87	E 813-81	E 813-87
PVDF	1	10.1	15.0	10.2	14.5
MDPE	0.5	26.5	28.5	26	31
HDPE	0.5	2.6	3.0	2.3	2.8
	1.0	2.6	2.9	2.8	2.8
	5.0	2.1	2.7	2.7	3.0

Discussion

Application of the ASTM E 813 Test Method

For results to be considered valid in this method, the J-controlled growth condition must be fulfilled, and this is achieved by limiting the maximum crack extension to less than 6% of the uncracked ligament [*14*]. In the ASTM E 813 standard, the 1.5 mm offset blunting line is used also for data exclusion. Combining these two restrictions, it can be implied that the specimen should have a minimum width of 50 mm and a thickness of 25 mm. This may impose problems in producing specimens of such a size for polymers. It is suspected that the 6% criteria is too stringent, and, on examination of the work performed by other authors [*1–4*] and the results from this study, it is apparent that a geometry independent R curve can exist at crack growths of up to about 10% of the uncracked ligament. It has been also proposed that the limit can be relaxed to 15% for metals, and a size independent R-curve still be obtained [*15*]. Therefore, it is suggested here that a maximum crack extension of 10% of the ligament is considered to be acceptable for polymers.

The nine point averaging technique used for crack extension measurements is considered to be more appropriate than the maximum point taken as the Δa by most other investigators [*1–5*] in the past. Since J is a two dimensional analysis a straight crack front is assumed so that the fracture area can be represented by the crack length. However, J is the energy per unit area and this area change is better described by the nine point averaging technique if the amount of curvature changes with Δa.

The data extrapolation procedure in the E 813-81 method can lead to an artificial size effect on the J_{Ic} value as observed in Ref *5*. The same effect could also result if the amount of crack extension is small [*9*], and this is illustrated in Fig. 20*a*. It can be seen that the J_{Ic} value depends on the amount of crack extension and the distribution of the data points. In order to reduce the bias on the J_{Ic} determination, δJ_{Ic}, it is suggested that the data exclusion and distribution schemes recommended in the standards should be followed if the E 813-81 protocol is adopted. However, the curve fitting practice in the E 813-87 method will provide a more consistent J_{Ic} value [*9*] as shown in Fig. 20*b*.

Blunting Line

In E 813, the blunting line plays a crucial role in defining the J_{Ic} value. However, it has been reported that the conventional blunting line does not adequately reflect the blunting mechanisms for polymers [*1,2,8,9*] and the same phenomenon can be seen in Figs. 3 to 5. The reasons for this are still uncertain, but it has been explained as the effect of plastic constraint at the crack tip [*2*]. From the results, this is considered to be inappropriate for

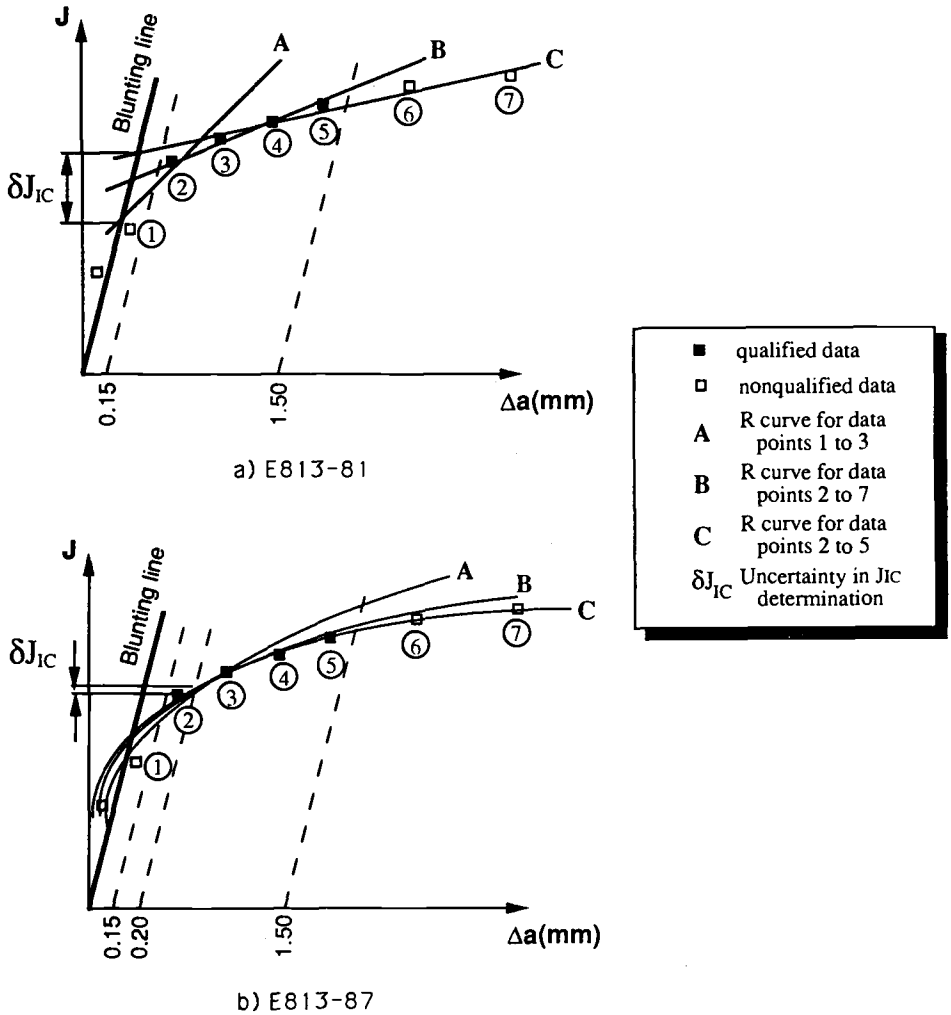

FIG. 20—*Error in determination of the* J_{Ic} *value.*

the materials tested here since the constraint factor will be less than 1 in the cases of HDPE and PVDF. It is believed that the problem lies on the crack length measurement and the properties of the materials. Crack extension measurements from the fracture surfaces are always difficult since the changes of fracture surface morphology are taken as crack advance. For materials such as HDPE which craze before fracture, the craze zone is usually included in the crack length measurements, and this is bound to give a less steep blunting line as shown in Fig. 21*a* in which $\Delta a_b > \delta/2$. In case of the tougher polymers such as MDPE, the material at the crack tip flows due to viscoelasticity, a layer of plastically deformed and strain hardened material will be formed, and a larger crack opening displacement δ, COD, and a steeper blunting line will result, as shown in Fig. 21*b* in which $\Delta a_b < \delta/2$. Figure 21*c* shows the usual assumption of smooth blunting in which $\Delta a_b = \delta/2$ together with the other two types of blunting line. Crack blunting measured from the side of the midsection by

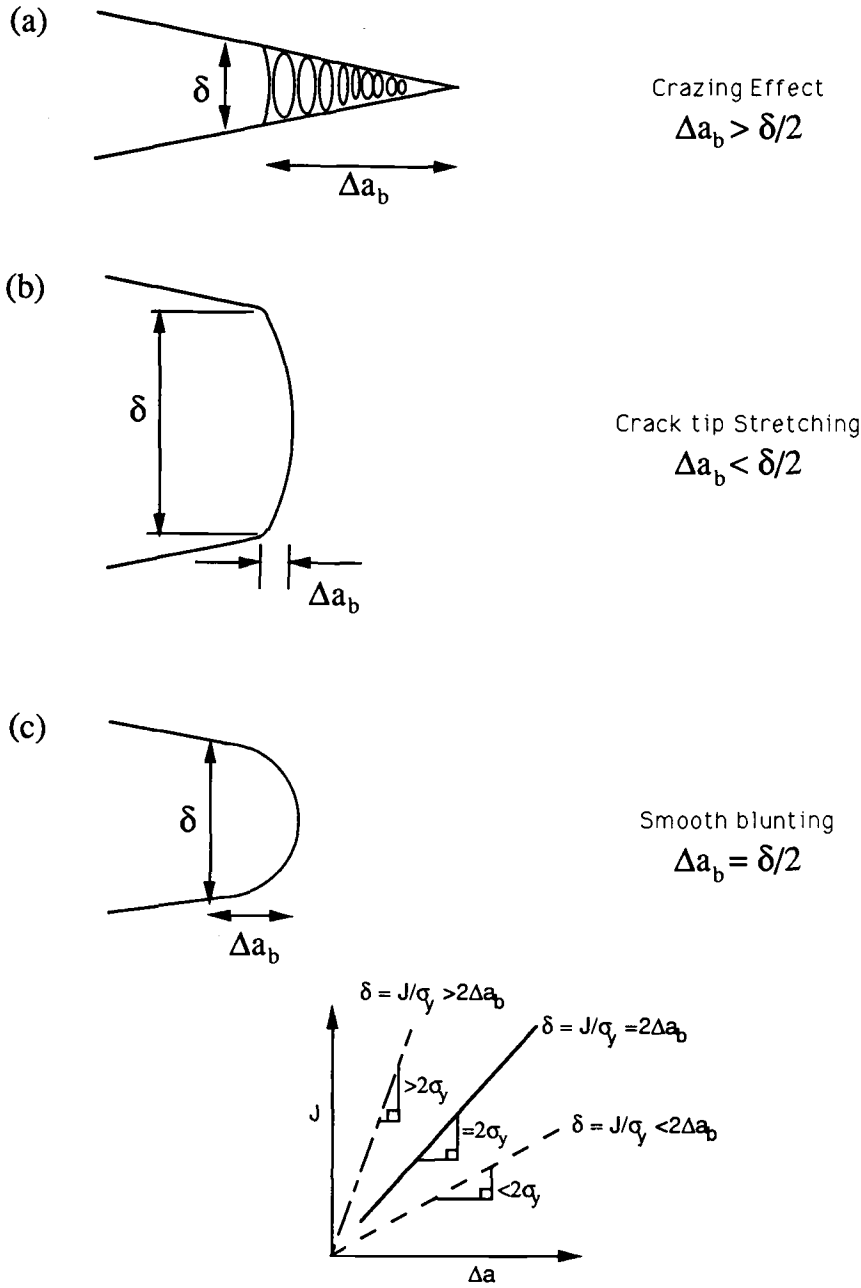

FIG. 21—*Illustration of blunting processes for polymers.*

sectioning of the specimen [*9*] provides an alternative, but the crack tip must be opened to attain the same COD as before unloading took place since the crack tip will close up at the relaxed state and no crack extension will be observed. The major difficulty with the application of the J method to polymers is to define a suitable measurement point for J_{Ic}, and

the properties of the materials vary greatly from nearly elastic to highly viscoelastic. Direct visualization of the initiation point is often impossible for opaque materials and the crack tends to initiate at the middle. Since the blunting process is material dependent, a formulation of the blunting line for polymers is difficult to establish. As long as the blunting line still plays a role in defining the J_{Ic}, further investigation on the blunting process is necessary.

Comparison of E 813-81 with E 813-87

By comparing the new and old ASTM E 813 protocols, it is apparent that each has its own advantages and drawbacks. The old protocol seems to reflect the initiation point more correctly, but the representation of the *R*-curve by a regression line will cause some degree of uncertainty in determining the J_{Ic}, especially for toughened polymers where the *R*-curve rises gradually, and a distinct change of slope, as expected in the protocol, will not be observed. For the new E 813 procedures, the power law fit gives a better description of the *R*-curve but the 0.2 mm offset blunting line for the J_{Ic} determination actually describes the fracture toughness at 0.2 mm ductile crack growth which will always give a higher J_{Ic} value. However, the 0.2 mm offset blunting line offers an advantage of excluding the data in the blunting region, which are often too small to be measured accurately for polymers, and the lack of knowledge in the blunting mechanisms of polymers also makes the validity of data in this region questionable. The new E 813 standard gives more consistent J_{Ic} values, albeit it does not characterize the initiation point satisfactorily.

Effect of Loading Rate

The J_{Ic} values and the *J-R* curve for the HDPE did not show a strong dependence on the loading rate, but it can be seen from Figs. 6 and 15 that the *J-R* curves tend to flatten with increasing loading rate. This indicates that the energy for crack propagation reduces as strain rate increases. However, extra experiments are considered to be necessary because of the restricted range of loading rate used in the tests and the amount of scatter in the data.

Single Specimen J *Method*

For the single specimen method, the point where compliance was taken for crack length prediction was determined empirically, and it worked well for the materials tested here which represent the characteristics of a range of thermoplastics. The results agreed well with the ones from the multiple specimen method within the experimental scatter. Because the compliance was measured manually, scatter in the data could not be avoided, and the accuracy could not be evaluated quantitatively. Nevertheless, the single specimen method was judged to be a possible alternative to the multiple specimen method.

Conclusions

The results from the multiple specimen tests and the single specimen tests were in good agreement. The regions on the unloading and loading hysteresis loops for compliance measurements were determined empirically, and it was observed that the friction of the support rollers can change the appearance of the loops. For the use of the E 813-81 standard, the data exclusion and distribution scheme suggested in the protocols must be followed in order to gain an unbiased estimate of J_{Ic} values. The maximum Δa of 6% of uncracked ligament recommended for attaining *J* controlled growth conditions was considered to be too stringent for polymers. The conventional blunting line, which plays an important role in J_{Ic} deter-

mination, was found to be inadequate for predicting the crack blunting behavior of polymers. The *J-R* curves for HDPE tended to flatten slightly as the loading rate increased, but the effect of it was still not clear due to insufficient data and the limited range of loading rate used in this study.

Acknowledgments

The authors wish to thank DSM Research for their generous financial support of this project. The study was motivated by the work of C. Tahon and A. Kelecom of Solvay & Cie which was first presented in the European Group on Fracture (EGF) Task Group meeting in Switzerland in 1987 and which provided valuable information for this study. We also wish to thank BP Chemicals and Solvay & Cie for providing the materials tested.

References

[1] Chan, M. K. V. and Williams, J. G., "*J*-Integral Studies of Crack Initiation of a Tough High Density Polyethylene," *International Journal of Fracture*, Vol. 19, 1983, pp. 145–159.

[2] Hashemi, S. and Williams, J. G., "A Fracture Toughness Study of Low Density and Linear Low Density Polyethylenes," *Polymer*, Vol. 27, 1986, pp. 384–392.

[3] Hashemi, S. and Williams, J. G., "Fracture Characterization of Tough Polymers Using the *J* Method," *Polymer Engineering and Science*, Vol. 26, No. 11, 1986, pp. 760–767.

[4] Hashemi, S. and Williams, J. G., "The Effects of Specimen Configuration and Notch Tip Radius on the Fracture Toughness of Polymers using J_c," *Plastics and Rubber Processing and Applications*, Vol. 6, No. 4, 1986, pp. 363–375.

[5] Huang, D. D. and Williams, J. G., "*J* Testing of Toughened Nylons," *Journal of Material Science*, Vol. 22, 1987, pp. 2503–2508.

[6] Jones, R. E. and Bradley, W. L., "Fracture Toughness Testing of Polyethylene Pipe Materials," *Nonlinear Fracture Mechanics: Volume I—Time Dependent Fracture, ASTM STP 995*, American Society for Testing and Materials, Philadelphia, 1989, pp. 447–456.

[7] Huang, D. D., "A Comparison of Multispecimen *J*-Integral Methods as Applied to Toughened Polymers," *Advances in Fracture Research, Vol. 4, Seventh International Conference on Fracture*, University of Houston, Houston, TX, 1989, pp. 2725–2732.

[8] Takemori, M. T. and Narisawa, I., "*J*-Integral Characterization of Impact-modified Polymers," *Advances in Fracture Research, Vol. 4, Seventh International Conference on Fracture*, University of Houston, Houston, TX, 1989, pp. 2733–2737.

[9] Narisawa, I. and Takemori, M. T., "Fracture Toughness of Impact-Modified Polymers Based on the *J*-Integral," *Polymer Engineering and Science*, Vol. 29, No. 10, 1989, pp. 671–684.

[10] Tada, H., Paris, P. C., and Irwin, G. R., *The Stress Analysis of Cracks Handbook*, Del Research Corporation, Hellertow, PA, 1973.

[11] Kapp, J. A., Leger, G. S., and Gross, B., "Wide-Range Displacement Expressions for Standard Fracture Mechanics Specimens," *Fracture Mechanics: Sixteenth Symposium, ASTM STP 868*, M. F. Kanninen and A. T. Hopper, Eds., American Society for Testing and Materials, Philadelphia, 1985, pp. 27–44.

[12] Bakker, A., "Compatible Compliance and Stress Intensity Expressions for the Standard Three-Point Bend Specimen," to be published in *International Journal of Fatigue and Fracture of Engineering Materials and Structures*.

[13] Heerens, J., Schwalbe, K.-H., and Cornec, A., "Modification of ASTM E 813-81 Standard Test Method for an Improved Definition of J_{Ic} Using New Blunting Line Equation," *Fracture Mechanics: Eighteenth Symposium, ASTM STP 945*, D. T. Read and R. P. Reed, Eds., American Society for Testing and Materials, Philadelphia, 1988, pp. 374–389.

[14] Shih, C. F., Andrews, A. H., and De Lorenzi, H. G., "Crack Initiation and Growth Under Fully Plastic Conditions: A Methodology for Plastic Fracture," Report NP-701-SR, Electric Power Research Institute, Palo Alto, CA, Feb. 1978, pp. 6.1–6.63.

[15] Gordon, J. R. and Jones, R. L., "The Effect of Specimen Size on the *J-R* Curve Behaviour of a Titanium Alloy," *Fatigue and Fracture of Engineering Material Structure*, Vol. 12, No. 4, 1989, pp. 295–308.

Author Index

A

Albrecht, P., 178

B

Bar-On, I., 260
Bernstein, H. L., 306

C

Chung, W. N., 320

D

Dodds, R. H., 19

F

Farrara, R. A., 197

G

Gallant, A. D., 260
Gordon, J. R., 81
Graham, S. M., 213

H

Herrera, R., 42, 114
Hiser, A. L., Jr., 102
Hu, J. M., 178
Huang, D. D., 290

J

John, S. J., 133
Jones, R. L., 81
Joyce, J. A., 57, 273

L

Landes, J. D., 42, 114
Landow, M. P., 163, 238
Lee, K., 42
Lloyd, W. R., 213
Lowe, A. L., Jr., 225

M

Macdonald, B. D., 102
Marschall, C. W., 163, 238
Miglin, M. T., 273

O

O'Hara, G. P., 197
Oberdick, R. H., 102
Ohtsuka, N., 150

R

Reuter, W. G., 213
Rolfe, S. T., 19

S

Senick, J. R., 197
Sharobeam, M. H., 114
Sorem, W. A., 19

T

Tuler, F. R., 260

U

Underwood, J. H., 197

V

Van Der Sluys, W. A., 2, 225, 273

W

Wade, C. S., 2, 273
Williams, J. G., 320

Y

Yoon, K. K., 225

Z

Zalinka, J. J., 197
Zhou, Z., 42

Subject Index

A

ASTM Standards
  E 8-86, 275
  E 399, 102
  E 399-83, 2, 274, 275
  E 813, 2, 42, 102
  E 813-81, 2, 163, 238–239, 263, 268, 290–291, 306, 313, 320
  E 813-87, 2, 3, 8, 60, 197, 213–219, 263, 274, 275, 290–291, 306, 313, 320
  E 1152, 42
  E 1152-87, 3, 7, 60–61, 150, 161, 228, 238, 277
  E 1290, 185
Austenitic stainless steels, 213, 238

B

Behavior
  elastic-plastic fracture, 114
  elastic-plastic materials, 19
  metals, 114
  test methods, load separation technique, 114
Blunt notch testing standard test method, 114
Blunting line, 320
British Standards
  BS 5762, 20
Brittle fracture testing, 19

C

Calibration, 133, 225
Carbon steel pipe, 238
Cleavage, 273
Compact tension, 133, 178
Compliance, 133
Computer interaction, 133
Crack extension
  data instability, 102, 163
  growth limit, 63–68
  J-resistance curves, 150
  measurement, 42, 57, 61–62
  nuclear piping materials, 238
  plastic CTOD, 190–191
  stainless steel welds, 213
Crack growth, 57, 150, 163, 290
Crack growth—polycarbonate, 306–307
Crack growth resistance curves, 81
Crack initiation, 57, 163, 197, 199
Crack initiation toughness, 213
Crack instabilities, 238
Crack length, 181–183, 188–189
Crack testing, 19, 42
Crack tip opening displacement (CTOD)
  deformation behavior, 178
  resistance curves, 81, 92–94, 185, 178
  specimen testing, 19, 34–36
CTOD (*see* Crack tip opening displacement)

D

Data instability
  fracture, 102
Deep crack testing, 19
Deformation behavior, 178
Deformation curve, 42
Deformation plasticity, 57
Deformation theory *J*, 150
Design
  use of *J*-resistance curves, 133
Direct current electric potential
  use to monitor crack growth, 163, 238
Displacement, 42
Ductile-brittle transition, 273
Ductile crack growth, 238
Ductile fracture
  crack growth resistance curves, 81
  eta factor, 114
  load separation, 114
  test methods, 19, 42, 57, 114
  toughness, 273
Ductile instability
  use of *J*-resistance curves, 133
Ductile metals, crack growth, 163
Ductile tearing, 273
Ductile-to-brittle transition, 273
Dynamic fatigue toughness tests, 277
Dynamic tension tests, 277

E

Elastic compliance, 42, 114
Elastic-plastic fracture
  behavior, 19
  crack growth resistance curves, 81
  crack initiation tests, 197
  ductile crack growth, 57, 273
  instability data, 102
  J-resistance curves
    nonincremental evaluation, 150
    residual stress, 260
    specimen size requirements, 81
  key-curves, 225
  Linde 80 welds, 225
  nuclear piping materials, 238
  polycarbonate, 306
  stainless steel weldment, 213
  test methods, 2, 42, 57, 114, 133
  toughened polymers, 290
Elastic unloading compliance, 42, 133
Electric potential method, 163–164, 165, 238
Electric Power Research Institute (EPRI), 3
Engineering applications
  J-control, 57–80
EPRI (*see* Electric Power Research Institute)
Eta factor, 114

F

Fatigue analysis
  notch method, to analyze crack initiation test results, 197
Fatigue crack initiation tests, 197
Ferrous materials—fracture toughness, 273
Finite element analysis, 19, 24
Fracture analysis, 57
Fracture behavior of polycarbonates, 306
Fracture mechanics
  crack growth resistance curves, 81
  key-curve analysis, 225
  plastic deformation, 260
  test methods, 133, 164
  toughness, 273, 290
Fracture tests
  crack growth, 290
  crack initiation, 197
  crack resistance curves, 81
  ferrous materials, 273
  J-R curves, 19, 42, 133, 199
    data instability, 102
  key-curves, 133, 225
  load separation technique, 114
  methods, 2, 42, 114
  polycarbonate, 306
  toughness, 19, 42, 81, 150, 163
    data instability, 102
Fracture toughness
  polycarbonate, 306
  stainless steel, 197, 260, 273
  toughened polymers, 290

H

HY 100 steel
  crack growth resistance curves, 81

I

Initiation toughness, 213
Instability, fracture
  data qualification, 102
Integrity assessment
  test methods, 133

J

J_{1c}
  test standards, 2
J-integral test methods
  analysis, 26–27, 42, 57
  crack growth, 81
  ductile crack growth, 57
  elastic unloading compliance, 114, 197
  engineering applications, 57–80
  fracture toughness, 197
  load separation technique, 114
  nuclear piping, 238
  polycarbonate, 306
  polymers, 320
  resistance curves, 57, 114, 133, 150, 197
  short crack specimens, 19
  stainless steel weldment, 213
  steels, 260
  test methods, 2, 133, 197, 238
  toughened polymers, 290
Johnson equation, modification, 163, 172

K

Key-curves, 133, 150, 225

L

Ligament depth, 290
Limit load, 178
Linear elastic behavior, 19, 290

Load, 42, 178
Load-line displacement, 186–188
Load separation
  test method for elasti-plastic fracture, 114
Low-alloy steels, 273

M

Material behavior, 260
Material properties, 23, 180–181, 100
Metallic materials
  test methods for fracture toughness, 2
Multiple specimen *J* tests, 320

N

Nonincremental evaluation
  J-resistance curve, 150
Normalization test methods
  crack growth resistance curves, 81
  J-R curves, 43, 44–47, 133
Nuclear piping materials, 238

O

Oak Ridge National Laboratory, 3
ORNL (*see* Oak Ridge National Laboratory), 3

P

Plane strain conditions, 290
Plastic CTOD R-curves, 191, 194–195
Plastic deformation, 260
Plastic fracture, 178
Plastic rotation factor, 178
Polycarbonate
  fracture toughness, 306
  J-integral fracture criteria, 315
  load displacement behavior, 308
  tensile properties, 308
Polyethylene, 320
Polymers, 290
Polyvinylide difluoride, 320
Precipitation-hardening stainless steel, 197
Pressure-vessel steels, 273
Prestrained specimens, 260, 268

R

R-curves (*see* Resistance curves)
Reactor vessel weldments, 225
Residual stress, 260
Resistance curves
  plastic crack growth, 81, 92–94, 97–98
Rubber-toughened polymers, 290

S

Safety analysis, 57
Short crack
  testing, 19
Single specimen J test, 320
Standard test methods
  load separation technique, 114
Stainless steel pipe, 238
Stainless steels
  fracture and fatigue testing, 197, 204
  material properties, 200
Steels, 260, 273

T

Tensile properties—polycarbonate, 308
Test methods
  blunt notch testing standard, 114
  elastic-plastic fracture, 2, 114, 150, 197, 273
  elastic unloading compliance, 133, 201
  fracture instability
    data qualification limit, 102
  HY-100 steel, 260
  J-resistance curves, 19, 42, 133, 150, 213
  key curves, 133, 150, 225
  load separation technique, 114
  nuclear piping materials, 238
  plastic fracture, 178
  polycarbonate, 306
  polymeric materials, 290
  short crack specimens, 19
  stainless steel welds, 213, 225
  three-point bend, 213
  unloading compliance, 197
    equipment, 201
Three-point bend, 133, 197, 213
Toughened polymers, 290
Toughness
  crack growth resistance curves, 81
  eta factors, 114
  J-resistance curve, 150
  load separation technique, 114
  test methods, 2, 19, 114, 213, 273
  test results, 103
  stainless steel weld, 213
Transition fracture
  instability data qualification, 102
  toughness, 19
Tunneling growth, 213

U

Unloading compliance
  key curves, 133, 225
  nuclear piping materials, 238
  welded steel, 197, 213

V

Von Mises stress distribution, 20

W

Welds
  fracture and fatigue testing, 197, 204
  material properties, 200
  Linde 80 metals, 225
  stainless steel, 213

ISBN 0-8031-1418-4